

**ADVANCES IN CHEMICAL PHYSICS**  
**VOLUME XXXVII**

## EDITORIAL BOARD

- C. J. BALLHAUSEN, Kobenhaven Universitets Fysisk-Kemiske Institut, Kemisk Laboratorium IV, Kobenhaven, Denmark
- J. J. M. BEENAKKER, Rijksuniversiteit te Leiden, Kamerlingh Onnes Laboratory, Leiden, Netherlands
- RICHARD B. BERNSTEIN, Department of Chemistry, University of Texas at Austin, Austin, Texas, U.S.A.
- H. HAKEN, Institut für Theoretische und Angewandte Physik der Technischen Hochschule, Stuttgart, Germany
- YU L. KLIMONTOVITCH, Moscow State University, Moscow, USSR
- RYOGO KUBO, Department of Physics, University of Tokyo, Tokyo, Japan
- M. MANDEL, Chemie-Complex der Rijks-Universiteit, Wassenaarseweg, Leiden, Netherlands
- PETER MAZUR, Institute Lorentz voor Theoretische Natuurkunde, Nieuwsteeg, Leiden, Netherlands
- GREGOIRE NICOLIS, Pool de Physique, Faculte de Sciences, Universite Libre de Bruxelles, Bruxelles, Belgium
- S. ONO, Institute of Physics, University of Tokyo, (College of General Education), Tokyo, Japan
- MICHAEL PHILPOTT, IBM Research Center, San Jose, California, U.S.A.
- J. C. POLANYI, Department of Chemistry, University of Toronto, Toronto, Ontario, Canada
- YVES POMEAU, Commissariat a l'Energie Atomique, Centre d'Etudes nucleares de Saclay, Division de la Physique, Gif sur Yvette, France
- B. PULLMAN, Institute de Biologie, Physico-Chimique, Universite de Paris, Paris, France
- C. C. J. ROTHAAAN, Departments of Physics and Chemistry, The University of Chicago, Chicago, Illinois, U.S.A.
- IAN ROSS, Department of Chemistry, Australian National University, Canberra, Australia A.C.T.
- JOHN ROSS, Department of Chemistry, Massachusetts Institute of Technology, Cambridge, Massachusetts, U.S.A.
- R. SCHECTER, Department of Chemical Engineering, University of Texas at Austin, Austin, Texas, U.S.A.
- I. SHAVITT, Battelle Memorial Institute, Columbus, Ohio, U.S.A.
- JAN STECKI, Institute of Physical Chemistry of the Polish Academy of Sciences, Warszawa, Poland
- GEORGE SZASZ, General Electric Corporate R & D, Zurich, Switzerland
- KAZUHISA TOMITA, Department of Physics, Faculty of Science, Kyoto University, Kyoto, Japan
- M. V. VOLKENSTEIN, Institute of Molecular Biology, Academy of Science, Moscow, USSR
- E. BRIGHT WILSON, Department of Chemistry, Harvard University, Cambridge, Massachusetts, U.S.A.

# Advances in CHEMICAL PHYSICS

EDITED BY

**I. PRIGOGINE**

University of Brussels  
Brussels, Belgium  
and  
University of Texas  
Austin, Texas

AND

**STUART A. RICE**

Department of Chemistry  
and  
The James Franck Institute  
The University of Chicago  
Chicago, Illinois

**VOLUME XXXVII**

AN INTERSCIENCE® PUBLICATION

JOHN WILEY AND SONS

NEW YORK • CHICHESTER • BRISBANE • TORONTO

An Interscience ® Publication

Copyright © 1978 by John Wiley & Sons, Inc.

All rights reserved. Published simultaneously in Canada.

Reproduction or translation of any part of this work beyond that permitted by Sections 107 or 108 of the 1976 United States Copyright Act without the permission of the copyright owner is unlawful. Requests for permission or further information should be addressed to the Permissions Department, John Wiley & Sons, Inc.

**Library of Congress Catalog Number: 58-9935**

ISBN 0-471-03459-2

Printed in the United States of America

10 9 8 7 6 5 4 3 2 1



# CONTRIBUTORS TO VOLUME XXXVII

- G. DE BROUCKERE, Foundation for Fundamental Research on Matter, Lucas Bolwerk 4, Utrecht, The Netherlands
- G. D. CARNEY, North American Carbon Company, P.O. Box 19737, Columbus, Ohio
- R. R. CHANCE, Materials Research Center, Allied Chemical Corporation, Morristown, New Jersey
- Y.-D. CHEN, Laboratory of Molecular Biology, National Institute of Arthritis, Metabolism, and Digestive Diseases, National Institutes of Health, Bethesda, Maryland
- C. W. KERN, Department of Chemistry, The Ohio State University, Columbus, Ohio
- J. J. KOZAK, Department of Chemistry, University of Notre Dame, Notre Dame, Indiana
- R. DE LEVIE, Department of Chemistry, Georgetown University, Washington, D.C.
- K. D. LUKS, Department of Chemical Engineering, University of Notre Dame, Notre Dame, Indiana
- A. PROCK, Department of Chemistry, Boston University, Boston, Massachusetts
- R. SILBEY, Department of Chemistry and Center for Materials Science and Engineering, Massachusetts Institute of Technology, Cambridge, Massachusetts
- L. L. SPRANDEL, Department of Chemistry, The Ohio State University, Columbus, Ohio

# INTRODUCTION

Few of us can any longer keep up with the flood of scientific literature, even in specialized subfields. Any attempt to do more, and be broadly educated with respect to a large domain of science, has the appearance of tilting at windmills. Yet the synthesis of ideas drawn from different subjects into new, powerful, general concepts is as valuable as ever, and the desire to remain educated persists in all scientists. This series, *Advances in Chemical Physics*, is devoted to helping the reader obtain general information about a wide variety of topics in chemical physics, which field we interpret very broadly. Our intent is to have experts present comprehensive analyses of subjects of interest and to encourage the expression of individual points of view. We hope that this approach to the presentation of an overview of a subject will both stimulate new research and serve as a personalized learning text for beginners in a field.

ILYA PRIGOGINE

STUART A. RICE

# CONTENTS

MOLECULAR FLUORESCENCE AND ENERGY TRANSFER NEAR INTERFACES <i>by R. R. Chance, A. Prock and R. Silbey</i>	1
NOISE ANALYSIS OF KINETIC SYSTEMS AND ITS APPLICATIONS TO MEMBRANE CHANNELS <i>by Yi-der Chen</i>	67
MATHEMATICAL MODELING OF TRANSPORT OF LIPID-SOLUBLE IONS AND ION-CARRIER COMPLEXES THROUGH LIPID BILAYER MEMBRANES <i>by Robert de Levie</i>	99
THE STATISTICAL MECHANICS OF SQUARE-WELL FLUIDS <i>by Kraemer D. Luks and John J. Kozak</i>	139
CALCULATIONS OF OBSERVABLES IN METALLIC COMPLEXES BY THE MOLECULAR-ORBITAL THEORY <i>by G. de Brouckère</i>	203
VARIATIONAL APPROACHES TO VIBRATION-ROTATION SPECTROSCOPY FOR POLYATOMIC MOLECULES <i>by Grady D. Carney, Ludwig L. Sprandel and C. William Kern</i>	305
AUTHOR INDEX	381
SUBJECT INDEX	393

**ADVANCES IN CHEMICAL PHYSICS**

**VOLUME XXXVII**

# MOLECULAR FLUORESCENCE AND ENERGY TRANSFER NEAR INTERFACES

R. R. CHANCE

*Materials Research Center, Allied Chemical Corporation,  
Morristown, New Jersey*

A. PROCK\*

*Department of Chemistry, Boston University, Boston, Massachussets,*

R. SILBEY\*

*Department of Chemistry and Center for Materials Science and Engineering,  
Massachusetts Institute of Technology, Cambridge, Massachussets*

## CONTENTS

I.	Introduction . . . . .	2
II.	Dipole Emission Near Interfaces . . . . .	3
	A. Theory for a Single Mirror . . . . .	3
	B. Comparison to Experiment. . . . .	13
	C. Energy Transfer. . . . .	21
III.	Dyadic Green's Function Method . . . . .	26
	A. General Formulation . . . . .	26
	B. Higher Multipoles Near Single Interfaces . . . . .	29
	C. Multiple Interfaces. . . . .	30
	1. Finite Metal Film. . . . .	31
	2. Double Mirror. . . . .	33
	3. General Stratified Media . . . . .	35
	D. Appendix. Decay Rate of Multipole Emitters Near a Mirror A check by Other Methods . . . . .	37
IV.	Energy Transfer and Surface Plasmons . . . . .	39
	A. Isotropic Media. . . . .	39
	B. Anisotropic Media. . . . .	46
	1. Dipole Near an Anisotropic Absorbing Medium . . . . .	46
	2. Dipole Embedded in Anisotropic Nonabsorbing Medium. . . . .	56
	3. Appendix. . . . .	61
V.	Summary . . . . .	63
	Acknowledgments . . . . .	63
	References . . . . .	64

\*Work of this author was partially supported by the National Science Foundation.

## I. INTRODUCTION

The lifetime of an excited molecule fluorescing near an interface between two media can be altered substantially owing to reflection and absorption at the surface. The perfection of the fatty-acid monolayer assembly technique by Kuhn and co-workers<sup>1-4</sup> led to a series of beautiful experiments by Drexhage et al.,<sup>5-9</sup> in which the fluorescent lifetime of an excited molecule was measured near gold, silver, and copper surfaces. By the Langmuir-Blodgett dipping technique,<sup>11,12</sup> a number of layers of fatty acid were placed on a metal surface, and a layer of dye molecules was then put on top of this assembly. In this way the dye molecules were a known fixed distance from the metal. The dye molecules were then excited and their fluorescence was monitored. It was found that for large distances from the metal surface the fluorescence lifetime oscillated as a function of distance, while for small distances the lifetime went monotonically towards zero. The oscillations are explained qualitatively as being due to the metal surface acting as a mirror for the electric field of the emitter. The interference between the reflected wave and the initial wave gives rise to the observed oscillations in the lifetime.<sup>5-8,12</sup> The decrease in the lifetime when the distance becomes small is due to nonradiative transfer of energy from the excited molecule to the metal.<sup>13,14</sup> The nature of the states of the metal that accept this energy was unclear until the analogy between these experiments and the problem of radio-wave propagation near the surface of the earth became apparent.<sup>13-15</sup> The emitting molecule acts as an oscillating dipole (antenna) near a partially absorbing and partially reflecting surface (earth). Sommerfeld<sup>16</sup> provided the first theoretical treatment of the radio problem in 1909 and pointed out the possibility of a surface wave being present for the antenna close to the earth. In the same way it has been shown that the *surface-plasmon* modes of the metal dielectric interface are those that couple to the near field of the emitting molecule.<sup>17-19</sup> These modes have become of interest in recent years because of the experiments of Otto<sup>20</sup> and Burstein,<sup>21</sup> and the theoretical work of Ritchie<sup>22</sup> and others.<sup>23</sup>

In the present article the classical theory of an oscillating charge distribution near a dielectric interface is applied to the problem of molecules fluorescing near a surface. The experiments of Drexhage et al.<sup>5-9</sup> are explained quantitatively, and the connection between energy transfer and the surface modes is stressed. In addition, the possibility of resonant coupling to the surface plasmons is discussed for a variety of experimental situations.

In Section II the theory of a dipole antenna near a metal surface is given in detail and the terms in the decay-rate constant are separated into those due to energy transfer and those due to "radiative" effects. Detailed comparisons to the available experimental data are made. In Section III the dyadic Green's function method is used to derive damping rates for oscillating charge distributions near a single interface and near multiple interfaces. This method proves to be the most direct and elegant way to derive most of the formulas. In Section IV the coupling of the emitting molecule to the surface-plasmon modes of the metal/dielectric interface is discussed in detail for both isotropic and anisotropic media. Both nonresonant and resonant coupling are considered. Some experiments to test these predictions are suggested.

## II. DIPOLE EMISSION NEAR INTERFACES

### A. Theory for a Single Mirror

In this section we describe two methods for calculating the lifetime of an emitting dipole near a single interface (mirror). The first involves the use of Kuhn's model,<sup>12</sup> which requires the calculation of the reflected electric field at the dipole position. The second is the energy flux method.<sup>18</sup> Though the two approaches are physically equivalent, the energy-flux method has the advantage of allowing a rigorous separation of radiative and nonradiative lifetime components.

Following Kuhn<sup>12</sup> we first write the equation of motion of the dipole (assumed to be a harmonically bound charge)

$$\ddot{\mu} + \omega^2 \mu = \frac{e^2}{m} E_R - b_0 \dot{\mu} \quad (2.1)$$

where  $\omega$  is the oscillation frequency in the absence of all damping,  $m$  is the effective mass of the dipole,  $E_R$  is the reflected field at the dipole position, and  $b_0$  is the damping constant (inverse lifetime) in the absence of the mirror. The dipole moment  $\mu$  and the reflected field  $E_R$  oscillate at the same (complex) frequency:

$$\mu = \mu_0 e^{-i(\omega + \Delta\omega)t} e^{-bt/2} \quad (2.2)$$

and

$$E_R = E_0 e^{-i(\omega + \Delta\omega)t} e^{-bt/2} \quad (2.3)$$

where  $\Delta\omega$  and  $b$  are the frequency shift and the lifetime in the presence of the mirror. The problem is then one of a driven harmonic oscillator where the resonant external force is the reflected radiation field of the emitting dipole.

Substituting into (2.1) and recognizing<sup>18</sup> that  $b^2$  and the magnitude of  $(e^2/\mu_0 m)E_0$  are very small compared to  $\omega^2$ , we have

$$\Delta\omega = \frac{b^2}{8\omega} + \left[ \frac{e^2}{2\mu_0 m\omega} \right] \text{Re}(E_0) \quad (2.4)$$

and

$$b = b_0 + \left[ \frac{e^2}{2\mu_0 m\omega} \right] \text{Im}(E_0) \quad (2.5)$$

The frequency shift is found to be quite small<sup>24</sup> and so is unimportant for the purposes of the discussion in this section. We return to  $\Delta\omega$  in Section IV. We now introduce the quantum yield of emitting state,  $q \equiv b_r/b$  and the classical formula for the radiative decay constant<sup>12,14</sup>

$$b_r = \frac{2}{3} \frac{e^2 k_1^3}{m\omega n_1^2} \quad (2.6)$$

where  $n_1$  is the refractive index of the medium containing the dipole and  $k_1$  is the propagation constant ( $k_1 = \omega n_1/c$ ). Equation 2.5 can now be rewritten in a more convenient form

$$\hat{b} \equiv \frac{b}{b_0} = 1 + \frac{3qn_1^2}{2\mu_0 k_1^3} \text{Im}(E_0) \quad (2.7)$$

The problem is now reduced to that of calculating the reflected electric field at the dipole position.

The geometry of the problem of the single mirror is shown in Fig. 1. The two regions are half spaces with dielectric constants given as  $\epsilon_1 = n_1^2$  and  $\epsilon_2 = n_2^2 - \kappa_2^2 + i2n_2\kappa_2$ , where  $n_2$  and  $\kappa_2$  are the real and imaginary parts of the refractive index of region 2. The electric field at any point in region 1 can be found as

$$\mathbf{E} = \frac{1}{\epsilon_1} [k_1^2 \Pi_1 + \nabla(\nabla \cdot \Pi_1)] \quad (2.8)$$

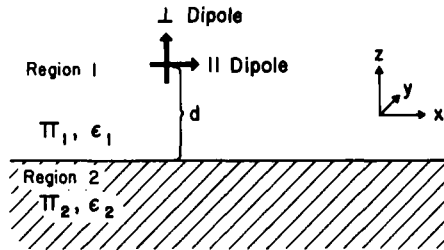


Fig. 1. Geometry for the single-mirror problem. Region 1 is a non-absorbing dielectric of refractive index  $n_1$  ( $\epsilon_1 = n_1^2$ ). Region 2 is a half-space with no restrictions on the dielectric constant except that it be isotropic.



where  $\Pi_1$  is the Hertz vector of region 1, which we now construct.

We first consider the dipole oriented perpendicular to the interface. Following Sommerfeld<sup>16</sup> we write the Hertz vectors in the two media as follows (in cylindrical coordinates  $r, z, \phi$ ):

$$\Pi_1 = \hat{e}_z \mu k_1 \int_0^\infty du J_0(ur) \frac{u}{l_1} (e^{\pm l_1(z-\hat{d})} + f_1 e^{-l_1 z}) \quad (2.9)$$

$$\Pi_2 = \hat{e}_z \mu k_1 \int_0^\infty f_2 e^{l_2 z} J_0(ur) \frac{u}{l_1} du \quad (2.10)$$

where  $\hat{d} \equiv k_1 d$ ,  $l_j \equiv -i(\epsilon_j/\epsilon_1 - u^2)^{1/2}$  and  $J_0(ur)$  is the zeroth-order Bessel function. The first term in (2.9) is the source term for the dipole; we take the minus sign in the region  $z > \hat{d}$  and the plus sign in the region  $z < \hat{d}$ , which is the region of interest here for the reflected field calculation. The terms  $f_1$  and  $f_2$  are to be determined by fitting the boundary conditions at  $z=0$ :

$$\epsilon_1 \Pi_1 = \epsilon_2 \Pi_2 \quad (2.11)$$

and

$$\frac{\partial \Pi_1}{\partial z} = \frac{\partial \Pi_2}{\partial z} \quad (2.12)$$

On solving, we find

$$f_1 = -R^{\parallel} e^{-l_1 \hat{d}} \quad (2.13)$$

$$f_2 = \frac{\epsilon_1}{\epsilon_2} (1 - R^{\parallel}) e^{-l_1 \hat{d}} \quad (2.14)$$

where  $R^{\parallel}$  is the reflection coefficient for an incident ray polarized parallel to the plane of incidence (p-polarized)<sup>25</sup>:

$$R^{\parallel} = \frac{\epsilon_1 l_2 - \epsilon_2 l_1}{\epsilon_1 l_2 + \epsilon_2 l_1} \quad (2.15)$$

Note that for the case of a perfect mirror ( $R^{\parallel} = -1$ ),  $f_1$  becomes  $e^{-l_1 \hat{d}}$  and gives the image term in Sommerfeld's treatment.<sup>16</sup> Substituting into (2.8) and omitting the source term, we obtain the reflected field at the dipole position as

$$E_R^{\perp} = -\frac{k_1^3}{\epsilon_1} \mu \int_0^\infty R^{\parallel} e^{-2l_1 \hat{d}} \frac{u^3}{l_1} du \quad (2.16)$$

Finally from (2.7), we have

$$\hat{b}_1 = 1 - \frac{3}{2} q \operatorname{Im} \left( \int_0^\infty R^{\parallel} e^{-2l_1 \hat{d}} \frac{u^3}{l_1} du \right) \quad (2.17)$$

We next consider the dipole oriented parallel to the  $x$ -axis and the interface (Fig. 1). Again, following Sommerfeld we write the Hertz vectors as follows:

$$\Pi_1 = \hat{e}_x \mu k_1 \int_0^\infty (e^{\pm l_1(z-d)} + f_1 e^{-l_1 z}) \frac{u}{l_1} J_0(ur) du + \hat{e}_z \mu k_1 \frac{x}{r} \int_0^\infty g_1 e^{-l_1 z} J_1(ur) du \quad (2.18)$$

and

$$\Pi_2 = \hat{e}_x \mu k_1 \int_0^\infty f_2 e^{l_2 z} J_0(ur) \frac{u}{l_1} du + \hat{e}_z \mu k_1 \frac{x}{r} \int_0^\infty g_2 e^{l_2 z} J_1(ur) du \quad (2.19)$$

The boundary conditions at  $z=0$  are

$$\frac{\partial \Pi_{1z}}{\partial z} - \frac{\partial \Pi_{2z}}{\partial z} = \frac{\partial \Pi_{2x}}{\partial x} - \frac{\partial \Pi_{1x}}{\partial x} \quad (2.20)$$

$$\epsilon_1 \frac{\partial \Pi_{1x}}{\partial z} = \epsilon_2 \frac{\partial \Pi_{2x}}{\partial z}, \quad (2.21)$$

$$\epsilon_1 \Pi_{1x} = \epsilon_2 \Pi_{2x}, \quad (2.22)$$

and

$$\epsilon_1 \Pi_{1z} = \epsilon_2 \Pi_{2z}. \quad (2.23)$$

On solving we find, again in agreement with Sommerfeld,<sup>16</sup>

$$f_1 = R^\perp e^{-l_1 d} \quad (2.24)$$

$$f_2 = \frac{\epsilon_1}{\epsilon_2} (1 + R^\perp) e^{-l_1 d} \quad (2.25)$$

and

$$g_1 = (R^\parallel - R^\perp) e^{-l_1 d}; \quad g_2 = \frac{\epsilon_1}{\epsilon_2} g_1 \quad (2.26)$$

where  $R^\perp$  is the reflection coefficient for the incident ray polarized perpendicular to the plane of incidence (s-polarized)

$$R^\perp = \frac{l_1 - l_2}{l_1 + l_2} \quad (2.27)$$

Note again for a perfect reflector ( $R^\perp = R^\parallel = -1$ ), we are left in (2.8) with source and image terms only, as expected.

On substituting into (2.8) and omitting the source term, we obtain

$$E_R^\parallel = \frac{k_1^3 \mu}{2\epsilon_1} \int_0^\infty [(1 - u^2) R^\parallel + R^\perp] e^{-2l_1 d} \frac{u du}{l_1} \quad (2.28)$$

and

$$\hat{b}_{\parallel} = 1 + \frac{3q}{4} \operatorname{Im} \int_0^{\infty} [(1-u^2)R^{\parallel} + R^{\perp}] e^{-2t_1 d} \frac{u du}{l_1} \quad (2.29)$$

(Equations 2.17 and 2.29 with some minor, but tedious, manipulation are in agreement with our previous work and with that of Tews.<sup>15</sup>)

Though we now have the theoretical description of the effect of a single mirror on the lifetime, the mirror has significant effects both on the radiative and nonradiative components of the lifetime—the latter being a result of nonradiative energy transfer. The method that we now describe gives a rigorous separation of these two effects. The geometry is the same as in Fig. 1, except now we imagine a plane above the dipole ( $z > d$ ) and a plane below the dipole ( $0 < z < d$ ). The total energy flux through these planes is now calculated. Since the planes are infinite in extent, this calculation accounts for all the energy flowing away from the dipole by way of the radiation field. The flux through each plane,  $F_{\uparrow}^{\dagger}$  or  $F_{\downarrow}^{\dagger}$ , is calculated by integrating the normal component of the complex Poynting vector,  $\mathbf{S}^*$ , over the plane<sup>25</sup>:

$$F_{\uparrow, \downarrow} = \operatorname{Re} \int_{A_{\uparrow, \downarrow}} \mathbf{S}^* \cdot \mathbf{n} dA \quad (2.30)$$

where

$$\mathbf{S}^* = \left( \frac{c}{8\pi} \right) \mathbf{E} \times \mathbf{H}^*$$

$$\mathbf{H} = -i \left( \frac{\omega}{c} \right) \operatorname{curl} \mathbf{\Pi}$$

and  $\mathbf{E}$  is given by (2.8). The Hertz vector  $\mathbf{\Pi}$  is given by (2.9) for the perpendicular dipole and by (2.18) for the parallel dipole. We begin with a detailed discussion of the perpendicular dipole. In that case we have

$$\mathbf{S}^* \cdot \mathbf{n} = -\frac{i\omega}{8\pi\epsilon_1} \left[ \frac{\partial}{\partial r} \left( \frac{\partial \Pi_{1z}}{\partial z} \right) \right] \left( \frac{\partial \Pi_{1z}^*}{\partial r} \right) \quad (2.31)$$

Substituting from (2.9) for  $\Pi_{1z}$  and integrating over the plane, we have for  $F_{\uparrow}$  (take minus sign in exponent of source term in  $\Pi_1$ ):

$$F_{\uparrow} = k_1^3 |\mu| \operatorname{Re} \int_{A_{\uparrow}} dr r d\phi \int_0^{\infty} \frac{i\omega}{8\pi\epsilon_1} [e^{-l_1(z-\hat{d})} - R^{\parallel*} e^{-l_1(z+\hat{d})}]$$

$$\times u'^2 J_1(u'r) du' [e^{-l_1^*(z-\hat{d})} - R^{\parallel*} e^{-l_1^*(z+\hat{d})}] \frac{u^2}{l_1^*} J_1(ur) du \quad (2.32)$$

On changing the order and integrating over  $\phi$ , we have

$$\begin{aligned}
F_1 = & k_1^3 |\mu|^2 \operatorname{Re} \int_0^\infty \int \frac{i\omega}{4\epsilon_1} [e^{-l_1(z-\hat{d})} - R^{**} e^{-l_1^*(z+\hat{d})}] \\
& \times [e^{-l_1^*(z-\hat{d})} - R^{**} e^{-l_1^*(z+\hat{d})}] \\
& \times u'^2 \frac{u^2}{l_1^*} du' du \int_0^\infty dr r J_1(u'r) J(ur) \quad (2.33)
\end{aligned}$$

The last integral equals  $\delta(u' - u)/u'$  and the integration over  $u'$  can be done to yield

$$F_1 = k_1^3 |\mu|^2 \operatorname{Re} \int_0^\infty \left( \frac{i\omega}{4\epsilon_1} \right) \frac{u^3}{l_1^*} |e^{-l_1(z-\hat{d})} - R^{**} e^{-l_1(z+\hat{d})}|^2 du \quad (2.34)$$

After noting that the  $1 \rightarrow \infty$  portion of the integral is imaginary and carrying out some minor manipulation, we divide by the total energy of the dipole ( $\frac{1}{2}\omega^2 m |\mu|^2 / e^2$ ) to obtain  $b_1$

$$b_1 = \left( \frac{2e^2 k_1^3}{3m\omega n_1^2} \right) \left[ 1 - \frac{3}{4} \operatorname{Im} \int_0^1 (1 - |R^{**}|^2) \frac{u^3 du}{l_1} - \frac{3}{2} \operatorname{Im} \int_0^1 R^{**} e^{-2l_1 \hat{d}} \frac{u^3 du}{l_1} \right] \quad (2.35)$$

Note that the first term in parentheses is just  $b_r$  from (2.6) and that for  $R^{**} = 0$ ,  $b = b_r/2$  as it should. Normalizing to the decay rate in the absence of mirror,  $b_0 = b_r/q$ , we have the final form:

$$\hat{b}_1 = q - \frac{3}{4} q \operatorname{Im} \int_0^1 (1 - |R^{**}|^2) \frac{u^3 du}{l_1} - \frac{3}{2} q \operatorname{Im} \int_0^1 R^{**} \frac{e^{-2l_1 \hat{d}}}{l_1} u^3 du \quad (2.36)$$

A similar prescription may be followed to obtain  $\hat{b}_i$  (the only modifications necessary are to change signs from minus to plus in the exponent of the source term for  $\Pi_1$  and to change the sign of  $S^*$ )

$$\hat{b}_i = \frac{3}{4} q \operatorname{Im} \int_0^1 (1 - |R^{**}|^2) \frac{u^3 du}{l_1} - \frac{3}{2} q \operatorname{Im} \int_1^\infty R^{**} e^{-2l_1 \hat{d}} \frac{u^3 du}{l_1} \quad (2.37)$$

These results can be compared with our results from the earlier calculation for  $\hat{b}_1$  of (2.17) according to the relation<sup>18</sup>

$$\hat{b} = b_1 + b_i + (1 - q) \quad (2.38)$$

where we have included the intrinsic nonradiative damping constant,  $b_{nr}/b_0 \equiv 1 - q$ . Equation 2.38 correctly reproduces (2.17) and the same is true for the parallel dipole. We only give the results for the parallel case:

$$\begin{aligned}\hat{b}_\uparrow = & q - \frac{3}{8} q \operatorname{Im} \int_0^1 du \frac{u}{l_1} [(1 - |R^\perp|^2) + (1 - u^2)(1 - |R^\parallel|^2)] \\ & + \frac{3}{4} q \operatorname{Im} \int_0^1 du \frac{u}{l_1} e^{-2l_1 \hat{d}} [R^\perp + (1 - u^2)R^\parallel]\end{aligned}\quad (2.39)$$

and

$$\begin{aligned}\hat{b}_\downarrow = & \frac{3}{8} q \operatorname{Im} \int_0^1 du \frac{u}{l_1} [(1 - |R^\perp|^2) + (1 - u^2)(1 - |R^\parallel|^2)] \\ & + \frac{3}{4} q \operatorname{Im} \int_1^\infty du \frac{u}{l_1} [R^\perp + (1 - u^2)R^\parallel] e^{-2l_1 \hat{d}}\end{aligned}\quad (2.40)$$

We now have enough information to calculate an apparent quantum yield,  $q_a \equiv \hat{b}_\uparrow / \hat{b}$ , which is the value that could be determined experimentally by measuring the emission intensity integrated over the half space of region 1 in Fig. 1. We show in Fig. 2 the variation of  $q_a$  with distance from a silver mirror (optical constants taken for an emission wavelength of 612 nm).<sup>26</sup> At large distances  $q_a$  approaches a value less than 1.0 because of "trivial" transfer to the silver mirror.<sup>18</sup> The dip in  $q_a$  at  $\hat{d} \sim 1.7$  is caused by a dramatic decrease in  $\hat{b}_\uparrow$  in this region (see Refs. 2 and 27). We return to this point later in this section. There are no experimental data for  $q_a$  available at this time.

Both Kuhn's model and the energy flux method give the effect of the mirror on the lifetime of the dipole. However, with the energy flux method we have separated and can now identify the individual terms. In (2.36), (2.37), (2.39), and (2.40), the first integral expression is, in each case, directly related to the transfer of energy to the mirror by way of the far field of the dipole ("trivial" transfer). This is obvious from the behavior of these terms in a number of limiting cases. For example, it is important to note that these terms are independent of distance, so that for large  $\hat{d}$  they are dominant in the equations for  $\hat{b}_\downarrow$ . Therefore, the transfer must be by way of the far field of the dipole. We have verified this assignment by a direct calculation of the absorption of photons from the far field of a dipole placed in front of the mirror.<sup>18</sup>

With the assignment of these distance-independent terms clear, we can now write expressions for the radiative,  $b_r$ , and nonradiative,  $b_{nr}$ , decay-rate constants in the presence of the mirror:

$$\hat{b}_r(\perp) = q - \frac{3}{2} q \operatorname{Im} \int_0^1 R^\parallel e^{-2l_1 \hat{d}} \frac{u^3 du}{l_1} \quad (2.41)$$

and

$$\hat{b}_{nr}(\perp) = (1 - q) - \frac{3}{2} q \operatorname{Im} \int_1^\infty R^\parallel e^{-2l_1 \hat{d}} \frac{u^3 du}{l_1} \quad (2.42)$$

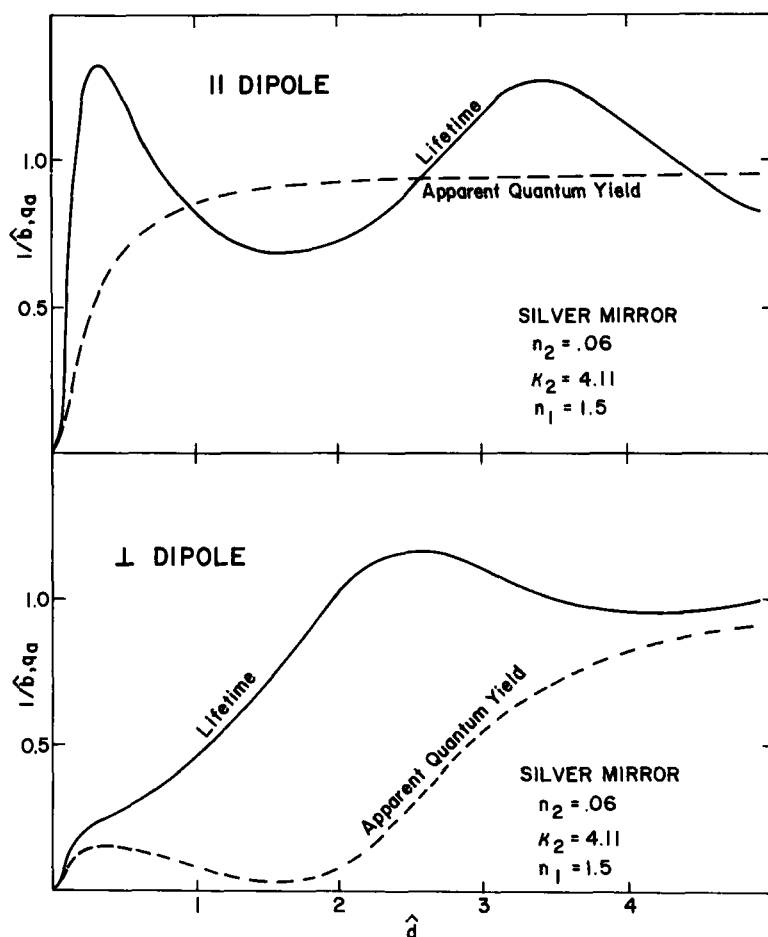


**Fig. 2.** Apparent quantum yield  $q_a$  and normalized lifetime  $1/\hat{b}$  versus distance  $\hat{d}$  ( $\hat{d} = 2\pi n_1 d/\lambda$ ) from a silver mirror ( $n_2 = 0.06 + i4.11$ ) from (2.36 through 2.40). Results are shown for electric dipoles oriented perpendicular to the interface and parallel to the interface. The quantum yield of the emitting state,  $q$ , is taken to be unity here and in the figures to follow unless noted otherwise.

Analogous expressions can be written, by inspection, for the parallel dipole. Our results for  $\hat{b}_r(\perp)$  and  $\hat{b}_r(\parallel)$  are the same as those given previously by Drexhage<sup>6-9</sup> who used a method based on the far field of the dipole (the interference method). This approach involves looking at the interference between the primary ray exiting directly from the dipole and the reflected ray from the mirror. The amplitude that results is converted to intensity and integrated over all angles  $\theta$ . After normalizing to the result in the absence of

the mirror and changing variables so that  $u = \sin \theta$ , we obtain (2.36) in the perpendicular case, and by neglecting  $d$  independent terms we get (2.41) as before. The same is true for the parallel case, as well as for more complicated mirror configurations and for multipole emission, which are discussed later. It is now clear that the interference method gives the effect of the mirror on the *radiative* decay-rate constant of the emitter. Furthermore, the interference method is a useful and sometimes convenient technique (see appendix, Section III.D) for obtaining the total decay-rate expression  $\hat{b}_{\perp, \parallel}$ , since we only need in that case to extend the integration to complex angles of incidence ( $\cos \theta = 0$  to  $i\infty$  or  $u = 1$  to  $\infty$ ).

Finally, the integral expression in (2.42) for  $\hat{b}_{nr}(\perp)$  gives the nonradiative rate constant for energy transfer to the mirror. At small  $\hat{d}$ ,  $\hat{b}_{nr}$  is proportional to  $\hat{d}^{-3}$  as expected from the dimensionality of the problem. We discuss the small distance behavior in more detail later in this section and in Section IV.

We now discuss briefly how our results compare to earlier approximate theories.<sup>27</sup> We showed earlier that Drexhage's formulas are identical to ours in the radiation zone limit ( $\hat{d}$  large). Other approaches have used image methods, assuming perfect reflection ( $R^{\perp} = R^{\parallel} = -1$ ). Taking this limit for (2.17) and (2.29), we find

$$\hat{b}_{\perp} = 1 - 3q \operatorname{Im} \left[ \left( \frac{1}{(2\hat{d})^3} - \frac{i}{(2\hat{d})^2} \right) e^{i2\hat{d}} \right] \quad (2.43)$$

and

$$\hat{b}_{\parallel} = 1 + \frac{3}{2} q \operatorname{Im} \left\{ \left[ \frac{1}{(2\hat{d})^3} - \frac{i}{(2\hat{d})^2} + \frac{1}{(2\hat{d})} \right] e^{i2\hat{d}} \right\} \quad (2.44)$$

in agreement with other work—including quantum mechanical treatments of the perfect mirror problem.<sup>17,28,29</sup>

None of these approximate theories mentioned above takes energy transfer into account. Kuhn<sup>12</sup> modified the image theory in a manner that, for the first time, reproduces some of the aspects of energy transfer—principally that  $\hat{b}$  varies as  $\hat{d}^{-3}$  at small  $\hat{d}$ . He inserted an amplitude and phase factor into the perfect-mirror equations to obtain, for example, in the parallel case

$$\hat{b}_{\parallel} = 1 + \frac{3}{2} q |R| \operatorname{Im} \left\{ \left[ \frac{-1}{(2\hat{d})^3} + \frac{i}{(2\hat{d})^2} + \frac{1}{(2\hat{d})} \right] e^{i(2\hat{d} - \delta)} \right\} \quad (2.45)$$

where  $Re^{-i\delta}$  is the reflection coefficient of the mirror at normal incidence, that is,  $R^{\parallel}$  or  $R^{\perp}$  at  $\theta = 0$  ( $u = 0$ ). For a perfect mirror  $|R| = 1$  and  $\delta = \pi$ , so that (2.44) and (2.45) agree in this limit. Equation 2.45 can be shown to be an asymptotic limit of (2.29) for large  $\hat{d}$ . The same is true for the perpendicular dipole case.

In Fig. 3 we compare results from the exact classical theory,<sup>14,15</sup> Kuhn's

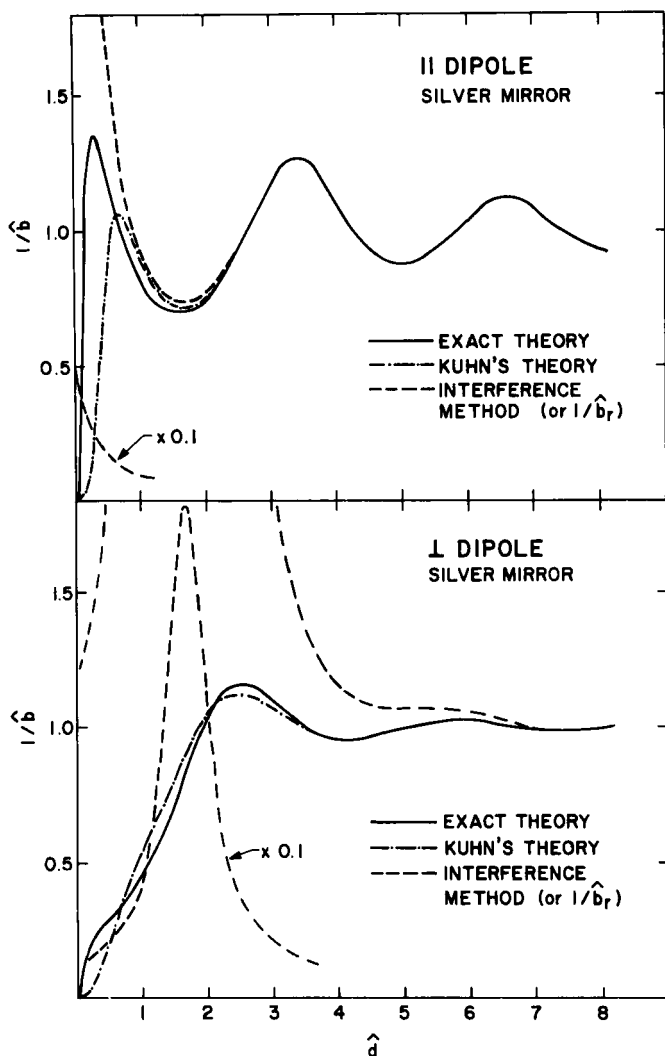


**Fig. 3.** Comparison of the exact classical theory [see (2.17) and (2.29)], Kuhn's approximate theory [see (2.45)], and the interference method. The interference method gives identical results to our (2.41) for the effect of the mirror on the radiative lifetime of the dipole,  $1/\hat{b}_r$ .

approximate theory,<sup>12</sup> and the interference method for a silver mirror. All three theories approach the same limiting values at large  $\hat{d}$ . However, at small  $\hat{d}$  Kuhn's theory fails to reproduce the exact result because of an overestimation (in this particular instance) of the importance of energy

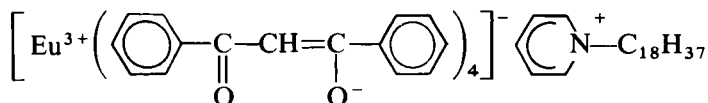


transfer. As is shown earlier the interference method yields  $\hat{b}_r$  only and, therefore, completely ignores energy transfer. Referring back to Fig. 2, the dip in  $q_a$  at  $\hat{d} \sim 1.7$  for the perpendicular dipole can now be understood. The large increase in the radiative lifetime in this region (a result of destructive interference), which is evident in Fig. 3, allows energy transfer to the mirror to compete more favorably and the apparent quantum yield decreases, reaching a minimum where  $1/\hat{b}_r$  is maximum.

### B. Comparison to Experiment

In this section we compare the theory to the experimental results of Drexhage et al.<sup>5-9</sup> and Tews et al.<sup>30</sup> for the  $\text{Eu}^{3+}$ /mirror systems. Other experimental results that emphasize the energy transfer region are considered separately in Section II.C.

The Langmuir-Blodgett technique<sup>10,11</sup> of monolayer deposition has been utilized by Kuhn and co-workers in the study of a variety of physical processes that require dimensional control on a molecular scale.<sup>1-4,31-33</sup> Their perfection of the monolayer assembly technique led to the  $\text{Eu}^{3+}$ /mirror experiments discussed in this section. The lifetime of a europium complex,



(emission at 612 nm) was measured as a function of distance from silver, gold, copper, and air mirrors. As a number of mirror configurations were investigated, the experimental data provided a thorough test of theory.

We first consider the  $\text{Ag}/\text{Eu}^{3+}$ /air system, since the experimental data for this system have appeared in numerous publications with a corresponding number of theoretical descriptions.<sup>4-9,12-15,27,34,35</sup> The construction of this system proceeds as follow<sup>6</sup>: (1) silver is evaporated onto a glass support to a thickness that is much greater than the absorption depth at 612 nm, (2) the desired number of fatty-acid spacers (each layer 26.4 Å thick) are added by the monolayer assembly technique, and (3) a final layer is added containing  $\text{Eu}^{3+}$  complex, so that, in this case, the emitter is located at or very near a fatty acid/air interface. The excitation energy is absorbed by the four ligands and is transferred nonradiatively to  $\text{Eu}^{3+}$  on a time scale that is very short compared to the lifetime of  $\text{Eu}^{3+}$  ( $\sim 1$  msec). Finally, the lifetime of the 612 nm  $\text{Eu}^{3+}$  emission is measured and the assembly process is repeated for another  $d$  value. It is important to note that this experimental arrangement requires a double-mirror (Ag and air) theory. In earlier theoretical treatments, the presence of the fatty acid/air interface was ignored. Two examples of such single-mirror, theoretical treatments are shown in Fig. 4 along with the experimental data for the  $\text{Ag}/\text{Eu}^{3+}$ /air systems. We have used Kuhn's

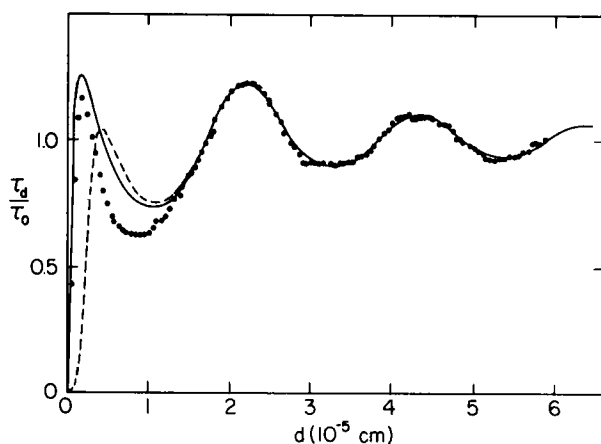


**Fig. 4.** Normalized lifetime versus distance for the Ag/Eu<sup>+</sup><sup>3</sup>/air double-mirror system. The solid curve is the best fit using exact classical theory<sup>14,15</sup> for a single-mirror configuration. The dashed curve is from Kuhn's approximate theory.<sup>12</sup> Both curves assume a parallel dipole configuration with  $q=0.85$  and  $\tau_0=820 \mu\text{sec}$ . (After Chance et al.<sup>14</sup> used with permission.)

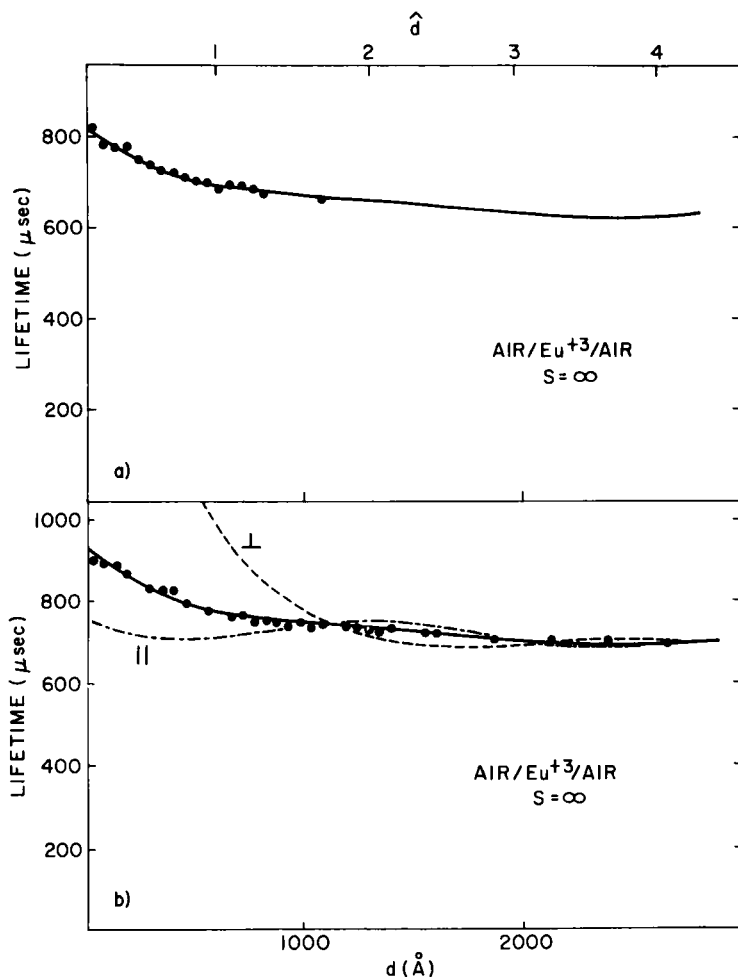
theory (2.45)<sup>12</sup> and the exact single-mirror theory (2.29)<sup>14</sup> with  $n_1=1.50$ ,<sup>3</sup>  $n_2=0.06$ , and  $\kappa_2=4.11$  (Table I),<sup>26</sup>  $q$  and  $\tau_0$  variable. Both theories give good agreement for  $d > 1500 \text{ \AA}$ . At short distance ( $d \leq 100 \text{ \AA}$ ) the lifetime is dominated by nonradiative energy transfer to the mirror. The exact treatment gives a satisfactory representation of the data in this region. Kuhn's approximate

TABLE I  
Optical Constants of Silver, Copper,  
and Gold at 612 nm

Metal	$n_2^a$	$\kappa_2^a$
Silver	0.06 (0.10)	4.11 (4.00)
Gold	0.215 (0.047)	3.22 (3.60)
Copper	0.327 (0.35)	3.14 (2.60)

<sup>a</sup>Taken from Johnson and Christy<sup>26</sup> (with small interpolation). The values shown in parentheses were used previously by Tews<sup>15</sup> in fitting the lifetime data.

theory greatly overestimates the importance of energy transfer. Both theories give poor fits in the 200–1500 Å region. However, the major shortcoming of this and all single mirror treatments of these data is that, to obtain reasonable agreement with experiment, the dipole must be assumed to be primarily in a parallel orientation (fractional perpendicular contribution <0.11).<sup>14</sup> This



**Fig. 5.** Lifetime versus distance for the air/Eu<sup>3+</sup> single-mirror system; (a) experimental data from Drexhage et al.<sup>6,7</sup> and (b) experimental data from Tews et al.<sup>30</sup> In both cases the solid curves represent best fits to the data; (a)  $\tau_0 = 637$  μsec and  $q = 0.777$  and (b)  $\tau_0 = 709$  μsec and  $q = 0.857$ . Also shown in b are theoretical results obtained with the best fit values of  $\tau_0$  and  $q$  but with pure parallel and perpendicular dipole orientations. In the perpendicular case the theoretical curve will approach a value of 2078 μsec at  $d = 0$ .

conclusion is in direct conflict with the results for the air/Eu<sup>3+</sup> system<sup>7-9,30</sup> in Fig. 5, which indicate quite clearly a random, or near random, distribution of dipole orientations (two-thirds parallel and one-third perpendicular).

These two problems, dipole orientation and poor fit at small distances, are eliminated when the second interface is included in the theory.<sup>34,35</sup> The formulation of the double-mirror problem is quite similar to that described in detail earlier and is treated by the Green's function method in the next section. The geometry of the problem is shown in Fig. 6. The results can be conveniently summarized with the following formulas<sup>35</sup>:

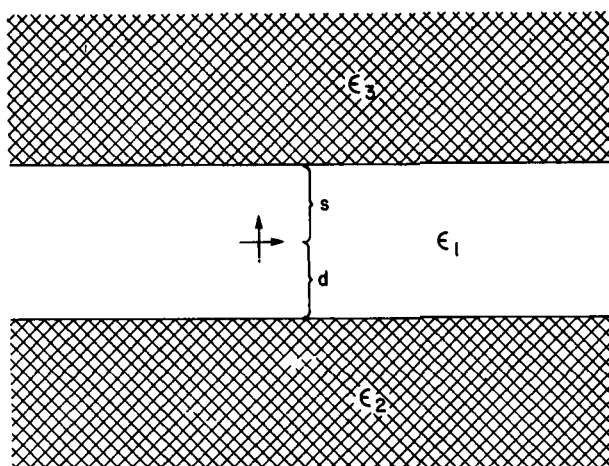


Fig. 6. Geometry of the double-mirror problem. Region 1 is a nonabsorbing dielectric. Regions 2 and 3 are half spaces with dielectric constants  $\epsilon_2$  and  $\epsilon_3$ .

$$b_{\perp, \parallel} = b_0(1 - qZ_{\perp, \parallel}) \quad (2.46)$$

where

$$Z_{\perp} = 1 - \frac{3}{2} \operatorname{Im} \int_0^{\infty} \frac{F(\hat{d}, -R_{12}^{\parallel})F(\hat{s}, -R_{13}^{\parallel})}{F(\hat{d} + \hat{s}, -R_{12}^{\parallel}R_{13}^{\parallel})} u^3 \frac{du}{l_1} \quad (2.47)$$

and

$$\begin{aligned} Z_{\parallel} = 1 - \frac{3}{4} \operatorname{Im} \int_0^{\infty} du \frac{u}{l_1} & \left[ \frac{F(\hat{d}, R_{12}^{\perp})F(\hat{s}, R_{13}^{\perp})}{F(\hat{d} + \hat{s}, -R_{12}^{\parallel}R_{13}^{\parallel})} \right. \\ & \left. + (1 - u^2) \frac{F(\hat{d}, R_{12}^{\parallel})F(\hat{s}, R_{13}^{\parallel})}{F(\hat{d} + \hat{s}, -R_{12}^{\parallel}R_{13}^{\parallel})} \right] \end{aligned} \quad (2.48)$$

where  $F(x, y) = 1 + y \exp(-2l_1x)$ ,  $\hat{d} = k_1d$ , and  $\hat{s} = k_1s$ . The reflection coefficients are defined like those in (2.15) and (2.27):

$$R_{ab}^{\parallel} = \frac{\epsilon_a l_b - \epsilon_b l_a}{\epsilon_a l_b + \epsilon_b l_a} \quad (2.49)$$

and

$$R_{ab}^{\perp} = \frac{l_a - l_b}{l_a + l_b} \quad (2.50)$$

with  $l_j \equiv -i(\epsilon_j/\epsilon_1 - u^2)^{1/2}$  as before. The quantities  $q$  and  $\tau_0$  ( $\equiv 1/b_0$ ) are varied to obtain the best fit to experiment, with  $\tau_0$  being simply a normalization factor, leaving  $q$  as the primary fit parameter. In most of the systems discussed here  $q$  and  $\tau_0$  can be determined essentially independently from the theoretical fits to the data. (They are completely independent at large distances where nonradiative energy transfer to the mirror is unimportant.)

The results for the  $\text{Eu}^{3+}/\text{Ag}$  system are shown in Fig. 7. The agreement is essentially quantitative at all distances. Also, the results require an isotropic,

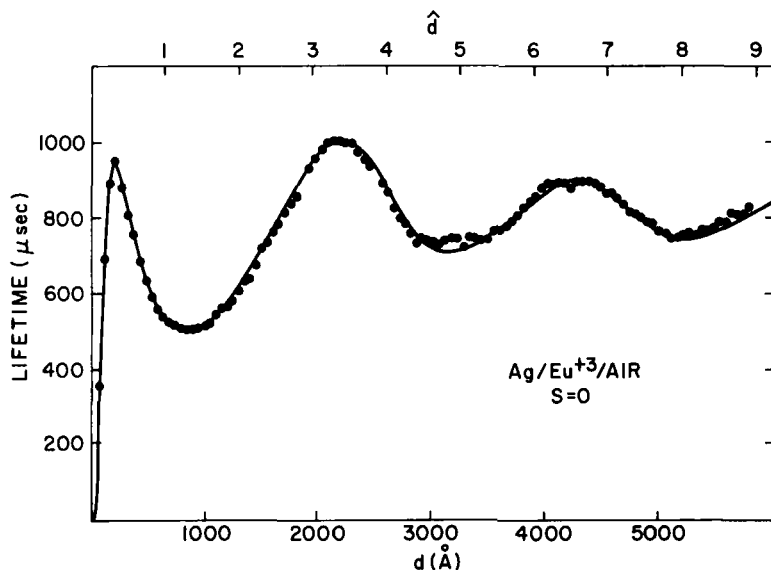


**Fig. 7.** Lifetime versus distance for the  $\text{Ag Eu}^{3+}/\text{air}$ , double-mirror system. Experimental data from Drexhage et al.<sup>5-8</sup> The solid curve represents the best fit of (2.46) to the data:  $\tau_0 = 632 \mu\text{sec}$  and  $q = 0.760$ . (After Chance et al.<sup>35</sup> used by permission.) In this figure and those to follow an isotropic distribution is assumed. In most cases only this distribution will give a good fit to the data.

or near isotropic, distribution of dipole configurations in agreement with the  $\text{Eu}^{3+}/\text{air}$  results

$$[\tau_{\text{iso}} = \tau_0(\frac{2}{3}\hat{b}_{\parallel} + \frac{1}{3}\hat{b}_{\perp})^{-1}]$$

If the fatty acid/air interface is removed to larger distances in the  $\text{Eu}^{3+}/\text{Ag}/\text{air}$  experiment, the results shown in Fig. 8 are obtained.<sup>36</sup> The only modifica-

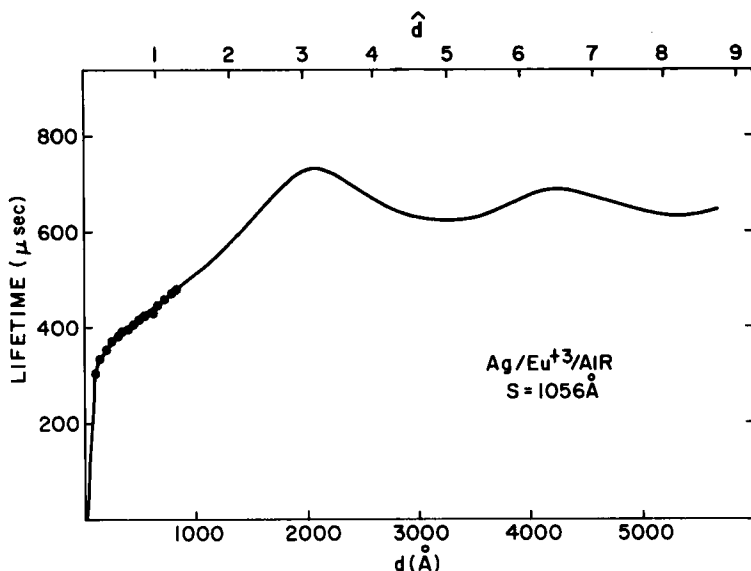


Fig. 8. Lifetime versus distance for the  $\text{Ag}/\text{Eu}^{3+}/40 \text{ CdC layers}/\text{air}$  double-mirror system. Experimental data from Drexhage.<sup>36</sup> The theoretical curve is obtained with  $\tau_0 = 625 \text{ sec}$  and  $q = 0.795$ . (After Chance et al.<sup>35</sup> used by permission.)

tion of the experiment is the addition of 40 fatty-acid layers after the  $\text{Eu}^{3+}$  layer, that is,  $s = 1056 \text{ Å}$ . Note that the first large peak in the Fig. 7 data at  $d \sim 200 \text{ Å}$  has disappeared completely with the addition of the fatty-acid cover layer. The theoretical curve predicts this dramatic effect and is in good agreement with the experimental data with little change in  $q$  or  $\tau_0$ . Again, these results can be explained only with the isotropic dipole orientation.

Experimental and theoretical results for gold and copper mirrors are shown in Figs. 9 to 12. In all calculations reported here we have used optical constants from Johnson and Christy<sup>26</sup> (Table I), with the exception of the  $\text{Cu}/\text{Eu}^{3+}/\text{air}$  system shown in Fig. 12. In that case we also included results for an alternate set of optical constants that were used previously by Tews<sup>15</sup> in his analysis of the same data. (If we use the alternate set of optical constants for Au shown in Table I, the fit improves only slightly.) It is apparent from Fig. 12 that adjustment of the optical constants would improve the fit particularly in the small-distance (energy-transfer) regime where the measurements could be quite sensitive to surface contamination, for example. We have

made no further attempt to find the "best" optical constants for the Cu (or Au) experiments.

The results of the fitting procedure are summarized in Table II. Note first that the quantum yield varies from 0.69 to 0.86. However, the experiments giving the extreme values in this range both have features in the preparative details that set them apart from the remaining six experiments. The air/Eu<sup>3+</sup>

TABLE II  
Summary of Results (after Chance et al.<sup>35</sup>)

Mirror	$d$ (Å) (range)	$s$ (Å)	$q^a$	$\tau_0$ (μsec) <sup>a</sup>	$\tau_r$ (μsec) <sup>d</sup>	S.D. (%) <sup>e</sup>	Figure	References
Air	26-1082	$\infty$	0.777	637	820	1.1	5a	6, 7
Air	26-2666	$\infty$	0.857	709 <sup>b</sup>	827	1.4	5b	30
Silver	53-5861	0	0.760	632	832	2.2	7	5-8
Silver	105-845	1056	0.795	625 <sup>c</sup>	786	3.5	8	36
Gold	158-5438	0	0.818	639	781	2.9	9	6
Gold	158-2534	1056	0.767	625 <sup>c</sup>	815	2.4	10	36
Gold	264-5280	$\infty$	0.688	536	779	2.1	11	9
Copper	158-3379	0	0.801	620	774	3.7	12	6

<sup>a</sup>Except where noted  $q$  and  $\tau_0$  are obtained as best fits of (2.46) to the experimental data.

<sup>b</sup>Tews obtained 720 μsec experimentally.<sup>30</sup>

<sup>c</sup>Since the experimental data for these two systems were restricted primarily to short distances, a number of  $q$  and  $\tau_0$  combinations give an adequate representation of the data. Therefore, for these two cases only, Drexhage's estimate<sup>6</sup> of  $\tau_0$  was corrected for the presence of the air layer and was used without further adjustment.

<sup>d</sup>Radiative lifetime ( $\tau_r = \tau_0/q$ ) of Eu<sup>3+</sup> (612 nm emission) in a dielectric medium with a refractive index of 1.50.

<sup>e</sup>Relative standard deviation.

system of Fig. 5b<sup>30</sup> is the only one of the eight experiments that was not performed by Drexhage. It is not unlikely that there were differences in the preparative procedure, though details are not available. The Au/Eu<sup>3+</sup> system of Fig. 8 utilized a dielectric matching immersion liquid and was performed at 0°C, while the rest of the experiments were conducted at room temperature.<sup>36</sup> The variation in  $q$  for the remaining six experiments is quite small.

The radiative lifetime of Eu<sup>3+</sup> ( $\tau_r \equiv \tau_0/q$ ) should be less sensitive to the details of the experiment, and the results in Table II show  $\tau_r$  to be relatively constant for the eight experiments, for an average value of  $803 \pm 20$  μsec. This variation in  $\tau_r$  is quite small when one considers the precision of the lifetime measurements (3-4%)<sup>30,36</sup> and the uncertainty in the choice of the

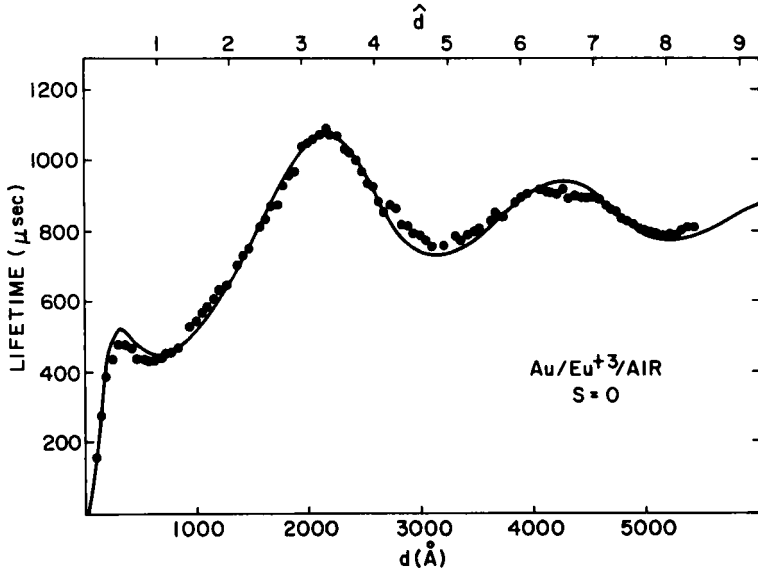


Fig. 9. Lifetime versus distance for the Au/Eu<sup>3+</sup>/air, double-mirror system. Experimental data from Drexhage et al.<sup>6</sup>; theoretical curve:  $\tau_0 = 639 \mu\text{sec}$  and  $q = 0.818$ . (After Chance et al.<sup>35</sup> used by permission.)

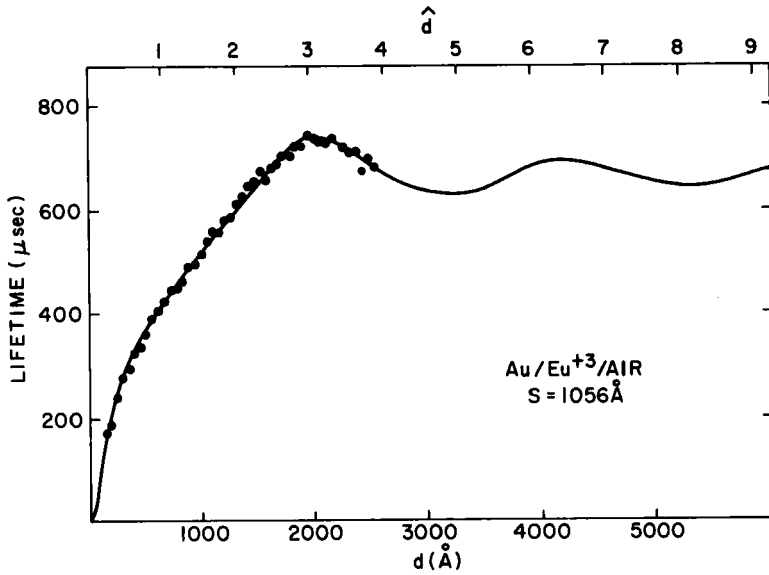


Fig. 10. Lifetime versus distance for the Au/Eu<sup>3+</sup>/40 CdC layers/air double-mirror system. Experimental data from Drexhage<sup>36</sup>; theoretical curve:  $\tau_0 = 625 \mu\text{sec}$  and  $q = 0.767$ . (After Chance et al.<sup>35</sup> used by permission.)



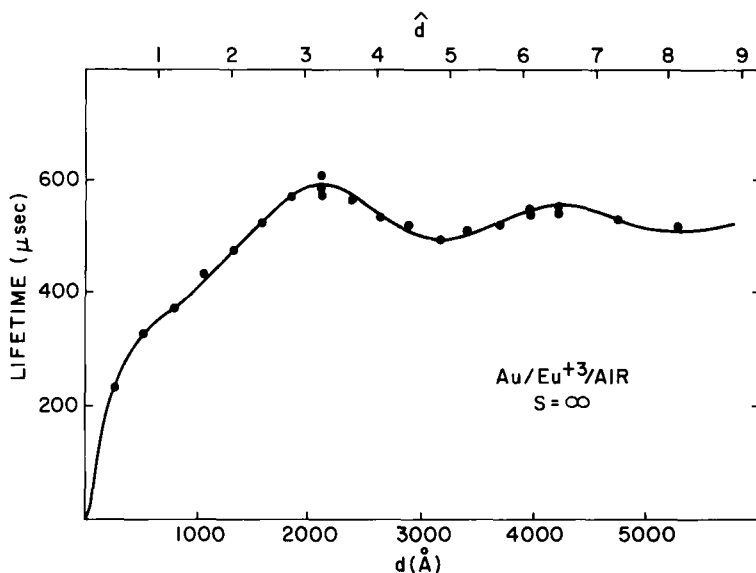


Fig. 11. Lifetime versus distance for the Au/Eu<sup>3+</sup> single-mirror system. Experimental data from Drexhage<sup>9</sup>; theoretical curve:  $\tau_0 = 536$  sec and  $q = 0.688$ . A dielectric matching immersion liquid was used to remove the second interface. (After Chance et al.<sup>35</sup> Used by permission.)

most appropriate values for the optical constants of the gold and copper systems.

The quantitative agreement between theory and experiment for the individual systems and the constancy of  $\tau$ , for all eight experiments provide a gratifying confirmation of our basic premise that a purely classical theory provides a quite satisfactory theoretical description of these systems, even when the distance scale is only tens of angstroms. In the next section we consider the short-distance, energy-transfer regime in some detail.

Before closing this section, it should be pointed out that we have ignored a fairly large birefringence ( $n_e - n_o \approx 0.07$ )<sup>6</sup> in the fatty-acid layers. However, we include this effect in a theoretical description given in Section IV. Since it can be shown that the major effect of this birefringence is only a few percent change in our  $q$  values,<sup>35</sup> we have not bothered to refit the data with the more complete theory.

### C. Energy Transfer

Nonradiative energy transfer has been discussed by a number of authors<sup>37-40</sup> as an effective decay channel for an excited molecule near a metal mirror. Simple dimensionality considerations for dipole-dipole trans-

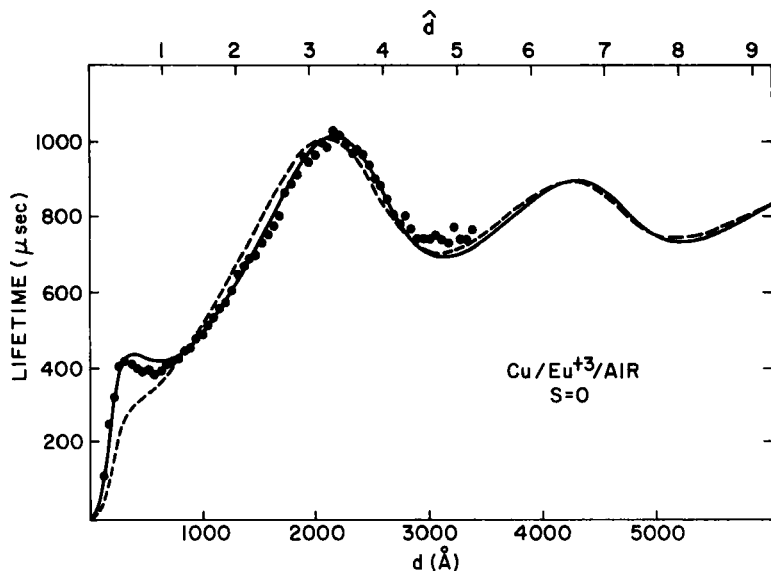


Fig. 12. Lifetime versus distance for the Cu/Eu<sup>3+</sup>/air double-mirror system. Experimental data from Drexhage et al.<sup>6</sup>; theoretical curves:  $\tau_0 = 620 \mu\text{sec}$  and  $q = 0.801$ . The solid curve results when Johnson and Christy's values<sup>26</sup> for the optical constants of copper are used. The dashed curve results when the alternate set given in Table I is used. (After Chance et al.<sup>35</sup> Used by permission.)

fer (Förster transfer) predict an inverse cubic dependence on distance, and the experimentally determined decay-rate constant is generally written as

$$\hat{b}_{ET} = \beta d^{-3} \quad (2.51)$$

A theoretical estimate of  $\beta$  could proceed along the lines of Förster transfer theory.<sup>12</sup> This procedure is valid for weak absorbers but fails in the case of metals, as we show here.

In (2.42) we give the energy-transfer rate constant for a perpendicular dipole that is valid for all distances and for both weak and metallic acceptors. We have examined the short distance behavior of (2.42) and the analogous expression for a parallel dipole and find

$$\hat{b}_{ET} = -\frac{q\theta}{4d^3} \text{Im}(R_{d \rightarrow 0}) = \frac{q\theta}{4d_1^3} \text{Im}\left(\frac{\epsilon_2 - \epsilon_1}{\epsilon_2 + \epsilon_1}\right) \quad (2.52a)$$

so that

$$\beta = \frac{q}{k_1^3} \frac{\theta \epsilon_1 n_2 \kappa_2}{|\epsilon_1 + \epsilon_2|^2} \quad (2.52b)$$

where the orientational parameter  $\theta$  is  $\frac{3}{2}$ ,  $\frac{3}{4}$ , or 1 for perpendicular, parallel, and isotropic dipole configurations, respectively.<sup>18,19</sup> If the emission is not confined to a narrow band, (2.52) may be rewritten as an integral over the emission spectrum in a fashion analogous to the well-known Förster expression.<sup>41</sup> This expression is quite different from that derived from Kuhn's treatment (2.45), but both agree in the limit of a weak absorber ( $\kappa_2$  small,  $n_1 \approx n_2$ ).

We have seen in the  $\text{Eu}^{3+}$  systems that agreement with experiment is essentially quantitative even at the smallest distances (about 50 Å). However, since energy transfer was not the emphasis of these experiments, the data are limited in the energy-transfer region and a thorough test of our limiting case formulas [see (2.52)] is not possible. As is obvious from the theoretical fits to these data,  $\beta$ 's that are in reasonable agreement with (2.52) can be extracted.<sup>18</sup>

Some tests of the predictions of (2.52) are possible from other work.<sup>37,39,40</sup> The  $\beta$  values derived from those experiments are shown in Table III along with theoretical estimates from (2.52). The agreement is satisfactory in the anthracene/Au case but quite poor in the anthracene/Al case. One explanation for this large discrepancy is that the Al layer was actually quite thin.<sup>37</sup> We now present theoretical results for thin films and return later to the anthracene/Al experiment.

Energy transfer with emphasis on surface-plasmon coupling is discussed in Section IV. In particular, the thin-film case is discussed in detail. Here we need only the expression for  $\beta$  (small  $d_1$  limit)

$$\beta \equiv \hat{b}_{ET} d_1^3 = \frac{2q\theta}{k_1^3} \text{Im } \epsilon_2 \int_0^\infty du e^{-2u} u^2 \frac{(\epsilon_1 + \epsilon_2) + (\epsilon_1 - \epsilon_2) e^{-2u(d_2/d_1)}}{(\epsilon_1 + \epsilon_2)^2 - (\epsilon_1 - \epsilon_2)^2 e^{-2u(d_2/d_1)}} \quad (2.53)$$

where  $d_1$  is the distance from dipole emitter to mirror and  $d_2$  is the mirror thickness. We have taken the dielectric constant to be  $\epsilon_1$  on both sides of the metal layer. For large values of  $d_2$  (thick films), the energy-transfer rate constant varies as  $d^{-3}$ , so that  $\beta$  is truly a constant and (2.53) reduces to (2.52). However, again from simple considerations of dimensionality for small  $d_2$  (thin films), the energy-transfer rate constant should vary as  $d^{-4}$ , or  $\beta$  will be proportional to  $d^{-1}$ , as we show shortly. For intermediate thicknesses a smooth transition from  $d^{-3}$  to  $d^{-4}$  behavior is *not* observed. Instead, we find a peak in  $\beta$  versus  $d_2/d_1$ , as shown in Fig. 13. The physical origin of this surprising effect is discussed in Section IV. The example of Fig. 13 is chosen for application to the anthracene/Al experiment discussed earlier. In Figure 14 we have replotted these data along with the experimental results from Vaubel et al.<sup>37</sup> for anthracene/Al. The large discrepancy between theory and experiment, discussed in reference to Table III, is illustrated again here by comparison of a curve *a* with the experimental data. As can be seen, the thin-film enhancement effect can explain the magnitude of the dis-

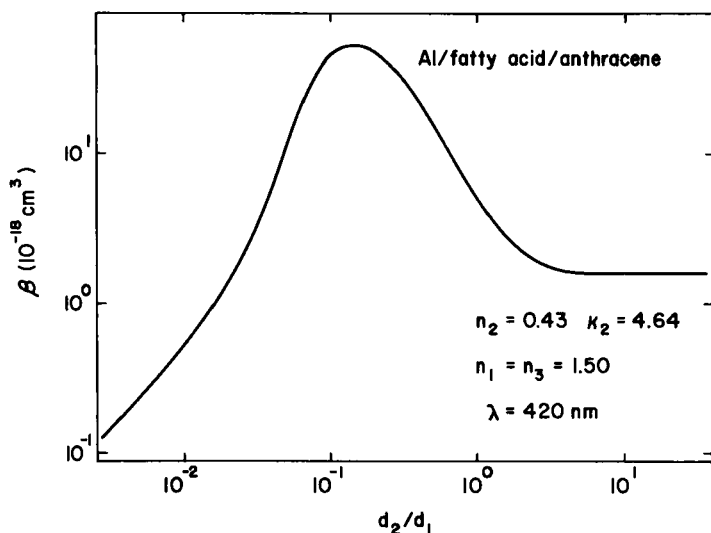


Fig. 13. Energy-transfer parameter  $\beta$  [see (2.53)] versus  $d_2/d_1$ , where  $d_2$  is the thickness of the metal film (Al in this case) and  $d_1$  is the distance between the electric dipole and the metal. The results shown are for an isotropic dipole orientation. The dielectric constants on either side of the metal film have been taken to be equal ( $\epsilon_1 = 2.25$ ).

crepancy (though possibly not the observed distance dependence). A  $d_2$  value of 50 Å is quite reasonable, since the evaporated films were only about 100 Å thick and Al is known to oxidize under ambient conditions to form oxide layers up to about 50 Å.<sup>42</sup> Though these experimental data should not be taken as proof of thin-film enhancement effect, they do show that some care is necessary in controlling the acceptor-layer thickness. In later experiments by Kurczewska and Bässler,<sup>40</sup> precautions were taken to insure that the layer was “infinitely” thick and good agreement with our theory was found (Table III).

In the limit that  $d_1$  is small and  $d_2/d_1$  is much less than 1, a formula can be derived that resembles the formula of Kuhn<sup>12</sup> and Bücher et al.<sup>31</sup> in that it gives the correct  $d^{-4}$  dependence. The result is

$$\hat{b}_{ET} = \frac{d_0^4}{d^4} \quad (2.54)$$

where  $d_0$  is the critical transfer distance,

$$d_0 = \frac{\alpha\lambda}{n_1} (Aq)^{1/4} \left[ \frac{n_2}{2n_1} \left( 1 + \frac{\epsilon_1^2}{|\epsilon_2|^2} \right) \right]^{1/4}, \quad (2.55)$$

TABLE III  
Comparison of Theory and Experiment for  
Energy-Transfer-Rate Parameter  $\beta$

System	$n_1$	$n_2^c$	$\kappa_2^c$	$\beta(\text{exptl})^a$	$\beta(\text{theory})^{a,b}$
Anth/A1	1.5	0.43	4.64	$9.6 \pm 2.0^d$	1.1
Anth/Au	2.1	1.46	1.96	$\geq 2.6^e$	10.0
Anth/Au	1.5	1.46	1.92	$16.3 \pm 3.0^f$	16.9

<sup>a</sup>Units for  $\beta$  are  $10^{-18} \text{ cm}^3$ .

<sup>b</sup>From (3.52). The dipole orientation is assumed to be isotropic; the quantum yield is taken to be unity.

<sup>c</sup>Optical constants taken from Johnson and Christy<sup>26</sup> and Hass and Waylonis.<sup>42</sup>

<sup>d</sup>Experimental system was A1/fatty acid/anthracene.<sup>37</sup>

<sup>e</sup>Indirect measurement for Au/anthracene system allowing only a lower limit estimate of  $\beta$ .<sup>39</sup>

<sup>f</sup>Experimental system was Au/fatty acid/anthracene.<sup>40</sup>

and  $A$  is the absorbance of the layer,

$$A = \frac{4\pi\kappa_2 d_2}{\lambda} \quad (2.56)$$

The geometric factor  $\alpha$  equals  $(1/4\pi)(9)^{1/4}$  for a perpendicular dipole and  $(1/4\pi)(\frac{9}{2})^{1/4}$  for a parallel dipole. When  $n_1 = n_2 \gg \kappa_2$  this expression reduces to that of Kuhn,<sup>12</sup> that is the term in brackets in (2.55), which is the correction factor added by our theory, goes to 1.0. The  $q$  value derived from an energy-transfer experiment using Kuhn's theory will be underestimated by this correction factor. This is unimportant for the weakly absorbing acceptor layers used in the majority of the energy-transfer experiments. However, when a metal acceptor layer is employed, the effect can be substantial. For example, in the experiments described in Ref. 33 using a gold acceptor layer, the  $q$  values derived should be increased by factors of 2.1 for the 460-nm fluorescence emitter and 6.7 for the 550-nm phosphorescence emitter. The principal conclusions of this article<sup>33</sup> are not changed.

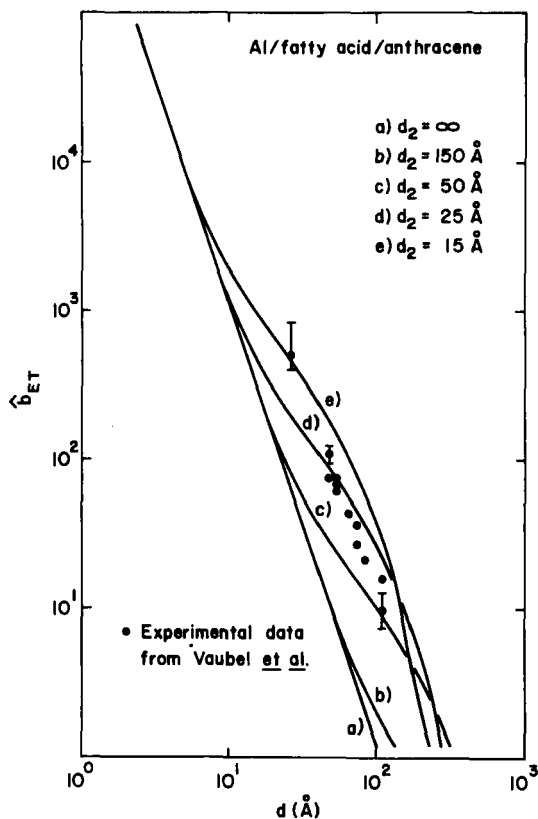


Fig. 14. Comparison of experimental data from Vaubel et al.<sup>37</sup> with thin-film theory [see (2.53)] for various values of film thickness. The theoretical curves are constructed from the results displayed in Fig. 13. The results illustrate that the observed energy-transfer rate constant can be as much as an order of magnitude greater than that expected for a thick mirror as a result of the thin-film enhancement effect.

### III. DYADIC GREEN'S FUNCTION METHOD

#### A. General Formulation

The elegant and powerful dyadic Green's function method<sup>43</sup> may also be used to compute the decay rate of an oscillating charge distribution near a surface. This method allows for a straightforward extension to higher multi-

pole charge distributions, as well as to stratified media. Our notation in this section is constructed to follow that of Tai<sup>43</sup> as closely as possible; we make the appropriate connections to the notation and results in previous sections. The calculation proceeds as follows: The equation for the electric field due to an oscillating current density  $\mathbf{J}(\mathbf{R})$  is

$$\nabla \times \nabla \times \mathbf{E} - k_1^2 \mathbf{E} = i\omega \mathbf{J}(\mathbf{R}) \quad (3.1)$$

where  $k_1$  is the propagation constant ( $\omega n/c$ ) in the region of interest. To solve this equation in the presence of surfaces, the usual boundary conditions must be imposed on the general solution. The electric field is given by

$$\mathbf{E}(\mathbf{R}) = i\omega \int \mathbf{G}(\mathbf{R}|\mathbf{R}') \cdot \mathbf{J}(\mathbf{R}') d\mathbf{R}' \quad (3.2)$$

where  $\mathbf{G}(\mathbf{R}|\mathbf{R}')$ , the dyadic Green's function, satisfies the equation

$$\nabla \times \nabla \times \mathbf{G}(\mathbf{R}|\mathbf{R}') - k_1^2 \mathbf{G}(\mathbf{R}|\mathbf{R}') = I \delta(\mathbf{R} - \mathbf{R}') \quad (3.3)$$

with the appropriate boundary conditions now built into  $G(\mathbf{R}|\mathbf{R}')$ . Thus for any geometry one finds  $\mathbf{G}(\mathbf{R}|\mathbf{R}')$  and the calculation of decay rates for any oscillating charge distribution is straightforward. To solve (3.3)<sup>43</sup> the vector eigenfunctions of the homogeneous equation

$$\nabla \times \nabla \times \mathbf{F} - k_1^2 \mathbf{F} = 0 \quad (3.4)$$

are found for the appropriate boundary conditions. For the case of a *single planar interface* the two independent sets of eigenfunctions of (3.4) can be written in cylindrical coordinates  $\hat{r}, \hat{\phi}, \hat{z}$

$$\begin{aligned} \mathbf{M}_{e_{n\lambda}}(h) &= e^{ihz} \left[ \mp \frac{nJ_n(\lambda r)}{r} \frac{\sin n\phi \hat{r}}{\cos} - \frac{\partial J_n(\lambda r)}{\partial r} \frac{\cos n\phi \hat{\phi}}{\sin} \right] \\ \mathbf{N}_{o_{n\lambda}}(h) &= \frac{e^{ihz}}{k_1} \left[ ih \frac{\partial J_n(\lambda r)}{\partial r} \frac{\cos n\phi \hat{r}}{\sin} \mp inh \frac{J_n(\lambda r)}{r} \frac{\sin n\phi \hat{\phi}}{\cos} + \lambda^2 J_n(\lambda r) \frac{\cos n\phi \hat{z}}{\sin} \right] \end{aligned} \quad (3.5)$$

where  $h^2 + \lambda^2 = k_1^2$  and the  $e$  and  $o$  refer to even and odd. Using these functions, the Green's function for our problem can be split into a zeroth-order (nonscattering) piece  $\mathbf{G}_0$  and a scattering piece  $\mathbf{G}_s$ :

$$\begin{aligned} \mathbf{G}_0(\mathbf{R}|\mathbf{R}') &= \frac{i}{4\pi} \int_0^\infty d\lambda \sum_{n=0}^\infty \frac{2 - \delta_{n0}}{\lambda h_1} \left[ \begin{aligned} &\mathbf{M}_{jn\lambda}(h_1) \mathbf{M}'_{jn\lambda}(-h_1) \\ &\mathbf{M}_{jn\lambda}(-h_1) \mathbf{M}'_{jn\lambda}(h_1) \\ &+ \mathbf{N}_{jn\lambda}(h_1) \mathbf{N}'_{jn\lambda}(-h_1) \end{aligned} \right] \begin{aligned} &z \geq z' \\ &+ \mathbf{N}_{jn\lambda}(-h_1) \mathbf{N}'_{jn\lambda}(h_1) \end{aligned} \quad \begin{aligned} &z \geq z' \\ &z \leq z' \end{aligned} \end{aligned} \quad (3.6)$$

where  $h_1 = (k_1^2 - \lambda^2)^{1/2}$  and the primed functions are functions of  $\mathbf{R}'$ , and

$$\mathbf{G}_s(\mathbf{R}|\mathbf{R}') = \frac{i}{4\pi} \int_0^\infty d\lambda \sum_{\substack{n=0 \\ j=e,o}}^\infty \frac{2-\delta_{n0}}{\lambda h_1} [R^\perp \mathbf{M}_{jn\lambda}(h_1) \mathbf{M}'_{jn\lambda}(h_1) - R^\parallel \mathbf{N}_{jn\lambda}(h_1) \mathbf{N}'_{jn\lambda}(h_1)] \quad (3.7)$$

where  $R^\perp = (h_1 - h_2)/(h_1 + h_2)$  and  $R^\parallel = (k_2^2 h_1 - k_1^2 h_2)/(k_2^2 h_1 + k_1^2 h_2)$ . Using these Green dyadics, we can compute the electric field in region 1 (where the charge distribution is placed). The scattered or reflected field comes from the piece  $G_s$  alone:

$$\mathbf{E}_s(\mathbf{R}) = i\omega \int \mathbf{G}_s(\mathbf{R}|\mathbf{R}') \cdot \mathbf{J}(\mathbf{R}') d\mathbf{R}' \quad (3.8)$$

Note that the Fresnel coefficients  $R^\perp$  and  $R^\parallel$  enter in the usual way.

The calculation of the decay rate of the charge distribution is accomplished by noting that the energy  $W$  of an oscillating charge distribution in a field  $E(r)$  is proportional to<sup>25</sup>

$$\text{Re} \int \mathbf{P}(\mathbf{r}) \cdot \mathbf{E}(\mathbf{r}) d\mathbf{r} \quad (3.9)$$

where  $\mathbf{P}(\mathbf{r})$  is the moment of the charge distribution

$$\mathbf{P}(\mathbf{r}) = \sum_i \mathbf{r}_i q_i \delta(\mathbf{r} - \mathbf{r}_i) = \mathbf{r} \rho(\mathbf{r}) \quad (3.10)$$

The decay rate then obeys the following proportionality<sup>25</sup>

$$\text{Re} \left[ \int \mathbf{J}(\mathbf{r}) \cdot \mathbf{E}(\mathbf{r}) d\mathbf{r} \right] \propto \text{Im} \left[ \int \mathbf{P}(\mathbf{r}) \cdot \mathbf{E}(\mathbf{r}) d\mathbf{r} \right] \quad (3.11)$$

for a harmonically oscillating charge distribution. For example, an oscillating dipole  $p^{(1)}$  at  $\mathbf{R}_0$ ,

$$\mathbf{J}^{(1)}(\mathbf{R}) = -i\omega \mathbf{p}^{(1)} \delta(\mathbf{R} - \mathbf{R}_0) \quad (3.12)$$

so the decay rate obeys the following proportionality:

$$\text{Im} \mathbf{p}^{(1)} \cdot \mathbf{E}(\mathbf{R}_0) \propto \text{Re} \mathbf{p}^{(1)} \cdot \mathbf{G}(\mathbf{R}_0/\mathbf{R}_0) \cdot \mathbf{p}^{(1)} \quad (3.13)$$

The proportionality constant depends on the electromagnetic constants of region 1 alone, and thus drops out when ratios are taken. We have then for the normalized decay rate constant of the dipole at  $d$ ,

$$b = 1 + \frac{\text{Re} \mathbf{p}^{(1)} \cdot \mathbf{G}_s(\mathbf{R}_0/\mathbf{R}_0) \cdot \mathbf{p}^{(1)}}{\text{Re} \mathbf{p}^{(1)} \cdot \mathbf{G}_0(\mathbf{R}_0/\mathbf{R}_0) \cdot \mathbf{p}^{(1)}} \quad (3.14)$$



For a dipole perpendicular to the surface,

$$b = 1 - \frac{\text{Im } R'' \int_0^\infty d\lambda (\lambda^3/k_1 h_1) e^{i2h_1 d}}{\text{Im } \int_0^\infty d\lambda (\lambda^3/k_1 h_1)} \quad (3.15)$$

with  $h_1^2 = k_1^2 - \lambda^2$ . This is identical to (2.17). The power of this method is now evident. For a dipole parallel to the surface we find (2.29) directly from (3.14) above, without having to impose the boundary conditions again. In the next section we use this method to compute the decay rates for oscillating quadrupoles and magnetic dipoles.

### B. Higher Multipoles Near Single Interfaces

Using the dyadic Green's function method, we can easily derive expressions for the decay rate of higher multipole moments near single interfaces, since the Green's function remains the same and the current density  $J(r)$  can be expanded into multipole moments in the usual way. As an example we consider an oscillating quadrupole moment  $\mathbf{D}$  at the point  $\mathbf{d} = (0, 0, d)$  above a half space (see Fig. 1); the energy of interaction of this with the field is given by

$$\begin{aligned} W \propto \lim_{R \rightarrow R_0} \mathbf{D} : \nabla_R \mathbf{E}(\mathbf{R}) &\propto \lim_{R \rightarrow R_0} \mathbf{D} : \int d\mathbf{R}' \mathbf{G}(R/R') \cdot \mathbf{D} \cdot \nabla_{R'} \delta(\mathbf{R}' - \mathbf{R}_0) \\ &= \lim_{R \rightarrow R_0} \{ -\mathbf{D} : \nabla_R \nabla_{R_0} \mathbf{G}(\mathbf{R}/\mathbf{R}_0) : \mathbf{D} \} \end{aligned} \quad (3.16)$$

The decay rate is given by the rate of energy loss as before. For  $\mathbf{D} = \hat{z}\hat{z}$ , a unit quadrupole component in the  $z$  direction, the decay rate constant due *only* to the presence of the mirror ( $b_s$ ) is [using  $G$  as given in (3.6)]

$$b_s = \text{Re} \frac{1}{2} \int_0^\infty d\lambda h_1 \lambda^3 (-R'') e^{i2h_1 d} \quad (3.17)$$

Thus the normalized decay rate is given by

$$\begin{aligned} b_{zz} &= 1 - q \frac{\text{Re} \int_0^\infty d\lambda \lambda^3 h_1 R'' e^{i2h_1 d}}{\text{Re} \int_0^\infty d\lambda \lambda^3 h_1} \\ &= 1 - \frac{15}{2} q \text{Im} \int_0^\infty du u^3 l_1 R'' e^{-2l_1 k_1 d} \end{aligned} \quad (3.18)$$

where

$$R'' = \frac{\epsilon_1 l_2 - \epsilon_2 l_1}{\epsilon_1 l_2 + \epsilon_2 l_1}, \quad l_1 = -i(1 - u^2)^{1/2} = -i(\epsilon_2/\epsilon_1 - u^2)^{1/2}$$

as in Section II. This calculation is easily repeated for all the quadrupole

components giving the results in Table IV, where  $b$  is written as  $\hat{b} = 1 + q \operatorname{Im} X$ .

The decay rate of a magnetic dipole near an interface can also be calculated in this method. Since the magnetic dipole current for such a dipole at  $R_0$  will be proportional to  $\mathbf{m} \times \nabla \delta(\mathbf{R} - \mathbf{R}_0)$ , we find the decay rate proportional to

$$\lim_{R \rightarrow R_0} [\operatorname{Im} \mathbf{m} \cdot \{\nabla_R \times \nabla_{R_0} \times \mathbf{G}(R|R_0)\} \cdot \mathbf{m}] \quad (3.20)$$

TABLE IV  
Decay Rates of Quadrupole Moments and  
Magnetic Dipole Moments near Single Interface

Component	X
$\frac{3}{2} \hat{z}\hat{z} - \frac{1}{2}$	$-\frac{15}{2} \int_0^\infty du u^3 l_1 R'' e^{-2l_1 d}$
$\hat{x}\hat{y} + \hat{y}\hat{x}$ $\hat{x}\hat{x} - \hat{y}\hat{y}$	$\frac{5}{4} \int_0^\infty du \frac{u^3}{l_1} e^{-2l_1 d} (R^\perp - l_1^2 R'')$
$\hat{x}\hat{z} + \hat{z}\hat{x}$ $\hat{y}\hat{z} + \hat{z}\hat{y}$	$\frac{5}{4} \int_0^\infty du u e^{-2l_1 d} \left[ R^\perp l_1 - R'' \frac{(1-2u^2)}{l_1} \right]$
Magnetic dipoles	
$\hat{z}$	$\frac{3}{2} \int_0^\infty R^\perp e^{-2l_1 d} \frac{u^3 du}{l_1}$
$\hat{x}\hat{y}$	$-\frac{3}{4} \int_0^\infty \left( \frac{R''}{u^2} + \frac{R^\perp}{u^2} (1-u^2) \right) e^{-2l_1 d} \frac{u^3 du}{l_1}$

The decay rate due to the mirror is found by putting  $\mathbf{G}_s$  in (3.20) and that for a dipole in the absence of the mirror is found from (3.20) by substituting  $\mathbf{G}_0$ . We find that the normalized decay rate for magnetic dipoles is then

$$\hat{b} = 1 + q \operatorname{Im} X \quad (3.21)$$

where  $X$  is given in Table IV.

### C. Multiple Interfaces

In the experiments of Drexhage et al.,<sup>5-9</sup> the presence of several planar interfaces (surfaces of discontinuity in the dielectric function) was shown to have a significant effect on the fluorescent lifetime of the dye molecule. The theory of the previous section can be extended to this situation without

difficulty by computing the Green's function for this geometry. In the present section the theory is generalized to two problems: a finite metal film and two interfaces surrounding the emitter ("double mirror"); then the general problem of multiple interfaces is solved.

### 1. Finite Metal Film

In the case of a metal film of thickness  $d_2$ , the dyadic Green's function can be computed by satisfying the boundary conditions at both interfaces in Fig. 15. The scattering part of the Green's function in region I,  $\underline{G}_S^{(I)}$ , is written as before

$$\underline{G}_S^{(I)} = \left( \frac{i}{4\pi} \right) \int_0^\infty d\lambda \sum_{\substack{n=0 \\ j=e,o}}^\infty \left( \frac{2-\delta_{n0}}{\lambda h_1} \right) [c'_1 \mathbf{M}_{jn\lambda}(h_1) \mathbf{M}'_{jn\lambda}(h_1) + f'_1 \mathbf{N}_{jn\lambda}(h_1) \mathbf{N}'_{jn\lambda}(h_1)] \quad (3.22)$$

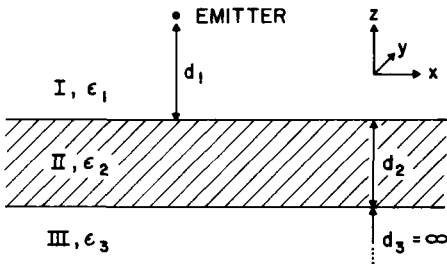


Fig. 15. Geometry of the finite-film problem. Region II has a thickness  $d_2$ ; regions I and II are half spaces. The normal to the interfaces is the  $z$  direction.

In region II (the metal with dielectric function  $\epsilon_2$ ), the Green's function is written

$$\begin{aligned} \underline{G}_S^{(II)} = & \left( \frac{i}{4\pi} \right) \int_0^\infty d\lambda \sum_{\substack{n=0 \\ j=e,o}}^\infty \left( \frac{2-\delta_{n0}}{\lambda h_1} \right) \{ [c_2 \mathbf{M}_{jn\lambda}(-h_2) + c'_2 \mathbf{M}_{jn\lambda}(h_2)] \mathbf{M}'_{jn\lambda}(h_1) \\ & + [f_2 \mathbf{N}_{jn\lambda}(-h_2) + f'_2 \mathbf{N}_{jn\lambda}(h_2)] \mathbf{N}'_{jn\lambda}(h_1) \} \end{aligned} \quad (3.23)$$

Similarly, in region III (nonabsorbing material of dielectric function  $\epsilon_3$ ),

$$\begin{aligned} \underline{G}_S^{(III)} = & \left( \frac{i}{4\pi} \right) \int_0^\infty d\lambda \sum_{\substack{n=0 \\ j=e,o}}^\infty \left( \frac{2-\delta_{n0}}{\lambda h_1} \right) \{ c_3 \mathbf{M}_{jn\lambda}(-h_3) \mathbf{M}'_{jn\lambda}(h_1) \\ & + f_3 \mathbf{N}_{jn\lambda}(-h_3) \mathbf{N}'_{jn\lambda}(h_1) \} \end{aligned} \quad (3.24)$$

where  $h_j^2 = k_j^2 - \lambda^2$ ,  $k_j^2 = \epsilon_j(\omega/c)^2$ . The absence of  $\mathbf{M}_{jn\lambda}(h_3)$  and  $\mathbf{N}_{jn\lambda}(h_3)$  in  $\underline{G}_S^{(III)}$

ensures that the fields satisfy the radiation condition as  $z \rightarrow -\infty$ ,<sup>43</sup> just as the absence of those vector functions of argument  $-h_1$  in  $\mathbf{G}_S^{(I)}$  guarantees that the fields satisfy the radiation condition as  $z \rightarrow +\infty$ .

The boundary conditions on  $\mathbf{E}$  and  $\mathbf{H}$  at an interface can be written as the continuity of both  $\hat{e}_z \times \mathbf{G}$  and  $\hat{e}_z \times \nabla \times \mathbf{G}$  across the interface. In the present case the interfaces occur at  $z=0$  and  $z=-d_2$ , so we have

$$\left. \begin{aligned} \hat{e}_z \times (\mathbf{G}_0 + \mathbf{G}_S^{(I)}) &= \hat{e}_z \times \mathbf{G}_S^{(II)} \\ \hat{e}_z \times \nabla \times (\mathbf{G}_0 + \mathbf{G}_S^{(I)}) &= \hat{e}_z \times \nabla \times \mathbf{G}_S^{(II)} \end{aligned} \right\} \quad z=0 \quad (3.25)$$

and

$$\left. \begin{aligned} \hat{e}_z \times \mathbf{G}_S^{(II)} &= \hat{e}_z \times \mathbf{G}_S^{(III)} \\ \hat{e}_z \times (\nabla \times \mathbf{G}_S^{(II)}) &= \hat{e}_z \times (\nabla \times \mathbf{G}_S^{(III)}) \end{aligned} \right\} \quad z=-d_2 \quad (3.26)$$

We find

$$\begin{aligned} 1 + c'_1 &= c_2 + c'_2 \\ \frac{h_1}{k_1} (-1 + f'_1) &= \frac{h_2}{k_2} (-f_2 + f'_2) \\ -h_1 + c'_1 h_1 &= -c_2 h_2 + c'_2 h_2 \\ k_1(1 + f'_1) &= k_2(f_2 + f'_2) \\ c_2 e^{ih_2 d} + c'_2 e^{-ih_2 d} &= c_3 e^{ih_3 d_2} \\ \frac{h_2}{k_2} (-f_2 e^{ih_2 d_2} + f'_2 e^{-ih_2 d_2}) &= \frac{h_3}{k_3} (-d_3 e^{ih_3 d_2}) \\ -c_2 h_2 e^{ih_2 d_2} + c'_2 h_2 e^{-ih_2 d_2} &= c_3 h_3 e^{ih_3 d_2} \\ k_2(f_2 e^{ih_2 d_2} + f'_2 e^{-ih_2 d_2}) &= k_3 f_3 e^{ih_3 d_2} \end{aligned} \quad (3.27a)$$

when solved for  $c'_1$  and  $f'_1$ , we find

$$\begin{aligned} c'_1 &= \frac{h_1 R_1 - h_2}{h_1 R_1 + h_2}, \quad f'_1 = \frac{S_1 h_1 \varepsilon_2 - h_2 \varepsilon_1}{S_1 h_1 \varepsilon_2 + h_2 \varepsilon_1} \\ R_1 &= \frac{h_2 - ih_3 \tan \varphi}{h_3 - ih_2 \tan \varphi}, \quad S_1 = \frac{h_2 \varepsilon_3 - ih_3 \varepsilon_2 \tan \varphi}{h_3 \varepsilon_2 - ih_2 \varepsilon_3 \tan \varphi} \end{aligned} \quad (3.27b)$$

and  $\varphi = h_2 d_2$ , so that as  $d_2 \rightarrow \infty$ , both  $S_1$  and  $R_1 \rightarrow 1$ , giving the result for a single interface.

The calculation of the emission rate of any oscillating charge distribution now proceeds just as before with  $c'_1$  and  $f'_1$  replacing  $R^I$  and  $-R^II$  in earlier equations. For example, the final form for the perpendicular case is

$$\hat{b}_1 = 1 - \frac{3}{2} q \int_0^\infty \left( \frac{R_{12}^{II} + R_{23}^{II} e^{-2l_2 d_2}}{1 + R_{12}^{II} R_{23}^{II} e^{-2l_2 d_2}} \right) e^{-2l_1 d_1} \frac{u^3 du}{l_1} \quad (3.28)$$

## 2. Double mirror

In this case the oscillating dipole is between two semi-infinite half spaces of different dielectric constant (see Fig 6). The scattered part of the dyadic Green's function in region I is given by

$$\mathbf{G}_S^{(I)} = \left( \frac{i}{4\pi} \right) \int_0^\infty d\lambda \sum_{\substack{n=0 \\ j=e,0}}^\infty \left( \frac{2-\delta_{n0}}{\lambda h_1} \right) \{ [c_1 \mathbf{M}_{jn\lambda}(-h_1) + c'_1 \mathbf{M}_{jn\lambda}(h_1)] \mathbf{M}'_{jn\lambda}(h_1) \\ + [f_1 \mathbf{N}_{jn\lambda}(-h_1) + f'_1 \mathbf{N}_{jn\lambda}(h_1)] \mathbf{N}'_{jn\lambda}(h_1) \} \quad (3.29)$$

while in medium II (above the dipole)

$$G_S^{(II)} = \left( \frac{i}{4\pi} \right) \int_0^\infty d\lambda \sum_{\substack{n=0 \\ j=e,0}}^\infty \left( \frac{2-\delta_{n0}}{\lambda h_1} \right) [c'_2 \mathbf{M}_{jn\lambda}(-h_2) \mathbf{M}'_{jn\lambda}(h_1) \\ + f'_2 \mathbf{N}_{jn\lambda}(-h_2) \mathbf{N}'_{jn\lambda}(h_1)] \quad (3.30)$$

and in medium III (below the dipole)

$$G_S^{(III)} = \left( \frac{i}{4\pi} \right) \int_0^\infty d\lambda \sum_{\substack{n=0 \\ j=e,0}}^\infty \left( \frac{2-\delta_{n0}}{\lambda h_1} \right) [c_3 \mathbf{M}_{jn\lambda}(-h_3) \mathbf{M}'_{jn\lambda}(h_1) \\ + f_3 \mathbf{N}_{jn\lambda}(-h_3) \mathbf{N}'_{jn\lambda}(h_1)] \quad (3.31)$$

with all definitions as before. The boundary conditions are now applied as before at  $z=0$  and at  $z=z_0$  ( $=s+d$  in Fig. 6). At  $z=0$  we find

$$\begin{aligned} 1 + c_1 + c'_1 &= c_3 \\ \frac{h_1}{k_1} (-1 - f_1 + f'_1) &= \frac{h_2}{k_3} (-f_3) \\ -h_1(1 + c_1) + c'_1 h_1 &= -h_3 c_3 \\ k_1(1 + f_1 + f'_1) &= k_3 f_3 \end{aligned} \quad (3.32)$$

while at  $z=z_0$ , we find

$$\begin{aligned} c_1 e^{-ih_1 z_0} + (1 + c'_1) e^{ih_1 z_0} &= c'_2 e^{ih_2 z_0} \\ \frac{h_1}{k_1} [-f_1 e^{-ih_1 z_0} + (1 + f'_1) e^{ih_1 z_0}] &= f'_2 \frac{h_2}{k_2} e^{ih_2 z_0} \end{aligned}$$

$$\begin{aligned}
 h_1[-c_1 e^{-ih_1 z_0} + (1 + c'_1) e^{ih_1 z_0}] &= h_2 c'_2 e^{ih_2 z_0} \\
 k_1[f_1 e^{-ih_1 z_0} + (1 + f'_1) e^{ih_1 z_0}] &= k_2 f'_2 e^{ih_2 z_0}
 \end{aligned} \tag{3.33}$$

which give

$$\begin{aligned}
 c_1 &= e^{i2h_1 z_0} R_{12}^{\perp} \frac{1 + R_{13}^{\perp}}{1 - R_{12}^{\perp} R_{13}^{\perp} e^{i2h_1 z_0}} \\
 c'_1 &= R_{13}^{\perp} \frac{1 + R_{12}^{\perp} e^{i2h_1 z_0}}{1 - R_{12}^{\perp} R_{13}^{\perp} e^{i2h_1 z_0}} \\
 f_1 &= R_{12}^{\parallel} \frac{e^{i2h_1 z_0} (1 - R_{13}^{\parallel})}{1 - R_{12}^{\parallel} R_{13}^{\parallel} e^{i2h_1 z_0}} \\
 f'_1 &= R_{13}^{\parallel} \frac{(1 - R_{12}^{\parallel} e^{i2h_1 z_0})}{1 - R_{12}^{\parallel} R_{13}^{\parallel} e^{i2h_1 z_0}}
 \end{aligned} \tag{3.34}$$

where

$$R_{ij}^{\parallel} = \frac{\varepsilon_i h_j - \varepsilon_j h_i}{\varepsilon_i h_j + \varepsilon_j h_i} \tag{3.35}$$

$$R_{ij}^{\perp} = \frac{h_i - h_j}{h_i + h_j} \tag{3.36}$$

For an oscillating dipole oriented perpendicular to the planes of the two interfaces ( $\parallel z$ ) and a distance  $d$  from II and  $s$  from III, we find the normalized decay rate from (2.14).

$$\hat{b}_1 = 1 - q + \frac{3}{2} q \operatorname{Im} \int_0^{\infty} du \frac{u^3 k_1}{(-ih_1)} F(u) \tag{3.37}$$

where

$$F(u) = \frac{(1 - R_{12}^{\parallel} e^{i2h_1 d})(1 - R_{13}^{\parallel} e^{i2h_1 s})}{1 - R_{12}^{\parallel} R_{13}^{\parallel} e^{i2h_1 (d+s)}} \tag{3.38}$$

This reduces to (2.47) (Section II.B). In the limit that regions II and III become perfectly conducting, we find ( $L = d + s$  and  $d \leq s$ )<sup>44</sup>

$$\hat{b}_1 = (1 - q) + 3q \left( \frac{\pi}{k_1 L} \right) \left[ \frac{1}{2} + \sum_{j=1}^{\lfloor k_1 L / \pi \rfloor} \left( \frac{1 - j^2 \pi^2}{k_1^2 L^2} \right) \cos^2 j \frac{\pi d}{L} \right] \tag{3.39}$$

where  $\lfloor k_1 L / \pi \rfloor$  is the greatest integer part of  $k_1 L / \pi$ . This is in agreement with the work of Philpott<sup>28</sup> and Milonni and Knight,<sup>29</sup> who used quantum mechanical treatments of the same problem but restricted their studies to perfect reflectors.

By the same technique we find for a dipole oriented parallel to the interfaces (distance  $d$  from II and  $S$  from III).

$$\hat{b}_{\parallel} = 1 - q + \frac{3}{4} q \operatorname{Im} \int_0^{\infty} du \frac{uk_1}{(-ih_1)} G(u) \quad (3.40)$$

where

$$G(u) = \frac{(1 - R_{12}^{\perp} e^{i2h_1 d})(1 - R_{13}^{\perp} e^{i2h_1 s})}{1 - R_{12}^{\perp} R_{13}^{\perp} e^{i2h_1(d+s)}} + (1 - u^2) \frac{(1 + R_{12}^{\parallel} e^{i2h_1 d})(1 + R_{13}^{\parallel} e^{i2h_1 d})}{(1 - R_{12}^{\parallel} R_{13}^{\parallel} e^{i2h_1(d+s)})} \quad (3.41)$$

in agreement with (2.46) after some minor rearrangement. In the limit that both metals are perfectly conducting ( $\varepsilon_2 = \varepsilon_3 \rightarrow \infty$ ), we find<sup>44</sup>

$$\hat{b}_{\parallel} = (1 - q) + \frac{3}{2} q \frac{\pi}{k_1 L} \sum_{j=1}^{[k_1 L/\pi]} \left( \frac{1 + j^2 \pi^2}{k_1^2 L^2} \right) \sin^2 j\pi d \quad (3.42)$$

also in agreement with previous work.<sup>28,29</sup> Therefore, our purely classical treatment correctly reproduces the quantum mechanical results but is sufficiently general to apply to nonideal reflectors, as is in Section II.

### 3. General Stratified Media

Consider an oscillating charge distribution embedded in a dielectric below which is a stratified medium as in Fig. 16. The dyadic Green's function

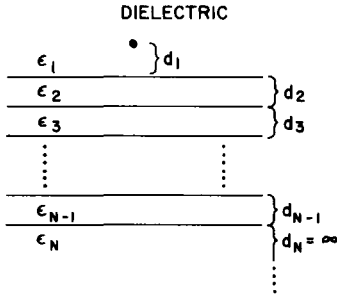


**Fig. 16.** Geometry of the stratified media problem. The emitter is a distance  $d_1$  from a multilayer system of  $N-1$  layers—the last layer being semi-infinite in extent.

may be found in the same way as before by matching boundary conditions at each planar interface and satisfying the radiation condition as  $z \rightarrow \pm \infty$ . In each stratum the scattered Green's function has the usual form [see (3.29)] with unknowns  $c_n$ ,  $c'_n$ ,  $f_n$ , and  $f'_n$ . The boundary conditions at an interface between  $n$  and  $n+1$  (where  $n \neq 1$ ) are

$$\begin{aligned}
c_n e^{-ih_n z_n} + c'_n e^{ih_n z_n} &= c_{n+1} e^{-ih_{n+1} z_n} + c'_{n+1} e^{ih_{n+1} z_n} \\
\frac{h_n}{k_n} (-f_n e^{-ih_n z_n} + f'_n e^{ih_n z_n}) &= \frac{h_{n+1}}{k_{n+1}} (-f_{n+1} e^{-ih_{n+1} z_n} + f'_{n+1} e^{ih_{n+1} z_n}) \\
-c_n h_n e^{-ih_n z_n} + c'_n h_n e^{ih_n z_n} &= -h_{n+1} c_{n+1} e^{-ih_{n+1} z_n} + c'_{n+1} h_{n+1} e^{ih_{n+1} z_n} \\
k_n f_n e^{-ih_n z_n} + k_n f'_n e^{ih_n z_n} &= k_{n+1} f_{n+1} e^{-ih_{n+1} z_n} + k_{n+1} f'_{n+1} e^{ih_{n+1} z_n}
\end{aligned} \tag{3.43}$$

where  $z_n$  is the distance in the  $z$  direction to the  $n/n+1$  boundary. In the  $N$ th (lowest) stratum,  $c'_N = f'_N = 0$ , so the equations can be solved for  $c_{N-1}$  and  $c'_{N-1}$  in terms of  $c_N$  and for  $f_{N-1}$  in terms of  $f_N$ . Then the next set is solved for  $c_{N-2}$ ,  $c'_{N-2}$ ,  $f_{N-2}$ , and  $f'_{N-2}$ , and so on until  $c_1$ ,  $c'_1$ ,  $f_1$ , and  $f'_1$  are known in terms of  $c_N$  and  $f_N$ . It proves convenient to solve for  $c_n + c'_n$  and  $c_n - c'_n$  so that

$$T_n \equiv \frac{c_n + c'_n}{c_n - c'_n} = \frac{T_{n+1} - i(h_{n+1}/h_n) \tan \varphi_n}{(h_{n+1}/h_n) - T_{n+1} \tan \varphi_n} \tag{3.44}$$

where  $\varphi_n = h_n(z_n - z_{n+1}) \equiv h_n d_n$ . Similarly,

$$S_n \equiv \frac{f_n + f'_n}{f_n - f'_n} = \frac{S_{n+1} - i(h_{n+1} k_n^2 / h_n k_{n+1}^2) \tan \varphi_n}{(h_{n+1} k_n^2 / h_n k_{n+1}^2) - i S_{n+1} \tan \varphi_n} \tag{3.45}$$

Note that  $T_N = S_N = 1$  so that the number of equations is  $N$ . Once  $T_1$  and  $S_1$  are found,  $c'_1$  and  $f'_1$  can be found from

$$c'_1 = \frac{h_1 T_1 - h_2}{h_1 T_1 + h_2} \tag{3.46}$$

$$f'_1 = \frac{h_1 k_2^2 S_1 - h_2 k_1^2}{h_1 k_2^2 S_1 + h_2 k_1^2} \tag{3.47}$$

If there is another boundary (or stratified medium) above the oscillating charge distribution, a further set of equations must be solved for the upper boundaries.

These equations can be put into another form by noting that  $h_n = ik_1 l_n$  with  $l_n = -i(\epsilon_n/\epsilon_1 - u^2)^{1/2}$  and by defining, for example,

$$\mathcal{S}_n = \frac{1 - S_n}{1 + S_n} \tag{3.48}$$

Then

$$f'_1 = -\frac{R_{12}^{\parallel} - \mathcal{S}_1}{1 - R_{12}^{\parallel} \mathcal{S}_1} \tag{3.49}$$

$$\mathcal{S}_n = \frac{(-R_{n,n+1}^{\parallel} + \mathcal{S}_{n+1})e^{-2l_n \hat{d}_n}}{1 - R_{n,n+1}^{\parallel} \mathcal{S}_{n+1}} \tag{3.50}$$



where  $\hat{d}_n = k_1 d_n$ , as before.

A similar manipulation for  $c'_1$  gives

$$c'_1 = -\frac{R_{12}^\perp + \mathcal{R}_1}{1 - R_{12}^\perp \mathcal{R}_1} \quad (3.51)$$

where

$$\mathcal{R}_n = \frac{1 - T_n}{1 + T_n}, \quad \mathcal{R}_N = 0 \quad (3.52)$$

so that

$$\mathcal{R}_n = \frac{(-R_{n,n+1}^\perp + \mathcal{R}_{n+1})e^{-2i\alpha\hat{d}_n}}{1 - R_{n,n+1}^\perp \mathcal{R}_{n+1}} \quad (3.53)$$

This representation shows the simple connection to the Fresnel reflection coefficients ( $R_{ij}^\perp$  and  $R_{ij}^\parallel$ ).

These equations have been solved<sup>45</sup> for the case of an emitting dipole above a liquid mercury surface for various models of the surface conductivity.<sup>46</sup>

#### D. Appendix. Decay Rate of Multipole Emitters Near a Mirror: A Check by Other Methods

The formulation for decay rate of a multipole emitter near a mirror can be checked by a method similar to the interference method of Drexhage. The reason for this is given in Section II, where it is shown that the interference term in (2.41) is the  $0 \rightarrow 1$  part of the total integral from  $0 \rightarrow \infty$  (which describes the effect of the mirror on emitter decay rate). We use this result in our calculations below by first writing the components of the radiation (far) electric field of the emitter, introducing the partially reflecting mirror, and then writing the expression for interference between primary rays from the emitter and rays reflected from the surface. Finally, the integration limit is extended to infinity.

Only the highlights of the calculation for electric quadrupole emitters is given. The Hertz vector describing the far field can be written

$$\Pi = \mathbf{p}^{(2)} \frac{e^{iR}}{R} \quad (3.54)$$

where distance  $R$  includes the magnitude of the wave vector and thus is dimensionless, and  $p^{(2)}$  is given by

$$\mathbf{p}^{(2)} = \mathbf{D} \cdot \nabla R \quad (3.55)$$

and  $\mathbf{D}$  is the particular quadrupole tensor.<sup>25</sup>

Using (2.8) we find for the radiation field,

$$\begin{aligned} E_\theta &= \Pi_\theta \equiv f(\phi) E^\parallel \\ E_\phi &= \Pi_\phi \equiv g(\phi) E^\perp \end{aligned} \quad (3.56)$$

where  $\theta$  and  $\phi$  are polar angles (the longitudinal component  $E_R$  is zero). Then, depending on the phase relation between the two rays from the emitter—one towards the mirror, the other away from it, we can write for the non-normalized rate (where  $q = 1$ )

$$b_1 = \text{Im} \int_0^1 R^2 (c^{\parallel} |\pm 1 - R^{\parallel} e^{-2id}|^2 |E^{\parallel}|^2 + c^{\perp} |\pm 1 + R^{\perp} e^{-2id}|^2 |E^{\perp}|^2) \frac{u du}{l} \quad (3.57)$$

where  $c^{\parallel}$  and  $c^{\perp}$  arise from the integrals over  $\phi$ ,  $u = \sin \theta$ , and  $l = -i \cos \theta$ .

The prescription to obtain the normalized decay rate follows from section II:

1. Normalize such that when  $R^{\parallel} = R^{\perp} = 0$ ,  $b^{\dagger} = \frac{1}{2}$ .
2. Retain only the distance-dependent terms of (3.57).
3. Multiply by  $q$ , extend the integration limit to infinity, and add 1 to the result.

As an example we give the intermediate quantities in the calculation for the square quadrupole  $Q^{xz}$ , which corresponds to the last component in Table IV of Section III.

$$\begin{aligned} \mathbf{P}^{(2)} &= \left( \hat{e}_x \frac{z}{R} + \hat{e}_z \frac{x}{R} \right) \\ [E_{\theta}, E_{\phi}] &= \left[ (1 - 2 \sin^2 \theta) \cos \phi \frac{e^{iR}}{R}, -\cos \theta \sin \phi \frac{e^{iR}}{R} \right] \\ (c^{\parallel}, c^{\perp}) &= (\pi, \pi) \\ (\text{phase } E^{\parallel}, \text{phase } E^{\perp}) &= (1 - R^{\parallel} e^{i2d \cos \theta}, -1 + R^{\perp} e^{i2d \cos \theta}) \end{aligned}$$

The calculated values of  $\hat{b}$  for this and all other cases are in agreement with those of Table IV.

The magnetic dipole can be discussed in the same way where for each orientation the corresponding quantities  $E_{\theta}$ ,  $E_{\phi}$ ,  $c^{\parallel}$  and  $c^{\perp}$  and the phase relations are determined and combined according to the prescription given above.

The decay-rate expressions can also be checked by deriving them from the dipole formulas. For a given quadrupole emitter the Hertz vector is obtained by differentiation of the dipole Hertz vectors. Then in the framework of Kuhn's<sup>1,2</sup> model it is only necessary to insert the derivative of the reflected field at the emitter position. The constant multiplying the integral in the expression for normalized decay rate is readily evaluated through a limiting condition: for a perfect reflector ( $R^{\parallel} = R^{\perp} = -1$ ) when  $q = 1$ , then for  $d \rightarrow 0$  we require for the first three quadrupoles of Table IV that  $b \rightarrow 0$ , and for that last two, that  $b \rightarrow 2$ .

As an example we consider the  $xz$  quadrupole. The Hertz vector is

$$\Pi^{xz} = -\frac{\partial}{\partial x} \Pi_d^\perp + \frac{\partial}{\partial d} \Pi_d^\parallel \quad (3.58)$$

where  $\Pi_d^\perp$  and  $\Pi_d^\parallel$  are given by (2.9) and (2.18), respectively. The field  $\mathbf{E}$  is calculated from (2.8), and the derivative of  $\mathbf{E}$  along the diagonal of  $\mathbf{D}^{xz}$  at the emitter position is

$$\frac{1}{2} \left( \frac{\partial E_x}{\partial z} + \frac{\partial E_z}{\partial x} \right) \quad (3.59)$$

This is proportional to the integral  $X$  in the last line of Table IV. The requirement that  $b \rightarrow 2$  means that this term must equal unity. The integral becomes  $\frac{4}{3}$  in this case, so that the constant is  $\frac{5}{4}$ , in agreement with Table IV.

The magnetic dipole decay rates can also be derived from the Hertz vectors of the electric dipole by making the changes  $\mathbf{E} \rightarrow \mathbf{H}$ ,  $\mathbf{H} \rightarrow -\mathbf{E}$ ,  $\mu \rightarrow \epsilon$ ,  $\epsilon \rightarrow \mu$ . The boundary conditions for  $\Pi$  are similar and are also derived from the continuity conditions for  $E$  and  $H$ . The reflection coefficients are found to be related to those of the electric dipole through the changes  $R^\perp \rightarrow -R^\perp$ ,  $R^\parallel \rightarrow -R^\parallel$ . Alternately, the reflected *magnetic* field at the dipole position can be found for use in Kuhn's model and the result for  $\hat{b}$  follows.

## IV. ENERGY TRANSFER AND SURFACE PLASMONS

### A. Isotropic Media

As pointed out in Section II, nonradiative energy transfer to a nearby metal surface can be an effective decay channel for an excited molecule. In this section we discuss the dependence of this transfer rate on frequency and the connection between this dependence and the surface-plasmon modes.

Consider an emitting molecule (oscillating dipole) near a metallic half space; the normalized energy-transfer rate at small distances ( $k_1 d = \hat{d} \ll 1$ ) from the surface is [see (2.52)]<sup>18</sup>

$$\hat{b}_{ET} = \left[ \frac{\theta}{4\hat{d}^3} \right] \text{Im} \left( \frac{\epsilon_2(\omega) - \epsilon_1}{\epsilon_2(\omega) + \epsilon_1} \right) \quad (4.1)$$

where  $\epsilon_2(\omega)$  is the dielectric function of the metal,  $\epsilon_1$  is that of the dielectric in which the dipole is embedded, and  $\theta$  is an orientational parameter ( $\theta = \frac{3}{2}$  for a perpendicular dipole and  $\theta = \frac{3}{4}$  for a parallel dipole). This result can also be derived easily from image theory, since the *reflected* field at the dipole (due to the metallic surface) is given from image theory<sup>25</sup> as:

$$\mathbf{E}_R(\omega) = \left( \frac{\epsilon_2(\omega) - \epsilon_1}{\epsilon_2(\omega) + \epsilon_1} \right) \mathbf{E}_R^{\text{ideal}}(\omega) \quad (4.2)$$

where  $\mathbf{E}_R^{\text{ideal}}(\omega)$  is the electric field from a perfect image dipole in the metal. In the case of a dipole parallel to the surface

$$\mathbf{E}_R^{\text{ideal}}(\omega) = \mu \frac{k_1^3}{n_1^2} e^{i2\hat{d}} \left[ \frac{1}{(2\hat{d})^3} - \frac{i}{(2\hat{d})^2} - \frac{1}{(2\hat{d})} \right] \quad (4.3a)$$

while for a dipole perpendicular to the surface,

$$E_R^{\text{ideal}}(\omega) = \frac{2\mu k_1^3}{n_1^2} e^{i2\hat{d}} \left[ \frac{1}{(2\hat{d})^3} - \frac{i}{(2\hat{d})^2} \right] \quad (4.3b)$$

Thus at very small  $\hat{d}$ , we have from (2.7)

$$\hat{b}_{ET} = \frac{3q\epsilon_1}{2k_1^3} \text{Im} \left[ \frac{\mathbf{E}_R(\omega)}{\mu} \right] \quad (4.4)$$

which gives the above result (4.1).

This result immediately shows the strong frequency dependence of  $\beta$  ( $\equiv \hat{b}_{ET} d^3$ ). Consider the case of a Drude metal with  $\epsilon_2(\omega) = 1 - \omega_p^2/\omega(\omega + i\delta)$ , where  $\delta$  is the inverse relaxation time and  $\omega_p$  the plasma frequency. Then, for small  $\delta$

$$\beta \propto \frac{\omega_p^2 \omega \epsilon_1 \sigma}{(1 + \epsilon_1)^2 \left[ \left( \omega^2 - \frac{\omega_p^2}{1 + \epsilon_1} \right)^2 + \frac{\omega_p^4 \delta^2}{\omega^2} \right]} \quad (4.5)$$

so that  $\beta$  has a resonance at  $\omega_{sp} = \omega_p(1 + \epsilon_1)^{-1/2}$ , which is the surface-plasmon frequency of this interface.<sup>47</sup> Note that this result has been derived in the small  $\hat{d}$  limit, which corresponds to the  $c \rightarrow \infty$  limit, so the effects of retardation are not included. In this limit the surface-plasmon mode has no dispersion; the effect of this dispersion on energy transfer is in the higher-order terms, which are not treated in this section. We see later when anisotropic media are discussed that this limit rules out the effects of the “ $k$ -limited” modes discussed by Kliwer and Fuchs.<sup>48</sup>

The decay-rate constant of electric quadrupole and magnetic dipole transitions near a thick mirror also can have surface-plasmon resonances. The expressions for  $\hat{b}_{ET}$  for such transitions in the small  $\hat{d}$  limit are<sup>19</sup>

$$\hat{b}_{ET}^Q = \frac{12q}{d^5} \frac{\theta \epsilon_1 n_2 \kappa_2}{|\epsilon_1 + \epsilon_2|^2} \quad (4.6)$$

$$\hat{b}_{ET}^M = \frac{qn_2 \kappa_2}{4\epsilon_1 \hat{d}} \left( \frac{4\theta \epsilon_1^2}{|\epsilon_1 + \epsilon_2|^2} + \theta' \right) \quad (4.7)$$

where  $\theta$  and  $\theta'$  are given in Table V. A resonance at the surface plasmon frequency is predicted in every case except the perpendicular ( $z$ ) orientation of the magnetic dipole ( $\theta = 0$  from Table V); there is no coupling in this case,

TABLE V  
Energy-Transfer Parameters

	$\theta$	$\theta'$
Electric dipole component (4.1)		
$z$	$\frac{3}{2}$	0
$y, x$	$\frac{3}{4}$	0
Magnetic dipole component (4.7)		
$z$	0	$\frac{3}{2}$
$y, x$	$\frac{3}{2}$	$\frac{3}{4}$
Electric quadrupole component (4.6)		
$zz$	$\frac{15}{8}$	0
$zx, zy$	$\frac{5}{4}$	0
$x^2 - y^2, yx$	$\frac{5}{16}$	0

since the radiation field contains no component normal to the mirror surface. Note the distance dependence of the magnetic dipole decay rate is  $d^{-1}$ , because the electric field falls off as  $R^{-2}$ , so that the absorption of energy by the metal is proportional to  $R^{-4}$  integrated over the half space, producing the  $d^{-1}$  behavior.

The effect of the nearby surface on the *frequency* of the emission can also be treated in this way. Arguments similar to the above<sup>24</sup> indicate that the change in frequency for an electric dipole are, in the small  $\hat{d}$  limit, given by

$$\Delta\omega = q\gamma(\omega)\hat{d}^{-3}\tau_0^{-1} \quad (4.8)$$

where  $\tau_0 (= 1/b_0)$  is the fluorescence lifetime in the absence of the mirror, and

$$\gamma(\omega) = \frac{\theta}{8} \operatorname{Re} \left[ \frac{\epsilon_1 - \epsilon_2(\omega)}{\epsilon_1 + \epsilon_2(\omega)} \right] \quad (4.9)$$

$\theta$  is the orientational parameter for an electric dipole given earlier. Using the Drude dielectric function above, we predict a dispersionlike curve for  $\gamma(\omega)$  near  $\omega = \omega_p(1 + \epsilon_1)^{-1/2}$ .

The coupling of the short-range dipole field to surface waves was first noted by Sommerfeld in his famous study<sup>16</sup> of radio-wave propagation near the earth's surface. In recent years interest has grown in the surface modes of the metal/dielectric interface (surface plasmons) and the dielectric/dielectric

interface (surface polaritons), and a variety of clever experiments<sup>20,21</sup> have been performed to measure the dispersion of the surface modes.

In the context of the fluorescence lifetime of excited molecules near surfaces, Morawitz and Philpott<sup>17</sup> and Chance et al.<sup>18,19</sup> have noted the coupling of the surface plasmons to the emitting molecule. Quantum-mechanical treatments of this coupling have been given by Philpott<sup>17</sup> for the decay rate (which agrees with the classical formula) and by Agarwal,<sup>49</sup> Barton,<sup>50</sup> and Babiker and Barton,<sup>51</sup> for the frequency shifts (which show some nonclassical effects). In addition, there have been experimental studies of vibrational lineshapes of adsorbed molecules by Kirtley et al.<sup>52</sup> that show the effects of *nonresonant* coupling to surface plasmons.

The calculated values of  $\gamma$  and  $\beta$  are given in Fig. 17 and 18 for the fatty acid/silver mirror interface. From the curve for  $\gamma(\omega)$ , it is clear that frequency shifts will be much too small to measure for distances greater than a few

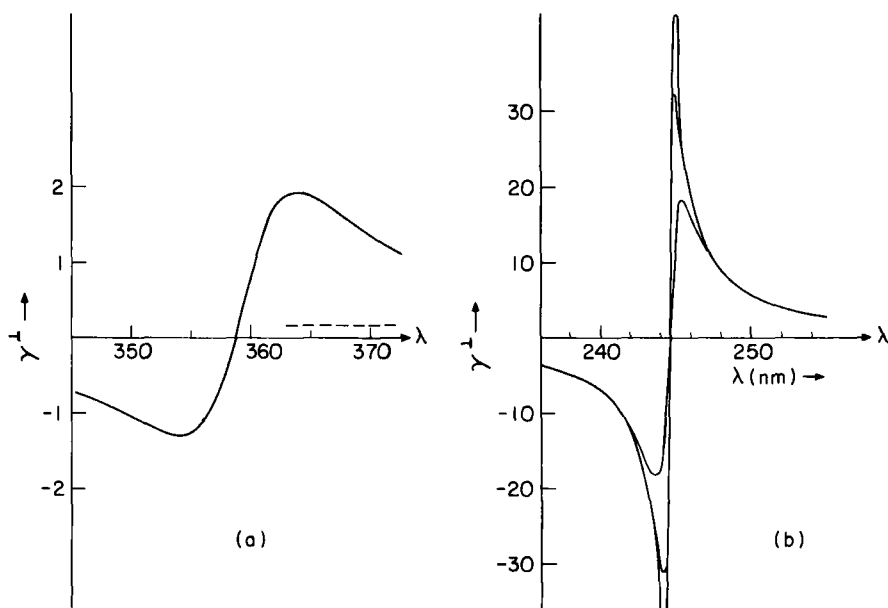


**Fig. 17.** Frequency-shift parameter  $\gamma^{\perp}$  [see (4.9)] for a dipole oriented perpendicular to a silver mirror in a dielectric of refractive index  $n_1 = 1.50$ : (a) dielectric function of Ag from experimental data in reference<sup>26</sup>; (b) dielectric function of Ag based on Drude model<sup>26</sup> with  $\omega_p = 13.9 \times 10^{-15}$  sec<sup>-1</sup> and relaxation times  $\tau$  equal to 19, 31, and  $43 \times 10^{-15}$  sec (the lower  $\tau$ , the lower the peak in  $\gamma^{\perp}$ ). The dashed line in a shows the perfect mirror result. Results for a parallel dipole can be obtained as  $\gamma^{\parallel} = \gamma^{\perp}/2$ . (After Chance et al.<sup>24</sup> Used by permission.)

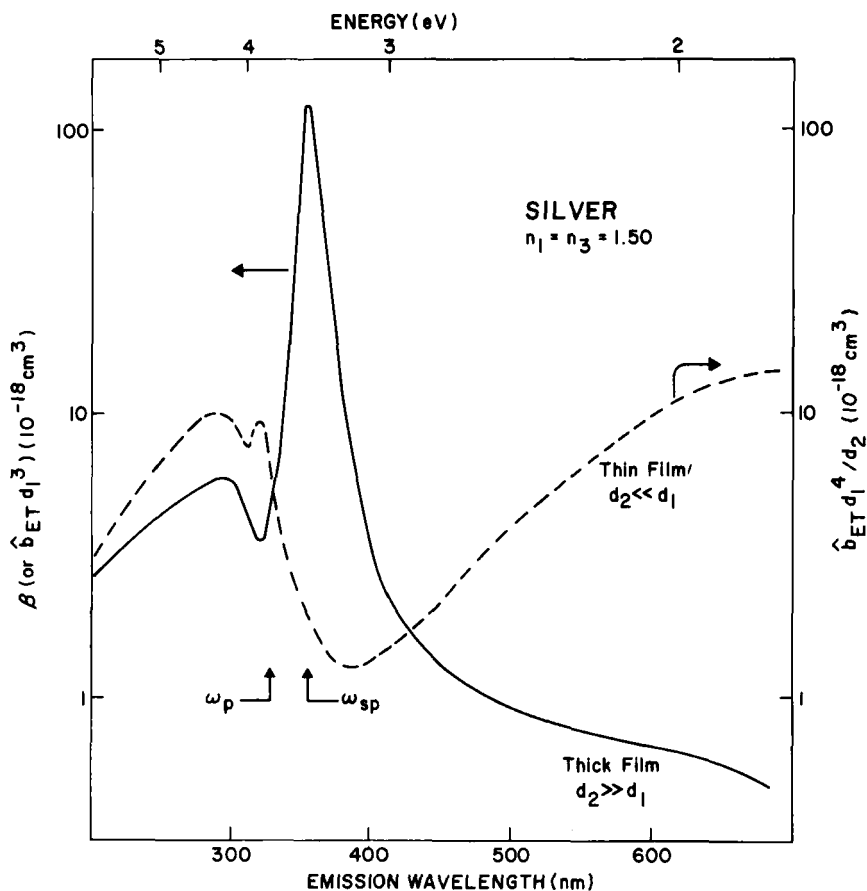


**Fig. 18.** Energy-transfer rate parameter versus emission wavelength for a silver mirror. The thick-mirror results ( $\beta = \hat{\beta}_{ET} d_1^3$ ) have a resonance near the surface-plasmon frequency,  $\omega_{sp} (\epsilon_2 \approx -\epsilon_1 = -2.25)$ . The thin-film ( $d_2 \ll d_1$ ) results show a resonance at the bulk-plasmon frequency  $\omega_p (\epsilon_2 \approx 0)$ . The results shown are for an isotropic dipole orientation.

angstroms. Note that  $\beta$  in Fig. 18 increases by a factor of  $10^3$  as the wavelength decreases from 600 (where the Drexhage experiments<sup>5-9</sup> are done) to 360 nm (near the surface plasmon mode). This implies a Förster energy-transfer length of  $\sim 1000 \text{ \AA}$ . That is, energy transfer competes successfully with emission within  $1000 \text{ \AA}$  of the surface.

If the metal half space is replaced by a thin film, an interesting phenomenon can occur. Consider an emitting molecule (embedded in a nonabsorbing dielectric of dielectric constant  $\epsilon_1$ ) near a thin metal film (dielectric constant

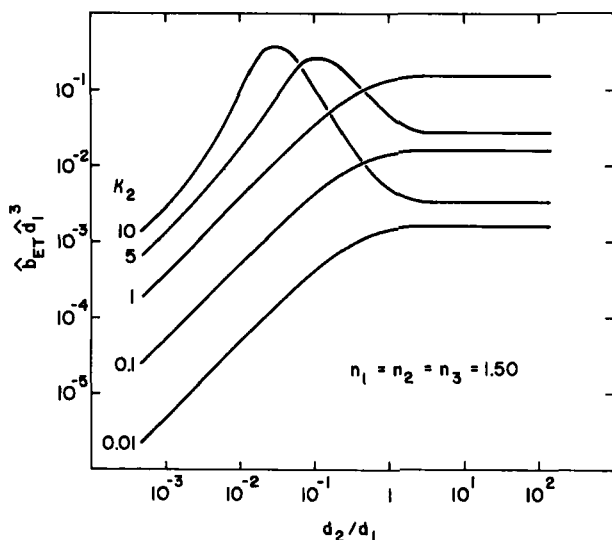


Fig. 19. Energy-transfer parameter  $\beta$  versus  $d_2/d_1$ , where  $d_2$  is the metal-film thickness and  $d_1$  is the electric dipole-metal distance. The peak in  $\beta$  that develops as  $\kappa_2$  becomes large ( $\kappa_2 > n_1$ ) illustrates the thin-film enhancement effect. The results shown are for an isotropic dipole orientation.

$\epsilon_2$ ). The small-distance decay-rate constant is given in (2.53). From this equation an expression for the maximum in  $\beta$  as a function  $\epsilon_2$  and  $(d_2/d_1)$  can be found. If  $\epsilon_2$  is written as  $|\epsilon_2|e^{i(\pi-\alpha)}$  and  $\alpha$  is taken to be small (i.e.,  $\kappa_2$  large),  $\beta_{\max}$  is found to be  $\approx 0.8$  at  $d_2 d_1^{-1} = \frac{4}{3} \epsilon_1 / |\epsilon_2|$ . When  $\beta$  is computed, using (2.53), a maximum in  $\beta$  is found for  $\kappa_2 \gg 1$ . A plot of  $\beta$  versus  $d_2/d_1$  for various  $\kappa_2$  is given in Figure 19 for the case  $n_1 = n_2 = n_3 = 1.50$ . Notice that in the weak absorber limit, there is a smooth transition from  $d^{-3}$  to  $d^{-4}$  behavior, but in the strong absorber limit ( $\kappa_2$  large), a thin film may be a *better* acceptor of energy than a thick film. This indicates that the Förster energy-transfer law only works for this system in the weak-absorber range.

A qualitative explanation of this effect can be found by examining the formula for  $\beta$  in terms of the surface-plasmon modes of thin films. From (3.28) for a perpendicular dipole, we take the case  $\epsilon_1 = \epsilon_3$  (or  $R_{12}^{\parallel} = -R_{23}^{\parallel}$ ),  $d_1 \ll 1$ , and change variables  $-x = (u^2 - 1)^{1/2}$ , to give

$$\hat{b}_{ET}^{\perp} = \frac{3q}{k_1^3} \text{Im} \left\{ \epsilon_2 \int_0^{\infty} dx x^2 e^{-2xd_1} \left[ \frac{(\epsilon_1 + \epsilon_2) + (\epsilon_1 - \epsilon_2)e^{-2xd_2}}{(\epsilon_1 + \epsilon_2)^2 - (\epsilon_1 - \epsilon_2)^2 e^{-2xd_2}} \right] \right\} \quad (4.10)$$

[alternately we could begin with (2.52) and substitute  $x = u/d$ ]. For the parallel case,  $\hat{b}_{ET}^{\parallel} = \frac{1}{2} \hat{b}_{ET}^{\perp}$ .



The resonance condition for  $\hat{b}_{ET}$  becomes (for fixed  $d_1$ )

$$(\varepsilon_1 + \varepsilon_2) = \pm(\varepsilon_1 - \varepsilon_2)e^{-x d_2} \quad (4.11)$$

If  $x$  is interpreted as  $k_1 \sin \theta$ , where  $\theta$  is the angle of incidence, then  $x$  is the component of the wave vector in the surface plane,  $k_{\parallel}$ , and the resonance condition becomes the equation for the surface-plasmon modes of the thin film.<sup>22,23,53</sup> If the Drude formula for  $\varepsilon_2(\omega)$  is substituted, then the formula for the surface-plasmon frequencies is

$$\omega_{sp}^2(k_{\parallel} d_2) = \frac{\omega_p^2(1 \mp e^{-k_{\parallel} d_2})}{(1 + \varepsilon_1) \mp (1 - \varepsilon_1)e^{-k_{\parallel} d_2}}$$

Thus for any  $d_2$  there will be a surface mode in resonance with the emitter; however, the *coupling* of the emitter to the surface and the density of surface states will depend strongly on  $d_2$ . As  $d_2$  decreases there will be a value of  $d_2$  to maximize the effective coupling to the surface modes, giving rise to a peak in  $\beta$ . The value of  $\hat{b}_{ET} \hat{d}_1^3$  at the peak in Fig. 19 is almost as large as the resonant value of  $\beta$  for thick films of the same dielectric function, thereby lending support to this explanation.

As  $d_2 \rightarrow 0$  the low-frequency surface mode will couple less effectively to the emitter so that the strength of the resonance is reduced (that is, the residue at the pole is smaller). This is shown by taking the limit of  $\beta$  for  $d_2 \ll d_1$ ; the results for electric dipoles, electric quadrupoles, and magnetic dipoles are given by (4.12) and Table V. Results from (4.12a) for an electric dipole emitter are shown in Fig. 18 as a function of frequency for the fatty acid/silver system. Note that the only resonance occurs for  $\varepsilon_2 = 0$  ( $\omega = \omega_p$ ) in (4.12) and in Fig. 18, which is one of the limiting values of  $\omega_{sp}(k_{\parallel} d_2)$  for  $d_2 \rightarrow 0$ . The other surface-mode branch ( $\omega_{sp} \rightarrow 0$ ) does not contribute to the energy transfer rate in this limit. Ferrell<sup>23</sup> points out how strongly these modes are changed by retardation (i.e., the photon/plasmon coupling), so these results are valid only for the  $(\omega d_2/c) \rightarrow 0$  limit.

$$\hat{b}_{ET}^{ED} = \frac{3q\hat{d}_2}{8\hat{d}_1^4} \frac{\theta n_2 \kappa_2}{\varepsilon_1} \left( 1 + \frac{\varepsilon_1^2}{|\varepsilon_2|^2} \right) \quad (4.12a)$$

$$\hat{b}_{ET}^{MD} = \frac{q\hat{d}_2 n_2 \kappa_2}{4\hat{d}_1^2 \varepsilon_1} \left[ \frac{\theta}{2} \left( 1 + \frac{\varepsilon_1^2}{|\varepsilon_2|^2} \right) + \theta' \right] \quad (4.12b)$$

$$\hat{b}_{ET}^{QD} = \frac{15q\theta n_2 \kappa_2 \hat{d}_2}{2\hat{d}_1^5 \varepsilon_1} \left[ 1 + \frac{\varepsilon_1^2}{|\varepsilon_2|^2} \right] \quad (4.12c)$$

Although the coupling of fluorescence to the surface plasmon of the interface has been treated theoretically and the expressions for  $\beta$  (for the various cases treated in this section) have been derived, there has been little experimental confirmation to date of these predictions.

## B. Anisotropic Media

In recent years there has been a growing interest in one- and two-dimensional conductors (and anisotropic conductors in general)<sup>54</sup> owing to their unusual properties. In this section the interaction of fluorescing molecules with such systems is treated to explore the possibility of studying them with these techniques. The introduction of such anisotropy increases the theoretical labor considerably and produces some surprising results. We consider first the dipole near an anisotropic absorbing medium (with cylindrically symmetric  $\epsilon$ ); then for completeness we discuss the dipole embedded in an anisotropic nonabsorbing medium.

### 1. Dipole Near an Anisotropic Absorbing Medium

We consider a dipole emitter embedded in an isotropic nonabsorbing medium of dielectric constant  $\epsilon$  and located at a distance  $d$  from the interface with the anisotropic absorbing medium. The interface is regarded as the  $x,y$ -plane and  $d$  lies along the  $z$ -axis. The normalized decay rate of the dipole, whatever the orientation, can be expressed in terms of integrals involving  $R^{\parallel}$  and  $R^{\perp}$  as in the isotropic cases discussed previously. It is necessary to determine these expressions for  $R^{\parallel}$  and  $R^{\perp}$  and then to insert them into the integrals with appropriate geometric weighting factors for the various dipole orientations. In this section we use the plane-wave spectrum method,<sup>55</sup> which allows an evaluation of  $R^{\parallel}$  and  $R^{\perp}$  most easily in the anisotropic cases treated here. This method proceeds by expanding the dipole field in plane waves, matching boundary conditions in this representation to get  $R^{\parallel}$  and  $R^{\perp}$  for each ray. These expressions are then put into the equation for  $\hat{b}_{ET}$  (for small  $\hat{d}$ ). First we derive the expressions for  $R^{\parallel}$  and  $R^{\perp}$ . We need consider only two cases: (a) the unique axis lying in the  $xy$ -plane—it may lie along  $x$  with no loss in generality, and (b) the unique axis lying along the  $z$ -axis.

a. Case *a* Unique Axis in Plane (Along  $x$ -axis). The dielectric tensor of the absorber has the form

$$\epsilon_2 = \begin{pmatrix} \epsilon_x & 0 & 0 \\ 0 & \epsilon_z & 0 \\ 0 & 0 & \epsilon_z \end{pmatrix} \quad (4.13)$$

Figure 20 shows the geometry of the problem. The emitting dipole is located in the upper half space at a distance  $d$  from the interface. A p-polarized electromagnetic wave from the dipole is first considered. On reflection from the interface the ray remains in the plane of incidence as required by phase matching, but the polarization is changed by an angle designated  $\gamma$  in Fig. 20.

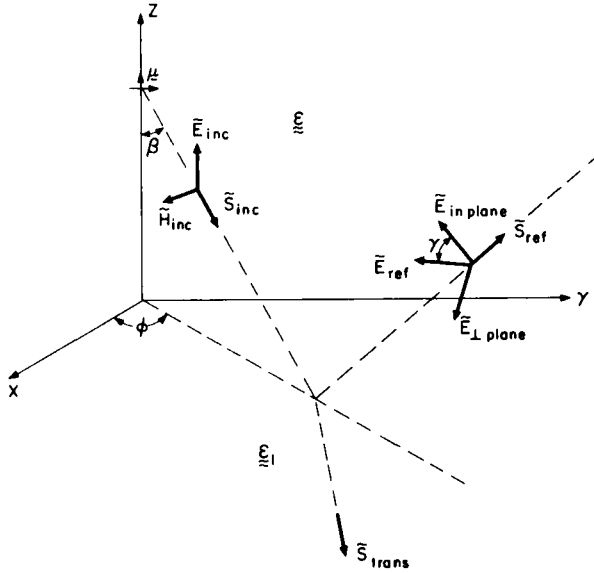


Fig. 20. Geometry of incident, reflected, and transmitted rays for the interface between an isotropic and anisotropic medium.

The incident ray has a unit wave vector  $S_1$  given by

$$S_1 = \frac{l\hat{e}_x + m\hat{e}_y + n\hat{e}_z}{n_A} \quad (4.14)$$

where  $\hat{e}_x$ ,  $\hat{e}_y$ , and  $\hat{e}_z$  are unit vectors in the  $x$ ,  $y$  and  $z$  directions. Then we may write for the incident electric vector,

$$\mathbf{E}_{\text{inc}} = S_1 \times \frac{\hat{l}_z \times S_1}{|\hat{l}_z \times S_1|} = \frac{-ln\hat{e}_x - mn\hat{e}_y + (l^2 + m^2)\hat{e}_z}{n_A(e^2 + m^2)^{1/2}} |\mathbf{E}_{\text{inc}}| \quad (4.15)$$

The reflected ray has an electric-field component in the plane of incidence and a component perpendicular to this plane as determined by the value of  $\gamma$ . In these terms we write

$$\mathbf{E}_{\text{ref}} = \left\{ \frac{\cos \gamma}{n_A} [ln\hat{e}_x + mn\hat{e}_y + (e^2 + m^2)\hat{e}_z] + \sin \gamma (m\hat{e}_x - l\hat{e}_y) \right\} \frac{|\mathbf{E}_{\text{ref}}|}{(l^2 + m^2)^{1/2}} \quad (4.16)$$

The magnetic-field components are vectors rotated  $90^\circ$  from their corresponding electric-field components around the ray direction. The magnetic fields are  $n_A$  times as large as the electric fields, or

$$\mathbf{H}_{\text{inc}} = \frac{m\hat{e}_x - l\hat{e}_y}{(m^2 + l^2)^{1/2}} n_A |\mathbf{E}_{\text{inc}}| \quad (4.17)$$

and

$$\mathbf{H}_{\text{ref}} = \left\{ -\sin \gamma [\ln \hat{e}_x + mn\hat{e}_y + (l^2 + m^2)\hat{e}_z] + n_A \cos \gamma (m\hat{e}_x - l\hat{e}_y) \right\} \frac{|\mathbf{E}_{\text{ref}}|}{(l^2 + m^2)^{1/2}} \quad (4.18)$$

The transmitted wave vector is also coplanar, as demanded by congruence of phases at the boundary. This also demands that the values of  $l$  and  $m$  be those of the incident wave. There are actually two transmitted waves with different velocities and different directions (different only in their values of  $n$ ). One wave has  $E_x = 0$ , the other has  $H_x = 0$ , and each is characterized by its own refractive index. The electric field vectors are calculated below.

*Case where  $E_x = 0$ .* The components  $l$ ,  $m$ , and  $n_1$  satisfy the relation

$$l^2 + m^2 + n_1^2 = \epsilon_z = n_{21}^2 \quad (4.19)$$

It follows that

$$\mathbf{D}_1 = \frac{\mathbf{S}_{21} \times \hat{e}_x}{|\mathbf{S}_{21} \times \hat{e}_x|} |\mathbf{D}_1| = \frac{n_1 \hat{e}_y - m\hat{e}_z}{(n_1^2 + m^2)^{1/2}} |\mathbf{D}_1| \quad (4.20)$$

and since  $\tilde{\mathbf{D}}_1$  and  $\tilde{\mathbf{E}}_1$  are parallel for this wave (i.e.,  $\tilde{\mathbf{D}}_1 = \epsilon_z \tilde{\mathbf{E}}_1$ ), we can write also

$$\mathbf{E}_1 = \frac{(n_1 \hat{e}_y - m\hat{e}_z)}{(n_1^2 + m^2)^{1/2}} |\mathbf{E}_1| \quad (4.21)$$

Finally,

$$\mathbf{H}_1 = n_2 \mathbf{S}_{21} \times \mathbf{E}_1 = \frac{-(m^2 + n_1^2)\hat{e}_x + lm\hat{e}_y + ln_1\hat{e}_z}{(m^2 + n_1^2)^{1/2}} |\mathbf{E}_1| \quad (4.22)$$

*Case where  $H_x = 0$ .* Here the components  $l$ ,  $m$ , and  $n_2$  satisfy

$$\frac{\epsilon_x}{\epsilon_z} l^2 + m^2 + n_2^2 = \epsilon_x \quad (4.23)$$

We can write for the field  $\mathbf{H}_2$ ,

$$\mathbf{H}_2 = \frac{\mathbf{S}_{22} \times \hat{e}_x}{|\mathbf{S}_{22} \times \hat{e}_x|} |\mathbf{H}_2| = \frac{n_2 \hat{e}_y - m\hat{e}_z}{(m^2 - n_2^2)^{1/2}} |\mathbf{H}_2| \quad (4.24)$$

Because  $\mathbf{E}$  has an  $x$  component in this case, we need the tensor relation

between **E** and **D**, so we write

$$\begin{aligned} \mathbf{D}_2 = -n_{22}\mathbf{S}_{22} \times \mathbf{H}_2 &= \frac{(m^2 + n_2^2)\hat{e}_x - lm\hat{e}_y - ln_2\hat{e}_z}{n_{22}(m^2 + n_2^2)^{1/2}} |\mathbf{D}_2| \\ &= \varepsilon_x E_{2x}\hat{e}_x + \varepsilon_z E_{2y}\hat{e}_y + \varepsilon_z E_{2z}\hat{e}_z \end{aligned} \quad (4.25)$$

where  $n_{22} = l^2 + m^2 + n_2^2$ . At the interface between the two media, the tangential components of **E** and **H** must be continuous. Equations 4.27 to 4.30 state the continuity of  $E_x$ ,  $E_y$ ,  $H_x$ , and  $H_y$ , respectively. These have been divided by  $E_{\text{inc}}$  and the ratio  $E_{\text{ref}}/E_{\text{inc}}$  has been replaced by  $R$ . The following substitutions have also been made.

$$\cos \beta = \frac{n}{n_A}; \quad \cos \phi = \frac{l}{(l^2 + m^2)^{1/2}}; \quad \sin \phi = \frac{m}{(l^2 + m^2)^{1/2}} \quad (4.26)$$

$$-\cos \beta \cos \phi + (\cos \beta \cos \phi \cos \gamma + \sin \phi \sin \gamma)R = \frac{D_2}{E_{\text{inc}}\varepsilon_x n_{22}} (m^2 + n_2^2)^{1/2} \quad (4.27)$$

$$\begin{aligned} -\cos \beta \sin \phi + (\cos \beta \sin \phi \cos \gamma - \cos \phi \sin \gamma)R &= \frac{E_1}{E_{\text{inc}}} \frac{n_1}{(m^2 + n_1^2)^{1/2}} \\ &\quad - \frac{D_2}{E_{\text{inc}}\varepsilon_z n_{22}} \frac{lm}{(m^2 + n_2^2)^{1/2}} \end{aligned} \quad (4.28)$$

$$n_A \sin \phi - n_A(\cos \beta \cos \phi \sin \gamma - \sin \phi \cos \gamma)R = -\frac{E_1}{E_{\text{inc}}} (m^2 + n_1^2)^{1/2} \quad (4.29)$$

$$\begin{aligned} -n_A \cos \phi - n_A(\cos \beta \sin \phi \sin \gamma + \cos \phi \cos \gamma)R \\ = \frac{E_1}{E_{\text{inc}}} \frac{lm}{(m^2 + n_1^2)^{1/2}} + \frac{D_2}{E_{\text{inc}}n_{22}} \frac{n_2}{(m^2 + n_2^2)^{1/2}} \end{aligned} \quad (4.30)$$

This set of four equations can be solved for the four unknowns,  $R$ ,  $E_1/E_{\text{inc}}$ ,  $D_2/E_{\text{inc}}$ , and  $\gamma$ , by first eliminating the right-hand sides to yield two equations in  $R$  and  $\gamma$ , and then solving these. In doing so, the following relations are helpful.

$$\begin{aligned} m^2 + n_1^2 &= \varepsilon_z - l^2 \\ m^2 + n_2^2 &= \frac{\varepsilon_x}{\varepsilon_z} (m^2 + n^2) \end{aligned} \quad (4.31)$$

The solution for  $\gamma$  is given by

$$\begin{aligned} \tan \gamma = \\ \frac{-2\varepsilon_z l m n_A n_1 (n_1 - n_2) \cos \beta}{\cos^2 \beta \cdot \varepsilon_z n_A (l^2 n_1 n_2 + \varepsilon_z m^2) + \cos \beta (l^2 n_1^2 + m^2 \varepsilon_z)(\varepsilon_z n_2 - n_A^2 n_1) - n_A n_1 (l^2 n_1^2 + \varepsilon_z m^2 n_2)} \end{aligned} \quad (4.32)$$

and it is seen that  $\gamma$  is zero when  $n_1 = n_2$  (i.e.,  $E_x = E_z$ ) or when the plane of incidence includes the unique axis ( $l = \text{zero}$ ) or else is perpendicular to it ( $m = \text{zero}$ ). The solution for  $R$  is given by

$$R = (1 + \tan^2 \gamma)^{1/2} \frac{\epsilon_z n_2 \cos \beta - n_A n_1^2}{(m/l) \epsilon_z \tan \gamma (n_2 + n_A \cos \beta) + \epsilon_z n_2 \cos \beta + n_A n_1^2} \quad (4.33)$$

We are interested only in the energy-transfer region and therefore in the limiting forms taken by these equations when  $d$  approaches zero. We let  $x \equiv \tau d$  where  $\tau$  is  $\sin \beta$  and let  $d$  go monotonically to zero, and we find

$$\begin{aligned} n_1 &= -\frac{1}{d} (\epsilon_z d^2 - n_A^2 \tau^2 d^2)^{1/2} \rightarrow -i \frac{x}{d} n_A \\ l &= n_A \cos \phi \sin \beta \rightarrow n_A \cos \phi \frac{x}{d} \\ m &= n_A \sin \phi \sin \beta \rightarrow n_A \sin \phi \frac{x}{d} \\ \cos \beta &= \frac{1}{d} (d^2 - \tau^2 d^2)^{1/2} \rightarrow -\frac{ix}{d} \\ n_2 &= -\frac{1}{d} \left( \epsilon_x d^2 - \frac{\epsilon_x}{\epsilon_z} n_A^2 \tau^2 d^2 \cos^2 \phi - n_A^2 \tau^2 d^2 \sin^2 \phi \right)^{1/2} \rightarrow \\ &\quad -in_A \frac{x}{d} \left( \frac{\epsilon_x}{\epsilon_z} \cos^2 \phi + \sin^2 \phi \right)^{1/2} \end{aligned} \quad (4.34)$$

We note first in (4.32) that the numerator will contain the term  $(x/d)^5$ , while the denominator will contain  $(x/d)^6$ . In the limit of vanishing  $d$  this quotient will vanish, or  $\tan \gamma$  will approach zero. In this limit the reflected electric field will lie in the plane of incidence and we may replace  $R$  with  $-R_{d \rightarrow 0}^{\parallel}$ ,

$$-R_{d \rightarrow 0}^{\parallel} = \frac{\epsilon_z \{1 + [(\epsilon_x - \epsilon_z)/\epsilon_z] \cos^2 \phi\}^{1/2} - n_A^2}{\epsilon_z \{1 + [(\epsilon_x - \epsilon_z)/\epsilon_z] \cos^2 \phi\}^{1/2} + n_A^2} \quad (4.35)$$

Note that in the case of an isotropic absorber, where  $\epsilon_z = \epsilon_x$ , the expression for  $R^{\parallel}$  reduces to the proper form.

We treat the calculation of  $R^{\perp}$  briefly, since it makes no contribution to the energy-transfer limit of a dipole emitter. The incident electric vector is now s polarized and can be written as

$$\mathbf{E}_{\text{inc}} = \frac{m \hat{e}_x - l \hat{e}_y}{(m^2 + l^2)^{1/2}} |\mathbf{E}_{\text{inc}}| \quad (4.36)$$

while the incident magnetic vector is now

$$\mathbf{H}_{\text{inc}} = \frac{\ln \hat{e}_x + mn\hat{e}_y - (l^2 + m^2)\hat{e}_z}{(l^2 + m^2)^{1/2}} |\mathbf{E}_{\text{inc}}| \quad (4.37)$$

We let  $\gamma$  be the angle of rotation around the reflected ray of the vector  $E_{\text{ref}}$  from its original s polarization.

Then

$$\mathbf{E}_{\text{ref}} = \frac{|\mathbf{E}_{\text{ref}}|}{(l^2 + m^2)^{1/2}} \left[ \cos \delta (m\hat{e}_x - l\hat{e}_y) + \frac{\sin \delta}{n_A} (\ln \hat{e}_x + mn\hat{e}_y + (l^2 + m^2)\hat{e}_z) \right] \quad (4.38)$$

$$\mathbf{H}_{\text{ref}} = \frac{|\mathbf{E}_{\text{ref}}|}{(l^2 + m^2)^{1/2}} \{ n_A \sin \delta (m\hat{e}_x - l\hat{e}_y) - \cos \delta [\ln \hat{e}_x + mn\hat{e}_y + (l^2 + m^2)\hat{e}_z] \} \quad (4.39)$$

Matching boundary conditions using the substitutions of (4.26) and dividing by  $E_{\text{inc}}$  and calling  $R_1$  the ratio of  $E_{\text{ref}}$  to  $E_{\text{inc}}$ , we find

$$\sin \phi + R_1 (\sin \phi \cos \delta + \cos \phi \cos \beta \sin \delta) = \frac{D_2}{E_{\text{inc}} \epsilon_x n_{22}} (m^2 + n_2^2)^{1/2} \quad (4.40)$$

$$\begin{aligned} -\cos \phi - R_1 (\cos \phi \cos \delta - \sin \phi \cos \beta \sin \delta) \\ = \frac{E_1}{E_{\text{inc}}} \frac{n_1}{(m^2 + n_1^2)^{1/2}} - \frac{D_2}{E_{\text{inc}} \epsilon_z n_{22}} \frac{lm}{(m^2 + n_2^2)^{1/2}} \end{aligned} \quad (4.41)$$

$$n_A \cos \phi \cos \beta + n_A (\sin \phi \sin \delta - \cos \phi \cos \beta \cos \delta) R_1 = -\frac{E_1}{E_{\text{inc}}} (m^2 + n_1^2)^{1/2} \quad (4.42)$$

$$\begin{aligned} n_A \sin \phi \cos \beta - n_A (\cos \phi \sin \delta + \sin \phi \cos \beta \cos \delta) R_1 \\ = \frac{E_1}{E_{\text{inc}}} \frac{lm}{(m^2 + n_1^2)^{1/2}} + \frac{D_2}{E_{\text{inc}} n_{22}} \frac{n_2}{(m^2 + n_2^2)^{1/2}} \end{aligned} \quad (4.43)$$

On solving we find that  $\tan \delta$  is found from  $\tan \gamma$  [see (4.32)] by changing  $\cos \beta$  to  $-\cos \beta$  and that

$$R_1 = (1 + \tan^2 \delta) \frac{-n_1 n_A \cos \beta + n_1^2}{(m/l) \tan \delta (\epsilon_z \cos \beta + n_1 n_A) - (n_1^2 + n_1 n_A \cos \beta)} \quad (4.44)$$

In the energy-transfer limit the set of equations (4.34) may be employed. It is found that  $\tan \delta$  approaches zero and that  $R_1$  becomes  $R_{(d \rightarrow 0)}^1$ ; however, this quantity approaches zero as in the isotropic case and makes no contribution to energy transfer.

We may now consider energy transfer to the anisotropic absorber from an electric dipole emitter in each of its three orientations. We must determine the weighted average (over  $\phi$ ) of the reflectivity in the short-distance limit,  $R_{(d \rightarrow 0)}^{\parallel}$ , to be used in the following relation for decay rate of the dipole emitter [see (2.52)]

$$\hat{b}_{ET} = \frac{-3q}{8d_1^3} \text{Im} \{R_{(d \rightarrow 0)}^{\parallel}\} \quad (4.45)$$

The weighting factor is proportional to the dependence of the square of the p-polarized electric field on the azimuthal angle  $\phi$ . For a dipole-emitter parallel to the  $x$  direction (unique axis) the p-polarized electric field  $E^{\parallel}$  is proportional to  $\cos \phi$ , the weighting factor is  $\cos^2 \phi$  and the average is taken over the range of  $\phi$ , which is  $2\pi$ .

When the dipole emitter is oriented parallel to the  $y$ -axis instead, the weighting factor becomes  $\sin^2 \phi$ ; and when the dipole is parallel to the  $z$ -axis, by symmetry the weighting factor is unity. Finally, an ensemble of randomly oriented dipoles behaves like an equal mixture of all three orientations with a weighting factor equal to one-third their sum, or  $\frac{2}{3}$ . Table VI shows a summary of weighting factors, designated  $A$  which are used in the expression to calculate the reflectivity for the dipole field,

$$R_{(d \rightarrow 0)}^{\parallel} = \frac{-1}{2\pi} \int_0^{2\pi} \frac{\epsilon_z \{1 + [(\epsilon_x - \epsilon_z)/\epsilon_z] \cos^2 \phi\}^{1/2} - \epsilon_1}{\epsilon_z \{1 + [(\epsilon_x - \epsilon_z)/\epsilon_z] \cos^2 \phi\}^{1/2} + \epsilon_1} A d\phi \quad (4.46)$$

where we have written  $\epsilon_1$  for  $n_A^2$ .

*Limiting Case of Small Absorption.* Equation 4.46 takes a simple form when the absorber consists of a low concentration of molecules whose transition dipole moments point in the  $x$  direction. The molecules are embedded in a medium of the same dielectric function as that containing the emitter. We have the case that  $\epsilon_z$  is  $n_A^2$  and  $\epsilon_x$  is  $(n_A + i\kappa_x)^2$ , which is approximately

TABLE VI  
Parameters for Anisotropic Media (4.46)

Dipole orientation	A	$\theta$
$x$	$\cos^2 \phi$	$(\frac{9}{128})$
$y$	$\sin^2 \phi$	$(\frac{3}{128})$
$z$	1	$(\frac{3}{32})$
Isotropic	$\frac{2}{3}$	$(\frac{1}{16})$



$n_A^2 + 2in_A\kappa_x$ , since  $\kappa_x$  is small. The integrand of (4.46) becomes (where  $\varepsilon_1$  is  $n_A^2$ )

$$\frac{\varepsilon_z \{1 + [(\varepsilon_x - \varepsilon_z)/\varepsilon_z] \cos^2 \phi\}^{1/2} - \varepsilon_1}{\varepsilon_z \{1 + [(\varepsilon_x - \varepsilon_z)/\varepsilon_z] \sin^2 \phi\}^{1/2} + \varepsilon_1} \rightarrow \frac{i\kappa_x}{2n_A} \cos^2 \phi \quad (4.47)$$

Upon inserting the weighting factors  $A$  from Table VI and doing the integration, we obtain for  $b_{ET}$

$$b_{ET} = \frac{\theta_q \kappa_x}{d_1^3 n_A} \quad (4.48)$$

where the geometrical factor  $\theta$  is given in Table VI.

The rate of energy transfer is seen to increase with increasing  $\kappa_x$ . As in the case of an isotropic absorber this is only for the weak absorption case and does not hold for large values of  $\kappa_x$ . Here also it is to be noted that the condition is *not* met by merely considering a thin film of absorber. On the contrary, the film thickness must be much larger than  $d_1$  for this formula to be valid.

Resonant coupling to the surface plasmons is predicted by (4.46) if both  $\varepsilon_x$  and  $\varepsilon_z$  are negative. In addition, such coupling is present when the absorber is a two-dimensional conductor in the plane perpendicular to the unique axis and an insulator along the unique axis ( $\varepsilon_x > 0$  and real and  $\varepsilon_y = \varepsilon_z$  complex with a negative real part). To see that a surface-plasmon resonance occurs in  $R_{(d \rightarrow 0)}^{\parallel}$ , note that if  $\varepsilon_z = -\varepsilon_1$  (the surface-plasmon-frequency condition), then

$$\begin{aligned} R_{(d \rightarrow 0)}^{\parallel} &= -\frac{1}{\pi} \int_0^{\pi} d\phi A \left\{ 1 + \frac{2}{\{1 + [(\varepsilon_x + \varepsilon_1)/\varepsilon_1] \cos^2 \phi\}^{1/2} - 1} \right\} \\ &= -\frac{1}{\pi} \int_0^{\pi} d\phi A \left\{ 1 + \frac{2 + 2[1 + [(\varepsilon_x + \varepsilon_1)/\varepsilon_1] \cos^2 \phi]^{1/2}}{[(\varepsilon_x + \varepsilon_1)/\varepsilon_1] \cos^2 \phi} \right\} \end{aligned} \quad (4.49)$$

Therefore, if  $A \neq \cos^2 \phi$  there will be a pole in the integrand at  $\phi = \pi/2$ . To determine the behavior of  $R_{(d \rightarrow 0)}^{\parallel}$  near the surface plasmon frequency, we examine the case  $\varepsilon_z = -\varepsilon_1 + i\varepsilon_z^{\parallel}$  where  $\varepsilon_z^{\parallel}$  is the small (compared to  $\varepsilon_1$ ) absorptive part of  $\varepsilon_z$ . Then expanding the denominator of (4.46) about  $\phi = \pi/2$  and keeping quadratic terms only, we find

$$\begin{aligned} \text{Im } R_{(d \rightarrow 0)}^{\parallel} &\doteq -\frac{1}{\pi} \int_{-\infty}^{+\infty} \frac{(-2\varepsilon_1) d\theta}{(i\varepsilon_z^{\parallel}) + \frac{1}{2}(\varepsilon_x + \varepsilon_1 - i\varepsilon_z^{\parallel})^{1/2} \theta^2} \\ &= \frac{-2\varepsilon_1}{|\varepsilon_z + \varepsilon_1|^{1/2} [(\varepsilon_x + \varepsilon_1)/2]^{1/2}} \end{aligned} \quad (4.50)$$

In the case of an isotropic absorber near the surface-plasmon frequency we

find that

$$\text{Im } R_{(d \rightarrow 0)}^{\parallel} = \frac{-2\varepsilon_1}{|\varepsilon_z + \varepsilon_1|} \quad (4.51)$$

It can be noted by inspection of (4.46) and Table VI that this coupling is absent when the emitter dipole lies along the  $x$ -axis (parallel to the unique axis) as a result of a term in  $\sin^2 \theta (= \cos^2 \phi)$  in the numerator of the integrand. The coupling is restored when the dipole lies along the  $y$ -axis (perpendicular to the unique axis) owing to the term  $\cos^2 \theta$  (which is essentially unity) in the numerator of the integrand. Furthermore, in this approximation the coupling is the same as that for the dipole along the  $z$ -axis (which is also perpendicular to the unique axis).

b. Case b. Unique axis perpendicular to surface plane. The dielectric tensor of the absorber has the form

$$\varepsilon_2 = \begin{pmatrix} \varepsilon_x & 0 & 0 \\ 0 & \varepsilon_x & 0 \\ 0 & 0 & \varepsilon_z \end{pmatrix} \quad (4.52)$$

We consider only  $p$ -polarized radiation since we are concerned with the energy-transfer limit. From symmetry considerations it is clear that both the reflected electric field and the ray direction will lie in the plane of incidence. The incident and reflected fields are the same as in (4.15) to (4.18), except that the angle  $\gamma$  is zero here. The two transmitted waves are now characterized by vanishing  $\mathbf{E}_z$  or  $\mathbf{H}_z$ . In the first case

$$\mathbf{E}_1 = \frac{m\hat{e}_x - l\hat{e}_y}{(m^2 + l^2)^{1/2}} |\mathbf{E}_1| \quad (4.53)$$

and

$$\mathbf{H}_1 = \frac{l n_1 \hat{e}_x + m n \hat{e}_y - (l^2 + m^2) \hat{e}_z}{(l^2 + m^2)^{1/2}} |\mathbf{E}_1| \quad (4.54)$$

where  $l$ ,  $m$ , and  $n$  are related by (4.19).

In the second case

$$\mathbf{D}_2 = \frac{-l n_2 \hat{e}_x + m n_2 \hat{e}_y - (l^2 + m^2) \hat{e}_z}{(l^2 + m^2)^{1/2}} |\mathbf{H}_2| = \varepsilon_x E_{2x} \hat{e}_x + \varepsilon_x E_{2y} \hat{e}_y + \varepsilon_z E_{2z} \hat{e}_z \quad (4.55)$$

and

$$|\mathbf{H}_2| = \frac{m\hat{e}_x - l\hat{e}_y}{(l^2 + m^2)^{1/2}} |\mathbf{H}_2| \quad (4.56)$$

where  $l$ ,  $m$ , and  $n_2$  are related by

$$n_2 = \left( \frac{\varepsilon_x}{\varepsilon_z} \right)^{1/2} (\varepsilon_z - l^2 - m^2)^{1/2} \quad (4.57)$$

The boundary conditions, that is, matching of tangential components of  $\mathbf{E}$  and  $\mathbf{H}$ , yield a set of equations that are solved to yield

$$R^{\parallel} = \frac{\varepsilon_x \cos \beta - n_A n_2}{\varepsilon_x \cos \beta + n_A n_2} \quad (4.58)$$

In the limiting case as  $d$  approaches zero we have

$$\cos \beta \rightarrow -\frac{ix}{d} \quad n_2 \rightarrow -\left(\frac{\varepsilon_x}{\varepsilon_z}\right)^{1/2} in_A \frac{x}{d} \quad (4.59)$$

and

$$R^{\parallel} = \frac{(\varepsilon_x \varepsilon_z)^{1/2} - \varepsilon_1}{(\varepsilon_x \varepsilon_z)^{1/2} + \varepsilon_1} \quad (4.60)$$

It is evident that when  $\varepsilon_x = \varepsilon_z$  we return to the isotropic case, and  $R^{\parallel}$  reduces to the corresponding limiting form.

The expression for decay rate of a dipole emitter oriented along the  $z$ -axis at a distance  $d$  from the interface follows directly from (4.45), namely,

$$\hat{b}_{ET} = \frac{3}{8} \frac{q}{d_1^3} \operatorname{Im} \left[ \frac{(\varepsilon_x \varepsilon_z)^{1/2} - \varepsilon_1}{(\varepsilon_x \varepsilon_z)^{1/2} + \varepsilon_1} \right] \quad (4.61)$$

Because of symmetry no averaging over  $\phi$  is required. We can write (4.61) as

$$\hat{b}_{ET} = \frac{\theta q}{2d_1^3} \frac{\varepsilon_1 \operatorname{Im} (\varepsilon_x \varepsilon_z)^{1/2}}{[(\varepsilon_x \varepsilon_z)^{1/2} + \varepsilon_1]^2} = \frac{\theta q}{2d_1^3} \frac{\varepsilon_1 (n_x \kappa_z + n_z \kappa_x)}{[(\varepsilon_x \varepsilon_z)^{1/2} + \varepsilon_1]^2} \quad (4.62)$$

where  $\theta$  has the value  $\frac{3}{2}$ ,  $\frac{3}{4}$ , or 1 for emitter dipoles oriented along  $z$ , in the  $xy$ -plane, or isotropically. The pair of terms in the numerator reduces to  $n_z \kappa_x$  for the two-dimensional conductor case, that is, when  $\varepsilon_x$  and  $\varepsilon_y$  are equal and complex and when  $\varepsilon_z$  is real. For the one-dimensional conductor case, that is, where  $\varepsilon_z$  is complex and  $\varepsilon_x$  and  $\varepsilon_y$  are equal and real, the pair of terms reduces to  $n_x \kappa_z$ . The reader should note for either case where the numerator contains only one term, the absorber transition moments are either in the  $xy$ -plane or along the  $z$ -axis, and the expression for energy transfer is reduced by a factor of 2 relative to the isotropic case where all three components of  $\varepsilon$  are equal and complex. This will occur for electric quadrupole emitters in any orientation also, because  $R^{\parallel}$  describes the interaction of their  $p$ -polarized radiation with the interface.

Resonant surface-plasmon coupling is seen to be possible from (4.61). Like an isotropic absorber in the energy-transfer ( $d_1 \rightarrow 0$ ) limit, the denominator of (4.61) can become very small in a certain frequency range. However, it is necessary that both  $\varepsilon_x$  and  $\varepsilon_z$  lie almost along the negative real axis, that is, that the medium be highly absorbing (conducting) along all three principal directions. In this case the behavior is that of an isotropic medium

whose dielectric function is the geometric mean of  $\epsilon_x$  and  $\epsilon_z$ . If the medium behaves as a one- or two-dimensional conductor, then the denominator of (4.61) cannot be made small and surface-plasmon coupling is precluded.

It was found above that there is a surface-plasmon resonance in  $b_{ET}$  for small  $d$  in the case of some anisotropies in  $\epsilon_2$  and dipole orientations. However, the conditions for a surface plasmon resonance in the case of two principal components of  $\epsilon$  negative and one positive are (1)  $\epsilon_x > 0$  and  $\epsilon_y, \epsilon_z < 0$ , and (2) the dipole not parallel to  $x$ . Thus only if the conductivity plane is perpendicular to the surface is there a surface-plasmon resonance. (Of course, if all three components of  $\epsilon_2$  are negative, there is always a resonance.)

The explanation for this behavior can be found in the discussion of surface polaritons (or plasmons) in anisotropic media by Kliever and Fuchs.<sup>48</sup> In this work it is shown that for a cylindrically symmetric  $\epsilon_2$  there are surface-plasmon modes of frequency  $\omega$  and surface wavevector  $\mathbf{k}$ , for the following cases (excluding the trivial case  $\epsilon_x, \epsilon_y, \epsilon_z < 0$ ):

Case 1

$$\epsilon_z < 0; \quad \epsilon_x = \epsilon_y > 0$$

only for  $\epsilon_1(\omega/c)^2 < k^2 < \epsilon_x(\omega/c)^2$ .

Case 2

$$\epsilon_y = \epsilon_z < -\epsilon_1; \quad \epsilon_x > 0$$

and  $\mathbf{k} \perp \hat{x}$ .

Case 3

$$\epsilon_y = \epsilon_z > 0; \quad \epsilon_x < 0$$

and  $\mathbf{k} \parallel \hat{x}$  and only for  $\epsilon_1(\omega/c)^2 < k^2 < \epsilon_z(\omega/c)^2$ .

Thus in the  $c \rightarrow \infty$  limit, which will correspond to  $\omega d/c \rightarrow 0$  (or  $d \rightarrow 0$ ), only in case 2 will surface-plasmon modes exist. This corresponds to the conditions derived above for surface-plasmon resonances in  $b_{ET}$  from (4.46) and (4.62).

## 2. Dipole Embedded in Anisotropic Nonabsorbing Medium

In the experiments<sup>1-9</sup> that have measured dipole emitter lifetime, non-absorbing fatty-acid monolayers have been employed as spacers. The optical properties of these layers have been described in detail.<sup>1-4</sup> One of the most frequently used, a CdC<sub>20</sub> layer, has an ordinary and extraordinary refractive index given by  $n_x = 1.52$  and  $n_z = 1.59$ . The effect of this anisotropy on the angular dependence of fluorescence emission has been discussed by Drexhage, who only needed to consider the radiation zone of the emitter in his calculation. In this section we present a calculation valid for all distances of the

emitter dipole from the absorber interface, though we are primarily interested in the energy-transfer region and the effect on surface-plasmon coupling.

The approach to this problem is through the plane-wave-spectrum method,<sup>55</sup> whereby the Hertzian vectors can be immediately written, and the form taken by the boundary conditions can be easily derived following the same approach that is employed in the isotropic case.

a. Dipole parallel to anisotropic axis (perpendicular to interface)

We begin with this simpler problem of a perpendicular dipole at a distance  $z$  above the interface with a medium of dielectric function  $\epsilon_z$ . The medium containing the dipole has the dielectric tensor

$$\underline{\epsilon}_1 = \begin{pmatrix} \epsilon_x & 0 & 0 \\ 0 & \epsilon_x & 0 \\ 0 & 0 & \epsilon_z \end{pmatrix} \quad (4.63)$$

The components of  $n_1 \hat{S}$ , where  $\hat{S}$  is a unit wavefront vector belonging to the plane wave spectrum, are  $l$ ,  $m$ , and  $n$ . The latter satisfy a relation similar to (4.23), where in the present case  $H_z$  is zero,

$$\frac{l^2}{\epsilon_z} + \frac{m^2}{\epsilon_z} + \frac{n^2}{\epsilon_x} = 1 \quad (4.64)$$

Then, following Clemmow we may write for the dipole in the absence of the interface

$$\Pi_z = \frac{\mu_0 k_0}{2\pi i} \int_{-\infty}^{+\infty} \int_{-\infty}^{+\infty} \exp \{ ik_0 [lx + my + n(z - z_0)] \} \frac{dl \, dm}{n} \quad (4.65)$$

A standard type of substitution is now used<sup>25,55,56</sup> to find

$$\Pi_z = \frac{\mu_0 k_0}{i} \int_0^\infty J_0(k_0 r \epsilon_z^{1/2} u) \frac{\epsilon_z}{\epsilon_x^{1/2}} \frac{\exp ik_0(z_0 - z)\epsilon_x^{1/2}(1 - u^2)^{1/2}}{(1 - u^2)^{1/2}} u \, du \quad (4.66)$$

where  $J_0$  is a Bessel function. We note in passing that (4.66) can be integrated at once to yield

$$\Pi_z = \mu_0 \left( \frac{\epsilon_z}{\epsilon_x} \right) \frac{\exp \{ ik_0 [\epsilon_z(x^2 + y^2) + \epsilon_x(z_0 - z)^2]^{1/2} \}}{[\epsilon_z(x^2 + y^2) + \epsilon_x(z - z_0)^2]^{1/2}} \quad (4.67)$$

which in the isotropic case ( $\epsilon_x = \epsilon_z = \epsilon$ ) gives the proper result,

$$\Pi_z = \mu_0 \frac{e^{ik_1 R}}{R} \quad (4.68)$$

where  $k_1$  is  $\epsilon^{1/2} k_0$ , and  $R$  is  $[x^2 + y^2 + (z_0 - z)^2]^{1/2}$ .

We can now write the appropriate Hertz vector for the present purposes,

namely, we include the reflected field and omit the primary source,  $0 \leq z \leq z_0$

$$\Pi_z^{\text{ref}} = -\mu_0 k_0 \int_0^\infty J_0(k_0 r \varepsilon_z^{1/2} u) R^{\parallel}(u) \frac{\varepsilon_z}{\varepsilon_x^{1/2}} \frac{\exp \{ik_0(1-u^2)^{1/2} \varepsilon_x^{1/2}(z+z_0)\}}{i(1-u^2)^{1/2}} \quad (4.69)$$

The reflectivity  $R^{\parallel}(u)$  is determined by matching the boundary conditions that, at  $z=0$ ,  $H_x$  and  $E_x$  are continuous across the boundary. This leads to

$$R^{\parallel} = \frac{-\varepsilon_2 \cos \beta + \varepsilon_x [(\varepsilon_2/\varepsilon_1) - \sin^2 \beta]^{1/2}}{\varepsilon_2 \cos \beta + \varepsilon_x [(\varepsilon_2/\varepsilon_1) - \sin^2 \beta]^{1/2}} \quad (4.70)$$

where

$$\cos \beta = \left(\frac{\varepsilon_x}{\varepsilon_1}\right)^{1/2} (1-u^2)^{1/2}; \quad \sin \beta = \left(\frac{\varepsilon_z}{\varepsilon_1}\right)^{1/2} u \quad (4.71)$$

so that (4.70) may be written as

$$R^{\parallel} = \frac{-\varepsilon_2(1-u^2)^{1/2} + (\varepsilon_x \varepsilon_z)^{1/2} (\varepsilon_2/\varepsilon_z - u^2)^{1/2}}{\varepsilon_2(1-u^2)^{1/2} + (\varepsilon_x \varepsilon_z)^{1/2} (\varepsilon_2/\varepsilon_z - u^2)^{1/2}} \quad (4.72)$$

We may now return to (4.69), finish the calculation in the same manner as for the isotropic case, and evaluate the field at the dipole position. We further use the result that the radiative lifetime (see Appendix)  $b_r^{\perp}$  is

$$b_r^{\perp} = \frac{2\omega^2 e^2 \varepsilon_z^{1/2}}{3c^3 m} \quad (4.73)$$

The normalized emitter lifetime can be written as

$$\hat{b}_1 = 1 + \frac{3qc^3}{2\omega^3 \varepsilon_z^{1/2}} \text{Im} \left( \frac{E_{\text{ref}}}{\mu_0} \right). \quad (4.74)$$

Substitution for the reflected field at the dipole position gives

$$\frac{E_{\text{ref}}}{\mu_0} = -k_0^3 \frac{\varepsilon_z}{\varepsilon_x^{1/2}} \int_0^\infty du \frac{u^3 R^{\parallel}}{-i(1-u^2)^{1/2}} \exp \{i\varepsilon_x^{1/2} k_0 2z_0(1-u^2)^{1/2}\} \quad (4.75)$$

As in the isotropic case, the following definitions are introduced:

$$l_1 \equiv -i(1-u^2)^{1/2}, \quad l_2^{\parallel} \equiv -i(\varepsilon_2/\varepsilon_z - u^2)^{1/2}, \quad \hat{d}_0 \equiv k_0 z_0 \quad (4.76)$$

which leads to the result that

$$b^{\perp} = 1 - \frac{3}{2} q \left(\frac{\varepsilon_z}{\varepsilon_x}\right)^{1/2} \text{Im} \int_0^\infty R^{\parallel} \exp \{-2l_1 \varepsilon_x^{1/2} \hat{d}_0\} \frac{u_3 du}{l_1} \quad (4.77)$$

with

$$R^{\parallel} = \frac{-\varepsilon_2 l_1 + (\varepsilon_x \varepsilon_z)^{1/2} l_2^{\parallel}}{\varepsilon_2 l_1 + (\varepsilon_x \varepsilon_z)^{1/2} l_2^{\parallel}} \quad (4.77)$$

Equation 4.77 differs from the corresponding equation for the isotropic case in two aspects; first the distance scale factor is determined by  $\varepsilon_x^{1/2}$ , the refractive index perpendicular to the anisotropic axis, and second, the effect of quantum yield  $q$  is enhanced by the factor  $(\varepsilon_z/\varepsilon_x)^{1/2}$ , which is around 5% in the case of a CdC<sub>20</sub> fatty acid.

The energy-transfer region is described as in the isotropic case by taking the limit as  $d$  approaches zero. The main result is that  $R^{\parallel}$  approaches the limit

$$R_{(d \rightarrow 0)}^{\parallel} = \frac{-\varepsilon_2 + (\varepsilon_x \varepsilon_z)^{1/2}}{\varepsilon_2 + (\varepsilon_x \varepsilon_z)^{1/2}} \quad (4.79)$$

which is the same as would be produced if the medium were isotropic with dielectric function equal to the geometric mean of  $\varepsilon_x$  and  $\varepsilon_z$ . The complete expression is

$$\hat{b}_{ET} = \frac{3q}{2\hat{d}_1^3} \frac{\varepsilon_z n_2 \kappa_2}{|\varepsilon_2 + (\varepsilon_x \varepsilon_z)^{1/2}|^2} \quad (4.80)$$

where  $\hat{d}_1$  is  $\varepsilon_x^{1/2} \hat{d}_0$ . Surface-plasmon coupling is then expected on the same basis as for isotropic media.

#### b. Dipole Perpendicular to Anisotropic Axis (Parallel to Interface).

For this orientation of the dipole  $\mathbf{H}_z$  is different from zero and we must consider the two kinds of waves that propagate in this medium. The procedure of Clemmow<sup>55</sup> is well suited for this problem and requires introducing two different Hertz vectors.

Following Clemmow<sup>55</sup> we write

$$\tilde{\mathbf{H}} = \tilde{\mathbf{H}}_1 + \tilde{\mathbf{H}}_2 \quad (4.81)$$

where

$$\tilde{\mathbf{H}}_1 = \text{curl curl } \tilde{\mathbf{M}} \quad \tilde{\mathbf{H}}_2 = ik_0 \text{ curl } \tilde{\mathbf{\Pi}} \quad (4.82)$$

with  $\mathbf{M}$  and  $\mathbf{\Pi}$  being vectors along the  $z$ -axis that are given by

$$M = -\mu_0 \int_{-\infty}^{+\infty} \int_{-\infty}^{+\infty} \frac{m}{n_1(l^2 + m^2)} \exp \{ik_0[lx + my + n(z - z_0)]\} dl dm \quad (4.83)$$

$$\Pi = \mu_0 \int_{-\infty}^{+\infty} \int_{-\infty}^{+\infty} \frac{l}{l^2 + m^2} \exp \{ik_0[lx + my + n(z - z_0)]\} dl dm$$

where

$$l^2 + m^2 + n_1^2 = \epsilon_x \quad (4.84)$$

and

$$\frac{l^2}{\epsilon_z} + \frac{m^2}{\epsilon_z} + \frac{n_2^2}{\epsilon_x} = 1 \quad (4.85)$$

By making use of the boundary conditions on the electric and magnetic fields, we derive an equation for the reflected electric field at the dipole position in terms of the reflection coefficients,  $R^{\parallel}$  and  $R^{\perp}$  where

$$R^{\perp} = \frac{l_1 - l_2^{\perp}}{l_1 + l_2^{\perp}} \quad (4.86)$$

and

$$R^{\parallel} = \frac{\epsilon_2 l_1 - (\epsilon_x \epsilon_z)^{1/2} l_2^{\parallel}}{\epsilon_2 l_1 + (\epsilon_x \epsilon_z)^{1/2} l_2^{\parallel}} \quad (4.87)$$

where  $l_1$  is given by (4.76) above and in this case

$$l_2^{\perp} = -i \left( \frac{\epsilon_2}{\epsilon_x} - u^2 \right)^{1/2} \quad (4.88)$$

$$l_2^{\parallel} = -i \left( \frac{\epsilon_2}{\epsilon_z} - u^2 \right)^{1/2} \quad (4.89)$$

and  $u$  is an integration variable. With these definitions the formula for the normalized radiative decay rate is found to be

$$\hat{b}^{\parallel} = 1 - q \left( \frac{3\epsilon_x}{3\epsilon_x + \epsilon_z} \right) \text{Im} \int_0^{\infty} \left[ -R^{\perp} + \frac{\epsilon_z}{\epsilon_x} R^{\parallel} (1 - u^2) \right] \exp \{ -2l_1 \epsilon_x^{1/2} \hat{d}_0 \} \frac{u du}{l_1} \quad (4.90)$$

where in the absence of the interface the decay rate is given by (see Appendix)

$$b_r^{\parallel} = \frac{2\omega^2 e^2}{3mc^3} \frac{3}{4} \epsilon_x^{1/2} \left( 1 + \frac{1}{3} \frac{\epsilon_z}{\epsilon_x} \right) \quad (4.91)$$

As is pointed out for the case of the vertical emitter, the distance scale factor is determined by  $\epsilon_x^{1/2}$ , and in comparison to the isotropic case the effect of quantum yield  $q$  is altered by the factor  $4\epsilon_x/(3\epsilon_x + \epsilon_z)$ . This amounts to about a 2% reduction for the CdC<sub>20</sub> fatty acid.

The energy-transfer result [the limit of (4.90) as  $d_0$  approaches zero] is

$$\hat{b}_{ET}^{\parallel} = \left( \frac{3}{3 + \epsilon_z/\epsilon_x} \right) \frac{q}{\hat{d}_1^3} \left( \frac{\epsilon_z}{\epsilon_x} \right)^{1/2} \frac{\epsilon_x n_2 \kappa_2}{|(\epsilon_z \epsilon_x)^{1/2} + \epsilon_2|^2} \quad (4.92)$$



Surface-plasmon coupling is expected here also, and for both dipole orientations the condition is the same, namely, that the sum  $\varepsilon_2 + (\varepsilon_x \varepsilon_z)^{1/2}$  approaches zero.

### 3. Appendix

For completeness, we append here some simple discussions for anisotropic media.

a. **Determination of Energy Flux for a Dipole Embedded in a Nonabsorbing Anisotropic (Uniaxial) Medium: Dipole Parallel to Anisotropic Axis.** We consider a dipole embedded in this medium very far removed from the interface. The Hertz vector is given by (4.65) and  $H$  and  $E$  are given as in Section II. We need to retain only the radiation fields, that is, those terms that depend on the first power of the inverse of the distance from the emitter. The power flux density is given by  $\frac{1}{2} \text{Re} [\tilde{\mathbf{E}} \times \tilde{\mathbf{H}}^*]$ , where the asterisk means complex conjugate. Owing to the symmetry of the problem the latter is given by  $\frac{1}{2} \text{Re} [E_\theta H_\phi^*]$ , where  $\theta$  and  $\phi$  are the polar and azimuthal angles, respectively. Integration over a large sphere surrounding the dipole yields the total rate of energy flux  $P$ .

$$P = \text{const } \varepsilon_x \varepsilon_z^2 \int_0^\pi \frac{\sin^3 \theta d\theta}{(\varepsilon_x \cos^2 \theta + \varepsilon_z \sin^2 \theta)^{5/2}} \quad (4.93)$$

where integration over  $\phi$  has been done. The constant is determined by the condition that for an isotropic medium ( $\varepsilon_x = \varepsilon_z \equiv \varepsilon$ )  $P$  is  $\frac{1}{3} \mu_0^2 \omega^4 / c^3 \varepsilon^{1/2}$ . The constant is, then,  $\frac{1}{4} \mu_0^2 \omega^4 / c^3$ . Thus we can write

$$P = \frac{\mu_0^2 \omega^4 \varepsilon_x \varepsilon_z^2}{4c^3} \int_0^\pi \frac{\sin^3 \theta d\theta}{(\varepsilon_x \cos^2 \theta + \varepsilon_z \sin^2 \theta)^{5/2}} \quad (4.94)$$

One way to evaluate the integral is to transform it by letting  $y = C \cos \theta$ , where  $C = (\varepsilon_z - \varepsilon_x) / \varepsilon_z$ . The integral  $I$  becomes

$$I = \frac{1}{C} \int_{-C}^{+C} \frac{dy}{(1-y^2)^{5/2}} - \frac{1}{C^3} \int_{-C}^{+C} \frac{y^2 dy}{(1-y^2)^{5/2}} \quad (4.95)$$

Then on substituting  $Z = y/(1-y^2)^{1/2}$

$$I = \frac{1}{C} \int (1+z^2) dz - \frac{1}{C^3} \int z^2 dz \quad (4.96)$$

The integrations are easily done, and on substituting in terms of the original variable,  $\theta$ , we find

$$I = \frac{4}{3} \frac{1}{\varepsilon_x \varepsilon_z^{3/2}} \quad (4.97)$$

Then the power can be written

$$P = \frac{1}{3} \mu_0^2 \frac{\omega^4}{c^3} \varepsilon_z^{1/2} \quad (4.98)$$

b. Radiative Lifetime. The dipole is considered to be a charge  $e$  of mass  $m$  oscillating harmonically with  $\mu_0$  equal to  $e x_{\max}$  where  $x_{\max}$  is the amplitude (instantaneous) of the motion. Power is radiated continuously and the dipole energy decreases asymptotically to zero with a characteristic lifetime. We calculate here the lifetime and the inverse, which is the radiative decay rate  $b_r$ .

At given time we can write for both the instantaneous energy  $\mathcal{E}$  and the radiated power  $P$  (equal to  $-d\mathcal{E}/dt$ )

$$\mathcal{E} = \frac{1}{2} k x_{\max}^2 = \frac{1}{2} \omega^2 m \left( \frac{\mu_0}{e} \right)^2 \quad (4.99)$$

$$P = -\frac{d\mathcal{E}}{dt} = \frac{1}{3} \mu_0^2 \frac{\omega^4}{c^3} \varepsilon_z^{1/2} \quad (4.100)$$

where  $\omega$  is the frequency of oscillation. On eliminating  $\mu_0$  between (4.99) and (4.100) we find

$$\frac{d\mathcal{E}}{\mathcal{E}} = -\frac{2}{3} \frac{\omega^2 e^2 \varepsilon_z^{1/2}}{m c^3} dt \quad (4.101)$$

which on integration from zero to  $t$  yields

$$\mathcal{E} = \mathcal{E}_0 e^{-t/\tau} \quad (4.102)$$

where

$$\tau^{-1} = b_r^{-1} = \frac{2\omega^2 e^2 \varepsilon_z^{1/2}}{3mc^3}$$

c. Rate of Energy Flux for a Dipole Moment in a Nonabsorbing Uniaxial Medium: Dipole Perpendicular to Anisotropic Axis. This is sketched briefly, since the calculation is much like that of Section a of this appendix. Clemmow<sup>55</sup> gives the expression for the component of  $\pi$ . We need retain only the few terms that describe the radiation field. Using the relation

$$\varepsilon \cdot \mathbf{E} = \text{curl } \mathbf{H} \quad (4.103)$$

we can readily write the components of  $\mathbf{E}$ . Then on using (4.93) for power emitted we find

$$P = \frac{\mu_0^2 \omega^4 \varepsilon_x^{1/2}}{8c^3} \left[ 2 + \varepsilon_x^{1/2} \varepsilon_z^2 \int_0^{2\pi} \frac{\cos^2 \theta \sin \theta d\theta}{(\varepsilon_z \sin^2 \theta + \varepsilon_x \cos^2 \theta)^{5/2}} \right] \quad (4.104)$$

Integration proceeds as in Section A with the substitutions as shown. On

writing power as  $-d\mathcal{E}/dt$  and expressing  $\mathcal{E}$  by (4.99) we find through the reasoning of (4.101) and (4.102) that lifetime is

$$\tau^{-1} \equiv b_r'' = \frac{2\omega^2 e^2}{3mc^3} \left[ \frac{3\epsilon_x^{1/2}}{4} \left( 1 + \frac{\epsilon_z}{3\epsilon_x} \right) \right] \quad (4.105)$$

where the term in brackets replaces the refractive index for the isotropic case.

## V. SUMMARY

The classical description of fluorescence and energy transfer from excited molecules to layered systems that is presented here has been shown to be in quantitative agreement with all the experiments to date on these systems. In addition, the results of a quantum-mechanical treatment of lifetime variations<sup>13,17,28,29</sup> are in complete agreement with the classical results. Our energy-transfer formulas are of general applicability to many experimental situations in photoconductivity and dye sensitization,<sup>38,39,57</sup> where an important limitation on efficiency is deactivation of the excited state by means of energy transfer to a metallic electrode.

The experiments of Drexhage et al.<sup>5-9</sup> have provided a thorough quantitative test of the theory. In these experiments the molecule/mirror separation varied from about 6000 to 50 Å. However, the surprising theoretical predictions in the short-distance (energy-transfer) region have not been experimentally tested as yet. Of particular importance is the resonant effect due to surface plasmon coupling in the emitter/silver system (Fig. 18). The experiment is complicated by the need to scan emission frequency; however, the effect is so dramatic that it could easily be revealed by a comparison to a metal (e.g., gold) where there is a weaker effect predicted. In addition, the thin-film enhancement effect (again due to surface plasmon coupling) could be investigated at a single emitter frequency, since the surface plasmon frequency and coupling depend on mirror thickness. These experiments take on added significance with the recent proposal by Bonifacio and Morawitz<sup>59</sup> of a new laser device based on excited molecule/surface plasmon coupling.

In addition, the coupling of excited molecules to surface plasmons in anisotropic media (see Section IV) may be used as a probe of these modes in lower-dimensional materials.

## Acknowledgments

We are grateful to H. Kuhn, K. H. Drexhage, K. H. Tews, H. Morawitz, and M. R. Philpott for their help and cooperation throughout this work. We are particularly grateful to Dr. Drexhage for providing us with his experimental data and with previously unpublished data. We also thank Alan Miller for carrying out many of the calculations described herein.

## References

1. H. Kuhn, *Pure Appl. Chem.*, **11**, 345 (1965); H. Kuhn, *Naturwissenschaften*, **54**, 429 (1967).
2. H. Kuhn in *Structural Chemistry and Molecular Biology* A. Rich and N. Davidson Eds., Freeman, San Francisco, 1968, p. 566.
3. H. Kuhn and D. Möbius, *Angew. Chem. (Int. Ed. Engl.)*, **10**, 620 (1971).
4. H. Kuhn, D. Möbius, and H. Bucher, in *Physical Methods of Chemistry*, Vol. I, Part 3B, A. Weissberger and B. Rossiter Eds., Wiley, New York, 1972, p. 577.
5. K. H. Drexhage, M. Fleck, F. P. Schafer, and W. Sperling, *Ber. Bunsenges. Phys. Chem.*, **70**, 1179 (1966); K. H. Drexhage, H. Kuhn, and F. P. Schafer, *Ber. Bunsenges. Phys. Chem.*, **72**, 329 (1968).
6. K. H. Drexhage, "Optische Untersuchungen an neuartigen monomolekularen Farbstoffschichten, Habilitations-Schrift, Marburg, 1966, unpublished.
7. K. H. Drexhage, *J. Lumin.*, **1/2**, 693 (1970).
8. K. H. Drexhage, *Sci. Am.*, **222**, 108 (1970).
9. K. H. Drexhage in *Progress in Optics XII*, E. Wolf, Ed., North-Holland, Amsterdam, 1974, p. 165.
10. I. Langmuir, *J. Am. Chem. Soc.*, **39**, 1848 (1917).
11. K. B. Blodgett, *J. Am. Chem. Soc.*, **57**, 1007 (1935).
12. H. Kuhn, *J. Chem. Phys.*, **53**, 101 (1970).
13. H. Morawitz, *Phys. Rev.*, **187**, 1792 (1969).
14. R. R. Chance, A. Prock, and R. Silbey, *J. Chem. Phys.*, **60**, 2184, 2744 (1974).
15. K. H. Tews, *Ann. Phys. Leipz.*, **29**, 97 (1973); thesis, Marburg/Lahn, 1972.
16. A. Sommerfeld, *Ann. Phys. Leipz.*, **28**, 665 (1909); A. Sommerfeld, *Ann. Phys. Leipz.* **81**, 1135 (1926); A. Sommerfeld, *Partial Differential Equations of Physics*, Academic Press, New York, 1949.
17. H. Morawitz and M. R. Philpott, *Phys. Rev.*, **B10**, 4863 (1974); M. R. Philpott, *J. Chem. Phys.*, **62**, 1812 (1975).
18. R. R. Chance, A. Prock, and R. Silbey, *J. Chem. Phys.*, **62**, 2245 (1975).
19. R. R. Chance, A. Prock, and R. Silbey, *J. Chem. Phys.*, **65**, 2527 (1976); *ibid.*, **66**, 1765 (1977).
20. A. Otto, *Phys. Stat. Sol.*, **26**, K99 (1968); A. Otto, *Z. Physik*, **216**, 398 (1968).
21. J. Schoenwald, E. Burstein, and J. Elson, *Sol. State Comm.*, **12** 185 (1973).
22. R. Ritchie, *Phys. Rev.* **106**, 874 (1957); a good survey is given by R. H. Ritchie in *Surf. Sci.*, **34**, 1 (1973).
23. E. Stern and R. Ferrell, *Phys. Rev.*, **120**, 130 (1960); R. Ferrell, *Phys. Rev.*, **111**, 1214 (1958).
24. R. R. Chance, A. Prock, and R. Silbey, *Phys. Rev.*, **A12**, 1448 (1975).
25. J. Stratton, *Electromagnetic Theory*, McGraw-Hill, New York, 1941.
26. P. Johnson and R. Christy, *Phys. Rev.*, **B6**, 4370 (1973).
27. K. H. Tews, *J. Lumin.*, **9**, 223 (1974); K. H. Tews, *Z. Naturforsch.*, **29a**, 712 (1974).
28. M. R. Philpott, *Chem. Phys. Lett.*, **19**, 435 (1973).
29. P. W. Milonni and P. L. Knight, *Opt. Commun.*, **9**, 119 (1973).
30. K. H. Tews, O. Inacker, and H. Kuhn, *Nature*, **228**, 276 (1970).
31. H. Bucher, K. H. Drexhage, M. Fleck, H. Kuhn, D. Möbius, F. P. Schafer, J. Sondermann, W. Sperling, P. Tillman, and J. Wiegand, *Mol. Cryst.*, **2**, 199 (1967); L. Scentpaly, D. Möbius, and H. Kuhn, *J. Chem. Phys.*, **52**, 4618 (1969).
32. O. Inacker, H. Kuhn, H. Bucher, H. Meyer, and K. H. Tews, *Chem. Phys. Lett.*, **7**, 213 (1970).
33. O. Inacker and H. Kuhn, *Chem. Phys. Lett.*, **27**, 317 (1974).
34. R. R. Chance, A. H. Miller, A. Prock, and R. Silbey, *Chem. Phys. Lett.*, **33**, 590 (1975).
35. R. R. Chance, A. H. Miller, A. Prock, and R. Silbey, *J. Chem. Phys.* **63**, 1589 (1975).
36. K. H. Drexhage, personal communication.
37. G. Vaubel, H. Bässler, and D. Möbius, *Chem. Phys. Lett.*, **10**, 334 (1971).

38. H. Kallman, G. Vauhel, and H. Bässler, *Phys. Stat. Sol. (b)*, **44**, 813 (1971).
39. R. R. Chance and A. Prock, *Phys. Stat. Sol. (b)*, **57**, 597 (1973).
40. H. Kurczewska and H. Bässler, preprint "Energy Transfer across an Anthracene-Gold Interface," *J. Luminescence*, in press.
41. T. Förster, *Ann. Phys.*, **2**, 55 (1948); T. Förster in *Modern Quantum Theory*, Vol. III. O. Sinanoglu Ed., Academic Press, New York 1965.
42. G. Hass and J. Waylonis, *J. Opt. Soc. Am.*, **51**, 719 (1961).
43. See, for example, C. T. Tai, *Dyadic Green's Function in Electromagnetic Theory*, Intext, New York, 1971.
44. R. R. Chance, A. Prock, and R. Silbey, *J. Chem. Phys.*, **62**, 771 (1975).
45. R. R. Chance, A. Prock, and R. Silbey, *Sol. State. Commun.*, **18**, 1259 (1976).
46. S. A. Rice, D. Guidotti, H. L. Lemberg, W. C. Murphy, and A. N. Block, in *Advances in Chemical Physics*, Vol. 27, I. Prigogine and S. A. Rice Eds., Wiley-Interscience, New York 1974, p. 543.
47. E. Stern and R. A. Ferrell, *Phys. Rev.*, **178**, 372 (1969).
48. K. L. Klierer and R. Fuchs in *Advances in Chemical Physics*, Vol. 27 I. Prigogine and S. A. Rice, Eds., Wiley-Interscience, New York 1974, p. 355.
49. G. S. Agarwal, *Phys. Rev. A*, **12**, 1475 (1975).
50. G. Barton, *J. Phys.*, **B7**, 2134 (1974).
51. M. Babiker and G. Barton, *J. Phys. A*, **9**, 129 (1976).
52. J. Kirtley and P. K. Hansma, *Phys. Rev. B*, **13**, 2910 (1976).
53. R. Fuchs and K. Klierer, *Phys. Rev.*, **140**, 2076 (1965).
54. (a) A. Garito and A. Heeger, *Acc. Chem. Res.*, **7**, 232 (1974); (b) R. Greene, G. Street, and L. Suter, *Phys. Rev. Lett.*, **34**, 577 (1975) and references therein; (c) W. Scherman and G. Wegner, *Makromol. Chem.*, **125**, 667 (1974); (d) R. R. Chance and R. Baughman, *J. Chem. Phys.*, **64**, 3889 (1976).
55. P. Clemmow, *The Plane Wave Spectrum Representation of Electromagnetic Fields*, Pergamon, Oxford, 1966.
56. A. Banos, *Dipole Radiation in the Presence of a Conducting Half Space*, Pergamon, New York 1966.
57. P. Melman, D. O'Stein, A. Prock, and R. R. Chance, *Chem. Phys.*, **22**, 71 (1977).
58. H. Gerischer and F. Willig in *Topics Curr. Chem.*, **61** (Springer-Verlag, 31 (1976)).
59. R. Bonifacio and H. Morawitz *Phys. Rev. Lett.*, **36**, 1559 (1976).

# NOISE ANALYSIS OF KINETIC SYSTEMS AND ITS APPLICATIONS TO MEMBRANE CHANNELS

YI-DER CHEN

*Laboratory of Molecular Biology, National Institute of Arthritis,  
 Metabolism and Digestive Diseases, National Institutes of Health,  
 Bethesda, Maryland*

## CONTENTS

I.	Introduction . . . . .	68
II.	General Concepts of Noise and Fluctuations . . . . .	69
	A. Time Correlation Functions . . . . .	69
	B. Noise-Power Spectrum . . . . .	70
III.	General Properties of a Kinetic System . . . . .	71
	A. Elementary Chemical Reactions . . . . .	71
	B. Conservation Relations and Independent Stochastic Variables . . . . .	73
IV.	Master-Equation Approach to Noise Calculations . . . . .	74
	A. The Time Correlation Functions. . . . .	74
	B. The Relaxation Matrix and the Variances . . . . .	75
	C. The Noise-Spectrum Matrix . . . . .	78
	D. The Eigenvalue Method. . . . .	79
V.	Irreversible Thermodynamic Approach . . . . .	81
	A. The Thermodynamic Forces and Variances for Systems at Equilibrium . . . . .	82
	B. The Noise-Power-Spectrum Matrix. . . . .	84
	C. Nonequilibrium Steady-State Case . . . . .	85
VI.	Applications of Noise Analysis to General Kinetic Problems . . . . .	86
	A. Differentiation Between Systems. . . . .	86
	B. Determination of the Number of Independent Stochastic Variables in Kinetic Systems . . . . .	88
	C. Determination of Rate Constants . . . . .	89
VII.	Applications to Channel Conductance Noise in Membranes. . . . .	89
	A. Lipid Bilayer Membranes with Ionic Channels. . . . .	90
	B. Conductance Fluctuations at Postsynaptic End-plates of Neuromuscular Junctions . . . . .	91
	C. Model Differentiation of Potassium Channels in Nerve Membranes . . . . .	93
	Acknowledgment . . . . .	96
	References . . . . .	96

## I. INTRODUCTION

The investigation of noise or fluctuations in nerve membranes started in 1965 with the publication by Verveen and Derksen<sup>1</sup> on electrical voltage noise of frog nodes of Ranvier, the small cylindrical surfaces (area 10 to 20  $\mu\text{m}^2$ ) of excitable membranes in myelinated nerve fibers. Originally this work was not undertaken primarily to investigate membrane properties for their own sake, but to search for and to describe the processes underlying the stochastic behavior of nerve fibers upon stimulation. However, as the noise or fluctuations of a kinetic system reflect the system's microscopic kinetic behavior, recent noise analyses on axon membranes,<sup>2-8</sup> postsynaptic end plates at neuromuscular junctions,<sup>9-11</sup> and lipid bilayer membranes with channel-forming materials<sup>12-14</sup> are all directed to the study of kinetic properties of the membrane.

Two review articles<sup>15,16</sup> dealing with measurements of current (or voltage) fluctuations and noise spectrum of nerve membranes have appeared recently that cover almost all existing experimental results. Thus it is not our intention to repeat the experimental side of the subject here. Instead, we concern ourselves with a general noise analysis on complex kinetic systems in which an arbitrary number of chemical species (subsystems) are undergoing coupled chemical reactions. We emphasize the following questions: (1) How does one calculate the noise-power spectrum of a complex kinetic system if all the rate constants are given? (2) How can noise measurements be used to elucidate the mechanism or to evaluate the rate parameters of a complex kinetic system? Applications to membrane-transport systems are illustrated as examples.

We are interested in general kinetic systems because most biological processes, no matter how complicated, can always be described in terms of chemical reactions. Thus channel-transport phenomena in nerve membranes or postsynaptic end plates, muscle contraction, DNA replication, and protein synthesis, and so forth can all be modeled with a set of chemical reactions. Recently, linear cycling steady-state models have been extensively studied by Hill<sup>17,18</sup> to interpret energy-transducing systems, such as active transport and muscle contraction. Thus the theoretical noise analysis presented in this paper might be useful in analyzing the kinetic properties in these biological processes in the future.

## II. GENERAL CONCEPTS OF NOISE AND FLUCTUATIONS

In this section the concept of fluctuations in a chemical kinetic system is introduced briefly.

Because a system undergoes rapid and repetitive transitions among its microstates, even if the system is at equilibrium, the thermodynamic parameters of a macroscopic system fluctuate from instant to instant. For example, if a system is in contact with a heat reservoir, the microscopic transitions will lead the macroscopic system sometimes to states of low energy and sometimes to states of high energy, as the (constant) total energy is shared in different proportions between system and reservoir. In general, the extensive parameters characterizing the system as a whole fluctuate only when the system is in contact with reservoirs, that is, the system is open. One must note that fluctuations of local quantities in a closed system do exist—such as local density fluctuations in fluids at the critical point (critical fluctuations). In this chapter we do not consider this case; we consider only fluctuations of thermodynamic parameters characterizing the whole system.

In chemical kinetic systems in which coupled chemical reactions are taking place, the concentrations of the species may fluctuate even if the system is *closed*, because microscopic reactive collisions constantly convert one type of molecule into another. The speed of fluctuations depends on the rate of reactive collisions. For illustration, let us consider the simple isomeric reaction



in a closed system with constant volume and temperature. If one follows the concentration of A as a function of time, one will find that  $N_A$  (we use  $N_A$  here to represent the number of molecules in a unit volume) is not constant, but fluctuates around the mean value  $\bar{N}_A$ , as indicated in Fig. 1. If the reaction is fast, the fluctuations are more rapid, and vice versa. Thus the speed of the reaction is reflected in the rate of fluctuations.

### A. Time Correlation Functions

To characterize the rate of fluctuations quantitatively, let us introduce the time correlation function  $C(t)$  defined by (see Fig. 1)

$$C(t) = \lim_{T \rightarrow \infty} \frac{1}{2T} \int_{-T}^T \alpha_A(t') \alpha_A(t' + t) dt' \quad (1)$$

where  $\alpha_A(t) = N_A(t) - \bar{N}_A$ .

This function gives us information about the coherence of the time series  $N_A(t)$ . For  $t=0$ ,  $C(0)$  is equal to the mean square fluctuation amplitude. As the value of  $t$  increases, the random nature of the fluctuations causes the



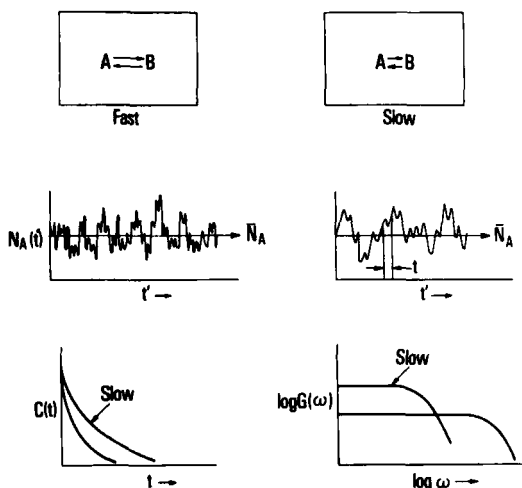


**Fig. 1.** Schematic drawing of fluctuations and noise functions of a hypothetical isomeric reaction  $A \rightleftharpoons B$ .  $N_A(t')$  represents the instantaneous concentration of A in the system and  $\bar{N}_A$  is the average value.  $C(t)$  denotes the time correlation function as defined by (1) in the text and  $G(\omega)$  is the noise power spectrum. If the reaction is fast,  $N_A$  fluctuates rapidly,  $C(t)$  rapidly decays to zero value, and  $G(\omega)$  extends to a higher frequency region.

coherence to decay. Thus at  $t = \infty$  there is no correlation between  $\alpha_A(t')$  and  $\alpha_A(t' + \infty)$  and, consequently,  $C(\infty)$  becomes zero. For fast fluctuating systems  $C(t)$  decays rapidly to zero as  $t$  increases. Thus  $C(t)$  can be used to measure the speed of a reaction system (see Fig. 1).

### B. Noise-Power Spectrum

The noise spectral density is a way of presenting the average frequency content of the fluctuating signal  $N_A(t)$ . It is obtained by filtering  $N_A(t)$  with band-pass filters with sharp cut-off characteristics followed by squaring and averaging of each filter output. In general, the noise spectrum  $G(f)$  where  $f$  is the frequency can be shown to be related to the time correlation function  $C(t)$  through Fourier transformation<sup>20,21</sup>:

$$\begin{aligned} G(\omega) &= 2 \operatorname{Re} \int_{-\infty}^{\infty} C(t) e^{-i\omega t} dt \\ &= 4 \int_0^{\infty} C(t) \cos \omega t dt \end{aligned} \quad (2)$$

where  $\omega = 2\pi f$ ,  $i = \sqrt{-1}$ , and Re represents taking the real part. Thus  $G(\omega)$  can also be used to characterize the speed of a chemical reaction (see Fig. 1).

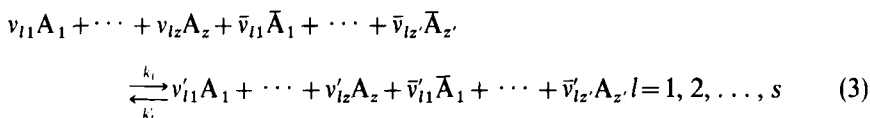
### III. GENERAL PROPERTIES OF A KINETIC SYSTEM

Since our main subject is the noise and fluctuations in kinetic systems, a brief discussion of properties of kinetic reactions seems appropriate.

#### A. Elementary Chemical Reactions

An elementary chemical reaction in a kinetic system is a true microscopic collision event between the molecules (or a true isomeric transition in first-order reactions) that converts one type of molecule into another.<sup>21</sup> Thus the mechanism of a kinetic system is determined by the set of elementary reactions.

In a most general way the elementary chemical reactions can be described by the equations



where  $A_i (i = 1, 2, \dots, z)$  are the species in the system that are free to fluctuate and  $\bar{A}_i (i = 1, 2, \dots, z')$  are the species that are held at constant concentrations by external control. The  $v$ ,  $\bar{v}$ , and so forth are the stoichiometric coefficients, and  $k_i$  and  $k'_i$  are the forward and backward rate constants of this elementary reaction. The  $s$  in (3) represents the total number of elementary reactions in the system. In general, the free-to-fluctuate species may also be in contact with their reservoirs (open system). Thus, in addition to (3), the system may have "exchange reactions" for all species:



where  $J_i^{\text{ex}}$  denotes the net rate of exchange with a positive value representing influx from reservoir into the system and a negative value representing outflux.  $J_i^{\text{ex}}$  may depend on the concentration of  $A_i$  in the system. For example, in a simple diffusion model,  $J_i^{\text{ex}}$  may be expressed as

$$J_i^{\text{ex}} = \eta_i - \mu_i N_i \quad (4)$$

with  $\eta_i$  representing the influx rate and  $\mu_i N_i$  the outflux rate. It is by fixing the concentrations  $[\bar{A}_i]$  in (3) and the influx rate  $\eta_i$  in (4) that a chemical "non-equilibrium" situation may be maintained as a steady state.

According to the principles of reaction kinetics, the corresponding rates of reaction (or transition probability per unit time in stochastic terms) in the  $l$ th elementary reaction are

$$\begin{aligned}
 v_l &= k_l [\bar{A}_1]^{\bar{v}_{1l}} \cdots [\bar{A}_z]^{\bar{v}_{zl}} [A_1]^{v_{1l}} \cdots [A_z]^{v_{zl}} & (\text{forward}) \\
 v'_l &= k'_l [\bar{A}_1]^{\bar{v}'_{1l}} \cdots [\bar{A}_z]^{\bar{v}'_{zl}} [A_1]^{v'_{1l}} \cdots [A_z]^{v'_{zl}} & (\text{backward}) \\
 l &= 1, 2, \dots, s
 \end{aligned} \tag{5}$$

Since the concentrations of  $\bar{A}_i$  are kept constant, we may absorb the product  $[\bar{A}_1]^{\bar{v}_{1l}} \cdots [\bar{A}_z]^{\bar{v}_{zl}}$  into  $k_l$  and rewrite (5) as

$$\begin{aligned}
 v_l &= k_l N_1^{v_{1l}} \cdots N_z^{v_{zl}} & (\text{forward}) \\
 v'_l &= k'_l N_1^{v'_{1l}} \cdots N_z^{v'_{zl}} & (\text{backward}) \\
 l &= 1, 2, \dots, s
 \end{aligned} \tag{6}$$

with  $k_l$  and  $k'_l$  here denoting the new rate constants. Here we have used  $N_i$  to represent the number concentration  $[A_i]$ .

The rate of change of species in the system is then equal to

$$\frac{dN_i}{dt} = \sum_{l=1}^s (v'_{li} - v_{li})(v_l - v'_l) + \eta_i - \mu_i N_i \quad i = 1, 2, \dots, z \tag{7}$$

For any stationary state, one has  $dN_i/dt = 0$ , that is the respective concentrations constitute a time-independent solution of (7). In the special case of chemical equilibrium, each elementary rate must vanish. Thus

$$\begin{aligned}
 (v_l)^{\text{eq}} &= (v'_l)^{\text{eq}} & l = 1, 2, \dots, s \\
 J_i^{\text{ex}} &= 0 & i = 1, 2, \dots, z
 \end{aligned}$$

that is, the “detailed balance” condition<sup>22</sup> must be obeyed by each elementary reaction and each exchange reaction. In this case every  $\bar{A}_i$  in (3) must be either absent or held at its equilibrium concentration for all elementary reactions.

For convenience, we call an elementary reaction “regular” if it does not have species  $\bar{A}_i$  or all  $\bar{A}_i$ ’s are held at their equilibrium values. Otherwise, we call it a “nonregular” reaction. One must note that we denote a system to be “open” or “closed” according to whether or not, its free-to-fluctuate species are in contact with their reservoirs irrespective of whether or not the system has species  $\bar{A}_i$  (an  $\bar{A}_i$  is held at constant concentration by an external source and must be in contact with some sort of reservoir). Thus closed systems with nonregular elementary reactions are always at steady state. For example, the simple enzymatic reactions involving substrate S and product P can be described by the following set of reactions,



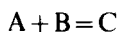
where ES and EP are enzyme-substrate and enzyme-product complexes. The net reaction of the above set of reactions is



Thus if S and P are held at their equilibrium concentrations, the reactions in (8) are all regular reactions. On the other hand, if S is not at equilibrium with P, the first and third reactions in (8) become nonregular reactions and the system is at a cycling steady state.<sup>18,23</sup> If E is in contact with a reservoir, the system becomes an open system.

### B. Conservation Relations and Independent Stochastic Variables

To discuss fluctuations we must find the stochastic variables that characterize the fluctuations of the system. In chemical reactions the stochastic variables are simply the number of molecules of each species in the system that are free to fluctuate,  $\{N_1, N_2, \dots, N_z\}$ . However, not all these variables are linearly independent, because some species in the system may have mass conservation relations. For example, in the simple reaction



there are three species and two conservation relations:  $N_A - N_B = \text{constant}$  and  $N_A + N_C = \text{constant}$ . Thus two of these three species will not fluctuate independently. In general, the number of independent stochastic variables (hereafter denoted as ISV) is obtained by eliminating all the conservation relations from the set of  $\{N_1, \dots, N_z\}$ . Thus in the above example there is only one independent stochastic variable.

The conservation relations of a system are determined by the elementary reactions (3) and (4). If one can find a set of constants  $\{b_1, b_2, \dots, b_z\}$ , which are not all zero, such that  $\sum_{i=1}^z b_i (dN_i/dt) = 0$ , where  $dN_i/dt$  can be obtained

from (7), then the system has a conservation relation,  $\sum_{i=1}^z b_i N_i = \text{constant}$ .

Suppose that there are  $r$  sets of such  $b_i$  constants that are *linearly independent*; the number of ISV of the system is then equal to  $z - r$ . From now on, we use  $\{N_1, N_2, \dots, N_x\}$  (where  $x = z - r$ ) to represent the set of independent stochastic variables. The rest of the  $r(z - x)N_j$ 's can be expressed as linear combinations of  $\{N_1, N_2, \dots, N_x\}$  by the relations

$$dN_j = \sum_{i=1}^x \lambda_{ji} dN_i \quad j = x+1, \dots, z \quad (9)$$

where the  $\lambda_{ji}$ 's are determined by the conservation relations.

#### IV. MASTER-EQUATION APPROACH TO NOISE CALCULATIONS

A general stochastic master-equation approach to the calculation of the noise-power spectrum has been developed by Lax<sup>24</sup> and others.<sup>20</sup> We present an application of the general theory to complex kinetic systems.

##### A. The Time Correlation Functions

For a one-variable system, the time correlation function has been defined by (1). Using ensemble averages, (1) becomes

$$C(t) = \sum \alpha_A(t') \alpha_A(t+t') P[N_A(t+t'); N_A(t')] \quad (10)$$

where  $P[N_A(t+t'); N_A(t')]$  is the joint probability of finding the system having  $N_A(t')$  molecules of A at time  $t'$  and  $N_A(t+t')$  at time  $t+t'$ .

For multivariate systems the time correlation function  $C(t)$  in (10) becomes a matrix. In general, we are interested in the fluctuation of the macroscopically measured quantity  $X_\beta$  defined as<sup>19</sup>

$$X_\beta = \sum_{i=1}^z a'_{\beta i} N_i, \quad \beta = 1, 2, \dots, y \quad (11)$$

where the coefficient  $a'_{\beta i}$  is a constant representing the  $\beta$ th measurement index of species  $i$ . For example,  $a'_{\beta i}$  could be the unit conductivity in a conductance measurement or the extinction coefficient in an optical absorbance measurement.  $y$  is the total number of independent sets of  $a'$  values (independent measurements). If the system has conservation relations some of the  $N_i$ 's in (11) can be replaced by the independent set  $\{N_1, N_2, \dots, N_x\}$ . Thus after substituting the integrated form of (9) into (11),  $X_\beta$  becomes

$$\begin{aligned} X_\beta &= \sum_{i=1}^x \left( a'_{\beta i} + \sum_{j=x+1}^z a'_{\beta j} \lambda_{ji} \right) N_i + K_\beta \\ &= \sum_{i=1}^x a_{\beta i} N_i + K_\beta \end{aligned} \quad (12)$$

where  $a_{\beta i}$  is defined by the quantity inside the brackets and  $K_\beta$  is a constant.

The time correlation matrix in the measured quantity  $\mathbf{X}$  becomes

$$\mathbf{C}(t) = \langle [\mathbf{X}(t') - \mathbf{X}^s][\tilde{\mathbf{X}}(t'+t) - \tilde{\mathbf{X}}^s] \rangle \quad (13)$$

where  $\tilde{\mathbf{X}}(t)$  (row vector) is the transpose of  $\mathbf{X}(t)$  (column vector) and  $\mathbf{X}^s$  is the steady-state value of  $\mathbf{X}$ . The notation  $\langle \rangle$  means taking an ensemble average as in (10). Note that the order of matrix  $\mathbf{C}(t)$  is  $y$  by  $y$ . For a stationary process (steady state or equilibrium),  $\mathbf{C}(t)$  is independent of  $t'$ . Thus (13) can

be rewritten as

$$C(t) = \langle [X(0) - X^s][\tilde{X}(t) - \tilde{X}^s] \rangle \quad (14)$$

Substituting (12) into (14), we get

$$C(t) = \mathbf{a} \langle \alpha(0) \tilde{\alpha}(t) \rangle \tilde{\mathbf{a}} \quad (15)$$

where  $\alpha = N - N^s$ .

It is more convenient to use a conditionally averaged quantity defined by

$$\langle \alpha(t) \rangle_{\alpha(0)} = \sum (N(t) - N^s) P(N, t | N(0)) \quad (16)$$

with  $P(N, t | N(0))$  denoting the conditional probability of finding the system to have  $N$  at time  $t$  if it has exactly  $N(0)$  at time zero. Use of (16) now gives for (15)

$$C(t) = \mathbf{a} \langle \alpha(0) \langle \tilde{\alpha}(t) \rangle_{\alpha(0)} \rangle \tilde{\mathbf{a}} \quad (17)$$

## B. The Relaxation Matrix and the Variances

As shown in the previous section the central part of the noise calculation is the evaluation of the conditionally averaged quantity  $\langle \alpha(t) \rangle_{\alpha(0)}$ . The master equation describing the conditional probability  $P(N(t) | N(0))$  can be shown to be<sup>20</sup>

$$\frac{\partial P(N, t | N(0))}{\partial t} = \sum_{N'} P(N', t | N(0)) Q(N; N') - \sum_{N'} P(N, t | N(0)) Q(N'; N) \quad (18)$$

where  $Q(N; N')$  is the transition probability per unit time from state  $N'$  to state  $N$ . In the stochastic formulation of chemical reactions,  $Q$  can be expressed in terms of  $v_i$ ,  $v'_i$ ,  $\eta_i$  and so forth as defined in Section III.A<sup>25</sup> (see below).

If one multiplies (18) by  $N$  and sums over all  $N$ , we have, interchanging the summations in the last sums,

$$\frac{\partial \langle N(t) \rangle_{N(0)}}{\partial t} = \sum_{N'} A(N') P(N', t | N(0)) \equiv \langle A(N) \rangle_{N(0)} \quad (19)$$

where

$$A(N') = \sum_N (N - N') Q(N; N') \quad (20)$$

When we expand about the steady-state (or equilibrium) value  $N^s$  and neglect terms higher than first order (quasilinearization approximation),  $A(N)$  in (20) becomes

$$A(N) = A(N^s) - M\alpha + O(\alpha^2) \quad (21)$$

where  $\mathbf{M}$  is a square matrix (of order  $x$  by  $x$ ), the phenomenological matrix:

$$\mathbf{M} = - \left[ \frac{\partial A(\mathbf{N})}{\partial \mathbf{N}} \right]_{\mathbf{N} = \mathbf{N}^s} \quad (22)$$

Averaging (21) over a steady state (or equilibrium) ensemble, we get

$$\langle A(\mathbf{N}) \rangle = \langle A(\mathbf{N}^s) \rangle = A(\mathbf{N}^s) \quad (23)$$

By taking the limit  $t \rightarrow \infty$  in (19), it is easy to show that

$$\langle \mathbf{N}(t) \rangle_{\mathbf{N}(0)} \rightarrow \langle \mathbf{N} \rangle \quad \text{and} \quad \langle A(\mathbf{N}) \rangle_{\mathbf{N}(0)} \rightarrow \langle A(\mathbf{N}) \rangle = 0$$

Thus

$$A(\mathbf{N}^s) = 0 \quad (24)$$

After substitution with (21) and (24), (19) becomes

$$\frac{\partial \langle \mathbf{N}(t) \rangle_{\alpha(0)}}{\partial t} = -\mathbf{M} \langle \alpha \rangle_{\alpha(0)} \quad (25)$$

Equation 25 is the relaxation equation to be used in the noise calculation. However, one needs an explicit expression for the relaxation matrix  $\mathbf{M}$ . By comparing (20) and (22), it is easy to show that the elements of  $\mathbf{M}$  can be expressed as

$$M_{ij} = \left\{ -\frac{\partial}{\partial N'_j} \sum_{\mathbf{N}} (N_i - N'_i) Q(\mathbf{N}; \mathbf{N}') \right\}_{\mathbf{N}' = \mathbf{N}^s} \quad (26)$$

For chemical kinetic systems, the sum over  $\mathbf{N}$  in (26) can be replaced by the sum over all elementary chemical reactions and all exchange reactions. Thus

$$M_{ij} = \left\{ -\frac{\partial}{\partial N'_j} \left[ \sum_{l=1}^s (N_i - N'_i) R_l(N_i; N') + (N_i - N'_i) R^{\text{ex}}(N_i; N'_i) \right] \right\}_{\mathbf{N}' = \mathbf{N}^s} \quad (27)$$

where  $R_l(N_i; N'_i)$  is the transition probability per unit time for species  $i$  to change from  $N'_i$  to  $N_i$  in the  $l$ th elementary chemical reaction and  $R^{\text{ex}}(N_i; N'_i)$  is the transition probability per unit time for species  $i$  to change from  $N'_i$  to  $N_i$  in the exchange reactions. Thus

$$\begin{aligned} N_i &= N'_i + (v'_{li} - v_{li}) & \text{when } R_l(N_i; N'_i) &= v_{li} \\ N_i &= N'_i + (v_{li} - v'_{li}) & \text{when } R_l(N_i; N'_i) &= v'_{li} \\ N_i &= N'_i + 1 & \text{when } R^{\text{ex}}(N_i; N'_i) &= \eta_i \\ N_i &= N'_i - 1 & \text{when } R^{\text{ex}}(N_i; N'_i) &= \mu_i N'_i \end{aligned} \quad (28)$$

As a result the  $M_{ij}$  can be expressed as

$$\begin{aligned} M_{ij} &= \left\{ \frac{\partial}{\partial N_j} \left[ \sum_l (v'_{li} - v_{li})(v'_l - v_l) - \eta_i + \mu_i N_i \right] \right\}_{\mathbf{N} = \mathbf{N}^s} \\ &\equiv \left\{ \frac{\partial}{\partial N_j} \left( -\frac{dN_i}{dt} \right) \right\}_{\mathbf{N} = \mathbf{N}^s} \end{aligned} \quad (29)$$

One must note that, in carrying out the differentiation in (29), (9) has to be taken into consideration for dependent variables (see the examples of Ref. 25).

Multiplying (18) by  $\mathbf{N}\tilde{\mathbf{N}}$  and summing over  $\mathbf{N}$ , we get

$$\frac{\partial \langle \mathbf{N}\tilde{\mathbf{N}} \rangle_{\mathbf{N}(0)}}{\partial t} = \sum_{\mathbf{N}'} \sum_{\mathbf{N}} (\mathbf{N}\tilde{\mathbf{N}} - \mathbf{N}'\tilde{\mathbf{N}}') P[\mathbf{N}', t | \mathbf{N}(0)] Q(\mathbf{N}; \mathbf{N}') \quad (30)$$

Now we replace  $\mathbf{N}\tilde{\mathbf{N}}$  by

$$\mathbf{N}\tilde{\mathbf{N}} = (\mathbf{N} - \mathbf{N}')(\tilde{\mathbf{N}} - \tilde{\mathbf{N}}') + \mathbf{N}'\tilde{\mathbf{N}}' + \mathbf{N}'(\tilde{\mathbf{N}} - \tilde{\mathbf{N}}') + (\mathbf{N} - \mathbf{N}')\tilde{\mathbf{N}}' \quad (31)$$

and introduce

$$\mathbf{B}(\mathbf{N}') = \sum_{\mathbf{N}} (\mathbf{N} - \mathbf{N}')(\tilde{\mathbf{N}} - \tilde{\mathbf{N}}') Q(\mathbf{N}; \mathbf{N}') \quad (32)$$

Then we have

$$\frac{\partial \langle \mathbf{N}\tilde{\mathbf{N}} \rangle_{\mathbf{N}(0)}}{\partial t} = \langle \mathbf{B} \rangle_{\mathbf{N}(0)} + \langle \mathbf{N}\tilde{\mathbf{A}}(\mathbf{N}) \rangle_{\mathbf{N}(0)} + \langle \mathbf{A}(\mathbf{N})\tilde{\mathbf{N}} \rangle_{\mathbf{N}(0)} \quad (33)$$

Now expanding  $\mathbf{A}(\mathbf{N})$  about the steady-state (or equilibrium)  $\mathbf{N}^s$  and taking the values at  $t \rightarrow \infty$ , we have, from (33), for the variance matrix  $\sigma \equiv \langle \alpha\tilde{\alpha} \rangle$ :

$$\langle \alpha\tilde{\alpha} \rangle \tilde{\mathbf{M}} + \mathbf{M} \langle \alpha\tilde{\alpha} \rangle = \mathbf{B}(\mathbf{N}^s) \quad (34)$$

In thermal equilibrium systems,  $\langle \alpha\tilde{\alpha} \rangle \tilde{\mathbf{M}} = \mathbf{M} \langle \alpha\tilde{\alpha} \rangle$ . Therefore,

$$\sigma \equiv \langle \alpha\tilde{\alpha} \rangle = \frac{1}{2} \mathbf{M}^{-1} \mathbf{B}(\mathbf{N}^s) \quad (35)$$

where  $\mathbf{M}^{-1}$  denotes the inverse of  $\mathbf{M}$ .

As we did for  $\mathbf{M}$  in the previous section, we are able to express  $\mathbf{B}(\mathbf{N}^s)$  in terms of the rate terms  $v_i$ ,  $v'_i$ , and so forth.

From (32) we can write the elements of  $\mathbf{B}(\mathbf{N}')$  as

$$B_{ii}(\mathbf{N}') = \sum_{\mathbf{N}} (N_i - N'_i)^2 Q(\mathbf{N}; \mathbf{N}') \quad (36)$$

$$B_{ij}(\mathbf{N}') = \sum_{\mathbf{N}} (N_i - N'_i)(N_j - N'_j) Q(\mathbf{N}; \mathbf{N}') \quad (37)$$



In terms of elementary reactions, (36) and (37) become

$$B_{ii}(N') = \sum_{l=1}^s (N_i - N'_i)^2 R_l(N_i; N'_i) + (N_i - N'_i)^2 R^{\text{ex}}(N_i; N'_i) \quad (38)$$

$$B_{ij}(N') = \sum_{l=1}^s (N_i - N'_i)(N_j - N'_j) R_l(N_i, N_j; N'_i, N'_j) \quad (39)$$

Here  $R_l(N_i, N_j; N'_i, N'_j)$ , in contrast to  $R_l(N_i; N'_i)$ , represents the transition probability of the  $l$ th reaction from  $(N'_i, N'_j)$  to  $(N_i, N_j)$ , which involves species  $i$  and  $j$  *simultaneously*.

Substitution with (28) gives for (38) and (39):

$$B_{ii}(N) = \sum_{l=1}^s (v_{li} - v'_{li})^2 (v_l + v'_l) + \eta_i + \mu_i N_i \quad (40)$$

$$B_{ij}(N) = \sum_{l=1}^s (v_{li} - v'_{li})(v_{lj} - v'_{lj})(v_l + v'_l) \quad (41)$$

### C. The Noise-Spectrum Matrix

When extended to multivariate cases, (2) becomes

$$\begin{aligned} \mathbf{G}(\omega) &= 2 \operatorname{Re} \int_{-\infty}^{\infty} \mathbf{C}(t) e^{-i\omega t} dt \\ &= 2 \operatorname{Re} \left[ \int_0^{\infty} \mathbf{C}(t) e^{-i\omega t} + \int_0^{\infty} \tilde{\mathbf{C}}(t) e^{i\omega t} dt \right] \end{aligned} \quad (42)$$

The formal solution of (25) is

$$\langle \alpha(t) \rangle_{\alpha(0)} = e^{-\mathbf{M}t} \alpha(0) \quad (43)$$

or

$$\langle \tilde{\alpha}(t) \rangle_{\alpha(0)} = \tilde{\alpha}(0) e^{-\tilde{\mathbf{M}}t} \quad (44)$$

Substituting (44) into (17) gives for the time correlation matrix:

$$\mathbf{C}(t) = \mathbf{a} \sigma e^{-\tilde{\mathbf{M}}t} \tilde{\mathbf{a}} \quad (45)$$

After  $\mathbf{C}(t)$  from (45) is inserted into (42) and the integration is carried out, the noise-spectrum matrix  $\mathbf{G}(\omega)$  can be expressed as

$$\mathbf{G}(\omega) = 2 \operatorname{Re} [\mathbf{a}(\mathbf{M} - i\omega \mathbf{E})^{-1} \sigma \tilde{\mathbf{a}} + \mathbf{a} \sigma (\tilde{\mathbf{M}} + i\omega \mathbf{E})^{-1} \tilde{\mathbf{a}}] \quad (46)$$

or, as shown by Chen,<sup>19</sup>

$$\mathbf{G}(\omega) = 2 [\mathbf{a}(\mathbf{M}^2 + \omega^2 \mathbf{E})^{-1} \mathbf{M} \sigma \tilde{\mathbf{a}} + \mathbf{a} \sigma (\tilde{\mathbf{M}}^2 + \omega^2 \mathbf{E})^{-1} \tilde{\mathbf{M}} \tilde{\mathbf{a}}] \quad (47)$$

where  $\mathbf{E}$  denotes the unity matrix. Equation 47 is the desired result.  $\mathbf{G}(\omega)$  can

be calculated when  $\mathbf{a}$ ,  $\mathbf{M}$ , and  $\sigma$  are given. In case  $\mathbf{a}$  is a one-row matrix (corresponding to one measurement),  $\mathbf{G}(\omega)$  becomes the "auto" noise-power spectrum. In deducing (46) the condition of detailed balance has never been used. Therefore, (47) is applicable to steady state as well as equilibrium. However, if an equilibrium system is considered, the microscopic reversibility condition gives<sup>24</sup>

$$\mathbf{M}\sigma = \sigma\tilde{\mathbf{M}} \quad (48)$$

or

$$\tilde{\mathbf{M}} = \sigma^{-1}\mathbf{M}\sigma \quad (49)$$

and

$$\tilde{\mathbf{M}}^2 = \sigma^{-1}\mathbf{M}^2\sigma \quad (50)$$

With (49) and (50) the second term on the right-hand side of (47) can be shown to be equivalent to the first term and  $\mathbf{G}(\omega)$  becomes

$$\mathbf{G}(\omega) = 4\mathbf{a}(\mathbf{M}^2 + \omega^2\mathbf{E})^{-1}\mathbf{M}\sigma\tilde{\mathbf{a}} \quad (51)$$

As shown in (34)  $\sigma$  is directly related to  $\mathbf{M}$  and  $\mathbf{B}$ . Thus, for systems whose  $\sigma$  is not readily obtainable, the  $\sigma$  in (47) and (51) must be replaced with  $\mathbf{B}$ . With the aid of (34),  $\mathbf{G}(\omega)$  has been shown to be<sup>25</sup>

$$\mathbf{G}(\omega) = 2\mathbf{a}(\mathbf{M}^2 + \omega^2\mathbf{E})^{-1}\mathbf{M}\mathbf{B}\tilde{\mathbf{M}}(\tilde{\mathbf{M}}^2 + \omega^2\mathbf{E})^{-1}\tilde{\mathbf{a}} + 2\omega^2\mathbf{a}(\mathbf{M}^2 + \omega^2\mathbf{E})^{-1}\mathbf{B}(\tilde{\mathbf{M}}^2 + \omega^2\mathbf{E})^{-1}\tilde{\mathbf{a}} \quad (52)$$

and

$$\mathbf{G}(\omega) = 2\mathbf{a}(\mathbf{M}^2 + \omega^2\mathbf{E})^{-1}\mathbf{B}\tilde{\mathbf{a}} \quad (\text{equilibrium}) \quad (53)$$

Since  $\mathbf{M}$  and  $\mathbf{B}$  are explicitly expressed in terms of the rate constants of the system, as shown in (29), (40), and (41),  $\mathbf{G}(\omega)$  can be readily calculated when all the rate constants and the measurement index matrix  $\mathbf{a}$  are given.

#### D. The Eigenvalue Method

The  $\mathbf{G}(\omega)$  in (47) and (51) through (53) are expressed explicitly in terms of matrices  $\mathbf{M}$  and  $\mathbf{B}$  (or  $\sigma$ ). Alternatively, (25) can be directly solved to obtain  $\langle\alpha(t)\rangle_{\alpha(0)}$  using the eigenvalue-eigenfunction method. In general, the solution of (25) is

$$\langle\alpha(t)\rangle_{\alpha(0)} = \Phi(t)\alpha(0) \quad (54)$$

where  $\Phi(t) \equiv e^{-\mathbf{M}t}$  is the fundamental matrix of the linear differential equation (25).<sup>26,27</sup> With (54) and (17) the correlation matrix  $\mathbf{C}(t)$  becomes

$$\mathbf{C}(t) = \mathbf{a}\sigma\tilde{\Phi}(t)\tilde{\mathbf{a}} \quad (55)$$

One way to get  $\Phi(t)$  is to find the set of linearly independent special solutions of (25).<sup>28</sup> If  $\Lambda(t)$  represents the set of special solutions, then

$$\Phi(t) = \Lambda(t)\mathbf{H} \quad (56)$$

where  $\mathbf{H} = \Lambda(0)^{-1}$  is the inverse of  $\Lambda(t)$  when  $t=0$ . For the nondegenerate case  $\Lambda(t)$  can be obtained by finding the eigenvalues and corresponding eigenfunctions of matrix  $-\mathbf{M}$ .<sup>26</sup> Thus we let  $\xi_i$  and  $\mathbf{r}_i$  represent the real eigenvalues and corresponding eigenfunctions of  $\mathbf{M}$ , respectively,  $\xi_n + \theta_n \bar{i}$  ( $\bar{i} = \sqrt{-1}$ ,  $\theta_n$  is positive, real) and  $\mathbf{r}_n + \mathbf{w}_n \bar{i}$  represent the positive complex eigenvalues and eigenfunctions, and  $\xi_m - \theta_m \bar{i}$  ( $\theta_m$  is positive, real) and  $\mathbf{r}_m + \mathbf{w}_m \bar{i}$  represent the conjugate negative complex eigenvalues and eigenfunctions. Then  $\Lambda(t)$  can be constructed as<sup>28</sup>

$$\begin{aligned} (\Lambda)_i &= \mathbf{r}_i e^{\xi_i t} \\ (\Lambda)_n &= (\mathbf{r}_n \sin \theta_n t + \mathbf{w}_n \cos \theta_n t) e^{\xi_n t} \\ (\Lambda)_m &= (\mathbf{r}_m \cos \theta_m t + \mathbf{w}_m \sin \theta_m t) e^{\xi_m t} \end{aligned} \quad (57)$$

Thus the  $(i, j)$  element of  $\Phi(t)$  can be expressed as

$$\begin{aligned} \phi_{ij}(t) &= \sum_i r_{ii} h_{ij} e^{\xi_i t} + \sum_n (r_{in} \sin \theta_n t + w_{in} \cos \theta_n t) h_{nj} e^{\xi_n t} \\ &\quad + \sum_m (r_{im} \cos \theta_m t + w_{im} \sin \theta_m t) h_{mj} e^{\xi_m t} \end{aligned} \quad (58)$$

where  $h_{kj}$  is the  $(k, j)$  element of  $\mathbf{H}$  and  $r_{ii}$  is the  $i$ th element of column matrix  $\mathbf{r}_i$ , and so forth.

Substituting (58) into (55), we obtain the  $(\gamma, \beta)$  element of  $\mathbf{C}(t)$ :

$$\begin{aligned} C_{\gamma\beta}(t) &= \sum_{ijk} a_{\gamma k} \sigma_{kj} \phi_{ij}(t) a_{\beta i} \\ &= \sum_i \tilde{r}_{\beta i} \tilde{h}_{\gamma i} e^{\xi_i t} + \sum_n (\tilde{r}_{\beta n} \sin \theta_n t + \tilde{w}_{\beta n} \cos \theta_n t) \tilde{h}_{\gamma n} e^{\xi_n t} \\ &\quad + \sum_m (\tilde{r}_{\beta m} \cos \theta_m t + \tilde{w}_{\beta m} \sin \theta_m t) \tilde{h}_{\gamma m} e^{\xi_m t} \end{aligned} \quad (59)$$

where

$$\begin{aligned} \tilde{\gamma}_{\beta\alpha} &= \sum_j^x a_{\beta j} r_{j\alpha} \\ \tilde{h}_{\gamma\alpha} &= \sum_{kj}^x a_{\gamma k} \sigma_{kj} h_{\alpha j} \\ \tilde{w}_{\beta\alpha} &= \sum_j^x a_{\beta j} w_{j\alpha} \\ \alpha &= l, n, m \end{aligned} \quad (60)$$

By substituting (59) into (42), the  $(\beta, \gamma)$  element of  $\mathbf{G}(\omega)$  can be shown to be

$$\begin{aligned}
 G_{\beta\gamma}(\omega) = & \sum_l \frac{-2(\tilde{r}_{\beta l} \tilde{h}_{\gamma l} + \tilde{r}_{\gamma l} \tilde{h}_{\beta l}) \xi_l}{\xi_l^2 + \omega^2} \\
 & + \sum_n \left[ (\tilde{r}_{\beta n} \tilde{h}_{\gamma n} + \tilde{r}_{\gamma n} \tilde{h}_{\beta n}) \left( \frac{\theta_n - \omega}{\xi_n^2 + (\theta_n - \omega)^2} + \frac{\theta_n + \omega}{\xi_n^2 + (\theta_n + \omega)^2} \right) \right. \\
 & \left. - (\tilde{w}_{\beta n} \tilde{h}_{\gamma n} + \tilde{w}_{\gamma n} \tilde{h}_{\beta n}) \left( \frac{\xi_n}{\xi_n^2 + (\theta_n - \omega)^2} + \frac{\xi_n}{\xi_n^2 + (\theta_n + \omega)^2} \right) \right] \\
 & + \sum_m \left[ (\tilde{w}_{\beta m} \tilde{h}_{\gamma m} + \tilde{w}_{\gamma m} \tilde{h}_{\beta m}) \left( \frac{\theta_m - \omega}{\xi_m^2 + (\theta_m - \omega)^2} + \frac{\theta_m + \omega}{\xi_m^2 + (\theta_m + \omega)^2} \right) \right. \\
 & \left. - (\tilde{r}_{\beta m} \tilde{h}_{\gamma m} + \tilde{r}_{\gamma m} \tilde{h}_{\beta m}) \left( \frac{\xi_m}{\xi_m^2 + (\theta_m - \omega)^2} + \frac{\xi_m}{\xi_m^2 + (\theta_m + \omega)^2} \right) \right] \quad (61)
 \end{aligned}$$

This equation explicitly expresses  $\mathbf{G}(\omega)$  in terms of eigenvalues and eigenfunctions of  $\mathbf{M}$  and presents an alternate method for numerical calculation of  $\mathbf{G}(\omega)$ . Since  $\mathbf{G}(\omega)$  is expressed as a function of  $\omega$  in a closed form, (61) is particularly useful in a qualitative discussion of  $\mathbf{G}(\omega)$ . If the matrix  $\mathbf{M}$  does not have complex eigenvalues, the second and third summations in (61) drop out. In this case  $\mathbf{G}(\omega)$  contains only terms proportional to  $(\xi_n^2 + \omega^2)^{-1}$  and is a typical Lorentzian curve centered at zero frequency. If the matrix  $\mathbf{M}$  has complex eigenvalues, then  $\mathbf{G}(\omega)$  contains nonzero Lorentzians  $(\theta_n \pm \omega, \text{etc.})$  and may have "peaking" in the spectrum.<sup>26</sup> This property is useful in differentiating kinetic systems, as is discussed in Section VI.A.

## V. Irreversible Thermodynamic Approach

For systems at equilibrium the noise-power-spectrum matrix can be approached from another point of view, namely, irreversible thermodynamics.<sup>20,29</sup> The formulation is based on the so-called fluctuation-dissipation theorem or the generalized Nyquist formula as established by Callen and Greene<sup>30</sup> and others.<sup>31</sup> This theorem states that the spectral densities of the fluctuating extensive thermodynamic parameters are simply  $4k_B\omega^{-2}$  times the real part of admittance functions that relate the thermodynamic forces and fluxes in a periodically perturbed system, where  $k_B$  = Boltzmann constant and  $\omega = 2\pi f$ . Thus, from a purely experimental point of view, if the admittance functions can be determined, the noise spectrum can be readily obtained. Or, if the macroscopic linear transport equations of the system are known, the admittance function can be calculated and hence also the noise spectrum. It is easy to show that the noise-spectrum matrix obtained by the thermodynamic approach is identical to that found by the master-equation method. Extension of this approach to systems at steady

state far from equilibrium can be easily carried out if the Nyquist theorem is properly generalized and a generalized entropy function is properly defined (see below).

### A. The Thermodynamic Forces and Variances for Systems at Equilibrium

Einstein founded the macroscopic theory of thermodynamic fluctuations by suggesting that the entropy of a fluctuating system can be considered to be a function of the instantaneous extensive variables and that the probability distribution function can be considered to be related to the entropy by<sup>24</sup>

$$W(N) = C \exp \left[ \frac{S(N) - S(N^e)}{k_B} \right] \quad (62)$$

where  $C$  is a factor chosen to provide normalization. In the neighborhood of equilibrium, the entropy may be expanded as

$$S = S^e - \frac{1}{2} \sum_{ij} s_{ij}^0 \alpha_i \alpha_j + \text{higher terms} \quad (63)$$

where  $s_{ij}^0 \equiv - \left( \frac{\partial S}{\partial N_i \partial N_j} \right)_e$ . The Einstein treatment of fluctuations then yields

$$W(\alpha) = C \exp \left( - \frac{1}{2k_B} \alpha \cdot s^0 \cdot \alpha \right) \quad (64)$$

It is thus a purely mathematical exercise to calculate the moments of this distribution,

$$\sigma_{ij} = \langle \alpha_i \alpha_j \rangle = k_B (s^0)_{ij}^{-1} \quad (65)$$

or, in matrix form

$$\sigma = \langle \alpha \tilde{\alpha} \rangle = k_B (s^0)^{-1} \quad (66)$$

where  $\tilde{\alpha}$  is a row matrix.

The extensive variable conjugate to  $\alpha_i$  may be defined by<sup>24</sup>

$$F_i \equiv \frac{\partial S}{\partial \alpha_i} \quad (67)$$

The thermodynamic force  $X_i$  [the  $X_i$  here should not be confused with  $X_\beta$  in (11)] conjugate to  $\alpha_i$  and tending to restore the latter to equilibrium is

$$X_i = F_i(N) - F(N^e) = - \sum_j s_{ij}^0 \alpha_j \quad (68)$$

Equation 68 is used later in deriving  $G(\omega)$  through the linear transport equation. Here we want to express  $s^0$  explicitly in terms of equilibrium  $N^e$ .

For chemical reactions, the infinitesimal change of entropy of the system can be expressed by

$$dS = \frac{dE}{T} + \frac{P dV}{T} - \frac{1}{T} \sum_{i=1}^z \mu_i dN_i \quad (69)$$

Substituting (9) into (69), to eliminate the dependent variables, we get

$$dS = \frac{dE}{T} + \frac{P dV}{T} - \frac{1}{T} \sum_{i=1}^x \left\{ \mu_i + \sum_{k=x+1}^z \lambda_{ki} \mu_k \right\} dN_i \quad (70)$$

Thus the intensive variables  $F_i$  can be shown to be

$$F_i \equiv \frac{\partial S}{\partial N_i} = -\frac{1}{T} \left\{ \mu_i + \sum_{k=x+1}^z \lambda_{ki} \mu_k \right\} \quad i = 1, 2, \dots, x \quad (71)$$

Also, the thermodynamic forces become

$$X_i = -\frac{1}{T} \left[ (\mu_i - \mu_i^e) + \sum_{k=x+1}^z \lambda_{ki} (\mu_k - \mu_k^e) \right] \quad i = 1, 2, \dots, x \quad (72)$$

In dilute solutions the chemical potential can be expressed by

$$\mu_i = \mu_i^0 + k_B T \ln N_i \quad (73)$$

where  $\mu_i^0$  is the standard chemical potential of species  $i$ . Near equilibrium

$$\frac{1}{T} (\mu_i - \mu_i^e) = k_B \ln \frac{N_i}{N_i^e} = \frac{k_B \alpha_i}{N_i^e} \quad (74)$$

where  $\alpha_i = N_i - N_i^e$  and  $N_i^e$  is the equilibrium value of  $N_i$ . Substituting (74) into (72), we get

$$X_i = -k_B \left( \frac{\alpha_i}{N_i^e} + \sum_{k=x+1}^z \frac{\lambda_{ki} \alpha_k}{N_k^e} \right) \quad (75)$$

Since the  $\alpha_i$ 's are the deviations from equilibrium values, they must also obey conservation relations similar to (9):

$$\alpha_k = \sum_{j=1}^x \lambda_{kj} \alpha_j \quad k = x+1, x+2, \dots, z \quad (76)$$

Thus, after substituting (76) into (75), we get

$$X_i = -k_B \sum_{j=1}^x \left( \frac{\delta_{ij}}{N_i^e} + \sum_{k=x+1}^z \frac{\lambda_{ki} \lambda_{kj}}{N_k^e} \right) \alpha_j \quad (77)$$

where  $\delta_{ij}$  is the usual Kronecker delta.

From (68) and (77), the  $(i, j)$  element of  $\mathbf{s}^0$  can be identified as

$$s_{ij}^0 = k_B \left( \frac{\delta_{ij}}{N_i^e} + \sum_{k=x+1}^z \frac{\lambda_{ki}\lambda_{kj}}{N_k^e} \right) \quad (78)$$

The variance matrix  $\sigma$  can thus be obtained from (66) with the use of (78).

### B. The Noise-Power-Spectrum Matrix

Near equilibrium the approach toward equilibrium of  $N_i$  follows the linear equation<sup>23</sup>

$$J_i \equiv \frac{dN_i}{dt} = \dot{\alpha}_i = \sum_{j=1}^x L_{ij} X_j \quad (79)$$

where the  $L_{ij}$  are constants that depend on the mechanism and rate constants of the system.

Equation 79 can be inverted to yield

$$X_i = \sum_{j=1}^x R_{ij} \dot{\alpha}_j \quad (80)$$

Substituting (68) into (80), we have, in matrix form,

$$\mathbf{R}\dot{\alpha} + \mathbf{s}^0\alpha = 0 \quad (81)$$

If an external periodic force  $\mathbf{V}(t) = \mathbf{V}_m e^{\bar{i}\omega t}$  ( $\bar{i} = \sqrt{-1}$ ) is applied to the system, the kinetic equations become

$$\mathbf{R}\dot{\alpha} + \mathbf{s}^0\alpha = \mathbf{V}(t) \quad (82)$$

Equation 82 is the basic equation to be solved to obtain the admittance between  $\mathbf{V}(t)$  and  $\dot{\alpha}$ . Differentiating (82) with respect to time, we get

$$\mathbf{R} \frac{d\dot{\alpha}}{dt} + \mathbf{s}^0\dot{\alpha} = \bar{i}\omega \mathbf{V}_m e^{\bar{i}\omega t} \quad (83)$$

The solution of (83) can be easily shown to be<sup>20,29</sup>

$$\dot{\alpha}(t) = \left( \mathbf{R} + \frac{\mathbf{s}^0}{\bar{i}\omega} \right)^{-1} \mathbf{V}(t) \quad (84)$$

Thus the admittance  $\mathbf{Y}(\omega)$  between  $\dot{\alpha}(t)$  and  $\mathbf{V}(t)$  is

$$\mathbf{Y}(\omega) = \left( \mathbf{R} + \frac{\mathbf{s}^0}{\bar{i}\omega} \right)^{-1} \quad (85)$$

The noise-power-spectrum matrix for the variables  $\alpha$  is

$$\mathbf{G}_\alpha(\omega) = 4k_B\omega^{-2} \text{Re} [\mathbf{Y}(\omega)] \quad (86)$$

From (85) it is easy to show that

$$\text{Re } (\mathbf{Y}) = (\mathbf{R}^2 \omega^2 + \mathbf{s}^0 \mathbf{R}^{-1} \mathbf{s}^0)^{-1} \omega^2 \quad (87)$$

as a result

$$\mathbf{G}_a(\omega) = 4k_B(\mathbf{R}\omega^2 + \mathbf{s}^0 \mathbf{R}^{-1} \mathbf{s}^0)^{-1} \quad (88)$$

In general we are interested in the measured quantity  $\mathbf{a}\mathbf{N}$  where  $\mathbf{a}$  is the matrix of measurement indices. Thus (88) becomes

$$\mathbf{G}(\omega) = 4k_B \mathbf{a}(\mathbf{R}\omega^2 + \mathbf{s}^0 \mathbf{R}^{-1} \mathbf{s}^0)^{-1} \tilde{\mathbf{a}} \quad (89)$$

Equation 89 is the final expression for the noise-spectrum matrix. From a purely thermodynamic point of view,  $\mathbf{R}$  can be measured experimentally. However, for chemical reactions with a given mechanism (elementary reactions), the relaxation (or regression) equation is

$$\dot{\alpha} = -\mathbf{M}\alpha \quad (90)$$

Thus, from (81) and (90), one has

$$\mathbf{M} = \mathbf{R}^{-1} \mathbf{s}^0 \quad (91)$$

or

$$\mathbf{R} = \mathbf{s}^0 \mathbf{M}^{-1} \quad (92)$$

and

$$\mathbf{R}^{-1} = \mathbf{M}(\mathbf{s}^0)^{-1} \quad (93)$$

Substituting (92) and (93) into (89) and rearranging the equations, we get

$$\mathbf{G}(\omega) = 4k_B \mathbf{a}(\mathbf{M}^2 + \omega^2 \mathbf{E})^{-1} \mathbf{M}(\mathbf{s}^0)^{-1} \tilde{\mathbf{a}} \quad (94)$$

That (94) is equivalent to (51) can be readily verified with the use of (66).

### C. Nonequilibrium Steady-State Case

For systems at steady state far from equilibrium, the generalized Nyquist theorem in (86) can be shown to become<sup>29</sup>

$$\mathbf{G}_a(\omega) = 2k_B \text{Re } \{ \mathbf{Y}(\omega) + \tilde{\mathbf{Y}}(\omega) \} \quad (95)$$

where  $\tilde{\mathbf{Y}}(\omega)$  is the transpose of  $\mathbf{Y}(\omega)$ . Thus, if the thermodynamic forces of the system are properly defined, the noise spectrum matrix can be obtained by measuring the admittance function  $\mathbf{Y}(\omega)$ .

In general, thermodynamics is not applicable to systems far from equilibrium. However, it has been suggested recently that steady-state thermodynamic functions may be defined by a generalized entropy function  $\Sigma$ , which in turn is determined by the variances of the extensive variables of the



system by<sup>32,33</sup>

$$k_B(\sigma^{-1})_{ij} = \left( \frac{\partial^2 \Sigma}{\partial N_i \partial N_j} \right)_s \equiv \Sigma_{ij}^0 \quad (96)$$

where  $\sigma$  is the variance matrix of the system, which may be measured experimentally. In particular, the forces in this case can be derived from (96):

$$X_i = - \sum_j \Sigma_{ij}^0 \alpha_j \quad (97)$$

where  $\alpha_j = N_j - N_j^s$  and  $N_j^s$  is the steady-state value. Thus we have a formal way of defining the forces in a nonequilibrium steady state. One must note that the forces defined by (97) and (96) are very dependent on the mechanism of the system under consideration and that the forces are, in general, not related to the usual chemical potentials as shown in (72). Linear first-order kinetic systems are exceptions. In this case both (73) for the chemical potentials and (72) for the forces are applicable to each species in the system.<sup>33</sup>

To show that the noise-spectrum matrix obtained from (95) is identical to (47) from the stochastic approach, we follow the same procedure as developed in the previous section. With the replacement of  $s^0$  by  $\Sigma^0$ , (79) to (85) are applicable to steady state as well. Thus the admittance function becomes

$$Y(\omega) = \left( \mathbf{R} + \frac{\Sigma^0}{i\omega} \right)^{-1} \quad (98)$$

It must be pointed out here that the difference in  $\mathbf{R}$  between an equilibrium state [see (85)] and a nonequilibrium steady state [see (98)] is that  $\mathbf{R}$  is symmetrical (Onsager's reciprocal relations)<sup>34</sup> in the former case and unsymmetrical in the latter case. Thus, for an equilibrium system,  $\tilde{\mathbf{Y}}(\omega) = \mathbf{Y}(\omega)$  and (95) reduces to (86).

Substituting (98) into (95) and taking into account the measurement index matrix  $\mathbf{a}$  gives for the noise-spectrum matrix

$$\mathbf{G}(\omega) = 2k_B \mathbf{a} \{ (\mathbf{R}\omega^2 + \Sigma^0 \mathbf{R}^{-1} \Sigma^0)^{-1} + (\tilde{\mathbf{R}}\omega^2 + \Sigma^0 \tilde{\mathbf{R}}^{-1} \Sigma^0)^{-1} \} \tilde{\mathbf{a}} \quad (99)$$

With the aid of (96), equation 99 can easily be proved to be identical to (47).

## VI. APPLICATIONS OF NOISE ANALYSIS TO GENERAL KINETIC PROBLEMS

### A. Differentiation Between Systems

As is mentioned in Section IV.D, the existence of complex eigenvalues in the matrix  $\mathbf{M}$  may cause  $\mathbf{G}(\omega)$  to show "peaking" at a frequency other than zero (Fig. 2). It is well known in the field of relaxation theory<sup>35</sup> that, for systems whose elementary reactions are *regular*, the complete relaxation

matrix, involves all species in the system, can always be reduced to a real symmetrical matrix by a similarity transformation. Since the eigenvalues of a real symmetric matrix are always real, matrix  $\mathbf{M}$  has only real eigenvalues. That is, the noise spectrum of an equilibrium system (linear or nonlinear) is always of the simple Lorentzian type (Fig. 2a). On the other hand, for systems with *nonregular* reactions, the matrix  $\mathbf{M}$  may have complex eigenvalues and the noise spectrum may be of the "peaking" Lorentzian type. One must note that not all *nonregular* kinetic systems will give peaking spectra. However, if the noise spectrum shows peaking the underlying elementary reactions are definitely not regular.

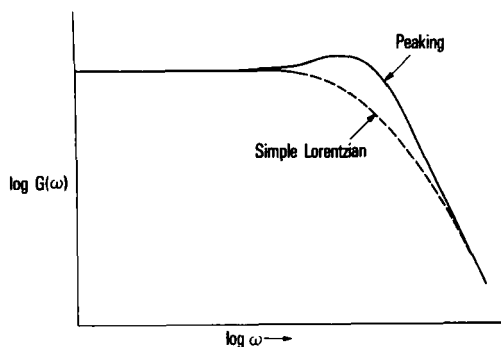


Fig. 2. Schematic drawing of an ordinary Lorentzian power spectrum and a "peaking" spectrum.

Recently Fishman and his collaborators<sup>6</sup> have observed the peaking phenomenon in some current and voltage noise-power spectra of squid axon membranes. If these phenomena are really derived from the conductance fluctuations of potassium (or sodium) channels, then the usual Hodgkin-Huxley model<sup>37</sup> (see below) cannot be right because it is a linear equilibrium model<sup>38</sup> and involves only regular reactions.

Another function that is capable of differentiating between various systems is the time correlation matrix  $\mathbf{C}(t)$ . As shown in (45),  $\mathbf{C}(t)$  is symmetric when  $\mathbf{M}\sigma = \sigma\tilde{\mathbf{M}}$ . That is,  $\mathbf{C}(t)$  ( $t \neq 0$ ) is an unsymmetric matrix, except the system is at equilibrium. Thus, by testing the symmetry of  $\mathbf{C}(t)$ , one can determine whether or not the system is at equilibrium.

The results of this section are summarized in Table I according to the classification of kinetic systems discussed in Section III.A.

TABLE I  
Differentiation of Kinetic Systems by  $G(\omega)$  and  $C(t)$

	Regular system			Nonregular system		
	Closed	Open $J_i^{ex}=0$	Open $J_i^{ex}\neq 0$	Closed	Open $J_i^{ex}=0$	Open $J_i^{ex}\neq 0$
Stationary state	Equilibrium	Equilibrium	Steady state	Steady state (cycling)	Steady state	Steady state
$G(\omega)$	Nonpeaking	Nonpeaking	Nonpeaking	May have peaking	May have peaking	May have peaking
$C(t)$ $t > 0$	Symmetric	Symmetric	May be non-symmetric	May be non-symmetric	May be non-symmetric	May be non-symmetric

### B. Determination of the Number of Independent Stochastic Variables in Kinetic Systems

For systems at equilibrium, the number of independent stochastic variables (ISV) is exactly equal to the number of independent elementary reactions of the system. In general, the number of ISV of a complex system is determined by the number of species and the number of elementary reactions in the system. Thus a knowledge of the number of ISV is important in characterizing the mechanism of an unknown kinetic system.

Since the number of independent stochastic variables is a kinetic property of the system, it can never be obtained by equilibrium measurements. However, fluctuation measurements are able to provide this information. This result is based on a theorem recently proved by Plesner and Chen,<sup>36</sup> which states: the variance matrix  $C(0)$  is nonsingular [the determinant of  $C(0)$  is not zero] if the order of  $C(0)$  is less than or equal to the number of independent stochastic variables of the system and becomes singular if the order of  $C(0)$  exceeds this number. Thus the largest rank of  $C(0)$  is exactly the number of ISV of the system.

As shown in Section VI.A, the order of  $C(0)$  is equal to the number of independent measurements. Thus, if the number of ISV of the system is large, the main difficulty of this method will be to find sufficient numbers of independent fluctuation measurements. Provided this barrier is overcome, the present method should be very useful in model differentiation in biological

systems. For example, the number of subunits in a potassium (or sodium) channel, which determines the number of transition reactions among the states, may be obtained by this method. In usual Hodgkin–Huxley models the number of subunits in a potassium channel is taken to be four.<sup>37</sup> However, as shown by Hill and Chen,<sup>38</sup> models with the number of subunits ranging from 3 to 10 can all fit Hodgkin–Huxley's voltage clamp data.

### C. Determination of Rate Constants

A most interesting and useful application of the present formalism may be in the evaluation of the kinetic rate constants of complex chemical reactions from the noise-power spectra of concentration fluctuations at equilibrium or at steady state. As shown in (47) and (51), there exists a direct relation between the relaxation matrix  $\mathbf{M}$  and the noise-power spectrum matrix. In particular, when  $\omega = 0$ , (47) and (51) become

$$\mathbf{G}(0) = 2\mathbf{a}\mathbf{M}^{-1}\boldsymbol{\sigma}\tilde{\mathbf{a}} + 2\mathbf{a}\boldsymbol{\sigma}\tilde{\mathbf{M}}^{-1}\tilde{\mathbf{a}} \quad (100)$$

$$\mathbf{G}(0) = 4\mathbf{a}\mathbf{M}^{-1}\boldsymbol{\sigma}\tilde{\mathbf{a}} \quad (\text{equilibrium case}) \quad (101)$$

The variance matrix  $\boldsymbol{\sigma}$  in the above equations can be replaced by  $\mathbf{C}(0)$  [see (45)]. Thus

$$\mathbf{G}(0) = 2\mathbf{a}\mathbf{M}^{-1}\mathbf{a}^{-1}\mathbf{C}(0) + 2\mathbf{C}(0)\tilde{\mathbf{a}}^{-1}\tilde{\mathbf{M}}^{-1}\tilde{\mathbf{a}} \quad (102)$$

$$\mathbf{G}(0) = 4\mathbf{a}\mathbf{M}^{-1}\mathbf{a}^{-1}\mathbf{C}(0) \quad (\text{equilibrium case}) \quad (103)$$

With given  $\mathbf{a}$  and measured  $\mathbf{G}(0)$  and  $\mathbf{C}(0)$ , the matrix  $\mathbf{M}$  can in principle be evaluated from (102) and (103), thus yielding the rate constants of the reactions.

It should be noted that, to be able to evaluate all the rate constants from noise measurements, one must have the complete  $\mathbf{a}$  matrix so that the order of matrix  $\mathbf{G}(0)$  is equal to the order of  $\mathbf{M}$  [ $y = x$ , where  $y$  is the total number of independent  $\mathbf{a}$  values; see (11)]; that is, a complete set of multi-spectral noise measurements is required.<sup>19</sup> Optical methods, such as optical absorbance, fluorescence, optical rotation, and circular dichroism, are most suitable for future experiments, since several wavelengths can be monitored simultaneously.

## VII. APPLICATIONS TO CHANNEL CONDUCTANCE NOISE IN MEMBRANES

In this section we present some examples illustrating how to obtain the kinetic parameters of an ionic channel in membranes by noise analysis. We consider “channel conductance noise”—the type of noise caused by fluctuations in the number of channels of different conductance states. As shown in the previous section, kinetic parameters of a complex kinetic system can be

obtained from noise analysis only when sufficient simultaneous and independent noise measurements are available. Thus, except for simple systems with only one ISV, electrical-noise measurement alone is unable to yield all the kinetic parameters of a complex system. However, noise data may still be useful in differentiating kinetic models.

### A. Lipid Bilayer Membranes with Ionic Channels

It is well known that artificial lipid bilayer membranes, although being almost impermeable to inorganic ions, can acquire electrical conductances comparable to those of natural biological membranes in the presence of a large number of substances that form channels (or pores) across the hydrocarbon region of the membranes.<sup>39</sup> The materials so far known to have this channel-forming ability include EIM<sup>40</sup> (excitation inducing material), gramicidin A,<sup>41</sup> alamethicin,<sup>41,42</sup> nystatin,<sup>43</sup> and monozomycin.<sup>44</sup> According to the number of conducting states of a channel, as resolved from single-channel studies, these channel-forming materials may be classified as single-conductance type (EIM, gramicidin A) and multiconductance type (alamethicin, nystatin, monozomycin). Currently, conformational transitions and aggregation reactions of these materials inside the membrane are considered to be the mechanism of the formation of channels. For simple systems such as EIM and gramicidin A, the kinetic properties of channels may be obtained from single-channel studies. Noise analysis on a large number of channels can also yield kinetic parameters. For gramicidin A this has been discussed recently using time correlation functions.<sup>12,13</sup> An application of the noise-power-spectrum method as developed in previous sections is presented here.

The formation of a gramicidin channel is assumed to follow the reaction<sup>12</sup>:



where A is a gramicidin monomer and D is a dimer in the membrane. D is the state in which ions can be transported. The exchanges of the A and D inside the membrane with those in the bathing solution are assumed to be negligible.<sup>12</sup> Thus the total number of gramicidin molecules inside the membrane is considered to be constant. The unit conductance  $\bar{g}$  of D can be obtained from single-channel studies. It has been found that  $\bar{g}$  is fairly independent of membrane thickness (varied by changing the membrane composition) and of temperature ( $Q_{10} \simeq 1.4$ ) and has typical values of  $2 \times 10^{-11}$  and  $4.8 \times 10^{-11}$  mho in 1 M NaCl and 1 M KCl, respectively.<sup>41</sup> The rate constants  $k$  and  $k'$  are to be obtained from noise spectral analysis.

In (104) the system has two species, A and D but has one conservation relation,  $dN_A + 2dN_D = 0$ . Thus it has only one ISV. The relaxation matrix M

becomes a scalar quantity in this case. According to (29), and with  $N_D$  as the independent variable,

$$M = 4kN_A^e + k' = 4(kk'N_D^e)^{1/2} + k' \quad (105)$$

where  $N_D^e$  is the equilibrium (or stationary) value of  $N_D$  in the membrane. The mean conductance of the membrane at equilibrium is

$$X = \bar{g}N_D^e \quad (106)$$

Substituting (106) into (105), we get

$$M = 4\left(\frac{kk'}{\bar{g}}\right)^{1/2} X^{1/2} + k' \quad (107)$$

Thus, if the values of  $M$  and  $X$  at two gramacidin A concentrations can be measured, the rate constants  $k$  and  $k'$  can be calculated from (107). Alternatively, one may obtain the rate constants by plotting  $M$  versus  $X^{1/2}$ . The value of  $M$  at  $X=0$  is exactly equal to  $k'$  and the slope of the straight line is equal to  $4(kk'/\bar{g})^{1/2}$ . With given  $\bar{g}$ ,  $k$  can be calculated from the slope.

The mean conductance  $X$  is obviously a measurable quantity. We have to show that  $M$  can also be obtained experimentally. From (103)  $M$  can be shown to be related to  $G(0)$  and  $C(0)$  as

$$M = 4a^{-1}C(0)G(0)^{-1}a$$

For the one ISV case,  $M$  becomes a scalar quantity:

$$M = 4C(0)G(0)^{-1} \quad (109)$$

Thus  $M$  can be directly obtained from the measured  $G(0)$  (conductance noise-power spectrum at zero frequency) and  $C(0)$  (total conductance fluctuations).

In general, for aggregation reactions involving  $n$  monomers



Equation 107 becomes

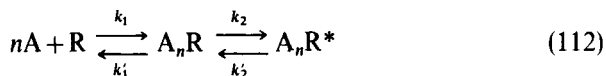
$$M = 2nk\left(\frac{k'}{k\bar{g}}\right)^{(n-1)/n} X^{(n-1)/n} + k' \quad (111)$$

Thus a plot of  $M$  versus  $X^{(n-1)/n}$  will yield  $k$  and  $k'$  (with given  $\bar{g}$ ).

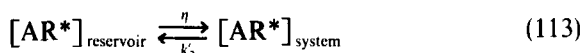
### B. Conductance Fluctuations at Postsynaptic End Plates of Neuromuscular

A current kinetic model for the activation of ionic channels at postsynaptic end-plates by transmitter (acetylcholine, ACh) molecules can be represented

by<sup>9,10,45,46</sup> (for a comprehensive treatise see Ref. 45)



where A denotes the acetylcholine and R the receptor.  $A_nR^*$  represents the open conformation of the complex in which ion transport takes place. If the concentration of ACh in the junctional space is very low and the binding reaction of ACh to receptors is assumed to be very fast ( $k_1, k'_1 \gg k_2, k'_2$ ), Equation 112 can be reduced to a simpler one-ISV *open* system as<sup>1,10</sup>



where  $\eta = k_1 k_2 [A]^n / k'_1$  and  $[A]$  is the concentration of ACh. Equation 113 is equivalent to a random process fluctuating between open and closed states with Poisson statistics and is used by Stevens and his colleagues to interpret the kinetic and noise data.<sup>10,46</sup> Since there is only one ISV in (113), the rate parameters  $\eta$  and  $k'_2$  can be elucidated by noise analysis. Unlike the lipid bilayer membrane case, fluctuations of a single channel are difficult to measure at neuromuscular junctions (single-channel fluctuations at extra-junctional membranes of denervated muscle cells have been reported recently<sup>47</sup>). Therefore, the unit conductance of  $A_nR^*$ ,  $\bar{g}$ , is also an unknown quantity to be evaluated from noise analysis.

Let  $N^e$  be the number of  $A_nR^*$  at the end plate (the system) at stationary (equilibrium) state. The total conductance of the system is

$$X = aN^e = \bar{g}N^e \quad (114)$$

From (29), we have for the reaction in (113)

$$M = \left[ -\frac{\partial}{\partial N} (\eta - k'_2 N) \right]_{N^e} = k'_2 \quad (115)$$

Thus  $k'_2$  can be obtained from (109) and (115) with measured  $G(0)$  and  $C(0)$ .

From (38) we get  $B$  for the scheme in (113):

$$B = \eta + k'_2 N^e = 2k'_2 N^e \quad (116)$$

With (115) and (116), the variance  $\sigma$  can be obtained from (35):

$$\sigma = \frac{1}{2} M^{-1} B = N^e \quad (117)$$

Equation 117 confirms that the kinetic scheme in (113) is a Poisson process. Substituting (117) into (15), we get the total fluctuations

$$C(0) = a^2 \sigma = \bar{g}^2 N^e \quad (118)$$

With the aid of (114), the unit conductance becomes

$$\bar{g} = \frac{C(0)}{X} \quad (119)$$

Thus  $\bar{g}$  can be obtained from the slope of the linear relation between  $C(0)$  and  $X$  by varying the ACh concentration or the membrane potential.

Alternatively, one may obtain  $k'_2$  and  $\bar{g}$  from the noise-power spectrum. The noise-power spectrum can be obtained from (51):

$$G(\omega) = \frac{4a^2 M \sigma}{M^2 + \omega^2} = \frac{4\bar{g}^2 k'_2 N^e}{(k'_2)^2 + \omega^2} = \frac{4\bar{g} k'_2 X}{(k'_2)^2 + \omega^2} \quad (120)$$

It is obvious that  $G(\omega_c) = \frac{1}{2}G(0)$  where  $\omega_c = k'_2$ . That is,  $k'_2$  is exactly equal to the frequency at which  $G(\omega)$  is one-half of  $G(0)$ . With the  $k'_2$  value known,  $\bar{g}$  can be calculated easily from (120) with given  $X$ .

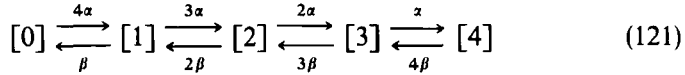
### C. Model Differentiation of Potassium Channels in Nerve Membranes

For systems with more than one ISV, electrical conductance noise analysis alone cannot yield rate parameters. However, it may be useful in model differentiation. For linear (first-order) multistate channel models, one important question is whether the channels have only one conducting state or many conducting states with different unit conductances. For example, in the original Hodgkin-Huxley formalism of nerve membranes,<sup>37</sup> a potassium channel can be viewed as a complex unit composed of four independent subunits, each of which can exist in one of two states,  $i$  and  $ii$ . The channel is open to  $K^+$  only when all four subunits are in state  $ii$ . Thus an HH  $K^+$  channel is a multistate linear kinetic system with a single-conducting state.<sup>48</sup> But it is somewhat unreasonable, physically, to assume that a  $K^+$  channel is "open" only if all subunits are in state  $ii$ . Let us suppose instead that if one subunit of the complex is in state  $i$ , there is an additional steric or electrostatic energy barrier  $W$  to passage of a potassium ion, with the result that the conductance of an all- $ii$  channel is reduced by a factor  $\kappa = e^{-W/kT} < 1$ . If two subunits are in state  $i$ , the simplest and most likely assumption is that the barrier is  $2W$  and hence that the conductance reduction factor is  $\kappa^2$ , and so forth. Thus the single-conductance HH model is extended to a *multiconductance* model. Another simple alternative is that the reduction factors are  $\kappa, \kappa/2, \kappa/3, \dots$ . We hereafter refer to the former case as a  $\kappa$  model and to the latter as a  $\kappa'$  model. Note that the original HH model is a special case of these models with  $\kappa = 0$ . As shown by Chen and Hill,<sup>27</sup> it is always possible to fit the potassium conductance kinetics of the Hodgkin-Huxley voltage-clamp experiment with a  $\kappa$  (or  $\kappa'$ ) model of arbitrary  $\kappa$  value if the kinetic parameters of the subunits are adequately adjusted. That is, it is not possible to distinguish between a single-conducting model and a multiconducting



model using kinetic data alone. However, it has been shown recently that differentiation may be accomplished by noise analysis.<sup>8</sup> A brief discussion is given below.

The kinetic scheme describing the transitions among the channel states of a four-subunit channel (HH formalism) can be expressed as<sup>4,8</sup>



where [0] represents the channel state with all four subunits in  $i$ , [1] represents the state with one subunit in  $ii$  and the other three subunits in  $i$ , and so forth. The rate constants  $\alpha$  and  $\beta$  refer to the first-order transitions of a subunit between  $i$  and  $ii$  and are functions of membrane potential. Thus, at fixed membrane potential, the conductance of the membrane is determined by the values of  $\alpha$  and  $\beta$ . In the Hodgkin-Huxley model, only [4] is open for  $K^+$  transport. In general we assume all five states in (121) can conduct  $K^+$ , but with varying conductivities ( $\kappa$  or  $\kappa'$  models, see above).

Let [4] be the state that has the largest unit conductance  $\bar{g}_K$  and  $a_j = \bar{g}_K e_j$  with  $e_j = a_j/a_4$  ( $j=0, 1, \dots, 4$ ). Then the total conductance of the membrane can be expressed as

$$X = \sum_{j=0}^4 a_j N_j^e = N \sum_{j=0}^4 a_j p_j^e = N \bar{g}_K \bar{e} \quad (122)$$

where

$$\bar{e} = \sum_{j=0}^4 e_j p_j^e$$

$N$  is the total number of channels in the membrane and  $p_j^e$  is the stationary-state (equilibrium) probability of a channel in state  $j$ . The variance  $\sigma_{ij}$  for the kinetic system in (121) has been shown to have the form<sup>19,27</sup>

$$\sigma_{ij} = N p_i^e \delta_{ij} - N p_i^e p_j^e \quad (123)$$

where  $\delta_{ij}$  is the Kronecker delta. With (123) and using  $\mathbf{a} = \bar{g}_K(e_0, e_1, e_2, e_3, e_4)$ , we can obtain the total conductance fluctuation  $C(0)$  from (15):

$$C(0) = \mathbf{a} \sigma \mathbf{a} = N [\bar{e}^2 - \bar{e}^2] \bar{g}_K^2 \quad (124)$$

where

$$\bar{e}^2 = \sum_{j=0}^4 e_j^2 p_j^e$$

After eliminating  $N$  from (124) with the use of (122), we get

$$\bar{g}_K \gamma(V) = E(V) \quad (125)$$

with

$$\gamma(V) = \frac{\overline{e^2} - \bar{e}^2}{\bar{e} - \bar{e}^2} \quad (126)$$

and

$$E(V) = \frac{C(0)}{X(1 - \bar{e})} \quad (127)$$

As discussed in Ref. 8, the  $E(V)$  function in (127) can be measured experimentally and is thus model independent. On the contrary,  $\gamma(V)$  is a completely model-dependent quantity. Since  $\bar{g}_K$  is a constant, (125) implies that the functional form of  $\gamma(V)$  must be identical to that of  $E(V)$ . Thus, if the measured  $E(V)$  is available, the  $\gamma(V)$  in (126) can be used to differentiate models. After the model is determined, the single-channel conductance  $\bar{g}_K$  can be evaluated from (125) and the total number of channels  $N$  in the membrane can be obtained from (122).

To show that  $\gamma(V)$  is model dependent, the  $\gamma(V)$  functions of the  $K^+$  channels of both the squid axon and the frog node of Ranvier have been calculated for both  $\kappa$  and  $\kappa'$  models mentioned above. As shown in Fig. 3,

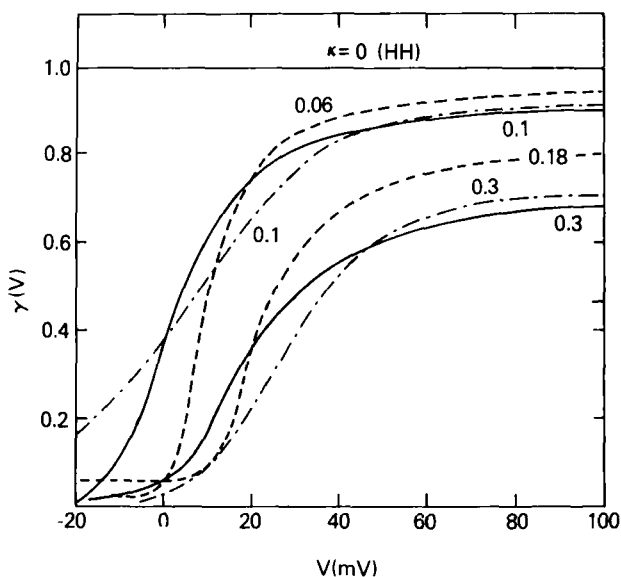


**Fig. 3.**  $\gamma(V)$  as a function of  $V$  for  $K^+$  channels with  $x=4$ .  $V=0$  at rest;  $V>0$  for depolarizations. The values of  $\kappa$  are shown in the figure: (—) modified  $\kappa$  model for the squid axon; (---) modified  $\kappa'$  model for the squid axon; (- - -)  $\kappa$  model for the frog node of Ranvier. The  $\gamma(V)$  for the Hodgkin-Huxley model ( $\kappa=0$ ) is a constant independent of  $V$ .

$\gamma(V)$  for the HH model (or single-conductance model) is independent of membrane potential. For all nonzero  $\kappa$  (or  $\kappa'$ ) values considered,  $\gamma(V)$  is very small near and below the rest potential and rises very rapidly upon depolarization. At high depolarizations  $\gamma(V)$  is almost constant and parallel to the horizontal line of the HH model. It is not unexpected that  $\gamma(V)$  is very small at resting potential or below since the channels will stay mostly in states with small  $e$  values so that  $\bar{e}^2$  is very small compared to  $\bar{e}$ . The sharp increase of  $\gamma(V)$  upon depolarization means that the equilibrium distribution of channel states changes in such a way that  $\bar{e}^2$  increases faster than  $\bar{e}$  [see (126)]. At high depolarizations the main channel state is state 4 with  $e_4 = 1$ . Thus the increase of  $\bar{e}^2$  is roughly equal to that of  $\bar{e}$ , which is in turn roughly equal to the change of  $p_4$ . This accounts for the leveling-off behavior of  $\gamma(V)$  at high depolarizations. Undoubtedly, the sigmoid shape of  $\gamma(V)$  as found in Fig. 3 derives from the sigmoid nature of the potassium channel conductance at stationary state.

The fact that the  $\gamma(V)$  curve for a nonzero  $\kappa$  model is very different from a horizontal line at moderate depolarizations ( $V < 20$  mV, for example) suggests that this function can be used to distinguish an HH (single-conductance) model from a  $\kappa$  or  $\kappa'$  (multiconductance) model. Or, if the measured noise data are accurate enough, one may even be able to determine the  $\kappa$  values by comparing the measured  $E(V)$  and the calculated  $\gamma(V)$ . Note that the crucial region for model differentiation is near the rest potential area. Therefore, for practical model testing, it is important to have noise measurements in that region.

As discussed in Ref. 8, when the present analysis was applied to the frog node of Ranvier, it was found that the potassium channels may have multiconductance states and are therefore not of the Hodgkin-Huxley type.

#### ACKNOWLEDGMENT

I am much indebted to Dr. Terrell Hill for his valuable suggestions and encouragement during the writing of this chapter and for his reading of the manuscript.

#### References

1. A. A. Verveen and H. E. Derksen, *Kybernetik*, **2**, 152 (1965).
2. H. M. Fishman, *Proc. Natl. Acad. Sci. US*, **70**, 876 (1973).
3. E. Siebenga, A. Meyer, and A. A. Verveen, *Pflügers Arch. Ges. Physiol.*, **341**, 97 (1973); E. Siebenga, J. De Goede, and A. A. Verveen, *op. cit.*, **351**, 25 (1974).
4. E. Wanke, L. J. De Felice, and F. Conti, *Pflügers Arch. Ges. Physiol.*, **347**, 63 (1974).
5. F. Conti, L. J. De Felice, and E. Wanke, *J. Physiol.*, **248**, 45 (1975).
6. H. M. Fishman, L. E. Moore, and D. J. M. Poussart, *J. Membrane Biol.*, **24**, 305 (1975).
7. T. Begenisich and C. F. Stevens, *Biophys. J.*, **15**, 843 (1975).
8. Y. Chen, *Biophys. J.*, **16**, 965 (1976).
9. B. Katz and R. Miledi, *J. Physiol.*, **224**, 665 (1972); **230**, 707 (1973); **231**, 549 (1973); **249**, 269 (1975).

10. C. R. Anderson and C. F. Stevens, *J. Physiol.*, **235**, 655 (1973).
11. D. Colquhoun, V. E. Dionne, J. H. Steinbach, and C. F. Stevens, *Nature*, **253**, 204 (1975).
12. H. A. Kolb, P. Läuger, and E. Bamberg, *J. Membrane Biol.*, **20**, 133 (1975).
13. H. P. Zingsheim and E. Neher, *Biophys. Chem.*, **2**, 197 (1974); E. Neher and H. P. Zingsheim, *Pflügers Arch. Ges. Physiol.*, **351**, 61 (1974).
14. L. E. Moore and E. Neher, *J. Membrane Biol.*, **27**, 347 (1976).
15. A. A. Verveen and L. J. De Felice, *Prog. Biophys. Mol. Biol.*, **28**, 189 (1974).
16. F. Conti and E. Wanke, *Q. Rev. Biophys.*, **8**, 451 (1975).
17. T. L. Hill, *Proc. Natl. Acad. Sci. US*, **64**, 267 (1969); **65**, 409 (1970).
18. T. L. Hill, *Free Energy Transduction in Biology*, Academic Press, New York, 1977.
19. Y. Chen, *Proc. Natl. Acad. Sci. US*, **72**, 3807 (1975).
20. K. M. Van Vliet and J. R. Fassett, in *Fluctuation Phenomena in Solids*, R. E. Burgess, Ed., Academic Press, New York, 1965, Chap. 7.
21. J. Keizer, *J. Theoret. Biol.*, **49**, 323 (1975); *J. Chem. Phys.*, **63**, 398 (1975).
22. R. H. Fowler, *Statistical Mechanics*, Cambridge University Press, London, 1929.
23. T. L. Hill, *Thermodynamics for Chemists and Biologists*, Addison-Wesley, Reading, Mass., 1968 Chap. 7.
24. M. Lax, *Rev. Mod. Phys.*, **32**, 25 (1960).
25. Y. Chen, *J. Theoret. Biol.*, **65**, 357 (1977).
26. Y. Chen, *J. Theoret. Biol.*, **55**, 229 (1975).
27. Y. Chen and T. L. Hill, *Biophys. J.*, **13**, 1276 (1973).
28. S. L. Ross, *Differential Equations*, Blaisdell, New York 1964, Chap. 7.
29. Y. Chen, manuscript in preparation.
30. H. B. Callen and R. F. Greene, *Phys. Rev.*, **86**, 141 (1952); R. F. Greene and H. B. Callen, *op. cit.*, **88**, 150 (1952).
31. R. Kubo and K. Tomita, *J. Phys. Soc. Japan*, **9**, 888 (1954).
32. J. Jähnig and P. H. Richter, *J. Chem. Phys.*, **64**, 4645 (1976).
33. J. Keizer, *J. Chem. Phys.*, **65**, 4431 (1976).
34. S. R. De Groot and P. Mazur, *Nonequilibrium Thermodynamics*, North-Holland, 1962, Chap. 4.
35. G. Schwarz, *Rev. Mod. Phys.*, **40**, 206 (1968).
36. I. W. Plesner and Y. Chen, *J. Chem. Phys.* in press.
37. A. L. Hodgkin and A. F. Huxley, *J. Physiol.*, **117**, 500 (1952).
38. T. L. Hill and Y. Chen, *Biophys. J.*, **12**, 948 (1972).
39. R. Fettiplace, L. G. M. Gordon, S. B. Hladky, J. Requena, H. P. Ringsheim, and D. A. Haydon, in *Methods in Membrane Biology*, Vol. 4, E. D. Korn, Ed., Plenum Press, New York, 1975.
40. P. Mueller and D. O. Rudin, *J. Theoret. Biol.*, **4**, 268 (1963).
41. S. B. Hladky and D. A. Haydon, *Nature*, **225**, 451 (1970); *Biochim. Biophys. Acta*, **274**, 294 (1972).
42. M. Eisenberg, J. E. Hall, and C. A. Mead, *J. Membrane Biol.*, **14**, 143 (1973); L. G. M. Gordon and D. A. Haydon, *Biochim. Biophys. Acta*, **255**, 1014 (1972).
43. A. Case, A. Finkelstein and V. Krespi, *J. Gen. Physiol.*, **56**, 100 (1970); A. Finkelstein and R. Holz, in *Membranes: A Series of Advances*, G. Eisenman, Ed., Dekker, New York, 1972.
44. R. U. Muller and A. Finkelstein, *J. Gen. Physiol.*, **60**, 263, 285 (1972).
45. P. W. Gage, *Physiol. Rev.*, **56**, 177 (1976).
46. K. L. Magleby and C. F. Stevens, *J. Physiol.*, **223**, 151, 173 (1972).
47. E. Neher and B. Sakmann, *Nature*, **260**, 799 (1976).
48. T. L. Hill and Y. Chen, *Proc. Natl. Acad. Sci. US*, **68**, 1711, 2488 (1971).

# **MATHEMATICAL MODELING OF TRANSPORT OF LIPID-SOLUBLE IONS AND ION-CARRIER COMPLEXES THROUGH LIPID BILAYER MEMBRANES**

**ROBERT DE LEVIE**

*Department of Chemistry, Georgetown University,  
Washington, D.C.*

## **CONTENTS**

I. Introduction . . . . .	100
II. The Continuum Model . . . . .	101
A. General Relations . . . . .	101
B. The Steady-State Constant-Field Approximation . . . . .	103
C. Constant-Field Approximation for Potential-Step Measurements . . . . .	105
D. Constant-Field Approximation for Small-Amplitude Sinusoidal Signals . . . . .	105
E. Boundary Conditions . . . . .	106
F. Example: Ionic Displacement Charge Density for Membrane-Soluble Ions . . . . .	110
G. Example: Low-Frequency Admittance for Membrane-Soluble Ions . . . . .	111
III. The Single-Barrier Model . . . . .	114
A. General Approach . . . . .	114
B. Boundary Conditions . . . . .	116
C. Example: Steady-State and Transient Response for Ion Transport by Membrane-Confined Carriers . . . . .	116
D. Example: Admittance for Membrane-Soluble Ions . . . . .	117
IV. More Elaborate Models . . . . .	118
A. Comparison of the Preceding Models . . . . .	118
B. Physical Basis for Modifications . . . . .	120
C. Modified Models . . . . .	122
D. Complicating Factors . . . . .	123
E. Adsorption Isotherm . . . . .	125
V. Conclusion . . . . .	126
Appendix A. Second-Order Estimate of the Electric Field . . . . .	127
Appendix B. The Constant Concentration Approximation . . . . .	128
Appendix C. On the Ionic-Displacement Charge Density . . . . .	128
Appendix D. Response to Various Small-Amplitude Perturbations . . . . .	129
Appendix E. Equivalent Circuit Representations . . . . .	130
Appendix F. The Shape of Intrinsic Current-Voltage Curves . . . . .	131
Appendix G. Glossary of symbols used . . . . .	133
Acknowledgment . . . . .	135
References . . . . .	135

\*This work was supported by NIH grant GM 22296-02 and by AFOSR grant 76-3027.

## I. INTRODUCTION

Biological membranes provide a hydrophobic barrier to transport of ions from one aqueous solution to another. Ions can penetrate such barriers by one of several mechanisms. We focus attention here on the solution of ions in the hydrophobic phase, and their subsequent motion through that phase. Another mechanism makes use of special molecular structures, so-called channels or pores, which reach from one side of the hydrophobic barrier to the other and provide a hydrophilic pathway for ion transport. In both cases the potential-energy profile along the path traveled by the ion will determine its permeation speed. With pores, however, the statistics of pore opening and closing are superimposed and are often the predominant effect. The detailed description of the latter is still unfolding.<sup>1-15</sup>

In biological membranes the hydrophobic barrier to ion permeation is believed to be located inside a layer only two molecules thick, the plasma membrane or lipid bilayer.<sup>16-18</sup> Since 1962 its properties have also been studied in a convenient model system, the artificial black lipid membrane,<sup>19-25</sup> which is of comparable dimensions, that is, two monolayers of lipid plus a residue<sup>26,27</sup> of some nonpolar solvent (chloroform, decane, vaseline, etc.) used in its formation. As a consequence of the extreme thinness (a few nanometers) of the hydrophobic barrier, electroneutrality requirements are relaxed, so that ions of one kind can permeate the membrane, unaccompanied by counterions. As most studies of ion transport through ultrathin lipid membranes have been concerned with ions of one kind only, we restrict the discussion to that case.

Since the membranes considered here are so thin, they can be considered from two extreme points of view, namely, that of a thin, homogeneous, macroscopic phase and that of a mere interfacial barrier. The former characterization would be most appropriate for a membrane thickness of, for example, 30 nm, and the latter for one of, say, 0.3 nm, but neither one can be expected to be very satisfactory for a membrane thickness of 3 nm. We outline here both limiting approaches, and then briefly discuss a sampling of the many intermediate models that incorporate some more detailed aspects of the hydrophobic barrier in lipid membranes.

The present treatment is concerned with the mathematical description of nonconvective ion transport, as measured most conveniently in terms of electrical properties, and dependence of these properties on chemical and physical parameters such as concentration and time. This topic has been discussed in several recent reviews.<sup>28-33</sup> We focus here mostly on the mathematical modeling of the continuum approach. For more chemical and mechanistic aspects the reader might want to consult Refs. 34 to 42.

## II. THE CONTINUUM MODEL

### A. General Relations

In its simplest form, the continuum model is based on a description in terms of distance-invariant macroscopic parameters, such as dielectric constant  $\epsilon$ , ionic diffusion coefficient  $D$  and standard chemical potential  $\mu^\ominus$ . Taking into account only diffusion and migration, but not osmotic forces or activity coefficients, we have the Poisson equation

$$\epsilon \operatorname{div} \operatorname{grad} \psi = -4\pi \sum_i n_i F c_i$$

and the continuity equations for the membrane-soluble species  $i$

$$\frac{\partial c_i}{\partial t} = D_i \operatorname{div} \left( \operatorname{grad} c_i + \frac{n_i F c_i}{RT} \operatorname{grad} \psi \right) \quad (2)$$

where  $c$  denotes concentration,  $n$  ionic valency, and  $\psi$  potential. Substitution of (1) into the left-hand side of (2) as summed over all species  $i$ , and subsequent integration with respect to distance, yields

$$\sum_i n_i F D_i \left( \operatorname{grad} c_i + \frac{n_i F c_i}{RT} \operatorname{grad} \psi \right) + \frac{\epsilon}{4\pi} \frac{\partial}{\partial t} \operatorname{grad} \psi = I \quad (3)$$

where the integration constant  $I$  represents the total (ionic plus dielectric displacement) current.

When the radius of curvature of the membrane is much larger than its thickness, such curvature may be neglected. When the treatment is further restricted to the presence, in the membrane, of ions of only one kind, and dimensionless quantities are introduced to simplify the notation, (1) through (3) transform into

$$\frac{d^2 \varphi}{ds^2} = \frac{dE}{ds} = -\gamma \quad (4)$$

$$\frac{\partial \gamma}{\partial \tau} = \frac{\partial}{\partial s} \left( \frac{\partial \gamma}{\partial s} + \gamma E \right) \quad (5)$$

$$i = \frac{\partial \gamma}{\partial s} + \gamma E + \frac{\partial E}{\partial \tau} \quad (6)$$

where

$$\varphi \equiv \frac{nF\psi}{RT} \quad (7)$$

$$E \equiv \frac{nFd}{RT} \frac{d\psi}{dx} = \frac{d\varphi}{ds} \quad (8)$$

$$\gamma \equiv \frac{4\pi n^2 F^2 d^2 c}{\epsilon R T} \quad (9)$$

$$i \equiv \frac{4\pi n F d^3 I}{D \epsilon R T} \quad (10)$$

$$s \equiv \frac{x}{d} \quad (11)$$

$$\tau \equiv \frac{D t}{d^2} \quad (12)$$

in which  $d$  denotes the membrane thickness, Here  $\psi$ ,  $E$ , and  $\gamma$  are functions of the dimensionless distance  $s$ , but  $i$  is not. Note that we have adopted here a somewhat simpler sign convention for  $\varphi$  and  $i$  than that used in our earlier papers.<sup>44,46-48</sup> Elimination of  $\gamma$  between (4) and (6) yields

$$i = -\frac{\partial^2 E}{\partial s^2} - E \frac{\partial E}{\partial s} + \frac{\partial E}{\partial \tau} \quad (13)$$

For the steady-state behavior, we may set  $\partial E / \partial \tau = 0$ , so that (13) can be integrated to

$$\frac{dE}{ds} + \frac{1}{2} E^2 = A - is \quad (14)$$

where  $A$  is an integration constant (see Appendix A).

The analytical solution of (14) for  $i=0$  reads<sup>43,44</sup>

$$E = \sqrt{2A} \frac{C_1 \cosh s\sqrt{A/2} + C_2 \sinh s\sqrt{A/2}}{C_1 \sinh s\sqrt{A/2} + C_2 \cosh s\sqrt{A/2}} \quad (15)$$

except for the special case  $A=0$ , where

$$E = \frac{2}{s+C} \quad (16)$$

For  $i \neq 0$ , one obtains<sup>45,46</sup> for  $A - is < 0$

$$E = \frac{-i}{|i|} [2(is - A)]^{1/2} \frac{C_1 J_{2/3}(\beta) - J_{-2/3}(\beta)}{C_1 J_{-1/3}(\beta) + J_{1/3}(\beta)} \quad (17)$$

$$\beta \equiv \frac{-\sqrt{2}}{3i} (is - A)^{3/2} \quad (18)$$

and, for  $A - is > 0$

$$E = \frac{-i}{|i|} [2(A - is)]^{1/2} \frac{C_2 I_{2/3}(\alpha) + I_{-2/3}(\alpha)}{C_2 I_{-1/3}(\alpha) + I_{1/3}(\alpha)} \quad (19)$$



$$\alpha \equiv \frac{-\sqrt{2}}{3i} (A - is)^{3/2} \quad (20)$$

Here  $C$ ,  $C_1$  and  $C_2$  are integration constants;  $J_\nu$  and  $I_\nu$  are a Bessel and modified Bessel function, respectively, both of the first kind and of order  $\nu$ . For the special case  $A - is = 0$ , (16) applies.

The dimensionless concentration  $\gamma$  and potential  $\varphi$  are obtained from (15) through (20) through the Poisson equation, (4), and the membrane conductance follows from (6), which, in the steady state ( $\partial E / \partial \tau = 0$ ), can be integrated<sup>49</sup> to

$$i \int_0^1 \frac{ds}{\gamma} = \ln \frac{\gamma_1}{\gamma_0} + (\varphi_1 - \varphi_0) = v - v_{eq} \quad (21)$$

where

$$v \equiv \varphi_1 - \varphi_0 \quad (22)$$

and  $v$  denotes the corresponding equilibrium potential difference,  $\ln \gamma_0 / \gamma_1$ . The dimensionless conductance  $g$  follows from (21) as

$$g \equiv \frac{i}{v - v_{eq}} = \frac{1}{\int_0^1 (ds/\gamma)} \quad (23)$$

Closed-form, analytical solutions for the general, time-dependent case ( $\partial E / \partial \tau \neq 0$ ) are not available. (An earlier claim to this effect for the special case of small-amplitude sinusoidal signals<sup>47</sup> was incorrect, since the constant-field approximation had been introduced tacitly in going from the homogeneous to the general solution.<sup>50</sup>)

## B. The Steady-State Constant-Field Approximation

Inspection of profiles<sup>44,46</sup> of electric field versus distance show that, when  $\gamma \ll 1$ ,  $E$  is essentially constant throughout the membrane. This result can be obtained from (14) by assuming that the term  $dE/ds = -\gamma$  is negligible with respect to  $\frac{1}{2}E^2$  and that, likewise,  $|is| \ll |A|$ , so that

$$\frac{1}{2}E^2 \approx A \quad (24)$$

Integration of  $d\varphi/ds = E$  for constant  $E$  then yields<sup>51</sup>

$$v \equiv \varphi_1 - \varphi_0 = E \quad (25)$$

Substitution of (25) into (6) for a time-independent value of  $v$  results in  $i = d\gamma/ds + v\gamma$  or

$$d \ln \left( \gamma - \frac{i}{v} \right) = -d(vs) \quad (26)$$

which can be integrated<sup>52</sup> to

$$\gamma = \left( \gamma_0 - \frac{i}{v} \right) e^{-vs} + \frac{i}{v} \quad (27)$$

where  $\gamma_0$  denotes the value of  $\gamma$  at  $s=0$ . Substitution of  $s=1$  yields

$$\gamma_1 = \left( \gamma_0 - \frac{i}{v} \right) e^{-v} + \frac{i}{v} \quad (28)$$

from which the current follows as

$$i = \frac{(\gamma_0 - \gamma_1 e^v) v}{1 - e^v} \quad (29)$$

Elimination of  $i/v$  between (27) and (28) leads to

$$\gamma = \frac{(\gamma_0 - \gamma_1) e^{-vs} + \gamma_1 - \gamma_0 e^{-v}}{1 - e^{-v}} \quad (30)$$

One readily verifies that (25), (29), and (30) satisfy (6) (without the term  $\partial E / \partial \tau$ ) and (5) (without the term  $\partial \gamma / \partial \tau$ ) but not the Poisson equation, (4). By combining (4) and (5) to

$$\frac{\partial \gamma}{\partial \tau} = \frac{\partial^2 \gamma}{\partial s^2} + E \frac{\partial \gamma}{\partial s} - \gamma^2 \quad (31)$$

the Poisson equation introduces a term in  $\gamma^2$  in the continuity equation that is neglected in the constant-field approximation. Clearly, the constant-field approximation expresses the notion that the electric field has an effect on the ionic concentration in the membrane but that the latter is so small that its reciprocal effect on the field can be neglected. In fact, the constant-field approach replaces the actual field  $E$  by its space-average value  $E_{av}$ , as follows directly from

$$E_{av} \equiv \frac{\int_0^1 E ds}{\int_0^1 ds} = \int_0^1 E ds = \int_0^1 d\varphi = \varphi_1 - \varphi_0 = v \quad (32)$$

An estimate of the difference between the actual and the average field is given in Appendix A.

The approximation  $-dE/ds \ll \frac{1}{2} E^2$  is not justified when  $E$  becomes very small, as happens when  $v$  tends to zero. In this case the constant concentration approximation<sup>44</sup> given in Appendix B is more appropriate.

### C. Constant-Field Approximation for Potential-Step Measurements

The description of the transient response following a potential step (voltage clamp) is most readily handled in terms of the Laplace transformation

$$\bar{f}(t) = \{f(t)\} \equiv \int_0^\infty e^{-pt} f(t) dt \quad (33)$$

When the dimensionless electric field jumps at time  $t = 0$  to the value  $E = v$ , we obtain from (5)

$$\frac{d^2 \bar{\gamma}}{ds^2} + v \frac{d\bar{\gamma}}{ds} - \frac{pd^2}{D} \bar{\gamma} = -\frac{d^2}{D} \gamma_{t=0} \quad (34)$$

$$\bar{\gamma} = C_1 e^{-vs(1+r)/2} + C_2 e^{-vs(1-r)/2} + \frac{\gamma_{t=0}}{p} \quad (35)$$

$$r \equiv \left(1 + \frac{4pd^2}{Dv^2}\right)^{1/2} \quad (36)$$

where  $C_1$  and  $C_2$  denote integration constants.

Inverse Laplace transformation of (35) is rather simple in two limiting cases. When  $4pd^2/Dv^2 \gg 1$  (corresponding to time  $t \gg 4d^2/Dv^2$ ) (35) assumes the form of a pure diffusion problem,

$$\bar{\gamma} = C_1 e^{-x(p/D)^{1/2}} + C_2 e^{x(p/D)^{1/2}} + \frac{\gamma_{t=0}}{p} \quad (37)$$

On the other hand, after a time  $t$  much longer than  $4d^2/Dv^2$  (i.e., for  $4pd^2/Dv^2 \gg 1$  or  $r \approx 1$ ), the ions have had time to redistribute themselves and one obtains the steady-state result (30). These two limiting cases,  $4pd^2/Dv^2 \gg 1$  and  $4pd^2/Dv^2 \ll 1$ , correspond to neglecting in (5) the terms  $\partial(\gamma E)/\partial s$  or  $\partial\gamma/\partial\tau$ , respectively. The complete solution of (34) for the redistribution of the continuum ionic charge in the membrane, following a stepwise change in applied potential, is characterized<sup>53,130</sup> by time constants  $4d^2/[D(v^2 + 4n^2\pi^2)]$  where  $n = 1, 2, 3, \dots$

### D. Constant-Field Approximation for Small-Amplitude Sinusoidal Signals

Here it is convenient to use for the quantities  $\phi$ ,  $E$ , and  $\gamma$  expressions of the type

$$\gamma = \gamma'(s) + \gamma''(s)e^{j\omega t} \quad (38)$$

$$j \equiv \sqrt{-1} \quad (39)$$

and, after substitution in (4) through (6), to separate direct and alternating terms and to neglect harmonics, that is, terms of the type  $Ae^{mj\omega t}$  where

$m > 1$ . By such a procedure, (5) yields

$$\frac{d^2\gamma''}{ds^2} + E' \frac{d\gamma''}{ds} - (2\gamma' + \nu)\gamma'' = -\frac{d\gamma'}{ds} E'' \quad (40)$$

$$\nu \equiv \frac{j\omega d^2}{D} \quad (41)$$

We now make the constant-field assumptions [ $E' = v'$ ,  $E'' = v''$ , neglect of the term  $-2\gamma'\gamma''$  which corresponds with the term  $-\gamma^2$  in (31)] and substitute for  $\partial\gamma'/\partial s$  the explicit solution obtained from (30) to get

$$\frac{d^2\gamma''}{ds^2} + v' \frac{d\gamma''}{ds} - \nu\gamma'' = \frac{v'v''(\gamma'_0 - \gamma'_1)e^{-v's}}{1 - e^{-v'}} \quad (42)$$

$$\gamma'' = C_1 e^{\lambda_1 s} + C_2 e^{\lambda_2 s} - \frac{v'v''(\gamma'_0 - \gamma'_1)e^{-v's}}{v(1 - e^{-v'})} \quad (43)$$

$$\lambda_{1,2} = -\frac{1}{2}v' \pm \frac{1}{2}[(v')^2 + 4\nu]^{1/2} \quad (44)$$

where  $C_1$  and  $C_2$  denote integration constants. As in the preceding section, a high-frequency approximation can be found by neglecting the term  $v'\partial\gamma''/\partial s$  in (42), whereas the low-frequency limit is obtained by neglecting the term  $-\nu\gamma''$ , which leads to<sup>47</sup>

$$\gamma'' = C_1 e^{-v's} + C_2 - \frac{v''s(\gamma'_0 - \gamma'_1)e^{-v's}}{1 - e^{-v'}} \quad (45)$$

where  $C_1$  and  $C_2$  are integration constants [not necessarily the same as those in (43)]. This low-frequency approximation corresponds to neglecting  $\partial\gamma/\partial\tau$  in (5), setting  $r$  equal to 1 in (35) or, in physical terms, using sufficiently low frequencies so that the ionic adjustment to the electric field does not contribute appreciably to the membrane admittance.

### E. Boundary Conditions

The expressions derived so far for permeation through the membrane phase require boundary conditions that must reflect interfacial stoichiometries, such as those encountered with carrier-mediated transport, as well as other transport-limiting processes outside the membrane phase, such as aqueous diffusion. Below we briefly outline the corresponding mathematical formulations and subsequently illustrate the approach with a few worked-out examples.

A general boundary condition follows from the requirement of continuity of the dielectric displacement at the water/membrane interfaces,

$$\epsilon_w E_w = \epsilon(E \pm q) \quad (46)$$

$$q \equiv \frac{4\pi n F d Q}{\epsilon R T} \quad (47)$$

where the top and bottom signs refer to  $s=0$  and  $s=1$ , respectively, the subscript  $w$  identifies the water phase, and  $Q$  denotes any surface-charge density present. The fields  $E_w$  are associated with the aqueous space-charge layers. The simplest model for such space-charge layers is that of Gouy and Chapman which, for a symmetrical  $n,n$  electrolyte, leads to dimensionless "diffuse double-layer" potentials<sup>48</sup>

$$\varphi_d = 2 \operatorname{arsinh} \left[ \frac{\epsilon(q \pm E)}{2\kappa d \epsilon_w} \right] \quad (48)$$

where  $\kappa$  is the reciprocal Gouy-Chapman (or Debye-Hückel) length,

$$\kappa \equiv \left( 4\pi F^2 \sum_i n_i^2 c_i^* / \epsilon_w R T \right)^{1/2} \quad \text{with } c_i^* \text{ representing the individual ionic}$$

concentrations in the bulk of the aqueous solutions.

The Gouy-Chapman model does not take into account the finite size of the ions making up the diffuse double layer, a deficiency that Stern<sup>54</sup> remedied through the simple expedient of a charge-free region interposed between the aqueous space-charge region and the plane through the surface charges. Such a charge-free region is not field-free, and the dimensionless potential difference  $\varphi_c$  across it follows from the continuity of dielectric displacement as<sup>55</sup>

$$\varphi_c = \frac{\epsilon d_c (q \pm v)}{\epsilon_c d} \quad (49)$$

The double-layer potentials  $\varphi_c$  and  $\varphi_d$  enter the mathematical formalism in two ways. First, all interfacial aqueous concentrations must be multiplied by a Boltzmann factor,  $\exp[-\varphi_d]$ , in all expressions involving interfacial kinetics. Second, the dimensionless applied voltage  $v_a$  across the membrane and its adjacent aqueous space-charge layers is given by

$$v_a = \varphi_{c0} + \varphi_{d0} + v - \varphi_{c1} - \varphi_{d1} \quad (50)$$

and experimental current-voltage curves are relations between  $i$  and  $v_a$  rather than between  $i$  and  $v$ . Often, however, the term in  $E$  is very small,<sup>48,56</sup> and the surface-charge densities  $Q$  do not vary with applied potential, so that the difference between  $v_a$  and  $v$  is approximately constant. However, (49) and (50) must be taken into account explicitly when  $Q$  varies with  $v$ , as is the case, for example, when membrane-permeable ions are adsorbed at the water/membrane interfaces (see Section II.H).

An often-studied permeation mechanism for ions that, by themselves,

are insufficiently membrane soluble, is that of carrier-facilitated transport. For example, a neutral, membrane-soluble molecule such as valinomycin can chelate a potassium ion, whereby the ion-carrier complex so formed becomes membrane-soluble. In this example the equilibrium concentrations of both carrier and ion-carrier complex in the membrane are very much higher than those in the adjacent aqueous solutions, so that they can be idealized as membrane-confined. For a neutral carrier, here indicated with the subscript T for translocator, (2) reduces for planar geometry to Fick's law,

$$\frac{\partial c_T}{\partial t} = D_T \quad (51)$$

When interconversion between carrier and ion-carrier complex is possible only at the interfaces (since it involves an aqueous ion), then

$$D \left( \frac{\partial c}{\partial x} + \frac{nFc}{RT} \frac{\partial \psi}{\partial x} \right) = -D_T \left( \frac{\partial c_T}{\partial x} \right) \quad x=0, d \quad (52)$$

or, in dimensionless form,

$$\frac{\partial \gamma}{\partial s} + \gamma E = -\frac{D_T}{D} \frac{\partial \gamma_T}{\partial s} \quad s=0, 1 \quad (53)$$

If we consider the carrier and its complex as membrane-confined, then  $\int_0^1 (\gamma + \gamma_T) ds$  must be a constant. In this case the constant-field approximation leads to a further simplification. The total (ionic and dielectric displacement) current  $i$  is independent of distance [compare (3)]. In the constant-field approximation, the dielectric displacement current is also independent of distance, hence the same must apply to the ionic displacement current. Specifically,  $i - \partial E / \partial \tau = \partial \gamma / \partial s + \gamma E$  must have the same value at  $s=0$  and

$s=1$ . In view of (53),  $(\partial \gamma_T / \partial s)_{s=0} = (\partial \gamma_T / \partial s)_{s=1}$  so that  $\int_0^1 \gamma ds$  and  $\int_0^1 \gamma_T ds$  must each be constant.

Transport of ions through the adjacent aqueous phases can usually be described to sufficient accuracy by planar diffusion,

$$\frac{\partial c_w}{\partial t} = D_w \frac{\partial^2 c_w}{\partial x^2} \quad (54)$$

where the subscript  $w$  denotes the water phase. Neglected in (54) are effects due to electric fields and those resulting from gradients in ionic-activity coefficients, which are both quite negligible in aqueous solutions of sufficiently large ionic strength, except in the space-charge layers at the membrane interfaces. For the latter a Boltzmann-type equilibrium correction based on

the Gouy-Chapman model usually suffices.<sup>48</sup> In the steady state,  $\partial c_w / \partial t = 0$  and (54) can be integrated to correspond to Nernst diffusion layers of thickness  $d_w$ .

Artificial ultrathin lipid membranes are often surrounded by a torus, in which case diffusion to and from such torus may complicate the diffusion geometry.<sup>57</sup> For steady-state experiments, description in terms of diffusion layers of fixed (but stirring-dependent) thickness is usually adequate. Potential step measurements are mostly restricted to rather short (typically sub-second) times, so that semi-infinite diffusion suffices, and the same applies to admittance measurements.

In the case of membrane-soluble weak acids and their conjugated bases, (54) must be modified to take into account the acid-base reactions  $\text{HA} \rightleftharpoons \text{H}^+ + \text{A}^-$ , so that<sup>58-60</sup>

$$\frac{\partial c_{\text{HA}}}{\partial t} = D_{\text{HA}} \frac{\partial^2 c_{\text{HA}}}{\partial x^2} + k_c c_{\text{H}^+} c_{\text{A}^-} - k_d c_{\text{HA}} \quad (55)$$

$$\frac{\partial c_{\text{A}^-}}{\partial t} = D_{\text{A}^-} \frac{\partial^2 c_{\text{A}^-}}{\partial x^2} - k_c c_{\text{H}^+} c_{\text{A}^-} + k_d c_{\text{HA}} \quad (56)$$

For the rather large organic anions  $\text{A}^-$  usually involved, one can often put  $D_{\text{HA}} \approx D_{\text{A}^-}$ , which greatly simplifies the mathematics; otherwise, an approximation due to Koutecký<sup>61</sup> can be used. As a rule the neutral form HA is much more membrane permeable than the anion  $\text{A}^-$ . The situation is then very much like that described by Brdicka<sup>62,63</sup> for the water/mercury interface, where, in a certain range of potentials, HA can be removed from the interface by electroreduction (rather than membrane permeation) whereas  $\text{A}^-$  cannot.

For time-dependent measurements, one may have to consider possible interfacial accumulation of ions, that is, adsorption. This can be incorporated into the formalism by modifying the interfacial mass-balance equations. For membrane-soluble ions, for example, the mass-balance equations will then take the form

$$D \left( \frac{\partial c}{\partial x} + \frac{nFc}{RT} \frac{\partial \psi}{\partial x} \right)_{x=0} - \frac{\partial \Gamma_0}{\partial t} = D_w \left( \frac{\partial c_w}{\partial x} \right)_{x=0} \quad (57)$$

$$D \left( \frac{\partial c}{\partial x} + \frac{nFc}{RT} \frac{\partial \psi}{\partial x} \right)_{x=d} + \frac{\partial \Gamma_1}{\partial t} = D_w \left( \frac{\partial c_w}{\partial x} \right)_{x=d} \quad (58)$$

where the subscripts 0 and 1 denote the value of  $s = x/d$ . In experiments in which one varies the concentration of the adsorbable ion, the consequent change in membrane-surface-charge density and the corresponding change in all ionic concentrations immediately adjacent to the membrane must of course be taken into account.<sup>64-66</sup>

When slow interfacial kinetics are involved, a rate expression must be introduced, for example,

$$D \left( \frac{\partial c}{\partial x} + \frac{nFc}{RT} \frac{\partial \psi}{\partial x} \right)_{x=0} = kc_0 - k_w c_{w0} = D_w \left( \frac{\partial c_w}{\partial x} \right)_{x=0} \quad (59)$$

(and a similar one for  $x=d$ ) for membrane-soluble ions. In the simplest model the first-order heterogeneous rate constants  $k$  and  $k_w$  are taken to be independent of applied potential.

### F. Example: Ionic Displacement Charge Density for Membrane-Soluble Ions

As a first example of the application of the foregoing relations, we consider the ionic displacement charge density that results from a change in dimensionless potential from 0 to  $+v$ . For the sake of simplicity, we assume experimental conditions such that ion transfer into and out of the membrane is negligible during the ionic redistribution process, so that  $(\partial\gamma/\partial s + \gamma E)_{s=0,1} = 0$ . The corresponding charge density then follows from (6) as

$$\Delta q = \int i d\tau = \int \left( \frac{\partial E}{\partial \tau} \right)_{s=0,1} d\tau = \Delta E_{s=0,1} \quad (60)$$

where the integration encompasses the time during which displacement current flows.

Estimates of the values of  $E_{s=0,1}$  before and after the stepwise change in applied potential can be found (see Appendix A) from

$$E = E_{av} + \int_0^1 \int_0^s \gamma ds' ds - \int_0^s \gamma ds \quad (61)$$

where  $E_{av} = v$ , see (32), in which case the ionic component of the displacement current can clearly be identified with the two integrals on the right-hand side of (61). A somewhat simpler formalism is obtained when one considers that

$$-\int_0^1 s \gamma ds = \int_0^1 s dE = sE \Big|_0^1 - \int_0^1 E ds = E_1 - E_{av} = E_1 - v \quad (62)$$

Consequently, the ionic displacement charge density is simply given by the change in the quantity  $-\int_0^1 s \gamma ds$ . From (27) one obtains the equilibrium distribution ( $i=0$ )

$$\gamma = \gamma_0 e^{-vs} = \frac{v\gamma^* e^{-vs}}{1 - e^{-v}}$$

where  $\gamma^* \equiv \int_0^1 \gamma ds$ , and consequently the ionic displacement current following a change in applied potential from 0 to  $v$  is

$$\Delta q = - \int_0^1 \frac{sv\gamma^* e^{-vs}}{1 - e^{-v}} ds + \int_0^1 s\gamma^* ds = \Delta q_m \left( \coth \frac{v}{2} - \frac{2}{v} \right) \quad (63)$$



where

$$\Delta q_m = \lim_{v \rightarrow \infty} \Delta q = \gamma^*/2$$

On the other hand, when all the ions are adsorbed at the water/membrane interfaces, and assuming a Boltzmann equilibrium distribution for  $\Gamma$ , we obtain

$$s\gamma = \Gamma_1 = \Gamma_0 e^{-v} = \frac{\Gamma^* e^{-v}}{1 - e^{-v}}$$

where  $\Gamma^* = \Gamma_0 + \Gamma_1$ , from which it follows that

$$\Delta q / \Delta q_m = \frac{-\Gamma^* e^{-v} / (1 - e^{-v}) + \Gamma^* / 2}{\Gamma^* / 2} = \tanh \frac{v}{2} \quad (64)$$

The two expressions (63) and (64) correspond to the bottom and top curves, respectively, in Fig. 1. The other curves show the intermediate case in which some of the ions are adsorbed at the interfaces, while the remainder are dissolved in the membrane interior (see Appendix C). Note that different values of  $\phi_d$  apply before and after the experiment, so that (49) and (50) must be taken into account when comparing (64) with experiment.

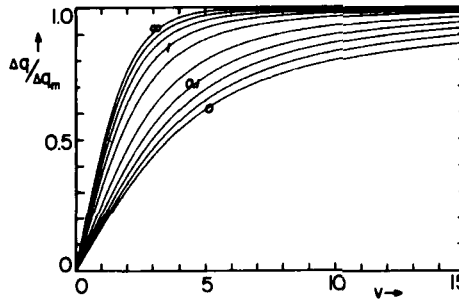


**Fig. 1.** The ionic displacement charge density  $\Delta q$  (in units of its maximum value  $\Delta q_m$ ) due to the voltage-dependent redistribution of ions in the membrane when the dimensionless potential is changed from zero to  $+v$ . Curves are drawn according to (C7) for the following values of  $B$  (from top to bottom):  $\infty$ , 5, 2, 1, 0.5, 0.2, 0.1, 0.05, 0.02 and 0, corresponding with a gradual transition from exclusively adsorption at the water/membrane interfaces (64) to a homogeneous ionic distribution in the membrane interior (63).

### G. Example: Low-Frequency Admittance for Membrane-Soluble Ions

As an illustration of the application of specific boundary conditions, we derive here an explicit expression for the admittance resulting from transport of membrane-soluble ions of one kind through the membrane. We use the

low-frequency approximation to the constant-field approach [i.e., we neglect the term  $-v\gamma''$  in (42)] and consider aqueous diffusion, slow interfacial ion transfer, and interfacial adsorption. For the sake of simplicity, we assume that all membrane properties are symmetrical with respect to the plane at  $s = \frac{1}{2}$  and that the dimensionless direct current  $i'$  and voltage  $v'$  are both zero. Also, to keep the number of rate parameters manageable, we assume that the adsorption and desorption processes are so fast that their kinetics need not be considered in the frequency range used. The interfacial transfer kinetics are taken to be of first order, with rate constants that are independent of applied potential.

• When phase transfer is measurably slow, a distinction between adsorption at the “membrane” or “water” side of the interface (denoted here by  $\Gamma$  and  $\Gamma_w$ , respectively) becomes operationally meaningful. The boundary conditions read (compare Fig. 2)

$$D \left( \frac{\partial c}{\partial x} + \frac{nFc}{RT} \frac{\partial \psi}{\partial x} \right)_{x=0} - \frac{\partial \Gamma_0}{\partial t} = k_m c_0 - k_w c_{w0} = D_w \left( \frac{\partial c_w}{\partial x} \right)_{x=0} + \frac{\partial \Gamma_{w0}}{\partial t} \quad (65)$$

$$D \left( \frac{\partial c}{\partial x} + \frac{nFc}{RT} \frac{\partial \psi}{\partial x} \right)_{x=d} + \frac{\partial \Gamma_1}{\partial t} = k_w c_{w1} - k_m c_1 = D_w \left( \frac{\partial c_w}{\partial x} \right)_{x=d} - \frac{\partial \Gamma_{w1}}{\partial t} \quad (66)$$

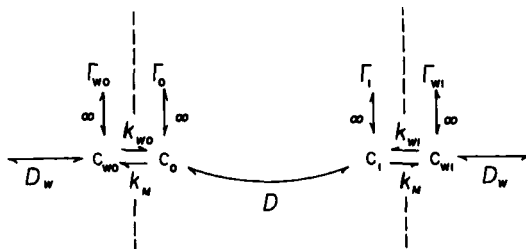


Fig. 2. The rate parameters considered in the example of Section II.G. Aqueous concentrations are indicated with the subscript  $w$ , and the two sides of the membrane with 0 and 1. Adsorption equilibrium is assumed to be established immeasurably fast.

In dimensionless form, restricted to the alternating component at angular frequency  $\omega$ , and using the constant-field approximation, that is,  $E' = v' = 0$ ,  $E'' = v''$ , and  $\gamma'_0 = \gamma'_1 = \gamma'$  (for reasons of symmetry), we obtain

$$\left( \frac{d\gamma''}{ds} \right)_{s=n} + \gamma'_n v'' \mp \frac{j\omega d}{D} \frac{\partial \Gamma_n}{\partial c_n} \gamma''_n = \pm k'(\gamma''_n - \gamma''_{wn}) = \pm \left[ \frac{(j\omega D_w)^{1/2} d}{DK} + \frac{j\omega d}{DK} \frac{\partial \Gamma_{wn}}{\partial c_{wn}} \right] \gamma''_{wn} \quad (67)$$

where  $k' \equiv dk_w/DK$ ,  $K \equiv k_w/k_m$ , and where the top sign is for  $n=0$  and the

bottom sign for  $n=1$ . The term in  $(j\omega D_w)^{1/2}$  originates in (54) which, for semi-infinite diffusion, leads<sup>47</sup> to  $(d\gamma_w/ds)_{s=n} = \pm(j\omega d^2/D_w)^{1/2}\gamma''_{wn}$ .

The right-hand side equality in (62) yields

$$\frac{k'\gamma''_n}{\gamma''_{wn}} = k' + \frac{(j\omega D_w)^{1/2}d}{DK} + \frac{j\omega d}{DK} \frac{\partial \Gamma_{wn}}{\partial s_n} \quad (68)$$

which can be used to eliminate  $\gamma''_{wn}$  from the left-hand side of (67),

$$\left(\frac{d\gamma''}{ds}\right)_{s=n} + \gamma'_n v'' = \pm F_n \gamma''_n \quad (69)$$

TABLE I

Equivalent Circuit Elements, Corresponding Physical Phenomena, and their Expression in Terms of Rate Parameters in the Constant-Field and Single-Barrier Models,

Respectively, for a Symmetrical Membrane at Zero Direct Current  $i$  and Voltage  $v'$ . The constant-field admittance  $Y$  follows from (68) and  $Y = D\varepsilon\gamma/4\pi d^3$ ; the single-barrier results follow from (85) with  $n'_1 = n'_0$ ,  $-\kappa_1 = \kappa_0$  and the notational simplification  $K = k_w/k_M$ . Note that the single-barrier results can be translated into the constant-field formalism, or vice versa, with the relations

$$n'_0 = c'd/2, \quad \kappa_0 = D/d^2, \quad k_0 = D/d, \quad c' = 2\kappa_0 n'_0/k_0, \quad D = k_0^2/\kappa_0, \quad d = k_0/\kappa_0$$

and that the single-barrier model implies that, in constant-field notation,  $\partial\Gamma/\partial c = 1$ .

Circuit element	Symbol	Physical phenomenon	Constant-field model (low-frequency approximation)	Single-barrier model
Membrane capacitance	$C$	Dielectric charge displacement	$\frac{\varepsilon}{4\pi d}$	$\frac{\varepsilon}{4\pi d}$
Membrane resistance	$R$	Ion transport across membrane	$\frac{RT}{n^2 F^2} \frac{d}{c' D}$	$\frac{RT}{n^2 F^2} \frac{1}{2\kappa_0 n'_0}$
Phase transfer resistance	$R_{pt}$	Ion transport across interface	$\frac{RT}{n^2 F^2} \frac{1}{c' k}$	$\frac{RT}{n^2 F^2} \frac{k_0}{2\kappa_0 n'_0 k_{m0}}$
Warburg (diffusion) impedance	$Z_w$	Diffusion through aqueous phase	$\frac{RT}{n^2 F^2} \frac{K}{c' \sqrt{j\omega D_w}}$	$\frac{RT}{n^2 F^2} \frac{k_0 K}{2\kappa_0 n'_0 \sqrt{j\omega D_w}}$
Adsorption capacitance	$C_a$	Ion adsorption at membrane side of interface	$\frac{n^2 F^2}{RT} \frac{c'}{c' \frac{\partial \Gamma}{\partial c}}$	$\frac{n^2 F^2}{RT} \frac{2\kappa_0 n'_0}{k_0}$
Aqueous adsorption capacitance	$C_{wu}$	Ion adsorption at water side of interface	$\frac{n^2 F^2}{RT} \frac{c'}{K \frac{\partial \Gamma_w}{\partial c_w}}$	$\frac{n^2 F^2}{RT} \frac{2\kappa_0 n'_0}{k_0 K} \frac{\partial \Gamma_{w0}}{\partial c_{w0}}$

$$F_n = \frac{j\omega d}{D} \frac{\partial \Gamma_n}{\partial c_n} + \left[ \frac{1}{k'} + \frac{1}{(j\omega D_w)^{1/2} d/DK + j\omega d(\partial \Gamma_{wn}/\partial c_n)/DK} \right]^{-1} \quad (70)$$

Comparison with (6) as restricted to angular frequency  $\omega$ ,

$$i'' = \frac{d\gamma''}{ds} + v''(\gamma' + v) \quad (71)$$

and with its integrated form,

$$i'' = \int_0^1 i'' ds = \gamma_1'' - \gamma_0'' + v''(\gamma' + v) \quad (72)$$

then yields for the admittance  $y$

$$y \equiv \frac{i''}{v''} = v + \frac{\gamma'}{1 + 1/F_0 + 1/F_1} \quad (73)$$

The fractional forms of (70) and (73) facilitate identification<sup>67</sup> of the corresponding equivalent circuit components shown in Fig. 3 and given in Table I.

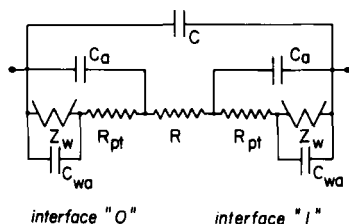


**Fig. 3.** Equivalent circuit representation of (73) and (89). The circuit parameters are given in Table I. If adsorption/desorption kinetics must be taken into account, these turn out to be represented by corresponding resistances in series with each of the adsorption capacitances  $C_a$  and  $C_{wa}$ . For a symmetrical membrane and identical surrounding aqueous solutions, analysis is simplest for zero direct current  $i'$  and voltage  $v'$ , in which case the corresponding interfacial circuit elements at the two-membrane interfaces are equal and can be considered together.

### III. THE SINGLE-BARRIER MODEL

#### A. General Approach

In this model<sup>68,69</sup> permeation through the hydrophobic region of the membrane is described as that across a simple activation energy barrier, such as depicted in Fig. 4. It is assumed that the applied voltage constitutes only a small perturbation of the barrier shape, so that the position of the potential-energy maximum along the reaction coordinate is not affected to any appreciable extent by the applied dimensionless voltage  $v$ . In this case the voltage only increases the barrier height at its maximum by an amount  $\alpha v$  where  $0 \leq \alpha \leq 1$  as long as its contribution is a monotonic function of the reaction coordinate. Such a formalism is common to electrochemical

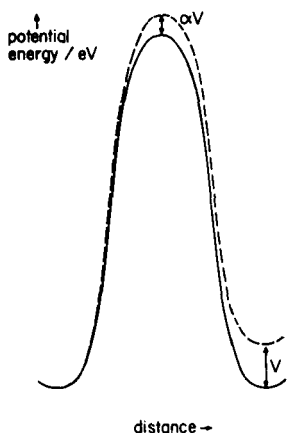


**Fig. 4.** Schematic representation of the energy barrier considered in the single-barrier model (—) and of the effect of an externally applied potential  $V$  (---).

kinetics<sup>70-72</sup> and has subsequently been incorporated into the “absolute” rate theory.<sup>73</sup> Consequently, the potential dependence of the rate constants describing transport from one side of the membrane to the other can be expressed by

$$k_0 = k_0^\ominus e^{\alpha v} \quad (74)$$

$$k_1 = k_0^\ominus e^{(1-\alpha)v} \quad (75)$$

where  $k^\ominus$  denotes a standard rate constant.

For an energy profile as shown in Fig. 4, only a negligible fraction of the ions will reside at any time in the region near the maximum, and a considerable simplification of the model description can be obtained by assuming that all ions are located in the region of the energy minima adjacent to the barrier. In this case we must use surface concentrations  $n_i$ , which can be related to volume concentrations  $c_i$  through division by appropriate distances. (If we assume that the energy maximum is located at  $s = \alpha'$ , the appropriate distances are  $\alpha'd$  and  $(1 - \alpha')d$ . Equating  $\alpha'$  to  $\alpha$  can be justified on the basis of a constant-field assumption.)

When the two sides of the membrane have identical chemical composition, symmetry requires that  $k_0^\ominus = k_1^\ominus = k^\ominus$  and  $\alpha = \alpha' = \frac{1}{2}$ . We use this simplification to focus more sharply on the basic properties of the model. The resulting formalism is now extremely simple, since the corresponding ionic flux  $J$  is given by

$$J = k^\ominus (n_0 e^{v/2} - n_1 e^{-v/2}) \quad (76)$$

### B. Boundary Conditions

The boundary value problem for the simple barrier formalism is very similar to that discussed earlier for the continuum approach (Section II.E), with only the following differences. Since the ions are supposed to be located at the membrane interfaces, there is no physical distinction between adsorption onto the membrane and partitioning into it, and consequently no need to consider adsorption separately.

Because surface concentrations  $n_i$  are used rather than bulk concentrations  $c_i$ , some rate constants associated with heterogeneous processes, such as that of leaving the membrane for the aqueous solution, have the dimensions of homogeneous rate constants. The correct dimensionality is obtained by multiplication by a suitable length ( $d/2$  for symmetrical membranes).

Transport of an uncharged species, such as a neutral carrier or weak acid, is also described in terms of rate constants (which are now voltage independent) rather than as a diffusion process.

The single-barrier model yields the ionic flux  $J$ , which can be converted into the corresponding ionic current density through multiplication by  $-nF$ . The model does not consider the (capacitive) dielectric displacement current density, which therefore must be added separately when appropriate.

### C. Example: Steady-State and Transient Response for Ion Transport by Membrane-Confined Carriers

As a first illustration of the single-barrier approach, we consider here the case of neutral membrane-confined carriers forming a 1:1 complex with otherwise membrane-insoluble ions. We assume that the transported ion is present in sufficiently large excess in the aqueous solutions bordering the membrane so that aqueous diffusion need not be taken into account, and formation of the ion-carrier complex can be considered a pseudo-first-order reaction. Also we take the aqueous concentrations of the transported ion to be the same on both sides of the membrane, which further simplifies the mathematics. We now have<sup>74</sup> (see Fig. 5)

$$\frac{dn_0}{dt} = k^\ominus n_1 e^{-v/2} - k^\ominus n_0 e^{v/2} + k_c n_{T0} - k_d n_0 \quad (77)$$

$$\frac{dn_1}{dt} = k^\ominus n_0 e^{v/2} - k^\ominus n_1 e^{-v/2} + k_c n_{T1} - k_d n_1 \quad (78)$$

$$\frac{dn_{T0}}{dt} = k_T (n_{T1} - n_{T0}) + k_d n_0 - k_c n_{T0} \quad (79)$$

$$\frac{dn_{T1}}{dt} = k_T (n_{T0} - n_{T1}) + k_d n_1 - k_c n_{T1} \quad (80)$$

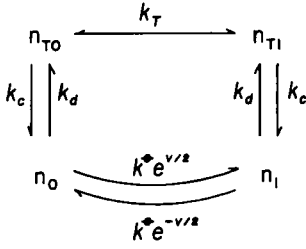


**Fig. 5.** The rate parameters considered in the example of Section III.C. Note that the complexation rate constant  $k_c$  is of pseudo first order and includes the concentration of the complexed aqueous ion, which is taken to be constant throughout both aqueous solutions.

Addition of (77) through (80) shows that  $n_0 + n_1 + n_{T0} + n_{T1} = N$ , a constant. Combination of (77) and (78) and subsequent integration yield the result<sup>41</sup> that  $n_0 + n_1 = k_c N / (k_c + k_d)$  and, likewise,  $n_{T0} + n_{T1} = k_d N / (k_c + k_d)$ , independent of time. (Compare Section II.E for the constant-field result regarding  $\int_0^1 \gamma ds$  and  $\int_0^1 \gamma_T ds$ .) Using these relations, the ionic flux following a jump

of dimensionless potential from zero to  $v$  is obtained from (77) through (80) as<sup>75</sup>

$$J = k^\ominus n_0 e^{v/2} - k^\ominus n_1 e^{-v/2} = J_1 e^{-v/2} = J_1 e^{-\eta_1 t} + J_2 e^{-\eta_2 t} + J_3 \quad (81)$$

where

$$\begin{aligned} \eta_{1,2} = & \frac{1}{2} \left( k_d + 2k^\ominus \cosh \frac{v}{2} + 2k_T + k_c \right) \\ & \pm \frac{1}{2} \left[ \left( k_d + 2k^\ominus \cosh \frac{v}{2} - 2k_T - k_c \right)^2 + 4k_c k_d \right]^{1/2} \end{aligned} \quad (82)$$

$$\begin{aligned} J_{1,2} = & \frac{k^\ominus}{2} \left( \frac{k_c}{k_d k_T} + \frac{2}{k_d} \right) \cosh \frac{v}{2} \\ & \pm \frac{k^\ominus}{2} \frac{(k_c/k_d k_T + 2/k_d)(k_c + k_d + 2k_T - 2k^\ominus \cosh(v/2)) - 4}{[(k_d + 2k^\ominus \cosh(v/2) - 2k_T - k_c)^2 + 4k_c k_d]^{1/2}} \cosh \frac{v}{2} \end{aligned} \quad (83)$$

and the steady-state component<sup>74</sup>

$$J_3 = \frac{k_c N}{k_c + k_d} \frac{\sinh(v/2)}{1/k^\ominus + (k_c/k_d k_T + 2/k_d) \cosh(v/2)} \quad (84)$$

#### D. Example: Admittance for Membrane-Soluble Ions

The case of membrane-soluble ions is discussed in an earlier section in connection with the continuum approach, and here we select equivalent

boundary conditions to facilitate comparison. By analogy with (38) we write

$$n = n' + n'' e^{j\omega t} \quad (85)$$

and similar expressions for  $J$  and  $v$ . Furthermore, we use

$$k = k' + \kappa v'' e^{j\omega t} \quad (86)$$

where  $\kappa \equiv \partial k / \partial v$ . We consider aqueous diffusion, first-order interfacial transfer kinetics, and adsorption on the aqueous side of the interface; as mentioned earlier, adsorption in the membrane is already taken into account automatically by the single-barrier formalism. Consequently, we have the material balance

$$\begin{aligned} J &= -D_w \left( \frac{\partial c_w}{\partial x} \right)_{x=0} - \frac{\partial \Gamma_{w0}}{\partial t} - \frac{\partial n_0}{\partial t} = k_{w0} c_{w0} - k_m n_0 - \frac{\partial n_0}{\partial t} \\ &= k_0 n_0 - k_1 n_1 = k_m n_1 - k_{w1} c_{w1} + \frac{\partial n_1}{\partial t} = -D_w \left( \frac{\partial c_w}{\partial x} \right)_{x=d} + \frac{\partial n_1}{\partial t} + \frac{\partial \Gamma_{w1}}{\partial t} \end{aligned} \quad (87)$$

from which the components at angular frequency  $\omega$  follow as

$$\begin{aligned} J'' &= -c''_{w0} (j\omega D_w)^{1/2} - j\omega c''_{w0} \frac{\partial \Gamma_{w0}}{\partial c_{w0}} - j\omega n''_0 = k_{w0} c''_{w0} - k_m n''_0 - j\omega n''_0 \\ &= k'_0 n''_0 - \kappa_0 n'_0 v'' - k'_1 n''_1 - \kappa_1 n'_1 v'' = k_m n''_1 - k_{w1} c''_{w1} + j\omega n''_1 \\ &= c''_{w1} (j\omega D_w)^{1/2} + j\omega c''_{w1} \frac{\partial \Gamma_{w1}}{\partial c_{w1}} + j\omega n''_1 \end{aligned} \quad (88)$$

Elimination of  $n''_0$ ,  $n''_1$ ,  $c''_{w0}$ , and  $c''_{w1}$  leads to the admittance

$$Y = j\omega C + \frac{n^2 F^2}{RT} \frac{J''}{v''} = j\omega C + \frac{n^2 F^2}{RT} \frac{\kappa_0 n'_0 - \kappa_1 n'_1}{1 + 1/G_0 + 1/G_1} \quad (89)$$

$$G_n = \frac{j\omega}{k_n} + \left[ \frac{k_n}{k_m} + \frac{1}{k_m (j\omega D_w)^{1/2} / k_n k_{wn} + j\omega k_m (\partial \Gamma_{wn} / \partial c_{wn}) / k_n k_{wn}} \right]^{-1} \quad n=0, 1 \quad (90)$$

which corresponds to the equivalent circuit shown in Fig. 3.

#### IV. MORE ELABORATE MODELS

##### A. Comparison of the Preceding Models

Before we go on to consider more elaborate models, it is useful to reflect on the two simple models discussed so far. The steady-state current-voltage curves predicted by either model are smooth and rather structureless and can be highly nonlinear. The nonlinearity often derives mostly from asym-



metric boundary conditions, and a more discriminating comparison can be made by keeping the aqueous concentrations of all species near the membrane constant and equal on both sides, and all interfacial kinetics infinitely fast. The resulting intrinsic current-voltage curve for membrane-soluble ions should be linear according to the (square-barrier) constant-field approximation, whereas the current should be proportional to  $\sinh(v/2)$  for a single (narrow) barrier. Intrinsic current-voltage curves extracted so far from experiments on membrane-soluble ions are all "superlinear" (i.e., the current increases with  $v$  faster than by strict proportionality), although the curvature is usually less (but in at least one case more<sup>76</sup>) pronounced than that predicted by the single-barrier model. With membrane-confined carriers, the other widely studied mechanism, current-voltage curves have been observed to be superlinear or sublinear, depending on the nature and concentration of the carrier, the nature of the lipid, and the composition of the surrounding aqueous solutions. Again, the simple (square-barrier) constant-field approximation cannot account for superlinear current-voltage curves, whereas both models can be made to fit sublinear ones.

Although the observation of experimental superlinear current-voltage curves would seem to fit the simple barrier model better, we do not attach much significance to such a preliminary conclusion, because simple modifications of both models, proposed to bring each of them in better quantitative agreement with experimental data, tend to obliterate the distinction and, more importantly, because neither model takes into account the effects of double-layer and dipole potentials discussed in Section IV.D.

For membrane-soluble ions the predicted membrane admittances at audio and subaudio frequencies are operationally indistinguishable (see Sections II.G and III.D). Although this may be disappointing when one is concerned primarily with choosing between various models, it is most useful for the experimentalist to have available a technique whose interpretation is largely insensitive to model assumptions. That is, the experimentally measured admittance can be analyzed according to the equivalent circuit of Fig. 3, and the circuit elements so obtained will indicate which physical phenomena are rate determining. One can also study the dependence of the individual circuit components on concentration, pH, temperature, membrane thickness, and so forth. Only when one wants to interpret these data in terms of specific rate parameters (e.g., as either a membrane diffusion coefficient or as a single-jump rate constant, rather than as a membrane resistance to ion transport across the hydrophobic barrier) must a model-dependent choice be made between the two columns on the right-hand side of Table I.

The above applies not only to admittance measurements, but to other small-amplitude perturbations as well, since all of these can be described in terms of the same equivalent circuit. In Appendix D we indicate how the

response to a voltage, current, or charge step can be derived immediately from the membrane admittance, so that these responses need not be derived *ab ovo* for every technique. Appendix E briefly discusses some aspects of equivalent circuit representations.

At higher frequencies the two models predict different admittances: the constant-field approximation leads to a frequency-dependent contribution from the ionic displacement current, whereas, in the small-amplitude single-barrier formalism, ion transport across the barrier representing the membrane interior remains resistive at all frequencies.

The two models also predict different transient and high-frequency ac behavior for membrane-confined carriers. The difference is in fact analogous to that obtained for membrane-soluble ions, accentuated by the circumstance that transport of the neutral component of the carrier system is described by diffusion laws in the continuum model, but as a kinetic step in the single-barrier approach.

Andersen and Fuchs<sup>77</sup> measured the ionic displacement charge density as a function of  $v$ . Their results can be represented in the form  $\Delta q/\Delta q_m = \tanh(\beta v/2)$  where, for tetraphenylborate,  $\beta$  seems to be somewhat smaller than one. [Reported values for  $\beta$  range from 0.86 at very low tetraphenylborate concentrations to up to 0.98 at micromolar concentration.<sup>78</sup> At the latter value even a small diffuse-layer contribution may affect the data significantly, see (50).] The experimental result that  $\beta$  is close to one must be interpreted within the framework of the constant-field formalism as resulting from dominant interfacial adsorption (see Fig. 1 and Appendix C). Of course, if the site of adsorption is somewhat more inside the membrane, then the difference in potential between  $\Gamma_0$  and  $\Gamma_1$  might be a fraction of the total applied potential, and such an interpretation would apply to (64) as well as to the single-barrier formalism, which, in its simple form, predicts adherence to (64). The experiment of Andersen and Fuchs<sup>77</sup> underlines the need to include ionic adsorption in the continuum description.<sup>47,79</sup>

## B. Physical Basis for Modifications

The lipid bilayer provides an efficient barrier to ion permeation because of the low dielectric permittivity of its paraffinic interior and the associated Born energy.<sup>80-82</sup> Consequently, the barrier height is inversely proportional to the effective radius of the permeating ion. Moreover, close to the membrane/water interfaces, ions will still be attracted towards the medium with the higher dielectric constant, as can be described in terms of image forces. Parsegian<sup>82</sup> calculated the image force on an ion in the very middle of the membrane, and Neumcke and Lauser<sup>83</sup> extended this to any position in a thin slab of low dielectric permittivity, sandwiched between two semi-infinite regions of high dielectric constant. They found that the abrupt

changes in dielectric constant at the boundaries of the slab introduce a substantial rounding-off of the potential-energy profile (see Fig. 6). More recently, Bradshaw and Robertson<sup>84</sup> included the effect of ionic polarizability in the calculation.

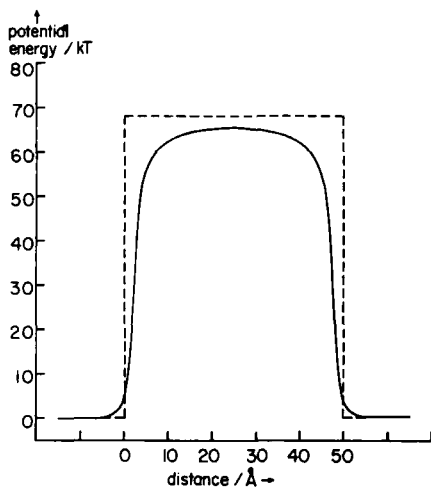


**Fig. 6.** The potential-energy barrier, in units of  $kT$ , for an ion of 2-Å radius in a 50-Å-thick membrane of relative dielectric constant  $\epsilon_r = 2$  sandwiched between aqueous phases ( $\epsilon_r = 78.5$ ). (---) Born energy barrier; (—) with image force contribution. Taken from Ref. 83.

Of course, the relative dielectric constant does not change discontinuously from 80 to 2 just beyond the hydrophilic headgroups of the membrane lipids, and a more gradual change leads to substantially reduced image potentials.<sup>85-87</sup> At the same time, however, the introduction of a more gradual variation of the dielectric constant introduces a corresponding profile in the Born energy, which again tends to round off the potential-energy profile, although it does not affect its height in the membrane interior.

Finally, studies of both lipid monolayers<sup>88</sup> and bilayers<sup>89-92</sup> yield persuasive evidence for the existence of a region of oriented dipoles in or near the hydrophilic headgroups. Again, such dipoles will modify the potential-energy profile near the membrane/water interfaces. The dipole potential depends on the nature of the membrane lipids and can be influenced by the presence of adsorbed ions and dipolar molecules (see Section IV.D).

Clearly, then, the potential-energy profile depends on the nature of both the membrane lipids and the permeating ions, and it exhibits a gradual rather than an abrupt change in going from the aqueous solution to the hydrocarbon core of the lipid bilayer membrane. This must be reflected in more realistic models.

(It is interesting to note here that, because of the image effect, membranes

thinner than about 1 nm would not provide much of a barrier to ion transport, whereas electroneutrality requirements would interfere for membranes thicker than about 10 nm. Thus the thickness range available for biologically useful bilayer membranes is rather small.)

### C. Modified Models

The continuum model can easily be modified to accommodate a specific potential-energy profile. Formally, the modification can be handled either by the introduction of a specific profile in  $\psi$  or by considering that the value of the standard chemical potential  $\mu^\ominus$  need not be constant near an interface, so that the usual expression for the electrochemical potential,

$$\bar{\mu}_i = \mu_i^\ominus + RT \ln c_i + n_i F \psi \quad (91)$$

leads to the somewhat generalized Nernst-Planck expression<sup>83</sup>

$$\frac{\partial c_i}{\partial t} = D_i \operatorname{div} \left( \frac{c_i}{RT} \operatorname{grad} \mu_i^\ominus + \operatorname{grad} c_i + \frac{n_i F c_i}{RT} \operatorname{grad} \psi \right) \quad (92)$$

to be used instead of (2). Combination with (1) now yields

$$\sum n_i F D_i \left[ \operatorname{grad} c_i + \frac{n_i F c_i}{RT} \operatorname{grad} \left( \psi + \frac{\mu_i^\ominus}{n_i F} \right) \right] + \frac{\epsilon}{4\pi} \frac{\partial}{\partial t} \operatorname{grad} \psi = I \quad (93)$$

or, restricted to ions of one kind, assuming negligible membrane curvature, and written in dimensionless form,

$$i = \frac{\partial \gamma}{\partial s} + \gamma \frac{\partial}{\partial s} (\varphi + w) + \frac{\partial E}{\partial \tau} \quad (94)$$

$$w \equiv \frac{\mu^\ominus}{RT} \quad (95)$$

Thus the effect of a change in  $\mu^\ominus$  is fully equivalent to the introduction of an additional potential  $w$ .

For steady-state measurements ( $\partial E / \partial \tau = 0$ ), (94) can be written as

$$i = \frac{\partial \gamma}{\partial s} + \gamma \frac{\partial}{\partial s} (\varphi + w) \equiv e^{-\varphi - w} \frac{d}{ds} (\gamma e^{\varphi + w}) \quad (96)$$

hence

$$i \int_0^1 e^{\varphi + w} ds = \gamma_1 e^{\varphi_1 + w_1} - \gamma_0 e^{\varphi_0 + w_0} \quad (97)$$

By our earlier notation,  $\varphi_0 = 0$  and  $\varphi_1 = v$ , so that we obtain for a symmetrical membrane ( $w_0 = w_1$ ),

$$i = \frac{\gamma_1 e^v - \gamma_0}{\int_0^1 e^{\varphi + w - w_0} ds} \quad (98)$$

Equation 98 can be used either to introduce model assumptions regarding the barrier profile<sup>83</sup> or to adjust the model parameters to fit experimental observation.<sup>93</sup> Using the latter method, Hall et al.<sup>93</sup> showed that nonactin-mediated potassium transport through membranes made from bacterial phosphatidylethanolamine in decane could be described quantitatively by a trapezoidal barrier. Appendix F illustrates the effect of the barrier profile on the current-voltage characteristics.

Instead of modifying the model for the membrane interior, one can consider as interfaces those regions where  $\mu^\ominus$  varies significantly and describe ion transport through such a region in terms of potential-dependent kinetics using, for example, the electrochemical formalism.<sup>94-97</sup> In its simplest form, a fixed fraction of the potential externally applied to the membrane is assumed to drive the interfacial kinetics, the balance being left for ion transport through the membrane interior. The data of Hall et al.<sup>93</sup> can be represented equally well by such a model<sup>97</sup> or, for that matter, by a number of other plausible ones.<sup>98</sup>

One can, of course, avoid making a choice between these two approaches by combining potential-dependent interfacial kinetics with, for example, a trapezoidal barrier profile.<sup>96,99</sup> Such a combination almost inevitably improves the fit between theoretical and experimental current-voltage curves, although it is not obvious how much of such improvement reflects a better physical model and how much derives merely from the larger number of adjustable parameters involved.

Since the single-barrier model cannot easily accommodate a specific barrier profile, it is most readily modified by the introduction of potential-dependent interfacial kinetics, so that ion permeation through the membrane is represented by three successive barriers, each with potential-dependent rate constants.<sup>96,100</sup> The effect of image force on barrier height can be taken into account explicitly.<sup>96</sup>

#### D. Complicating Factors

It might seem to be a relatively straightforward task to test some or all of the above models and to select the most appropriate one, but this is not quite the case. There are, of course, the difficulties that the current-voltage, current-time, and conductance-concentration curves are all rather structureless and that the measurement accuracy and precision are rather low (because of the limited stability and reproducibility of artificial black lipid membranes), so that no unique choice of model can be made solely on the basis of curve-fitting exercises.<sup>77,98</sup> This, however, is only part of the problem. More fundamental is the direct effect that some ions and molecules have on the kinetic parameters themselves.

Often the dependence of the membrane conductance (as measured in the

linear portion of the current-voltage curve near  $i' = v' = 0$ ) on the aqueous concentration of the permeating species does not reveal the appropriate stoichiometry. McLaughlin<sup>65</sup> showed that the near-linear conductance-concentration curve observed with 2,4-dinitrophenol results from the interplay of two opposing effects. The intrinsic conductance is a quadratic function of dinitrophenol concentration because the permeating species is the dinitrophenol-dinitrophenolate complex.<sup>101</sup> However, dinitrophenolate is strongly adsorbed at the water/membrane interface, and such adsorption produces a negative surface charge density, which in turn lowers the aqueous dinitrophenolate concentration adjacent to the membrane, the more so at higher concentrations where more is adsorbed. A similar case is observed with pentachlorophenol.<sup>102</sup> With both, at least part of the effect is due to the change in membrane charge density that accompanies the adsorption of ions, but it is likely that another effect also plays a significant role, namely, a modification of the dipole potential.

It has recently been shown that several neutral molecules, including salicylamide<sup>103</sup> and phloretin<sup>92</sup>, can have a dramatic effect on the membrane conductance of lipid-soluble ions as well as on carrier-mediated ion transport. In these cases cation conductance is decreased by about the same factor by which anion conductance is enhanced, which rules out the possibility that the effect is caused by, for example, a change in membrane fluidity.<sup>91</sup> Apparently, molecules such as phloretin are adsorbed in the membrane in such a way as to reduce, through their dipole moments, the membrane dipole potential.

Although the modification of the dipole potential is most easily studied with neutral molecules (which do not change the charge density), there is no reason to believe that the same effect cannot be caused by dipolar or polarizable ions. Indeed, the membrane conductance of cations is increased significantly by the presence of tetraphenylborate<sup>104</sup> in concentrations too low to cause a significant change of the surface charge density,<sup>69,77</sup> and the same appears to hold for picrate.<sup>105</sup>

The amount of adsorption of membrane-permeable ions may be potential dependent.<sup>77</sup> As a consequence, the current-voltage curves for such membrane-soluble anions as tetraphenylborate, dipicrylamine, picrate, dinitrophenol, and pentachlorophenol may reflect the effect of the potential-dependent adsorption of these ions on their own membrane permeation. A striking example is that of picrate, which exhibits a current-voltage curve far steeper<sup>76</sup> than accounted for even by the single-barrier model. Qualitatively, such a curve might be interpreted as resulting from the self-inhibition of adsorbed picrate (through its modification of the membrane charge density and/or dipole potential), decreasing with increasing applied potential, which reduces the amount adsorbed on that side of the membrane where the

picrate ions enter. Experimentally, the effect on the dipole potential can be distinguished from that on the diffuse double layer, since the latter depends on the ionic strength of the aqueous solutions. Moreover, dipole potentials can be correlated with Volta potential measurements on monolayers, and diffuse double-layer potentials can be correlated with electrophoretic mobilities of lipid suspensions or vesicles.<sup>90</sup>

### E. Adsorption Isotherm

To account quantitatively for such effects, an adsorption isotherm needs to be specified. Such an isotherm must be sufficiently general to account, within reasonable error, for the adsorption behavior of a number of ions, yet it should not be overparameterized. A plausible form of such an isotherm is<sup>55</sup>

$$\beta c_w = \frac{\Gamma_s \Gamma}{\Gamma_s - \Gamma} \exp [A\Gamma + \varphi_c + \varphi_d] \quad (99)$$

where the parameter  $\beta$  is related to the free energy of adsorption  $\Delta G$  by

$$\beta \equiv \exp \left[ \frac{-\Delta G_{\text{ads}}}{RT} \right] \quad (100)$$

In (99)  $\Gamma_s$  denotes the saturation value of  $\Gamma$ , and  $A$  is an interaction parameter. Since ion adsorption seldom approaches saturation coverage,  $\Gamma_s$  is not a very critical parameter, so that (99) contains three significant adjustable parameters:  $A$ ,  $\beta$ , and the ratio  $d_c/\epsilon_c$  [compare (49)]. The term  $\Gamma_s \Gamma / (\Gamma_s - \Gamma)$  represents monolayer adsorption at a fixed number of sites according to a Langmuir formalism and might be modified to account for different adsorption statistics, such as those of Flory<sup>106</sup> and Huggins.<sup>107</sup> The term  $\exp [A\Gamma]$  accounts for mutual, lateral interaction of the adsorbed particles,<sup>108</sup> and the term  $\exp [\varphi_c + \varphi_d]$  reflects the work required to bring an ion from the bulk of the aqueous solution to the adsorption site.<sup>55,109-111</sup> We note here that the simple electrostatic model used to obtain (49) does not take into account the discrete nature of the ionic charges.<sup>112-115</sup> It is not clear whether that is a serious deficiency, although a discreteness-of-charge effect might well be more significant for ions adsorbed deep inside the membrane (with low dielectric constant and little or no screening) than it is at the solution/mercury interface.

An isotherm at the water/membrane interface, of the form

$$\beta c_w = \Gamma \exp [A\Gamma] \quad (101)$$

was recently proposed by Andersen et al.<sup>116</sup> at low concentrations where  $\Gamma \ll \Gamma_s$  and when the contribution of  $\varphi_c + \varphi_d$  is insignificant. On the other hand, McLaughlin and Harary<sup>117</sup> emphasized the appropriateness of combining the diffuse double-layer correction,  $\exp [\varphi_d]$ , with the Langmuir

isotherm, leading to an expression of the form

$$\beta c_w = \frac{\Gamma_s \Gamma}{\Gamma_s - \Gamma} \exp [\varphi_d] \quad (102)$$

Clearly, (101) and (102) are special cases of (99). Combination of (99) with explicit expressions for the change in dipole potential upon adsorption should go a long way toward the mathematical description of the effects of adsorption on ion transport through bilayer membranes.

## V. CONCLUSION

The present chapter stresses the development of theory in connection with electrical measurements. Other techniques can be used to study ion transport, such as the movement of isotopes that can be followed by radiochemistry or mass spectroscopy. Such measurements can have great chemical specificity, but they lack the time resolution of their electrical counterpart. In fact, isotope transport is often limited by diffusion through the stagnant aqueous solutions next to the membrane rather than by membrane permeation itself, in which case it only carries qualitative information on the latter.

Of the models discussed in this review, the continuum model obviously operates near the limit of a macroscopic theory. (But then, the same is even more true for the Gouy-Chapman theory, which works well at a characteristic thickness  $1/\kappa$  of 3 Å!) Not only will the dielectric constant vary near the membrane interfaces, but the diffusion coefficient will not be constant either, since the middle of the membrane is more fluid than the region near the polar headgroups.<sup>118,119</sup> This difficulty is, of course, inherent in any macroscopic description of a structure that is little more than two adjacent interfaces, and is only seemingly avoided by lumping all unknown factors together in nondescript energy barriers. Other effects, such as possible mechanical deformation of the membrane ("dimpling") accompanying ion transport,<sup>120</sup> might further complicate matters.

The extensive work of Lauger and his co-workers using the single-barrier formalism has focused clearly on the interfacial rather than bulk properties of black lipid membranes and has emphasized that membrane-soluble ions may reside almost exclusively at the water/membrane interfaces rather than in the membrane interior. The equivalent continuum description explicitly takes into account specific adsorption.

The nonlinear nature of the Nernst-Planck-Poisson equations severely restricts their usefulness for the description of ion transport through ultrathin membranes. Mathematical simplifications valid at low ion concentrations, such as the constant-field and constant-concentration approximations, can provide an adequate description of most experimental observations, especi-



ally when the formalism recognizes adsorption effects and, possibly, potential-dependent interfacial kinetics. A more radical simplification, the single-barrier approach of Markin and Luger, yields even simpler mathematical relations but is also, at least in the opinion of this author, conceptually somewhat more restricted.

Studies of ion transport through membranes have gone through two main stages since the introduction of artificial black lipid membranes 15 years ago.<sup>19-21</sup> The first stage consisted of cataloging the major qualitative features and stoichiometries of ion transport; the second consisted of attempts to organize the information so assembled into a coherent mathematical framework, as sketched in this review. In the meantime, new qualitative features have been recognized, such as those discussed in Section IV.D, and these will require a revision of the mathematical models. In retrospect, virtually all membrane-soluble anions used so far to establish the shape of the current-voltage relation of black lipid membranes have now been implicated for their effect on the double-layer charge and/or dipole potential. Further progress is likely to come after such adsorption effects have been incorporated into the models in terms of adsorption isotherms. In many respects, then, the study of ion transport through membranes runs parallel to that of electrode kinetics, which is facing (and solving) strikingly similar problems.<sup>121,122</sup>

## APPENDIX A. SECOND-ORDER ESTIMATE OF THE ELECTRIC FIELD

To estimate the difference between the actual and the average field, while still assuming  $\gamma \ll 1$ , we combine (4) with the constant-field result (27)

$$E = E_0 + \int_0^s dE = E_0 - \int_0^s \gamma ds = E_0 + (\gamma_0 v - i) \frac{(e^{-vs} - 1)}{v^2} - \frac{is}{v} \quad (\text{A.1})$$

from which we obtain

$$E_{av} \equiv \int_0^1 E ds = E_0 - \frac{(\gamma_0 v - i)(e^{-v} + v - 1)}{v^3} - \frac{i}{2v} = v \quad (\text{A.2})$$

$$E = v + \frac{(\gamma_0 v - i)(ve^{-vs} + e^{-v} - 1)}{v^3} - \frac{i(s - 1/2)}{v} \quad (\text{A.3})$$

When the ionic current  $i$  is zero, (A3) reduces to

$$E = v + \gamma_0(v e^{-vs} + e^{-v} - 1)/v^2 \quad (\text{A.4})$$

which, for  $v = 0$ , further simplifies to (B.3). [A time-dependent expression such

as (35) should be used instead of the steady-state relation (27) for times of the order of, or shorter than,  $4d^2/Dv^2$ .] A second-order estimate of the integration constant  $A$  in (14) can be obtained by substitution of (A.3) into (14) or its integrated form

$$A = \int_0^1 A \, ds = E_1 - E_0 + \frac{1}{2} \int_0^1 E^2 \, ds + \frac{1}{2} i$$

## APPENDIX B. THE CONSTANT-CONCENTRATION APPROXIMATION

When the externally applied field tends to zero, it is no longer justifiable to neglect the small internal field resulting from the ionic charges in the membrane. Instead of (24) we can use in this case

$$\frac{dE}{ds} \approx A \quad (\text{B.1})$$

According to (4)  $dE/ds = -\gamma$  for all  $s$ ; hence we have  $\gamma = -A$ , a constant. Substitution of this result into (15) leads to

$$\varphi = \frac{1}{2} \gamma_0 s(s-1) \quad (\text{B.2})$$

$$E = -\gamma_0(s - \frac{1}{2}) \quad (\text{B.3})$$

$$\gamma = \gamma_0 = \gamma_1 \quad (\text{B.4})$$

$$\frac{d\gamma}{ds} = \gamma_0^2(s - \frac{1}{2}) \quad (\text{B.5})$$

Of course, the range of validity of this constant concentration approximation<sup>44</sup> is restricted to  $\gamma \ll 1$  and near-zero applied electric fields.

## APPENDIX C. ON THE IONIC DISPLACEMENT CHARGE DENSITY

We assume here that some of the membrane-soluble ions are adsorbed at the membrane/solution interfaces, while the remainder are dissolved in the membrane interior and distributed across the membrane according to the constant-field result [see (27) with  $i=0$ ]

$$\gamma = \gamma_0 e^{-\nu s} \quad (\text{C.1})$$

Furthermore, we assume, for mathematical convenience, a linear (Henry's law) relation between  $\Gamma_n$  and  $\gamma_n$  ( $n=0, 1$ ), as might be a reasonable first-order approximation to (99) at low values of  $\Gamma$  and with aqueous solutions of high

ionic strength,

$$\Gamma_0 = B\gamma_0 \quad \Gamma_1 = B\gamma_1 = B\gamma_0 e^{-v} \quad (\text{C.2})$$

For a constant total number of ions in the membrane (see Section II.F) we then have

$$\begin{aligned} \Gamma_0 + \Gamma_1 + \int_0^1 \gamma \, ds &= B\gamma_0(1 + e^{-v}) + \gamma_0 \int_0^1 e^{-vs} \, ds \\ &= \frac{\gamma_0}{v} [e^{-v}(Bv - 1) + (Bv + 1)] = C^* \end{aligned} \quad (\text{C.3})$$

so that

$$\gamma_0 = \frac{C^* v}{e^{-v}(Bv - 1) + (Bv + 1)} \quad (\text{C.4})$$

$$\Delta q = -\Gamma_1 - \int_0^1 \gamma s \, ds + \frac{C^*}{2} = \frac{C^* [(Bv^2 - 2)(1 - e^{-v}) + v(e^{-v} + 1)]}{2ve^{-v}(Bv - 1) + 2v(Bv + 1)} \quad (\text{C.5})$$

$$\Delta q_m = \lim_{v \rightarrow \infty} \Delta q = -\frac{C^*}{2} \quad (\text{C.6})$$

$$\frac{\Delta q}{\Delta q_m} = \frac{(Bv - 2/v)(e^{-v} - 1) - (e^{-v} + 1)}{e^{-v}(Bv - 1) + Bv + 1} \quad (\text{C.7})$$

For  $B \rightarrow 0$  and  $B \rightarrow \infty$ , (C.7) simplifies to (63) and (64), respectively. Equation (C.7) is plotted in Fig. 1 for various values of the adsorption parameter  $B$ .

The interpretation of the ionic displacement charge density is straightforward only when the aqueous concentration of the adsorbing ions is so low that aqueous diffusion into and out of the membrane need not be taken into account in the interpretation of the data. For this reason we have used here a Henry isotherm. At higher concentrations and corresponding surface excesses, a more realistic isotherm such as (99) should be used, and the effect of the aqueous double-layer potentials [see (50)] should also be considered.

#### APPENDIX D. RESPONSE TO VARIOUS SMALL-AMPLITUDE PERTURBATIONS

We indicate here how the response to various small-amplitude perturbations can be obtained directly from the membrane admittance  $Y(\omega)$ . We start by replacing all terms  $j\omega$  in  $Y(\omega)$  by  $p$ , and thus obtain the transfer admittance  $Y(p)$ . For a potential step of amplitude  $V$ , the current density then follows as

$$I(t) = V \mathcal{L}^{-1} \left\{ \frac{Y(p)}{p} \right\} \quad (\text{D.1})$$

where  $\mathcal{L}^{-1}$  denotes the inverse Laplace transformation. For a current

density step of amplitude  $I$ , the voltage transient is given by

$$V(t) = I \mathcal{L}^{-1} \left\{ \frac{1}{pY(p)} \right\} \quad (\text{D.2})$$

For a charge step, the voltage transient measured at open circuit after injection of a charge density  $Q$  is given by

$$V(t) = Q \mathcal{L}^{-1} \left\{ \frac{1}{Y(p)} \right\} \quad (\text{D.3})$$

Results such as the above can also be used to interrelate the responses to the various small-amplitude step function methods. For example, use of (D.1) and (D.3) shows that the voltage transient  $V(t)$  following a charge step of amplitude  $Q$  is related to the current transient  $I(t)$  following a voltage step of amplitude  $V$  by

$$V(t) = QV \mathcal{L}^{-1} \left\{ \frac{1}{p \mathcal{L}[I(t)]} \right\} \quad (\text{D.4})$$

## APPENDIX E. EQUIVALENT CIRCUIT REPRESENTATIONS

There are several ways in which an equivalent circuit can be obtained and used. One is to use it as a convenient, shorthand notation for experimentally observed behavior, in much the same way in which arbitrary parameters may often be represented by power laws or polynomial expansions. We do not deal with such use of equivalent circuits here, but only note that experimental observation per se seldom if ever leads to a unique equivalent circuit,<sup>123</sup> so that interpretation of the circuit parameters thus obtained in terms of physical phenomena is tenuous at best.

An alternative procedure is one in which the equivalent circuit is derived from a mathematical model. Such a circuit is sometimes unique in a physical sense in that each physical phenomenon is represented by a single circuit element.<sup>67</sup> Figure 3 is an example of such an equivalent circuit, which, incidentally, can be arrived at using different model assumptions (see Sections II.G and III.D). In this instance the physical interpretation of the various circuit elements happens to be the same for both models, although the translation from electrical into physicochemical parameters may differ: the membrane resistance  $R$  would be interpreted in terms of a diffusion coefficient in the continuum approach, but as a rate constant in the single-barrier formalism.

A somewhat intermediate approach is to derive a model that assumes a particular equivalent circuit representation for a specific physical phenomenon. Such a method may have some intuitive physical appeal. A prime

example of such an approach in electrochemistry can be found in the work of Barker,<sup>124</sup> and examples in the present context are, for example, Lauger's model of the effect of aqueous diffusion<sup>125</sup> and the three-capacitor model of Lebedev and Boguslavskii<sup>126</sup> and Markin et al.<sup>127</sup> A word of caution is in order. Intuitive use of circuit elements does not always result in their correct placement (cf. Refs. 47 and 125) or may lead to a circuit that is only seemingly, but not operationally, different. For instance, the three-capacitor model<sup>126,127</sup> yields the same transient and ac response as the single-barrier model of Ketterer et al.<sup>69</sup> or its constant-field counterpart.<sup>67</sup> Also, the interplay of various physical phenomena that, considered separately, are represented accurately by individual circuit elements, can lead to phenomenological "coupling" not represented by a mere combination of such circuit elements,<sup>97</sup> an effect well known in electrode kinetics.<sup>128,129</sup>

## APPENDIX F: THE SHAPE OF INTRINSIC CURRENT-VOLTAGE CURVES

The effect of the potential-energy profile on the shape of the current-voltage relation is readily appreciated by considering (98) with an assumed profile. We take here a symmetrical profile of the form

$$w = h e^{-a(|2s-1|)^m} \quad (\text{F.1})$$

where  $h$  denotes the barrier height in the middle of the membrane, and the parameter  $m$  ( $m \geq 2$ ) regulates the width of the essentially flat central portion of the profile (see Fig. 7). Finally, the parameter  $a$  defines the height at which the various profiles intersect, chosen here as about 5%, compare fig. 6. Corresponding current-voltage relations assuming  $\gamma_0 = \gamma_1 = \gamma$  can then be calculated by numerical integration of

$$\frac{i}{\gamma} = \frac{e^v - 1}{\int_0^1 e^{vs + h \exp[-a(|2s-1|)^m] - h \exp[-a]} ds} \quad (\text{F.2})$$

Although there is a unique relation between an assumed potential-energy profile  $w$  and the resulting current-voltage curve, the reverse is not true at all: there are an infinite number of possible profiles (including a fair number of plausible ones<sup>93,97,98</sup>) which will lead to the same integral in the denominator of (98), and hence to the same current-voltage curve, even in the absence of interfacial complications. Figure 8 illustrates the shape of the current-voltage curves calculated from (F.2).

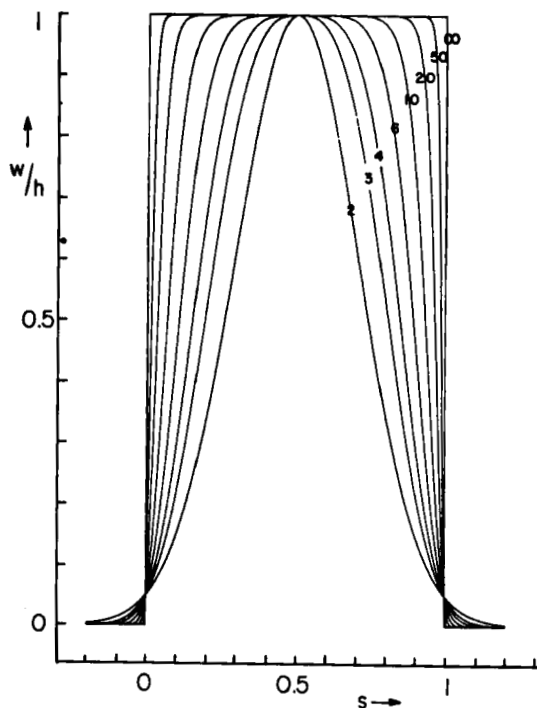


**Fig. 7.** The potential-energy profiles  $w/h$  of (F.1) as functions of the dimensionless distance parameter  $s$ , calculated for various values of the parameter  $m$  as indicated on the curves. The parameter  $a$  is taken to be 3.

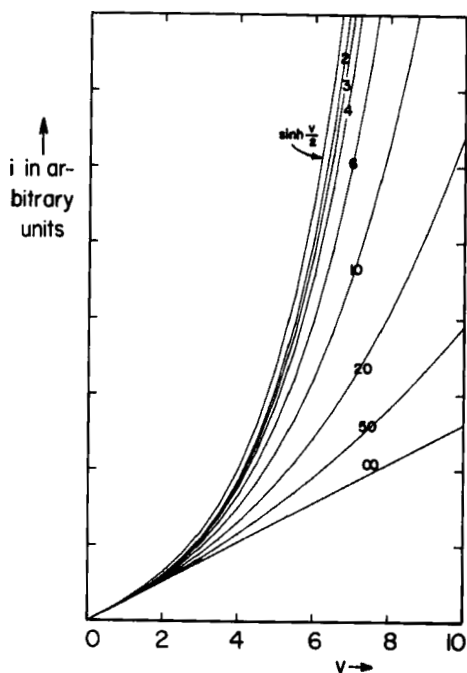


**Fig. 8.** Current-voltage curves calculated from (F.2) using  $A=3$ ,  $h=50$ , and the values of  $m$  indicated on the curves. All curves have been scaled so that their conductances at vanishingly small voltages are the same. Also shown on the same scale is the function  $\sinh v/2$  which is obtained from the single-barrier model, compare (76). Note that a relatively small rounding of the square profile in Fig. 7 (e.g., curve  $m=20$ ) causes a pronounced departure from linearity in the current-voltage curve.

# APPENDIX G. GLOSSARY OF SYMBOLS USED

<i>a</i>	Parameter; see (F.1)
<i>A</i>	Integration constant; see (14)
	Interaction coefficient; see (99)
<i>B</i>	$4\pi n^2 F^2 d^2 \beta / \epsilon RT$ , adsorption coefficient; see (C.2)
<i>C</i>	Integration constant
<i>c</i>	Concentration
<i>D</i>	Diffusion coefficient
<i>d</i>	Thickness
<i>E</i>	$(nFd/RT)/(d\psi/dx)$ , dimensionless electric field; see (8)
<i>F</i>	Faraday
<i>F<sub>n</sub></i>	Interfacial parameter; see (70)
<i>f</i>	Function
<i>G</i>	Conductance per unit area
<i>G<sub>n</sub></i>	Interfacial parameter; see (90)
$\Delta G$	Free energy of adsorption
<i>g</i>	$4\pi d^3 G / D\epsilon$ , dimensionless conductance; see (23)
<i>h</i>	Barrier height parameter; see (F.1)
<i>I</i>	Current density
<i>I<sub>v</sub></i>	Modified Bessel function; see (19)
<i>i</i>	$4\pi nFd^3 I / D\epsilon RT$ , dimensionless current density; see (10)
<i>J</i>	Ionic flux
<i>J<sub>v</sub></i>	Bessel function; see (17)
<i>j</i>	$(-1)^{1/2}$ , see (39)
<i>K</i>	Partition coefficient
<i>k</i>	Rate constant
$\mathcal{L}$	Laplace transform symbol; see (33), (D1)
<i>m</i>	Integer
<i>N</i>	Total concentration
<i>n</i>	Valence; see (1)
	Surface concentration; see (76)
	0 or 1; see (67)
<i>p</i>	Laplace transform operator; see (33)
<i>Q</i>	Charge density
<i>q</i>	$4\pi nFdQ/\epsilon RT$ , dimensionless charge density; see (47)
<i>R</i>	Gas constant
<i>r</i>	$(1 + 4pd^2/Dv^2)^{1/2}$ ; see (36)
<i>s</i>	$x/d$ , dimensionless distance across membrane; see (11)
<i>T</i>	Absolute temperature
<i>t</i>	Time
<i>V</i>	Potential
<i>v</i>	$nF(\psi_1 - \psi_0)/RT$ , dimensionless potential

$w$	$\mu^{\ominus}/RT$ , dimensionless standard chemical potential; see (95)
$Y$	Admittance per unit area; see (89)
$y$	$4\pi d^3 Y/D\epsilon$ , dimensionless admittance; see (73)
$\alpha$	$-(2A - 2is)^{3/2}/6i$ ; see (20) Transfer coefficient; see (74)
$\beta$	$-(2is - 2A)^{3/2}/6i$ ; see (18) Adsorption coefficient; see (100)
$\Gamma$	Surface excess; see (57)
$\gamma$	$4\pi n^2 F^2 d^2 c/\epsilon_w RT$ , dimensionless concentration; see (9)
$\epsilon$	Dielectric constant
$\eta$	Effective rate constant; see (82)
$\kappa$	$(4\pi F^2 \Sigma n^2 c^*/\epsilon_w RT)^{1/2}$ , reciprocal Gouy-Chapman length; see (48) $\partial k/\partial v$ , see (86)
$\lambda$	$-\frac{1}{2}v' \pm \frac{1}{2}[(v')^2 + 4v]^{1/2}$ , see (44)
$\mu$	Chemical potential; see (91)
$\nu$	$j\omega d^2/D$ , dimensionless frequency; see (41)
$\tau$	$Dt/d^2$ , dimensionless time; see (12)
$\varphi$	$nF\psi/RT$ , dimensionless potential; see (7)
$\psi$	Potential
$\omega$	Angular frequency

## Superscripts

—	Laplace-transformed function; see (33)
-	Electrochemical; see (91)
$\ominus$	Standard state
'	Direct component; see (38)
"	Alternating component; see (38)
*	Bulk aqueous solution

## Subscripts

0, 1	Value of $s$
$a$	Applied; see (51)
$av$	Average; see (32)
$c$	Compact double layer; see (49) Complexation; see (55) and (77)
$d$	Diffuse double layer, see (48) Dissociation; see (55) and (77)
$i$	Arbitrary species
$M$	Membrane, see (65) and (87)
$s$	Saturation, see (99)
$T$	Translocator = carrier; see (51)
$W$	Aqueous; see (46)



### Acknowledgment

The author gratefully acknowledges intensive discussions with Professor S. K. Rangarajan and helpful comments on earlier versions of this manuscript from Dr. K. M. Abbey, Dr. O. S. Andersen, Dr. J. A. Hashmall, Dr. S. McLaughlin, and Dr. A. Parsegian.

### References

1. P. Mueller and D. O. Rudin, *J. Theor. Biol.*, **4**, 268 (1963).
2. P. Mueller and D. O. Rudin, *Nature*, **217**, 713 (1968).
3. P. Mueller and D. O. Rudin, *J. Theor. Biol.*, **18**, 222 (1968).
4. P. Mueller and D. O. Rudin, *Curr. Topics Bioenerg.*, **13**, 157 (1969).
5. R. C. Bean, W. C. Shepherd, H. Chan, and J. Eichner, *J. Gen. Physiol.*, **53**, 741 (1969).
6. S. B. Hladky and D. A. Haydon, *Nature*, **225**, 451 (1970).
7. D. W. Urry, *Proc. Natl. Acad. Sci. U.S.*, **68**, 672 (1971).
8. S. Krasne, G. Eisenman, and G. Szabo, *Science*, **174**, 412 (1971).
9. R. Latorre, G. Ehrenstein, and H. Lecar, *J. Gen. Physiol.*, **60**, 72 (1972).
10. L. G. M. Gordon and D. A. Haydon, *Biochim. Biophys. Acta*, **274**, 313 (1972).
11. M. Eisenberg, J. E. Hall, and C. A. Mead, *J. Membrane Biol.*, **14**, 143 (1973).
12. E. Bamberg and P. Läuger, *J. Membrane Biol.*, **11**, 177 (1973).
13. G. Baumann and P. Mueller, *J. Supramol. Struct.*, **2**, 538 (1974).
14. P. Mueller, *MTP Int. Revs. Biochem.* (1)**3**, 75 (1975).
15. P. Mueller, *Ann. N.Y. Acad. Sci.*, **264**, 247 (1975).
16. E. Gorter and F. Grendel, *J. Exp. Med.*, **41**, 439 (1925).
17. J. F. Danielli and H. Davson, *J. Cell Comp. Physiol.*, **5**, 495 (1935).
18. J. D. Robertson, *Biochem. Soc. Symp.*, **16**, 3 (1959).
19. P. Mueller, D. O. Rudin, H. T. Tien, and W. C. Wescott, *Nature*, **194**, 979 (1962).
20. P. Mueller, D. O. Rudin, H. T. Tien, and W. C. Wescott, *Circulation*, **26**, 1167 (1962).
21. P. Mueller, D. O. Rudin, H. T. Tien, and W. C. Wescott, *J. Phys. Chem.*, **67**, 534 (1963).
22. M. Takagi, K. Azuma and U. Kishimoto, *Ann. Repts. Biol. Works, Fac. Sci., Osaka Univ.*, **13**, 107 (1965).
23. M. Montal and P. Mueller, *Proc. Nat. Acad. Sci. USA*, **69**, 3561 (1972).
24. M. Montal, *Methods Enzymol.*, **32**, 545 (1974).
25. S. H. White, D. C. Petersen, S. Simon, and M. Yafuso, *Biophys. J.*, **16**, 481 (1976).
26. R. E. Pagano, J. M. Ruysschaert, and I. R. Miller, *J. Membrane Biol.*, **10**, 11 (1972).
27. A. S. Bunce and R. C. Hider, *Biochim. Biophys. Acta*, **363**, 423 (1974).
28. D. A. Haydon and S. B. Hladky, *Q. Rev. Biophys.*, **5**, 187 (1972).
29. R. A. Arndt and L. D. Roper, *Simple Membrane Electrodifffusion Theory*, Phys. Biol. Sci. Misc., Blacksburg, Va. 1972.
30. P. Läuger and B. Neumcke, *Membranes*, **2**, 1 (1973).
31. S. M. Ciani, G. Eisenman, R. Laprade, and G. Szabo, *Membranes*, **2**, 61 (1973).
32. V. S. Markin and Yu. A. Chizmadzhev, *Induced Ion Transport*, Nauka, Moscow, 1974.
33. B. Neumcke and E. Bamberg, *Membranes*, **3**, 251 (1975).
34. M. K. Jain, *The Bimolecular Lipid Membrane*, Van Nostrand-Reinhold, New York, 1972.
35. G. Szabo, G. Eisenman, R. Laprade, S. M. Ciani, and S. Krasne, *Membranes*, **2**, 179 (1973).
36. W. Simon and W. E. Morf, *Membranes*, **2**, 329 (1973).
37. Yu. A. Ovchinnikov, V. T. Ivanov, and A. M. Shkrob, *Membrane-Active Complexones*, Elsevier, Amsterdam, 1974.
38. H. T. Tien, *Bilayer Lipid Membranes*, Dekker, New York, 1974.
39. S. McLaughlin and M. Eisenberg, *Ann. Revs. Biophys. Bioeng.*, **4**, 335 (1975).
40. E. Grell, T. Funck, and F. Eggers, *Membranes*, **3**, 1 (1975).

41. R. Laprade, S. M. Ciani, G. Eisenman, and G. Szabo, *Membranes*, **3**, 127 (1975).
42. R. de Levie, *J. Electroanal. Chem.*, **69**, 265 (1976).
43. S. M. Skinner, *J. Appl. Phys.*, **26**, 498 (1955).
44. R. de Levie and H. Moreira, *J. Membrane Biol.*, **9**, 241 (1972).
45. S. M. Skinner, *J. Appl. Phys.*, **26**, 509 (1955).
46. R. de Levie, N. G. Seidah, and H. Moreira, *J. Membrane Biol.*, **10**, 171 (1972).
47. R. de Levie, N. G. Seidah, and H. Moreira, *J. Membrane Biol.*, **16**, 17 (1974).
48. R. de Levie and N. G. Seidah, *J. Membrane Biol.*, **16**, 1 (1974).
49. T. Teorell, *Progr. Biophys. Biophys. Chem.*, **3**, 305 (1953).
50. S. K. Rangarajan, private communication, 1976.
51. D. E. Goldman, *J. Gen. Physiol.*, **27**, 37 (1943).
52. N. F. Mott, *Proc. Roy. Soc. (London)*, **A171**, 27 (1939).
53. K. S. Cole, *Physiol. Rev.*, **45**, 340 (1965).
54. O. Stern, *Z. Elektrochem.*, **30**, 508 (1924).
55. R. de Levie, *J. Electroanal. Chem.*, **82**, 361 (1977).
56. D. Walz, E. Bamberg, and P. Läuger, *Biophys. J.*, **9**, 1150 (1969).
57. S. B. Hladky, *Biochim. Biophys. Acta*, **307**, 261 (1973).
58. J. Koutecký and R. Brdicka, *Coll. Czech. Chem. Commun.*, **12**, 337 (1947).
59. O. H. LeBlanc Jr., *J. Membrane Biol.*, **4**, 227 (1971).
60. B. Neumcke, *T. I. T. J. Life Sci.*, **1**, 85 (1971).
61. J. Koutecký, *Coll. Czech. Chem. Commun.*, **19**, 857 (1954).
62. R. Brdicka, *Coll. Czech. Chem. Commun.*, **12**, 212 (1947).
63. R. Brdicka, *Coll. Czech. Chem. Commun.*, **19**, 41 (1954).
64. S. McLaughlin, G. Szabo, G. Eisenman, and S. M. Ciani, *Proc. Natl. Acad. Sci. US*, **67**, 1268 (1970).
65. S. McLaughlin, *J. Membrane Biol.*, **9**, 361 (1971).
66. S. McLaughlin, G. Szabo, and G. Eisenman, *J. Gen. Physiol.*, **58**, 667 (1972).
67. R. de Levie and D. Vukadin, *J. Electroanal. Chem.*, **62**, 95 (1975).
68. V. S. Markin, *Mol. Biol.*, **3**, 610 (1969).
69. B. Ketterer, B. Neumcke, and P. Läuger, *J. Membrane Biol.*, **5**, 225 (1971).
70. J. Tafel, *Z. Phys. Chem.*, **50**, 641 (1905).
71. J. A. V. Butler, *Trans. Faraday Soc.*, **19**, 729 (1924).
72. T. Erdey-Gruz and M. Volmer, *Z. Phys. Chem.*, **150**, 203 (1930).
73. S. Glasstone, K. J. Laidler, and H. Eyring, *The Theory of Rate Processes*, McGraw-Hill, New York, 1941.
74. P. Läuger and G. Stark, *Biochim. Biophys. Acta*, **211**, 458 (1971).
75. G. Stark, B. Ketterer, R. Benz, and P. Läuger, *Biophys. J.*, **11**, 981 (1971).
76. E. Bamberg, Dissertation, Basel, 1971 as quoted in ref. 30.
77. O. S. Andersen and M. Fuchs, *Biophys. J.*, **15**, 795 (1975).
78. O. S. Andersen, S. McLaughlin, and S. Feldberg, private communications, Dec. 1976.
79. R. de Levie, N. G. Seidah, and D. Larkin, *J. Electroanal. Chem.*, **49**, 153 (1974).
80. M. Born, *Z. Physik*, **1**, 45 (1920).
81. A. Finkelstein and A. Cass, *J. Gen. Physiol.*, **52**, 145 (1968).
82. A. Parsegian, *Nature*, **221**, 844 (1969).
83. B. Neumcke and P. Läuger, *Biophys. J.*, **9**, 1160 (1969).
84. R. W. Bradshaw and C. R. Robertson, *J. Membrane Biol.*, **25**, 93 (1975).
85. F. P. Buff and N. S. Goel, *J. Chem. Phys.*, **51**, 4983, 5363 (1969).
86. J. R. Clay, N. S. Goel, and F. P. Buff, *J. Chem. Phys.*, **56**, 4245 (1972).
87. J. W. Perram and N. M. Barber, *Mol. Phys.*, **28**, 131 (1974).
88. N. K. Adam, *The Physics and Chemistry of Surfaces*, Oxford University Press, London, 1941.

89. V. V. Denim, A. M. Shkrob, and Yu. A. Ovchinnikov, *Int. Biophys. Congr. Moscow*, **4**, 149 (1972).
90. D. A. Haydon and V. B. Myers, *Biochim. Biophys. Acta*, **307**, 429 (1973).
91. G. Szabo, *Nature*, **252**, 47 (1974).
92. O. S. Andersen, A. Finkelstein, I. Katz, and A. Cass, *J. Gen. Physiol.*, **67**, 749 (1976).
93. J. E. Hall, C. A. Mead, and G. Szabo, *J. Membrane Biol.*, **11**, 75 (1973).
94. L. Y. Wei and B. Y. Woo, *J. Biol. Phys.*, **1**, 50 (1973).
95. L. Y. Wei and B. Y. Woo, *Bull. Math. Biol.*, **36**, 229 (1974).
96. S. B. Hladky, *Biochim. Biophys. Acta*, **352**, 71 (1974).
97. R. de Levie and K. M. Abbey, *J. Theor. Biol.*, **56**, 151 (1976).
98. S. Ginsburg and D. Noble, *J. Membrane Biol.*, **29**, 211 (1976).
99. G. Eisenman, S. Krasne, and S. M. Ciani, *Ann. N.Y. Acad. Sci.*, **264**, 34 (1975).
100. W. Knoll and G. Stark, *J. Membrane Biol.*, **25**, 249 (1975).
101. E. J. A. Lea and P. C. Croghan, *J. Membrane Biol.*, **1**, 225 (1969).
102. P. Smejtek, K. Hsu and W. H. Perman, *Biophys. J.*, **16**, 319 (1976).
103. S. McLaughlin, *Nature*, **243**, 234 (1973).
104. Ye. A. Liberman and V. P. Topaly, *Biofiz.*, **14**, 452 (1969).
105. V. S. Markin, V. V. Klochkov, Ye. A. Liberman, and V. P. Topaly, *Biofiz.*, **16**, 626 (1971).
106. P. J. Flory, *J. Chem. Phys.*, **10**, 51 (1942).
107. M. L. Huggins, *J. Phys. Chem.*, **46**, 151 (1942); *Ann. N.Y. Acad. Sci.*, **43**, 1 (1942).
108. A. N. Frumkin, *Z. Physik*, **35**, 792 (1926).
109. D. C. Grahame, *J. Am. Chem. Soc.*, **80**, 4201 (1958).
110. J. M. Parry and R. Parsons, *Trans. Faraday Soc.*, **59**, 241 (1963).
111. M. A. V. Devanathan and B. V. K. S. R. A. Tilak, *Chem. Rev.*, **65**, 635 (1965); *Proc. Roy. Soc. (London)*, **A290**, 527 (1966).
112. O. A. Esin and V. M. Shikov, *Zh. Fiz. Khim.*, **17**, 236 (1943).
113. B. V. Ershler, *Zh. Fiz. Khim.*, **20**, 679 (1946).
114. S. Levine, G. M. Bell, and D. Calvert, *Can. J. Chem.*, **40**, 518 (1962).
115. C. A. Barlow and J. R. Macdonald, *J. Chem. Phys.*, **40**, 1535 (1964).
116. O. S. Andersen, S. Feldberg, H. Nakadomari, S. Levy, and S. McLaughlin, in *Ion Transport Across Membranes*, Raven Press, 1977.
117. S. McLaughlin and H. Harary, *Biochemistry*, **15**, 1941 (1976).
118. W. L. Hubbell and H. M. McConnell, *J. Am. Chem. Soc.*, **93**, 314 (1971).
119. P. B. Hitchcock, R. Mason, K. M. Thomas, and G. G. Shipley, *Proc. Natl. Acad. Sci. US*, **71**, 3036 (1974).
120. V. A. Parsegian, *Ann. N.Y. Acad. Sci.*, **264**, 161 (1975).
121. P. Delahay, *Double Layer and Electrode Kinetics*, Wiley, New York, 1965.
122. J. Albery, *Electrode Kinetics*, Clarendon Press, Oxford, 1975.
123. O. J. Zobel, *Bell Syst. Tech. J.*, **2**, 1 (1923).
124. G. C. Barker, *Pure Appl. Chem.*, **15**, 239 (1967).
125. P. Luger, J. Richter, and W. Lesslauer, *Ber. Bunsenges.*, **71**, 906 (1967).
126. A. V. Lebedev and L. I. Boguslavskii, *Biofiz.*, **16**, 221 (1971).
127. V. S. Markin, P. A. Grigorev, and L. N. Yermishkin, *Biofiz.*, **16**, 1011 (1971).
128. P. Delahay, *J. Phys. Chem.*, **70**, 2067, 2373 (1966).
129. S. K. Rangarajan, *J. Electroanal. Chem.*, **55**, 297, 329 (1974).
130. S. K. Ranjarajan and R. de Levie, in preparation.

# THE STATISTICAL MECHANICS OF SQUARE-WELL FLUIDS

KRAEMER D. LUKS

*Department of Chemical Engineering, University of Notre Dame,  
Notre Dame, Indiana*

JOHN J. KOZAK

*Department of Chemistry, University of Notre Dame,  
Notre Dame, Indiana*

## CONTENTS

I. Introduction . . . . .	140
II. Properties of the $\theta$ -Expanded YBG Equation for Square-Well Molecules . . . . .	145
A. Interpretation of the Expansion as a Perturbation Theory . . . . .	145
B. The $\theta$ Expansion of the YBG Equation for Square-Well Molecules. . . . .	146
C. Comparison of the Results of the $\theta$ -Expanded YBG Equation with Machine Calculations . . . . .	149
D. Other Results Using the $\theta$ -Expanded YBG Equation for Square-Well Molecules . . . . .	154
III. Properties of the Unexpanded YBG Equation for Square-Well Molecules . . . . .	155
A. The YBG Hard-Sphere Problem . . . . .	155
B. The YBG Square-Well Problem. . . . .	158
C. Analysis of the Solutions of the YBG Equation . . . . .	167
IV. Phase transitions in Square-Well Fluids. . . . .	172
V. Equation-of-State Behavior for Square-Well Fluids Near the Critical Point . . . . .	180
VI. Transport Properties of the Square-Well Dense Fluid . . . . .	185
A. A Perspective on the Square-Well Transport Problem . . . . .	185
B. Results Obtained From the Davis-Rice-Sengers Theory . . . . .	186
VII. Concluding Remarks . . . . .	194
References . . . . .	198

## I. INTRODUCTION

It is often taken as a fundamental axiom of statistical mechanics that if one were to incorporate a sensible potential function within the framework of that theory, there should result an essentially correct description of the states of matter. Further, it is believed that such a description should include, as well, a characterization of the possible transformations, that is, phase transitions, between or among the states of the system under study. Of course, such an assertion must be proved, and in recent years very considerable progress has been made in obtaining rigorous results on the problem of the thermodynamic limit, the stability of classical and quantum systems, and the nature of irreversibility.<sup>1</sup> Moreover, very beautiful theories have been developed to describe particular states of matter, and great strides have been taken in the understanding of cooperative phenomena. One need only recall, for example, the astonishing success of the recently developed theories of the liquid state, theories based on the century-old ideas of van der Waals<sup>2</sup> and given modern expression by Zwanzig<sup>3</sup>; particularly from the work of Barker and Henderson<sup>4</sup>, Verlet and Weis<sup>5</sup>, and Andersen et al.,<sup>6</sup> we now realize the important advantages gained by a proper interpretation of the hard-sphere fluid and the relationship of this system to one characterized by both attractive and repulsive interactions. And, with respect to cooperative phenomena, the significant advances, both qualitative and quantitative, in our understanding of critical phenomena,<sup>7-9</sup> have given a definite sense of progress, even in dealing with the old dilemma of how singularities can arise in thermodynamic functions that are otherwise analytic.

Despite these and other advances, a *conceptual* question that remains open is whether or not there exists in statistical mechanics a *single* theoretical framework within which the equilibrium and transport properties of the gaseous, liquid, and solid states of matter can be calculated with reasonable quantitative success, and which provides as well at least a qualitatively correct description of the possible transformations among the states of matter. It is to this question that the present review is addressed. We attempt to show that a distribution-function theory, in particular one version of the BBGKY formulation,<sup>10,11</sup> the Yvon-Born-Green (YBG) theory for the pair distribution function under the superposition approximation, when used in conjunction with the simplest intermolecular potential function that possesses both attractive and repulsive parts, the square-well potential (Fig. 1), does achieve a certain success in realizing the overall program described above.

Before proceeding with an exposition of the results per se, we must address two questions: (1) Why choose as the "single theoretical framework" the YBG equation for the pair distribution function when it is known that that theory does not enjoy great quantitative success in property calculations for the

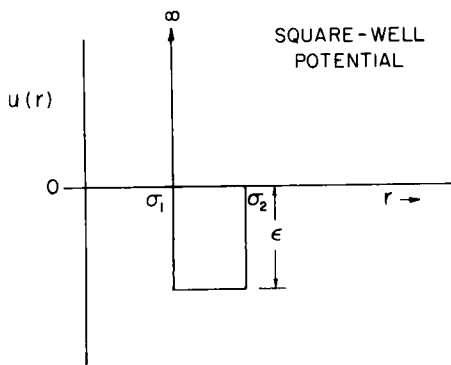


**Fig. 1.** The square-well intermolecular potential model. (From Ref. 66, "A comparative analysis of the Rice-Allnatt and square-well transport theories." Used by permission of Gordon and Breach Science Publishers.)

hard-sphere and Lennard-Jones fluids? and (2) Why choose as the potential function such a hopelessly approximate function as the square-well potential? With regard to the latter point, it is true that the square-well potential function hardly describes the kind of distance dependence one believes characterizes the spatial energetic relationship between pairs of atoms or molecules. Indeed, molecular-beam experiments have demonstrated convincingly that many-parameter fits are necessary to reproduce quantitatively the potential functions for even the simplest atomic systems. Yet, there is a belief, at least among those working in statistical mechanics, that if a many-parameter potential function were idealized as a square-well potential, but "the statistical mechanical consequences of such a potential were then determined without further approximation, there would undoubtedly result an essentially correct description of all the macroscopic properties of matter throughout a vast region of the  $P, T$  plane, including the neighborhoods of the triple and critical points," as stated by Widom<sup>12</sup>. He then goes on to say, "what matters is not the quantitative accuracy of the assumed  $\phi(r)$  but rather the qualitative accuracy of the resulting spatial correlations of molecular positions." These remarks represent a conceptual rationalization for statistical mechanical studies performed using the square-well potential. The more pragmatic (i.e., "experimental") rationale for this choice of potential function, however, is that the kind of broad program described above, whose objective is to characterize the equilibrium and transport properties of the gaseous, liquid, and solid states of matter, as well as the possible phase transformations among these states, would be quite impossible to realize for other choices of potential function (except the hard-sphere potential), given the computational facilities available at most institutions where such studies have been performed.

Turning next to the choice of theoretical framework, the equation for the

pair distribution function developed by Yvon, Born, and Green, it would seem that this choice is a bit out of step with the times, inasmuch as it is known, both for the hard-sphere fluid and the Lennard-Jones fluid, that the results generated by numerical solution of the YBG equation for  $g^{(2)}(r)$  are not as close to the molecular dynamics calculations (which provide the "experimental" data for these idealized potentials) as the hypernetted chain (HNC) results and compare even worse with the Percus-Yevick (PY) results. However, as pointed out a decade ago by Rice et al.,<sup>11,13</sup> there is "one consideration which weighs strongly for the YBG and against the PY and HNC theories: the existence of a phase transition. Solution of the latter two equations for the hard sphere fluid shows that the pressure continues to be a smooth function of the density even into the (unphysical) region more dense than a system of close-packed spheres. The YBG equation, on the other hand, becomes *divergent* [sic] beyond a certain critical density, and Kirkwood has shown that this density corresponds to the onset of long-range order in the system. We may take this as indicating that the Yvon-Born-Green-Kirkwood approach is qualitatively sound, and that it can be made quantitatively correct by improvements on the superposition approximation." We remark in passing that the possibility raised by Rice and Lekner was realized with some success by these authors in their study of the hard-sphere fluid, by Rice and Young in their study of the Lennard-Jones fluid,<sup>14</sup> and by Lee et al.<sup>15</sup> in their extensive calculations on the second equation of the YBG hierarchy (where pair- and triplet-distribution functions were used to make a superposition approximation to the quadruplet distribution function, and the equations for  $g^{(2)}$  and  $g^{(3)}$  were then solved simultaneously). Though more recent work (described later herein) has modulated somewhat Kirkwood's identification of a critical density, the main point to be stressed here is that the YBG equation under the superposition approximation can describe with a fair degree of success not only the solid-liquid transition, but also the gas-liquid transition, with the latter characterized by distinctly nonclassical critical exponents.

There are several ancillary features of the YBG equation, and the ever-present superposition approximation, which encourage, or at least do not discourage, continued examination of this equation for the pair distribution function. Firstly, the renaissance of interest in recent years in the theory of classical fluids<sup>16</sup> has led to a deeper understanding of the structure of such distribution-function theories as those of YBG, HNC, PY, and Cole-Fisher, as well as such perturbation theories as the Mayer expansion,<sup>10</sup> the Zwanzig expansion,<sup>3</sup> and the Brout-Carruthers expansion.<sup>17</sup> A detailed comparison of distribution-function theories has been presented by Percus,<sup>18</sup> and Stell,<sup>18</sup> and the diagrammatic bases of these theories has been discussed in the book by Rice and Gray<sup>11</sup>; a diagrammatic analysis of the relationship among the

three perturbation theories cited above has been presented by Moffat and Kozak.<sup>19,20</sup> From these studies the physical and theoretical meaning of the superposition approximation (a central approximation in the numerical solution of the YBG equation) has been clarified. For example, the classes of diagrams (interactions) neglected in adopting the superposition approximation<sup>11</sup> are the

$$\sum_{n=1}^{\infty} \rho^n \delta_{n+3}(1, 2, 3)$$

where  $\rho$  is the density and  $\delta_n(1, 2, 3)$  defines the irreducible cluster integral in which the molecules 1, 2, 3 are held fixed. This specification quantifies the usual statement that in expressing the potential of mean force, the superposition approximation neglects the effect of fixing a molecule at  $r_3$  on the distribution of the other  $(N-3)$  molecules around molecules fixed at  $r_1$  and  $r_2$ . However, the superposition approximation *does* sum a subset of diagrams to all orders in the density. Since it is known, for example, that the critical point is characterized by long-range correlations between the particles of the fluid, there is at least a hope that a theory that considers a subset of diagrams (correlations) to all orders in the density might provide a qualitatively correct picture of critical phenomena in particular, and phase transformations in general. The extent to which this hope is realized is discussed later in this chapter.

Another point to be made also relates to the problem of phase transitions and springs from the rather self-evident remark that the YBG (and Kirkwood) equation is a highly nonlinear mathematical object. Given that nonlinear equations can often exhibit multiple solutions, Vlasov<sup>21</sup> and Kirkwood and Monroe,<sup>22</sup> working quite independently, developed the idea that theorems on the stability of solutions to nonlinear equations might have considerable relevance to the problem of phase transformations. In the last few years, an enthusiastic activity has grown up around the possibility of identifying multiple solutions of the YBG and Kirkwood equations and interpreting the passage of the system being described from one branch of stable solutions to another branch of stable solutions at certain points (densities, activities), as the mathematical counterpart of a phase transition. Certain of these efforts are mentioned in our later discussion, but for the moment the very least one can say is that the YBG (and Kirkwood) equation *does* have a sufficiently rich mathematical structure (namely, an integral equation possessing an exponential nonlinearity) to warrant a detailed investigation of the existence and uniqueness of the solutions obtained, their bifurcation properties, and their physical interpretation. It might be remarked here that the possible existence of multiple solutions of the YBG (and Kirkwood) equation should be regarded as a two-edged sword; if it turns out, for example, that bifurcation points



have nothing whatever to do with phase transitions or instabilities, then their occurrence in the YBG theory would be something of an embarrassment.

To offer some encouragement to the perspective described in the preceding paragraph, we may cite the exact results currently available on a related system of (linear) integral equations, the Kirkwood-Salsburg (KS) equations. As it happens, the structure of this hierarchy of equations is particularly well suited to a study of the mathematical properties of correlation functions at small activity. Principal among the results obtained here are those reported in 1963 by Ruelle,<sup>23</sup> who established for the KS system a lower bound on the limit of stability for a pure phase for a given class of potential functions. (Note that a lower bound on the limit of stability of a pure phase is *not* of necessity a point of phase transformation!) Subsequent work by Gallavotti and Miracle-Sole<sup>24</sup> established a relationship between KS correlation functions and lattice systems, and later Cheng and Kozak<sup>25</sup> demonstrated that Ruelle's lower bound on the limit of stability of a pure phase coincided with the bifurcation point in a simple case (a one-dimensional line of hard rods). A more recent contribution of great interest is the result of Pastur,<sup>26</sup> generalized by Moraal,<sup>27</sup> that the spectrum of the Kirkwood-Salsburg operator consists of the inverses of the zeros of the grand-canonical partition function; this result clarifies further the relationship between the structure of the KS distribution function theory and the Yang-Lee theory of phase transitions.<sup>28</sup> The importance of the above studies, relative to the problem under discussion here, is that they shed light on the *precise* meaning of several concepts that have been used quite figuratively in describing the existence and uniqueness properties of solutions to the YBG (and Kirkwood) equations for the pair distribution function.

In Sections II and III we focus on the YBG equation with superposition approximation for square-well fluids, first in the  $\theta$ -expanded formalism (Section II), then in the unexpanded form (Section III). Particular attention in Section III is paid to the YBG hard-sphere problem. Mathematical analysis of this problem and the square-well problem is developed as a prelude to the discussion of phase transitions in Section IV. Section V attends to the behavior of the YBG equation in the vicinity of the critical point, that is, the critical exponents. Section VI discusses the transport properties of square-well fluids, for which formalism has existed for over a decade. Concluding remarks in Section VII attempt to evaluate the work herein in terms of its significance and to identify those areas of research where the authors feel that future endeavor will be both enlightening and fruitful.

## II. PROPERTIES OF THE $\theta$ -EXPANDED YBG EQUATION FOR SQUARE-WELL MOLECULES

### A. Interpretation of the Expansion as a Perturbation Theory

It is of interest to adopt a historical perspective in discussing the solutions and properties of the YBG equation. For this reason we consider first in this review the evolution in our understanding of the  $\theta$ -expanded YBG equation.

In 1952 Kirkwood et al.,<sup>29</sup> obtained solutions to the YBG equation with superposition approximation by first separating the intermolecular potential into a hard-sphere part and an attractive part, according to

$$\begin{aligned} u(x) &= +\infty, & x \leq 1 \\ &= 4\epsilon(x^{-12} - x^{-6}), & x > 1 \end{aligned} \quad (2.1)$$

(called a "modified" Lennard-Jones 12-6 intermolecular potential), and then expanding the pair correlation function according to

$$g^{(2)}(x) = \exp \left[ \sum_{i=0}^{\infty} \frac{\psi_i(x)}{x} \theta^i \right] \quad (2.2)$$

where  $\theta = \epsilon/kT$ . Substitution of (2.2) into the YBG equation led to determination of the density-dependent functions  $\{\psi_i(x)\}$ , where  $\psi_0(x)$  yields the hard-sphere pair correlation function. One first solves for  $\psi_0(x)$ , and then for  $\psi_1(x)$ , where

$$\psi_1 = \psi_1(\psi_0) \quad (2.3)$$

and  $\psi_2(x)$ , where

$$\psi_2 = \psi_2(\psi_1, \psi_0) \quad (2.4)$$

and so on, successively. Given the form of (2.2), any property can be expressed as a power series in  $\theta$ , for example, the Helmholtz energy  $A$ :

$$A = \sum_{i=0}^{\infty} A_i \theta^i \quad (2.5)$$

where  $A_0$  is the Helmholtz energy of the hard-sphere fluid.

In 1954 a different use of perturbation theory for determining the thermodynamic properties of the liquid state was proposed by Zwanzig.<sup>3</sup> In his approach knowledge of the properties of a reference system of molecules was assumed, and the properties of a system of molecules characterized by a different intermolecular potential function from the reference system were determined by calculating averages of the (perturbation) potential that take the reference system into the system of interest. In Zwanzig's theory particular thermodynamic properties are developed as a power series in the reciprocal

temperature, as in (2.5). In recent years investigators using the Zwanzig theory have achieved remarkable success in determining the properties of simple liquids by effecting ingenious separations of the full intermolecular pair potential into perturbed and unperturbed parts. In particular, the methods introduced by Barker and Henderson,<sup>4</sup> Verlet and Weis,<sup>5</sup> and Anderson et al.,<sup>6</sup> lead to a rapid convergence of the expansion [see (2.5)].

There are two basic differences in carrying out a  $\theta$  expansion of the YBG equation with superposition approximation and employing a Zwanzig-type approach to generating properties. First of all, the Zwanzig approach requires incorporation of some arbitrarily chosen  $g^{(2)}(x)$  input, while the YBG approach is self-contained with respect to acquisition of  $g^{(2)}(x)$  data. Secondly, in the YBG approach, only *pair*-correlation-function data is required, since the superposition approximation is applied prior to  $\theta$  expansion. In the Zwanzig-type perturbation expansions, for example, correlation functions as high as  $g^{(4)}$  are formally required to obtain the contribution  $A_2$  in (2.5). Thus, in the latter case, superposition is applied *after* introduction of the  $\theta$  expansion to enable use of the  $g^{(2)}$  input.

It is worthwhile to compare the results of the YBG theory with superposition approximation to machine calculations, such as those generated by Monte Carlo or molecular dynamics techniques, as these comparisons provide an absolute evaluation of the approximations inherent in the YBG scheme as outlined above. For the well-width parameter  $R = \sigma_2/\sigma_1 = 1.5$  for the square-well intermolecular potential, Henderson et al. have carried out the evaluation of  $A_1$  and  $A_2$  by the Monte Carlo method.<sup>30,31</sup> Alder et al.<sup>32</sup> have determined  $A_1$  through  $A_4$  by molecular dynamics. Also provided is the opportunity to compare the corresponding results of the Barker-Henderson (BH) and Andersen-Chandler-Weeks (ACW) perturbation approaches for the same intermolecular potential. These comparisons are explored in Section II.C.

### B. The $\theta$ -Expansion of the YBG Equation for Square-Well Molecules

The YBG equation for  $g^{(2)}(x)$  with superposition approximation is

$$\ln g^{(2)}(x) = -\theta\gamma(x) + \frac{\lambda_0}{4x} \int_{-\infty}^{\infty} K(x-s)s[g^{(2)}(s)-1] ds \quad (2.6)$$

where

$$\lambda_0 = 4\pi n\sigma_1^3 = 4\pi n^* = 24\gamma \quad (2.7)$$

$$K(t) = \theta \int_{|t|}^{\infty} (\omega^2 - t^2) g^{(2)}(\omega) \frac{d\gamma(\omega)}{d\omega} d\omega \quad (2.8)$$

$$\gamma(x) = \frac{u(x)}{\varepsilon} \quad (2.9)$$

Adoption of the square-well potential (where  $R = 1.5$ ) and employment of the expansion in (2.2) lead to a hierarchy of equations for  $\{\psi_i(x)\}$ , related as suggested earlier by (2.3) and (2.4):

$$\psi_i(x) = -x\gamma(x)\delta_{i-1} + \frac{\lambda_0}{4} \sum_{j=0}^{\infty} \sum_{k=0}^{\infty} \int_{-\infty}^{+\infty} [B_j^{(0)}(x-s) + B_{j-1}^{(1)}(x-s)] C_k(s) \delta_{j+k-i} ds \quad (2.10)$$

in which

$$B_j^{(0)}(t) = - \int_{|t|}^{\infty} d\omega (\omega^2 - t^2) g_0(\omega) D_j(\omega) \delta(\omega - 1_+) \quad (2.11)$$

$$B_l^{(1)}(t) = + \int_{|t|}^{\infty} d\omega (\omega^2 - t^2) g_0(\omega) \sum_{m=0}^l \frac{1}{(m+1)!} D_{l-m}(\omega) \delta(\omega - R_+), \quad l \geq 0$$

$$= 0, \quad l < 0 \quad (2.12)$$

$$C_0(s) = s[g_0(s) - 1] \quad (2.13)$$

$$C_k(s) = s g_0(s) D_k(s), \quad k > 0 \quad (2.14)$$

and

$$g_0(x) = \exp \left[ \frac{\psi_0(x)}{s} \right] \quad (2.15)$$

The Kronecker  $\delta_m$  dictates term selection according to

$$\begin{aligned} \delta_m &= 0, & m &\neq 0 \\ &= 1, & m &= 0 \end{aligned} \quad (2.16)$$

The  $\delta$  functions in  $B_j^{(0)}$  and  $B_l^{(1)}$  are Dirac delta functions. The family of  $D$  functions are coefficients of  $\theta$  in the expansion

$$\begin{aligned} \frac{g^{(2)}(x)}{g_0(x)} &= \exp \sum_{i=1}^{\infty} \frac{\theta^i \psi_i(x)}{x} \\ &\equiv \sum_{j=0}^{\infty} \theta^j D_j \end{aligned} \quad (2.17)$$

It is apparent that

$$\psi_i = \psi_i(\psi_j), \quad j = 0, \dots, i-1 \quad (2.18)$$

as suggested earlier in (2.3) and (2.4).

Successive solution of (2.10) for  $\psi_i$  for increasing  $i$  can be carried out (see Refs. 33 and 34 for details of such computations), and the resulting  $\{\psi_i(x)\}$

can be used to evaluate  $\{A_i\}$  in (2.5). It can be shown that<sup>35</sup>

$$\frac{A - A_0}{NkT} = 12y \int_0^\theta \int_0^\infty \frac{u(x)}{\varepsilon} x^2 g^{(2)}(x) dx d\theta \quad (2.19)$$

where  $A_0$  is the Helmholtz energy for a system of hard spheres. For a system of square-well molecules, (2.19) becomes

$$\frac{A - A_0}{NkT} = -12y \int_0^\theta \int_1^R x^2 g^{(2)}(x) dx d\theta \quad (2.20)$$

Since  $g^{(2)}(x)$  can be expressed, using (2.2), as

$$g^{(2)}(x) = \sum_{i=0}^{\infty} \theta^i g_i(x) \quad (2.21)$$

it follows that

$$\frac{A_i}{NkT} = -12 \left( \frac{y}{i} \right) \int_1^R g_{i-1}(x) x^2 dx \quad (2.22)$$

where

$$g_1(x) = g_0(x) \left\{ \frac{\psi_1(x)}{x} \right\} \quad (2.23)$$

$$g_2(x) = g_0(x) \left\{ \frac{\psi_2(x)}{x} + \frac{\psi_1^2(x)}{2x^2} \right\} \quad (2.24)$$

$$g_3(x) = g_0(x) \left\{ \frac{\psi_3(x)}{x} + \frac{\psi_1^3(x)}{6x^3} + \frac{\psi_1(x)\psi_2(x)}{x^2} \right\} \quad (2.25)$$

and so on.

For use with machine calculations, such as the Monte Carlo technique<sup>30,31</sup> and molecular dynamics,<sup>32</sup> appropriate formulas for  $\{g_i(x)\}$  and  $\{A_i\}$  can be written in terms of spatial distributions of interacting pairs of particles in the "experimental" system. Smith et al.<sup>31</sup> have used such formulas to generate  $g_0(x)$  and  $g_1(x)$  using Monte Carlo results and then computed  $A_1$  and  $A_2$ . Alder et al.<sup>32</sup> computed  $A_1$  through  $A_4$  directly, using molecular dynamics and appropriate spatial distribution formulas for interacting pairs in the equilibrium limit. These studies can be used as a basis of comparison to evaluate the "goodness" of the YBG equation with superposition approximation *when cast in a  $\theta$ -expanded form* as detailed above. (In Section III, the YBG equation with superposition approximation, but *unexpanded*, is discussed.)

### C. Comparison of the Results of the $\theta$ -Expanded YBG Equation with Machine Calculations

The functions  $\{\psi_i(x)\}$  can be obtained from (2.10) and used to construct  $\{g_i\}$ , which in turn can be used to generate  $\{A_i/NkT\}$  according to (2.22) to (2.25). Tables I and II compare the density-dependent  $\{A_i/NkT\}$  as a function of  $n^*$  with the results of Alder, Young and Mark<sup>32</sup> (AYM). Figures 2 to 4 are graphical demonstrations of the same through  $A_3/NkT$ . The results of  $A_1/NkT$  and, particularly,  $A_2/NkT$  are quite good up to and including  $n^*=0.7$ , and  $A_3/NkT$  and  $A_4/NkT$  are encouraging. It should be noted that the formal representation of  $A_2/NkT$  in the Zwanzig-type expansions requires knowledge of  $g^{(3)}$  and  $g^{(4)}$ . Smith et al.<sup>36</sup> have demonstrated how difficult it is to achieve agreement at the level of  $A_2/NkT$  using superposition in the formal result. However, any claim as to the relative success of the YBG approach must be tempered by cognizance of the uncertainty in the molecular dynamics calculations (see error bar in Fig. 3).

One frequent point of criticism of the YBG equation with superposition approximation, *vis-a-vis* the Percus-Yevick equation, is the lack of agreement of hard-sphere results, say  $g_0$ , with those of machine experiments. Figures 5 and 6 compare the YBG  $g_0$  and  $g_1$  with the Monte Carlo<sup>30,31</sup>  $g_0$  and  $g_1$  at

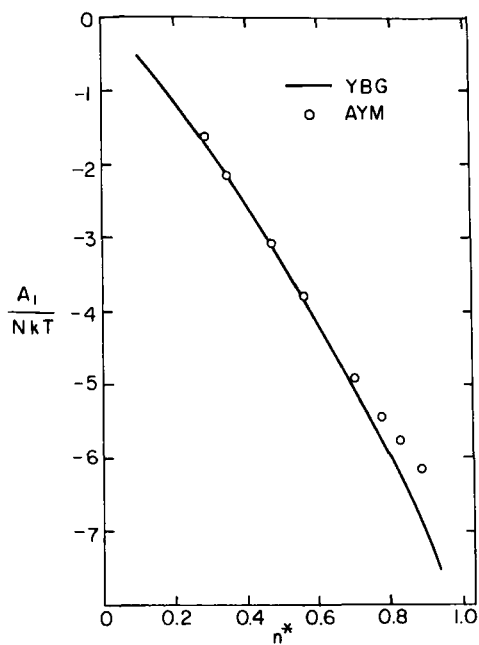
TABLE I  
Values of  $A_i/NkT$ ,  $i = 1, 2, 3$  for the YBG Theory as a Function of  $n^*$  Compared with Values from Alder et al. (AYM)<sup>a</sup>

$n^*$	$A_1/NkT$		$A_2/NkT$		$A_3/NkT$	
	YBG	AYM	YBG	AYM	YBG	AYM
0.1	-0.53348	--	-0.18744	—	-0.055696	—
0.2	-1.1367	-1.14	-0.28642	-0.288	-0.078349	-0.065
0.3	-1.8055	-1.8	-0.32429	-0.32	-0.082538	-0.05
0.4	-2.5350	-2.5	-0.32771	-0.32	-0.073834	-0.035
0.5	-3.3199	-3.3	-0.31829	-0.31	-0.057587	-0.03
0.6	-4.1571	-4.1	-0.31067	-0.31	-0.040133	-0.02
0.7	-5.0463	-5.0	-0.31205	-0.31	-0.026848	-0.01
0.8	-5.9962	-5.5	-0.32164	-0.3	-0.022747	+0.01
0.85	-6.5008	-6.3	-0.32532	-0.27	-0.028096	+0.013
0.9	-7.0328	-6.4	-0.32050	-0.26	-0.047779	+0.02

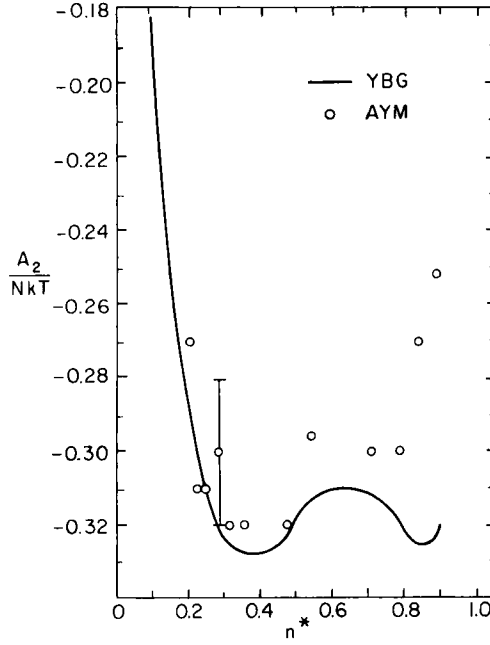
<sup>a</sup>The AYM values listed here were obtained from interpolations and graphs in Ref. 32.

TABLE II  
A Comparison of  $A_4/NkT$  for the YBG  
Theory at Two Densities with the Values  
Computed by Alder et al. (AYM)<sup>32</sup>

$n^*$	$A_4/NkT$	
	YBG	AYM
0.2020		$-0.032 \pm 0.010$
0.2357		$-0.028 \pm 0.007$
0.2453		$-0.035 \pm 0.010$
0.2828		$-0.032 \pm 0.007$
0.3000	$-0.0299$	
0.3143		$-0.030 \pm 0.005$
0.3536		$-0.019 \pm 0.004$
0.4041		$-0.017 \pm 0.007$
0.4714		$-0.019 \pm 0.003$
0.6000	$+0.0774$	
0.7071		$+0.004 \pm 0.004$
0.8839		$-0.002 \pm 0.002$



**Fig. 2.**  $A_1/NkT$  from the YBG theory compared with the values computed by Alder et al. (AYM)<sup>32</sup>. (From Ref. 34. Used by permission of the American Institute of Physics.)



**Fig. 3.**  $A_2/NkT$  from the YBG theory compared with the values computed by Alder et al. (AYM)<sup>32</sup>. A typical error bar for AYM is shown. (From Ref. 34. Used by permission of the American Institute of Physics.)

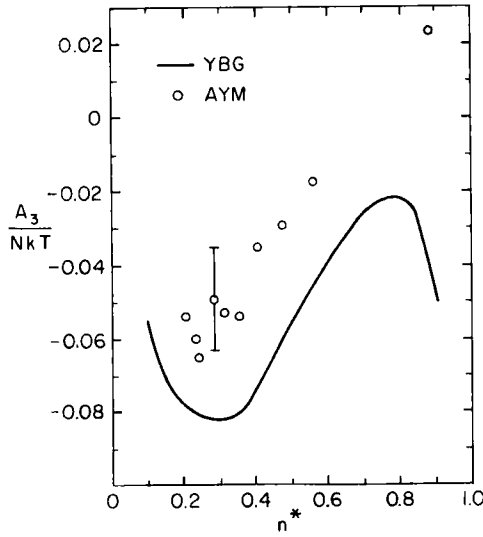


**Fig. 4.**  $A_3/NkT$  from the YBG theory compared with values computed by Alder et al. (AYM).<sup>32</sup> A typical error bar for AYM is shown. (From Ref. 34. Used by permission of the American Institute of Physics.)



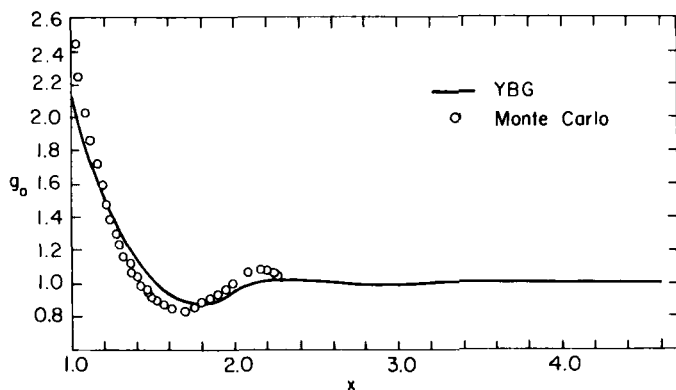


Fig. 5.  $g_0(x)$  for the YBG theory as compared to Monte Carlo calculations<sup>30</sup> at  $n^*=0.6$ . (From Ref. 34. Used by permission of the American Institute of Physics.)

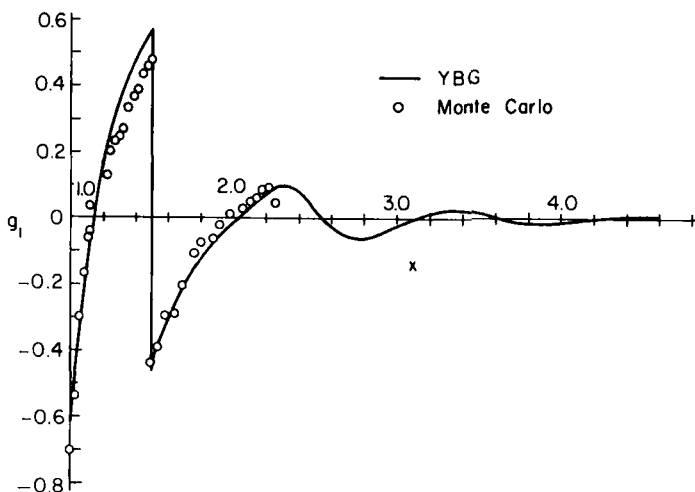


Fig. 6.  $g_1(x)$  for the YBG theory as compared to Monte Carlo calculations<sup>31</sup> at  $n^*=0.6$ . (From Ref. 34. Used by permission of the American Institute of Physics.)

$n^*=0.6$ . The YBG  $g_0$  differs quite noticeably from the Monte Carlo  $g_0$ , but the YBG  $g_1$  more closely mimics the Monte Carlo  $g_1$ . Since agreement between YBG and machine  $A_1/NkT$  is quite good, one might speculate that dissimilarities in  $g_0$  are "washed out" by the double integration in (2.20) when  $n^* \leq 0.7$ . However, it appears that the YBG theory fares better with respect to "attractive" contributions, such as  $g_1$  and higher, and one can

properly claim that the agreement of  $A_2/NkT$  is directly related to the goodness of  $g_1$ . The relative importance of higher-order contributions can be seen by examining  $A_3/NkT$  and  $A_4/NkT$ . The YBG results are encouraging. Figures 7 and 8 show  $g_2$  and  $g_3$  from the YBG theory at  $n^*=0.6$ . The discontinuities in  $g_1$ ,  $g_2$ , and  $g_3$  are due to the discontinuous nature of the square-well potential.

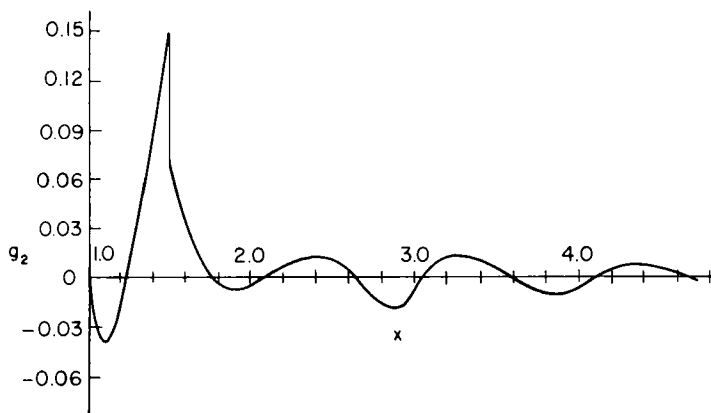


Fig. 7.  $g_2(x)$  for the YBG theory at  $n^*=0.6$ . (From Ref. 34. Used by permission of the American Institute of Physics.)

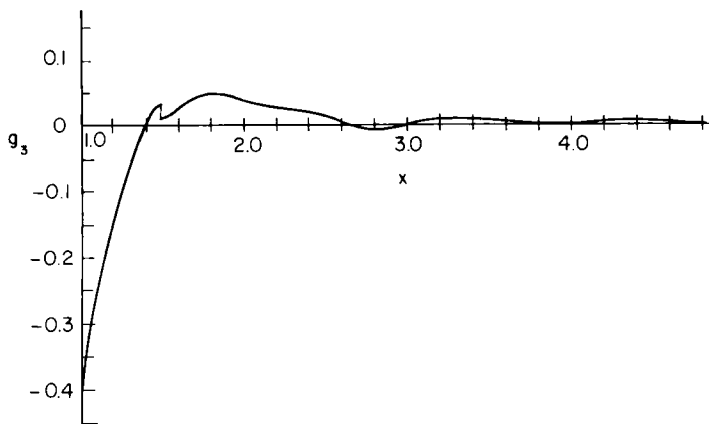


Fig. 8.  $g_3(x)$  for the YBG theory at  $n^*=0.6$ . (From Ref. 34. Used by permission of the American Institute of Physics.)

### D. Other Results Using the $\theta$ -Expanded YBG Equation for Square-Well Molecules

Schrodt et al.<sup>33,37,38</sup> solved the YBG equation in  $\theta$ -expanded form for square-well molecules with  $R = 1.85$  up through  $\psi_2$  terms in (2.2) for densities as high as  $n^* = 0.938$ . Properties such as the compressibility factor  $z = Pv/RT$  and excess internal energy  $E^E/NkT$  were tabulated throughout  $\theta - n^*$  space. The transport properties shear viscosity  $\eta$  and thermal conductivity  $\kappa$  were also computed<sup>38</sup> (see Section VI). More significantly, an attempt to delineate the gas-liquid coexistence region was made<sup>33</sup> and is discussed in Section IV. The critical point was located and critical exponents were evaluated.<sup>37</sup> These are discussed in Section V. The Schrodt studies focused on using and analyzing the pressure equation of state

$$z = 1 - 4y\theta \int_0^\infty x^2 \frac{d\gamma(x)}{dx} g^{(2)}(x) dx \quad (2.26)$$

A later study by Lincoln et al.<sup>39</sup> repeated the Schrodt studies using analysis of the energy equation of state, specifically

$$z = y \left( \frac{\partial(A/NkT)}{\partial y} \right)_T \quad (2.27)$$

where (2.20) is used for  $(A - A_0)/NkT$  and the Carnahan-Starling equation-of-state<sup>40</sup> is used for hard spheres:

$$z_0 = \frac{1 + y + y^2 - y^3}{1 - y^3} \quad (2.28)$$

The Lincoln results are discussed further in Sections IV and V.

Schrodt et al.<sup>41</sup> later modified the Kirkwood superposition approximation (KSA) into a "truncated superposition approximation" (TSA):

$$g^{(3)}(123) = g^{(2)}(12)A^{(2)}(13)A^{(2)}(23) \quad (2.29)$$

where

$$\begin{aligned} A^{(2)}(x) &= g^{(2)}(x), & x \leq D \\ &= \exp \left[ \frac{-u(x)}{kT} \right], & x > D \end{aligned} \quad (2.30)$$

For the square-well potential,  $D$  was chosen to be the well-width parameter  $R$ , and (2.30) became simply:

$$\begin{aligned} A^{(2)}(x) &= g^{(2)}(x), & x \leq R \\ &= 1, & x > R \end{aligned} \quad (2.31)$$

The philosophy adopted was that the KSA "overcorrelated" the third-particle

effect, and the TSA was an attempt to lessen that effect. The TSA results are evaluated in Sections IV and V in the discussion of the gas-liquid coexistence envelope, the critical point and related critical exponents.

Finally, Schrodtr and Luks<sup>33</sup> have pointed out the simplicity of employing (2.26) for equation-of-state analysis, as only  $g^{(2)}(1_+)$  and  $g^{(2)}(R_-) = e^{\theta} g^{(2)}(R_+)$  information is required. They fitted  $\psi_i(1_+)$  and  $\psi_i(R_-)$ ,  $i=0, 1, 2$ , as functions of density to simplify equation-of-state analysis. Later, Lincoln and Luks<sup>42</sup> attempted to use the pressure equation-of-state of Schrodtr and Luks to correlate the thermodynamic properties of supercritical simple fluids at very high pressures. Qualitative trends were correctly predicted by this square-well equation-of-state, but parametric modifications were required to develop a quantitative corresponding-states description consistent with the experimental corresponding-states charts developed by Breedveld and Prausnitz<sup>43</sup> for such species as Ar, N<sub>2</sub>, He, H<sub>2</sub>, Ne, Xe, CO, and CH<sub>4</sub>.

### III. PROPERTIES OF THE UNEXPANDED YBG EQUATION FOR SQUARE-WELL MOLECULES

#### A. The YBG Hard-Sphere Problem

A salient advantage of using a  $\theta$ -expanded form of the YBG equation with superposition approximation is that once  $\{\psi_i\}$  have been determined at a density, all properties at that density can be calculated as a function of temperature immediately, as temperature is explicit in the expansion parameter  $\theta$ . The zeroth-order term in the expansion for  $g^{(2)}(x)$  is the hard-sphere pair correlation function  $g_0(x)$ , which is related to  $\psi_0(x)$  through (2.15). The function  $g_0(x)$  is obtained from (2.6) expressed in the form

$$\ln g_0(x) = \frac{\lambda_0}{4x} \int_{-\infty}^{\infty} K_0(x-s)s[g_0(s)-1] ds \quad (3.1)$$

which can be reexpressed as

$$\ln g_0(x) = \frac{\lambda}{4x} \int_{-\infty}^{\infty} K'_0(x-s)s[g_0(s)-1] ds \quad (3.2)$$

where

$$K'_0(t) = -(1-t^2)\phi(t; |1|) \quad (3.3)$$

in which

$$\phi(t; |1|) = \eta(t+1) - \eta(t-1) \quad (3.4)$$

and  $\eta$  is the Heavyside step function. All later  $\{\psi_i\}$ ,  $i > 0$ , are directly dependent on  $g_0(x)$ , that is,  $\psi_0(x)$ .

Equation 3.2 is called either the Kirkwood or YBG equation, depending

on the definition of the  $\lambda$  parameter:

$$\lambda = \lambda_0 g_0(1+) \quad (\text{YBG}) \quad (3.5)$$

$$[g_0(1+; \lambda)]^{-1/2} \int_0^\lambda [g_0(1+; \lambda')]^{-1/2} d\lambda' = \lambda_0 \quad (\text{Kirkwood}) \quad (3.6)$$

The difference in the way in which  $\lambda$  relates to the reduced density  $\lambda_0$  in (3.5) and (3.6) is due to the different ways in which the superposition approximation is entered into the hierarchy equation for  $g^{(2)}(x)$ . From here on,  $\lambda_0$  in (3.6) is denoted by  $\lambda_0^K$ .

The solution to the hard-sphere problem not only serves as a basis for perturbation expansions, such as detailed in Section II, but also is the square-well result in the limit of  $\theta \rightarrow 0$ . Understanding the nature of  $g_0(x)$  is fundamental to its proper use as a basis function in perturbation expansions and provides a beginning to the understanding of the (unexpanded) YBG equation's behavior for an intermolecular potential with an attractive well such as the square well. At the same time, through (3.2) one can make a comparison between the YBG and Kirkwood versions of the hard-sphere problem.

Kirkwood et al.<sup>44</sup> first generated solutions to (3.2) but restricted their regime to  $\lambda < 34.8$  or, roughly,  $\lambda_0 = 12.5$ . They speculated that solutions beyond  $\lambda = 34.8$ , if they existed, would point to a "periodic" fluid structure and that the transition from dense fluid to this periodic fluid was possibly second-order. In two recent studies Co and the present authors<sup>45,47</sup> generated  $g_0(x)$  from (3.2) for  $\lambda$  values ranging from 30.2830 to 47.6136, which, when combined with earlier computations performed by Lincoln and the present authors,<sup>46</sup> present a detailed portrait of the behavior of  $g_0(x)$  as a function of  $\lambda$ . The Co computations were done over a range of 30 diameters of separation [ $g_0(x) \equiv 1$  for  $x > 30$  diameters] to aid in clarifying long-range phenomena, if present, in the  $g_0(x)$  function.

Co and the authors found that while (3.2) had solutions for each and every value of  $\lambda$  up through at least 47.6136 (the highest value of  $\lambda$  studied), there could be as many as three values of  $\lambda$  consistent with a value of the density  $\lambda_0$  or  $\lambda_0^K$  (see Fig. 9). Beyond a certain density  $\lambda_0 \approx 12.5$  (corresponding to  $\lambda_0^K \approx 14.7$ ), only one solution exists, while for a limited region of density space below this point, three solutions can exist. Figure 10 shows two of the  $g^{(2)}(x)$  functions for  $\lambda_0 = 7.0334$  for the YBG equation corresponding to  $\lambda = 14.60$  and 37 (points A and B, respectively) in Fig. 9. The  $g^{(2)}(x)$  function corresponding to point C in Fig. 9 is similar to the one at B in the sense that it is also nondamped and periodic in nature. In summary,  $g_0(x)$  is a damped function up to the vicinity of  $\lambda \approx 34.8$  (actually the authors found a damped function at  $\lambda = 34.925$ , a discrepancy that can be attributed to the approxima-

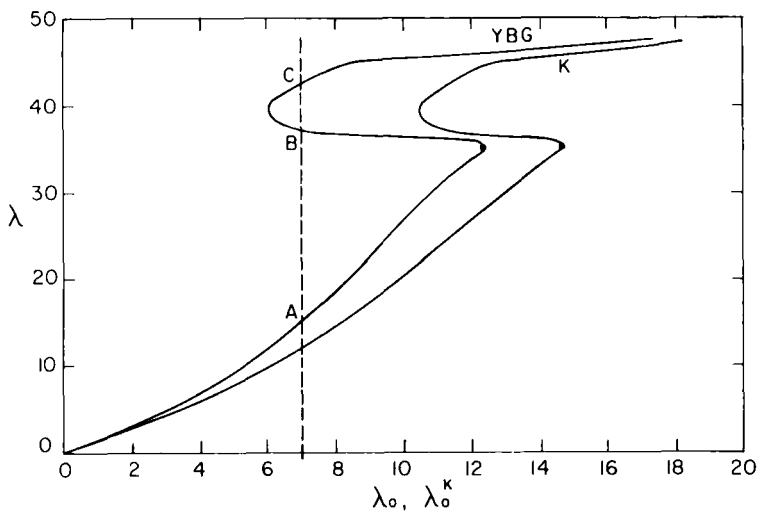


**Fig. 9.**  $\lambda$  versus  $\lambda_0$  and  $\lambda_0^K$  for the YBG and Kirkwood (K) equations for a system of hard spheres. The vertical dashed line denotes a typical density ( $\lambda_0 = 7.0334$ ) at which multiple solutions  $A, B, C$  exist for the YBG equation. The transition points (densities) are denoted by a filled circle for each curve. (From Ref. 45. Used by permission of the American Institute of Physics.)

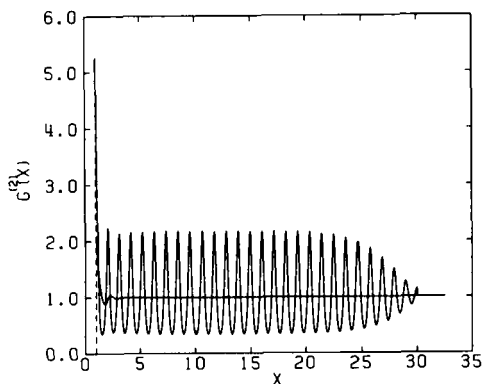


**Fig. 10.** The pair correlation functions  $g^{(2)}(x)$  for points  $A$  and  $B$  in Fig. 9. Point  $B$  is characterized by the nondamped periodic function, while point  $A$ 's function reaches unity within five diameters to  $\pm 0.003$ . (From Ref. 45. Used by permission of the American Institute of Physics.)

tions inherent in a finite difference calculus iterative computation), after which  $g_0(x)$  becomes a periodic function, with the amplitude of the period increasing with increasing values of  $\lambda$ . Figure 11 shows  $g_0(x)$  for  $\lambda = 46.6935$  (equivalent to  $\lambda_0 = 15$ ). Both this function and the function in Fig. 10 at  $\lambda = 37$  are shown to damp out to unity only because the numerical solutions had the boundary condition of  $g_0(x) = 1$  for  $x > x_{\text{MAX}} = 30$  diameters.

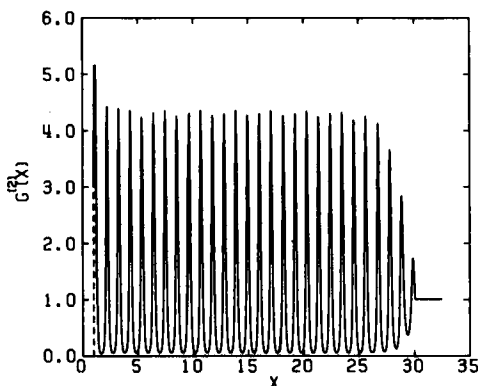


Fig. 11.  $g_0(x)$  at  $\lambda_0 = 15$  for  $x_{\text{MAX}} = 30$ . (From Ref. 47. Used by permission of the American Institute of Physics.)

Co et al.<sup>47</sup> identified similar phenomena for systems of square-well molecules at high densities, and these are discussed in the Section III.B. Possible reasons for finding multiple values of  $\lambda$  occurring within a certain range of  $\lambda_0$  or  $\lambda_0^k$  are discussed in Ref. 45. It is conjectured that the YBG hard-sphere equation, solved *without* imposing the superposition approximation, might undergo a point-transition in behavior at a certain value of  $\lambda_0$  corresponding to a discontinuity in  $\lambda$ , that is, the region of multiple solutions in  $\lambda_0$  space would collapse to a single  $\lambda_0$  point. On this premise, it is argued further that the Kirkwood equation is inherently less approximate than the YBG equation in dealing with this discontinuity for two reasons: (1) the Kirkwood theory fares better in comparison with the extended YBG theory of Rice and Lekner<sup>13</sup>, which incorporated an improved superposition approximation; (2) the Kirkwood theory, relatively speaking predicts a narrower region of multiple solutions in density space.

### B. The YBG Square-Well Problem

From a pragmatic standpoint, the YBG equation has experienced more popularity than the Kirkwood equation, simply because it is more easily expressible (i.e., solvable) as an equation for an intermolecular potential

with an attractive well. There is no analog to (3.2) for attractive molecules that allows one to solve both the Kirkwood and the YBG equation using a single common equation.

At high densities, a phenomenon was found<sup>47</sup> for square-well molecules that was similar to that found for hard-sphere molecules, namely, beyond a certain density, periodic  $g^{(2)}(x)$  functions were found upon solution of (2.6) in which

$$\begin{aligned} \gamma(x) &= +\infty & x \leq 1 \\ &= -1 & 1 < x \leq R \\ &= 0 & x > R \end{aligned} \quad (3.7)$$

where  $R = 1.85$ . Figure 12 demonstrates this sudden transition in behavior for

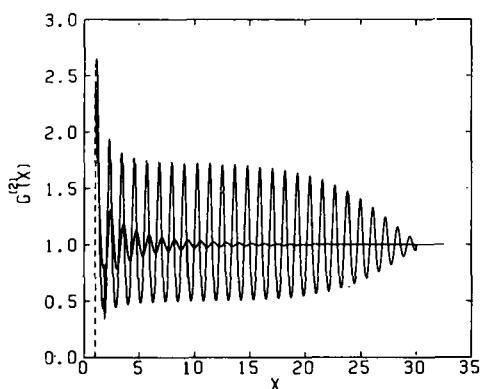


**Fig. 12.** Comparison of  $g^{(2)}(x)$  functions for  $\theta = 0.45$  at  $\lambda_0 = 12.5$  (damped dense-fluid region) and  $\lambda = 13.0$  (non damped "periodic" region), with  $x_{\text{MAX}} = 30$ . The  $g^{(2)}(x)$  function at  $\lambda_0 = 13.0$  has the higher peaks. (From Ref. 47. Used by permission of the American Institute of Physics.)

$\theta = 0.45$ . Table III documents this transition for  $\theta = 0.45, 0.20$ , and  $0.0$  (i.e., hard spheres) by presenting  $g^{(2)}(1_+)$ ,  $g^{(2)}(R_-)$ ,  $\kappa$ , where

$$\kappa = 1 + \lambda_0 \int_0^\infty [g^{(2)}(x) - 1] x^2 dx \quad (3.8)$$

is the isothermal compressibility. Also included for the "periodic" functions are the peak, trough, and periodic values one sees when one is "away" from the well region (say,  $x \approx 10$  diameters). Noteworthy is the fact that the  $\kappa$  function becomes singular in the periodic region. To support this contention, a periodic boundary was applied to  $g^{(2)}(x)$  for  $\theta = 0.45$  at  $\lambda_0 = 15$ , by matching



TABLE III

Comparison of  $g^{(2)}(1+)$ ,  $g^{(2)}(R_-)$ , and  $\kappa$  as a function of  $\lambda_0$  Obtained from the Solution of the Unexpanded YBG Equation at High Densities ( $x_{\text{MAX}} = 30$ ) for  $\theta = 0.0, 0.20$ , and  $0.45$

$\lambda_0$	$g^{(2)}(1+)$	$g^{(2)}(R_-)$	$\kappa$	Peak <sup>a</sup>	Trough <sup>a,b</sup>	Period <sup>a</sup>
$\theta = 0.0$						
11	2.7526	0.7174	0.3175	—	—	—
12	2.8004	0.6139	0.6782	—	—	—
13	3.5641	0.1743	6683.69	4.288	0.0531	1.069
15	3.1028	0.1502	7803.14	4.323	0.0521	1.066
17	2.8026	0.1236	9538.26	4.530	0.0427	1.066
$\theta = 0.20$						
11	2.6237	0.8170	0.4548	—	—	—
12	2.6723	0.7383	0.7834	—	—	—
12.5	2.6529	0.6890	1.3319	—	—	—
13	2.7345	0.4443	983.61	1.924	0.420	1.104
14	2.5679	0.3986	1353.46	2.041	0.377	1.103
15	2.4211	0.3628	1734.86	2.145	0.342	1.102
16	2.2948	0.3311	2176.80	2.257	0.312	1.101
$\theta = 0.45$						
11	2.4172	0.9546	1.8739	—	—	—
12	2.4415	0.8709	2.5478	—	—	—
12.5	2.4140	0.8218	3.9892	—	—	—
13	2.5679	0.5336	776.33	1.727	0.494	1.133
14	2.4142	0.4811	1132.45	1.848	0.445	1.131
15	2.2786	0.4394	1523.84	1.944	0.407	1.129
16	2.1545	0.4073	1912.32	2.024	0.377	1.128
18	1.9473	0.3556	2781.16	2.171	0.328	1.126
21	1.7041	0.3018	4227.65	2.357	0.275	1.123
24	1.5185	0.2639	5861.85	2.516	0.236	1.121

<sup>a</sup>Seen for the "periodic"  $g^{(2)}(x)$  at about  $x \approx 10$ .

<sup>b</sup>In contrast to the Percus-Yevick results,<sup>52</sup> the YBG  $g^{(2)}(x)$  function never attains negative values at high densities.

at  $x > 30$  diameters the periodic behavior at  $x$  between 9 and 14 diameters, until convergence and agreement were obtained. Figures 13 and 14 show  $g^{(2)}(x)$  computed without and with the periodic boundary condition, respectively, along with the  $\kappa$  function of (3.8) as a function of the upper limit of its integral.

Reference 45 suggests that multiple solutions, such as those shown in Fig. 9, should also occur for the square-well problem. An exploratory study

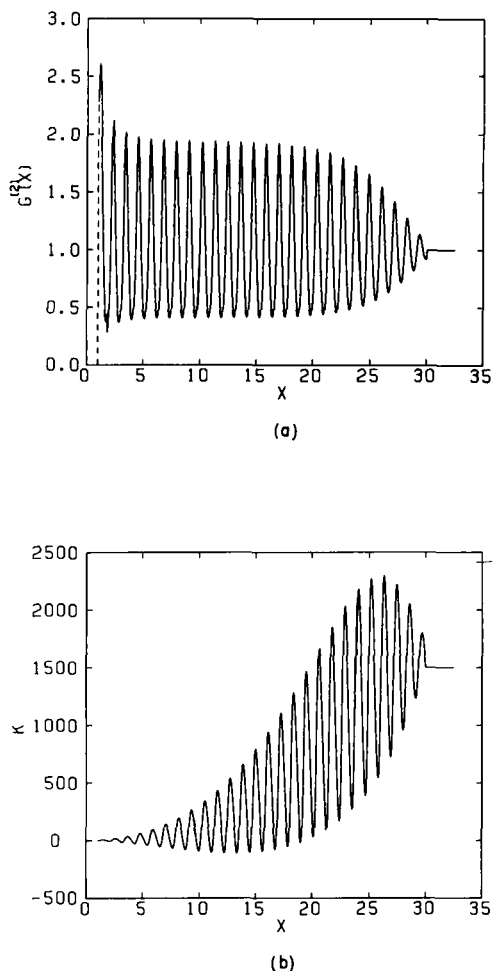


**Fig. 13.** (a)  $g^{(2)}(x)$  at  $\theta=0.45$ ,  $\lambda_0=15$  for  $x_{\text{MAX}}=30$  [ $g^{(2)}(x) \equiv 1$  at  $x > x_{\text{MAX}}$ ]. (From Ref. 47.)  
 (b) The value of the  $\kappa$  function as a function of the upper limit of the  $\kappa$  function integral for  $g^{(2)}(x)$  in a. (From Ref. 47. Used by permission of the American Institute of Physics.)

has been made by the authors to investigate this point and their existence has been confirmed.

As shown above, one can pass from a region of damped periodic to undamped periodic  $g^{(2)}(x)$  functions in the  $\theta$ - $\lambda_0$  thermodynamic space. The undamped functions are presumably infinite in range and occur only at high

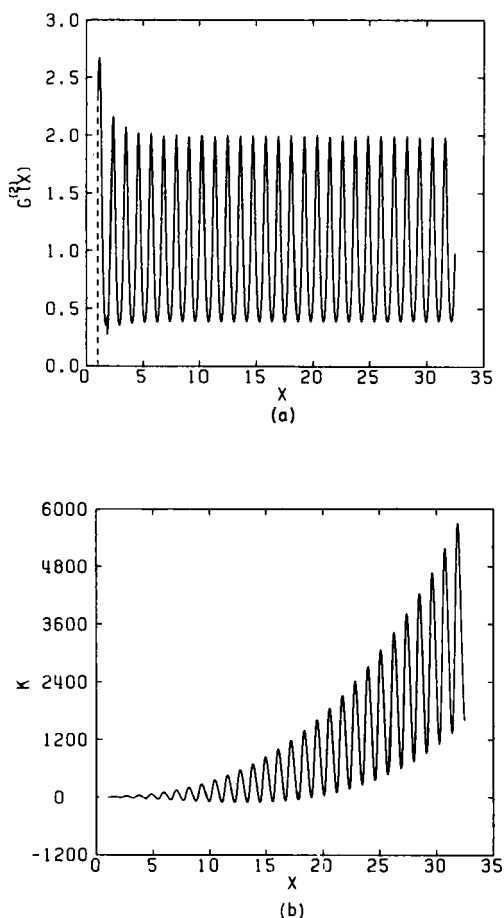


**Fig. 14.** (a)  $g^{(2)}(x)$  at  $\theta=0.45$ ,  $\lambda_0=15$  for a devised periodic boundary condition [ $g^{(2)}(x) \equiv$  periodic function at  $x > x_{\text{MAX}}$ ] at  $x_{\text{MAX}} = 30$ . (From Ref. 47.) (b) The value of the  $\kappa$  function as a function of the upper limit of the  $\kappa$ -function integral for  $g^{(2)}(x)$  in a. (From Ref. 47. Used by permission of the American Institute of Physics.)

densities. Furthermore, Co et al.<sup>47</sup> have shown, as indicated by Table III, that there does not seem to be an upper bound densitywise (i.e., a close-packing density such as  $\lambda_0=17.77$ ) to the existence of these solutions. Investigation of the  $\theta$ - $\lambda_0$  space at lower values of  $\lambda_0$  for values of  $\theta > 0.37$  reveals a region of  $\theta$ - $\lambda_0$  space with functions of extended range as well. These functions, which appear to have a relation to gas-liquid coexistence, are characterized by "positive tailing": the  $g^{(2)}(x)$  function, instead of damping out to unity in an oscillatory manner, tails off with  $g^{(2)}(x) > 1$  out to the bounds of the

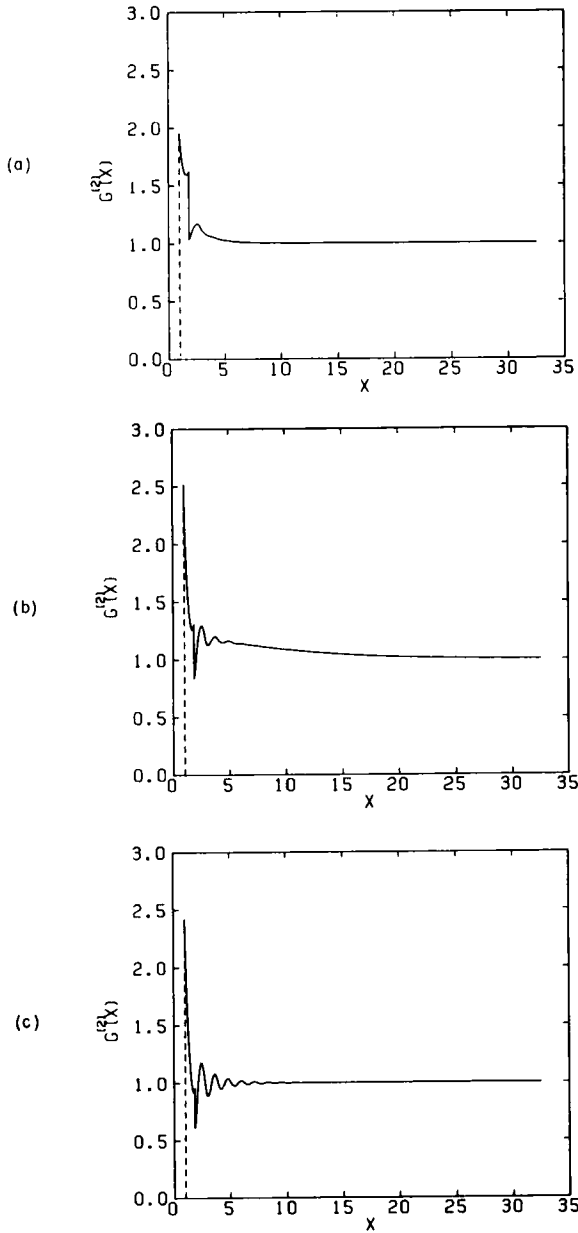


**Fig. 15.** (a)  $g^{(2)}(x)$  at  $\theta=0.45$ ,  $\lambda_0=1.5$  for  $x_{\text{MAX}}=30$  [ $g^{(2)}(x) \equiv 1$  at  $x > x_{\text{MAX}}$ ]. (b)  $g^{(2)}(x)$  at  $\theta=0.45$ ,  $\lambda_0=6.0$  for  $x_{\text{MAX}}=30$  [ $g^{(2)}(x) \equiv 1$  at  $x > x_{\text{MAX}}$ ]. For this function,  $g^{(2)}(x)=1.0011$  at  $x=30$  owing to the positive tailing phenomenon. (c)  $g^{(2)}(x)$  at  $\theta=0.45$ ,  $\lambda_0=11.0$  for  $x_{\text{MAX}}=30$  [ $g^{(2)}(x) \equiv 1$  at  $x > x_{\text{MAX}}$ ].

problem, say  $x = x_{\text{MAX}} = 30$  diameters, as set by the problem statement. Figure 15 compares three  $g^{(2)}(x)$  functions for  $\theta = 0.45$ , showing  $g^{(2)}(x)$  for the gas region, the "coexistence" region, and the liquid region. Adding consideration of the function shown in Figure 14, one has a visual spectrum of the kinds of  $g^{(2)}(x)$  functions the YBG equation can yield, depending on the  $(\theta, \lambda_0)$  specification. Figure 16 maps out the regions of behavior for the square-well fluid with  $R = 1.85$ .

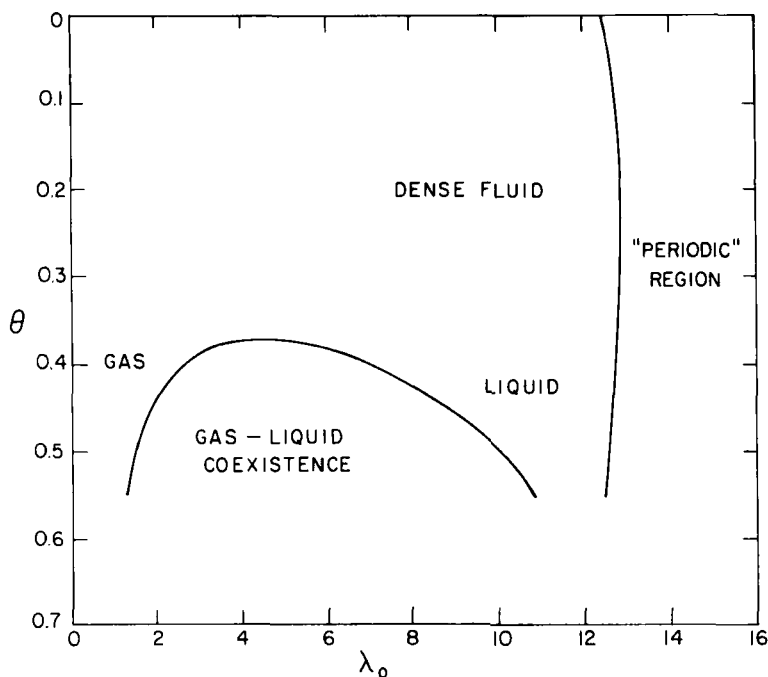


**Fig. 16.** A map in  $\theta$ - $\lambda$  space of the behavioral regimes of  $g^{(2)}(x)$  for the square-well fluid with  $R = 1.85$  based on analysis of the YBG equation with superposition approximation. The "periodic" region extends beyond "close-packing." See Table III. (From Ref. 47. Used by permission of the American Institute of Physics.)

Young and Rice<sup>48</sup> first pointed out the positive-tailing phenomenon and the accompanying rapid increase in  $\kappa$  in (3.8) associated with such functions. Lincoln and the present authors<sup>46</sup> examined this phenomenon in some detail, establishing that there is a locus in  $\theta$ - $\lambda_0$  space within which the range of  $g^{(2)}(x)$  is indefinite. Figure 17 shows how  $\kappa$  varies with  $v^* = n^*-1$  for several values of  $\theta$  and how it is affected by the range imposed on the solution, that is, the value of  $x_{\text{MAX}}$  at which  $g^{(2)}(x)$  is set equal to unity for  $x > x_{\text{MAX}}$ . It is

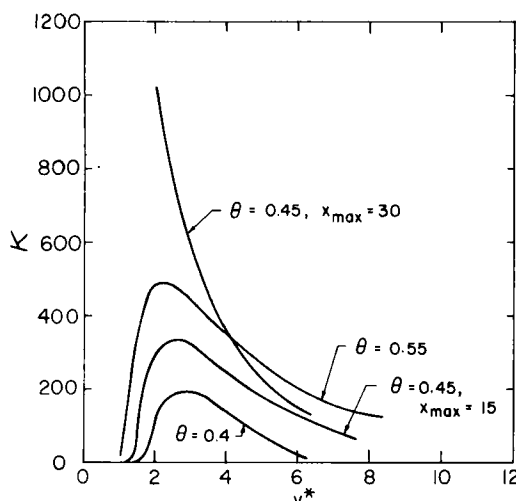


**Fig. 17.** The compressibility function  $\kappa$  for  $\theta = 0.4, 0.45, 0.55$  with  $x_{\text{MAX}} = 15$ , and  $\theta = 0.45$  with  $x_{\text{MAX}} = 30$ , where  $g^{(2)}(x) \equiv 1$  when  $x > x_{\text{MAX}}$ . (From Ref. 46. Used by permission of the American Institute of Physics.)

assumed that within this region of "coexistence,"  $\kappa \rightarrow \infty$  as  $x_{\text{MAX}} \rightarrow \infty$ . At this point it is to be understood that use of the term "coexistence" is merely for convenience, as the  $\theta$ - $\lambda_0$  region in question corresponds roughly to that region of space where one would expect gas-liquid coexistence behavior.

It is the unique nature of the coexistence region that differentiates the  $g^{(2)}(x)$  obtained from (2.6) in unexpanded form with that obtained from (2.10) when that expression, truncated at  $\theta^2$ , is substituted in (2.2) as follows:

$$g^{(2)}(x) = \exp \left\{ \frac{\psi_0(x) + \theta \psi_1(x) + \theta^2 \psi_2(x)}{x} \right\} \quad (3.9)$$

Outside the coexistence region, there is little difference between  $g^{(2)}(x)$  in (3.9) and  $g^{(2)}(x)$  in unexpanded form. Table IV shows  $P^*(P)$  as a function of  $\lambda_0$  at several  $\theta$  values, where

$$P^*(P) = \frac{n^*}{\theta} \left\{ 1 - \frac{2}{3} \pi n^* [R^3(1 - e^{-\theta})g^{(2)}(R_-) - g^{(2)}(1_+)] \right\} \quad (3.10)$$

for the square-well potential, which is obtained from

$$P^*(P) = \frac{n^*}{\theta} \left\{ 1 - \frac{2}{3} \pi n^* \int_0^\infty x^3 \frac{d\gamma(x)}{dx} g^{(2)}(x) dx \right\} \quad (3.11)$$

In the expanded form,  $g^{(2)}(x)$  causes  $P^*(P)$  to exhibit a van der Waals-type of loop in the coexistence region, which does not occur with the unexpanded

TABLE IV  
 $P^*(P)$  for Unexpanded and Expanded (3.9)  $g^{(2)}(x)$  as a  
Function of  $\lambda_0$  at Several Values of  $\theta$

$P^*(P)$		
$\lambda_0$	Unexpanded $g^{(2)}(x)$	Expanded $g^{(2)}(x)$
$\theta = 0.3$		
1	0.2331	0.2328
2	0.4250	0.4221
3	0.6093	0.5988
4	0.8230	0.8015
5	1.1151	1.0860
6	1.5554	1.5283
8.4736	3.8795	3.8891
$\theta = 0.4$		
1	0.1513	0.1514
2	0.2309	0.2282
3	0.3067	0.2543
4	0.4026	0.2545
5	0.4937	0.2681
6	0.5829	0.3542
8.4736	1.3930	1.3794
10	2.8981	2.9455
12	5.8853	6.1933
$\theta = 0.45$		
0.5	0.0742	0.0742
1	0.1228	0.1236
1.5	0.1490	0.1518
2	0.1911	0.1620
3	0.2810	0.1373
4	0.3662	0.0695
5	0.4475	-0.0082
6	0.5253	-0.0426
7	0.6006	0.0371
8.4736	0.7436	0.5295
10	1.6802	1.7001
12	4.0059	4.3950

TABLE IV (Contd.)

$\lambda_0$	$P^*(P)$	
	Unexpanded $g^{(2)}(x)$	Expanded $g^{(2)}(x)$
$\theta=0.55$		
0.5	0.0562	0.0556
1	0.0814	0.0820
1.5	0.1237	0.0833
2	0.1617	0.0627
3	0.2352	-0.0370
4	0.3054	-0.2046
5	0.3728	-0.4167
6	0.4377	-0.6294
9	0.6262	-0.5958
10	0.7088	-0.1407
12	1.4838	1.7906

$g^{(2)}(x)$  function. Although  $P^*(P)$  in (3.10) only reflects the behavior of  $g^{(2)}(1+)$  and  $g^{(2)}(R_-)$ , the entire  $g^{(2)}(x)$  function is quite different when expanded as compared to unexpanded. Specifically, there is no positive tailing and accompanying  $\kappa$  singularity in the coexistence region when one solves for (3.9). This is not surprising when one recognizes that for  $\theta=0$ ,  $g^{(2)}(x)=g_0(x)$  does not exhibit an extended range at moderate densities in the manner that  $g^{(2)}(x)$  does at  $\theta=0.45$  from (2.6) as is discussed earlier. Recalling (2.3) and (2.4), one can see that the expansion will not lead to infinite-ranged functions if  $\psi_0(x)$  is not infinite ranged.

### C. Analysis of the Solutions of the YBG Equation

Lincoln and the present authors<sup>46</sup> using (2.6) found that as one approached the region of coexistence, the change in the *short-range* values of  $g^{(2)}(x)$ , say, in the vicinity of the attractive well, was uniform and gradual, even though the overall change over a range of  $\lambda_0$  for some  $\theta$  value could be sizable. More significant was the feature that the  $g^{(2)}(x)$  function suddenly acquired a positive-tailing of indefinite range. Focusing on this feature, they attempted to analyze for a locus that enveloped the coexistence region in  $\theta$ - $\lambda_0$  space, a locus that would be characterized by *two* solutions for  $g^{(2)}(x)$ , differing only in the nature of their *long-range* behavior.

Let  $\bar{g}^{(2)}(x)$  be the solution with the positive tail and  $g^{(2)}(x)$  be the solution without the positive tail. It is postulated that both  $\bar{g}^{(2)}(x)$  and  $g^{(2)}(x)$  would



satisfy (2.6) at each point on the locus:

$$\ln g^{(2)}(x) = -\theta \dot{\gamma}(x) + \frac{\lambda_0}{4x} \int_{-\infty}^{\infty} K(x-s)s[g^{(2)}(s)-1] ds \quad (2.6)$$

$$\ln \bar{g}^{(2)}(x) = -\theta \gamma(x) + \frac{\lambda_0}{4x} \int_{-\infty}^{\infty} \bar{K}(x-s)s[\bar{g}^{(2)}(s)-1] ds \quad (2.6a)$$

If

$$\chi(x) = \ln \bar{g}^{(2)}(x) - \ln g^{(2)}(x) \quad (3.12)$$

then it follows that

$$\begin{aligned} \chi(x) = & \frac{\lambda_0}{4x} \int_{-\infty}^{\infty} [K(x-s) - \bar{K}(x-s)]s ds \\ & + \frac{\lambda_0}{4x} \int_{-\infty}^{\infty} g^{(2)}(s)[\bar{K}(x-s)e^{x(s)} - K(x-s)]s ds \end{aligned} \quad (3.13)$$

If the short-range behavior of  $\bar{g}^{(2)}(x)$  and  $g^{(2)}(x)$  is the same, then

$$\chi(x) = \frac{\lambda_0}{4x} \int_{-\infty}^{\infty} g^{(2)}(x)K(x-s)[e^{x(s)} - 1]s ds \quad (3.14)$$

If  $g^{(2)}(x) \rightarrow 1$  as  $x$  becomes large, then one can rewrite (3.14) as

$$Y(x) = \frac{\theta \lambda_0}{4x} \int_{-\infty}^{\infty} L(x-s)[e^{Y(s)} - 1]s ds \quad (3.15)$$

where

$$Y(x) = \ln \bar{g}^{(2)}(x) \quad (3.16)$$

and

$$L(x-s) = \int_{|x-s|}^{\infty} d\omega (\omega^2 - t^2) \frac{d\gamma(\omega)}{d\omega} \quad (3.17)$$

The possibility of finding nonvanishing solutions of (3.15) can be explored by examining known existence theorems on nonlinear integral equations. The problem may be approached as follows: Given that  $Y(x)=0$  is a solution of (3.15), one can apply a basic theorem, due to Krasnosel'skii,<sup>49</sup> provided certain conditions are satisfied. Firstly, the Krasnosel'skii theorem requires that the nonlinear equation under study be an equation defined over a bounded, closed set. Although the integral appearing in (2.6) was specified with limits  $(-\infty, +\infty)$ , note that the YBG equation in the canonical ensemble is an equation defined over a bounded, closed set. (The usual procedure of extending the range of the YBG equation to  $\pm\infty$  is justified by the observa-

tion that the kernel of this equation damps rapidly to zero with increasing argument.)

A second requirement of the Krasnosel'skii theorem may be stated as follows: Suppose we regard the right-hand side of (3.15) as a nonlinear operator  $A$ , that is,

$$Y = AY \quad (3.18)$$

Then, the theorem requires that  $A$  be completely continuous and possess a Fréchet derivative  $B$  at the point  $\theta_0$ , that is, the null point of the space on which the operator  $A$  is defined. In the square-well problem, the continuity condition will be satisfied if one thinks of the square-well (or hard-sphere) potential as representable with negligible error by continuous functions. Finally, note that the Fréchet derivative of the nonlinear operator at the point  $\theta_0$  is given by

$$Y(x) = \frac{\theta\lambda_0}{4x} \int_{-\infty}^{\infty} L(x-s)Y(s)ds \quad (3.19)$$

Under the conditions stated above, Krasnosel'skii proves that every eigenvalue of odd multiplicity of the operator  $B$  is a bifurcation point of the operator  $A$ , and to every such bifurcation point there corresponds a continuous branch of eigenvectors of nonzero norm. To apply the Krasnosel'skii theorem, one must therefore determine the eigenvalues (if any) of the linear integral equation (3.19).

In searching for eigenvalues (i.e., solutions) of the linear integral equation (3.19), it is convenient to use the Fourier-transform method.<sup>50</sup> Equation 3.19 can be rewritten as

$$Z(x) = \mu \int_{-\infty}^{\infty} L(x-s)Z(s)ds \quad (3.20)$$

where

$$\mu = \frac{\theta\lambda_0}{4} \quad (3.21)$$

$$Z(x) = xY(x) \quad (3.22)$$

One can then construct

$$\tilde{Z}(u) - \mu \tilde{Z}(u) \tilde{L}(u) = 0 \quad (3.23)$$

where

$$\tilde{Z}(u) = (2\pi)^{-1/2} \int_{-\infty}^{\infty} Z(x)e^{ixu}dx \quad (3.24)$$

$$\tilde{L}(u) = \int_{-\infty}^{\infty} L(t)e^{itu}dt \quad (3.25)$$

Nontrivial solutions  $\tilde{Z}(u)$  of (3.23) will occur whenever the following relation involving the Fourier-transformed kernel  $L(u)$  is satisfied:

$$1 - \mu \tilde{L}(u) = F(u; \lambda_0, \theta) = 0 \quad (3.26)$$

The  $F$  function for the square-well problem is

$$F(u; \lambda_0, \theta) = 1 - \lambda_0 g^{(2)}(1_+) F_1(u) + \lambda_0 (e^\theta - 1) g^{(2)}(R_+) F_2(u) \quad (3.27)$$

where

$$F_1(u) = \frac{u \cos u - \sin u}{u^3} \quad (3.28)$$

$$F_2(u) = \frac{Ru \cos(Ru) - \sin(Ru)}{u^3} \quad (3.29)$$

Figure 18 shows the functions  $F_i(u)$ ,  $i = 1, 2$ .

It should be noted that the condition  $F(u; \lambda_0, \theta) = 0$  is a necessary but *not* sufficient condition for the existence of a bifurcation point of (3.15). To insure bifurcation the eigenvalue of the associated linear operator must be of odd multiplicity. Our numerical calculations have shown that the solutions of the YBG equation are unique for the range of  $(\theta, \lambda_0)$  considered. From this fact one would expect that nonvanishing solutions of (3.13), if they exist, will be unique, and the eigenvalue spectrum of this equation, as well as that of the reduced (3.15), and its associate linear equation (3.20), will be simple.

The loci shown in Fig. 16 earlier were found from examination of (3.27).

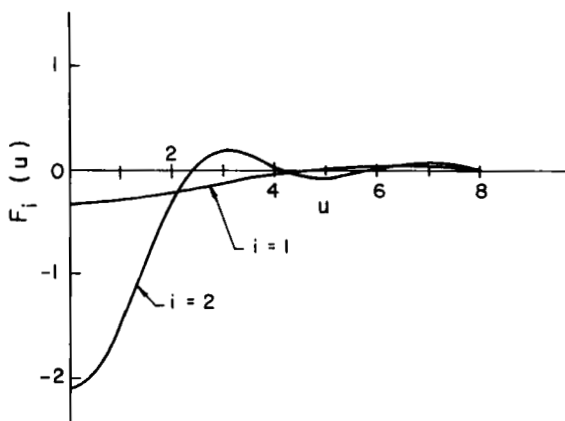


Fig. 18.  $F_i(u)$  versus  $u$  for  $i = 1, 2$ . See (3.28) and (3.29).

Worth noting is that the boundary of the periodic region is found for values of  $u$  in the vicinity of 5.4. On the other hand, the boundary of the coexistence region is found for  $u=0$ . If one interprets  $\tilde{\lambda}=2\pi/u$  as a wavelength, it turns out that the  $\tilde{\lambda}$  for the periodic boundary corresponds roughly to an average separation of molecules in a very dense fluid. This had been pointed out by Young and Rice.<sup>48</sup> To identify a  $\tilde{\lambda}$  signaling a low-density limit of stability of a pure-fluid phase, one recalls that in the neighborhood of a critical point, interparticle correlations are known to become extremely long ranged. It seems logical that the associated wavelength be  $\tilde{\lambda} \rightarrow \infty$  (i.e.,  $u=0$ ) for this locus. Reference 46 provides considerable detail on the specific behavior of the  $F$  function in (3.27).

One must be careful in attaching an interpretation to the loci in Fig. 16. An analysis of the Kirkwood-Salsburg hierarchy of integral equations<sup>25</sup> has shown that the existence of a bifurcation point may have nothing whatever to do with a phase transition; rather, the bifurcation point appears to be related to a *lower bound* on the stability of a pure phase. A similar result was found in a recent study on the asymptotic behavior of the  $D$ -dimensional Ising model.<sup>51</sup> Consequently, the points  $(u; \lambda_0, \theta)$  for which (3.26) is satisfied cannot be regarded as indicating the onset of a phase transition, but rather must be regarded as signaling a lower bound on the limit of stability of a pure phase. This observation must be kept in mind in our later discussion of phase transitions in Section IV.

Equation 3.26 is mathematically identical to the Kirkwood stability criterion<sup>22</sup> as extended by Young and Rice<sup>48</sup> to the case of the square-well intermolecular potential at very high densities. But, whereas the former criterion was developed with the view that it provided an upper limit to the dense fluid regime beyond which solutions might not exist, our derivation points to an alternative interpretation. Namely, the criterion signals the onset of a sudden change in the long-range, but not the short-range, behavior of  $g^{(2)}(x)$ . In truth, there appears to be a discontinuity in the short-range values of  $g^{(2)}(x)$  at the "periodic" boundary, but this is only because we are using  $\lambda_0$  to guide our search for solutions. Recalling the earlier discussion on hard spheres in Section II.A, one must remember that  $g_0(x)$  was continuous in  $\lambda$  but not in  $\lambda_0$ , that is, that following the  $\lambda_0$ -coordinate resulted in a step jump in  $\lambda = \lambda_0 g_0(1+)$ . Further investigation, however, uncovered a family of solutions for  $g_0(x)$  that were in one-to-one correspondence with intermediate values of the  $\lambda$  parameter. Consequently, the premises set forth in the derivation of (3.26) seem valid both at the coexistence region boundary locus and the dense fluid/periodic region boundary locus.

#### IV. PHASE TRANSITIONS IN SQUARE-WELL FLUIDS

While Sections II and III discuss the mathematical and some thermodynamic properties of the YBG equation with superposition approximation for square-well molecules in both the  $\theta$ -expanded and unexpanded forms, attention is now focused on these YBG equations as vehicles for describing phase transitions. Of specific interest are the gas-liquid transition and dense liquid-solid transition. Discussion of the critical point and the equation-of-state behavior in its immediate vicinity is taken up in Section V.

More than a century ago, van der Waals proposed an equation-of-state containing parameters that account for the attractive and repulsive features of a fluid's intermolecular potential. Although it lacks the quantitateness of more modern macroscopic semitheoretical (e.g., the Redlich-Kwong equation and its many offspring) equations-of-state, it is noteworthy for its qualitative features, particularly its ability to provide delineation of a gas-liquid coexistence region, including the location of the critical point and the spinoidal and binoidal loci that branch downward temperaturewise from that point.

The YBG equation, a statistical mechanical equation, has a goal in common with the van der Waals theory, namely, the translation of the attractive and repulsive forces between interacting molecules into a comprehensive equation of state, capable of handling the phase-transition properties, as well as the pure fluid properties. In other words, for a pure fluid, the end result is common in the sense of achieving a functionality

$$P = P(v, T) \quad (4.1)$$

In the case of van der Waals (or some other phenomenological) theory, the starting point in developing an equation of the form of (4.1) is the statement:

$$P = P_R + P_A \quad (4.2)$$

where  $P_R$  and  $P_A$  are the repulsive and attractive contributions, respectively, to the pressure function. The corresponding starting point in statistical mechanics can be one of three: (1) (2.26), the "pressure" equation-of-state; (2) (2.27), the "energy" equation-of-state; (3) the "compressibility" equation-of-state:

$$z = -v^*\theta \int_{\infty}^{v^*} (\theta v^{*2}\kappa)^{-1} dv^* \quad (4.3)$$

where  $\kappa$  is given in (3.8). Formally speaking, these three equations for the pressure should yield identical results, but the inevitable approximations that enter into a workable development of the  $g^{(2)}(x)$  function (e.g., the superposition approximation) cause these three equation-of-state expressions to

yield different numerical values of pressure at a given state point. In fact, variations among the results of these three equations of state for a given  $g^{(2)}(x)$  theory are often construed as a measure of the formal validity of the theory.

It has already been pointed out that using the pressure equation (3.10), with  $\theta$ -expanded  $g^{(2)}(x)$  data will produce a van der Waals-type loop. This was first observed by Kirkwood et al.<sup>29</sup> Recognizing that, at coexistence

$$\mu_{\text{gas}} = \mu_{\text{liquid}} \quad (4.4)$$

Schrodt and Luks<sup>33</sup> applied Maxwell construction techniques and computed the gas-liquid coexistence region for (3.10) (see Fig 19 and Table V). Schrodt

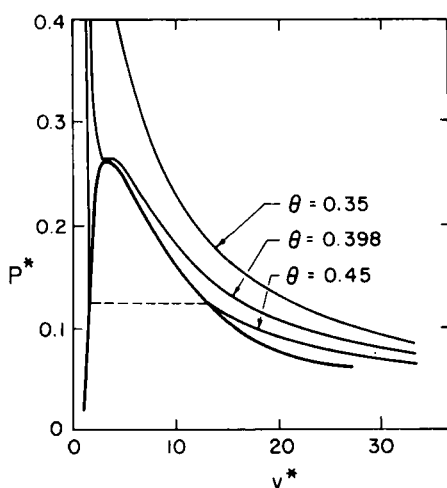


**Fig. 19.** The coexistence region in  $P^*-v^*$  space with representative isotherms as determined by the  $\theta$ -expanded YBG theory for the square-well potential with  $R = 1.85$ . (From Ref. 33. Used by permission of the American Institute of Physics.)

et al.,<sup>41</sup> using the truncated superposition approximation (2.29) repeated the same type of analysis. The locus of the coexistence region is given in Table VI. Lincoln et al.,<sup>39</sup> using the energy equation-of-state (2.27), also computed a gas-liquid coexistence region, which should be judged in comparison with that of Ref. 33, since each method employs the same data input (see Table VII). The energy equation-of-state approach yielded a value of the critical compressibility factor  $z_c = P_c^* v_c^* \theta_c = 0.3384$ , as compared with  $z_c = 0.3494$  using the pressure equation in Ref. 33. The TSA approach mentioned above<sup>41</sup> predicts  $z_c = 0.3398$ .

Figure 20 shows the gas-liquid  $T^* - v^*$  coexistence loci for the above three approaches, where  $T^* = \theta^{-1}$ . Also included is a plot of the experimental

TABLE V  
 $\theta$  Versus  $v^*$  of the Gas and Liquid Phases for  
the Gas-Liquid Coexistence Region for the  
 $\theta$ -Expanded YBG Equation with Kirkwood  
Superposition Approximation<sup>a</sup>

$\theta$	$v^*(\text{gas})$	$v^*(\text{liq})$	$P^*(P)$
0.39862 ( $=\theta_c$ )	3.3665	3.3665	0.2603
0.399	3.50	3.12	0.2590
0.400	3.95	2.95	0.2552
0.410	5.50	2.48	0.2225
0.420	7.10	2.10	0.1917
0.440	10.3	1.82	0.1449
0.450	12.4	1.70	0.124
0.500	27.2	1.40	0.060

<sup>a</sup>From analysis of  $P^*(P)$ , which is also given.

TABLE VI  
 $\theta$  Versus  $v^*$  of the Gas and Liquid Phases for  
the Gas-Liquid Coexistence Region for the  
 $\theta$ -Expanded YBG Equation with Truncated  
Superposition Approximation (TSA)<sup>a</sup>

$\theta$	$v^*(\text{gas})$	$v^*(\text{liq})$	$P^*(P)$
0.431423 ( $=\theta_c$ )	3.9155	3.9155	0.2011
0.4315	4.025	3.76	0.2009
0.4316	4.15	3.72	0.2007
0.4319	4.29	3.59	0.1999
0.44	5.90	2.83	0.1801
0.46	9.10	2.30	0.1398
0.48	12.6	2.04	0.1092
0.50	17.0	1.88	0.0848
0.52	22.5	1.76	0.0657

<sup>a</sup>From analysis of  $P^*(P)$ , which is also given.

TABLE VII  
 $\theta$  Versus  $v^*$  of the Gas and Liquid Phases for  
 Gas-Liquid Coexistence Region for  
 the  $\theta$ -Expanded YBG Equation with Kirk-  
 wood Superposition Approximation<sup>a</sup>

$\theta$	$v^*(\text{gas})$	$v^*(\text{liq})$	$P^*(E)$
0.4404 ( $=\theta_c$ )	3.97	3.97	0.1935
0.4406	4.18	3.77	0.1931
0.441	4.59	2.78	0.1920
0.442	5.24	2.75	0.1900
0.444	5.59	2.71	0.1850
0.45	7.27	2.57	0.1660
0.46	7.93	2.30	0.1520
0.50	15.00	1.89	0.0930
0.53	22.58	1.73	0.0650

<sup>a</sup>From analysis of  $P^*(E)$ , which is also given.

$T^*-v^*$  locus using parameters obtained from second virial coefficient data. Figure 21 offers a comparison of the saturated liquid loci for the  $\theta$ -expanded YBG equation with Kirkwood and truncated superposition approximations with the experimental locus using the same intermolecular potential parameters. As is emphasized later in Section VI, parameters apropos to the dilute-gas region are not necessarily appropriate nor effective for dense or critical region fluids. Figures 20 and 21 appear to reinforce this viewpoint. However,  $z_c=0.291$  experimentally for argon and is independent of parameter choice, except that the authors have chosen to adopt  $R=1.85$  as a "third" parameter to be characteristic of spherical nonpolar molecules. All in all, the predicted value of  $z_c$  appears to be a stiff test of theory, with a sort of bounds being provided by the experimental  $z_c=0.291$  and the van der Waals  $z_c=0.375$ , between which the three above-cited studies using  $R=1.85$  fall. Except for Ref. 34, all the work-to-present in which the authors have generated square-well  $g^{(2)}(x)$  data has adopted the choice of  $R=1.85$ .

As discussed in Section III.B, the *unexpanded* YBG square-well equation with superposition approximation does not require the application of Maxwell construction techniques. Specifically, the "pressure" equation-of-state  $P^*(P)$  and the "energy" equation-of-state  $P^*(E)$  yield monotonically increasing functions  $P^*$  with increasing density. The singular nature of  $\kappa$  in the "coexistence" region offers the prospect of flat isotherms in



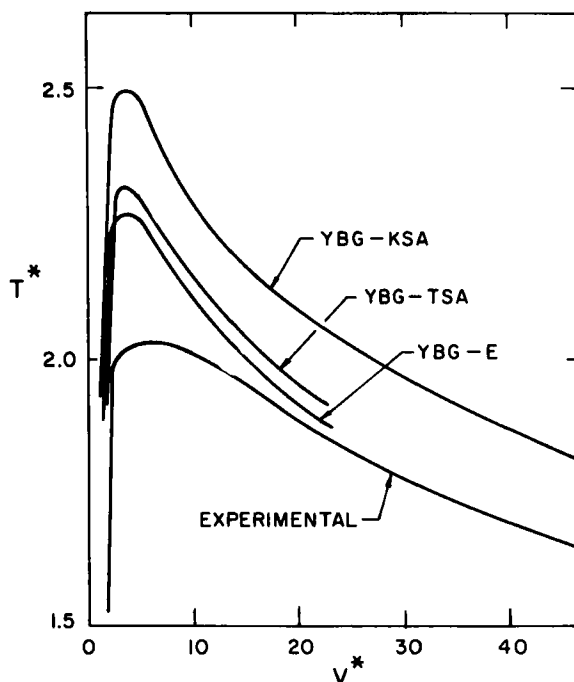
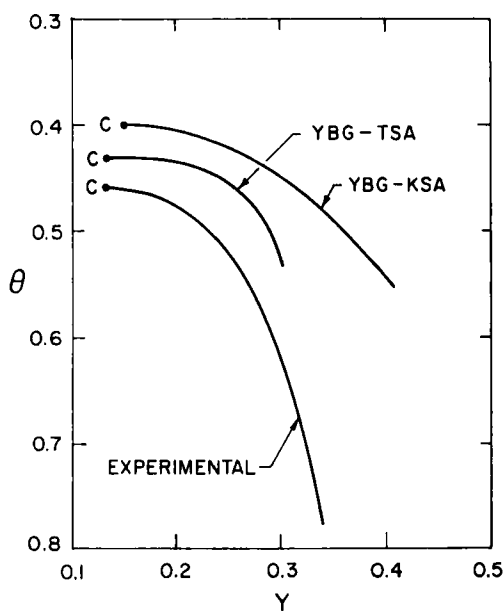
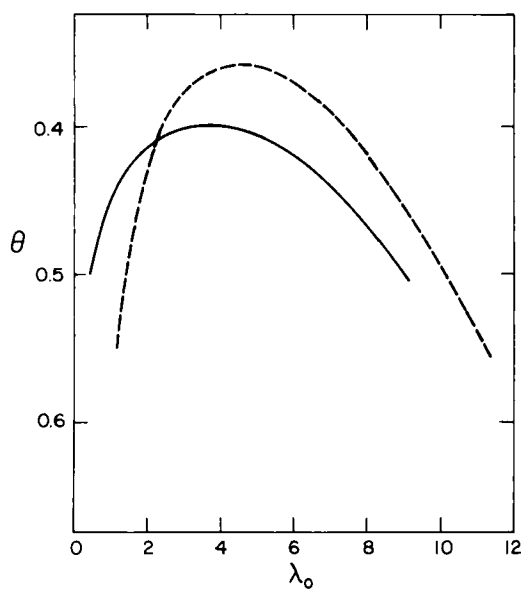


Fig. 20. A comparison of the coexistence envelopes in  $T^*-v^*$  space for the  $\theta$ -expanded YBG equation with Kirkwood superposition approximation (YBG-KSA) and truncated superposition approximation (YBG-TSA), both computations using the pressure equation, with that envelope arising from energy analysis of the YBG equation (YBG-E). Reduced experimental data for argon are also plotted, using  $\sigma_1 = 3.162 \text{ \AA}$ ,  $\epsilon/k = 69.4^\circ \text{K}$ ,  $R = 1.85$ . (From Ref. 39. Used by permission of the American Institute of Physics.)

that region according to (4.3). Lincoln, Co and the present authors<sup>46,53</sup> have computed the upper portion of this coexistence region.  $z_c$  was estimated to be  $0.3249 \pm 0.0087$ , which is an improvement over the  $\theta$ -expanded results. This result is noteworthy in several respects: (1) the coexistence locus found here does not coincide at all closely with that of the  $\theta$ -expanded approach in Ref. 33 [see Fig. 22]; (2) the flat isotherms [see Fig. 23] resulting from  $P^*(C)$ , i.e., (4.3) are consistent with arguments put forth by Hill<sup>54</sup> supporting the absence of "loops" in  $P-v$  space for an exact theory of first-order phase transitions; (3) stability analysis such as was performed on the unexpanded YBG results using (3.27) can also be applied to  $\theta$ -expanded results and yields remarkably similar results when compared with the unexpanded results. Figure 24 compares the loci of the lower bound on the stability of a pure phase, both with respect to the gas-liquid and liquid-



**Fig. 21.** A comparison of the saturated liquid loci in  $\theta$ - $\gamma$  space corresponding to YBG-KSA, YBG-TSA, and experimental data for argon in Fig. 20. (From Ref. 41. Used by permission of the American Institute of Physics.)



**Fig. 22.** Comparison of the coexistence envelope obtained in Ref. 33 with the locus obtained from analysis using (3.27). (—) Ref. 33; (---) (3.27). (From Ref. 53. Used by permission of the American Institute of Physics.)

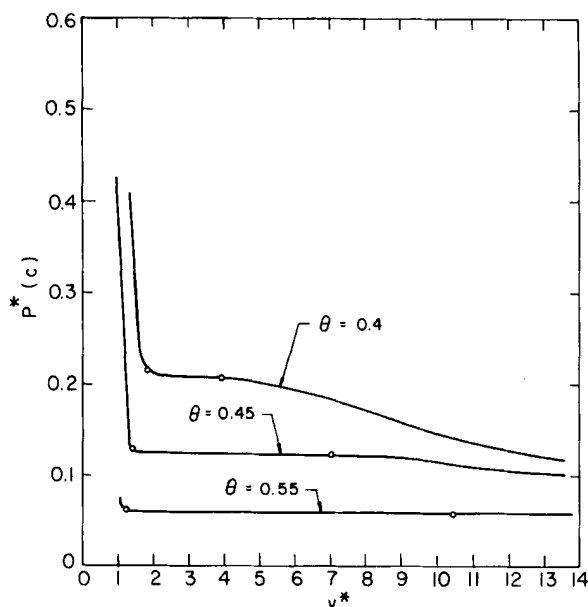


**Fig. 23.**  $P^*(C)$  as a function of  $v^*$  at  $\theta=0.4$ ,  $0.45$ , and  $0.55$ . The open circles denote lower bounds on the limit of stability of the pure fluid, as determined from (3.27). (From Ref. 46. Used by permission of the American Institute of Physics.)

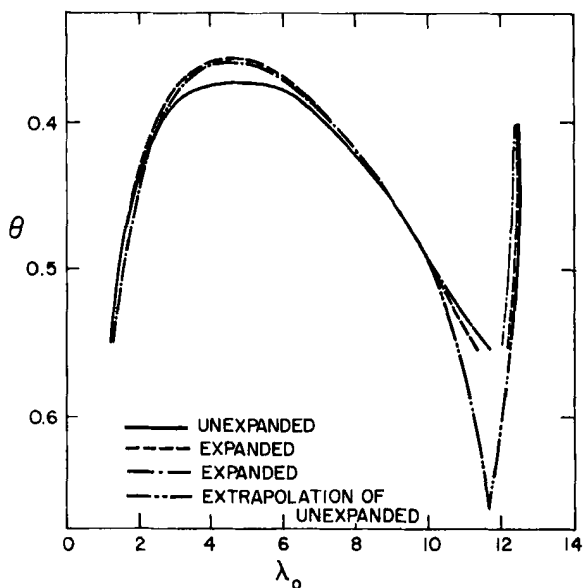


**Fig. 24.** Loci of stability limits determined from analysis of (3.27) in  $\theta-\lambda_0$  space for gas-liquid and liquid-solid coexistence regions. (—) unexpanded; (---) expanded [see (3.9)]; (-·-) expanded [see (4.5)]; (---) extrapolation of unexpanded. (From Ref. 53. Used by permission of the American Institute of Physics.)

“periodic” transitions shown in Fig. 16, for three applications of (3.27):

- a. Unexpanded  $g^{(2)}(x)$  data.
- b.  $\theta$ -Expanded  $g^{(2)}(x)$  data, according to (3.9).
- c.  $\theta$ -Expanded  $g^{(2)}(x)$  data, according to a perturbation-type expansion of (3.9):

$$g^{(2)}(x) = g_0(x) \left\{ 1 + \frac{\theta\psi_1(x)}{x} + \theta^2 \left[ \frac{\psi_1^2(x)}{2x^2} + \frac{\psi_2(x)}{x} \right] \right\} \quad (4.5)$$

Case a deviates from cases b and c, which are virtually identical, only in the critical-point region. Taking into account the comparison provided by Fig. 22, there certainly appears to be a nontrivial difference between the locus of the lower bound of stability of case b and the Maxwell construction results of the same data using either  $P^*(P)$  or  $P^*(E)$ . This difference strongly suggests that care must be exercised in the *physical* interpretation of bounds such as provided by the criterion (3.27).

Two remarks, one historical and one declarative, can be made in conclusion. First, in earlier work on the unexpanded YBG square-well problem with superposition approximation, Young and Rice<sup>48</sup> reported a value of  $z_c = 0.48 \pm 0.02$ , using a value of  $R = 1.5$  for the third square-well intermolecular potential parameter. One should hesitate to criticize the work of Young and Rice with respect to their value of  $z_c$ . First of all, the calculation of  $z_c$  was performed using  $P_c^*(P)$ , while it was earlier noted that only the function  $P^*(C)$  made sense in the context of analyzing the gas-liquid coexistence region in the case of the unexpanded YBG equation. Turning the problem around, one would find a poor (too high) result for  $z_c$  from the work of Co et al.<sup>53</sup> if  $P_c^*(P)$  had been used instead of  $P_c^*(C)$ . Simply, one must establish some sort of internal consistency between the mode of analysis of the coexistence problem and the associated computation of properties in the coexistence region. In fact, we speculate that had Young and Rice used  $P^*(C)$  instead of  $P^*(P)$ , they would have obtained a value of  $z_c$  much closer to experiment for inert gases. This is tantamount to proposing that the value of  $z_c$  is relatively insensitive to the parameter  $R$  for square-well molecules. (In *real* systems, there is only minor variation in  $z_c$  values between different molecules.)

The second comment to be made is that the loci displayed in Fig. 24, and the underlying  $g^{(2)}(x)$  data reviewed and discussed in the preceding section, provide a basis for the claim that the YBG equation under the superposition approximation can differentiate among the gaseous, liquid, and solid states of matter. Certainly, from a *qualitative* point of view, this assertion would seem to be justified; in the following section we evaluate the extent to which the assertion can be made *quantitative* by analyzing the equation-of-state behavior for the square-well fluid in a regime of thermodynamic space that has received much attention in recent years, namely, the critical point.

## V. EQUATION-OF-STATE BEHAVIOR FOR SQUARE-WELL FLUIDS NEAR THE CRITICAL POINT

Since Section IV provides one with the gas-liquid coexistence envelope by use of Maxwell construction techniques for several variations of the YBG square-well problem, as well as a lower bound on the stability of the pure fluid in the case of the unexpanded YBG equation with superposition approximation, one now has the opportunity to evaluate the equation-of-state behavior near the critical point. Specifically, the interest here lies in whether the values of the critical exponents are classical, in the van der Waals sense, or whether the YBG equation yields agreement with commonly accepted experimental values of, say, xenon, whose exponents appear to be quite similar to those of several other simple fluids that have been experimentally studied. As in the case of  $z_c$  the critical exponents are dimensionless, and therefore theory can be compared with experiment without specifying the intermolecular potential parameters ( $\sigma_1$ ,  $\epsilon/k$ ). Of course, the theory is certainly affected by our aforementioned choice of  $R=1.85$  for the square-well intermolecular potential, but how intimate the interaction is between equation-of-state behavior and choice of parameter  $R$  is difficult to evaluate.

The critical exponents of interest are defined as follows:

$$(\rho - \rho_c) \propto |T - T_c|^\beta \quad (5.1)$$

along the coexistence envelope, approaching the critical point from both sides, that is, one has a  $\beta_G$  and a  $\beta_L$ ;

$$(P - P_c) \propto |\rho - \rho_c|^\delta \quad (5.2)$$

along the critical isotherm, again from both sides of the critical point, yielding  $\delta_G$  and  $\delta_L$ ; and

$$\kappa \propto (T - T_c)^{-\gamma} \quad (5.3)$$

along the isochore  $\rho = \rho_c$  at  $T > T_c$ . Table VIII compares the experimental and classical values of  $\beta_G$ ,  $\beta_L$ ,  $\delta_G$ ,  $\delta_L$ , and  $\gamma$ .

Table IX is a listing of the critical exponents computed from four gas-liquid coexistence studies:

1. The YBG equation with Kirkwood superposition approximation in  $\theta$ -expanded form—the “pressure” equation-of-state (KSA-P).<sup>37</sup>
2. Same as 1, but using the “energy” form of the pressure equation-of-state (KSA-E).<sup>39</sup>
3. Same as 1, but using the truncated superposition approximation (TSA).<sup>41</sup>

4. The unexpanded YBG equation, where the critical point is located from stability analysis, providing a locus of the lower bound on the stability of the pure phase (SAL). See Section III.C and Ref. 53.

TABLE VIII  
A Comparison of Classical and Experimental  
Critical Exponents, Where the Latter Were  
Measured for Xenon

Exponent	Classical <sup>a</sup>	Experimental <sup>b</sup>
$\beta_G$	0.5	0.35
$\beta_L$	0.5	0.35
$\delta_G$	3.0	4.4
$\delta_L$	3.0	4.4
$\gamma$	1.0	1.3

<sup>a</sup>Based on the van der Waals equation.

<sup>b</sup>See p. 47 of Ref. 8.

Also tabulated are the reduced properties  $P_c^*$ ,  $v_c^*$ , and  $\theta_c$ . Examination of Table IX reveals that the  $\beta$ 's are definitely nonclassical, falling between "classical" and experimental values. On the other hand, the  $\delta$ 's are closer to the classical values, although within computational accuracy they are not necessarily classical. On the average, they too fall between classical and experimental values. The  $\gamma$  exponent provided mixed results, but it is worth noting that the SAL (stability analysis locus) value is definitely nonclassical and lies between the classical and experimental values.

One might criticize the computation of the  $\beta_G$  and  $\beta_L$  exponents in the SAL case, as it is not clear that the stability locus in question and the true coexistence envelope are coincident even near the critical point. (It is assumed, however, that the critical point itself is unequivocally located. The results suggest that any discrepancy does not strongly affect the computations of  $\beta_G$  and  $\beta_L$ , as they are relatively similar for all the different treatments.) On the other hand, it is noteworthy that the SAL-exponents are the best overall, as the  $g^{(2)}(x)$  data input used would be expected to be the least approximate, comparatively speaking, simply because  $\theta$  expansion was not invoked in the solution of the YBG equation.

We now comment on the relevance of the results reviewed above to the

TABLE IX  
The Critical Exponents and Reduced Thermodynamic Properties  
Computed from Four Different YBG Theories.<sup>a</sup>

	KSA-P	KSA-E	TSA <sup>b</sup>	SAL
$\beta_G$	$0.425 \pm 0.002$	$0.379 \pm 0.01$	0.433	$0.34 \pm 0.01$
$\beta_L$	$0.435 \pm 0.005$	$0.409 \pm 0.001$	0.4256	$0.44 \pm 0.01$
$\delta_G$	$2.99 \pm 0.01$	$3.02 \pm 0.01$	3.19	$2.95 \pm 0.01$
$\delta_L$	$3.10 \pm 0.02$	$3.11 \pm 0.01$	3.10	$3.15 \pm 0.01$
$\gamma$	$0.793 \pm 0.002$	$1.002 \pm 0.002$	0.8252	$1.09 \pm 0.02$
$\theta_c$	0.39862	0.4404	0.431423	0.3743
$v_c^*$	3.3665	3.97	3.9155	$2.73 \pm 0.05$
$P_c^*$	0.2603457	0.193534	0.2011311	$0.318 \pm 0.002$

<sup>a</sup>KSA-P = Kirkwood superposition approximation, "pressure" equation-of-state; KSA-E = Kirkwood superposition approximation, "energy" equation-of-state; TSA = truncated superposition approximation, "pressure" equation-of-state; SAL = located from stability analysis according to Ref. 53.

<sup>b</sup>The precision of these exponents is comparable to that of the KSA-P exponents.

scaling hypothesis in the theory of the critical point. As indicated in our discussion, the values of  $\delta_G$ ,  $\delta_L$  are nearly classical, but the other exponents are nonclassical. If to the list of critical exponents in Table I (case 4 above) we add the value  $\alpha = 0.20 \pm 0.02$  obtained by Alder et al.,<sup>32</sup> we find that the Griffith inequalities,<sup>8</sup>  $\alpha + \beta(1 + \delta) \geq 2$  and  $\alpha + 2\beta + \gamma \geq 2$  are remarkably well satisfied on the liquid side of the critical point; specifically,  $2 - \alpha = 1.80 \pm 0.02$ ,  $\beta(\delta + 1) = 1.82$ , and  $(\gamma + 2\beta) = 1.97$ . This near coincidence deteriorates on the gas side of the critical envelope where  $2 - \alpha = 1.88 \pm 0.02$ ,  $\beta(\delta + 1) = 1.34$ , and  $(\gamma + 2\beta) = 1.77$ . Nonetheless, one is led to the tentative conclusion that the scaling hypothesis seems to be working, at least on the liquid side of the critical point. Whether  $\delta$ ,  $\beta$ , and  $\gamma$  would be better determined, and the scaling hypothesis satisfied more exactly, given even more accurate  $g^{(2)}(x)$  data may be inferred by noticing that the critical exponents obtained using expanded  $g^{(2)}(x)$  data yield estimates of  $\gamma + 2\beta$  and  $\beta(\delta + 1)$  that are less satisfactory, namely,  $\gamma + 2\beta = 1.65$  and  $\beta(\delta + 1) = 1.73$ , than those derived from the unexpanded  $g^{(2)}(x)$  data cited above. This may indicate that the YBG equation under the superposition approximation is capable of describing critical behavior correctly provided sufficiently accurate  $g^{(2)}(x)$  data are available.

Here, however, one is on the horns of a dilemma, since we believe that the unexpanded  $g^{(2)}(x)$  data reported in Ref. 46 cannot be improved significantly without an enormous increase in computer time, for the next step to be taken in the refinement of the  $g^{(2)}(x)$  data for the square-well fluid would be to break the hierarchy at the level of  $g^{(4)}$ , in the manner of Lee et al.,<sup>15</sup> and then determine  $g^{(2)}$  and  $g^{(3)}$  simultaneously for the problem at hand.

A second point to be made concerns the use of perturbation expansions of  $g^{(2)}(x)$  in determining phase-transition loci within the framework of the YBG equation. The data presented in Fig. 24 indicate that the  $\theta$ -expanded  $g^{(2)}(x)$  function can lead to a surprisingly accurate determination of the phase-transition loci, as compared with the more accurate, unexpanded  $g^{(2)}(x)$  data. This result is interesting in light of the considerable success of modern perturbation theories<sup>4-6</sup> in describing the properties of pure-phase, classical liquids. In this regard the results derived from the expanded  $g^{(2)}(x)$  data, shown in Fig. 24, represent the first demonstration that a perturbative approach, when used within the context of the second equation in the YBG hierarchy, can lead to an essentially correct identification of the stability limits for two phases, gas and liquid, in "coexistence," and can yield non-classical values for the attendant critical exponents (see Table IX).

Finally, although the critical exponents determined for the square-well fluid by means of the YBG equation for the pair distribution function are somewhat displaced from the exact experimental values, the fact that the theoretically determined critical exponents are *nonclassical* at all seems, to the authors, to be of considerable significance. One can speculate on the underlying conceptual reason that this qualitatively correct physical behavior is demonstrated by the square-well fluid, and in this regard the insights of Widom<sup>12</sup> are particularly valuable. In his 1967 paper Widom pointed out certain similarities between the square-well fluid on the one hand and the lattice-gas model on the other, the latter model known to predict with near-quantitative accuracy the experimentally observed critical exponents of a simple, classical fluid. In a certain sense the square-well fluid may be thought of as a continuum analogue of the lattice gas, and it is this relationship that may be responsible for the success realized in determining critical exponents by means of the YBG theory. The most fundamental distinction between these two models, as stressed by Widom, is that the distance dependence of the square-well potential is usually handled within a continuum representation of the problem (in the development reviewed here, the YBG equation for the pair distribution function, as solved using the superposition approximation), whereas in the lattice gas the radial dependence is, by the very nature of the model, treated as discrete. One consequence of this distinction is that in the lattice gas, correlations are propagated only by the attractive forces, the repulsive forces serving only to establish a metric, whereas in the square-



well fluid both attractive and repulsive forces contribute to the propagation of correlations. Given the success of the lattice-gas model in describing real fluids in the neighborhood of the critical point, Widom suggested that it is the propagation of attractive correlations that determines the character of critical phenomena. On the other hand, the wholly unphysical predictions of the lattice gas model in other state regions of the  $\rho$ - $T$  plane, for example, the nonexistence of a fluid-solid transition, suggest that repulsive forces are not being treated properly in this model. It is in this rather restricted sense that the square-well fluid is superior to the lattice-gas model in describing physical systems, for, as documented in this review, the former exhibits both a gas-liquid and a liquid-solid transition.

At a somewhat different level, one can ask whether the emergence of nonclassical critical exponents for the square-well fluid, as determined by the YBG equation for the pair distribution function, is a manifestation of an essentially mathematical property of the representation per se. The kind of stability analysis that led to the identification of the lower bound on the limit of stability of the pure fluid phase (both with respect to the liquid-gas and the fluid-solid transition) suggests, at the very least, that the understanding of the critical point and its characterization is in some way related to the analytic properties of the YBG nonlinear integral equation, and, in particular, the fact that that equation yields  $g^{(2)}(x)$  functions that undergo important qualitative changes in their structure at certain points of the  $\rho$ - $T$  plane. It must be emphasized, however, that an explicit and rigorous correlation between the topological properties of the YBG (or Kirkwood) nonlinear integral equation and the existence of critical exponents has never been realized, although there are certainly aspects of Ruelle's earlier work<sup>23</sup> and the more recent renormalization group theories<sup>55,56</sup> that make the prospect tantalizing.

There is, however, a second kind of mathematical nonanalyticity present when the square-well fluid is characterized by means of the YBG equation, and it may be that this nonanalyticity as well plays a role in determining the character of the critical point. Examination of the  $g^{(2)}(x)$  data reveals that the pair distribution function suffers a discontinuity at the distance of 1.85 diameters. In other words, when the square-well potential is used within the framework of the YBG equation, the overall effect of the attractions and repulsions is manifested in a pair distribution function that is discontinuous at a certain reduced distance. One concludes that, in this continuum representation, correlations are not propagated smoothly, even when one is away from the critical point. It is tempting to turn this argument around and suggest that when incorporated within the YBG equation, the square-well potential displays at the level of *correlations* the kind of discontinuity in the potential per se that characterizes the lattice gas, and that this could contrib-

ute in part to the nonclassical nature of the exponents found in the study of the YBG equation. Just how important the discontinuous nature of the square-well potential is in affecting the values of the exponents can probably only be evaluated by comparing these present results with those of a similarly detailed study of the YBG equation using, say, the modified Lennard-Jones 12-6 potential mentioned earlier.

## VI. TRANSPORT PROPERTIES OF THE SQUARE-WELL DENSE FLUID

### A. A Perspective on the Square-Well Transport Problem

In 1961 Davis et al.<sup>57</sup> (DRS) developed a kinetic equation for square-well molecules, extending the well-known Enskog theory of transport for dense hard-sphere fluids<sup>58</sup> to the square-well intermolecular potential. The early successes of this comparatively simple transport theory and its resulting equations for the transport properties, such as shear viscosity  $\eta$ , and thermal conductivity  $\kappa_T$  have been documented in reviews elsewhere.<sup>59,60</sup>

The DRS theory has simplicity in its favor when compared to theories (e.g., see Ref. 60), which attempt to deal with more general attractive interactions. However, from the outset the DRS theory and its counterparts are hampered by several problems as follows:

1. The approximations within the transport dynamical description itself.
2. The lack of rigorously-obtained, say, by machine calculation, pair-correlation-function data over a broad range of density-temperature space.
3. The necessity to choose intermolecular interaction parameters. These parameters are present in the literature<sup>61,62</sup> in some profusion for simple molecules but are invariably based on dilute-gas properties, such as dilute-gas viscosity and second virial coefficient data. These data properly account for binary interactions within the limitations of the intermolecular potential chosen, but are not necessarily appropriate for the "many-body" description mandated by a dense fluid.

At present one can safely say that the quality and quantity of pair-correlation-function data have improved dramatically in the last decade; the earlier parts of this article are a partial testimony to this status. As is shown later, there are some fundamental limitations to the DRS theory itself that are troublesome in the investigation of transport phenomena in certain regions of the  $\rho$ - $T$  phase space, specifically near the critical region. As for what intermolecular potential parameters to use, this problem will always be with investigators who attempt to describe physical systems with mathematical

models. With respect to this latter point, there is much room for ingenuity. Suffice it to say, the state-of-the-art in the generation of equilibrium pair-correlation-function data presently permits an investigator to formulate new, more sophisticated transport theories capable of providing, at least in the medium of corresponding states, more accurate descriptions of real fluid transport property behavior. Viewed in another way, evaluation of the merits of a theory can now be better isolated from, rather than dictated by, the question of the pair correlation-function input.

### B. Results Obtained from the Davis-Rice-Sengers Theory

In this chapter the discussion is limited to pure systems; only the properties of shear viscosity  $\eta_s$  and thermal conductivity  $\kappa_T$  are examined as their expression in the context of the DRS theory is less ambiguous than that of the self-diffusivity. In addition there are only limited data available on bulk viscosity. The available data in the dense fluid region for  $\eta_s$  and  $\kappa_T$  provide a more complete picture of the overall dense fluid behavior with respect to these properties.

Diller et al.<sup>63</sup> have pointed out that the characteristic transport behavior of classical fluids (e.g., subcooled liquid argon) is represented by increases in  $\kappa_T$  and decreases in  $\eta_s$  with increasing temperature along constant density loci:

$$\left(\frac{\partial \eta_s}{\partial T}\right)_{n^*} < 0 \quad (6.1)$$

$$\left(\frac{\partial \kappa_T}{\partial T}\right)_{n^*} > 0 \quad (6.2)$$

(Actually they examined the behavior of  $\Delta\xi = \xi - \xi^*$ , where  $\xi$  is the liquid transport property and  $\xi^*$  is the dilute real-gas transport property.) Investigation of the shear viscosity data of de Bock et al.<sup>64</sup> and Cook,<sup>65</sup> indicates that (6.1) holds up to 120 to 125° K, at which point an inversion occurs, that is

$$\left(\frac{\partial \eta_s}{\partial T}\right)_{n^*} > 0, \quad T > 125^\circ \text{K} \quad (6.3)$$

One would expect a good transport theory to predict at least qualitatively these temperature dependencies of  $\eta_s$  and  $\kappa_T$ . The Enskog theory for hard spheres<sup>58</sup> predicts that

$$\left(\frac{\partial \xi}{\partial T}\right)_{n^*} > 0 \quad (6.4)$$

for both  $\xi = \eta_s$  and  $\kappa_T$ . Thus the role of the addition of a square well should be to create the above-mentioned inversion in the  $\eta_s$  function. It does not

appear that an inversion in  $\kappa_T$  occurs for classical fluids, although there exist no strong formal arguments to rule out the possibility of inversion for this property in all dense fluids.

The square-well transport-property formulas are given below.<sup>60,66</sup>

Shear viscosity:

$$\eta_s = \eta^* \left\{ \frac{\{1 + (8/5)y[g^{(2)}(1_+) + R^3 g^{(2)}(R_+) \Xi_1]\}^2}{g^{(2)}(1_+) + R^2 g^{(2)}(R_+) [\Xi_2 + (1/6)\theta^2]} + \frac{768}{25\pi} [g^{(2)}(1_+) + R^4 g^{(2)}(R_+) \Xi_2] \right\} \quad (6.5)$$

Thermal conductivity:

$$\kappa_T = \kappa^* \left\{ \frac{\{1 + (12/5)y[g(1_+) + R^3 g^{(2)}(R_+) \Xi_1]\}^2}{g^{(2)}(1_+) + R^2 g^{(2)}(R_+) [\Xi_2 + (11/16)\theta^2]} + \frac{512y^2}{25\pi} [g^{(2)}(1_+) + R^4 g^{(2)}(R_+) \Xi_2] \right\} \quad (6.6)$$

where

$$\eta^* = \frac{5}{16\sigma_1^2} \left( \frac{mkT}{\pi} \right)^{1/2} \quad (6.7)$$

$$\kappa^* = \frac{75}{64\sigma_1^2} \left( \frac{k^3 T}{\pi m} \right)^{1/2} \quad (6.8)$$

$$\Xi_1 = 1 - e^\theta + \frac{\theta}{2} \left( 1 + \frac{4}{\pi^{1/2}} e^\theta \int_{\theta^{1/2}}^{\infty} e^{-x^2} x^2 dx \right) \quad (6.9)$$

$$\Xi_2 = e^\theta - \frac{\theta}{2} - 2 \int_0^\infty x^2 (x^2 + \theta)^{1/2} e^{-x^2} dx \quad (6.10)$$

Because of the impulsive nature of the square-well intermolecular potential, the kinetics lead to the requirement of the knowledge of only  $g^{(2)}(1_+)$  and  $g^{(2)}(R_+)$  of the pair correlation function, where

$$g^{(2)}(R_+) = e^{-\theta} g^{(2)}(R_-) \quad (6.11)$$

The several studies of (6.5) and (6.6), which are rearranged expressions of the original DRS results developed by Sengers<sup>67</sup>, basically differ only in how the pair-correlation-function input was generated.

Davis and Luks<sup>68</sup> performed computations of  $\eta_s$  throughout the dense fluid region by two separate methods:

1. Using  $\kappa_T$  data and (6.6) in concert with equation-of-state data and (3.10) to determine  $g^{(2)}(1_+)$  and  $g^{(2)}(R_+)$  empirically. These  $g^{(2)}$  values can then be used to calculate  $\eta_s$  from (6.5). The method is inexorably tied in, as pointed out earlier, to the choice of intermolecular potential parameters, which in this case were chosen to be those characteristic of second-virial-coefficient data<sup>61</sup>

$$\sigma_i = 3.162 \text{ \AA}$$

$$\frac{\epsilon}{k} = 69.4^\circ \text{ K}$$

$$R = 1.85$$

2. Using an abbreviated version of a perturbation technique developed by Lowry et al.,<sup>69</sup> the  $g^{(2)}$  inputs were calculated *a priori*, according to

$$g^{(2)}(1_+) = g_0(1_+)e^\theta \quad (6.12)$$

$$g^{(2)}(R_+) = g_0(R_+) \quad (6.13)$$

where  $g_0$  is the hard-sphere function. Here, Davis et al.<sup>68,70</sup> employed the Percus-Yevick hard-sphere pair correlation functions, which are analytically computable.<sup>52,71,72</sup>

The advantage of method 2 over method 1 is that property data are not required to generate the  $g^{(2)}(x)$  input in the former. Table X compares the results of methods 1 and 2 with experiment for saturated liquid argon.

Schrodtt et al.<sup>66</sup> redid the computations of Davis and Luks using YBG hard-sphere input in (6.12) and (6.13), with the aim of locating inversions in  $\eta_s$  and  $\kappa_T$  along isochores as temperature was varied. Figure 25 shows that inversion loci were found for *both*  $\eta_s$  and  $\kappa_T$ , with the former being at temperatures higher than observed experimentally for liquid argon. Despite these unfavorable qualitative trends, quantitative agreement with the  $\eta_s$  data of de Bock et al.<sup>64</sup> and Cook<sup>65</sup> and the  $\kappa_T$  data of Ikenberry and Rice<sup>73</sup> was respectable, a fact that perhaps lent the approach more credence than it deserved at that time.

The acquisition of square-well  $g^{(2)}(x)$  data from the YBG theory in the form of (2.2) by Schrodtt and Luks<sup>33</sup> to terms of order  $\psi_2$  offered the opportunity to examine the DRS theory further. Figure 26 shows that the temperature inversion in  $\eta_s$  (and the lack of one in  $\kappa_T$ ) is in closer agreement with the behavior of liquid argon, the predicted inversion temperature being about 108° K. The dashed lines in Fig. 26 are analytical extensions of the predictions into the regions of two-phase coexistence as dictated by experiment and the square-well parameters  $\sigma_1 = 3.162 \text{ \AA}$ ,  $R = 1.85$ , and  $\epsilon/k = 69.4^\circ \text{ K}$ . Schrodtt and

TABLE X  
A Comparison of  $\eta_s$  Predictions Using (1) Empirically Generated  $g^{(2)}(x)$  Data and (2)  $g^{(2)}(x)$  Data from (6.12) and (6.13) with Experiment for Argon Along the Saturated Liquid Locus<sup>a</sup>

$T$ (°K)	$\eta_s$ (cP)			$\kappa_T(10^{-4}\text{cal}/(\text{cm})(\text{sec})(^\circ\text{K}))$	
	Experimental <sup>b</sup>	1	2	Experimental <sup>c</sup>	2
87.5	0.246	0.199	0.241	2.92	3.43
91.0	0.220	0.194	0.223	2.85	3.21
105.6	0.148	0.159	0.171	2.43	2.54
120.3	0.113	0.113	0.113	1.99	1.96
136.3	0.077	0.0927	0.090	1.51	1.42
149.4	0.051	0.0599	0.0515	1.32	0.832

<sup>a</sup>Method 2 is also used for  $\kappa_T$  and compared with argon experimental data along the same locus.

<sup>b</sup>Reference 65.

<sup>c</sup>Reference 73 (extrapolated results).

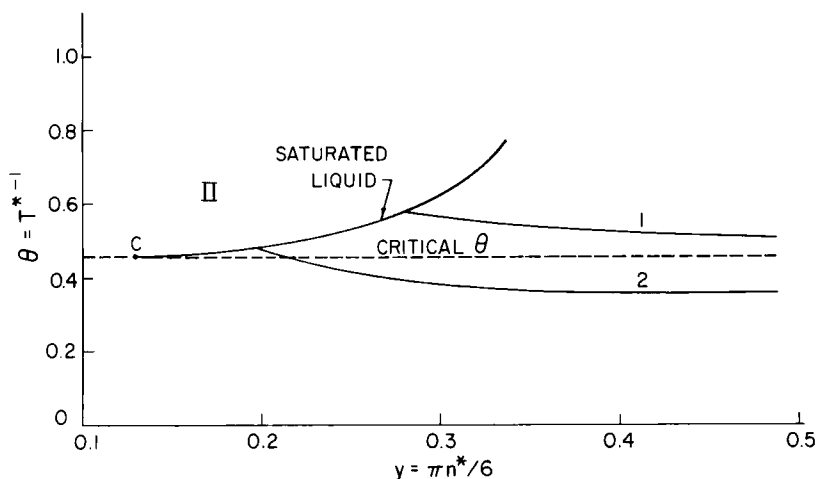


**Fig. 25.** A  $\theta$ - $y$  diagram for the square-well model of transport (DRS) denoting the liquid and dense-gas regimes (separated by the "critical  $\theta$ " line). Curve 1 denotes the line above which  $(\partial\kappa_T/\partial T)_{n*} < 0$  and below which  $(\partial\kappa_T/\partial T)_{n*} > 0$  for the square-well model. Curve 2 has a parallel interpretation for shear viscosity  $\eta_s$ .  $c$  is the critical point and II is the two-phase gas-liquid region. Equations 6.12 and 6.13 were used for data input. (From Ref. 66, "A comparative analysis of the Rice-Allnatt and square-well transport theories." Used by permission of Gordon and Breach Science Publishers.)

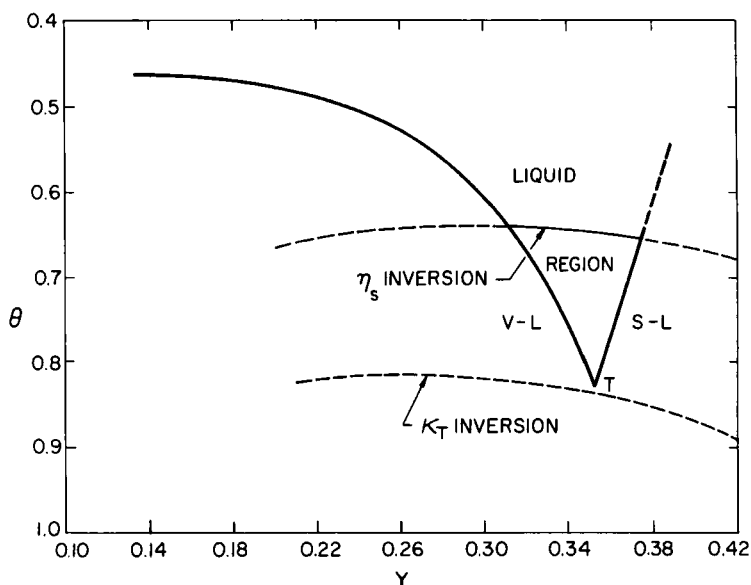


**Fig. 26.** Loci of the predicted inversions of  $\kappa_T$  and  $\eta_s$  in the liquid region in  $\theta$ - $y$  space. The liquid region is located using argon data and the parameters  $\sigma_1 = 3.162 \text{ \AA}$ ,  $\epsilon/k = 69.4^\circ \text{ K}$ . T denotes the triple point, and V-L and S-L denote the vapor-liquid and solid-liquid two-phase regions, respectively. The predictions were performed using data in the form of (2.2) to terms of order  $\psi_2$ . (From Ref. 38. Used by permission of the American Institute of Physics.)

Luks<sup>33</sup> have located a gas-liquid coexistence region based on this same  $g^{(2)}(x)$  data. If one were to match the location of theoretical and experimental critical points (holding  $R=1.85$  constant), one would replace the above  $\sigma_1$  and  $\epsilon/k$  with the revised parameters

$$\sigma_1 = 3.325 \text{ \AA}$$

$$\frac{\epsilon}{k} = 60.14^\circ \text{ K}$$

This "adjustment" is shown in Fig. 27, where one can see that the saturated liquid locus is ultimately matched closer to the YBG prediction. Use of these "adjusted parameters" would of course affect predictions. Table XI compares the effect of using the traditional parameters obtained from second-virial-coefficient data as opposed to these adjusted parameters for saturated liquid argon transport properties. Although both sets of predictions are weak, the ones using adjusted parameters are better.

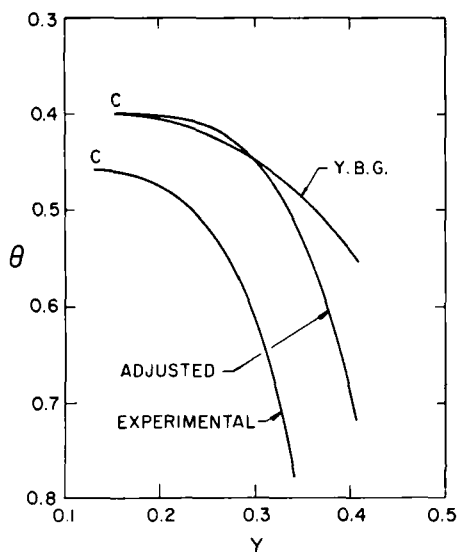


**Fig. 27.** A comparison of the theoretical (YBG  $\theta$ -expanded equation with Kirkwood superposition approximation to terms of order  $\psi_2$ ), experimental, and parametrically adjusted experimental saturated liquid loci for argon in the  $\theta$ - $y$  space. (From Ref. 38. Used by permission of the American Institute of Physics.)

If one examines the form of the  $g^{(2)}(x)$  function used for the predictions in Table XI:

$$g^{(2)}(x) = g_0(x) \exp \left[ \frac{\theta \psi_1(x) + \theta^2 \psi_2(x)}{x} \right]$$

and compares it with (6.12) and (6.13), one sees that the bracketed quantity in (3.9) goes to the limit of  $\theta$  as  $\lambda_0 \rightarrow 0$  (i.e., the ideal gas limit). Furthermore, computations show that

$$\theta \psi_1(1_+) + \theta^2 \psi_2(1_+) < \theta \quad (6.14)$$

for  $\lambda_0 > 0$ , so that  $g^{(2)}(1_+)$  in (3.9) will always be less than  $g^{(2)}(1_+)$  in (6.12). So, although using the YBG  $\theta$ -expanded results leads to a better qualitative description, it is not accompanied by quantitative improvement.

As described in Section II.D, the TSA modification of the YBG equation can lead to better quantitative agreement.<sup>41</sup> This is demonstrated in Table XII, it should be noted that the parameters  $\sigma_1 = 3.162 \text{ \AA}$ , and  $\epsilon/k = 69.4^\circ \text{ K}$  were used for predictive purposes. Since the TSA approximation moved the theoretical critical point much closer to the experimental critical point, parametric adjustment would offer only minor alteration in the predictions for  $\eta_s$  and  $\kappa_T$ .

Finally, with the existence of YBG square-well data in unexpanded form, additional computations can be made. For a given point in  $\theta$ - $y$  space, such as



TABLE XI  
A Comparison of the DRS Theory, With and Without  
Parametric Adjustment of  $\sigma_1$  and  $\epsilon/k$ , using the  $g^{(2)}(x)$   
Data of Ref. 33, Along the Saturated Liquid Argon Locus<sup>a</sup>

T (°K)	$\eta_s$ (cP)		$\kappa_T$ [ $10^{-4}$ cal/(cm) (sec) (°K)]	
	th <sup>b</sup>	pa <sup>c</sup>	th <sup>b</sup>	pa <sup>c</sup>
87.5	0.113	0.127	1.51	1.79
91.0	0.109	0.123	1.47	1.76
105.6	0.093	0.106	1.32	1.62
120.3	0.078	0.090	1.16	1.42
136.3	0.061	0.067	0.96	1.15
149.4	0.038	0.042	0.63	0.72

<sup>a</sup>Corresponding experimental data are presented in Table X.

<sup>b</sup>th refers to those computations performed without parametric adjustment.

<sup>c</sup>pa refers to parametric adjustment.

TABLE XII  
Predicted Values of  $\eta_s$  and  $\kappa_T$  for the DRS  
Theory Using YBG  $\theta$ -Expanded  $g^{(2)}(x)$  Data  
with Truncated Superposition Approximation  
Along the Saturated Liquid Argon Locus<sup>a</sup>

T (°K)	$\eta_s$ (cP)	$\kappa_T$ [ $10^{-4}$ cal/(cm) (sec) (°K)]
87.5	0.179	2.91
91.0	0.170	2.78
105.6	0.138	2.30
120.3	0.108	1.86
136.3	0.078	1.37
149.4	0.043	0.70

<sup>a</sup>Corresponding Experimental data are presented in Table X.

corresponds to the empirical saturated liquid locus, there will be little difference between the  $g^{(2)}(x)$  data of the unexpanded and  $\theta$ -expanded forms of the YBG equation. If one superimposes the experimental critical point of argon on the critical point of the locus denoting the lower limit on the bound of the stability of a pure phase, such as shown in Fig. 16, one finds that this latter locus falls well within the experimental vapor-liquid coexistence locus.<sup>74</sup> This observation was made earlier by Co and the present authors in a different context,<sup>75</sup> but their results apply here. Briefly, the experimental locus lies in a region where differences in  $g^{(2)}(x)$  from  $\theta$ -expanded and unexpanded YBG equations will be small if one does coincide the two critical points. However, this transformation will generate a new set of  $(\sigma_1, \epsilon/k)$ :

$$\sigma_1 = 3.565 \text{ \AA}$$

$$\frac{\epsilon}{k} = 56.47^\circ \text{K}$$

These new values will significantly alter the transport coefficient results one would get at a point in density-temperature space from those obtained earlier using  $(\sigma_1, \epsilon/k)$  determined from second-coefficient data. The rationale for performing such an alteration would be as before: to bring into correspondence to some degree theoretical and experimental information on the coexistence (i.e., critical point) region, recognizing that dilute-gas data are not necessarily apropos to generating intermolecular potential parameters that would be effective for dense-fluid properties.

Table XIII compares  $\eta_s$  and  $\kappa_T$  at three temperatures using unexpanded YBG pair-correlation-function data and the parameters cited above. The agreement is remarkably good. One might attribute this success to the

TABLE XIII  
Predicted Values of  $\eta_s$  and  $\kappa_T$  Along the Saturated Liquid Locus Using  
Unexpanded YBG Equation Data and Parametric Adjustment with  
the DRS Theory

$T$ (°K)	$\eta_s(\text{cp.})$		$\kappa_T[10^{-4}\text{cal}/(\text{cm})(\text{sec})(^\circ\text{K})]$	
	Predicted	Experimental	Predicted	Experimental
102.67	0.1418	0.160	2.246	2.59
125.48	0.1098	0.102	1.824	1.83
141.17	0.0786	0.068	1.346	1.42

ability of the unexpanded YBG equation to locate more realistically the critical point of the square-well fluid in  $\theta$ - $\lambda_0$  space. Figures 23 and 24 show (1) that the differences between the loci on the lower bounds of fluid stability are more pronounced near the critical point and (2) the locus related to the stability problem for the  $\theta$ -expanded YBG case is substantially removed from that obtained by Maxwell construction from the same data. But, although one may be pleased with the results achieved, one cannot leave this problem without admitting that the approximate nature of the data used, combined with the several equation-of-state methods available to establish the vapor-liquid coexistence locus, forces the user of the DRS equation to make a choice of methodology. However, it is encouraging that isotherms obtained from  $P^*(C)$  and the above-mentioned stability analysis for the unexpanded YBG equation offer a reassuring degree of consistency, as shown in Fig. 22, and at the same time, this same  $g^{(2)}(x)$  data can produce quite good transport-property predictions when used in an intuitively sensible manner (i.e., by first matching the location of theoretical and experimental critical points).

Finally, it is worth noting that there exists formalism for binary square-well transport properties,<sup>76</sup> for which some limited computations have been performed<sup>77</sup> for mixtures of simple fluids.

## VII. CONCLUDING REMARKS

The theory of the distribution function in statistical mechanics, and the application of this theory to the description of the states of matter have been under development for 40 years. A particular realization of this theory, that due to Yvon, Born, and Green, is the subject of this review, and the objective here is to assess the usefulness of the theory in characterizing the properties of a simple, classical system, namely, the square-well fluid. As regards our choice of the square-well fluid, the simplest model for which attractions and repulsions between the constituent molecules of a system are treated explicitly, the following point can be made. Because of their analytical and numerical convenience and the insights they provide, great emphasis is placed in statistical mechanics on the identification and elaboration of simple models. In dealing with critical phenomena one has the Ising model; for the solid state, the liquid state, and the gaseous state one has the harmonic solid, the hard-sphere fluid, and the perfect gas, respectively. We would like to suggest here, on the basis of the results gathered in this review, that the simplest model system that can account for the properties of all three states of matter is the square-well fluid. In light of the remarks presented in Section I, we would like to reemphasize that this does *not* mean that molecules really do interact by means of square-well intermolecular forces, but rather that such a

system displays all the essential features characterizing systems of molecules interacting by means of more realistic ( $n$ -parameter) potential functions.

Perhaps the main conclusion to be drawn from this review concerns the usefulness of the YBG equation for the pair distribution function per se. While acknowledging the success of other theories designed to describe a particular state of matter with quantitative accuracy, and recognizing of course the significant impact on our understanding of phase transitions derived from lattice theories and the more recent renormalization group theory of Wilson,<sup>55</sup> our view here is that the YBG equation does provide a single theoretical framework within which the equilibrium and transport properties of a classical system can be predicted with reasonable quantitative accuracy and also can describe the possible transformations among the gaseous, liquid, and solid states with at least qualitative success. This view is to be regarded not so much as an opinion, but as the necessary consequence of a *mathematical* point. In contrast to perturbation theories, however cleverly constructed,<sup>4-6</sup> only a distribution function theory, or perhaps an algebraic one (e.g., a  $B^*$  algebraic theory<sup>1,78</sup>), has a sufficiently rich *mathematical* structure to admit the possibility of considering, for example, phase transformations between the solid and liquid states *and* the liquid and gaseous states of matter within a *single* theoretical framework.

The work reviewed here provides a basis for claiming a certain success in achieving the overall objectives stated in Section I, though it is abundantly clear that much work has yet to be done. Accordingly, it may be useful to the reader at this point if we were to highlight areas of further study, both analytical and numerical, that we believe could extend significantly the results reported in this review.

One of the areas in which further progress would be welcome is in the application of the methods of nonlinear analysis in general, and in particular the careful use of theorems on the existence, uniqueness, or possible multiplicity of solutions to the YBG integro-differential equation or the Kirkwood integral equation. The contributions of Vlasov and Kirkwood, cited in the Section I, represent important first steps in this endeavor. Although a systematic review of the application of bifurcation theory to the nonlinear integral equations of classical-fluid theory would be out of place here, it should be emphasized that the kind of approach taken in Section III.C has its origins in the work of several authors. In addition to the references cited in that section, we may mention here especially the contributions of Khachatryan,<sup>79</sup> Gartenhaus and Stranahan,<sup>80</sup> and Jancovici<sup>81</sup> in the 1960s. At about the same time that Rice and his co-workers<sup>13,14</sup> were providing new insights regarding the analytic structure of the YBG equation, a program of study was initiated by Rice et al.,<sup>82-84</sup> in which Hammerstein theory was applied to the Kirkwood equation. Contributions of interest since then include the

developments by Raveché and Stuart,<sup>85</sup> Cheng and Kozak,<sup>86</sup> and especially the recent work of Lovett.<sup>87</sup> By carrying through an analysis based on a nonlinear equation relating the direct correlation function and the singlet density function (in contrast to an analysis based on similar relations between the singlet and pair densities), Lovett was able to investigate the mechanical stability of a system with a fluidlike pair distribution function. A numerical analysis of the three-dimensional hard-sphere system revealed that this system remained stable at all densities but that the addition of an attractive-pair interaction easily induced an instability. Lovett has pointed out<sup>88</sup> that the identification of the solid phase in our study of the square-well fluid at very high densities<sup>45,47</sup> is the same as the  $c(r)$ -based argument; that is, the square-well fluid becomes mechanically and thermodynamically unstable at the same density point. The apparent mechanical stability of the hard-sphere fluid, as determined by Lovett, may be interpreted in light of the relationship between  $\lambda$ ,  $\lambda_0$  for this system as calculated in Ref. 45 and displayed in Fig. 9. Although a traditional bifurcation-theoretical analysis in Ref. 45 attributes significance to the point  $\lambda_0 \sim 6$ , it should be noticed that the  $g^{(2)}(x)$  function changes *smoothly* with respect to the parameter  $\lambda$ , that is, there is no point in the  $(\lambda, \lambda_0)$  space at which the  $g^{(2)}(x)$  function changes discontinuously with respect to  $\lambda$ . However, a *discontinuous* change in the behavior of the  $g^{(2)}(x)$  function can occur if one follows the behavior of this function with respect to the  $\lambda_0$  coordinate, and, in fact, it was this dual behavior in the  $(\lambda, \lambda_0)$  space that was the main new insight derived from this study on the behavior of the YBG and Kirkwood equations at very high densities.

The progress made in interpreting the existence and uniqueness properties of solutions to the YBG equation is a direct consequence of having at ones disposal formal theorems on nonlinear integral equations,<sup>49,89</sup> theorems which, for the most part, have been available for a generation. More recently, Arthurs<sup>90</sup> has developed a theory of complementary variational principles that may prove to be as useful in studying integral equation theories of classical fluids as the theorems referred to above. The basic idea here, introduced by Noble,<sup>91</sup> is that one derives from the canonical form of the Euler-Lagrange variational theory certain functionals; given a trial solution, these functionals are then shown to bound from above *and* below a functional constructed from the *exact* solution to the problem, provided certain conditions are satisfied. Thus one has a systematic procedure for constructing better and better approximations to the formally exact solution to the problem by monitoring the success with which the functionals derived from the approximate solution bracket the functional constructed from the exact solution. Anderson et al.<sup>92</sup> were the first to apply the method in the theory of classical fluids; they determined an analytic approximation to the exact solution of the Kirkwood equation (under the superposition approximation)

for the hard-sphere fluid at  $\lambda = 5$ . Recently, Co and the present authors<sup>93</sup> have extended these calculations on the hard-sphere system into the very-high-density regime. At all  $\lambda$  values beyond the lower bound on the limit of stability of the pure, dense-fluid phase, identified previously in Ref. 45, variational analysis of the approximate analytical  $g^{(2)}(x)$  functions constructed suggested infinite periodicity in the formally exact  $g^{(2)}(x)$  function. This behavior was in agreement with the results presented in Ref. 45, where solutions to the Kirkwood equation were obtained by straightforward iterative methods. The important point here is that the analytic approximations to the exact  $g^{(2)}(x)$  function, identified by the theory of complementary variational principles, provide an *independent* corroboration of the principal result, that is, that the  $g^{(2)}(x)$  function experiences a dramatic change in its long-range behavior at about  $\lambda \simeq 34.9250$ .

Fundamental to the above application of complementary variational principles to the Kirkwood equation are the conditions on the kernel that must be satisfied, namely, the kernel must be symmetric and positive definite. It is evident that a generalization of the method presented by Arthurs to kernels that may have negative eigenvalues (perhaps in the manner in which Dolph and Minty<sup>94</sup> was able to generalize the earlier theorems of Hammerstein<sup>95</sup>) would allow the consideration of the square-well fluid per se. The immediate advantage of such a generalization would be that the method of complementary variational principles could be used to identify analytic approximations to the formally exact  $g^{(2)}(x)$  function in the neighborhood of the critical point. Since we already have numerical evidence for the non-classical behavior of the critical exponents as determined by direct solution of the YBG equation (under the superposition approximation) for the square-well model, it would be most interesting to see if nonclassical behavior is also predicted when the critical envelope is constructed from analytic approximations to the exact  $g^{(2)}(x)$  function.

In the area of transport properties, the DRS theory is limited in its accountability of many body effects, since it is an Enskog-type transport description. For example, it is difficult to envision the form of (6.6) for  $\kappa_T$  providing singularities in the region of coexistence, say near the critical point. In Section III.B,  $g^{(2)}(x)$  data that yield singularities in the isothermal compressibility throughout the coexistence region are discussed. These same  $g^{(2)}(x)$  data when inserted into (6.6) or (6.5) enhance the value of the transport property by about 60% in the coexistence region over the value obtained using  $g^{(2)}(x)$  from the  $\theta$ -expanded YBG equation.<sup>96</sup> One may conclude that, although insertion of appropriate data into transport formulas is necessary to make proper predictions in the vicinity of the coexistence region, the transport expressions themselves must also be appropriate to the problem description. The transport property enhancement just cited may be interpreted in an

academic sense in that there exists some limited amount of physics in the DRS theory apropos to the coexistence region problem. However, it is quite obvious that a less-restricted dynamical description leading to a more general kinetic equation is needed, a problem area that certainly deserves attention in the future, perhaps starting with an investigation of autocorrelation-function theory for square-well fluids.

Finally, one might challenge the wisdom of attributing too much importance to solutions generated within coexistence regions from equations such as (2.6) simply because one is attempting to extract conclusions from a homogeneous equation (i.e., one characterized by a single density at any state) about systems that are naturally heterogeneous; for example, a gas-liquid system should have *two* distinct densities associated with it. Proponents of this argument would prescribe coupling the singlet YBG equation with the doublet YBG equation to relax the constraint of homogeneity. However, a counterargument can be offered for maintaining interest in the homogeneous YBG equation within a coexistence region.<sup>97</sup> If one has an interface between two bulk phases of densities  $\rho_G$  and  $\rho_L$  for the gas-liquid problem and one wishes to study the properties of this interface, say, the surface-tension function, one must know the molecular-structure details of this admittedly inhomogeneous system at *all* intermediate densities to the bulk values  $\rho_G$  and  $\rho_L$ . These details have direct bearing on the singlet function  $g^{(1)}(z)$ , which in turn affects the interfacial properties. Using functions such as those discussed in Section III.B can yield proper qualitative descriptions of heterogeneous systems,<sup>75</sup> such as the gas-liquid interface, despite their being obtained from an integral equation for homogeneous  $g^{(2)}(x)$  and despite the several accompanying approximations that must be made to adapt homogeneous  $g^{(2)}(x)$  input to the heterogeneous formalism associated with an interfacial molecular description.

### References

1. D. Ruelle, *Statistical Mechanics*, Benjamin, New York, 1969.
2. For a rigorous derivation of the van der Waals equation, see: O. Penrose and J. L. Lebowitz, *J. Stat. Phys.*, **3**, 211 (1971), and the references cited therein.
3. R. W. Zwanzig, *J. Chem. Phys.*, **22**, 1420 (1954).
4. J. A. Barker and D. Henderson, *Rev. Mod. Phys.*, **48**, 587 (1976), and references contained therein.
5. (a) L. Verlet, *Phys. Rev.* **165**, 201 (1968); (b) L. Verlet and J. J. Weis, *Phys. Rev.*, **A5**, 939 (1972).
6. H. C. Andersen, D. Chandler and J. D. Weeks, *Adv. Chem. Phys.*, **34**, 103 (1976), and references cited therein.
7. M. E. Fisher, *Rep. Prog. Phys.*, **30**, 615 (1969).
8. H. E. Stanley, *Introduction to Phase Transitions and Critical Phenomena*, Oxford University Press, Oxford, 1971.
9. *Phase Transitions and Critical Phenomena*, Vols. 1-6, C. Domb and M. S. Green, Eds., Academic Press, New York, 1972.

10. T. L. Hill, *Statistical Mechanics*, McGraw-Hill, New York, 1956.
11. S. A. Rice and P. Gray, *The Statistical Mechanics of Simple Liquids*, Wiley, New York, 1965.
12. B. Widom, *Science*, **157**, 375 (1967).
13. S. A. Rice and J. Lekner, *J. Chem. Phys.*, **42**, 3559 (1965).
14. S. A. Rice and D. A. Young, *Discuss. Faraday Soc.*, **43**, 16 (1967).
15. (a) Y.-T. Lee, F. H. Ree, and T. Ree, *J. Chem. Phys.*, **48**, 3506 (1968); (b) F. H. Ree, Y.-T. Lee, and T. Ree, *J. Chem. Phys.*, **55**, 234 (1971).
16. H. L. Frisch and J. L. Lebowitz, *The Equilibrium Theory of Classical Fluids*, Benjamin, New York, 1964.
17. R. Brout and P. Carruthers, *Lectures on the Many-Electron Problem*, Interscience, New York, 1963.
18. J. L. Percus, in *The Equilibrium Theory of Classical Fluids*, H. L. Frisch and J. L. Lebowitz, Eds., Benjamin, New York, 1964, pp. II-33 to II-170, and G. Stell, *op. cit.* pp. II-171 to II-266.
19. M. J. Moffat and J. J. Kozak, *J. Chem. Phys.*, **55**, 3794 (1971).
20. M. J. Moffat and J. J. Kozak, *J. Chem. Phys.*, **58**, 876 (1973).
21. Vlasov applied the ideas of bifurcation theory to several different problems; the reader may consult: A. A. Vlasov, *Many-Particle Theory and Its Application to Plasma*, Gordon and Breach, New York, 1961.
22. J. G. Kirkwood and E. Monroe, *J. Chem. Phys.*, **9**, 514 (1941).
23. D. Ruelle, *Ann. Phys. (N.Y.)*, **25**, 109 (1963).
24. G. Gallavotti and S. Miracle-Sole, *Commun. Math. Phys.*, **7**, 274 (1968).
25. I.-Y. S. Cheng and J. J. Kozak, *J. Math. Phys.*, **14**, 632 (1973).
26. L. A. Pastur, preprint of the Academy of Sciences of the Ukrainian SSR, Kiev, 1973.
27. H. Moraal, *Physica*, **81A**, 469 (1975).
28. C. N. Yang and T. D. Lee, *Phys. Rev.*, **87**, 404 (1952).
29. J. G. Kirkwood, V. A. Lewinson, and B. J. Alder, *J. Chem. Phys.*, **20**, 929 (1952).
30. J. A. Barker and D. Henderson, *Mol. Phys.*, **21**, 187 (1971).
31. W. R. Smith, D. Henderson, and J. A. Barker, *J. Chem. Phys.*, **55**, 4027 (1971).
32. B. J. Alder, D. A. Young, and M. A. Mark, *J. Chem. Phys.*, **56**, 3013 (1972).
33. I. B. Schrodtt and K. D. Luks, *J. Chem. Phys.*, **57**, 200 (1972).
34. W. W. Lincoln, J. J. Kozak, and K. D. Luks, *J. Chem. Phys.*, **62**, 1116 (1975).
35. M. Chen, D. Henderson, and J. A. Barker, *Can. J. Phys.*, **47**, 2009 (1969).
36. W. R. Smith, D. Henderson, and J. A. Barker, *J. Chem. Phys.*, **53**, 508 (1970).
37. I. B. Schrodtt, J. J. Kozak, and K. D. Luks, *J. Chem. Phys.*, **57**, 206 (1972).
38. I. B. Schrodtt, J. S. Ku, and K. D. Luks, *J. Chem. Phys.*, **57**, 4589 (1972).
39. W. W. Lincoln, Y. Tago, and K. D. Luks, *J. Chem. Phys.*, **61**, 4129 (1974).
40. N. F. Carnahan and K. E. Starling, *J. Chem. Phys.*, **51**, 635 (1969).
41. I. B. Schrodtt, J. J. Kozak, and K. D. Luks, *J. Chem. Phys.*, **60**, 170 (1974).
42. W. W. Lincoln and K. D. Luks, *AIChE J.*, **19**, 1277 (1973).
43. G. J. F. Breedveld and J. M. Prausnitz, *AIChE J.*, **19**, 783 (1973).
44. J. G. Kirkwood, E. K. Maun, and B. J. Alder, *J. Chem. Phys.*, **18**, 1040 (1950).
45. K. U. Co, J. J. Kozak, and K. D. Luks, *J. Chem. Phys.*, **66**, 581 (1977).
46. W. W. Lincoln, J. J. Kozak, and K. D. Luks, *J. Chem. Phys.*, **62**, 2171 (1975).
47. K. U. Co, J. J. Kozak, and K. D. Luks, *J. Chem. Phys.*, **65**, 2327 (1976).
48. D. A. Young and S. A. Rice, *J. Chem. Phys.*, **47**, 4228 (1967).
49. M. S. Krasnosel'skii, *Topological Methods in the Theory of Nonlinear Integral Equation*, Pergamon, London, 1964.
50. P. M. Morse and H. Feshbach, *Methods of Theoretical Physics*, McGraw-Hill, New York, 1953.



51. R. A. Goldstein and J. J. Kozak, *Physica*, **71**, 267 (1974).
52. G. J. Throop and R. J. Bearman, *J. Chem. Phys.*, **42**, 2408 (1965).
53. K. U. Co, J. J. Kozak, and K. D. Luks, *J. Chem. Phys.*, **64**, 2197 (1976).
54. T. L. Hill, *Statistical Mechanics*, McGraw-Hill, New York, 1956, pp. 413 ff.
55. K. G. Wilson, *Phys. Rev.*, **B4**, 3174, 3184 (1971).
56. K. G. Wilson and M. E. Fisher, *Phys. Rev. Lett.*, **28**, 240 (1972).
57. H. T. Davis, S. A. Rice, and J. V. Sengers, *J. Chem. Phys.*, **35**, 2210 (1961).
58. S. Chapman and T. G. Cowling, *The Mathematical Theory of Non-Uniform Gases*, Cambridge University Press, London, 1961, Chap. 16.
59. S. A. Rice, J. P. Boon, and H. T. Davis in *Simple Dense Fluids*, H. L. Frisch and Z. W. Salsburg, Eds., Academic Press, New York, 1968.
60. H. T. Davis, in Vol. 24 of *Advances in Chemical Physics*, I. Prigogine and S. A. Rice, Eds., Wiley-Interscience, New York, 1973.
61. J. O. Hirschfelder, C. F. Curtiss, and R. B. Bird, *Molecular Theory of Gases and Liquids*, Wiley, New York, 1964.
62. T. M. Reed and K. E. Gubbins, *Applied Statistical Mechanics*, McGraw-Hill, New York, 1973.
63. D. E. Diller, H. J. M. Hanley, and H. M. Roder, *Cryogenics*, **August 1970**, p. 286.
64. A. de Bock, W. Grevendonk, and W. Herreman, *Physica*, **37**, 227 (1967).
65. G. A. Cook, *Argon, Helium and the Rare Gases*, Vol. I, Wiley, New York, 1961.
66. I. B. Schrod, J. S. Ku, and K. D. Luks, *Phys. Chem. Liq.*, **2**, 147 (1971).
67. J. V. Sengers, private communication.
68. H. T. Davis and K. D. Luks, *J. Phys. Chem.*, **69**, 869 (1965).
69. B. A. Lowry, H. T. Davis, and S. A. Rice, *Phys. Fluids*, **7**, 402 (1964).
70. K. D. Luks, M. A. Miller, and H. T. Davis, *AIChE J.*, **12**, 1079 (1966).
71. M. S. Wertheim, *Phys. Rev. Lett.*, **10**, 321 (1963).
72. E. Thiele, *J. Chem. Phys.*, **39**, 474 (1963).
73. L. D. Ikenberry and S. A. Rice, *J. Chem. Phys.*, **39**, 1561 (1963).
74. A. L. Gosman, R. D. McCarty, and J. G. Hust, *Natl. Stand. Ref. Data Ser.* **27**, (1969).
75. K. U. Co, J. J. Kozak, and K. D. Luks, *J. Chem. Phys.*, **66**, 1002 (1977).
76. I. L. McLaughlin and H. T. Davis, *J. Chem. Phys.*, **45**, 2020 (1966).
77. J. Palyvos, K. D. Luks, I. L. McLaughlin, and H. T. Davis, *J. Chem. Phys.*, **47**, 2082 (1967).
78. G. G. Emch, *Algebraic Methods in Statistical Mechanics and Quantum Field Theory*, Wiley-Interscience, New York, 1972.
79. A. G. Khachatryan, *Fiz. Tverd. Tela*, **5** (1963) [*Sov. Phys.—Solid State*, **5**, 16 (1963).]
80. S. Gartenhaus and G. Stranahan, *Phys. Rev.*, **A138**, 1346 (1965).
81. B. Jancovici, *Physica (Utr.)*, **31**, 1017 (1965); *Physica (Utr.)*, **32**, 1663 (1966).
82. J. J. Kozak, S. A. Rice, and J. D. Weeks, *Physica (Utr.)*, **54**, 573 (1971).
83. J. D. Weeks, S. A. Rice, and J. J. Kozak, *J. Chem. Phys.*, **52**, 2416 (1970).
84. H. L. Lemberg and S. A. Rice, *Physica (Utr.)*, **63**, 48 (1973).
85. H. J. Raveché and C. A. Stuart, *J. Chem. Phys.*, **63**, 1099 (1975); H. J. Raveché and C. A. Stuart, *J. Math. Phys.*, **17**, 1949 (1976).
86. I.-Y. Cheng and J. J. Kozak, *J. Math. Phys.*, **13**, 51 (1972).
87. R. Lovett, *J. Chem. Phys.*, **66**, 1225 (1977).
88. R. Lovett, private communication.
89. M. M. Vainberg, *Variational Methods for the Study of Nonlinear Operators*, Holden-Day, San Francisco, 1964.
90. A. M. Arthurs, *Complementary Variational Principles*, Clarendon Press, Oxford, 1970.
91. B. Noble, University of Wisconsin Mathematical Research Center Report No. 473 (1964).
92. N. Anderson, A. M. Arthurs, and P. O. Robinson, *Lett. Nuovo Cimento*, **IV**, 628 (1970).

93. K. U. Co, J. J. Kozak, and K. D. Luks, *J. Chem. Phys.*, **66**, 4306 (1977).
94. C. L. Dolph, *Trans. Am. Math. Soc.*, **66**, 289 (1949); C. L. Dolph and G. J. Minty, in *Nonlinear Integral Equations*, P. M. Anselone, Ed., The University of Wisconsin Press, Madison, 1964.
95. A. Hammerstein, *Acta Math.*, **54**, 117 (1930).
96. K. U. Co, private communication.
97. The substance of these remarks evolved from discussions with H. Ted Davis of the University of Minnesota.

# CALCULATIONS OF OBSERVABLES IN METALLIC COMPLEXES BY THE MOLECULAR ORBITAL THEORY

G. DE BROUCKÈRE

*Van der Waals Laboratory, University of Amsterdam,  
 Amsterdam, The Netherlands.*

## CONTENTS

Abstract . . . . .	204
I. Basic Elements. . . . .	205
A. Schrödinger Equation . . . . .	205
B. Hückel Hamiltonian . . . . .	207
C. The Goepfert-Mayer-Sklar Method . . . . .	210
D. Extended Hückel (EH) Method . . . . .	210
1. Integral Evaluations. . . . .	210
2. Explicit Forms of The Matrix Elements . . . . .	211
3. Evaluation of Repulsion Integrals . . . . .	211
4. Explicit Form of $\gamma_{pp}$ . . . . .	212
5. Off-Diagonal Elements $H_{pq}$ . . . . .	212
E. The Self-Consistent Field Method of Roothaan. . . . .	213
1. Spin Functions . . . . .	213
2. Hartree-Fock and Roothaan Equations . . . . .	213
3. Derivation of Hartree-Fock Equations . . . . .	214
4. Derivation of Roothaan Equations. . . . .	214
F. Our Molecular Orbital Model . . . . .	215
1. Choice of the Hamiltonian . . . . .	215
2. Derivation of the Diagonal, $H_{pp}$ , and Off-Diagonal, $H_{pq}$ , Elements of the Effective Hamiltonian . . . . .	216
3. Use of Spectroscopic Terms and Valence-State Ionization Energies (VSIE) for Evaluating the Effective Parameters $H_{pp}$ ; $W_p$ . . . . .	220
a. Use of Spectroscopic Terms. . . . .	220
b. Use of VSIE . . . . .	221
4. Unrestricted Hartree-Fock (UHF) Molecular Orbital Calculations . . . . .	221
5. About the Calculation of the Total Energy . . . . .	222
II. Theoretical Indices and Observables in the LCAO-SCF-MO Method . . . . .	224
A. Preliminaries. . . . .	224

B.	Theoretical Parameters of the Molecular Orbital Model . . . . .	225
1.	Population Analysis. . . . .	225
2.	Remarks about the General Use of the Mulliken-Ruedenberg Approximation Formulas in Deriving Molecular Observables . . . . .	227
C.	Electronic Structures and Related Parameters of Some Transition-Metal Complexes . . . . .	229
1.	Electronic Structure and Mono- and Bielectronic Observables . . . . .	229
2.	Charge Densities and Energy Levels Corresponding to the [Ti(6H <sub>2</sub> O)] <sup>3+</sup> (T <sub>h</sub> ) Cluster . . . . .	233
3.	NiL <sub>2</sub> System . . . . .	235
4.	CuCl <sub>4</sub> <sup>2-</sup> (D <sub>4h</sub> ) and Related Square-Planar Complexes . . . . .	237
D.	Calculations of Mono- and Bielectronic Observables . . . . .	240
1.	Preliminaries . . . . .	240
2.	Classification of Observables. . . . .	240
III.	About Some Other Semiempirical MO Treatments . . . . .	283
A.	Preliminaries. . . . .	283
B.	Wolfsberg-Helmholz Model . . . . .	284
C.	The X $\alpha$ -Model . . . . .	287
IV.	Electronic Transitions in Metallic Complexes and "The 10Dq Problem" . . . . .	290
A.	Preliminaries. . . . .	290
B.	d <sup>n</sup> Configuration . . . . .	291
C.	Solution by Crystal-Ligand Field Theory . . . . .	292
D.	Solution by the Molecular Orbital Theory . . . . .	293
V.	Conclusions. . . . .	296
	Acknowledgments . . . . .	297
	References . . . . .	297

### Abstract

The present review constitutes an original survey issued from our own research work of molecular orbital calculations mainly applied to transition-metal complexes. The emphasis is placed on the calculation of observables in metallic complexes, for example, the Fermi contact term, the nuclear quadrupole coupling constant, the  $g$  tensorial components and the spin-spin dipolar interactions. There has been no previous review devoted to the last subject.

## I. BASIC ELEMENTS

### A. Schrödinger Equation

The fundamental aim of molecular orbital (MO) calculations is the study of the electronic structure of molecules in their electronic ground state. The solution to the Schrödinger equation, in its time-independent form—the sole form considered in this review—constitutes a real mathematical challenge for solving rigorously second-order integrodifferential equations in three dimensions, a very small class of which permits solution in terms of standard functions, usually by separation of variables. Actually, only for closed-shell atoms, where this separation is possible, owing to the spherical symmetry field of forces (Delbrück theorem<sup>1</sup>) and leads to ordinary differential equations for the radial functions, have they been solved. For molecules, because of the absence of spherical symmetry, we are content to give the two, probably most well-known approximations, that is the Hückel approximation in its simple and extended form<sup>2</sup> and the Roothaan self-consistent field (SCF) method<sup>3</sup> using the LCAO approximation or linear combination of atomic orbitals. This method is no more than a way of getting a very reasonable solution to the Hartree-Fock equations, that is the precision of the approximate solution is only limited by the amount of computational work we can afford to do: in principle, one gets a solution of any precision's degree provided we agree to pay an unlimited price, compatible with a complete basis set of functions of infinite size!

The molecular spinless Hamiltonian operator occurring in the Schrödinger equation

$$\mathcal{H}\psi = E\psi \quad (1.1)$$

usually assumes the following form (in standard notations), in atomic units

$$\mathcal{H} = \sum_v \left\{ -\frac{1}{2} \nabla_v^2 - \sum_N \frac{Z_N}{r_{Nv}} \right\} + \sum_{\mu < \nu} \frac{1}{r_{\mu\nu}} + \sum_{M < N} \frac{Z_M Z_N}{r_{MN}} \quad (1.2)$$

The first two terms on the right-hand side of (1.2) represent the kinetic energy of an electron  $v$  and its attraction potential energy by the nuclei. The third and fourth terms represent the electrostatic repulsion of electrons  $\mu$  and  $\nu$  and of nuclei  $M$  and  $N$  respectively.

We consider below the last term of (1.2) as a constant, not as an operator, supposing the atoms immobile, their relative positions, in general, being known experimentally. This hypothesis, called the Born-Oppenheimer approximation,<sup>4</sup> is perfectly valid in most cases, owing to the great mass difference between the electron and the nucleus. Unless one is facing the study of very specific problems, such as the transition energy or transition moment calculation of a system having a linear and a bent geometry in its

ground and first excited state, respectively, or the calculation of a molecule's most stable geometry in its ground state, assuming variable bond lengths and valence angles, the last term of (1.2) is not relevant; all the ground-state energy quantities will be equally shifted by a definite amount. It must be noted, on the other hand, that the criteria guaranteeing the occurrence of an energy "absolute minimum" have still not been determined.

The function  $\psi$  is the total electronic wave function, embracing, in principle, the coordinates  $(x, y, z)$  and spin variables  $\sigma$  of all the electrons in the molecule

$$\psi \equiv \psi(x_1, x_2, x_3 \dots x_N) \quad \text{with } x_1 \equiv (x_1, y_1, z_1, \sigma_1) \dots \quad (1.3)$$

and

$$E = \int \psi^* \mathcal{H} \psi d\tau \quad \text{with } d\tau = dx_1 \cdot dx_2 \dots dx_N \quad (1.4)$$

assuming normalized functions  $\psi$ , such that

$$\int \psi^* \psi d\tau = 1 \quad (1.5)$$

Neglecting the repulsion interaction terms in (1.2) in the first instance, we can write the total electronic wave function as a product of independent mono-electronic functions, that is the molecular orbitals,

$$\psi(x_1, x_2, \dots, x_N) = \varphi_1(x_1) \cdot \varphi_2(x_2) \dots \varphi_N(x_N) \quad (1.6)$$

which is one of the fundamental postulates subjacent to almost the whole frame of molecular orbital calculations and to the construction of the so-called Slater determinant.

We postpone the development of the other assumptions until later in this section, as they are not necessary for introducing the Hückel approximation in its simple and extended form.

In empirical and semiempirical MO methods, a clear-cut separation is made between the inner and valence electrons. The former ones—supposed not to participate in the chemical bondings between atoms in the molecule—together with the nuclei, constitute the cores of the atoms. The "external" or "valence" electrons are supposed to be primarily responsible for the atomic bondings and do play an essential role in most molecular observables. Moreover, these electrons are, formally and mathematically speaking split into two categories according to whether their molecular orbitals are symmetric or antisymmetric relative to the principal plane of the molecule—one speaks of the  $\sigma$  or  $\pi$  electrons, respectively. This division, although formal, is most illuminating considering planar unsaturated molecules such as ethylene and benzene. We do not want to continue along these lines—in particular on

the debatable problem concerning the  $\sigma$ - $\pi$  separability<sup>5</sup>—well adapted usually to organic compounds but too restrictive for our purposes, as becomes evident later.

The Hückel method, in its simple form, applies to  $\pi$  electrons only; in its extended form,  $\sigma$ , as well as  $\pi$ , electrons are considered in the Hamiltonian. Let us briefly analyze the main features of both methods.

The  $\pi$ -electron Hamiltonian usually assumes the form

$$\mathcal{H}(1, 2, \dots, n_\pi) = \sum_{\mu} H_{\text{core}}(\mu) + \sum_{\mu < \nu} \frac{1}{r_{\mu\nu}} \quad (1.7)$$

$H_{\text{core}}(\mu)$  refers to the kinetic and potential energy of one  $\pi$  electron relative to the core of the molecule (including the attraction of  $\mu$  with the nuclei and its average interaction with the inner-shell and  $\sigma$ -framework electrons not included in the  $\pi$  system). The last term refers to repulsion energies among  $\pi$  electrons.

### B. Hückel Hamiltonian

In its simple form the Hückel Hamiltonian is simplified as

$$\mathcal{H}(1, 2, \dots, n_\pi) = \sum_{\mu} H_{\text{eff}}(\mu) \quad (1.8)$$

where  $H_{\text{eff}}(\mu)$  is some operator incorporating in some average way the effect of the electron repulsion terms of (1.7). Bearing in mind the product form [see (1.6)] of the  $\pi$  wave function, the Schrödinger equation (1.1) is immediately reduced to a series of one-electron equations,

$$\mathcal{H}_{\text{eff}}(\mu)\phi_i(\mu) = e_i\phi_i(\mu) \quad (1.9)$$

and the total energy, for closed-shell molecules, because of the analytical form of (1.8) is given by

$$E_{\pi} = 2 \sum_i e_i \quad (1.10)$$

$\phi_i$  is a molecular space orbital, which can formally accommodate two electrons. In writing (1.9) one already tacitly assumes, in the  $\pi$  wave function expansion, an “independence” between space and spin variables, although, at this level, there is no need whatsoever to use the concept of “spin-orbital.” A second assumption in the Hückel method is the so-called LCAO approximation or linear combination of atomic orbitals,

$$\phi_i = \sum_p c_{ip} \chi_p \quad (1.11)$$

The  $\chi_p$ 's are  $\pi$  atomic orbitals centered on the different cores or atoms in the

molecule ( $p_x, p_y$  orbitals in the case of benzene, for example). This approximation is an essential step in the Roothaan procedure (see below), as it permits a matrix solution of the Hartree-Fock equations that is otherwise impossible to reach for molecular systems.

Physically, this approximation is also very plausible and acceptable: if, for the sake of simplicity, one just thinks of the molecular ion  $H_2^+$ , it is quite plausible that the molecular orbital extending on both nuclei will be fairly well approximated by one of the two atomic orbitals (1s type), if the electron is to be found in a region very near either of the two nuclei. Therefore, in the more realistic case where the probability amplitude of finding the electron somewhere between the two cores will be the greatest, it is very reasonable and natural to put forward an analytical expression, such as (1.11), for the molecular orbital.

Equations 1.9 and 1.11 define a linear variational problem, the solutions of which—eigenfunctions, eigenvalues—are obtained by the resolution of a set of linear and homogeneous equations:

$$\sum_p c_{ip}(H_{pq}^{\text{eff}} - S_{pq}e_i) = 0 \quad (1.12)$$

which have nontrivial solutions when the  $e_i$ 's are roots of the secular equation

$$|H_{pq}^{\text{eff}} - S_{pq}e| = 0 \quad (1.13)$$

The determination of the best coefficients  $\{c\}$  in (1.11) and (1.12) rests on the well-known variational theorem stating that if  $\phi_1$  or  $\varphi_1$  (including spin function) is the molecular orbital corresponding to the lowest energy  $e_1$ , the energy corresponding to any other normalized function is greater than or equal to  $e_1$ . In the LCAO framework, the best  $c$ 's will be those for which a minimum value of the orbital energies is reached. The central problem, in any MO calculation, is therefore to evaluate the matrix elements,

$$H_{pq}^{\text{eff}} = \int \chi_p^*(1) \mathcal{H}(1) \chi_q(1) dv(1) \quad (1.14)$$

in the average field of the other electrons, and

$$S_{pq} = \int \chi_p^*(1) \chi_q(1) dv(1) \quad (1.15)$$

$dv(1)$  involving the spacial coordinates of electron 1, for given atomic orbitals  $\chi_p$ .

The latter integrals, often computed theoretically using Slater-type orbitals, are, in the Hückel simple scheme, ignored except when  $p$  equals  $q$

$$S_{pq} = \delta_{pq} \quad (1.16)$$



Neighboring  $\pi$ -overlap integrals in hydrocarbons are of the order of 0.3. So, superficially, this assumption is a poor one. However, it only leads to a small error, as can be easily shown, provided that it is made in conjunction with the next assumptions.

For the quantities  $H_{pq}^{\text{eff}}$ , we distinguish the cases  $p \neq q$  and  $p = q$  and, in the original Hückel method, regard the "Coulomb integral"

$$\alpha_p = H_{pp}^{\text{eff}} = \int \chi_p^*(1) \mathcal{H}^{\text{eff}}(1) \chi_p(1) d\tau(1) \quad (1.17)$$

as an empirical property of an atom and the "resonance integral"

$$\beta_{pq}^{\text{eff}} = H_{pq}^{\text{eff}} = \int \chi_p^*(1) \mathcal{H}^{\text{eff}}(1) \chi_q(1) dv(1) \quad (1.18)$$

as an empirical property of a bond, and we set

$$\beta_{pq} = 0 \quad (1.19)$$

when  $p$  and  $q$  are non-neighboring atoms.

It suffices to say here that ignoring overlap in the molecular orbital scheme introduces no error whatsoever if all integrals are reinterpreted as being over orthogonalized atomic orbitals or Löwdin orbitals.<sup>6</sup>

Hypothesis (1.16) and suitable evaluations of (1.17) and (1.18) are also related to the mathematical framework of the CNDO approximation<sup>7</sup> (CNDO = complete neglect of differential overlap); its serious shortcomings are discussed in Section III and I.D.3.

In the Hückel scheme, ethylene and benzene, for example, each involves a two-parameter problem, requiring the values of only  $\alpha_C$  and  $\beta_{CC}$  ( $C$  = carbon atom). For a comprehensive treatment of the Hückel method and its applications, we refer the reader to standard textbooks.<sup>8</sup>

The shortcomings of the Hückel method in its simple form are several. From a practical standpoint the values of the parameters required to fit one property often differ from those required to fit another, which should not be the case for a semiquantitative theory, the internal mathematics of which is consistent. It is also impossible to describe with this independent-particle model the splittings of several electron volts found between singlet and triplet states arising from the same electron configuration. From a theoretical point of view, it is just not valid to write (1.10) and (1.9). In the Hartree-Fock scheme, treated later in this section, it is also possible to consider the Fock operator as an effective Hamiltonian, like  $\mathcal{H}_{\text{eff}}(\mu)$  in (1.8) and (1.9), but  $E_\pi$  nevertheless would be given by

$$E_\pi = 2 \sum_i \frac{1}{2} (e_i + I_i) \quad (1.20)$$

Here,  $I_i$  is the mean value of the operator  $H_{\text{core}}$ , for the orbital  $\phi_i$ .

### C. The Goeppert-Mayer-Sklar Method

This method<sup>9</sup> seems, at first sight, very promising. It is based on the explicit use of the operator defined by (1.7) and of the LCAO approximation; the calculation is carried through in terms of molecular integrals  $I_{ij}$  representing the core contribution of (1.7), and molecular repulsion integrals  $\langle ij|kl \rangle$

$$I_{ij} = \int \phi_i^*(\mu) H_{\text{core}}(\mu) \phi_j(\mu) d\tau_\mu \quad (1.21)$$

$$\langle ij|kl \rangle \equiv \iint \phi_i^*(\mu) \phi_k^*(\nu) \frac{1}{r_{\mu\nu}} \phi_j(\mu) \phi_l(\nu) d\tau_\mu d\tau_\nu \quad (1.22)$$

both of these ultimately expressed in a  $\pi$  atomic basis set. It should be added that in the SCF theory of closed-shell ground states, the only molecular integrals playing a role are  $I_{ii}$ ,  $\langle ii|jj \rangle$ , and  $\langle ij|ij \rangle$ . Evaluation of the atomic integrals  $I_{pq}$  holds definite assumptions<sup>9</sup> on  $H_{\text{core}}$ . Although the singlet-triplet separation comes out, it tends to be too big if one uses purely theoretical atomic integrals with ordinary Slater screening constants. The very cumbersome problem in this method is the integral evaluation complexity as well as the great number of integrals, that is, of the order  $N^4$ ,  $N$  being the number of  $\pi$  electrons. This fact halts any attempt to carry out calculations on molecules larger than, say, naphthalene by this method.

### D. Extended Hückel (EH) Method

#### 1. Integral Evaluations

All the valence electrons are now included in the effective Hamiltonian operator (1.7). A vital point of the EH method, in contrast to the preceding one, is the ease with which the required integrals can be evaluated. As the ideas related to these integral evaluations are of central importance in the whole field of semiempirical MO calculations and as the mathematical formulation of these ideas often causes a definite semiempirical model to be preferred to a very elaborate *ab initio* model, we find it worthwhile to emphasize them briefly here.

According to Moffitt,<sup>10</sup> who first introduced this philosophy, these ideas can actually be summarized by the terms "atoms in a molecule." One should try to separate intra-atomic and interatomic correlation effects, to estimate the former by atomic spectroscopy and to calculate the latter by some orbital theory. To accomplish this, we must be able to separate matrix elements of the molecular Hamiltonian into intra- and interatomic pieces. That is the key to these methods.

Let us now briefly consider the main features and deficiencies of the EH method, for example, how it attempts to approach the above proposal.

## 2. Explicit forms of the matrix elements

By use of (1.7), (1.17), and (1.18) and by expliciting  $H_{\text{core}}$  as in the Goeppert-Mayer-Sklar method,<sup>9</sup> the following formula is obtained

$$\alpha^P \equiv H_{pp}^{\text{eff}} = -I_P - P_P - \sum_{q \neq p} \gamma_{pq} \quad (1.23)$$

$I_P$  is the ionization potential of an electron of atom P, in a definite valence-state configuration,

$$\gamma_{pq} = \langle pp|qq \rangle = \iint \chi_p^*(v) \chi_p(v) \frac{1}{r_{v\mu}} \chi_q^*(\mu) \chi_q(\mu) dv(v) dv(\mu) \quad (1.24)$$

the Coulomb electronic repulsion between valence electrons  $v$  and  $\mu$ , and the quantity

$$P_P = - \int \chi_p^*(v) H_{\text{core}}^0(v) \chi_p(v) dv(v) \quad (1.25)$$

called a penetration integral, describes the interaction of an electron in  $\chi_p$  with the neutral atom P itself ( $H_{\text{core}}^0$  refers to the neutral atom).

Equation 1.23, although approaching the Moffitt proposal, is still insufficient, as the atoms in the molecule might not necessarily retain their ground-state configurations, as in isolated atoms. On the other hand, the valence-state configuration of atom P must be chosen as close as possible to its actual configuration in the molecule, which of course is unknown at the outset. A remedy to this weakness is the relationship existing between  $H_{pp}^{\text{eff}}$  and the orbital population  $q_p$ , the value of which varies along the iterative process, the latter being pursued until a "self-consistent charge distribution" is obtained. This statement, derived in strong analogy with the Roothaan procedure, constitutes one of the foundations of calculation models discussed in this section.

## 3. Evaluation of Repulsion Integrals

A subject, which has been the starting point of a number of controversies, concerns the evaluation of the repulsion integrals  $\gamma_{pq}$  [see (1.24)]. In the EH method one invokes, in general, the zero-differential overlap approximation, that is,

$$\chi_p(v) \chi_q(v) dv(v) = 0 \quad \text{for } p \neq q \quad (1.26)$$

( $p$  and  $q$  being on the same or on two different centers). This eliminates a great number of atomic repulsion integrals in the general expression  $\langle pq|rs \rangle$ , leaving about  $N^2$  integrals ( $N^4$  integrals in the Goeppert-Mayer-Sklar model) of  $\gamma_{pq}$  type [see (1.24)]. The latter are computed in general from

theoretical formulas, or modified theoretical formulas of one kind or another,<sup>11</sup> subject to the condition  $\gamma_{pq} \rightarrow 1/R$  for large  $R$  ( $R = |\bar{r}_p - \bar{r}_q|$ ), making use occasionally of empirical data.

Approximation 1.26, used in one of Pople's models (Section III) that is the CNDO model,<sup>7</sup> ensures that the orbital charge figures, when subjecting the local atomic reference axes in a molecule to the same definite rotation, remain invariant, but at the cost of ignoring the angular dependence of the atomic orbitals in the repulsion-integral calculations—a result automatically reached in an *ab initio* MOLCAO framework where all the integrals are rigorously calculated within a set of normalized and linearly independent atomic orbitals. Preserving the rotational invariance of the orbital charges at such a price constitutes a questionable way of proceeding and discards *ipso facto* the study of important problems, such as the spatial conformations of certain molecules<sup>12</sup> (linear or bent). This point is treated in more detail in Section III.

#### 4 Explicit form of $\gamma_{pp}$

If  $p = q$  in (1.24), a formula, first proposed by Pariser,<sup>13</sup> and which is easily proved theoretically, is used

$$\gamma_{pp} = I_P - A_P \quad (1.27)$$

where  $A_P$  is the orbital-electron affinity of atom P. In general, the valence-state configuration determining the value of  $I_P$  may not be the same as that used in conjunction with (1.23), which again shows the ambiguity of choosing *one definite* valence state of the atom to match its actual configuration in the molecule.

In our model calculation, we give a way of achieving a reasonable solution to this problem, and therefore of better approaching the idea of "atoms in a molecule."

#### 5 Off-Diagonal Elements $H_{pq}$

Regarding the off-diagonal elements  $H_{pq}$  of the effective Hamiltonian, these are expressed, in the EH method, in terms of the atomic overlap integrals  $S_{pq}$  and the corresponding diagonal matrix elements  $H_{pp}$ . The relations used all suffer from a lack of mathematical coherence. Let us mention a few of them<sup>14-16</sup>:

$$H_{pq} = k \cdot S_{pq}(H_{pp} + H_{qq})/2 \quad (1.28)$$

$$H_{pq} = k \cdot S_{pq}(H_{pp} \cdot H_{qq})^{1/2} \quad (1.29)$$

$$H_{pq} = k \cdot S_{pq} \cdot \frac{H_{pp} \cdot H_{qq}}{(H_{pp} + H_{qq})/2} \quad (1.30)$$

$k$  is an arbitrary parameter whose values vary between 1.5 and 3. We point out, in Section I.F, a method, used by the present authors and originally proposed by Lipscomb et al.,<sup>17</sup> which, although not rigorous, is nevertheless mathematically more satisfactory for calculating the  $H_{pq}$  elements.

## E. The Self-Consistent-Field Method of Roothaan<sup>3</sup>

### 1. Spin Functions

It is, perhaps, rather surprising that until now the concept of "spin" has not played a role in the different MO schemes already considered, except as concerns the maximum number of electrons to be assigned to each orbital level, the reason being that the matrix elements of the Hamiltonian operator (1.2) have been approximated according to semiempirical relations of one kind or another, that is, not necessitating their effective derivations in a spin-space set of one-electron functions. When the latter objective is put forward, using the above operator, it results in what are called the Hartree-Fock equations<sup>18</sup> and the hypothesis of "spin-orbital" should be introduced at the outset of their derivations. The Roothaan equations result from expressing the Hartree-Fock equations in a suitable atomic orbital basis.

### 2. Hartree-Fock and Roothaan Equations

We briefly introduce the Hartree-Fock and the thereby derived Roothaan equations, as our MO model is directly inspired by the Roothaan procedure. The total electronic wave function [see (1.6)] is written as a product of molecular orbitals. Since the electrons or fermions obey the Fermi-Dirac Statistics, from which the Pauli exclusion principle derives, it can be straightforwardly shown that the wave function can be written as a determinant, the Slater determinant, having the antisymmetry properties required by the Pauli principle,

$$\psi(x_1, x_2, \dots, x_N) = \sum_p (-1)^p P \varphi_1(x_1) \cdot \varphi_2(x_2) \dots \varphi_N(x_N) \quad (1.31)$$

The summation acts on all the odd permutations compatible with a system of  $N$  electrons, according to the indistinguishability principle of the electrons. Formula 1.31 is, in shorthand notation, a Slater determinant.

Neglecting magnetic effects in the basic (spinless) Hamiltonian, that is (1.2), one supposes that each molecular orbital factors into a spatial MO function and a spin function

$$\varphi_1(x_1) = \phi_1(x_1, y_1, z_1) \cdot \alpha_1(\sigma)$$

or

$$\varphi_1(x_1) = \phi_1(x_1, y_1, z_1) \cdot \beta_1(\sigma) \quad (1.32)$$

$\alpha_1(\sigma)$  and  $\beta_1(\sigma)$  are two spin functions whose eigenvalues are  $+\frac{1}{2}$  and  $-\frac{1}{2}$ , respectively (in atomic units).

### 3. Derivation of Hartree-Fock Equations

The derivation of the Hartree-Fock equations rests on the variational method,<sup>19</sup> subjected, however, to two important restrictions:

1. The molecular orbitals must remain orthonormal.
2. The variational procedure involves just the first derivatives of the energy with respect to the orbitals  $\varphi_i$  themselves.

The above conditions are taken into account variationally by the usual Lagrange undetermined multipliers technique. A tedious but straightforward calculation shows that, for closed-shell systems, eliminating the off-diagonal Lagrange elements  $e_{ij}$  by a suitable unitary transformation, the latter leaving the Fock operator invariant, a simple monoelectronic set of equations results,

$$F\phi_i = e_i\phi_i$$

or in obvious notations

$$\left\{ H(v) + \sum_{j=1}^n [2J_j(v) - K_j(v)] \right\} \phi_i = \phi_i e_i \quad (1.33)$$

the so-called Hartree-Fock equations. The monoelectronic Coulomb and exchange operators  $J_j$  and  $K_j$  are those defined by Roothaan.<sup>3</sup>

### 4. Derivation of Roothaan Equations

Equations 1.33 are second-order integrodifferential equations, a small class of which can be solved exactly. Roothaan introduces, therefore, the LCAO approximation,  $\phi_i$  being expressed, without loss of generality, as

$$\phi_i = \sum_{p=1}^m c_{pi} \chi_p \quad (1.34)$$

Again for closed-shell systems, a straightforward set of linear and homogeneous equations results, the Roothaan equations, as is easily seen from the few following steps: multiplying both sides of (1.33) by  $\phi_i^*$  and using (1.34), one gets in standard notation,

$$\sum_{p,q=1}^m c_{pi}^* c_{qi} [I_{pq} + G_{pq} - S_{pq} e_i] = 0 \quad (1.35)$$

equations obviously valid for any occupied MO  $\phi_i$ .  $G_{pq}$  are the matrix elements of the operator  $\sum_j (2J_j - K_j)$ . The Roothaan equations therefore read

$$\sum_{p=1}^m c_p^* \sum_{q=1}^m c_q (L_{pq} - S_{pq}e) = 0 \quad (1.36)$$

with

$$L_{pq} = I_{pq} + G_{pq} \quad (1.37)$$

the solutions of which furnish the  $c_{pi}$  coefficients of the MO's  $\phi_i$  by solving the secular determinant

$$\det |L_{pq} - S_{pq}e| = 0 \quad (1.38)$$

The ground-state closed-shell wave function is built upon the first  $n$  lowest MO's ( $n \leq m$ ) and, as usual, an iterative procedure is used for solving the required equations, as these MO's enter the definition of the matrix elements  $G_{pq}$ .

For open-shell systems,<sup>3b</sup> the analytical forms of the Roothaan equations are more complicated, owing to the problem of eliminating the off-diagonal multipliers; the latter are, in fact, inserted into the Hamiltonian operator, the analytical form of which is more involved than in the preceding case, which permits ultimately the obtention of a set of linear and homogeneous equations similar to (1.36).

## F. Our Molecular Orbital Model

### 1. Choice of the Hamiltonian

Solving the Hartree-Fock equations for an open-shell system variationally, using a unique Hamiltonian for its closed- and open-shell parts, represents a very difficult task in a semiempirical formalism. To circumvent this difficulty, we have used the proposal of Longuet-Higgins and Pople,<sup>20</sup> treating tentatively the open- and closed-shell parts of the system with the same analytical form of the effective Hamiltonian operator, that is,

$$F(v) \equiv \mathcal{H}_{\text{eff}}(v) = H^{\text{core}}(v) + \sum_j \frac{n_j}{2} [2J_f(v) - K_f(v)] \quad (1.39)$$

where  $n_j$  is the number of electrons assigned to the orbital  $\phi_j$ .

In a comparison of the definition of the Fock operator (1.33) with the present equation, it should be noted that our identification holds true for the molecular occupation number  $n_j = 2$ . As noted in Section I.E.4, we know that such a simple expression (1.39) is variationally correct only for closed-shell systems ( $n_j = 2$ ). On the other hand, it can be easily shown, comparing the

present Hamiltonian for an open-shell system with the true one (see Roothaan paper<sup>3b</sup> on open-shell systems), that one ought to add to the former extra terms acting on partially occupied MO's  $j$  ( $n_j = 1$ ). Indeed, a simple calculation of the true total energy for an open-shell system, compared with that based on the above Hamiltonian reveals the occurrence of an extra term equal to one-fourth of the exchange molecular integral<sup>38</sup> ( $K_{jj} \equiv J_{jj}$ ) (see also Section I.F.5).

In the text below we retain the simple form of (1.39) above, as it is derived in complete agreement with the rigorous Roothaan treatment for closed-shell systems and also because in a very general way, and in particular for transition-metal complexes,<sup>21</sup> the exchange integrals are quite negligible compared to Coulomb ones. We have checked this point,<sup>39</sup> in particular, on the  $\text{CrCl}_4$  system (see Section I.F.5 and II.C.4). It is also interesting to note that the Longuet-Higgins and Pople proposal is directly inspired by the Hückel theory [see (1.7)].

$H^{\text{core}}(v)$  in (1.39) includes the kinetic energy and attraction potential energy of one valence electron in the field of the inner electrons and nuclei and in the average field of the other valence electrons, whereas the second term contains the interactions, Coulomb and exchange, among the occupied molecular orbitals of the system ( $n_j = 1$  or  $2$ ), in the average field of all other valence electrons.

## 2. Derivation of the Diagonal, $H_{pp}$ , and Off-Diagonal, $H_{pq}$ , Elements of the Effective Hamiltonian

**a. Diagonal Elements  $H_{pp}$ .** As is emphasized in Sections 1.D.2 and 1.F.1, adopting the operator (1.39), we are able to formulate a close analytical expression for the  $H_{pp}$ 's, derived in complete analogy with the Roothaan LCAO-SCF model. This point constitutes an improvement over other semiempirical treatments.

As the details of the mathematics have already been presented elsewhere,<sup>22a,22b</sup> we briefly summarize the main steps of this calculation.

The  $H_{pp}$  matrix element consists essentially of a two-term contribution as visualized from (1.39),

$$H_{pp} = I_{pp} + G_{pp} \quad (1.40)$$

The index  $p$  symbolizes an atomic orbital  $\chi_p$  centered on atom  $P$ , not included in the core of atom  $P$ . The physical content of these two components is stated in Section I.F.1. Factorizing the core contribution of a definite atom  $P$ , in the molecule, and replacing the core potential of the other atoms  $L$  ( $L \neq P$ ) of the molecule by their neutral potential (in analogy with the Goeppert-Mayer-Sklar<sup>9</sup> and EH procedures, see Section I.D.2), the matrix element



$I_{pp}$  takes the form

$$I_{pp} = W_P + \sum_{L \neq P} \left[ (V_{L,pp}^0) - \sum_{i(L)} n_L^i (J_{pi} - \frac{1}{2} K_{pi}) \right] \quad (1.41)$$

with

$$W_P = \int \chi_P^*(v) \left[ -\frac{1}{2} \nabla^2(v) + V_P(v) \right] \chi_P(v) dv(v) \quad (1.42)$$

$V_{L,pp}^0$  is the familiar penetration integral, seen in the extended Hückel method, referred to the neutral atom L itself.  $V_P(v)$ , on the other hand, refers to the potential of one valence electron  $v$ , outside the core of atom P, due to the inner electrons and nuclei or the core of atom P.  $n_L^i$  is the occupation number of the atomic orbital  $\chi_i$  of atom L in a definite valence-state configuration, the other symbols having their usual meanings.

The reason for having isolated in thought the core contribution of a definite atom in the molecule—atom P—is that we want, ultimately, to break down the components of the effective Hamiltonian matrix elements into “pure” atomic pieces, according to the Moffitt proposal “atoms in a molecule.”

Concerning the second component,  $G_{pp}$ , of  $H_{pp}$ , arising from the electron-repulsion terms of the total Hamiltonian  $\mathcal{H}_{\text{eff}}$ , we are faced with the problem of evaluating rigorously the multicenter, four centers at most, Coulomb and exchange integrals, in a suitable basis. Although this rather difficult mathematical task is nowadays carried through in *ab initio* model calculations, such a burden is never pursued at a semiempirical level. We have used the Mulliken-Ruedenberg approximations,<sup>23</sup> converting the tri- and quadricenter integrals into bicentric ones, easier to calculate:

$$\begin{aligned} (pp, rs) \in J_j &\simeq \frac{1}{2} S_{rs} [(pp, rr) + (pp, ss)] \\ (ps, rp) \in K_j &\simeq \frac{1}{2} S_{rs} [(pr, pr) + (ps, ps)] \end{aligned} \quad (1.43)$$

The convention adopted for a bielectronic integral is

$$(pq, rs) = \iint \chi_p^*(v) \chi_q(v) \frac{1}{r_{v\mu}} \chi_r^*(\mu) \chi_s(\mu) dv(v) dv(\mu) \quad (1.44)$$

and  $S_{rs}$  is the overlap integral between atomic orbitals  $\chi_r, \chi_s$ . The use of (1.43), although currently spread out in the whole field of semiempirical molecular orbital calculations, is fully accounted for only when the atomic centers involved in these multicenter integrals are of similar atomic numbers, or, equivalently, when the baricenter of any pair of atoms lies approximately in the middle of the interatomic distance. We come back to this point in Section II dealing, in particular, with the parameterization of our method.

As for  $I_{pp}$ , the P-atom contribution is put forward and the  $G_{pp}$  expression

now reads

$$G_{pp} = \sum_{r \in P} q_r^P (J_{pr} - \frac{1}{2} K_{pr}) + \sum_{l(L \neq P)} q_l^L (J_{pl} - \frac{1}{2} K_{pl}) \quad (1.45)$$

The first term of this equation is a monocentric term and, as a general rule, the approximations (1.43) cannot be applied to these integrals. However, in this case there is no harm in still using them formally, as if  $r = s$  or  $r \neq s$ , (1.43) reduce to an identity or vanish identically. The latter statement, aside from reasons of symmetry, is connected with the construction of the overlap matrix in our model: for monocenter elements only  $S_{rs} = 1$ , if  $r = s$  and  $S_{rs} = 0$  if  $r \neq s$ . Obviously, bicentric overlap elements are rigorously calculated through the whole atomic basis set (see also Section II). Summing up (1.41) and (1.45),  $H_{pp}$  reads

$$H_{pp} = W_P + \sum_{p \in r} q_r^P (J_{pr} - \frac{1}{2} K_{pr}) + \sum_{L \neq P} \left[ (V_{L,pp}^0) - \sum_{l(L)} (n_l^L - q_l^L) (J_{pl} - \frac{1}{2} K_{pl}) \right] \quad (1.46)$$

Neglecting the penetration integrals ( $V_{L,pp}^0$ ), which amount approximately to a displacement of the zero-point of the energy scale—not significant in our case—and supposing the atoms in the molecule to retain approximately their neutral electronic configurations, that is  $n_l^L \approx q_l^L$ , this equation reduces to a “sum” of pure atomic contributions, that is,

$$H_{pp} = W_P + \sum_{p \in r} q_r^P (J_{pr} - \frac{1}{2} K_{pr}) \quad (1.47)$$

This formula, aside from the fact that it fulfills nicely the concept atoms in a molecule, is, moreover, the basic expression in any iterative MO method. The parameter  $q_r$  embodies the usual dependence of the SCF matrix elements with respect to the coefficients  $c_{rj}$  of occupied MO's, as a consequence of the use of the Mulliken-Ruedenberg approximations for bielectronic integrals,

$$q_r = \sum_j \sum_s n_j c_{rj} c_{sj} S_{rs} \quad (1.48)$$

$q_r$  is called the gross atomic population of orbital  $r$ , following Mulliken.<sup>24</sup> By means of the theoretical overlap matrix elements calculation carried through the whole atomic basis, the long-range forces acting on the atoms in the molecule are automatically taken into account and embodied in the atomic-orbital charge distributions  $q_r$ .

The core parameters  $W_P$ , as well as the bielectronic integrals  $J_{pr}$ ,  $K_{pr}$ , are calculated from atomic spectroscopy and theoretical values of some Slater-Condon parameters,  $F^k$ ,  $G^k$ , as is explained below. By use of atomic spectroscopic data, the intra-atomic electronic correlation is naturally included in the MO calculation, which is one of the major reasons we are fairly confident

about the building-up of our wave function and which constitutes a good starting point for the calculation of a variety of observables to be analyzed in Section II.C.2.

The bicentric terms in (1.46), obviously important in the case of electrovalent or ionic crystals, have been approximated in two ways. Firstly, the quantity  $(J_{pl} - \frac{1}{2}K_{pl})$  is supposed to be equal to the inverse of the interatomic distance  $\frac{1}{R_{P-L}}$  for every pair of atomic orbitals  $\chi_p$  and  $\chi_l$ , which is the most common behavior for the bicentric Coulomb integrals  $J_{pl}$ . The quantity  $\sum_l (n_l^t - q_l^t)$  being the algebraic net charge of atom L, it is clear that this

bicentric term—a correction to the preceding one in (1.46)—is nothing but the Madelung potential due to interatomic transfers of charges. Jørgensen<sup>25</sup> has applied an equivalent correction using the Wolfsberg-Helmholtz model. At short distances, however, as  $J_{pl}$  takes a finite value, obviously related to the monocenter integrals  $J_{pp}$  and  $J_{ll}$ , a Mataga-Nishimoto relation type,<sup>26</sup> namely,

$$J_{pl} = \frac{1}{R_{P-L} + 1/\frac{1}{2}(J_{pp} + J_{ll})} \quad (\text{in atomic units}) \quad (1.49)$$

is more general and works better in actual computations than the former one. The bicentric exchange integrals in the case of transition-metal complexes being small compared to Coulomb integrals (this point is referred to in Sections I.F.5 and next II.C.4) are discarded throughout when use is made of approximation (1.49).

**b. Off-diagonal Elements  $H_{pq}$ .** These calculations constitute a weak point in any semiempirical MO model. A similar derivation, as in the case of the  $H_{pp}$  elements, is not easy, owing to the difficulty of evaluating rigorously the bielectronic potential parts  $V_{pq}$  of the  $H_{pq}$ 's and the great number of  $V_{pq}$  elements, that is, proportional to  $N^4$  ( $N$  = number of electrons). To preserve the simple character of our method and, at the same time, as much as possible the rigorous mathematical consistency of our procedure, we have adopted a proposition first introduced by Lipscomb et al.<sup>17</sup>

From a theoretical standpoint, the Wolfsberg-Helmholtz formula has serious shortcomings<sup>27</sup>: it is invariant, in general, neither with respect to linear transformations of the atomic basis nor to shift of the zero-point of the energy scale. Moreover, it implies that the kinetic part  $T_{pq}$  is proportional to the first power of the overlap integral  $S_{pq}$ , although  $T_{pq}$  is, in fact, a quadratic function of the orbital exponent. So, a square of the overlap integral, as Cusachs proposed,<sup>28</sup> should represent a better relationship between  $H_{pq}$  and  $T_{pq}$ .

Consequently, it seems to be advisable to abandon this approximation in favor of the Lipscomb et al. proposition.<sup>17</sup> All kinetic integrals,  $T_{pq}$ , with  $p=q$  and  $p \neq q$  within the basis set, are rigorously calculated—the latter amount to the derivation of a linear combination of ordinary overlap integrals—and the potential integrals,  $V_{pq}$ , are approximated by a Mulliken-type formula,<sup>23</sup>

$$V_{pq} \simeq \frac{1}{2} S_{pq} (V_{pp} + V_{qq}) \quad (1.50)$$

the diagonal elements  $V_{pp}$  and  $V_{qq}$  being easily evaluated with the help of the  $H_{pp}$ 's and  $T_{pp}$ 's.

This is, so far as we know, the best compromise that can be adopted for keeping our method simple enough, without being involved in quite cumbersome integral evaluations and at the same time preserving a reasonable mathematical coherence. We must, nevertheless, recognize that the resulting  $H_{pq}$  elements are not rigorously invariant to a rotation of the orbital coordinate axes, but we do feel that this slight lack of rotational invariance is to be greatly preferred to a rigorous invariance obtained, as in the CNDO model (see Section III), by simply ignoring the angular part of the atomic orbitals in the evaluation of the repulsion integrals, as already mentioned in Section I.D.3. This weakness of our method does not, however, prevent us from making good predictions on a great variety of observables, the latter not being affected in a tangible way by a slight variation of the local atomic axes.

### 3. Use of Spectroscopic Terms and Valence-State Ionisation Energies (VSIE) for Evaluating the Effective Parameters $H_{pp}$ : $W_p$

**a. Use of Spectroscopic Terms.** The atomic orbital charge  $q$ , in a molecule cannot be simply related to the occupation number of the atomic orbital in a definite valence-state configuration of the neutral atom or one of its ions (we refer the reader to the works of Jørgensen,<sup>29</sup> Basch,<sup>30</sup> Fenske,<sup>31</sup> etc., concerning this problem). We have used a procedure similar to that used by Pariser<sup>32</sup> for  $\pi$  electrons of conjugated systems.

The monocentric elements  $H_{pp}$  relative to a transition metal atom can be expressed, in the most general case, as a combination of average energies of some configurations<sup>33</sup> and a combination of Slater-Condon parameters<sup>32</sup>  $F^k$ ,  $G^k$ . The latter energies are, in their turn, expressed as a combination of spectroscopic terms and a few additional Slater-Condon parameters (correction term). These terms must be chosen in such a way that the latter correction term is minimized. In the most simple cases a difference of two spectroscopic terms, one corresponding to the neutral atom and the other to the ion suffice to evaluate the required  $H_{pp}$  matrix element.

Concerning the atomic core parameter  $W_p$ , it is possible to express easily

the difference of average energies of some configurations in terms of the required parameter and a few additional terms  $F^k, G^k$ . In choosing the appropriate spectroscopic terms, the same care as before must be exercised to minimizing the effect of these additional  $F^k, G^k$  terms. We refer the reader to the papers of Berthier,<sup>22a</sup> Di Sipio et al.,<sup>35</sup> and the present author<sup>22b</sup> for the details and some results of these calculations.

**b. Use of VSIE.** The  $H_{pp}$  matrix elements relative to ligand atoms are evaluated more simply by the use of valence-state configuration energies, given by, among others, Pilcher and Skinner,<sup>36</sup> Hinze and Jaffé,<sup>37</sup> and Basch et al.,<sup>30</sup> combining, as usual, the valence-state energies of the neutral atom and its ions. The core parameters  $W_p$  are easily derived from suitable combinations of the analytical expressions referring to the valence-state energies of the neutral atom and its ions. Results of such calculations are presented in Ref. 22b.

#### 4. *Unrestricted Hartree-Fock (UHF) Molecular Orbital Calculations*

As is well known in the case of open-shell systems, it is not a simple matter to eliminate the off-diagonal Lagrange multipliers by suitable unitary transformations. Roothaan<sup>3a</sup> gave a rigorous solution to this problem for closed-shell systems, by actually eliminating these off-diagonal parameters and constructing in this way a homogeneous set of equations equivalent to the primitive one. Unfortunately, the extension of the Roothaan elimination technique to open shells is very complicated.<sup>3b</sup>

Another way of proceeding, to avoid the above difficulty,<sup>40</sup> is to consider two families of spin-orbitals corresponding to two different space-spin functions<sup>41</sup>: the  $\alpha$  and  $\beta$  spin-orbital functions. The space orbitals for the  $\alpha$ -spin family are now different from those of the  $\beta$ -spin family, contrary to the case of a "closed-shell" system. Within each class of space-spin functions, one may assume orthogonality conditions among the space functions, whereas the orthogonality between the two classes of space-spin functions is realized through the spin functions. The Hartree-Fock equations separate into two systems:

$$\begin{aligned} & \left( H + \sum_{j=1}^N J_j - \sum_j^{\text{odd}} K_j \right) \phi_i = \sum_j^{\text{odd}} \phi_j e_{ji} \quad \text{with } i = 1, 3, 5, \dots \\ & \left( H + \sum_{j=1}^N J_j - \sum_j^{\text{even}} K_j \right) \phi_i = \sum_j^{\text{even}} \phi_j e_{ji} \quad \text{with } i = 2, 4, 6, \dots \end{aligned} \quad (1.51)$$

Within each system of equations, one can now eliminate the off-diagonal multipliers, giving rise to the usual set of homogeneous equations.

Using the approximation framework described above in the case of the restricted Hartree-Fock method, the diagonal elements of the effective

Hamiltonian for the  $\alpha$  spin-orbitals now read [see (1.46)]

$$H_{pp}^{\alpha} = W_{pp}^P + \sum_{r(P)} (q_r^{P,\alpha} + q_r^{P,\beta}) J_{pr} - \sum_{r(P)} q_r^{P,\alpha} K_{pr} - \sum_{l(L)} [n_l^{\downarrow} - (q_l^{\downarrow,\alpha} + q_l^{\downarrow,\beta})] J_{pl} \quad (1.52)$$

and for the  $\beta$  spin-orbitals

$$H_{pp}^{\beta} = W_{pp}^P + \sum_{r(P)} (q_r^{P,\alpha} + q_r^{P,\beta}) J_{pr} - \sum_{r(P)} q_r^{P,\beta} K_{pr} - \sum_{l(L)} [n_l^{\downarrow} - (q_l^{\downarrow,\alpha} + q_l^{\downarrow,\beta})] J_{pl}$$

neglecting as usual, the penetration integrals  $V_{L,pp}^0$  and the bicentric exchange integrals  $K_{pl}$ .

The charge densities in this method, as easily proved, are those resulting from the difference of the charge densities for the  $\alpha$  spin-orbitals and for the  $\beta$  spin-orbitals, respectively. Note that this difference may theoretically be negative, as is also well known from EPR hyperfine spectra (in the case of radicals, for example). For the off-diagonal elements, it is still possible to use the Wolfsberg-Helmholtz<sup>14</sup> relation.

We return (next section) to this theory, usually known as the UHF method, when discussing our calculations on the isotropic part of the hyperfine interactions (Fermi contact term) in copper and manganese complexes.

### 5. About the Calculation of the Total Energy

This quantity is somehow the touchstone in any model, semiempirical or *ab initio*, of MO calculations. We mean that the true energy of any system, except in the case of the hydrogen molecule, is never reached. Indeed, Kolos and Roothaan,<sup>42</sup> by using a 50-term function, including the interelectron distance, the analytical form of each term being similar to that proposed by James and Coolidge,<sup>43</sup> obtained an energy  $D_e^{H_2} = 4.7467$  eV to be compared to the experimental value  $4.7466 \pm 0.0007$  eV. "This truly remarkable work shows that for sufficiently small molecules, electronic computers have brought us to a situation where calculations may give a more accurate result than experiment! It is also not unreasonable to claim that these highly laborious calculations yielding such an excellent final result represent one of the most satisfactory 'proofs' of the validity of the original wave equation when applied to problems with more than one electron".<sup>44</sup> For large molecules, we must be content, however, with a much less rigorous treatment. By a comparison of the true energy expression with that derived from the use of the Longuet-Higgins effective Hamiltonian,<sup>20</sup> it can be shown that the following expression is theoretically equivalent:

$$E_i = \frac{1}{2} \left( \sum_i^D + \sum_i^P \right) [\langle i|I|i \rangle + e_i] - \frac{1}{4} \sum_i^P \sum_j^P K_{ij}$$

$D$  and  $P$  represent doubly and partially occupied MO's. In square brackets

appear the familiar one-electronic core operator  $I$  and the diagonal multiplier  $e_i$  or eigenvalue of the secular determinant. The last exchange term acting on partially occupied MO's makes this expression theoretically equivalent to the expression for an open-shell system represented by a single determinant built upon singly and doubly occupied orbitals.

We give in Table I a series of results on the total energy of the system  $\text{CrCl}_4$  considered as possessing 31 and 33 valence electrons. The latter case, that is  $[\text{Cr}(d^3)\text{Cl}_4]^{2-}$ , is considered in analogy with  $[\text{Cu}(d^9)\text{Cl}_4]^{2-}$ , the existence of which is well established (see next section). The configuration with three unpaired electrons, that is, resultant  $S = S_z = \frac{3}{2}$  (see table I) is related to ESR measurements on  $\text{Cr}^{3+}$  doped  $\text{CsCl}$  (see Sections II.C.1.a and II.D.2.b). In table I the possibly multiform character of the solutions of a set of standard

TABLE I  
Total Energy  $E_t$  (eV) Relative to the System  $[\text{CrCl}_4] (D_{4h})$

Total no. valence electrons	No. unpaired electrons	PS <sup>a</sup>	$e$	$i$	$c$	$E_t$
33	3	$a$	-355.773	-3331.508	-5.242	-3692.523
		$b$	-353.996	-3326.256	-5.828	-3686.080
31	3	$a$	-494.272	-3169.498	-4.505	-3668.275
		$b$	-488.260	-3162.734	-3.747	-3654.741
33	1	$[a; b]$	-358.592	-3335.280	-2.139	-3696.011
31	1	$a$	-497.040	-3173.629	-4.580	-3675.249
		$b$	-494.839	-3166.090	-0.925	-3661.854

<sup>a</sup>Under this column, two different plausible charge distributions, that is,  $a$  and  $b$ , among the basis set, corresponding to the configurations with 33 (1 or 3 unpaired  $\alpha$  electrons) and 31 valence electrons (1 or 3 unpaired  $\alpha$  electrons), respectively, are used at the outset of the iterative process.

$$\left. \begin{aligned}
 e &= \frac{1}{2} \left( 2 \sum_i^D + \sum_i^P \right) e_i && \text{(in electron volts)} \\
 i &= \frac{1}{2} \left( 2 \sum_i^D + \sum_i^P \right) \langle i | I | i \rangle && \text{(in electron volts)} \\
 c &= -\frac{1}{4} \sum_i^P \sum_j^P K_{ij} && \text{(in electron volts)}
 \end{aligned} \right\} E_t = e + i + c$$

The off-diagonal elements of the effective Hamiltonian are derived according to Section I.F.2.b (Wolfsberg-Helmholtz formula released). The  $K_{ij}$  and  $J_{ij}$  integrals are derived using the Mulliken-Ruedenberg formulas.<sup>23</sup>

Hartree-Fock equations appears clearly. As is well known, cancelling the total energy first derivative relative to any variation of the MO parameters and at the same time requiring the MO's to remain still orthogonal do not constitute enough restrictive conditions for getting a "stable" solution to the Hartree-Fock equations. As shown by Paldus et al.,<sup>45</sup> the variation of the total energy second derivative should also be considered.

Only a few comments are necessary concerning the values in Table I. The energy of the configuration with 33 electrons (or 31 electrons) with three decoupled electrons is always higher than the energy of the same configuration with one unpaired electron, as a consequence of the Aufbau principle in conjunction with the Pauli principle. The energy differences, however, are small.

A second point to be mentioned is related to the possible existence of several solutions to the Hartree-Fock equations: it is seen that two different sets of charge distributions for one particular electronic configuration give rise to two rather different total energies. In the language of group theory this means that the numbers of times that some definite irreducible representations are spanned by the occupied ground-state orbitals depend on the charge distributions ( $a, b$ ) used at the outset of the SCF iterative process. This is because these charge distributions lead to two different stationary states belonging to two different irreducible representations of the symmetry group  $D_{4h}$ . In one case, denoted by  $a$ ;  $b$  the same final state is reached whatever the charge distribution,  $a$  or  $b$ , chosen at the outset of the iterative process.

Let us finally say that the system  $[\text{CrCl}_4] (D_{4h})$  is the sole example we have met so far showing this ambivalence of the Hartree-Fock solutions. Well-known examples are, however, the  $\text{O}_3$  molecule<sup>46</sup> (three different stationary states) or even  $\text{O}^{2-}$ <sup>47</sup> and, more recently, the cluster (bis- $\pi$ -allyl)-Ni or  $[(\text{C}_3\text{H}_5)_2\text{Ni}]$ .<sup>48</sup>

## II. THEORETICAL INDICES AND OBSERVABLES IN THE LCAO-SCF-MO METHOD

### A. Preliminaries

Transition-metal complexes are currently the subject of extensive experimental work. Important fields of investigation include electron<sup>49</sup> and nuclear<sup>50</sup> spin resonance experiments, microwave solid-state maser and laser experiments,<sup>51</sup> and semiconductor and superconductor properties.<sup>52</sup> Very great interest in studying these systems with a wide range of experimental techniques has arisen because the unpaired electrons of the metal can be easily excited, thereby providing a natural means of interaction with the nuclear spin system. From a quantum mechanical point of view, using the



molecular orbital model, it becomes of central importance to have the best possible description of the molecular electronic wave function, with the help of which many experimental parameters can be theoretically predicted in a reliable way.

It therefore seems appropriate to comment on the parametrization of the MO model we use, before presenting and discussing some observable calculations derived from it.

## B. Theoretical Parameters of the Molecular Orbital Model

### 1. Population Analysis

As is pointed out in the previous section [see (1.46)], the molecular diagonal elements  $H_{pp}$  are functions of the individual atomic orbital charges  $q_r^p$ . These purely theoretical indices are not observables but constitute a satisfactory way of elucidating the molecular electronic structure in any molecular orbital calculation. Two sorts of "population analysis"—a term introduced by Mulliken—can be carried out through the use of a primitive set of orthogonal or nonorthogonal atomic basis functions. The use of an orthogonal basis characterizes the so-called Coulson and Longuet-Higgins<sup>53</sup> population analysis, the basic quantities being the atomic charge density ( $q_r$ ) and the bond order ( $p_{rs}$ ). Since all our calculations are carried out in a nonorthogonal basis set, these indices are defined below within the latter basis. The two distinct ways of expressing the population indices are discussed below.

1. Extending the Coulson and Longuet-Higgins proposal to a nonorthogonal primitive basis,  $\chi$ , the charge density reads

$$q_r = \sum_i n_i c_{ri} d_{ri} \quad (2.1)$$

with

$$d_{ri} = \sum_s S_{rs} c_{si} \quad (2.2)$$

The coefficients  $d_{ri}$  are the so-called Coulson-Chirgwin contravariant coefficients associated with the molecular orbital  $\varphi_i$ , the overlap matrix elements  $S_{rs}$  being considered as tensor components defined in the space spanned by the basis functions. The covariant coefficients  $c_{ri}$  are those involved in the analytical expressions of the basis functions themselves. Another basic quantity, introduced by Coulson, is the bond order  $p_{rs}$ , which, expressed in a nonorthogonal basis set, is analogous to the overlap population defined below.

2. The previous primitive basis set  $\chi$  is replaced by an equivalent orthonormal basis  $\lambda$ , obtained by the Löwdin orthonormalization procedure,<sup>54</sup> that is

$$\lambda = \chi S^{-1/2} \quad (2.3)$$

The molecular orbital coefficients  $b_{ri}$  relative to the new basis, the so-called Löwdin coefficients, now read

$$b_{ri} = \sum_s S_{rs}^{1/2} c_{ri} \quad (2.4)$$

the  $c_{ri}$ 's being those corresponding to the  $\chi$  primitive basis.

3. The so-called Mulliken population analysis,<sup>55</sup> according to Mulliken's own proposal, introduces mainly three population indices. The atomic population,

$$\rho^P = \sum_i \sum_{r \in P} n_i c_{ri}^2 \quad (2.5)$$

the overlap population between atoms P and Q,

$$\rho^{P-Q} = \sum_i \sum_{r \in P} \sum_{s \in Q} 2n_i c_{ri} c_{si} S_{rs} \quad (2.6)$$

and the gross atomic population,

$$q^P = \rho^P + \frac{1}{2} \sum_{P \neq Q} \rho^{P-Q} \quad (2.7)$$

In these relations  $n_i$  is the integer occupation number of molecular orbital  $\varphi_i$ . The Mulliken population analysis is carried out with the help of the primitive basis coefficients  $c_{ri}$  owing to the localized properties of the latter, as the MO coefficients usually resulting from the Löwdin orthonormalization procedure have a nonlocal character.<sup>56,57</sup> A parameter frequently utilized is the net atomic population

$$\delta_P = n_P - q_P \quad (2.8)$$

where  $n_P$  is the number of electrons carried by atom P in the molecule.

It is worthwhile to remember that all these indices obviously depend on the nature of the primitive basis chosen. Moreover, in most semiempirical MO models, the above indices do not remain rigorously invariant relative to a linear transformation of the atomic basis set (see Section I.D.3). However, in our case this fact does not alter (Section I.F.) the qualitative picture of the electronic structure of the molecule, confirmed by comparison with equivalent *ab initio* results (see below), nor does it prevent us from obtaining a fair agreement in the calculation of a variety of measured observables depending

on these population indices or related quantities, as is shown later in this section.

## 2. *Remarks about the General Use of the Mulliken–Ruedenberg Approximation Formulas in Deriving Molecular Observables*

**a. Reduction of Tri- and quadricenter Coulomb and Exchange Integrals into Bicentric Ones.** According to the Löwdin orthonormalization procedure, the molecular orbitals are expanded in terms of orthonormalized atomic orbitals  $\lambda$ , constructed from a set of atomic orbitals  $\chi$ , localized on the atoms in the molecule. Now, in most semiempirical model calculations the tri- and quadricenter Coulomb and exchange integrals are ultimately reduced to bicentric ones by virtue of the Mulliken formulas, that is, (1.43). This procedure is theoretically grounded for the following reason. Let us consider for the sake of simplicity just two atomic centers A and B. We use a one-center expansion of the basis sets  $\bar{\chi}$  and  $\bar{\lambda}$  on center B, in terms of the basis set  $\bar{\chi}$  on center A, where powers higher than 2 in  $S_{AB}$  ( $S_{AB} < 1$ ) appear in both expansions. If one retains at most the quadratic terms in  $S_{AB}^{57}$  within the primitive basis expansion  $\bar{\chi}$  and compares this result with the one resulting from the Löwdin basis expansion  $\bar{\lambda}$  including higher powers in  $S_{AB}$ , there appears to be very close agreement between both expansion results. This means that the multicenter integrals  $\langle \lambda_p^A \lambda_q^B; \lambda_r^C \lambda_s^D \rangle$  are negligible. Of course, if  $p = q$  and  $r = s$  no such conclusion can be drawn for the value of the resultant integral. If  $S$  is supposed sufficiently small, the Ruedenberg-Mulliken formula, where only the linear terms in  $S$  appear will constitute a quite satisfactory approximation for the corresponding tri- and quadricenter Coulomb and exchange integrals.<sup>58</sup>

**b. The Mulliken and Coulson and Longuet-Higgins Population indices and related quantities.** Aside from the fact that the physical meaning of these parameters is controverted and they constitute somehow a “plague of non-observables”,<sup>59</sup> they are nevertheless often used to calculate expectation values of a great variety of observables rather than to derive rigorously the operator expectation values themselves. Observables successfully derived by such a procedure are electric dipole moment, nuclear quadrupole coupling constant, spin-orbit coupling constants, and indirect nucleus-nucleus hyperfine interactions ( $J$  couplings; see Section II.D.2a). Theoretically, this procedure may be supported as follows: Many observables can be expressed unambiguously in terms of charge densities, bond orders, and related quantities, if the matrix elements of the corresponding operator with respect to the basis functions are approximated in terms of overlap integrals by a

Mulliken-type formula, namely,

$$\langle s|O|r\rangle \simeq \frac{1}{2}S_{rs}[\langle r|O|r\rangle + \langle s|O|s\rangle] \quad (2.9)$$

where  $O$  is some mono-electronic operator.

The latter relation, moreover, facilitates the calculations of the integrals considerably.

We have extended the field of application of this theoretical approach to an important class of mono- and bielectronic observables, that is, the molecular components of the  $g$  tensor occurring in the Zeeman term, and the spin-spin dipolar interactions occurring in the zero-field-splitting term. We briefly illustrate this method in the case of the electric dipole moment. More details can be found elsewhere.<sup>60</sup>

The MO-LCAO expression of the molecular dipole moment expectation value is (in atomic units)

$$\bar{\mu} = \sum_P \sum_Q \sum_{r \in P} \sum_{s \in Q} p_{rs}^{PQ} \int \chi_r \bar{r} \chi_s dr - \bar{\mu}_{\text{nucl}} \quad (2.10)$$

where

$$p_{rs}^{PQ} = \sum_i n_i c_{ir} c_{is} \quad (2.11)$$

$n_i$  is the occupation number of the MO  $\phi_i$  and the  $c$ 's are the usual LCAO expansion coefficients in the MO  $\phi_i$  corresponding to the orbitals in centers  $P$  and  $Q$ ;  $\bar{\mu}_{\text{nucl}}$  is the nuclear part of the dipole moment.

Equation 2.10, may be written unambiguously as a sum of three contributions, that is,

$$\bar{\mu} = \sum_P \delta_P \bar{r}_P + \bar{\mu}_{\text{hybrid}} + \bar{\mu}_{\text{overlap}} \quad (2.12)$$

with

$$\bar{\mu}_{\text{hybrid}} = \sum_P \sum_{r, r' \in P} p_{rr'} \bar{\xi}_{rr'}^P \quad (2.13)$$

$$\bar{\mu}_{\text{overlap}} = \sum_P \sum_{r \in P} \sum_{s \in Q} p_{rs}^{PQ} S_{rs}^{PQ} \bar{\eta}_{rs}^{PQ} \quad (2.14)$$

defining

$$\bar{\xi}_{rs}^P = \int \chi_r \bar{\xi} \chi_s d\tau \quad \eta_{rs}^{PQ} = \frac{\int \chi_r \bar{\eta} \chi_s d\tau}{S_{rs}^{PQ}} \quad (2.15)$$

where the vectors  $\bar{\xi}$  and  $\bar{\eta}$  are defined through the following relations

$$\bar{r} = \bar{r}_P + \bar{\xi} \quad \text{for those terms where } P=Q \quad (2.16)$$

$$\bar{r} = \frac{1}{2}(\bar{r}_P + \bar{r}_Q) + \bar{\eta} \quad \text{for those terms where } P \neq Q \quad (2.17)$$

$\bar{r}$  and  $\bar{r}_P$  are, respectively, the position vector of the electron and the atom P, both taken from the same, but otherwise arbitrary, origin, whereas  $\bar{\xi}$  and  $\bar{\eta}$  are radius vectors taken from the position of atom P and the center of the line PQ, respectively.  $\delta_P$  is the net charge upon atom P [see (2.8)]. We see that, provided  $\bar{\mu}_{\text{hybrid}}$  and  $\bar{\mu}_{\text{overlap}}$  vanish, the dipole moment is a function of the charges for which we are looking. If each atom P in the molecule contributes only atomic orbitals of the same symmetry species,  $\bar{\mu}_{\text{hybrid}}$  vanishes as a consequence of (2.15) and  $\bar{\mu}_{\text{overlap}}$  might vanish if  $\eta_{rs}=0$  or  $S_{rs}=0$ . This result might be obtained equally well using the Mulliken formula [see (2.9)], which is equivalent therefore to neglecting the two other contributions to  $\bar{\mu}$ . As is emphasized in Section I.F.2.a, the use of the Mulliken formula reducing the tri- or quadricenter integrals into bicentric ones is satisfactory only if the centroid of any atomic orbital pair lies approximately between the two atoms or, in other words, if the orbitals located on the two atoms are of a similar size. We refer the reader also to our remark in Section II.B.2.a.

### C. Electronic Structures and Related Parameters of Some Transition-Metal Complexes

#### 1. Electronic Structure and Mono- and Bielectronic Observables

First we study the electronic structure of some transition-metal complexes using the method described in Section I.F. Next we derive some mono-electronic and bielectronic observables related to these systems. The recent development of computer technology provides us with the possibility of making reliable comparisons with *ab initio* results in the case of transition-metal complexes on the following points:

1. Population analysis.
2. Symmetry species of the molecular electronic ground state.
3. Sequence of certain orbital energies.

These last two items are used in the discussion of our results on the cluster  $\text{CuCl}_4^{2-}$ : a number of semiempirical MO calculations have assessed different sequences of *d*-orbital energies in this type of compound, but very few of them are in agreement with the sequence found recently by *ab initio* calculations.

**a. Electronic Structure.** Before discussing these matters, we wish to comment on our choice of studying the electronic structure of definite clusters quantum mechanically. This will clarify our second task, that is, the calculation of some related molecular observables.

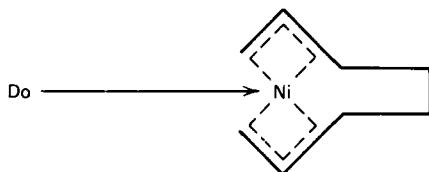
$[\text{Ti}(\text{6H}_2\text{O})]^{3+}(T_h)$  is supposed to obey the  $T_h$  point group. It is observed in aqueous solution of titanium chloride or in the crystal lattice of titanium

alums as  $\text{TiCs}(\text{SO}_4)_2 \cdot 12\text{H}_2\text{O}$ , subjected to the usual trigonal distortion.<sup>61</sup> This system has been investigated intensively by ESR methods,<sup>62</sup> as a simple  $d^1$  electronic configuration is involved, which is attributed to the central atom,  $\text{Ti}^{3+}$ , perturbed by an almost octahedral environment. The ground-state configuration is, moreover, experimentally assessed as being of the  $T_g$  symmetry species,<sup>63</sup> in agreement with crystal-field theory. An electronic transition  $T_g \rightarrow E_g$  is known with accuracy.<sup>64</sup>

We are mainly interested in the following questions:

1. How is the positive charge (3+) formally borne by the metal spread out in the cluster?
2. Would the electronic ground-state symmetry species according to our model calculation actually be the same as the one found experimentally?
3. How are the charge densities modified by the Madelung potential due to interatomic transfer of charges to be compared with a standard picture, that is, a Wolfsberg-Helmholz model where no such charge transfers are taken into account?

In the field of catalysis, it is well known that the oligomerization of butadiene  $[\text{CH}_2\cdots\text{C}(\text{CH}_3)\cdots\text{CH}_2]_2 - \text{M}(\text{C}_{2n})$  is catalyzed by transition-metal complexes (Ni, Fe, Co, Cr).<sup>65-68</sup> For example, in the cyclodimerization of butadiene, the following intermediate is isolated<sup>69</sup>:



where Do = donor. It is supposed that the ends of the  $\text{C}_8$  chain are bonded to the nickel through  $\pi$  bonds of the allyl groups. Further support for the above-mentioned hypothesis is also given by the synthesis of bis( $\pi$ -allyl)-Ni and bis( $\pi$ -methylallyl)-Ni. Curiously enough, the synthesis of these metallic compounds is impossible with any other transition-metal atom of the first period. These compounds are abbreviated here as  $\text{ML}_2$ . We are therefore interested in whether we can find some theoretical grounds predicting the stability of the  $\text{NiL}_2$  molecular system along the homologous series  $\text{NiL}_2$ ,  $\text{CoL}_2$ ,  $\text{FeL}_2$ ,  $\text{CrL}_2$ . The same spatial geometries for the unknown clusters are retained throughout the series and are referred to the existing  $\text{NiL}_2$  system for which an X-ray diffraction analysis<sup>70</sup> is available.

Aside from the peculiar electronic structures and sequences of the  $d$ -orbital energies in some of the following clusters  $\text{CuCl}_4^{2-}(D_{4h})$ ;  $\text{MnCl}_4^{2-}(D_{4h})$ ;  $\text{CrCl}_4(D_{4h})$ ;  $\text{CuCl}_4 \cdot 2\text{NH}_3(C_{2h})$  (see Section II.C.1), we are also interested in calculating quantum mechanically some coupling parameters currently measured by resonance techniques<sup>49,51</sup> (ESR, NMR, NQR, maser and laser spectroscopy) applied in particular to transition-metal complexes. These parameters occur in the phenomenological spin-Hamiltonian, the device of which has been proposed by Abragam and Pryce.<sup>71</sup> It seems to us that the calculation of some of these parameters may constitute good probes for testing our molecular orbital method. Very few *ab initio* calculations of these parameters have been published and such a work has never been undertaken within a semi-empirical formalism using an approximation level comparable to ours. A couple of years ago McWeeny<sup>72</sup> described a method for calculating these parameters *a priori* using spinless density functions of first and second order. However, no attempts of numerical evaluations of the relevant matrix elements seem to have been carried out.

The clusters  $\text{CuCl}_4^{2-}$ ,  $\text{MnCl}_4^{2-}$  are supposed to have the  $D_{4h}$  symmetry, in accordance with ESR measurements on  $\text{Cu}^{2+}$  and  $\text{Mn}^{2+}$  doped  $\text{NH}_4\text{Cl}$  single crystals.<sup>73,191</sup> The existence of those square-planar arrangements is also well established by other methods.<sup>75</sup> Room temperature ESR measurements<sup>74</sup> on  $\text{Cr}^{3+}$  ( $S_{\text{eff}} = \frac{3}{2}$ ) embedded in  $\text{CsCl}$  crystals strongly support the presence of the cation in an interstitial site in the host lattice. Experimental results also favor a planar configuration at the site  $\text{Cr}^{3+}$ . A planar arrangement, that is,  $\text{CrCl}_4$  ( $D_{4h}$ ), is considered in analogy with the well-known coplanar configurations occurring for the ions  $\text{Mn}^{2+}$  and  $\text{Cu}^{2+}$  in  $\text{NH}_4\text{Cl}$ . The last cluster, that is,  $\text{CuCl}_4 \cdot 2\text{NH}_3$ , observed in a  $\text{Cu}^{2+}$  doped  $\text{NH}_4\text{Cl}$  crystal containing an excess of  $\text{NH}_3$ ,<sup>73</sup> is in a crystal-field model supposed to have the  $D_{4h}$  symmetry too, assuming the  $\text{NH}_3$  groups to be two point charges placed above and below the square plane defined by the chlorine atoms at the center of which lies the copper atom. This model in particular is found to be responsible for the chlorine-transferred hyperfine interactions.<sup>73</sup> The molecular-orbital calculations, however, are based on a spatial model belonging to the  $C_{2h}$  symmetry,<sup>76</sup> the position in space of each hydrogen atom being well settled out (assuming usual valence angle and bond lengths) as shown in Fig. 5, Section II.D.2.a.

The quantum mechanical calculations of the following spin-Hamiltonian coupling parameters are described and discussed in this section.

1. The isotropic part of the hyperfine interaction parameter or the Fermi contact term, related to the  $\text{CuCl}_4^{2-}(D_{4h})$ ,  $\text{MnCl}_4^{2-}(D_{4h})$  clusters.
2. The molecular  $g$  components, appearing in the Zeeman term, related to the  $\text{CuCl}_4 \cdot 2\text{NH}_3(C_{2h})$  cluster.

3. The nuclear quadrupole coupling constant,  $eq^{\alpha}Q^{\alpha}$ , corresponding to the anion  $\alpha \equiv \text{Cl}^{-}$ , in the  $\text{CuCl}_4 \cdot 2\text{NH}_3(\text{C}_{2h})$  cluster.
4. The electronic spin-spin dipolar interaction,  $D_{SS}^{zz}$ , contributing the zero-field splitting parameter  $D^{zz}$ , related to the cluster  $\text{CrCl}_4(\text{D}_{4h})$ .

The molecular systems considered until now are all centrosymmetric, as is often the case when transition-metal atoms are involved in sometimes rather complicated atomic arrangements. With a view to testing our MO model in the case of the electric dipole moment, using the method described in paragraph II.B.2.b, we have chosen as our probe a very simple molecule, that is, HCl. We ought to remark that even for simple diatomic systems, involving transition-metal atoms, very few theoretical dipole-moment calculations have been reported. Known examples are TiN,<sup>92</sup> TiO,<sup>93,94</sup> and VO.<sup>96</sup> However, the electronic structures of these biatomic transition-metal oxides are known to be very peculiar. The ground-state symmetry species are still uncertain<sup>95</sup> and their electric dipole moments are not known experimentally.<sup>93-96</sup> Aside from these considerations, there are obviously no reasons why this calculation should not be as successful in the case of noncentrosymmetric transition-metal complexes with known electric dipole moments.

**b. Derivation of "Best" Ground-state Molecular Orbitals.** The derivation of the "best" SCF ground-state molecular orbitals is based, in a semi-empirical formalism, on the requirement of a "self-consistent charge distribution" related to a few consecutive iterations. Let us see, briefly, how this statement can be achieved according to our experience.

A plausible charge distribution among a minimum set of basis functions, that is, the valence orbitals, is selected at the outset of the calculation. These consist of nine orbitals [ $4s$ ,  $4p$  ( $\times 3$ ),  $3d$  ( $\times 5$ )] for a first-period transition-metal atom and four orbitals [ $2s$  or  $3s$ ,  $2p$  ( $\times 3$ ) or  $3p$  ( $\times 3$ )] for an atom of the second or third period. The primitive basis in all our MO calculations reported here consists of Slater orbitals or combinations of the latter. The charge densities, that is, (2.7), in general fractional numbers, are obviously unknown at the outset of the iterative process. Usually one chooses a molecular-charge repartition such that each atom retains approximately its neutral configuration, in conformity with the concept of valence state, the overall net charge, that is, (2.8), being zero. Now, the diagonal and off-diagonal elements of the effective Hamiltonian can be calculated, knowing the corresponding values of the integrals (see Section I (1.47) and (1.46) and Section I.F.2.b. A secular problem is set up, the solution of which is sought by the usual Löwdin orthonormalization procedure,

$$|S^{-1/2} \cdot H \cdot S^{-1/2} - E \cdot 1| = 0 \quad (2.18)$$



$S^{-1/2}$  is the inverse of the square root of the nonsingular overlap matrix. The latter is built up using a set of nonorthogonal basis functions (Slater type) and *all* the bicentric elements are calculated within this set.<sup>77</sup> The monocenter elements are set equal to zero except for the overlap of an orbital with itself, that is,  $[S_{pp'}]_{\text{monocenter}} = \delta_{pp'}$ .

A particular semiautomatic iterative procedure has been developed for solving the set of (2.18), that is, using a "variable" mean of the population indices of the  $n$ th and  $(n-1)$ th iterations according to the "extent" of convergence towards the stationary state. A self-consistent charge distribution is assumed to be reached among the ground-state occupied orbitals when the sets of orbital charge densities corresponding to a few consecutive iterations differ among themselves by less than 0.005 electron.

The theoretical indices available from our program, after having reached the charge self-consistency, are as follows:

1. Indices issued from the Mulliken population analysis, defined by (2.5) through (2.8).
2. Orbital energies  $H_{pp}$  corresponding to (1.47) and/or (1.46) (See Section I).
3. Sets of eigenvalues-eigenvectors (Löwdin coefficients) resulting from the last iteration.

## 2. Charge Densities and Energy Levels Corresponding to the $[\text{Ti}(\text{6H}_2\text{O})]^{3+}(T_h)$ Cluster

Table IA gives an illustrative example of the charge densities and energy levels<sup>78</sup> corresponding to the  $[\text{Ti}(\text{6H}_2\text{O})]^{3+}(T_h)$  cluster, sketched in Fig. 1. The Wolfsberg-Helmholz formula [Section I, (1.28)] for the  $H_{pq}$  elements is still used. For deriving the diagonal elements  $H_{pp}$  two approximations are used. First, the bicentric terms are neglected—denoted in Table I by the words "Standard MO method"—using (1.47). Second, using (1.46), the bicentric quantity  $\sum_{l(L)} (J_{pl} - \frac{1}{2}K_{pl})(n_l^{\uparrow} - q_l^{\uparrow})$  is approximated by  $\sum_L \xi_L/R_{P-L}$ , for every atomic-orbital pair.  $R_{P-L}$  is the interatomic distance and  $\xi_L$  the net charge upon atom L (see Section I.F.2.a). These results lead to the following conclusions:

1. The formal positive charge +3 is spread out in a more pronounced way when the interatomic Coulomb repulsions are included in the calculation.
2. Although the titanium atom remains almost neutral, the unpaired electron occupies a  $T_g$  energy level to which correspond molecular orbitals whose main components are the  $3d_{xy}$ ,  $3d_{xz}$ ,  $3d_{yz}$  of  $\text{Ti}^*$  in accordance with ligand-field predictions.<sup>64</sup>

\*The symmetry orbitals of the  $T_h$  point group are not ordinarily reported. They have been derived for the cluster  $[\text{Ti}(\text{6H}_2\text{O})]^{3+}$  using the well known projection operator technique<sup>78</sup>.

TABLE IA  
Charge Densities and Energy Levels of  $\text{Ti}(\text{H}_2\text{O})_6^{3+}$

		Standard MO method <sup>a</sup>			With interatomic Coulomb corrections		
Orbitals		$q_r$	$\rho_r$	Energy levels (eV)	$q_r$	$\rho_r$	Energy levels (eV)
Ti	$\left\{ \begin{array}{l} 4s \\ 3d_{z^2}, 3d_{x^2-y^2} \\ 3d_{xy}, 3d_{yz}, 3d_{zx} \\ \text{Net charge} \end{array} \right.$	0.03	0	$A_g$ -34.163	0.27	0	$A_g$ -63.550
		-0.11	0	$E_g$ -33.597	0.09	0	$E_g$ -61.513
		0.62	0	$T_u$ -32.973	0.64	0	$T_u$ -61.291
		0.68	0.230	$T_g$ -18.097	0.60	0.276	$A_g$ -44.249
		1.02		$A_g$ -16.711	0.38		$T_g$ -44.146
O	$\left\{ \begin{array}{l} 2s \\ 2p_x \\ 2p_y \\ 2p_z \\ \text{Net charge} \end{array} \right.$			$E_g$ -16.153			$T_u$ -42.205
		1.35	0	$T_u$ -15.624	1.28	0	$E_g$ -38.700
		1.63	0	$T_u$ -13.670	1.65	0	$T_u$ -35.895
		1.86	0.037	$T_g$ -12.741	1.87	0.021	$T_g$ -33.109
		1.37	0.006	$T_u$ -11.654	1.42	0.002	$T_u$ -30.404
		-0.21		$T_g^*$ -1.942	-0.22		$T_g^*$ -1.778
H	$\left\{ \begin{array}{l} 1s \\ \text{Net charge} \end{array} \right.$			$T_u$ 11.290			$T_u$ 23.511
		0.72	0.004	$E_g$ 18.350	0.67	0.003	$E_g$ 39.800
		0.28		$T_g$ 29.867	0.33		$A_g$ 70.893
				$T_u$ 33.229			$T_g$ 71.841
				$A_g$ 39.884			$T_u$ 75.182
				$E_g$ 49.666			$E_g$ 93.414
				$A_g$ 63.271			$T_u$ 138.066
				$T_u$ 64.557			$A_g$ 144.127

<sup>a</sup> $q_r$ : gross atomic populations;  $\rho_r$ : atomic populations in orbitals  $T_g^*$  occupied by an unpaired electron.

- The sequence of symmetry species of the first virtual molecular orbitals does not reproduce the sequence generally accepted for the excited states of  $\text{Ti}(\text{H}_2\text{O})_6^{3+}$ ; whereas the first absorption band is assigned to a transition  $T_g \rightarrow E_g$ ,<sup>64</sup> the nearest empty energy level in our calculation belongs to the representation  $T_u$ . One must remember, however, that the excited orbitals result from a variational treatment performed on the ground state orbitals alone. Furthermore, as is well known, the theoretical expressions for electronic transitions involve, in addition to orbital energies, repulsion and exchange terms that may be of considerable importance in the case of degenerate levels, where configuration interaction may contribute substantially.<sup>79</sup>

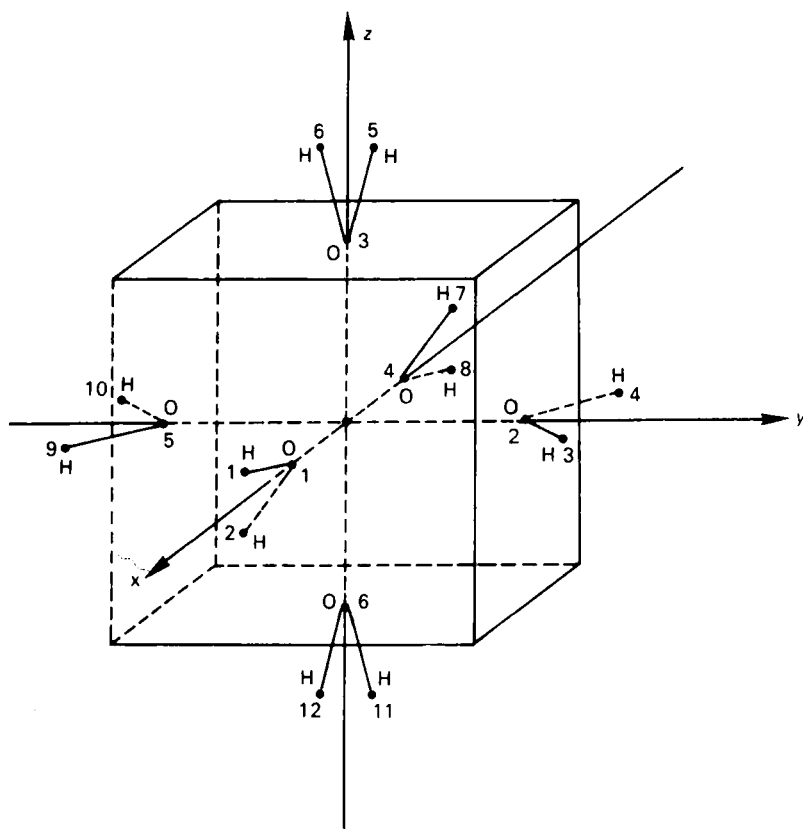


Fig. 1. Model for the complex  $\text{Ti}(\text{6H}_2\text{O})^{3+}(T_h)$ .

### 3. $\text{NiL}_2$ System

We are seeking some theoretical reasons<sup>80</sup> that may explain the successful synthesis of the  $\text{NiL}_2$  system alone in the homologous series bis- $\Pi$ -(methylallyl)- $\text{M}$  (with  $\text{M} = \text{Ni}, \text{Co}, \text{Fe}, \text{Cr}$ ) abbreviated as  $\text{NiL}_2, \text{CoL}_2, \text{FeL}_2, \text{CrL}_2$ , the spatial geometry ( $C_{2h}$ ) of which is shown in Fig. 2.

The special ability of Ni to give such complexes is perhaps best shown by Fig. 3, which shows a diagram of the orbital energies, that is, the values of the  $H_{pp}$ 's including the Nishimoto-Mataga relation (see (1.49)) for the  $J_{pl}$  integrals. It becomes striking that the following hold only in the case of the  $\text{NiL}_2$  system:

1. The usual sequence of the valence orbitals of the metal is found, the  $3d$  orbitals being the deepest, followed by the  $4s$  and the  $4p$ 's. A gradual

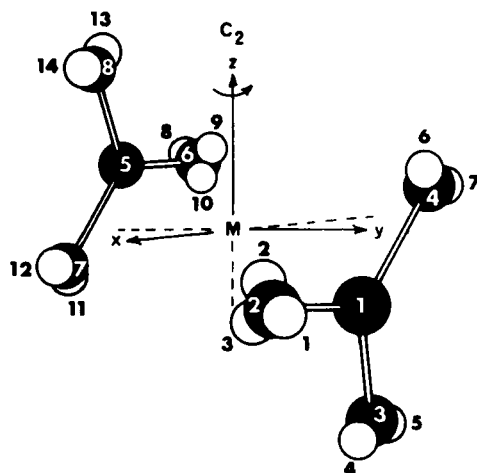


Fig. 2. Molecular geometry of the bis( $\pi$ -methylallyl) transition-metal complex ( $C_{2h}$  group of symmetry). ● = C, ○ = H.

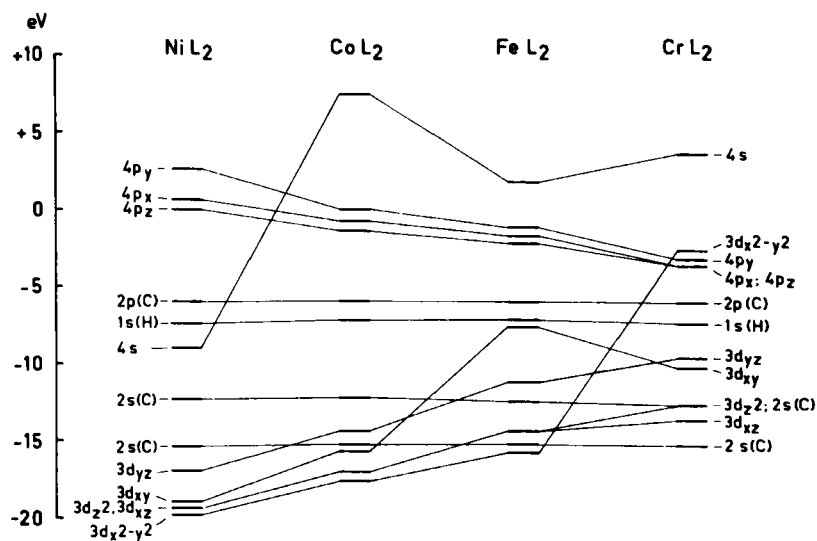


Fig. 3. Orbital energies corresponding to diagonal elements of the effective Hamiltonian (with  $J_{pl}$  contribution).

- dispersion among the  $3d$  orbital energies and a monotonous decrease of the  $4p$  orbitals are observed in the case of the hypothetical complexes.
2. The  $4s$  orbital has a relatively low energy, and the corresponding charge index  $q_{4s}$  is found to be positive for Ni, attesting the electroattractive character of this orbital.<sup>80</sup>

Including the  $J_{pl}$  integrals [see (1.49)] in the  $H_{pp}$  elements increases the net charges on the metal atoms, for example, 1.35 and 1.82 for Ni without and with  $J_{pl}$  contribution, respectively, and similar increases are obtained<sup>80</sup> for  $M = \text{Co, Fe, Cr}$ . Similar effects have been obtained by Jørgensen et al.<sup>81</sup> about another series of first-period transition-metal complexes by including the Madelung-energy (see Section I.F.2.a) in their standard Wolfsberg-Helmholtz model calculation. An *ab initio* work performed on the bis( $\pi$ -allyl)-Ni electronic ground state<sup>82</sup> reveals a charge of +1.92 on the nickel atom, in good agreement with our figure +1.82.<sup>80</sup> This emphasizes the importance of the  $J_{pl}$  integrals in the effective Hamiltonian used.

Let us finally stress that our results on the overlap population indices suggest for the metal-carbon bonds semipolar bonds,<sup>80</sup> with the weakest antibonding character for the Ni—C bonds. Similar results have been obtained by Stevenson et al. on  $\text{ScH}_3\text{NH}_3$  and  $\text{TiH}_3\text{F}$  for the Sc—N and Ti—H bonds<sup>83</sup> and by Berthier et al.<sup>84</sup> for organic molecules with known semipolar bonds.

#### 4. $\text{CuCl}_4^{2-} (D_{4h})$ and Related Square-Planar Complexes

Table II gives the charge densities<sup>85</sup>  $q_r$  for the cluster  $\text{CuCl}_4^{2-} (D_{4h})$  (see Fig 4a) containing 41 valence electrons. The net charges on copper and chlorine centers are in very good agreement with those obtained by *ab initio* calculations.<sup>86</sup>

TABLE II  
Charge Densities  $q_r^a$  and net Charges  $\delta_p$  in  $\text{CuCl}_4^{2-}$  Cluster

	Cu							Cl		
	$4s$	$d_{z^2}$	$d_{x^2-y^2}$	$d_{xy}$	$d_{xz}, d_{yz}$	$4p_x, 4p_y$	$4p_z$	$3s$	$3p_x, 3p_y$	$3p_z$
$q_r$	0.107	2.0	2.0	1.996	2.0	-0.127	+0.085	2.071	1.858	1.979
$\delta_p$				+1.066					-0.766	
$\delta_p^{*b}$				+1.05					-0.76	

<sup>a</sup>Calculated with  $J_{pl}$  contributions [see (1.49)].

<sup>b</sup>Issued from *ab initio* results.<sup>86</sup>

Moreover, the highest filled MO is predominantly of metallic character and obeys the  $B_{1g}$  symmetry, as confirmed by *ab initio* results.<sup>86</sup>

A rather tricky point to be mentioned is the different assessments of the *d*-level ordering for such square-planar complexes, reported in the literature and schematized in Fig. 4 (cases I through III). Case IV is the level ordering corresponding to our results.

$x^2-y^2$	—	—	$x^2-y^2$	—	$x^2-y^2$	—	$xy$
$xy$	—	—	$xy$	—	$z^2$	—	$z^2$
$z^2$	—	—	$\begin{cases} xz \\ yz \end{cases}$	—	$\begin{cases} xz \\ yz \end{cases}$	—	$\begin{cases} xz \\ yz \end{cases}$
$\begin{cases} xz \\ yz \end{cases}$	—	—	$z^2$	—	$xy$	—	$x^2-y^2$
	I	II	III		IV		

Fig. 4. Level orderings of the *d* orbitals in square-planar transition-metal complexes. In cases I through III the coordinate axes are located along the diagonals of the square spanned by the chlorine atoms,<sup>87-89</sup> whereas in case IV the level ordering refers to the reference frame of Fig. 4a.

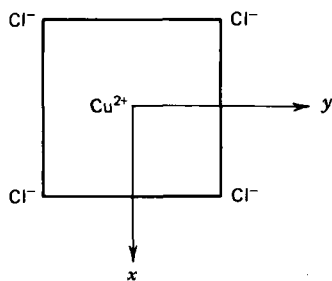


Fig. 4a. Model adopted for the  $\text{CuCl}_4^{2-}$  system.

The ordering noted I is proposed by Fenske et al.<sup>87</sup> for  $\text{Pt}^{2+}$  complexes. The ordering II results from a semiempirical MO calculation of Basch et al.<sup>88</sup> for the ion  $\text{PtCl}_4^{2-}$  and of Ros and Schuit<sup>89</sup> for the ion  $\text{CuCl}_4^{2-}$ . The ordering III has been reported qualitatively and tentatively by Figgis<sup>90</sup> to account for magnetic and spectral properties of square-planar complexes and is also found by *ab initio*<sup>86</sup> calculation. This *d*-level sequence is also in complete agreement with our results sketched in column IV, taking into account the two different assessments of the reference frame.

Table III gives the *d*-orbital energies. The energy differences amount in some cases to minor quantities, indeed. We refer the reader to one of our papers<sup>76</sup> for the results on the electronic structure and related parameters of the cluster  $\text{CuCl}_4 \cdot 2\text{NH}_3(\text{C}_{2h})$  (see also section II.D).

TABLE III  
Values of Some Diagonal Elements of the Effective  
Hamiltonian (eV) for  $\text{CuCl}_4^-$

$H_{z^2, z^2}$	$H_{x^2-y^2, x^2-y^2}$	$H_{yz, yz}$	$H_{xy, xy}$
-14.1758	-14.1844	-14.1786	-14.1366

As a last example, we draw a comparison between definite population indices for the complex  $\text{CrCl}_4(D_{4h})$ , using two distinct electronic hypotheses.<sup>91</sup> The ground-state configuration containing 31 valence electrons is assumed to possess three decoupled electrons, that is  $S = S_z = \frac{3}{2}$ , in accordance with ESR experiments on  $\text{Cr}^{3+}$  ions doped in CsCl monocrystals.<sup>74</sup>

The charge densities,  $q_r^I$  in Table IV, have been obtained without the Wolfsberg-Helmholz approximation. Instead, the atomic kinetic integrals,

TABLE IV  
Charge Densities in the Complex  $\text{CrCl}_4(D_{4h})$ <sup>191</sup> with Three Decoupled  
Electrons in Its Ground State

	Cr							Cl		
	4s	4p <sub>x</sub> =4p <sub>y</sub>	4p <sub>z</sub>	3d <sub>z</sub> <sup>2</sup>	3d <sub>x</sub> <sup>2</sup> -y <sup>2</sup>	3d <sub>xz</sub> =3d <sub>yz</sub>	3d <sub>xy</sub>	3s	3p <sub>x</sub> =3p <sub>y</sub>	3p <sub>z</sub>
q <sub>r</sub> <sup>I</sup>	0.6506	0.5530	0.4223	1.1024	0.5078	0.4260	0.9063	1.635	1.5233	1.6814
δ <sub>p</sub> <sup>I</sup>				+0.452					+0.636	
q <sub>r</sub> <sup>II</sup>	0.8131	0.6500	0.5296	1.9451	0.1771	0.0879	0.7983	1.6227	1.4344	1.8236
δ <sub>p</sub> <sup>II</sup>				+0.260					+0.685	

$T_{pp}$  and  $T_{pq}$  are rigorously calculated and the potential parts of  $H_{pq}$  are approximated by a Mulliken-type formula [see (1.50)]. The charge figures  $q_r^{II}$  are those obtained still retaining the Wolfsberg-Helmholz relation for the  $H_{pq}$ 's. Both sets of charges include the  $J_{pi}$  contributions [see (1.49)]. It is interesting to note that the molecular charge density is more uniformly distributed, especially among the  $d$  orbitals, when the Wolfsberg-Helmholz relation is released (see also Section I.F.S.b).

## D. Calculations of Mono- and Bielectronic Observables

### 1. Preliminaries

Actually, a relatively small number of calculations of molecular observables related to transition-metal complexes have been derived in the framework of *ab initio* or even semiempirical MO calculations. We hope that some of the results reported here, to be considered somehow as "a pioneer work," will stimulate other calculations of molecular observables in the case of transition-metal complexes, as they exist on a very large scale for organic compounds. The computer technology no longer constitutes an "insurmountable potential barrier" against this task. On the other hand, high-precision resonance measurements on transition-metal molecular compounds are currently being made in many laboratories, and these constitute excellent material for the theorists in testing their calculation methods and at the same time should provide the experimentalists with valuable predictions and a secure guide for future experiments.

### 2. Classification of Observables

It is convenient to distinguish one-electron molecular properties, which depend on one-electron operators, and two-electron molecular properties, which depend on operators involving the relative positions of the electrons. Moreover, among the one-electron properties, it is useful to distinguish properties directly associated with the expectation value of certain operators and those involving a second-order response to a one-electron perturbation operator. An example of the former one-electron property is the dipole moment, generally obtained by calculating the expectation value of the position operator for a given electronic state, usually the ground state. For the latter one-electron property, an example, among others involving an external magnetic field, is the indirect hyperfine nuclear spin-spin interactions. The calculation of this class of one-electron properties is complicated, as it involves, at least in principle, the wave functions and energies of virtual excited states. For the sake of clarity we present here an outline of the molecular observables to be treated subsequently.

#### I. Closed- or open-shell systems

- A. First-order one-electron properties (see Section II.D.2.a)
  - 1. Electric dipole moment  $\mu$  (Section II.D.2.a)
  - 2. Nuclear quadrupole coupling constant  $eQ$  (Section II.D.2.a)
- B. Second-order one-electron properties (Section II.D.2.a)
  - 1. Properties of electric origin
    - a. Electrical polarizability,  $\alpha$  (Section II.D.2.a)



2. Properties of magnetic origin
  - a. Magnetic susceptibility  $\chi$  (Section II.D.2.a)
  - b. Chemical shift  $\sigma$  (Section II.D.2.a)
  - c. Indirect nuclear spin-spin coupling,  $J_{NN'}$  (Section II.D.2.a)
  - d. Anisotropic hyperfine interactions (Section II.D.2.a)
- II. Open-shell systems (see Section II.D.2.b). Besides the above one-electron properties, one- and two-electron properties specific to open-shell systems have to be distinguished.
  - A. First-order one-electron properties (see Section II.D.2.b)
    1. Isotropic part of the magnetic hyperfine interactions or Fermi-contact term  $F$  (Section II.D.2.b) and total hyperfine interactions including their anisotropic parts (Section II.D.2.b)
  - B. Second-order one-electron properties (see Section II.D.2.b)
    1. Electronic gyromagnetic factor, or  $g$  factor (Section II.D.2.b)
  - C. Second-order two-electron properties (see Section II.D.2.b). As an example we treat the electronic spin-spin dipolar interaction  $D_{ss}^{zz}$  involved in the zero-field splitting parameter  $D^{zz}$  (Section II.D.2.b)

In the case of transition-metal complexes quite generally, only a few theoretical calculations have been reported on these observables. Therefore, we compare our theoretical results with experimental ones. In the case of molecular observable calculations carried out by other authors, the comparison is drawn occasionally between some theoretical results among which when possible, we quote the *ab initio* ones.

**a. Closed- or open-shell systems. First-Order One-Electron Properties.**

**ELECTRIC DIPOLE MOMENT  $\mu$ .** As is explained earlier in Section II.C.1.a we have chosen the simple diatomic molecule HCl for testing our calculation method (see Section II.B.2.b).

The computed ground-state properties of HCl are for obvious reasons numerous and reliable: electric dipole and quadrupole moment, magnetic susceptibilities, nuclei electric field gradients,<sup>97</sup> and so on. Therefore, we are in a position to compare our result with others based on much more involved methods of calculation.

First, the HCl ground-state molecular orbitals have been determined according to Section I.F and the corresponding Mulliken population analysis has been carried out.<sup>98</sup> The MO-LCAO expression previously quoted,

$$\bar{\mu} = \sum_P \delta_P \bar{r}_P + \sum_P \sum_{r,r' \in P} p_{rr'} \bar{\zeta}_{rr'}^P + \sum_P \sum_r \sum_{s \in Q} p_{rs}^{PQ} S_{rs}^{PQ} \bar{\eta}_{rs}^{PQ} \quad (2.19)$$

is then used. The symbols are defined through the expressions (2.8) and (2.12)

through (2.15). The different terms for convenience are labeled as

$$\begin{aligned}\bar{\mu}_1 &= \sum_P \delta_P \bar{r}_P \\ \bar{\mu}_2 &= \sum_P \sum_{r,r' \in P} p_{rr'} \bar{\zeta}_{rr'}^P \\ \bar{\mu}_3 &= \sum_P \sum_{r \in P} \sum_{s \in Q} p_{rs}^{PQ} S_{rs}^{PQ} \bar{\eta}_{rs}^{PQ}\end{aligned}\quad (2.20)$$

A Mulliken population analysis reveals that  $\delta_H = +0.23951e$  and  $\delta_{Cl} = -0.23951e$ . The origin of the reference frame is settled on chlorine, and taking  $\bar{r}_P \equiv H = 1.725 \text{ \AA}$ , we find a value  $\bar{\mu}_1 = 1.98432 \text{ D}$  ( $D = \text{Debye}$ ). For the hybridization moment  $\bar{\mu}_2$ , the only nonvanishing contribution comes from the chlorine center

$$\bar{\mu}_2 = p_{s,p_z}(\zeta_z)_{s,p_z}$$

(the corresponding MO coefficients  $p_{s,p_x}$ ,  $p_{s,p_y}$  vanish by symmetry).  $(\zeta_z)_{s,p_z}$  is the  $z$  component of  $\bar{\zeta}$ , corresponding to orbitals  $3s$ ,  $3p_z$ .

Using a Slater-type function

$$\chi_{nlm} = \left[ \frac{(2\xi_{nl})^{2n+1}}{(2n)!} \right]^{1/2} r^{n-1} e^{-\xi_{nl}r} Y_{lm}(\theta, \varphi)$$

it is straightforwardly shown that

$$(\zeta_z)_{s,p_z} = \sum_{i=1}^n \sum_{j=1}^m c_i c_j \sqrt{\frac{(2\xi_i)^{2n_i+1} (2\xi_j)^{2n_j+1}}{3(2n_i)!(2n_j)!}} \times \frac{(n_i + n_j + 1)!}{(\xi_i + \xi_j)^{n_i + n_j + 2}} \quad (2.21)$$

where  $c_i$  and  $c_j$  are the SCF expansion coefficients of the primitive basis set for the  $3s, 3p$  orbitals of Cl.

The value  $\bar{\mu}_2 = -0.320503 \text{ D}$  is found. The value has a negative sign because the orbitals corresponding to the lone pair electrons (for chlorine) are largely hybridized;<sup>99</sup> therefore, these electrons are not symmetrically arranged about the nucleus (as in pure  $s$  or  $p$  orbitals), their charge densities being oriented outwards on the side of the atom opposite that containing the bonded substituent.

For the overlap dipole moments  $\bar{\mu}_3$ , the nonvanishing matrix elements are

$$p_{3s,1s} S_{3s,1s}(\eta_z)_{3s,1s} \quad \text{and} \quad p_{3p_z,1s} S_{3p_z,1s}(\eta_z)_{3p_z,1s}.$$

The matrix elements of  $\eta_z$  are ultimately reducible to ordinary overlap matrix elements.<sup>77</sup> The final result is

$$\bar{\mu}_3 = -0.720869 \text{ D}$$

The interpretation of the negative value is similar to that given above.

Summing up the three contributions,  $\bar{\mu}_1, \bar{\mu}_2, \bar{\mu}_3$ , the value  $\bar{\mu} = +0.94295$  D is found, as compared to the observed value of  $+1.12$  D. The agreement is fair owing to the semiempirical nature of our wave function. It also proves that purely theoretical indices, for example,  $\delta_p$ , are quite reliable for predicting the value of the observable.

An *ab initio* molecular-orbital calculation of the ground-state dipole moment of HCl performed by McLean et al.,<sup>97</sup> calculating directly the expectation value of the position operator, gives the value  $\mu = 1.215$  D, in slightly better agreement with the experimental figure. Using configuration interaction, including about 200 mono- and biexcited configurations, Grimaldi et al.<sup>100</sup> obtain the figure 1.0426 D, as expected, a smaller value than the previous one, the discrepancy with the experimental result being, nevertheless, of about 7%.

**Nuclear Quadrupole Coupling Constant  $eq^{\alpha}Q^{\alpha}$ .** We have performed this calculation taking as an example the cluster  $\text{CuCl}_4 \cdot 2\text{NH}_3$  (see Fig. 5) introduced in Section II.C.1.a and obeying the point group  $C_{2h}$ . We refer to this spatial model later when discussing our  $g$  tensorial component calculations. We are interested in calculating the nuclear quadrupole coupling constant of the anion  $\text{Cl}^-$  and in comparing our result with those corresponding to similar transition-metal chlorinated compounds.

As outlined by Cotton et al.,<sup>101</sup> it is possible to obtain an analytical expression for  $eq^{\alpha}Q^{\alpha}$  in terms of certain population indices. For the sake of clarity we briefly sketch the main steps of this calculation; the reader is referred to the original work of Cotton et al.<sup>101</sup> for a full account.

In the MO-LCAO formalism, requiring the one-center atomic orbitals to be orthogonal, the field gradient  $q^{\alpha}$  at nucleus  $\alpha$  (or any other point in the molecule) may be written as

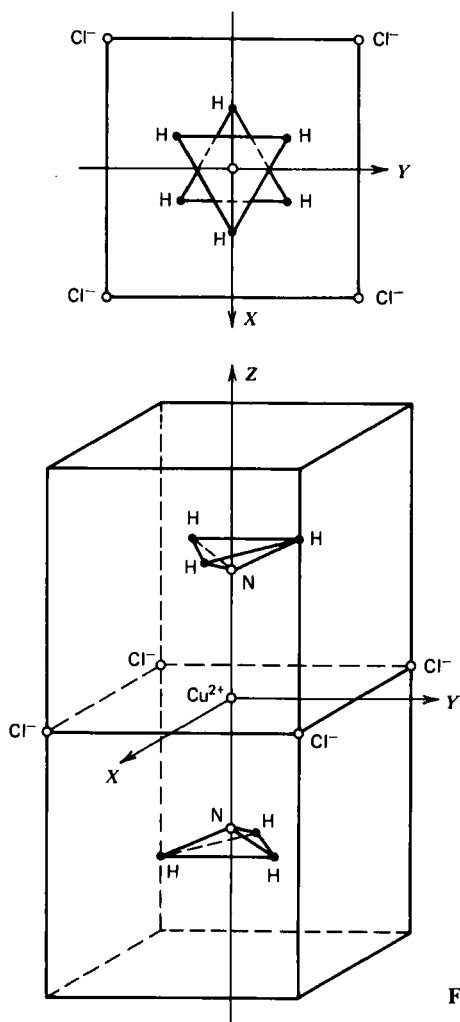
$$q^{\alpha} = \sum_j \sum_p \sum_q n_j c_{pj} c_{qj} q_{pq}^{\alpha} + q_{\text{nuc}}^{\alpha}$$

$$= \sum_j n_j \left[ \sum_p c_{pj}^2 q_{pp}^{\alpha} + \sum_q c_{qj}^2 q_{qq}^{\alpha} + \sum_{p,q} c_{pj} c_{qj} q_{pq}^{\alpha} + \sum_{q,l} c_{qj} c_{lj} q_{ql}^{\alpha} \right] + q_{\text{nuc}}^{\alpha} \quad (2.22)$$

with

$$q_{pq}^{\alpha} = e \int \chi_p^* \frac{3 \cos^2 \Theta - 1}{r_{\alpha}^3} \chi_q d\tau \quad (2.23)$$

The orthogonality of the one-center basis functions amounts to the appearance of only one term for the monocenter contribution, that is, the first one in the expression in square brackets.  $r_{\alpha}$  is the distance measured from nucleus  $\alpha$  and the angle  $\Theta$  is measured relative to a fixed direction (usually the  $z$  molecular axis).  $q_{\text{nuc}}^{\alpha}$  denotes the resultant field gradient on  $\alpha$  due

Fig. 5. Model for the complex  $\text{CuCl}_4 \cdot 2\text{NH}_3$ .

to the nuclear charges of the other atoms. The indices  $j$  and  $(p, q)$  are written for the molecular and atomic orbitals, respectively. The atomic orbital  $\chi_p$  belongs to atom  $\alpha$  such that  $q_{pp}^\alpha$  is a one-center integral. The next two terms represent the bicentric contributions, whereas the last one involves the tricentric contributions.

To limit the integral computational work, that is, by use of the valence orbitals only, (2.22) may be reduced to (2.24) under the following assumptions,

$$q^\alpha = \sum_j n_j \left[ \sum_p c_{jp}^2 q_{pp}^\alpha + \sum_{p < q} c_{jp} c_{jq} q_{pq}^\alpha \right] + P \quad (2.24)$$

where the summations on  $p$  and  $q$  act on the valence orbitals only.  $P$  designates the sum of all core orbitals of atom  $\alpha$ . These obviously undergo a polarisation, that is, the Sternheimer effect, which is taken to be the experimental value for the free atom (see below).

Furthermore, the quantity  $\left[ \sum_q^{\text{core}} q_{qq}^\alpha + q_{\text{nucl}}^\alpha \right]$  in (2.22) is set equal to  $q_{\text{core}}^\alpha$ , a result of the contributions of all atom cores, except atom core  $\alpha$ , in the molecule. This can be assumed to be correct to a high accuracy owing to the compactness of the cores, the electron density of the core of atom  $\alpha$  being supposed to lie outside the electron density of all other cores. On the other

hand,  $\left[ \sum_q^{\text{noncore}} q_{qq}^\alpha + \frac{1}{2} \sum_{p,q}^{\text{noncore}} c_{jp}^* c_{jq} q_{pq}^\alpha \right]$  in (2.22) is set equal to  $[-q_{\text{core}}^\alpha]$  defined

above. This is equivalent to assuming that the noncore valence electrons of all atoms but  $\alpha$ , together with half the overlap population of all bonds formed by atom  $\alpha$ , exactly screen the nucleus of atom  $\alpha$  from the potential due to the cores of all other atoms in the molecule. In the case of  $\text{PtCl}_4^{2-}$ ,<sup>101</sup> the error due to this assumption amounts to a few percent only. The tricenter contributions (last term in square brackets) of (2.22) are supposed to be negligible.

For  $q_{pq}^\alpha$  in (2.24), a Mulliken relationship is introduced:

$$q_{pq}^\alpha = S_{pq} q_{pp}^\alpha$$

if  $\chi_p$  and  $\chi_q$  are identical orbitals; otherwise

$$q_{pq}^\alpha = \frac{1}{2} S_{pq} (q_{pp}^\alpha + q_{qq}^\alpha) \quad (2.25)$$

Multiplying both sides of (2.24) by  $eQ^\alpha$ ,  $Q^\alpha$  being the nuclear quadrupole moment of atom  $\alpha$ , one gets

$$eq^\alpha Q^\alpha = \sum_p f_p \left[ q_{pp}^\alpha Q^\alpha + \left( \frac{eQ^\alpha P}{\sum_p f_p} \right) \right] \quad (2.26)$$

with

$$f_p = \sum_j n_j \left[ c_{jp}^2 + c_{jp} \sum_{q \neq p} c_{jq} S_{pq} \right] \quad (2.27)$$

that is, the Mulliken gross atomic population of the orbital  $\chi_p$ .

The Sternheimer correction  $P/\sum_p f_p$  is inserted into the observed value for the free atom, assuming that it varies slowly from molecule to molecule. Then, the term in brackets in (2.26) can be replaced by the observed nuclear quadrupole coupling constant of the free atom, that is to say, for  $p$  electrons in chlorine it can be replaced by 109.7 Mc/s. The final expression for chlorine,

having a hole in the  $p$  shell, is therefore

$$eqQ = 109.7 \sum_j \sum_p (2 - n_j) \left[ c_{jp}^2 + \sum_{q>p} c_{jp} c_{jq} S_{pq} \right] \quad (2.28)$$

Using the chlorine  $p$ -orbital charges determined according to Section I.F, in the case of the  $\text{CuCl}_4 \cdot 2\text{NH}_3$  cluster,<sup>102</sup> the value

$$eq^{\text{Cl}^-} Q^{\text{Cl}^-} = 109.7[6 - (1.911 + 1.570 + 2.007)] = +56.166 \text{ Mc/s}$$

is found for the anion  $\text{Cl}^-$ . This figure lies in the trend of values found for similar chlorinated complexes, that is  $\text{CsCl}_6^{2-}$ ,  $\text{IrCl}_6^{2-}$ ,  $\text{PtCl}_6^{2-}$ , the corresponding figures of which are 38, 44, 51 Mc/s respectively.<sup>101</sup>

Han et al.,<sup>103</sup> using a wave function derived within the extended Hückel framework (see Section I.D), as well as a similar calculation method, have computed the nitrogen nuclear quadrupole coupling constant in the hemin molecule. No experimental data seem to be available for this observable.

### Second-Order one-electron Properties.

PRELIMINARIES. Second-order one-electron properties, such as the magnetic shielding  $\sigma$ , magnetic susceptibility  $\chi$ , and electric polarizability  $\alpha$ , are, using *ab initio* model calculations, often derived by the so-called coupled or perturbed Hartree-Fock theory. To compare the formulation of this theory with that corresponding to the "usual" theory, let us give the expressions of the second-order energies, in the case of the susceptibility and magnetic shielding as derived by, respectively, Van Vleck<sup>104</sup> and Ramsey<sup>105</sup> using perturbation theory. The susceptibility is given by the expression (in standard notations)

$$E^{(2)} = \frac{e^2}{8mc^2} \left\langle \psi_0 \left| \sum_k \bar{H}(r_k^2 \bar{I} + \bar{r}_k \cdot \bar{r}_k) \cdot \bar{H} \right| \psi_0 \right\rangle - \frac{e^2}{4m^2 c^2} \sum_{n \neq 0} \frac{\left\langle \psi_0 \left| \sum_k \bar{H} \cdot \bar{L}_k \right| \psi_n \right\rangle \left\langle \psi_n \left| \sum_k \bar{L}_k \cdot \bar{H} \right| \psi_0 \right\rangle}{E_n - E_0}$$

the form of which is

$$E^{(2)} = -\frac{1}{2} \bar{H} \cdot \bar{\chi} \cdot \bar{H} \quad (2.29)$$

The magnetic shielding corresponds to the cross term between  $\bar{\mu}$  and  $\bar{H}$ , the result being

$$E^{(2)} = \frac{e^2}{2mc^2} \left\langle \psi_0 \left| \sum_k \frac{\bar{\mu}}{r_k^3} (r_k^2 \cdot \bar{I} - \bar{r}_k \cdot \bar{r}_k) \cdot \bar{H} \right| \psi_0 \right\rangle - \frac{e^2}{m^2 c^2} \sum_{n \neq 0} \frac{\left\langle \psi_0 \left| \sum_k \left( \frac{\bar{\mu}}{r_k^3} \right) \cdot \bar{L}_k \right| \psi_n \right\rangle \left\langle \psi_n \left| \sum_k \bar{L}_k \cdot \bar{H} \right| \psi_0 \right\rangle}{E_n - E_0}$$

which has the appropriate form

$$E^{(2)} = \bar{\mu} \cdot \bar{\sigma} \cdot \bar{H} \quad (2.30)$$

The calculation of the matrix elements  $\langle \psi_0 | L_x | \psi_n \rangle$ ,  $\langle \psi_0 | L_x / r_k^3 | \psi_n \rangle$ , or  $\langle \psi_0 | x_k | \psi_n \rangle$  are quite intractable if we require accurate wave functions of excited states of the unperturbed system, including the continuum. These functions are diffuse as compared to the ground state  $\psi_0$  of the unperturbed system, and a local perturbation of the orbitals by an external field is not well represented, with the result that an expansion in terms of such functions converges very slowly.<sup>106</sup>

In the perturbed or coupled Hartree-Fock theory, the basis of the method lies in the fact that the perturbing operators depend only on the coordinates of each electron separately so that the changes in the molecular wave function due to the perturbing field affect the  $e^2/r_{ij}$  terms indirectly through the self-consistent condition. Using *ab initio* calculation techniques, the atomic orbitals are optimized by varying their exponents as well as the MO's themselves by adjusting self-consistently the coefficients of the atomic orbital components (LCAO approximation). Thus the perturbations are made in suitable localized regions. We outline briefly the coupled Hartree-Fock theory and refer the reader to the review, and the references cited therein, written by Lipscomb<sup>106</sup> for more details, and in particular for the results on one-electron properties of certain biatomic *closed-shell* systems, such as LiH, BH, BF, CO.

The well-known quantities,  $F$ ,  $e_j$ , and  $\phi_j$ , appearing in the Schrödinger equation (see Section I.E.2) expand up to second order in the presence of a perturbing field

$$F = F^{(0)} + \lambda F^{(1)} + \lambda^2 F^{(2)}$$

$$e_j = e_j^{(0)} + \lambda e_j^{(1)} + \lambda^2 e_j^{(2)}$$

$$\phi_j = \phi_j^{(0)} + \lambda \phi_j^{(1)} + \lambda^2 \phi_j^{(2)}$$

with

$$\phi_j^{(1)} = \sum_k c_{kj}^{(1)} \phi_k^{(0)} \quad \phi_j^{(2)} = \sum_k c_{kj}^{(2)} \phi_k^{(0)} \quad (2.31)$$

The second-order energy is

$$E^{(2)} = \sum_{j=1}^n \left\{ 2h_{jj}^{(2)} + \sum_{p=1}^m [c_{pj}^{(1)*} h_{pj}^{(1)} + h_{jp}^{(1)} c_{pj}^{(1)}] \right\}$$

where  $N = 2n$  electrons and supposing  $m$  atomic orbitals. The  $c_{pi}^{(1)}$  coefficients of the first-order wave function have to fulfill the equation

$$[e_p^{(0)} - e_i^{(0)}] c_{pi}^{(1)} + A_{pi} + \sum_{j=1}^n \sum_{q=n+1}^m [4(jq|pi) - (ji|pq) - (qi|pj)] \times c_{qj}^{(1)} = 0 \quad (2.32)$$

where  $A_{pi}$  is the matrix element of a simple mono-electronic operator such as  $x$  and  $L_x$ ,

$$A_{pi} = \langle \phi_p^{(0)} | A | \phi_i^{(0)} \rangle$$

Notice that this procedure does not involve any excited state wave functions as in standard perturbation calculation. For example, in case of the magnetic shielding, cross term between  $\bar{\mu}$  and  $\bar{H}$ ,

$$\begin{aligned} \bar{h}^{(1)} &= \frac{e}{2mc} \bar{H} \cdot \bar{L} + \frac{e}{mc} \frac{\bar{\mu}}{r^3} \cdot \bar{L} \\ h^{(2)} &= \frac{e^2}{2mc^2} \bar{H} \cdot (r^2 \cdot \bar{I} - \bar{r} \cdot \bar{r}) \cdot \frac{\bar{\mu}}{r^3} \end{aligned} \quad (2.33)$$

and the  $c_{pi}^{(1)}$  have to verify the equation

$$(e_p^{(0)} - e_i^{(0)})c_{pi}^{(1)} + (L_x)_{pi} + \sum_{j=1}^n \sum_{q=n+1}^m [(qi|pj) - (ji|pq)]c_{qj}^{(1)} = 0 \quad (2.34)$$

Therefore, the shielding, averaged over all orientations takes the form<sup>106</sup>

$$\sigma_{av} = \frac{E^{(2)}}{\mu H} = \frac{2e^2}{3mc^2} \sum_{i=1}^n \left[ \left( \frac{1}{r} \right)_{ii} - \frac{2}{m} \sum_{p=n+1}^m c_{pi}^{(1)} \left( \frac{L_x}{r^3} \right)_{pi} \right] \quad (2.35)$$

The problem of gauge invariance occurring in the calculation of this observable, as in the case of the susceptibility, is taken up subsequently in Section II.D.2.a.

*Electrical polarizability  $\alpha$ .* Musher et al.<sup>109</sup> have calculated this observable in the case of the benzene molecule, using the Hartree-Fock perturbation theory, which is simpler to handle than the fully coupled method schematized in the previous paragraph. This work would seem to be of interest to us, because it seems to be particularly well adapted to large metallic complexes for which only a semiempirical treatment is possible. In view of this promising field, we briefly present the main steps of this method.

The perturbed orbital, in the presence of an electric field, can be divided into two parts: a nonlocal, or the molecular part, and a local part, which takes into account the effect of the field on the orbital basis itself. For saturated hydrocarbons the contribution due to nonlocal terms is negligible; for unsaturated molecules both local and nonlocal effects are considered. Let us see how these features arise in the method proposed by Musher et al.

The electric polarizability is given by

$$\alpha = -\varepsilon^{-1} \left. \frac{\partial E}{\partial \varepsilon} \right|_{\varepsilon=0} = -2(E_{02} + \lambda E_{12} + \lambda^2 E_{22} + \dots) \quad (2.36)$$



the total Hamiltonian being defined as

$$H = H_0 + \lambda H_1$$

with

$$H_0 = \sum_i h(i)$$

$h(i)$  is the ground-state effective one-electron Hamiltonian (i.e., the Fock operator) and  $H_1$  takes into account the effect of the perturbation. The subscripts in (2.36) correspond to the orders in  $\lambda$  and  $\varepsilon$ , respectively.

In the presence of an external electric field, in the  $x$  direction, for example,  $H_0$  is modified by the perturbing potential acting on particle  $i$ ,

$$\varepsilon H'_1 = \varepsilon \sum_i h'(i) = -\varepsilon \sum_i x(i) \quad (2.37)$$

( $x$  is measured from any convenient, but otherwise arbitrary, point in the molecule; the centroid of the electronic charge may be chosen in the case of a molecule with no dipole moment). The perturbed molecular orbitals  $\varphi'_i$  have to fulfill the set of equations

$$[h(1) - e_i] \varphi'_i(1) = [e'_i - h'(1)] \varphi_i(1) \quad (2.38)$$

$$[h(1) - e_i] \varphi'_i(1) = \sum_n (e'_i + X_n + x_n) c_{in} w_n(1) \quad (2.39)$$

In this last equation, the  $w_n$  functions form an orthonormal set and are the so-called equivalent orbitals, or bonding orbitals. These orbitals are obtained by applying a unitary transformation, belonging to the symmetry group of the molecule, to the occupied orbitals  $\varphi_i$ . The equivalent orbitals are supposed to be well localized<sup>192</sup> in the sense that the exchange integrals between any of them are negligible. Therefore,  $X_n$  is chosen to be the  $x$  component of the vector  $R_n$  taken from the origin to the center of the orbital  $w_n$ . In analogy with the right-hand side of (2.39), one seeks a solution for  $\varphi'_i$ , that breaks down into two parts: a local part  $\eta_i$ , corresponding to  $x_n$ , or the atomic part and a molecular part  $\xi_i$ , corresponding to  $X_n$ ,

$$\varphi'_i = \xi_i + \eta_i \quad (2.40)$$

Each term of  $\varphi'_i$  must fulfill an equation similar to (2.38). The first term,  $\xi_i$ , can best be found accurately by standard variational procedure in which it is expanded in a complete set of functions. In a semiempirical model, however, it is worthwhile to obtain an analytical expression approximating the rigorous solution reasonably well. This is obtained by retaining the leading terms of both sides of (2.38), that is,

$$\sum_{n=1}^m (h_{mn} - e_i \delta_{mn}) b_{in} \approx c_{im} (e_i^* + X_m) \quad m = 1, 2, \dots, M \quad (2.41)$$

( $M$  is the number of equivalent orbitals  $\xi_n$  involved in  $\xi_i$ ) with  $\xi_n \equiv w_n$  for  $n = 1, \dots, M$ .

The previous equation results from the fact that the secular equations of the variational procedure are of the form

$$\sum_{n=1}^{\infty} (h_{mn} - e_i \delta_{mn}) b_{in} = (e_i^{\dagger} + X_m) c_{im} \quad m = 1, 2, \dots \quad (2.42)$$

with

$$\xi_i = \sum_{n=1}^{\infty} b_{in} w_n \quad e_i^{\dagger} = \sum_n c_{in}^2 X_n$$

such that there is no term in  $X_m c_{im}$  for all equations with  $m > M$ . In a first approximation,  $h_{mn}$  can be considered to be small for  $m \leq M$  and  $n > N$  (where  $N$  is a large integer), and therefore  $b_{in}$  is small for  $n > M$  and  $m \leq M$ , which makes possible only the retention of the leading term in the perturbation equations determining the  $b_{in}$  coefficients. This term is the left-hand side of (2.41).

As far as the local contribution  $\eta_i$  is concerned, it may be split into two parts, as one of them is usually small compared to the other (see below)

$$\eta_i = \eta_{i,1} + \eta_{i,2} \quad (2.43)$$

where

$$\eta_{i,1} = \sum_n c_{in} w'_n$$

$w'_n$  is the electric field perturbed atomic orbital solution of

$$\left(-\frac{1}{2}\nabla^2 + V_n - e_n\right)w'_n = x_n w_n \quad (2.44)$$

and  $x_n$  is chosen such that  $\langle w_n | x_n | w_n \rangle = 0$ .

The equation governing the second component  $\eta_{i,2}$  contains the difference between the local potential for the orbital  $w_n$  and the usual self-consistent field potential corresponding to the long-range effects. When acting on an orbital  $w'_n$  localized mainly in the same region as  $w_n$ , it will give only a small value. Another cancellation arises from annihilation among the linear combination of eigenvalues occurring in the perturbation equations, that is,  $(-e'_{i,2} - e_i + e_n)$ . Neglecting the component  $\eta_{i,2}$ , and using orthogonality conditions for the orbitals  $w_n$  and  $w'_n$ ,  $\varphi_i$  and  $\varphi'_i$ , it may be shown that

$$\begin{aligned} E_{02} &= 2 \sum_{i=1}^N \langle \varphi_i | x | \xi_i + \eta_{i,1} \rangle \\ &= 2 \sum_{i=1}^N \sum_{m,n=1}^M [c_{in}^* b_{in} X_n \delta_{mn} + 2c_{in}^* b_{im} \langle w_n | x_n | w_m \rangle + c_{in}^* c_{im} \langle w_n | x_n | w'_m \rangle] \end{aligned} \quad (2.45)$$

The first term in brackets is merely the molecular contribution to the polarizability. The remaining two terms are the local contributions, the latter by assuming localized orbitals, that is

$$\langle w_n | x_n | w_m \rangle = 0 \quad \text{and} \quad \langle w_n | x_n | w'_m \rangle = 0 \quad \text{for} \quad m \neq n$$

simplify to  $2\langle w_n | x_n | w'_n \rangle \sum_{i=1}^N c_{in}^2$  for each orbital  $n$ .

An expression for  $E_{12}$  is similarly obtained, although it is more complicated. A considerable simplification occurs on the grounds of the localized-orbital approximation.

Let us note that the fully coupled Hartree-Fock method would give for the electric polarizability (in the  $x$  direction)

$$\alpha = -4 \sum_{i=1}^n \sum_{p=n+1}^m C_{pi}^{(1)} x_{pi} \quad (2.46)$$

mathematically equivalent to the previous results using the definition of  $\alpha$  (2.36). Musher et al. have calculated the local and molecular contributions in the plane and perpendicular to the plane spanned by the carbons of benzene. The agreement with experiment is fair despite the rather crude approximations used in the numerical computations. It seems to us that there is *a priori* no reason why successful calculations along these lines should not be reached for systems containing heavier atoms as transition metals. Electrical polarizabilities for diatomic systems, such as LiH, HF, F<sub>2</sub>, and HCl, using *ab initio* techniques of calculation in the frame of the coupled Hartree-Fock method have been reported by Lipscomb,<sup>106</sup> Amos et al.,<sup>108</sup> using second-order perturbation theory and localized orbitals derived from the zero-order wave function, report successful *ab initio* results on the polarizabilities of C—H and C—C bonds in CH<sub>4</sub>, C<sub>2</sub>H<sub>6</sub>, C<sub>2</sub>H<sub>4</sub>, and C<sub>2</sub>H<sub>2</sub>. Calculations of electric polarizabilities in a semiempirical framework (CNDO method, see next section) have been recently reported on simple hydrocarbons involving simple, double, and triple bonds,<sup>107</sup> using second-order perturbation theory.

**MAGNETIC SUSCEPTIBILITY  $\chi$ ; MAGNETIC SHIELDING  $\sigma$ .** Several formal methods have been proposed for calculating magnetic susceptibilities and nuclear magnetic shielding constants. Only the methods that utilize gauge-invariant atomic orbitals (GIAO) are independent of the choice of origin of the coordinate system.<sup>110</sup> The usual perturbed Hartree-Fock method, which uses any finite basis set of ordinary atomic orbitals, gives rise to magnetic shielding constants varying linearly with the choice of the origin.<sup>111</sup>

Use of the GIAO was first made by London<sup>112</sup> on problems of molecular diamagnetism in connection with ring currents in aromatic hydrocarbons,

and they have since been used in more general studies of magnetic properties by among others Hameka,<sup>110</sup> Pople,<sup>113</sup> Hall and Hardisson,<sup>114</sup> McWeeny,<sup>116</sup> and Amos and Roberts.<sup>115</sup>

The total Hamiltonian must now include the vector potential at electron  $j$ ,  $\bar{A}(r_j)$  and is defined as

$$\mathcal{H}(\bar{H}, \bar{\mu}_A, \bar{\mu}_B, \dots) = \frac{1}{2} \sum_j \left[ -i\nabla_j + \frac{1}{c} \bar{A}(r_j) \right]^2 + V \quad (2.47)$$

$V$  is the potential-energy term describing electron-nucleus and electron-electron interactions, and  $\bar{\mu}_A, \bar{\mu}_B, \dots$  are fixed nuclear moments on centers A, B, ... in the molecule.

$$\bar{A}(r_j) = \frac{1}{2} \bar{H} \wedge \bar{r}_j + \sum_B \frac{(\bar{\mu}_B \wedge \bar{r}_{jB})}{r_{jB}^3}$$

where  $r_j, R_A, R_B, \dots$  are defined with respect to some arbitrary origin and  $r_{jB} = r_j - R_B$ . The arbitrary choice of the origin of  $r_j$  leads to the gauge problems mentioned above. To ensure gauge invariance within the LCAO approximation, one defines the GIAO

$$\eta_i = \exp \left[ -\left( \frac{i}{c} \right) \bar{A}_i \cdot \bar{r} \right] \chi_i$$

$$\phi_j = \sum_s c_{js} \eta_s \quad (2.48)$$

where  $\bar{A}_i = \frac{1}{2} \bar{H} \wedge \bar{R}_i$  and  $\bar{R}_i$  is the distance vector taken from the arbitrary origin to the nucleus at which  $\eta_i$  is located;  $\chi_i$  is the usual atomic orbital in the absence of a magnetic field.

The molecular magnetic shielding and susceptibility tensors are defined as

$$(\sigma_B)_{\alpha\beta} = \left[ \frac{\partial^2 E(\bar{H}, \bar{\mu})}{\partial H_\alpha \partial \mu_{B\beta}} \right]_{H=\mu=0} \quad (2.49)$$

$$\chi_{\alpha\beta} = -\frac{1}{2} \left[ \frac{\partial^2 E(\bar{H}, \bar{\mu})}{\partial H_\alpha \partial H_\beta} \right]_{H=\mu=0} \quad \alpha, \beta = x, y, z \quad (2.50)$$

where

$$E(\bar{H}, \bar{\mu}_A, \bar{\mu}_B) = 2 \sum_j \sum_{p,q} c_{pj}^* c_{qj} (H_{pq}^{\text{core}} + \frac{1}{2} G_{pq}) \quad (2.51)$$

is the usual Hartree-Fock energy for a closed-shell system. We briefly sketch how to derive the analytical expression for  $(\sigma_B)_{\alpha\beta}$  in a GIAO theory.

Using the orthogonality conditions among the MO's, the first derivative

of the energy with respect to  $H_\alpha$ , reads

$$\frac{\partial E(\bar{H}, \bar{\mu})}{\partial H_\alpha} = \sum_j \sum_{p,q} c_{pj}^* \left[ 2 \frac{\partial}{\partial H_\alpha} (\langle \eta_p | H^{\text{core}} | \eta_q \rangle) + \sum_{r,s} P_{rs} \left( \frac{\partial}{\partial H_\alpha} G_{pqrs} \right) - 2 \frac{\partial S_{pq}}{\partial H_\alpha} e_j \right] c_{qj} \quad (2.52)$$

$$P_{rs} = 2 \sum_j c_{pj}^* c_{qj}$$

Noting that the derivatives of GIAO's with respect to  $\mu_B$  are equal to zero, since the atomic orbitals depend only on the external field  $\bar{H}$ , one gets from the previous equation and the definition of  $(\sigma_B)_{\alpha\beta}$

$$\begin{aligned} (\sigma_B)_{\alpha\beta} &= \sum_{p,q} \left[ P_{pq}(0) \left( \frac{\partial}{\partial H_\alpha} \left\langle \eta_p \left| \frac{\partial H^{\text{core}}}{\partial \mu_{B\beta}} \right| \eta_q \right\rangle \right) + \frac{\partial P_{pq}(H_\alpha)}{\partial H_\alpha} \left\langle \chi_p \left| \frac{\partial H^{\text{core}}}{\partial \mu_{B\beta}} \right| \chi_q \right\rangle \right] \\ &= \frac{1}{2c^2} \sum_{p,q} \left[ P_{pq}(0) \left\langle \chi_p \left| \frac{\bar{r}_B \cdot \bar{r}_q \delta_{\alpha\beta} - r_{B\alpha} r_{q\beta}}{r_B^3} \right| \chi_q \right\rangle \right. \\ &\quad \left. + P_{pq}(0) \left( \left\langle \frac{\partial \eta_p}{\partial H_\alpha} \left| \frac{L_{B\beta}}{r_B^3} \right| \chi_q \right\rangle + \left\langle \chi_p \left| \frac{L_{B\beta}}{r_B^3} \right| \frac{\partial \eta_q}{\partial H_\alpha} \right\rangle \right) \right. \\ &\quad \left. + \frac{\partial P_{pq}(H_\alpha)}{\partial H_\alpha} \left\langle \chi_p \left| \frac{L_{B\beta}}{r_B^3} \right| \chi_q \right\rangle \right] \quad \beta, \alpha = x, y, z \quad (2.53) \end{aligned}$$

with  $\bar{r}_q = \bar{r} - \bar{R}_q$ . All derivatives are taken at the limit  $\bar{H} = \bar{\mu}_B = 0$ . The first term is the diamagnetic contribution to  $(\sigma_B)_{\alpha\beta}$  depending on the unperturbed orbitals  $\chi$ ; the second and third terms are the paramagnetic contributions depending on the perturbed wave function. The derivatives  $\partial P_{pq}/\partial H_\alpha$  may be calculated numerically,<sup>117</sup> retaining only the first power terms in  $H_\alpha$  in the Fock matrix elements  $F_{pq}$ . This means

$$\int \eta_p^* \eta_q d\tau = \int \chi_p^* \chi_q d\tau - \frac{i}{2c} \left[ \bar{H} \wedge \bar{R}_p \cdot \bar{R}_q \int \chi_p^* \chi_q d\tau - \bar{H} \wedge R_{pq} \int \chi_p^* \bar{r}_p \chi_q d\tau \right] \quad (2.54)$$

No *ab initio* or semiempirical MO calculations of magnetic shielding or susceptibility seem to have been carried out on transition-metal complexes. An interesting case is the biatomic molecule AlH treated by Laws et al.,<sup>118</sup> where use is made of the coupled Hartree-Fock theory for determining the shielding  $\sigma$  and the magnetic susceptibility  $\chi$ . No experimental data are known for this molecule. The zero-order basis sets (Slater functions) were taken up from Cade and Huo.<sup>119</sup> The calculations assume a gauge origin at the

electronic centroid. Table V summarizes some of the results of Laws for the susceptibility.

TABLE V  
Magnetic Susceptibilities (ppm) of  
AlH<sup>118</sup> (gauge  
origin at electronic  
centroid)<sup>a</sup>

$\chi$	-1.37
$\chi^p$	32.56
$\chi^d$	-33.93
$\chi_{  }$	-21.87
$\chi_{\perp}$	9.17

<sup>a</sup> $\chi^p$  = paramagnetic part of  $\chi$ ;  $\chi^d$  = diamagnetic part of  $\chi$ ;  $\chi_{||}$ ,  $\chi_{\perp}$  = components of  $\chi$  parallel and perpendicular, respectively, to the external field.

The theoretical predictions are such that the paramagnetic and diamagnetic part of the susceptibility are great quantities that compensate each other. The experimental finding of a very small total susceptibility in AlH would provide strong evidence of the temperature-independent paramagnetism (remember that AlH is a closed-shell system) expected for the perpendicular component. Using GIAO's, Ditchfield<sup>121,120</sup> performed successful calculations for the total magnetic shielding and susceptibility of LiH and HF, using a Gaussian fit of the basis set (Slater orbitals) given by Ransil.<sup>122</sup>

Arrighini et al.<sup>123,111</sup> have computed within the coupled Hartree-Fock method, the magnetic susceptibilities for H<sub>2</sub>O, NH<sub>3</sub>, CH<sub>4</sub>, and H<sub>2</sub>O<sub>2</sub> and proton shielding constants in H<sub>2</sub>O, NH<sub>3</sub>, CH<sub>4</sub>, and CH<sub>3</sub>F. Some gauge dependence of the total susceptibility and shielding is present as a consequence of the necessarily limited basis set used. Karplus and Kolker<sup>124</sup> have developed a particular variation-perturbation method in which the first-order correction to the unperturbed wave function depends on a purely imaginary polynomial in suitable powers of  $x$ ,  $y$ ,  $z$ , avoiding the infinite summation upon excited states. Applied to simple biatomic systems such as H<sub>2</sub>, Li<sub>2</sub>, F<sub>2</sub>, CO, HF, LiH, this method is able to produce reliable results for the observed total susceptibilities. The magnetic anisotropies, however,  $\Delta\chi = \chi_{\perp} - \chi_{||}$  show rather large discrepancies (except in the case of H<sub>2</sub>),

which are overcome, as usual, by including the observed rotational magnetic moments in the evaluation of the paramagnetic susceptibilities.

There exists, of course, a vast amount of shielding semiempirical calculations in the case of medium-sized and large molecules. As an illustrative example, it is worth noting the  $^{13}\text{C}$  nuclear shieldings extensively tabulated by Ellis et al.<sup>125</sup> for olefinic and saturated hydrocarbons. They use the INDO approximation (see next section) for building up the molecular orbitals as well as GIAO's. It is necessary to adopt a new set of INDO parameters to obtain a reasonable agreement with experimental values. The tedious algebra inherent in this calculation is considerably reduced in a semiempirical framework, since  $(\sigma_M)_{\alpha\beta} - \alpha, \beta \equiv x, y, z$ —reduces to mono- and biatomic terms,

$$(\sigma_M)_{\alpha,\beta} = \sigma_{\alpha\beta}^d(M, M) + \sigma_{\alpha\beta}^p(M, M) + \sum_{K \neq M} [\sigma_{\alpha\beta}^d(M, K) + \sigma_{\alpha\beta}^p(M, K)] \quad (2.55)$$

the dominating terms being, in general, the monocentric ones.

Fluorine shielding constants in large organic systems have been the subject of numerous semiempirical calculations. In this respect, let us mention a very popular relation<sup>126</sup> linking the magnetic shielding and the charge density at a definite nucleus

$$\sigma_{\text{loc}}^p = -\frac{\mu_0}{4\pi} \frac{\hbar^2 e^2}{2m^2} \frac{1}{\Delta E} \langle r^{-3} \rangle_{np} \sum_B Q_{NB} \quad (2.56)$$

where loc = local; superscript  $p$  = paramagnetic part.

In this expression the distance  $\langle r^{-3} \rangle_{np}$  (for  $np$  valence shell orbitals) is taken from the nucleus N.  $\Delta E$  is a mean excitation energy, usually set equal to 10 eV for organic molecules, necessarily introduced owing to our present ignorance of excited-state wave functions;  $Q_{NB}$  accounts for the amount of unbalance in the orbital populations about the nucleus (zero for spherical symmetry). This relation is usually employed in conjunction with shielding changes at a nucleus N due to different substituents involved in a series of closely related compounds. The trend in the observed chemical shift is often qualitatively predicted as shown, for example, by Emsley.<sup>127</sup>

Actual mechanisms that contribute to  $\sigma_{\text{loc}}^p$  are electric field effects, van der Waals interactions, steric effects, both denominated as "through space effects." An approximate relation for the local diamagnetic part of  $\sigma$  is also frequently used.<sup>126</sup> The actual mechanisms that contribute the latter include inductive effects and intramolecular hydrogen bondings, both denominated as "through bond effects." Obviously, we cannot, in the scope of this review, enter into these considerations, but refer the reader to the Specialist Periodical Reports<sup>128</sup> (*Nuclear Magnetic Resonance*) for a general survey on these matters.

INDIRECT NUCLEAR SPIN-SPIN COUPLING  $J$ . The calculation and interpretation of indirect nuclear spin-spin coupling is based on the fundamental work of Ramsey,<sup>129</sup> according to which the perturbed Hamiltonian corresponding to the energy of electron-coupled spin-spin interactions of two nuclei A and B can be partitioned into three terms. The first one, and usually the largest in magnitude in the case of protons, is the contact term or the Fermi contact term. The second is the magnetic dipole-dipole interaction between nuclear and electron magnetic moments. The last term, that is, the so-called orbital term, describes the interaction between the magnetic field due to the electron orbital motion and the nuclear magnetic moment. A standard problem in the perturbation formula concerns the evaluation of the energy denominator in the second-order terms involving an infinite summation over excited states, including those of the continuum. Initially one has tried to circumvent this difficulty by introducing an empirical parameter, that is, an "average energy" for the quantity  $\sum_n^{\infty} (E_0 - E_n)^{-1}$  [see also (2.56)] and by then applying the closure theorem. The resulting matrix element contains the square of the perturbation operator, preventing a negative sign for  $J$ . The latter is nevertheless often experimentally observed.

Two methods are currently used to avoid the use of this empirical procedure and still circumvent the "infinite summation problem." One way consists of using the zero-order wave function in the absence of any perturbation; the other uses the SCF perturbed wave functions corresponding to a finite perturbing field (magnetic or electric field). The first method corresponds to the well-known coupled Hartree-Fock method<sup>106</sup>: one has to solve a set of coupled non-linear equations for determining the expansion coefficients, usually by use of an iterative process [see, for example, (2.32)]. In the second method the first-order wave function is calculated, for a finite value of the perturbing field,<sup>130</sup> by actual differentiation. Obviously, the two methods should give completely equivalent results.

We now discuss the *contact-term contribution* of the *indirect hyperfine interaction*. According to the Ramsey perturbation formula, the  $J$  coupling parameter has the following form

$$J_{X-Y} = A_{XY} \sum_k \frac{\int \psi_0^* \Theta(X) \psi_k d\tau \int \psi_k^* \Theta(Y) \psi_0 d\tau}{E_0 - E_k} \quad (2.57)$$

$A_{XY}$  is a constant depending on both the nature of the nuclei X and Y and of the units.  $\psi_0$  and  $\psi_k$  represent the total electronic wave functions for the ground state and the  $k$ th excited state of the molecule.  $\Theta(X)$  and  $\Theta(Y)$  are the perturbation operators corresponding to nuclei X and Y.



The monoelectronic contact or Fermi operators assume the following form

$$\begin{aligned}\Theta(X) &= \sum_{\mu} \delta(\bar{r}_{\mu X}) \bar{s}_{\mu} \\ \Theta(Y) &= \sum_{\nu} \delta(\bar{r}_{\nu Y}) \bar{s}_{\nu}\end{aligned}\quad (2.58)$$

where the summation signs run over all electrons  $\mu$  and  $\nu$ . The relation governing  $J_{XY}$  (supposing for the sake of simplicity the contact operators to be involved) has been analyzed in terms of symmetry components using the Wigner-Eckart theorem.<sup>131</sup> One can indeed define "normal" coupling constants using, on the one hand, symmetry-adapted vectors,  $\bar{X}_{lm}$ , belonging to the different irreducible representations of the point group of the molecule and, on the other hand, irreducible tensorial operators,  $\Theta_{lm}^*$ , characteristic of the molecular symmetry as well as of the sets of atoms X and Y. The vectors  $\bar{X}_{lm}$  are linear combinations of equivalent nuclei sets obtained by the well-known projection operator technique. It appears that these normal coupling constants are themselves linear combinations of internal coupling constants, characteristic of the individual nuclei. Inversely, a specific internal coupling constant  $J_{X_i-Y_i}$  is expressible as linear combination of symmetry-adapted, that is, normal coupling constants.

It should be added that it is necessary to give a definite value to the so-called "self-coupling constant" of the proton to evaluate a set of normal coupling constants for hydrogens. This quantity is not observable in molecules using nuclear spin-spin experiments but is known for the hydrogen atom.<sup>195</sup> If, however, a nonsingular operator is used instead of the standard Fermi contact term, the self-coupling constant  $J_{HH}$  can be calculated by variational methods<sup>196,197</sup> and a very much larger value is obtained for  $J_{HH}$  as compared to the actual  $J_{HH}$  measured in molecules, that is  $-0.291 \times 10^7$  Hz for  $H_2$ .

Molecular orbital calculations of nuclear coupling constants on systems involving transition-metal atoms have never been undertaken so far. However, many calculations have been reported for nuclei such as  $^1H$ ,  $^{13}C$ ,  $^{31}P$ ,  $^{15}N$ ,  $^{29}S$ ,  $^{11}B$ , and  $^{19}F$ , directly bonded or not, belonging to closed-shell molecules,<sup>128</sup> that is, involving triplet excited-state configurations. For electronic configurations of this type and within the assumptions involved in our semiempirical model calculation, we want to point out the rather elegant analytical expression one gets for  $J_{X-Y}$ . In the first place, note that as the operators  $\Theta(X)$  and  $\Theta(Y)$  are monoelectronic, (2.57) reduces to

$$J_{X-Y} = A'_{XY} \sum_{i,j} \frac{\int \varphi_i^*(\mu) \delta(\bar{r}_{\mu X}) \varphi_j(\mu) d\tau_{\mu} \int \varphi_j^*(\nu) \delta(\bar{r}_{\nu Y}) \varphi_i(\nu) d\tau_{\nu}}{E_0 - E_{ij}} \quad (2.59)$$

where  $\varphi_i$  and  $\varphi_j$  are the molecular orbitals pertaining to closed- and open-shell Slater determinants.  $E_{ij}$  is the energy of one of the triplet states  $\psi_k$ .  $A'_{XY}$  is a constant depending on the nuclei X and Y as well as of the units.

With a view to introducing the bicentric overlap integrals consistently, which is not generally the case,<sup>132</sup> use is made of the Ruedenberg expansion<sup>133</sup> of an atomic orbital centered on any atom in the molecule as a function of those centered on atom X. Furthermore, this expansion is limited to the linear terms in the overlap integrals. If one just retains the leading term, corresponding to orbitals of the same species, that is, two (2s), two (3s), and so on, the following approximate and rather elegant expression is found.<sup>131</sup>

$$J_{X-Y} = A'_{XY} \sum_{i,j} \frac{(c_{Xi}d_{Yi} + c_{Yi}d_{Xi})(c_{Xj}d_{Yj} + c_{Yj}d_{Xj})}{4(e_i - e_j + J_{ij})} \chi_X^2(X) \chi_Y^2(Y) \quad (2.60)$$

The denominator of this expression is the familiar Hartree-Fock singlet-triplet energy difference.  $c$  and  $d$  are, respectively, the covariant and contravariant coefficients to be associated with the LCAO-MO expansion, according to Chirgwin and Coulson [see Section II.B (2.2)].

As applications of the above relation, we should like to mention the work of Barbier et al.<sup>131</sup> on  $J_{H-H}$  and  $J_{13C-H}$  between atoms directly bonded, or not, in ethane, acetylene, methane and ethylene, using *ab initio* zero-order wave functions. The first set of results<sup>131</sup> is moderately successful, tending to emphasize that electronic correlation effects may be important. Barbier et al.<sup>134</sup> find indeed, using a minimal basis-set wave function and the usual second-order perturbation theory, a value of  $-1.27$  Hz for the geminal (H, H) coupling in methane (experimental value =  $-12.4$  Hz). The agreement with experiment is much improved, that is,  $-15.02$  Hz, if third-order contributions, which arise from correlation effects, are included. Since the contact-operator elements are very small unless both orbitals involved are localized on the same atom, the interpretation of the results is facilitated by carrying out the calculations in terms of localized MO's. In this way it may be shown that a one-electron SCF model cannot account for the rather large coupling constants  $J_{HH}$  observed between geminal protons.

Correlation effects and use of quasilocated orbitals have also been emphasized by Denis et al.<sup>135</sup> in a double-perturbation theory calculation of the coupling constants in some simple hydrocarbons. The wave functions used by Denis et al. are semiempirical, that is of the CNDO-type (see next section).

When all integrals appearing in the numerator of (2.59) are calculated, using the best available LCAO-SCF wave functions,<sup>136</sup> a rather tangible improvement of the results is achieved.<sup>137</sup> It is clearly evident that the contact interactions are very sensitive to a slight variation of the hydrogen orbital exponent, justifying the use of very good *ab initio* wave functions. Recently,

Barbier et al.,<sup>139</sup> using the double-perturbation technique (contact term and electronic correlation) and quasilocalized orbitals,<sup>192</sup> have derived the dependence of geminal spin-spin nuclear coupling constants in saturated compounds with respect to nuclear positions, bond angles, and substituent effects. Their results show that the use of a large atomic basis (Slater type), allowing in particular a variation of the hydrogen orbital exponent relative to a minimal basis set, is not really decisive for approximating the observation more closely. A comprehensive review on the analysis of NMR and EPR coupling constants (Fermi contact term contribution only) using localized orbitals and the double perturbation theory (see Section II.D.2.b) is presented by Ellinger et al.<sup>193</sup> The emphasis is placed upon NMR coupling between protons (geminal, vicinal, and long-range coupling constants).

In general the *dipolar and orbital contributions* to the *indirect hyperfine interactions* are smaller than those considered previously. The molecular orbital formulation in an approximate framework leads to analytical relations quite analogous to (2.60). In this respect, as shown by Barbier et al.,<sup>138</sup> the results of these observable calculations are significant only if use is made of the best available molecular wave functions, since their orders of magnitude, at least for simple organic molecules, are about one-tenth of the contact contributions (i.e., 1 eV). However, dipolar and orbital contributions might be important for coupling constants involving heavy atoms as is the case, for instance, for <sup>31</sup>P.<sup>198</sup>

**ANISOTROPIC HYPERFINE INTERACTIONS.** These types of observables arise from the anisotropies of both the shielding constant and the indirect nuclear spin-spin coupling. These anisotropies have been detected experimentally by NMR studies on nematic crystals where the probe molecules are partially oriented with respect to the applied field.<sup>140</sup> Typical molecules are CH<sub>3</sub><sup>19</sup>F, CH<sup>19</sup>F<sub>3</sub>, <sup>13</sup>CH<sub>3</sub>CN, and <sup>13</sup>CH<sub>3</sub>I.

The Hamiltonian for a set of spin  $\frac{1}{2}$  nuclei that are partially oriented with respect to a strong applied field, that is, they are tumbling anisotropically, is given by<sup>141</sup>

$$\langle \mathcal{H} \rangle = -\frac{H_a}{2\pi} \sum_i \gamma_i (\delta_{\alpha\beta} - \langle \sigma_{\alpha\beta} \rangle) I_{\beta i} + \sum_{i < j} (\langle T_{\alpha\beta ij} \rangle + J_{\alpha\beta ij}) \times I_{\alpha i} I_{\beta j} \quad (2.61)$$

$T_{\alpha\beta ij}$  is the direct nuclear dipole-dipole coupling tensor for nuclei  $i$  and  $j$ , whereas  $J_{\alpha\beta ij}$  is the indirect nuclear spin-spin coupling tensor, arising from electron spin and orbital motion.  $\alpha, \beta$  are the Cartesian coordinates ( $x, y, z$ ). The angle brackets denote average values of the quantities referred to space-fixed axes. The other symbols retain their usual meanings.

The nematic solvent is responsible for a constraint upon the probe molecule, resulting in an average anisotropic tumbling of the latter. It is usually

characterized by a parameter  $S_{\alpha\beta} = \frac{1}{2}(\langle 3 \cos \Theta_\alpha \cos \Theta_\beta \rangle - \delta_{\alpha\beta})$ , that is, the average orientation of the molecular axis with respect to the applied field.

As an illustrative example, we quote the papers of Morishima et al.<sup>142,143</sup> devoted to the calculation of the  $^{13}\text{C}$  anisotropic shielding constant in  $^{13}\text{CH}_3\text{I}$  and  $^{13}\text{CH}_3\text{CN}$ . The paramagnetic contribution of the shielding constant is computed by the method of Pople assuming an average excitation energy  $\Delta E$  equal to 10 eV [see (2.56)] and the  $\sigma$ 's anisotropy  $\Delta\sigma(\text{C}) = \sigma_{\parallel} - \sigma_{\perp}$  thereby derived. For  $\text{CH}_3\text{CN}$ , a qualitative agreement is reached, whereas the MO approach fails to reproduce the  $\Delta\sigma(\text{C})$  for  $\text{CH}_3\text{I}$ . Heavy-atom effects do alter the chemical shift because of the large spin-orbit interaction. A perturbation treatment involving this contribution brings a moderate agreement between the experimental and theoretical  $\Delta\sigma(\text{C})$  values.

### **b. Open-Shell Systems. *First- and Second-Order Properties.***

**PRELIMINARIES.** The observables described up to now are mainly calculated for closed-shell systems. However, there is no harm whatsoever in performing these calculations for open-shell systems. For example, indirect nuclear hyperfine coupling constants, as well as magnetic shieldings, have been derived for organic radicals. However, characteristic properties for a certain class of open-shell systems, that is, transition-metal complexes, have been subjected during the past decade to intensive experimental investigations. In the meantime, theoretical methods have been considerably developed predicting, often with great precision, the experimental observation.

The experimental parameters in which we are interested originate from the phenomenological spin-Hamiltonian developed by Abragam et al.<sup>71</sup> In nearly all cases it appears that the fine and hyperfine structure of molecular energy levels may be calculated using a basis of pure spin states, describing the total electron spin and all possible allocations of nuclear spins, both embedded in a spin-Hamiltonian. This formalism, aside from electron and nuclear spin operators, involves a set of parameters describing phenomenologically the strengths of coupling of the spins with each other and with the external field. In this framework one defines an effective electronic spin, usually associated with the unperturbed electronic ground state of the Hamiltonian operator, that is equal to the total electronic spin of the actual system including an infinite number of electronic states. By means of the spin Hamiltonian concept, the solution of a quantum-mechanical problem of great complexity, with a full Hamiltonian for all electrons and nuclei, is replaced by a relatively simple spin problem, containing a few spin-state functions, in which the fundamental theory has been absorbed into a set of parameters.

**THE HAMILTONIAN.** In quantum-mechanical language, the spin-Hamiltonian is a device that allows us to reproduce, using a basis of pure spin

functions, the results of a standard configuration interaction calculation to a given order of perturbation theory. One can write, indeed,

$$\mathcal{H} = \mathcal{H}_0 + \mathcal{H}'$$

where

$$\mathcal{H}' = H_{\text{ext}} + H_{SL} + H_{SS} + H_Z + H_N$$

where  $\mathcal{H}_0$  = molecular Hamiltonian excluding applied fields and all spin-dependent terms

$H_{\text{ext}}$  = potential energy arising from electrostatic environment effects

$H_{SL}$  = spin-orbit coupling terms

$H_{SS}$  = electron spin-spin coupling terms

$H_Z$  = Zeeman and other magnetic field terms (electronic)

$H_N$  = terms containing nuclear spins.

The analytical forms of these terms may be found in textbooks, for example in the treatise of Bethe and Salpeter.<sup>144</sup>

Owing to its application in resonance experiments, the spin-Hamiltonian assumes the following form (in standard notations)

$$\mathcal{H}_S = \bar{H} \cdot \bar{g} \cdot \bar{S} + \bar{S} \cdot \bar{D} \cdot \bar{S} + \bar{S} \cdot \bar{T} \cdot \bar{T} + \bar{T} \bar{P} \cdot \bar{T} - g_I \beta_N \bar{I} \cdot \bar{H}$$

where  $\bar{g}$ ,  $\bar{D}$ ,  $\bar{T}$ ,  $\bar{P}$  are second-order tensors related to the spatial part of the electronic ground-state wave function.

In the following text we mainly describe and comment in some detail on our molecular-orbital calculations of the following spin-Hamiltonian parameters:

1. Isotropic part of the hyperfine interactions,  $T_{\text{iso}} \equiv F$ , or the Fermi contact term.
2. Electronic gyromagnetic factor or the  $g$  tensor components occurring in the Zeeman term.
3. Spin-spin dipolar interactions  $D_{SS}^{zz}$ , contributing the zero-field splitting tensor  $D^{zz}$ .

The probe molecules are transition-metal complexes.

**FIRST-ORDER ONE-ELECTRON PROPERTIES.** The *Fermi contact term*  $F$  (*isotropic hyperfine interaction term*) may be defined as

$$F = \frac{8}{3} \pi g_M \beta_N I_M D_S(aa|r_M)$$

$D_S(aa|r_M)$  denotes the electronic spin density at the position of the transition metal nucleus  $M$ , the other symbols being defined as usual.

Although this term is not directly accessible to ESR experimental observation, it can nevertheless be derived from the measurements of the hyperfine parameters  $T_{\perp}$  and  $T_{\parallel}$  on paramagnetic crystals assuming an axial symmetry field around the paramagnetic center, that is the transition metal ion.  $T_{\parallel}$  denotes the  $T_{zz}$  component of the second-order tensor for which the  $z$  principal direction is chosen to coincide with the principal symmetry axis of the crystal;  $T_{\perp}$  denotes the  $T_{xx}$ ,  $T_{yy}$  components.

The ion  $\text{Cu}^{2+}$  embedded in an ammonium chloride lattice is one of the favorite systems for experimental studies<sup>145</sup> by means of resonance techniques (EPR, spinecho, etc.) in connection with the study of phase transitions, that is, the so-called  $T_{\lambda}$  transition.<sup>146</sup> We have also considered the case of the ion  $\text{Mn}^{2+}$  embedded in the lattice  $\text{NH}_4\text{Cl}$ , a well-known system in ESR measurements too.<sup>149,150</sup> From the EPR spectra, obtained in a large temperature scale, it appears that an axial field spin-Hamiltonian corresponding to the square-planar sublattice  $\text{CuCl}_4^{2-}(D_{4h})$  can adequately represent most features of the hyperfine spectra<sup>73</sup> (see also Section II.C.4). Table VI summarizes the "observed"  $F$  values, deduced from the  $T_{\parallel}$ ,  $T_{\perp}$  measurements, as a function of the ratio  $T_{\parallel}/T_{\perp}$  and according to the possible symmetry species of the electronic ground state. Neither the sign of the ratio  $T_{\parallel}/T_{\perp}$ , nor the ground-state symmetry can be unambiguously determined experimentally, using the standard crystal-field approach.<sup>73,147,145</sup> In view of these uncertainties, two basic spatial models for each system,  $\text{CuCl}_4^{2-}$  and  $\text{MnCl}_4^{2-}$ , are considered in the  $F$  theoretical calculation.

TABLE VI  
F Values (gauss) at 77°K for  $\text{NH}_4\text{Cl}$  Doped with  
 $\text{Cu}^{2+73}$

	$A_{1g}$		$B_{1g}$	
	$T_{\parallel}/T_{\perp} > 0$	$T_{\parallel}/T_{\perp} < 0$	$T_{\parallel}/T_{\perp} > 0$	$T_{\parallel}/T_{\perp} < 0$
F	+81.2	-40.8	-151.2	-82.5

In the first one, a square-planar model ( $D_{4h}$ ), the transition metal is placed at the center of a square spanned by the chlorine atoms. The interatomic distance  $R(\text{M}-\text{Cl}) = 2.749 \text{ \AA}$  is deduced from the size of the unit cell in  $\text{NH}_4\text{Cl}$ . The second one is a pyramidal model, the transition-metal being moved out of the chlorine's plane at a distance  $\frac{1}{2}R(\text{Cl}-\text{Cl}) = 1.944 \text{ \AA}$ .

The central problem of deriving the spin density at the copper nucleus can be worked out in two different ways. First, it is possible to use the coefficients arising from a restricted Hartree-Fock (RHF) calculation (Section I.F), where the contribution to the observable may be limited to the 4s atomic orbital or, alternatively, computed from the full nonorthogonal basis set. In either case the spin density at the transition metal nucleus is found negligible, the apparent reason being that the highest filled MO has a prominent *d* character and practically no *s* character, as later confirmed by an *ab initio* calculation.<sup>86</sup> Second, it is possible to choose an unrestricted Hartree-Fock model (see Section I.F.4) involving different space orbitals for different spins. Table VII summarizes the results<sup>148</sup> obtained in this way. The theoretical spin densities give a very good estimate of the contact terms *F* corresponding to  $\text{CuCl}_4^{2-}$  and  $\text{MnCl}_4^{2-}$  in the case of planar geometry. For  $\text{CuCl}_4^{2-}$  it is seen from Tables VI and VII, that the theoretical results strongly support a

TABLE VII  
Spin Densities and Fermi Contact Term Values in the Systems  
 $\text{CuCl}_4^{2-}$  and  $\text{MnCl}_4^{2-}$  According to UHF-MO<sup>148</sup> Scheme

Metal M	$I_M$	$g_M$	Spin densities at M ( $\text{cm}^{-3}$ )		Fermi contact term (gauss)		
			Planar sq.	pyramidal	Theoretical		Experimental
					Planar sq.	pyramidal	
Cu	$\frac{3}{2}$	1.4809	-0.2387	+0.12356	-151	+773	-151.2 <sup>a</sup>
Mn	$\frac{5}{2}$	1.384	-1.10311	-0.85660	-100	-835.5	-83; -88 <sup>b</sup>

<sup>a</sup>Taken from Table VI for  $B_{1g}$  and  $T_{//}/T_{\perp} > 0$ .

<sup>b</sup>The value -83 refers to a square planar model as proposed by Reed<sup>149</sup>; the value -88 refers to a pyramidal model proposed by Forman et al.<sup>150</sup>

ratio of  $T_{//}/T_{\perp} > 0$  as well as a  $B_{1g}$  ground state. The hypothesis of a sharp pyramidal complex is equally improbable for  $\text{CuCl}_4^{2-}$ , as well as for  $\text{MnCl}_4^{2-}$ , on the grounds of the great difference between "observed" and theoretical *F* values. A restricted Hartree-Fock *ab initio* calculation<sup>151</sup> on  $\text{CuCl}_4^{2-}$  ground state would tend to predict a flat tetrahedron obeying the  $D_{2d}$  symmetry, but no magnetic observable has been tentatively calculated with this wave function.

As is well known, the UHF wave function is not an eigenfunction of  $S^2$ .

Starting from the spin densities previously obtained and using the projection operator technique proposed by Amos et al.,<sup>152</sup> it is easy to annihilate the major contribution of the spin-multiplet's contamination, that is, the spin multiplet  $S+1$  ( $S=\frac{1}{2}$ ). This dramatically reduces the spin densities reported in Table VII. It is however, well known<sup>153</sup> that it is a poor approximation to project from the wave function the unwanted parts *after* having achieved self-consistency. It should be added that our problem is closely related to an atomic problem, as we are interested in the spin density at the metal nucleus; Bagus<sup>154</sup> reports a good agreement between the theoretical and experimental values for atomic transition metal spin densities in the UHF scheme, *without* using any projection operator technique. Watson et al.<sup>155</sup> have also used the spin densities directly issued from the UHF wave function for calculating some Fermi contact terms in transition metal atoms and the agreement with experimental values is fair.

As a last example we mention the *ab initio* UHF and RHF calculation on the cluster  $\text{NiF}_6^{4-}$  (see also next paragraph), using a basis of Gaussian orbitals.<sup>156</sup> The fluorine Fermi contact terms are calculated by both methods, in good agreement with the experimentally derived values:

$$F^{\text{RHF}} = 26.84 \cdot 10^4 \text{ cm}^{-1}; \quad F^{\text{UHF}} = 32.82 \cdot 10^4 \text{ cm}^{-1}; \\ F^{\text{exp}} = 33.91 \cdot 10^4 \text{ cm}^{-1}$$

No spin-projection-operator technique is utilized either.

We now discuss the calculation of the *total tensorial components*,  $T_{\parallel}$ ,  $T_{\perp}$  including their *anisotropic parts*  $A$ . A few papers have been devoted to the calculation of the matrix elements of the tensorial operator

$$A = \frac{3\bar{r}\bar{r} - r^2 \cdot \bar{i}}{r^5}$$

It is worthwhile mentioning the work of Ellis et al.<sup>157</sup> and that of Moskowitz et al.,<sup>156</sup> undertaken on the antiferromagnetic salt  $\text{KNiF}_3$ , with a view to elucidating some magnetic and optical properties of this crystal. The latter properties are related to the so-called "10Dq problem" treated in Section IV. These authors use the cluster approximation  $\text{Ni}^{2+}\text{F}_6^-$  or  $\text{NiF}_6^{4-}$  for determining the fluorine-transferred hyperfine interactions, that is the interaction of the delocalized electrons with the fluorine nuclei, besides the usual interactions with the metal nucleus. The fluorine anisotropic hyperfine tensorial components quantized along the molecular axis of symmetry  $T_{\parallel}$ , are derived using the RHF and the UHF wave function.

The results found by Moskowitz et al. are relatively good<sup>156</sup>:

$$T_{\parallel}^{\text{RHF}} = 10.29 \cdot 10^4 \text{ cm}^{-1}; \quad T_{\parallel}^{\text{UHF}} = 13.56 \cdot 10^4 \text{ cm}^{-1}; \quad T_{\parallel}^{\text{exp}} = 8.8 \times 10^4 \text{ cm}^{-1}$$



The authors also considered the linear  $\text{Ni}_2\text{F}^{3+}$  cluster, representing a different partitioning of the lattice, to make a comparison with the work of Ellis,<sup>157</sup> involving a special one-center expansion of Slater-type orbitals. Their final value for  $T$  is almost comparable to that of Ellis et al., although their UHF wave function is theoretically better, involving a much larger basis set where all types of integrals are calculated with an optimum accuracy.

**SECOND-ORDER ONE-ELECTRON PROPERTIES.** We now discuss the calculation of the  $g$  tensor components and their use in the case of the  $\text{CuCl}_4 \cdot 2\text{NH}_3(\text{C}_{2h})$  cluster.<sup>159</sup> Longuet-Higgins et al.<sup>158</sup> made, apparently for the first time, an actual MO estimation of the electronic gyromagnetic factor  $g$  in the system  $(\text{C}_5\text{H}_5)_3\text{Ni}_3(\text{CO})_2$ . This derivation is in a sense formal, as they do not numerically derive within the Hartree-Fock formalism the molecular orbital coefficients with which the  $g$  values are to be calculated. They used, moreover, crystal-field parameters, such as the atomic spin-orbit coupling constant and spectroscopic absorption energies, for the evaluation of the energy denominator appearing in the  $g$  expression (see below). Only the angular momentum monocentric diagonal elements relative to the atomic basis set are considered.

The procedure described here is not only completely free from crystal-field parameters, but it involves the computation of the relevant LCAO molecular angular momentum integrals, including the multicenter ones, whereas the energy denominators are expressed according to the Hartree-Fock procedure. No other work on transition-metal complexes seems to have been reported using equivalent approximations for the case of  $g$ -component evaluations.

The relations governing the  $g$  tensor components have been derived by Stone<sup>160</sup> up to the second order of perturbation theory, using the Dirac wave equation, which makes the derivation of a gauge invariant  $g$  tensor theory particularly convenient and directly applicable to molecules. The  $g$  relation quoted by Abragam<sup>71</sup> in his standard paper is not gauge invariant, and thus raises serious problems when applied to molecules.<sup>158</sup>

Using Stone's notations, the  $g^{a\beta}$  components read ( $\alpha, \beta = x, y, z$ , cyclic)

$$g^{a\beta} = 2 + \left(\frac{m}{h^2}\right) \left\langle \psi_0 \left| \sum_k (\alpha_k^2 + \beta_k^2) \xi_k(r_k) \right| \psi_0 \right\rangle + 2 \sum_{n \neq 0} \sum_k \frac{\langle \psi_0 | L_k^a | \psi_n \rangle \langle \psi_n | \xi_k(r_k) L_k^\beta | \psi_0 \rangle}{\epsilon_0 - \epsilon_n} \quad (2.62)$$

$\psi_0$  and  $\psi_n$  represent Slater determinants for the ground and excited states of the system, respectively;  $\alpha_k, \beta_k$  are the coordinates of the atom  $k$ ;  $\xi_k(r_k)$  is some function of the distance from the nucleus  $k$  occurring in the atomic spin-orbit coupling constant.  $L_k^a$  is the  $a$  component of the angular momentum operator centered on  $k$ . The second term, which is missing in the Abragam<sup>71</sup> standard

formula and which makes the above equation gauge invariant, is numerically negligible compared to the last one. In our semiempirical framework we have neglected this term. The molecular spin-orbit coupling constant  $\sum_k \xi_k$  has been calculated according to the Mulliken proposal,<sup>161</sup> that is,

$$\lambda^{(j)} \equiv \sum_k {}^{(j)}\xi_k = \sum_k {}^{(j)}n_k^{(j)} [ |q_k^{(j)}| a'_k + (1 - |q_k^{(j)}|) a_k ]$$

such that (2.62) now reads

$$g^{\alpha\beta} = 2 \left\{ \delta^{\alpha\beta} + \sum_n \sum_k {}^{(j)}n_k^{(j)} [ |q_k^{(j)}| a'_k + (1 - |q_k^{(j)}|) a_k ] \times \frac{\langle \psi_0 | L_k^\alpha | \psi_n \rangle \langle \psi_n | L_k^\beta | \psi_0 \rangle}{(\varepsilon_0 - \varepsilon_n)} \right\} \quad (2.63)$$

and the integrands no longer depend on the atomic spin-orbit constant.  $n_k^j$  and  $q_k^j$  are, respectively, the partial atomic population corresponding to the unpaired molecular orbitals and the net atomic charge.  $a'_k$  and  $a_k$  are the atomic spin-orbit coupling constants corresponding to the ions  $k^+$  or  $k^-$  and to the atom  $k$  in appropriate valence-state configurations. Through the dependence of the quantities  $n_k^j$  and  $q_k^j$  on the overlap atomic integrals, the interatomic transfer of charges are taken into account. A ligand-field treatment would take for the molecular spin-orbit constant that corresponding to the isolated ion as was done by Longuet-Higgins et al. in their  $g$ -value calculations.<sup>158</sup>

As is mentioned earlier, a detailed EPR investigation<sup>145</sup> has been carried out on ammonium chloride doped  $\text{Cu}^{2+}$  single crystals obtained from a growth solution containing an excess of  $\text{NH}_3$ . These experiments have been interpreted using an axial-field spin-Hamiltonian obeying the  $D_{4h}$  symmetry related to the basic cluster  $\text{CuCl}_4 \cdot 2\text{NH}_3$ . The copper and the chlorine atoms are coplanar, and the  $\text{NH}_3$  groups are assumed to be point charges, lying above and beyond the square plane such that in a crystal-field model this atomic arrangement retains the  $D_{4h}$  symmetry.

Several spin-Hamiltonian parameters have been measured<sup>147,145</sup> as a function of the temperature: the  $g$  values ( $g_{\parallel}$  and  $g_{\perp}$ ) and the hyperfine parameters ( $T_{\parallel}$  and  $T_{\perp}$ ), including the chlorine transferred hyperfine interactions. The zero-field splitting was found to be negligible. As is well known, one of the basic assumptions underlying the concept of the spin-Hamiltonian arises from the crystal-field model: the atoms are point charges, and localized (i.e., on the metal atom) mono-electronic states (solution of the Laplace equation  $\Delta V = 0$ ) fulfilling the symmetry requirements of the environment are solely used as basis functions for the evaluation of the spin-Hamiltonian parameters.<sup>162</sup>

As a matter of fact, the molecular-orbital approach is much more elaborate. We have considered the spatial model shown in Fig. 5 that obeys the

$C_{2h}$  point group. Usual N—H bond lengths and valence angle H—N—H have been used.<sup>191</sup> The two  $NH_3$  groups are images of each other through the inversion center  $i$ , origin of the cluster coordinate frame.  $R(Cu-N) = \frac{1}{2}R(Cl-Cl) = 1.944 \text{ \AA}$ . The ground state belongs to the  $B_g$  symmetry species with weak metallic components  $d_{xy}d_{yz}$ .<sup>76,\*</sup> Using (2.63), the remaining theoretical problems are as follows:

1. Calculation of the molecular spin-orbit coupling.
2. Calculation of the angular momentum matrix elements using a suitable set of excited-state configurations.
3. Calculation of the corresponding energy denominators.

The evaluation of the molecular spin-orbit coupling involves the following parameters:

$$a'_{Cu^{2+}} = -829 \text{ cm}^{-1}; \quad a_{Cl} = -587 \text{ cm}^{-1}; \quad a_N = 47.7 \text{ cm}^{-1}; \\ a'_N = 35.17 \text{ cm}^{-1} \quad (2.64)$$

and

$$n_{Cu}^i = -0.01572 \quad n_N^j = 0.00013 \quad n_{Cl}^i = 0.24598 \\ q_{Cu} = 0.821 \quad q_N = -0.208 \quad q_{Cl} = -0.330 \quad (2.65)$$

The spin-orbit coupling constants for  $Cu^{2+}$  and Cl are the experimental values. For nitrogen, as  $a_N$  is experimentally unknown, we have carried out a set of calculations corresponding to the neutral atom and its ions in appropriate valence state configurations, that is,  $N^{(0)}(^2D, ^2P, ^4S)$ ,  $N^+(^3P, ^1D, ^1S)$ ,  $N^-(^3P, ^1D, ^1S)$ . The results for  $N^{(0)}$  and  $N^+$  can be compared with those of Blume and Watson,<sup>163</sup> and the results for  $N^-$  can be compared with those of Malli and Fraga.<sup>164</sup> The analytical expressions for the atomic spin-orbit coupling constant including the spin-other orbit terms are given in the Blume and Watson work.<sup>165</sup> If Clementi's<sup>166</sup> and Jucys's<sup>167</sup> SCF atomic wave functions are used for these calculations, it is found that the best results are obtained by means of Clementi's functions.<sup>168</sup> In particular, our value  $a_N^{Clementi} = 35.17 \text{ cm}^{-1}$  is in excellent agreement with the value found by Malli and Fraga ( $a_N = 36.2 \text{ cm}^{-1}$ )<sup>164</sup> using their own tabulated SCF Hartree-Fock atomic function. These values correspond to the highest multiplicity configuration, and therefore to the lowest energy (Hund rule).

The parameters (2.65) result from a RHF calculation on  $CuCl_4 \cdot 2NH_3(C_{2h})$ .<sup>76</sup> The latter system possesses 55 valence electrons; the partial population indices  $n^j$  refer, therefore, to the twenty eighth MO.

\*A misprint occurs in Ref. 76: the cluster  $CuCl_4 \cdot 2NH_3$  obeys the  $C_{2h}$  symmetry point group (in place of  $D_2$ ) and the ground state wave function is of  $B_g$  symmetry (in place of  $B_1$ ).

We find the value  $-397.65 \text{ cm}^{-1}$  using the Mulliken formula for the molecular spin-orbit constant. This value is obviously very different from that corresponding to the ion  $\text{Cu}^{2+}$ , that is,  $-829 \text{ cm}^{-1}$ , that would be used in a crystal-field treatment.

The easiest way to evaluate the biatomic angular momentum matrix elements is to first transform them into spheroidal coordinates. Then it is easily seen that they reduce to a linear combination of ordinary overlap integrals.<sup>159</sup> The monocenter angular momentum integrals offer no problems. The tricentric (superscripts  $L, L', M$ ) integrals have been evaluated according to a Mulliken-type relation

$$\langle \chi^{nlm(L)} | \bar{L}^M | \chi^{n'l'm'(L')} \rangle \simeq \frac{1}{2} S^{LL'} [\chi^{nlm(L)} | \bar{L}^M | \chi^{nlm(L)} + \langle \chi^{n'l'm'(L')} | \bar{L}^M | \chi^{n'l'm'(L')} \rangle] \quad (2.66)$$

where  $\chi$  denotes a valence atomic orbital;<sup>166</sup> superscript  $M$  = transition metal atom; superscripts  $L, L'$  = ligand atoms.

Since  $L$  is a monoelectronic operator, a set of monoexcited electronic configurations have been used for the energy denominator evaluations of (2.63). As usual, these configurations (Fig. 6) are built up using the virtual

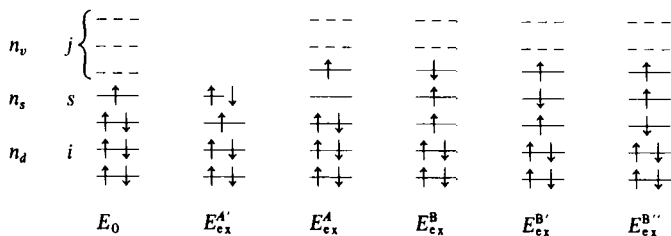


Fig. 6. Types of monoexcited configurations derived from the ground state with one unpaired electron.

MO's resulting from a variational treatment on the ground-state occupied orbitals. Actually,  $n_d = 27$ ,  $n_s = 1$ , as the ground state has 55 valence electrons, and  $n_v = 11$  with  $n_d + n_s + n_v = 39$ , that is, it is size of the basis set. It is readily seen that configurations  $B, B', B''$  are not eigenfunctions of  $S^2$ , and they have been replaced by the following orthonormal set, eigenfunctions of  $S^2$ :

$$\begin{aligned} \psi_{e_x}^I &= \frac{1}{\sqrt{2}} (\psi_B - \psi_{B'}) \\ \psi_{e_x}^{II} &= \frac{1}{\sqrt{6}} (\psi_B + \psi_{B'} - 2\psi_{B''}) \end{aligned} \quad (2.67)$$

Noting that only half-filled MO's contribute the  $g$  values, and expressing the energy differences within the SCF scheme, (2.63) after some algebra gives

$$g^{\alpha\beta} = 2 \left\{ \delta^{\alpha\beta} + \lambda \left[ \sum_i^{(d)} \frac{\langle \varphi_i | L_k^\alpha | \varphi_s \rangle \langle \varphi_s | L_k^\beta | \varphi_i \rangle}{e_i - e_s + J_{is} - \frac{1}{2} J_{ss}} + \sum_j^{(v)} \frac{\langle \varphi_s | L_k^\alpha | \varphi_j \rangle \langle \varphi_j | L_k^\beta | \varphi_s \rangle}{e_s - e_j + J_{sj} - \frac{1}{2} J_{ss}} \right. \right. \\ \left. \left. + \frac{2}{3} \sum_j^{(v)} \sum_i^{(d)} \frac{\langle \varphi_i | L_k^\alpha | \varphi_j \rangle \langle \varphi_j | L_k^\beta | \varphi_i \rangle}{e_i - e_j + J_{ij}} \right] \right\} \quad (2.68)$$

with

$$\lambda = \sum_k^{(j)} n_k^{(j)} [ |q_k^{(j)}| a'_k + (1 - |q_k^{(j)}|) a_k ]$$

The first, second, and third terms in square brackets refer to configurations  $A'$ ,  $A$  and  $(B, B', B'')$ , respectively. In the energy expressions, the molecular exchange terms,  $K_{ij}$  with  $i \neq j$ , may be neglected, since they are very small compared to the corresponding Coulomb terms. The incidence of this approximation on the values of the  $g$  components can be tested by introducing the following mean value, still preserving the degeneracy of the  $B$ -type configurations:

$$\varepsilon_0 - \frac{(\varepsilon_B + \varepsilon_{B'} + \varepsilon_{B''})}{3} = e_i - e_j + J_{ij} - \frac{1}{2} K_{ij} - \frac{1}{6} (K_{sj} - K_{si}) \quad (2.69)$$

In the case of configurations  $A$  and  $A'$  (no degeneracy problem) a rigorous treatment gives

$$\varepsilon_0 - \varepsilon_A = e_s - e_j + J_{sj} - \frac{1}{2} J_{ss} - \frac{1}{2} K_{sj} \quad (2.70)$$

As a first approximation the  $K_{ij}$ 's, with  $i$  different from  $j$ , which do not vanish for symmetry reasons, may be set equal to  $\frac{1}{2} J_{ij}$ . We have verified that this approximation always overestimates the values of the  $K_{ij}$ 's ( $i \neq j$ ). To be consistent with the whole approximation scheme, it is more advisable to evaluate these integrals with the help of the Mulliken-Ruedenberg formula, as in the case of the  $J_{ij}$ 's. It is found that the  $g$  values are not significantly affected by including the molecular exchange integrals, as seen by comparing the results of Tables VIII and IX.

The contributions to the  $g$  values according to the types of electronic configurations using the primitive basis coefficients are comparable to those obtained with the Löwdin coefficients. In the former case, all the mono-, bi-, and tricenter angular-momentum integrals are included in the calculation, whereas in the latter case only the monocentric integrals are retained, as a consequence of the well-known local and nonlocal character of the primitive basis and Löwdin coefficients, respectively.<sup>57</sup> In the results of Table VIII

TABLE VIII  
Values of the  $g$  Tensor Components in  $\text{CuCl}_4 \cdot 2\text{NH}_3(\text{C}_{2h})$

Component	Type of electronic configurations			Value of $g^{x\beta}$
	$A'$	$A$	$B, B', B''$	
With primitive basis coefficients <sup>a</sup>				
$g^{xx}$	$0.9698 \cdot 10^{-3}$	$0.3888 \cdot 10^{-9}$	$-0.1086 \cdot 10^{-3}$	2.713
$g^{yy}$	$0.7779 \cdot 10^{-5}$	$0.6769 \cdot 10^{-10}$	$-0.1154 \cdot 10^{-4}$	2.000
$g^{zz}$	$0.1076 \cdot 10^{-3}$	$-0.6524 \cdot 10^{-5}$	$-0.1565 \cdot 10^{-4}$	2.072
$g^{xz}$	$0.4857 \cdot 10^{-5}$	$0.1288 \cdot 10^{-6}$	$-0.2703 \cdot 10^{-5}$	0.0025
$g^{yz}$	$-0.7979 \cdot 10^{-9}$	0	$0.4670 \cdot 10^{-8}$	$1.841 \cdot 10^{-7}$
$g^{xy}$	$-0.1159 \cdot 10^{-6}$	0	$-0.5155 \cdot 10^{-6}$	$-3.655 \cdot 10^{-4}$
With Löwdin coefficients				
$g^{xx}$	$0.9878 \cdot 10^{-3}$	$-0.6861 \cdot 10^{-9}$	$-0.1044 \cdot 10^{-3}$	2.73
$g^{yy}$	$0.7524 \cdot 10^{-5}$	$0.1003 \cdot 10^{-9}$	$-0.1297 \cdot 10^{-4}$	2.000
$g^{zz}$	$0.1028 \cdot 10^{-3}$	$-0.6188 \cdot 10^{-5}$	$-0.1829 \cdot 10^{-4}$	2.067

<sup>a</sup>The figures under columns headed  $A'$ ;  $A$ ;  $B, B', B''$  represent the values of the first, second, and third terms of the part of (2.68) in square brackets. These figures are expressed in centimeters through the energy denominator, the numerator being dimensionless. The molecular spin-orbit coupling constant is expressed in reciprocal centimeters and the  $g^{a\beta}$  values are therefore dimensionless.

TABLE IX  
Values of the  $g$  Tensor Components in  $\text{CuCl}_4 \cdot 2\text{NH}_3(\text{C}_{2h})$ , Including the Estimated Molecular Exchange Integrals, that is,  $K_{ab} \approx \frac{1}{2}J_{ab}$  (if not = 0 by symmetry), Using the Primitive Basis Coefficients<sup>a</sup>

Component	Type of electronic configurations			Values of $g^{a\beta}$
	$A'$	$A$	$B, B', B''$	
$g^{xx}$	$0.9698 \times 10^{-3}$	$0.3888 \times 10^{-9}$	$-0.1514 \times 10^{-4}$	2.763
$g^{yy}$	$0.6054 \times 10^{-6}$	$0.6765 \times 10^{-10}$	$0.2201 \times 10^{-4}$	2.012
$g^{zz}$	$0.1076 \times 10^{-3}$	$-0.6524 \times 10^{-5}$	$-0.1005 \times 10^{-4}$	2.075

<sup>a</sup>See Table VIII.

given under "With Löwdin coefficients," it is assumed that the expression

$$\langle \varphi_i | \bar{L}^M | \varphi_j \rangle = \sum_p \sum_q C_{ip}^L C_{iq}^L \langle \lambda_p | \bar{L}^M | \lambda_q \rangle \quad (2.71)$$

can be written to a good approximation as

$$\langle \varphi_i | \bar{L}^M | \varphi_j \rangle \simeq \sum_{\text{atom}, i} \sum_{p, q \in \text{atom}} C_{ip}^L C_{iq}^L \langle \chi_p | \bar{L}^M | \chi_q \rangle \quad (2.72)$$

The  $\lambda$ 's and the  $\chi$ 's are the Löwdin orthonormal and the nonorthogonal Slater atomic orbitals, respectively, (see Section II.B.1). The  $C^L$ 's are the Löwdin coefficients derived by the usual Löwdin orthonormalization procedure.

Writing (2.72) involves the following suppositions:

1. The matrix elements of  $\bar{L}^M$  in the Löwdin basis set are negligible if the basis functions pertain to two different centers.
2. The remaining monocenter elements in the Löwdin basis differ negligibly from the corresponding elements using the primitive (Slater-type) basis.

The comparison of the results of Tables VIII and IX is considered as a justification *a posteriori* of the above two assumptions.

Another point to be stressed is that configuration *A* contributes negligibly to the  $g$  values, in contrast with the results of Longuet-Higgins et al.<sup>158</sup> in the case of  $(C_5H_5)_3Ni_3(CO)_2$ ,<sup>169-171</sup> where it contributes the most. On the other hand, configurations *A'* (which are not considered in the work of Longuet-Higgins et al. for some unknown reason<sup>158</sup>) and (*B*, *B'*, *B''*) contribute substantially and similarly to the  $g$  values.

A detailed analysis of the contributions of each of the 11 virtual levels to the  $g_{xx}$ ,  $g_{yy}$ , and  $g_{zz}$  values reveals that the configurations of types *A* and (*B*, *B'*, *B''*) contribute mainly to the final results through the two or three levels above the highest filled, that is, the twenty-eighth one, whereas rather "deep" levels contribute significantly in the case of configuration *A'* (see Fig. 6 and remember that  $n_d = 27$ ). The negligible contribution of configuration *A* in the case of the  $g_{xx}$  and  $g_{yy}$  values is to be ascribed to the simultaneously large values of the energy denominators and small values of the numerators in the  $g$  expression. Unfortunately, as the overall symmetry of the  $CuCl_4 \cdot 2NH_3$  cluster is rather low, that is,  $C_{2h}$ , it is not possible to explain the asymmetry in the diagonal  $g$  elements on grounds of symmetry considerations. The  $C_{2h}$  point group possesses four monodimensional irreducible representations. Therefore, no sets of coordinates ( $x$ ,  $y$ ), ( $x$ ,  $z$ ), ( $y$ ,  $z$ ), or ( $x$ ,  $y$ ,  $z$ ) can independently span such irreducible representations. The symmetry orbitals for each irreducible representation contain a linear combination of

atomic orbitals transforming as  $x$ ,  $y$ ,  $z$ , as well as some of their square and binary products ( $s$  and  $d$  functions). For this reason, and also because of the rather large dimension of the primitive basis, that is, 39, a great number of terms contribute the product of angular-momentum matrix elements, while no cancellations occur on grounds of symmetry.

Let us finally quote the experimental values<sup>73</sup>

$$g_{\perp} = 2.3 \pm 0.1; \quad g_{\parallel} = 2.0 \pm 0.1$$

to be compared with the theoretical values

$$g_{\perp} = 2.36; \quad g_{\parallel} = 2.07$$

The agreement is quite satisfactory.

Let us remark that off-diagonal elements of the  $g$  values have been calculated in the same reference frame (Table VIII). One of them, that is,  $g_{xz}$ , is not negligible. As far as we know, no ESR experiments have been reported on  $g$  off-diagonal matrix elements.

SECOND-ORDER TWO-ELECTRON PROPERTIES: SPIN-SPIN DIPOLAR INTERACTIONS CONTRIBUTING THE ZERO-FIELD SPLITTING PARAMETER. As the last observable in this section, we describe and comment on our calculation of the spin-spin dipolar interaction<sup>172</sup> involved in the zero-field splitting (ZFS),  $D^{zz}$ . This contribution is called  $D_{ss}^{zz}$  and is compared later with the experimental  $D^{zz}$  value (including moreover the spin-orbit contribution) observed in  $\text{Cr}^{3+}$  doped  $\text{CsCl}$  monocrystals. Only the  $z$  component of  $D$ , that is,  $D^{zz}$ , has been measured, the other components, related to exchange terms, being too small to be observed. We refer back to this point in Section II.D.2.b.

Room-temperature ESR measurements on  $\text{Cr}^{3+}$  embedded in cesium chloride are interpreted with the help of an axial field spin-Hamiltonian, corresponding to an effective spin  $S_{\text{eff}} = \frac{3}{2}$ . The hyperfine interactions are not measurable mainly because of the inhomogeneous broadening of the ESR lines. As is mentioned earlier, the planar arrangement (see earlier in this section) corresponding to the cluster  $\text{CrCl}_4$  obeying a  $D_{4h}$  symmetry is considered<sup>191</sup> by analogy with the well-known spatial arrangements occurring for  $\text{Mn}^{2+}$  and  $\text{Cu}^{2+}$  ions in  $\text{NH}_4\text{Cl}$  lattice.<sup>75</sup>

Theoretically,  $D_{ss}^{zz}$  may be evaluated on the basis of a first-order perturbation treatment of the spin-spin interaction. In a semiempirical formalism it is of fundamental importance to use reasonable values of the atomic integrals to get the right order of magnitude for  $D_{ss}^{zz}$ . A number of calculations have been performed in the last decade, using as zeroth-order wave functions different combinations of Slater determinants built on one-electron molecular orbitals using closed-shell ground state,<sup>173-175</sup> open-shell triplet state,<sup>178,176</sup> or unrestricted Hartree-Fock orbitals.<sup>179</sup> All these papers emphasize in one way or another the importance of using accurate atomic



integrals in a configuration-interaction calculation. This is the reason we have undertaken a very extensive derivation of the monocentric integrals of the spin-spin dipolar operator using the method of Geller et al.<sup>180</sup> These integrals, aside from contributing most significantly, are necessary in our procedure for deriving the multicenter integrals (see below). The extension of the work of Geller to principal quantum numbers 3 and 4 using Slater type orbitals to our knowledge has been undertaken for the first time.

In the first place, the molecular orbitals for  $\text{CrCl}_4(D_{4h})$  [31 valence electrons with 3 unpaired electrons in its ground state in agreement with  $S_{\text{eff}} = \frac{3}{2}$ ] have been derived according to the method outlined in Sections I.F and I.F.2.b, discarding the Wolfsberg-Helmholz approximation.

The method actually used to derive  $D_{ss}^{zz}$  rests on the double-perturbation technique proposed by Dalgarno et al.,<sup>181</sup> a technique apparently very little used in the case of bielectronic observable calculations. Let us mention, however, the work of Levy et al.<sup>182</sup> using this technique in the derivation of the spin-spin dipolar interactions in the naphthalene triplet ground state. No similar work is reported so far on clusters involving transition-metal atoms, probably because of the very complicated integral calculation needed for a basis set involving high principal quantum numbers (3s, 4s, 3p, 4p, 3d orbitals), aside from the fact that the spin-spin dipolar terms are themselves difficult to handle.

The principle of the double perturbation technique can be schematized as follows. We write the total Hamiltonian as

$$H = (H_0 + V) + T \quad (2.73)$$

$(H_0 + V)$  is the spinless Hamiltonian of the system;  $H_0$  is the Hartree-Fock ground-state unperturbed Hamiltonian operator whose eigenfunctions determine the zeroth-order wave function;  $V$  is the perturbation operator taking into account the electronic correlation not included in  $H_0$ . It is convenient to define  $H_0$  and  $V$  as the diagonal and off-diagonal parts of  $(H_0 + V)$  in such a way that for two elements  $\varphi_i$  and  $\varphi_j$  of the MO basis

$$\begin{aligned} \langle \varphi_i | H_0 | \varphi_j \rangle &= \langle \varphi_i | H_0 + V | \varphi_j \rangle \cdot \delta_{ij} \\ \langle \varphi_i | V | \varphi_j \rangle &= \langle \varphi_i | H_0 + V | \varphi_j \rangle \cdot (1 - \delta_{ij}) \end{aligned} \quad (2.74)$$

$\langle 0 | V | 0 \rangle = 0$  by construction of the Hartree-Fock operator,  $|0\rangle$  is the ground-state zeroth-order wave function.

$T$  represents the spin-spin dipolar operator whose matrix elements determine the perturbation on the uncoupled spins of the system (closed shells do not contribute to  $T$ ) and consequently are responsible for the spin-spin dipolar contribution of the ZFS. For an ensemble of  $N$  electrons<sup>144</sup>

$$T = \lambda \sum_{\alpha=1}^N \sum_{\beta=1}^N \sum_{i,j=1,2,3} S_{\alpha}^i \frac{R_{\alpha\beta}^2 \delta_{ij} - 3R_{\alpha\beta}^i R_{\alpha\beta}^j}{R_{\alpha\beta}^5} S_{\beta}^j \quad (2.75)$$

$\lambda$  is a factor depending on the units chosen:  $\lambda = 2.92842 \text{ cm}^{-1}$  per atomic unit of energy, using the values of the universal constants.<sup>183</sup>  $S_\alpha^i$  and  $R_{\alpha\beta}^i$  are the components along the  $i$ -axis of the spin operator of electron  $\alpha$  and the difference of position operators of electrons  $\alpha$  and  $\beta$ , respectively.

The perturbed energy corresponding to (2.73) may be written symbolically as a series of terms of different orders in  $V$  and  $T$

$$E = E_0 + T + V + T^2 + 2VT + V^2 + T^3 + 3T^2V + 3TV^2 + V^3 + TVTV + VTVV + \dots \quad (2.76)$$

The matrix elements of  $T$  being much smaller than those of  $V$ —typical orders of magnitude are  $10^{-5}$  and  $10^{-1}$  eV, respectively—one can just consider the terms linear in  $T$ . Then, the relation governing  $D_{ss}^{zz}$  is quite simple: using the Wigner-Eckart theorem,<sup>184</sup> one can easily show that there exists a particular choice of Cartesian coordinate axes (appearing in the expression of the  $T$  operator) such that the diagonal elements of the  $T$  matrix are all multiples of the same parameter  $D_{ss}^{zz}$ , with

$$D_{ss}^{zz} = \langle \psi_0^{3/2} | T | \psi_0^{3/2} \rangle + 2 \sum_i \frac{\langle \psi_0^{3/2} | V | \psi_i^{3/2} \rangle \langle \psi_i^{3/2} | T | \psi_0^{3/2} \rangle}{E_0 - E_i} \quad (2.77)$$

$\psi_i^{3/2}$  corresponds to some excited configuration  $i$  with  $S = S_z = \frac{3}{2}$ .

We now discuss the *components* in the *configuration interaction* calculation. A substantial reduction of the number of diexcited configurations occurs if the perturbation is limited to the order  $VT$ .

All possible monoexcited configurations one may build up from a three decoupled electron ground state give a nonvanishing value to  $D_{ss}^{zz}$ . These are exemplified in Fig. 7. Actually the number of doubly and singly occupied levels and virtual levels in the case of the  $\text{CrCl}_4$  ground state, are,  $\eta_d = 14$ ,  $\eta_s = 3$ ,  $\eta_v = 8$ , respectively. As usual the monoexcited configurations construct-

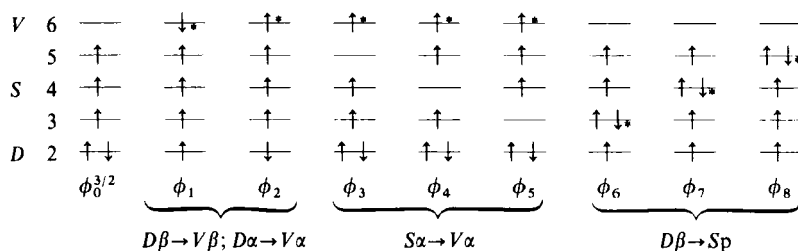


Fig. 7. Types of monoexcited configurations. The symbols  $D$ ,  $S$ , and  $V$  stand for double- and single-occupied and virtual levels. An asterisk indicates for each configuration the spin that has jumped. Furthermore, a "self-explaining" shorthand notation is introduced summing up a "group" of homologous configurations.

ed in this way (Fig. 7) are not necessarily eigenfunctions of  $S^2$ . They are replaced by the following orthonormal combination of functions, eigenfunctions of  $S^2$ ,

$$\begin{aligned}\phi_{\text{ex}}^{\text{I}} &= \frac{1}{\sqrt{2}} (\phi_1 - \phi_2) \\ \phi_{\text{ex}}^{\text{II}} &= \frac{1}{\sqrt{30}} (-3\phi_1 - 3\phi_2 + 2\phi_a + 2\phi_b + 2\phi_c) \\ \phi_{\text{ex}}^{\text{III}} &= \frac{1}{\sqrt{6}} (\phi_a - 2\phi_b + \phi_c) \\ \phi_{\text{ex}}^{\text{IV}} &= \frac{1}{\sqrt{2}} (-\phi_a + \phi_c)\end{aligned}\quad (2.78)$$

with (neglecting the normalization factor for the sake of simplicity)  $\phi_a = \|\mathbf{23456}\|$ ;  $\phi_b = \|\mathbf{23456}\|$ ;  $\phi_c = \|\mathbf{23456}\|$ . Furthermore, the configuration classes  $\phi_3$  up to  $\phi_5$  and  $\phi_6$  up to  $\phi_8$  are abbreviated in shorthand notation as  $\phi_{e\alpha}^V(S\alpha \rightarrow V\alpha)$  and  $\phi_{e\alpha}^V(D\beta \rightarrow Sp)$ , respectively ( $p = \text{paired}$ ).

Limiting the perturbation to the terms linear in  $T$ , the only biexcited configurations giving a nonvanishing contribution to  $D_{ss}^{zz}$  (see (2.77)) are shown in Fig. 8. They all possess three unpaired ( $\alpha$  spins) electrons and are automatically eigenfunctions of  $S^2$ . It can be shown that any other configuration with five or seven unpaired electrons, still corresponding to a resultant  $S=S_z=\frac{3}{2}$ , do not contribute to the second-order term in (2.77), as  $V_{0i}$ ,  $T_{0i}$ , or both  $T_{0i}$  and  $V_{0i}$  vanish identically ( $V_{0i}=\langle\psi_0^{3/2}|V|\psi_i^{3/2}\rangle$  with  $\psi_i^{3/2}$  representing a five or seven unpaired electron configuration. The  $T_{0i}$  element is defined analogously).

Among the configurations with three unpaired electrons only those of

[illegible]

**Fig. 8.** Biexcited configuration types. See legend to Fig. 7.

which the transiting pair of electrons leaves and reaches two different orbitals give a non-zero value to the second-order term in (2.77). This last statement arises from the symmetry properties of the spatial part of the  $T$  elements. The configurations shown in Fig. 8 are now written in compact form as

$$\begin{aligned}\phi_{\text{ex}}^{\text{VII}} &= [S\alpha^2 \rightarrow V\alpha^2] \\ \phi_{\text{ex}}^{\text{IX}} &= [D\beta^2 \rightarrow Sp^2] \\ \phi_{\text{ex}}^{\text{VIII}} &= [S\alpha \rightarrow V\alpha \text{ and } D\beta \rightarrow Sp]\end{aligned}\quad (2.79)$$

The virtual levels resulting from a variational treatment on the occupied ground-state orbitals are used for calculating the required  $V$  and  $T$  elements and their computation methods are described below.

We now discuss the *matrix elements* of the *correlation operator*. The correlation associated with the bielelectronic operator  $V$  comes from determinants  $\phi_k$ ,  $\phi_l$ , differing by at most two spin-orbitals. In the case where orbitals  $\phi_g(\mu)$ ,  $\phi_h(\nu)$  of  $\det \phi_k$  are distinct from orbitals  $\phi_f(\mu)$ ,  $\phi_j(\nu)$  of  $\det \phi_l$  it is easily seen that

$$\int |\text{diag } \phi_k|^* \sum_{\mu < \nu} H'(\mu\nu) |\det \phi_l| d\tau_\mu d\tau_\nu = (-1)^q [s_{\mu\nu} M_{gh}^{ij} - M_{gh}^{ji}] \quad (2.80)$$

with  $s_{\mu\nu} = 1$  if electrons  $\mu$  and  $\nu$  have the same spin functions, and otherwise,  $s_{\mu\nu} = 0$  ( $|\text{diag } \phi_k|$  is written for "diagonal elements of  $\phi_k$ "),  $q$  is the number of permutations on the spin-orbitals of  $\phi_l$  necessary to make them coincident with those in the diagonal of  $\phi_k$ , excluding electrons  $\mu$  and  $\nu$ , and

$$M_{gh}^{ij} = \int \phi_g^*(\mu) \cdot \phi_h^*(\nu) \cdot H'(\mu\nu) \cdot \phi_f(\mu) \phi_j(\nu) d\tau_\mu d\tau_\nu \quad (2.81)$$

In a second case, where  $\phi_k$  and  $\phi_l$  differ by one spin-orbital [i.e.,  $\phi_h(\mu)$  for  $\phi_k$  distinct from  $\phi_f(\nu)$  for  $\phi_l$ ], the integral reads

$$\int |\text{diag } \phi_k|^* \sum_{\mu < \nu} H'(\mu\nu) |\det \phi_l| d\tau_\mu d\tau_\nu = \sum_g (-1)^q [s_{\mu\nu} M_{gh}^{gj} - M_{gh}^{jq}] \quad (2.82)$$

the summation on  $g$  extending to all electrons  $\mu$  different from  $\nu$ .

The integrals  $M$  are further developed in the LCAO scheme. The tri- and quadricenter integrals are evaluated with the help of the Mulliken formula (Ref. 23). The bicentric ones are derived from the Nishimoto-Mataga relation (see Section I.F.2.a) (1.49), whereas the monocentric ones are evaluated by use of spectroscopic data (see Section I.F.3.a).

We discuss here the *matrix elements* of the *dipolar spin-spin operator*. Geller et al.<sup>180</sup> have derived the analytical forms of the one- and two-center Coulomb-type integrals corresponding to the two-particle operators

$$T \equiv T^{zz} = \frac{1}{2} r_{12}^{-5} (3z_{12}^2 - r_{12}^2) \quad \text{and} \quad T^{xy} = 3r_{12}^{-5} (x_{12}^2 - y_{12}^2)$$

using Slater type orbitals with principal quantum numbers  $n = 1$  and  $2$ .

To our knowledge we have extended this work for the first time to principal quantum numbers  $n = 3$  and  $4$ , i.e. Slater orbitals  $3s, 3p, 3d, 4s, 4p$ , considering in this case the monocentric Coulomb-type integrals corresponding to the operator  $T^{zz}$ . The matrix elements of the operator  $T^{xy}$  are not measurable in  $\text{Cr}^{3+}$  doped CsCl monocrystals as is mentioned earlier, as the selection rules for  $T^{xy}$  are  $\Delta m = \pm 2$ , giving rise to the exchange terms for  $T$  always being much smaller than the Coulomb ones occurring in  $T^{zz}$  for which  $\Delta m = 0$ .

In the actual evaluations of the  $T$  elements of (2.77) one may consider the bicentric Coulomb-type integrals only, the tri- and quadricenter integrals being converted into the latter by use of the Mulliken formula. Indeed Godfrey et al.<sup>177</sup> have shown in the case of benzene that the Coulomb-type bicentric integrals alone approximate very closely the exact value of the  $T$ 's integrals, including all other, Coulomb and exchange type, multicenter integrals. Here, the bicentric  $T$  elements have been derived by the use of a Mataga-type relation

$$T^{pl} = \frac{1}{2R_{pl}^5 / (3z_{pl}^2 - R_{pl}^2) + 2 / (T^{pp} + T^{ll})} \quad (\text{in atomic units}) \quad (2.83)$$

which for the planar geometry  $[\text{CrCl}_4](D_{4h})$  reduces to

$$T^{pl} = \frac{1}{-2R_{pl}^3 + 2 / (T^{pp} + T^{ll})} \quad (2.84)$$

$T^{pp}, T^{ll}$  being the Coulomb-type monocentric integrals.

The figures for the *monocentric Coulomb-type integrals* of the  $T^{zz}$  operator for  $n = 3$  and  $4$  are given in Table XI, as they do not seem to have been published yet in the relevant literature and we hope that they will be useful for related studies. We briefly summarize the main steps leading to these results. The derivations of the close analytical expressions of these integrals in terms of the effective charges  $Z, Z'$ , using Slater-type orbitals, are performed by computer and are available on request.

The integral to be evaluated is

$$\int \chi_a^2(\bar{r}_{a1}) O_1(\bar{r}_{12}) \chi_a'^2(\bar{r}_{a2}) d\bar{r}_{a1} d\bar{r}_{a2} \quad (2.85)$$

The atomic orbitals used on center  $a$  are linear combinations of Slater-type orbitals

and

$$O_1 = \frac{1}{2} r_{12}^{-5} (3z_{12}^2 - r_{12}^2) = r_{12}^{-3} \cdot P_2^0(\cos \theta_{12}) \quad (2.86)$$

Noting that a one-center product of two Slater functions can always be

expressed as a linear combination of basic charge distributions<sup>185</sup> (see Table X),

$$[N, L, M, Z] = \left(\frac{2L+1}{4}\right)^{1/2} \cdot 2^L \cdot Z^{N+2} [(N+L+1)!]^{-1} r^{N-1} e^{-Zr} \cdot S_{LM}(\theta, \varphi) \quad (2.87)$$

with

$$Z = \xi + \xi', \quad L = l + l', \quad N = n + n' - 1, \quad M = m + m'$$

denoted by NS, NPΣ, NPΠ, NPΠ̄, NDΣ, NDΠ, and so forth, integral (2.85) reduces to a linear combination of integrals

$$I_1 = \int [N \cdot L \cdot M \cdot Z]_a(\bar{r}_{a1}) O_1(\bar{r}_{12}) [N', L', M', Z']_a(\bar{r}_{a2}) d\bar{r}_{a1} d\bar{r}_{a2} \quad (2.88)$$

Their evaluation rests on the Fourier convolution theorem,<sup>186</sup> that is, after each component of the integrand of  $I_1$  is Fourier transformed, its value

TABLE X  
Expansion of Products of Slater Orbitals in Terms of  
Basic Charge Distributions<sup>a</sup>

---

$(ns) \cdot (n's) = V \cdot (NS).$
$(np\sigma) \cdot (n'p\sigma) = V \cdot \left[ (NS) + \frac{W}{10} (ND\Sigma) \right]$
$(np\pi) \cdot (n'p\pi) = V \cdot \left[ (NS) - \frac{W}{20} (ND\Sigma) \pm \frac{W\sqrt{3}}{20} (ND\Delta) \right]$
$(nd\sigma) \cdot (n'd\sigma) = V \cdot \left[ (NS) + \frac{W}{14} (ND\Sigma) + \frac{U}{56} (NG\Sigma) \right]$
$(nd\pi) \cdot (n'd\pi) = V \cdot \left[ (NS) + \frac{W}{28} (ND\Sigma) - \frac{U}{84} (NG\Sigma) \pm \frac{W\sqrt{3}}{28} (ND\Delta) \pm \frac{U\sqrt{5}}{168} (NG\Delta) \right]$
$(nd\delta) \cdot (n'd\delta) = V \cdot \left[ (NS) - \frac{W}{14} (ND\Sigma) + \frac{U}{336} (NG\Sigma) \pm \frac{U\sqrt{35}}{336} (NG\Gamma) \right]$

---

<sup>a</sup>  $N = n + n' - 1$ ;  $Z = \xi + \xi'$ ;  $V \equiv (2\xi)^{n+1/2} (2\xi')^{n'+1/2} (N+1)! (2n)!^{-1/2} (2n')!^{-1/2}$ ;  $W \equiv (N+2)(N+3)$ ;  $U \equiv W(N+4)(N+5)$ . When the sign  $\pm$  appears, the upper sign must be taken when both orbital species are of the  $\pi$  or  $\delta$  type, and the lower sign when both are of the  $\bar{\pi}$  or  $\bar{\delta}$  type.

remaining unchanged,  $I_1$  factors into an angular part

$$B(L, M, L, M') = (2\pi)^{-3} \left( -\frac{4}{3} \pi \right) \int_0^{2\pi} dv \begin{Bmatrix} \cos \\ \sin \end{Bmatrix} |M| V \begin{Bmatrix} \cos \\ \sin \end{Bmatrix} |M'| V \\ \times \int_0^\pi P_L^{|M|}(\cos u) \cdot P_2^0(\cos u) \cdot P_L^{|M'|}(\cos u) du \quad (2.89)$$

which vanishes unless  $M = M'$  and either  $\cos |M| V \cos |M'| V$  or  $\sin |M| V \sin |M'| V$  is chosen, and a radial part, which can be expressed as a linear combination of functions,

$$A(0, p, q) \equiv A(0, p, q, Z, Z') = \int dk k^2 (k^2 + Z^2)^{-p} (k^2 + Z'^2)^{-q} \quad (2.90)$$

Finally  $A(0, p, q)$  may be derived from  $A(0, 1, 1)$  as

$$A(0, p+1, q+1) = \left[ \left( -\frac{1}{2} R \right)^{p+q} (p!)^{-1} (q!)^{-1} \left( \alpha^{-1} \frac{\partial}{\partial \alpha} \right)^p \left( \beta^{-1} \frac{\partial}{\partial \beta} \right)^q \times A(0, 1, 1) \right]_{R=0} \quad (2.91)$$

with  $\alpha = ZR$  and  $\beta = Z'R$

$$A(0, 1, 1) = \frac{1}{2} \pi R \frac{(e^{-\alpha} - e^{-\beta})}{\beta^2 - \alpha^2}$$

These equations hold for bicentric integrals too,  $R$  being the internuclear distance; for monocentric integrals the limit  $R \rightarrow 0$  must be taken.

The SCF basis sets used in these calculations are for chromium (4s, 4p, 3d) those of Richardson et al.<sup>187</sup> and for chlorine (3s, 3p) those of Watson et al.<sup>188</sup> The figures of Table XI are subsequently used in the course of the derivation of the multicenter integrals as previously mentioned.

We now present an evaluation of the *energy denominators* in (2.77). Table XII summarizes the energy expressions corresponding to the different mono- and biexcited configurations shown schematically in Figs. 7 and 8. The molecular exchange integrals  $K_{ij}$  with  $i \neq j$  have been dropped as being very small (see Ref. 39, section I).

We are now in a position to evaluate all the components of the configuration interaction calculation just described [see (2.77) through (2.79), Figs. 7 and 8]. Table XIII presents our results.

It is seen that, within the second-order configurations,  $\phi_{ex}^{v11}(S\alpha^2 \rightarrow V\alpha^2)$  and  $\phi_{ex}^v(D\beta \rightarrow Sp)$  contribute, respectively, the least and the most to the  $D_{ss}^{zz}$  value, as expected.

Quite generally, we see that if the excitation involves a component within the occupied ground-state levels, the contribution to  $D_{ss}^{zz}$  is never negligible.

The ESR experimental results<sup>74</sup> on the zero-field splitting  $D^{zz}$  reveal the

TABLE XI  
Values of the Monocentric Integrals (in atomic  
units) of the Operator  $T^{zz}$  for  
Chromium (Cr<sup>I</sup>) and Chlorine (Cl<sup>I</sup>)

$\chi_a$	$\chi'_a$	Remark <sup>a</sup>	Value of the integral
Chromium			
4s	4pσ		$10^{-2} \times 0.1394580$
	4pπ	1	$-10^{-3} \times 0.6972902$
	3dσ		$10^{-3} \times 0.4359871$
	3dπ	1	$10^{-3} \times 0.2179936$
	3dδ	1	$-10^{-3} \times 0.4359871$
4pσ	4pσ		$-10^{-3} \times 0.2210256$
	4pπ	1	$10^{-3} \times 0.2934162$
	3dσ		$10^{-2} \times 0.3478764$
	3dπ	1	$10^{-2} \times 0.3478400$
	3dδ	1	$10^{-2} \times 0.3844616$
4pπ	4pπ	2	$10^{-3} \times 0.1105128$
	4p $\bar{\pi}$		$-10^{-3} \times 0.5868324$
	3dσ	1	$-10^{-2} \times 0.1798711$
	3dπ	2	$-10^{-2} \times 0.1604291$
	3d $\bar{\pi}$		$-10^{-2} \times 0.1933438$
3dσ	3dδ	3	$-10^{-2} \times 0.1862979$
	3dσ		$10^{-1} \times 0.5074125$
	3dπ	1	$10^{-1} \times 0.4013273$
	3dδ	1	$-10^{-2} \times 0.8907804$
	3dπ	2	$10^{-1} \times 0.1541949$
3dπ	3d $\bar{\pi}$		$-10^{-1} \times 0.4844092$
	3dδ	3	$10^{-1} \times 0.1218266$
	3dδ	2	$-10^{-1} \times 0.1139512$
3dδ	3d $\bar{\delta}$		$-10^{-1} \times 0.9931139$
Chlorine			
3s	3pσ		$10^{-1} \times 0.1678958$
	3pπ	1	$-10^{-2} \times 0.8394792$
3pσ	3pσ		$10^{-2} \times 0.1904398$
	3pπ	1	$10^{-1} \times 0.1315873$
3pπ	3pπ	2	$-10^{-3} \times 0.9521992$
	3p $\bar{\pi}$		$-10^{-1} \times 0.2631746$

<sup>a</sup>1 holds for  $\pi, \delta$  as well as for  $\bar{\pi}, \bar{\delta}$ ; 2 holds if functions are both  $\pi$  or both  $\bar{\pi}$  and both  $\delta$  or both  $\bar{\delta}$ ; 3 holds for all four combinations  $\pi\delta, \pi\bar{\delta}, \bar{\pi}\delta, \bar{\pi}\bar{\delta}$ .



TABLE XII  
Analytical Expressions for  $E_0 - E_i$  [see (2.77)] using Mono- and  
Biexcited Configurations Depicted in Figs. 7 and 8

Monoexcited configurations (One electron jumps from orbital $k$ to orbital $m$ ) $E_0 - E_i = e_k - e_m + R$		
Type of excitation	Excited functions	$R^a$
$D\beta \rightarrow V\beta$ ( $k\beta \rightarrow m\beta$ )	$\phi_1$	$J_{km}$
$D\alpha \rightarrow V\alpha$ ( $k\alpha \rightarrow m\alpha$ )	$\phi_2$	$J_{km}$
$S\alpha \rightarrow V\alpha$ and $D\beta \rightarrow S\beta$	$\phi_a, \phi_b, \phi_c$	$J_{km}^{(*)}$
$S\alpha \rightarrow V\alpha$ ( $k\alpha \rightarrow m\alpha$ )	$\phi_3$ up to $\phi_5$	$J_{km} - \frac{1}{2}J_{kk}$
$D\beta \rightarrow Sp$ ( $k\beta \rightarrow mp$ )	$\phi_6$ up to $\phi_8$	$J_{km} - \frac{1}{2}J_{mm}$
Biexcited configurations (Two electrons jump from orbitals $k, l$ to orbitals $m, n$ ) $E_0 - E_i = e_k + e_l - e_m - e_n + (J_{km} + J_{kn} + J_{lm} + J_{ln}) + S$		
Type of excitation	Excited functions	$S$
$S\alpha^2 \rightarrow V\alpha^2$ ( $k\alpha l\alpha \rightarrow m\alpha n\alpha$ )	$\phi_9$ up to $\phi_{11}$	$-\frac{1}{2}J_{kk} - J_{kl} - \frac{1}{2}J_{ll} - J_{mn}$
$S\alpha \rightarrow V\alpha$ and $D\beta \rightarrow Sp$ ( $k\alpha l\beta \rightarrow m\alpha np$ )	$\phi_{12}$ up to $\phi_{17}$	$-\frac{1}{2}J_{kk} - J_{kl} - J_{mn} - \frac{1}{2}J_{nn}$
$D\beta^2 \rightarrow Sp^2$ ( $k\beta l\beta \rightarrow mpnp$ )	$\phi_{18}$ up to $\phi_{20}$	$-J_{kl} - \frac{1}{2}J_{mm} - J_{nn} - \frac{1}{2}J_{nn}$

$a^{(*)}$  biexcited configurations forming a "complete" set of functions with the  $\phi_1, \phi_2$  functions.

presence of two different paramagnetic centers for  $\text{Cr}^{3+}$  doped in cesium chloride lattice, the values of which are  $|D^{zz}|_I = 0.2174 \text{ cm}^{-1}$  and  $|D^{zz}|_{II} = 0.1400 \text{ cm}^{-1}$  (the signs have not been determined experimentally). These values, including the spin-orbit effect, when compared with our theoretical value  $D_{ss}^{zz} = +0.07178 \text{ cm}^{-1}$ , suggest that the spin-spin contribution cannot be neglected in such clusters, contrary to common opinion.

Among the few other works devoted to the zero-field splitting evaluations in metallic complexes, it is worth mentioning the calculations of Sharma et al.<sup>189</sup> on S-state ions  $[\text{Mn}^{2+}(^6S)]$  doped in ionic crystals ( $\text{ZnF}_2$  and  $\text{MnF}_2$ ). We summarize in Table XIV part of their results for the case of  $\text{Mn}^{2+}$  doped  $\text{ZnF}_2$ .

As a first approximation, using an external-point-charge model as well as a point-multipole model, the different mechanisms contributing the  $D$  (in the presence of an axial crystal field) and  $E$  (in the presence of a rhombic crystal field) spin-Hamiltonian parameters are worked out. These mech-

TABLE XIII  
First- and Second-Order Contributions to  
 $D_{ss}^{zz}$  for the Cluster  $[\text{CrCl}_4]$  ( $\text{cm}^{-1}$ )

First-order term	
$\langle 0 T 0\rangle$	$10^{-1} \times 0.51074$
Second-order term	
Monoexcited configurations	
$\phi_{ex}^I = \frac{1}{\sqrt{2}} (\phi_1 - \phi_2)$	$-10^{-3} \times 0.98968$
$\phi_{ex}^{II} = \frac{1}{\sqrt{30}} (3\phi_1 + 3\phi_2 - 2\phi_a - 2\phi_b - 2\phi_c)$	$-10^{-2} \times 0.60886$
$\phi_{ex}^{III} = \frac{1}{\sqrt{6}} (\phi_a - 2\phi_b + \phi_c)$	$-10^{-3} \times 0.70913$
$\phi_{ex}^{IV} = \frac{1}{\sqrt{2}} (\phi_c - \phi_a)$	$-10^{-2} \times 0.184377$
$\phi_{ex}^V: D\beta \rightarrow Sp$	$10^{-1} \times 0.35163$
$\phi_{ex}^{VI}: S\alpha \rightarrow V\alpha$	$-10^{-2} \times 0.24106$
Biexcited configurations	
$\phi_{ex}^{VII}: S\alpha^2 \rightarrow V\alpha^2$	$-10^{-4} \times 0.77235$
$\phi_{ex}^{VIII}: D\beta^2 \rightarrow Sp^2$	$-10^{-2} \times 0.37113$
$\phi_{ex}^X: S\alpha \rightarrow V\alpha$ and $D\beta \rightarrow Sp$	$10^{-2} \times 0.137586$
Total value of $D_{ss}^{zz}$ up to second order	$10^{-1} \times 0.71783$

anisms refer to certain electronic-configuration-interaction processes (involving definite excited states of the metal). These processes arise from the nature of the crystal fields in the neighborhood of the metal and the analytical form of the spin-spin dipolar operator. In view of the crudeness of the above models, and owing to the unexpectedly good results (See Table XIV) obtained, that is, in contrast with most point-charge-model evaluations, these authors propose also a model inspired by the crystal-ligand-field theory. The metal-ligand orbital overlap and the charge-transfer parameters are introduced up to second order. All the relevant matrix elements of the spin-spin and spin-orbit operators are evaluated using SCF atomic Hartree-Fock orbitals. The result is, as seen in Table XIV, that this overlap model is not decisive for explaining the observed zero-field-splitting parameters. It shows a marked

TABLE XIV  
Point-Multipole and Overlap Contributions  
to the  $D$  and  $E$  Parameters for  $\text{Mn}^{2+}$   
in  $\text{ZnF}_2$  ( $10^{-4} \text{ cm}^{-1}$ )

Contributions	$D$	$E$
Point-multipole model		
Spin-orbit	+27.79	-99.25
Spin-spin	+6.35	+2.68
Total	+34.14	-96.51
Overlap model		
Spin-orbit	-5.29	-5.33
Spin-spin	+7.87	+54.06
Total	+2.58	+48.73
Experiment <sup>194</sup>	+10.5	-113.5

effect of the spin-spin contribution, partly cancelled by the spin-orbit contribution, such that the magnitude orders (and sometimes the signs) found for  $D$  and  $E$  are in disagreement with the experimental values.

Finally, we should like to mention the work of Han et al.<sup>190</sup> on the derivation of the  $D$ -parameters in the hemin molecule. Their MO calculations are not completely free from crystal-field parameters either (in connection with the evaluation of energy denominators) and lead using these parameters to a reasonable agreement with the observed values.

### III. ABOUT SOME OTHER SEMIEMPIRICAL MO TREATMENTS

#### A. Preliminaries

This section is devoted to a brief analysis of the main characteristics of some other semiempirical MO schemes capable of handling metallic complexes, as well as to a critical survey of some of the theoretical hypotheses involved in these MO schemes.

The models proposed by the following authors are retained, as they reflect the main trends of thought invoked in present semiempirical calculations: Wolfsberg and Helmholz; Pople; Basch, Viste, Gray, and Ballhausen;

Allen and Clark; Brown and Roby; Tossel and Lipscomb; Slater-Johnson ( $X\alpha$ -model).

The last item, the so-called  $X\alpha$ -model,—especially developed and adapted by Slater, Johnson and others for studying electronic structures of crystals—, is nowadays largely expounded in the relevant literature regarding energy band calculations and magnetic properties of solids and large polyatomic molecules<sup>199</sup>.

We should like to point out that it is beyond the scope of this review, mainly concerned with the calculations of observables in metallic complexes, to give an exhaustive account of the different MO formalisms and related problems existing at the present time. We refer the reader to the recent and comprehensive review article of Berthier<sup>200</sup> for a thorough and critical account on this subject for the case of metallic complexes, and to a somewhat old review covering, however, part of this matter.<sup>201</sup> Concerning the subject of organic molecules, the reader is referred to standard textbooks.<sup>202</sup>

### B. Wolfsberg-Helmholz Model

One of the first successful attempts to calculate certain observables in the case of metallic complexes is achieved within the Wolfsberg-Helmholz model.<sup>203</sup> The MO's are built up by simply postulating the Hamiltonian diagonal element  $H_{pp}$  to be equal to the ionization energy of the atom P, whereas the off-diagonal element  $H_{pq}$  is calculated according to the well-known Wolfsberg-Helmholz relation (see section I, (1.28)). The merits of this model lie in its simplicity—large molecules can be handled easily—as well as in the use of a suitable combination of semiempirical relations, none of which is fully justified theoretically, such that this model is capable of making reliable predictions on observables for inorganic molecules, a point about which the Hückel theory in its primitive form was not concerned. This formalism leads to more elaborate methods of calculation.

A striking feature in many semiempirical MO schemes is the lack of invariance of the occupied MO's towards linear transformations of the basis set. A remedy to this deficiency is proposed within the various Pople models.<sup>204–206</sup> Three methods of that sort, at least, are in current use. They differ from each other by the extent to which the zero-differential-overlap (ZDO) approximation [i.e.,  $\int \chi_p^*(v)\chi_q(v) dv(v)=0$  for  $p \neq q$ ,  $p$  and  $q$  being centered or not centered on two different atomic centers; see Section I.D.3] is invoked in deriving the Coulomb integrals. In the first stage, the so-called “complete neglect of differential overlap (CNDO) model”,<sup>204</sup> a rather crude algorithm, is used to satisfy the above symmetry requirements on the MO's (see also Section I.D.3). One simply postulates for the atomic bielectronic integrals ( $pq, rs$ )

$$(pq, rs) = \delta_{pq}\delta_{rs}\gamma_{pr} \quad (3.1)$$

irrespective of the allocation of the orbitals in the molecule and their species, and the bielectronic integrals  $\gamma_{pr}$  are set equal to  $\gamma_p$  for any orbitals  $\chi_p$  on atom P and any orbital  $\chi_r$  on atom R: the actual orbital species are fully ignored, only the nature of the atoms determines the  $\gamma_{pr}$  value. In the second stage, that is, "the intermediate neglect of differential overlap (INDO) model,"<sup>205</sup> the monocenter differential overlap distributions are merely retained, providing some account of the exchange terms in the usual effective Hamiltonian. Finally, in the so-called "neglect of diatomic differential overlap (NDDO) model,"<sup>206</sup> the ZDO approximation applies only to those orbitals  $\chi_p$  and  $\chi_q$  or  $\chi_r$  and  $\chi_s$  located on distinct atoms, in which case the corresponding bielectronic integrals are neglected. Expressions of the Fock matrix elements for the above MO schemes, as well as the evaluation<sup>207</sup> of the corresponding parameters, can be found in the original papers.<sup>204-207</sup> The last two methods are often used in the case of unrestricted Hartree-Fock calculations, simply setting the charge density  $P_{pq} = P_{pq}^\alpha + P_{pq}^\beta$ .

The major deficiency of these methods lies at the level of the CNDO scheme—very recently this model was shown from first principles to be physically unreasonable<sup>236</sup>—since it ignores completely the angular dependence of the basis set. The determination of spatial conformations of molecules (linear or bent) cannot be handled by this method. A striking example is the molecule  $\text{MgF}_2$ : the CNDO model predicts an energy minimum for an apex angle  $\theta = 140^\circ$ , in disagreement with experimental data<sup>234</sup> and *a priori* calculations,<sup>235</sup> which both confirm an almost linear spatial conformation. On the other hand, in both Pople models the off-diagonal Hamiltonian elements still involve the first power of the corresponding overlap elements, which is not theoretically satisfactory, as discussed in Section I.F.2.b. It should be added that none of these models provides fully for itself concerning all the parameter values to be used: an *ab initio* calculation may be necessary to fix the values of certain parameters. For large metallic complexes, this requirement may raise serious problems. Let us finally stress that usually for organic molecules containing *ns*, *np* ( $n=1, 2, 3$ ) orbitals elementary properties, such as equilibrium distances, dipole moment, and dissociation energies, are well reflected by the theory, provided that a good *ab initio* calculation exists for calibration (for a criticism of calibration processes based on experimental data as developed in the MINDO model of Dewar, see a recent dispute between Pople-Hehre<sup>237</sup> and Dewar<sup>238</sup>).

The use of the CNDO scheme, to maintain the calculation framework as simple as possible, in the case of metallic complexes necessitates some revision of the thereby involved assumptions. In the case of the transition atom the bielectronic integrals  $\gamma_{pr}$  (one- and two-center types) are now allowed to depend on the principal quantum number ( $n=3$  or 4). This formalism has been developed by Allen and Clack<sup>208</sup> and applied to certain homologous series of complex ions, such as  $[\text{MF}_6]^{4-}$ ,  $[\text{M}(\text{H}_2\text{O})_6]^{2+}$ , and  $[\text{M}(\text{H}_2\text{O})_6]^{3+}$ ,

where M replaces a set of first-period transition elements.<sup>208,209</sup> The results corresponding to some ground-state properties (bond lengths, symmetry species of the highest filled level, etc.) are compared with observed data. It should be added that this method still does not consider the overlap integrals and it has been shown that the ZDO approximation is ungrounded when applied to bonds in metallic complexes<sup>210</sup> if the latter approximation is not formulated in an orthogonalized basis set (see Ref. 6).

A restricted and an unrestricted Hartree-Fock MO method connected to the NDDO model have also been proposed by Brown et al. for treating metallic complexes.<sup>211</sup>

Discarding the problem of rotational invariance of the MO's (according to our experience this lack of invariance is small and in any case does not have a sensible incidence in predicting the values of a great variety of observables) and still wishing to maintain the theory easily manageable for practical applications, as well as preserving the qualitative features of the molecular electronic configuration, an efficacious process in the framework of a semiempirical scheme in accordance with the preceding statements consists of improving the original proposal of Wolfsberg-Helmholz. In this respect let us mention the precursor works of Ballhausen et al.<sup>212</sup> fitting the Hamiltonian diagonal elements to a linear combination of valence-state ionization energies (VSIE) or valence-orbital ionization potential (VOIP) corresponding to definite electronic configurations of the atoms.

In evaluating the Hamiltonian off-diagonal elements  $H_{pq}$ , no important improvements of the standard expressions (see Section I.D.5) have been made, as the bielectronic integrals occurring in the potential part of  $H_{pq}$  are difficult to handle properly. In this respect Lipscomb et al.<sup>213</sup> have proposed an "optimum way" of overcoming part of the theoretical weaknesses involved in the usual formulation, without sacrificing too much of the original simplicity of the semiempirical scheme. We would like to end this section by briefly schematizing their recent all-electron theory<sup>214</sup> free from empirical or semiempirical data (See also Sections I.F.2.b, I.F.5, and II.D.2.b). The clue to this method consists of using the values of certain matrix elements issued from an *a priori minimal basis* calculation on small molecules for the treatment of larger systems chemically analogous, allowing in a self-consistent way for fine adjustments in the new molecular environments. A number of intuitive<sup>216</sup> and approximate relations, for example, the Mulliken-Ruedenberg formula, are still used (for limiting the amount of computational work), but they are free from empirical parameters, that is, necessitating the care to maintain them rotationally invariant. It should be observed, however, that in this theory the rotational-invariance requirement is fulfilled for a certain class of linear transformations of the basis set only. Calculations on organic and inorganic systems, such as  $\text{CH}_4$ ,  $\text{C}_2\text{H}_4$ , and  $\text{C}_2\text{H}_2$  and  $\text{TiH}_3\text{F}$ ,

$\text{CuF}$ ,  $\text{GaH}_3$ , and  $\text{CuF}_4^{2-}$ ,<sup>215</sup> support the fact that this formalism can give at least qualitatively correct results for charge distributions and energy trends in metallic compounds too. No observable calculations have been reported so far. Finally it must be added that this formalism is presently restricted to the use of a minimum basis set and observables depending critically on the Hartree-Fock energy limit should be better reflected through extended-basis calculations.

### C. The $X\alpha$ -Model

At the end of this section, we discuss some characteristics of a molecular orbital theory with a structure different from the preceding ones. This theory, called the " $X\alpha$ -model," developed independently by Slater and co-workers,<sup>217</sup> Gombas and Gaspar,<sup>218</sup> Kohn and Sham,<sup>219</sup> and others between the 1950s and 1960s, has spread out these last years to a number of research institutes. Its subjacent central idea is to replace the very difficult nonlocal exchange-correlation term in the many-body problem by a statistical approximation with essentially a local character first introduced by Bloch,<sup>220</sup> Dirac<sup>221</sup> and Wigner,<sup>221</sup> in about the 1930s, in a form adapted for practical calculations. It involves a monoelectronic exchange-correlation potential acting on the position of the electron with a spherical distribution in space such that at the electron position it neutralizes its charge density. This is equivalent to withdrawing the self-interaction effects from the Coulomb potential corresponding to all electrons of a system. This function is defined by

$$\langle V_{XHF\uparrow i}(1) \rangle = - \sum_{i\uparrow} \sum_{j\uparrow} n_i n_j \frac{\int \varphi_i^*(1) \varphi_j^*(2) \frac{1}{r_{12}} \varphi_i(2) \varphi_j(1) dv_2}{\sum_{k\uparrow} n_k \varphi_k^*(1) \varphi_k(1)} \quad (3.2)$$

(and analogously for a spin-down orbital) where integration over  $dv_2$  includes summation over spins of the second electron. The denominator is the total charge density at position 1. Equation 3.2 can be expressed in close form in the case of a Lorentz electron gas, using exponential functions.<sup>217,220,221</sup> The result reads:

$$\langle V_{XHF\uparrow i}(1) \rangle = -3 \left[ \frac{3}{8\pi} \rho(1\uparrow) \right]^{1/3} \quad (3.3)$$

However, some doubt has been cast on the numerical coefficient obtained, which should be only two-thirds as great.<sup>218,219</sup> This coefficient is now left in practical applications as an adjustable parameter called  $\alpha$ , from which the  $X\alpha$ -model name derives.

A striking consequence of introducing this local potential into the Schrödinger equation is that the correct asymptotic value of the energy corres-

ponding to infinitely separated atoms in a crystal or a molecule is always found using a one-determinant function,<sup>199</sup> in contrast to the usual Hartree-Fock theory.

Another central ingredient of the  $X\alpha$ -theory is the introduction of the so-called "muffin-tin potential" for describing the corresponding one-electron potential inside a crystal. This approximation is rather crude and has been revealed to be quite unsatisfactory in some applications.<sup>222</sup> One divides the crystal potential essentially into three parts: a spherical potential inside spheres, of arbitrary radii, surrounding each atom; a constant potential (often taken to be zero) between the, initially, nonoverlapping spheres; and again a spherical potential outside a definite cluster of atoms leading to a limiting value at infinite distance. This potential choice simplifies the boundary-values problem considerably compared, for example, to the Wigner-Seitz cellular model.

For cubic close-packed or hexagonal face-centered crystals the muffin-tin potential can easily be argued, each sphere surrounding a neutral atom. For covalent semiconductors with only a few near-neighbors (impurity-doped crystals), the muffin-tin potential is certainly not justified. The arbitrariness in the muffin-tin potential lies in the fact that the radius of the sphere to be chosen cannot be determined variationally and is empirically settled. The departure from this potential has been taken into account in a variety of ways and is referred to later.

Generally the usual ground-state  $X\alpha$ -one-determinant function fails to reproduce the observed crystal excitation energies (ESCA measurements) using the corresponding eigenvalues of the secular equation according to the Koopman theorem, just as the Hartree-Fock theory fails in the one-determinant approximation. If, however, one defines a "transition state," the corresponding eigenvalue differences between the final and initial states are often in agreement with the observed data. This transition state is a state in which the occupation numbers of the relevant spin-orbitals are halfway between those of the initial and final states. Fair agreements with the observed X-ray spectra and optical transition energies have been obtained for systems (among others) such as  $\text{SF}_6$ ,<sup>223</sup>  $\text{MnO}_4^-$ ,<sup>224</sup>  $\text{VO}_4^{2-}$ , and  $\text{CrO}_4^{2-}$ <sup>225</sup> within the transition-state concept. As a matter of fact, such a state is certainly suitable in the case of a localized perturbation, that is, an atomic excited state within the crystal (exciton), in contrast to the case where the initial and final state wave functions would be fairly spread throughout many atoms, that is, where the corresponding individual atomic potential-energy changes would be small. In the latter case the eigenvalue differences obtained by the transition-state method would not be relevant for predicting any crystal excitation energies.

Something remains to be said about the solution of the secular problem



reached within a rather different framework compared to the LCAO scheme, as well as about some of the new perspectives for describing the one-electron potential function in a crystal.

A recent proposal to set up and solve the secular problem is included in the so-called "multiple-scattering wave method," developed by Johnson and Smith.<sup>226</sup> The general solution of the Schrödinger equation is sought within the muffin-tin approximation by expanding the wave functions in the respective regions around a definite atom in the crystal as linear combinations of spherical harmonics depending on the positions of the atoms. Continuity relations are then set up for points immediately inside and outside the different regions. The secular problem solutions are contained in a set of coefficients, functions of certain energy eigenvalues and of the scattered wavelets emitted by each atom.<sup>227</sup> The number of simultaneous equations to be solved is equal to the number of wavelets.

It is evident that this procedure does not involve a direct use of the familiar LCAO expansion. Of course, the connection with the latter exists, as within each atomic sphere or intersphere region an analysis into contributions of different  $l$  values determines the amount of  $s$ ,  $p$ ,  $d$ , and so on character of each molecular orbital.

An interesting point to note is that the  $X\alpha$ -model is able, without hard labor, to handle systems involving heavy elements as a consequence of the local character of the  $X\alpha$ -potential [i.e., (3.3)]. Let us mention the calculation of the electronic structure and of some electronic transitions in the uranyl ion,  $\text{UO}_2^{2+}$  using the transition-state concept.<sup>228</sup> The experimental ground state,  $^1\Sigma_g^+$ , is reproduced and the calculated transition energies fall in the region of the experimental absorption spectrum. However, the use of the "discrete variational method" discarding the use of the muffin-tin approximation, leads to a different sequence of some occupied orbitals.<sup>229</sup>

Ways are now being investigated to make it possible to avoid the use of the muffin-tin potential completely or at least in its original form.

In the discrete variational method<sup>230</sup> no use of the muffin-tin potential is made. The one-electron eigenfunctions are derived by means of the LCAO concepts; however, the secular equation is solved in a different way, than in the usual Hartree-Fock-Roothaan theory. The solution is obtained by minimizing a suitable error function, containing a number of parameters, over a set of sample points chosen in the space spanned by the molecule. This error function is obviously related to the approximate solution of the Hartree-Fock-Slater equation (involving the  $X\alpha$ -exchange-correlation term), but the matrix elements are now given in discrete form and not in integral form (usual Hartree-Fock theory), as a consequence of the use of a discrete number of sample points.

Avoiding the use of both the muffin-tin potential and the exchange-cor-

relation potential has recently been realized using the usual LCAO expansion in the calculation of some excitation energies for simple molecules, for example,  $N_2$ ,  $F_2$ ,  $CO$ , and  $H_2O$ ,<sup>231</sup> using the transition-state technique. Both of these functions of the one-electron SCF- $X\alpha$  Hamiltonian are fitted by least squares to suitable linear combinations of simple Gaussian functions.

A recent calculation of ionization energies derived within a standard self-consistent charge method based on the Hartree-Fock-Slater formalism and using the LCAO approximation has been reported on simple molecules, for example,  $AlCl$  and  $InCl$ , and the cluster  $Ni_5O$  with a fair overall accuracy of 1 eV.<sup>232</sup> Actually, this calculation avoids the use of arbitrary parameters (sphere radii).

Nevertheless, numerous papers still exist based on the use of the muffin-tin potential, but this potential involves overlapping spheres, the sphere radii still being left as arbitrary parameters. Charge-transfer excitations and  $d-d$  transition energies in the ferrocene molecule have been reported in good agreement with observed data using the transition-state concept and the muffin-tin potential.<sup>233</sup> Also, energy-band calculations and related properties are still often undertaken using the muffin-tin potential in the frame of the multiple-scattering-wave method or the augmented plane-wave method.

However, the present state of development of the  $X\alpha$ -model clearly shows that the LCAO approximation is more and more to be preferred relative to the muffin-tin approximation in numerous applications and at the same time an *ad hoc* SCF computational technique, coupled to the former approximation, is being sought for solving the secular equation at a "reasonable price".<sup>239</sup>

#### IV. ELECTRONIC TRANSITIONS IN METALLIC COMPLEXES AND "THE $10Dq$ PROBLEM"

##### A. Preliminaries

It is a known experimental fact that numerous metallic compounds absorb light in the far UV region or the visible region, giving rise to characteristic absorption bands. Studying the nature of the corresponding transition energies denominated in crystal-field theory by the quantity  $10Dq$  (see below) constitutes an adequate means of getting useful information about the symmetry species of both the ground state and the excited state(s) involved in the excitation process(es). The occurrence of these "molecular" excited states is merely a consequence of a natural physical phenomenon, for example, vibronic excitations.<sup>240</sup> Electronic transitions often allowed as a result of such excitation processes have to be carefully distinguished from the ones envisaged until now, that is, those involving "virtual excited states," their occurrence being essentially a consequence of the use of a mathematical

device (perturbation theory). For this reason we consider the analysis of these observables as a subject somewhat apart from the preceding ones.

Since calculations of the relevant transition energies have puzzled many people during these last two decades, we would like to comment briefly on them here.

### B. $d^n$ Configuration

Considering the simple case of a  $d^n$  configuration ( $n < 10$ ) involved in a point-charge octahedral field, it is elementary to show that this fivefold orbital degenerate level will split up into a doubly and triply degenerate sublevel belonging to the  $e_g$  and  $t_{2g}$  representations, respectively; the energy gap is given by<sup>241</sup>

$$e_M(d_{z^2}, d_{x^2-y^2}) - e_M(d_{xy}, d_{yz}, d_{xz}) = 6Dq - (-4Dq) = 10Dq$$

In the weak-field approximation, that is, the total angular momentum  $J$  still being a good quantum number, the occupation numbers of the levels  $t_{2g}$  and  $e_g$  will satisfy to a maximum value of the total spin quantum number  $S$ . For obvious energetic reasons, the  $t_{2g}$  levels will, in the first place, be filled assuming an environment of negative point charges. In the strong-field case, in contrast to the weak-field limit, the  $t_{2g}$  and  $e_g$  levels have to be occupied independently, in conformity with the Hund rules and the Pauli principle.

The expansion of the octahedral potential field in terms of Legendre polynomials leads to the well-known result, that is,

$$[Dq]_{\text{oct}} = \frac{35}{4} \frac{Ze}{R^5} \overline{r^4}$$

$R$  is the distance between the central metallic cation and the anion, whose charge is  $Ze$ , and  $\overline{r^4}$  is the mean value of the fourth power of the electron radius.

Similar relationships can easily be derived for other symmetry fields, for example,

$$[Dq]_{\text{oct}} = -\frac{9}{4} [Dq]_{\text{tet}} = -\frac{9}{8} [Dq]_{\text{cub}}$$

The first relationship is experimentally verified through thermal expansion and pressure experiments, producing an exponent of the distance dependence of 5 or 6.<sup>242</sup> This does not mean, however, that  $[Dq]$  may be calculated for an ion in a definite lattice by simply inserting a new radius. The  $[Dq]$  derivation is a rather involved one.

### C. Solution by Crystal-Ligand Field Theory

For historical reasons, a solution has first been sought in the frame of the crystal-ligand field theory. A preliminary and important remark has to be put forward prior to our critical survey on the  $10Dq$  calculations. The parameter  $10Dq$  is an empirical quantity that rests on a purely phenomenological ground, characterizing essentially the orbital splitting of the unfilled  $d^n$  shells of the central ion, for example, an ion of the iron or rare-earth group, by the surrounding electric field (crystalline field). According to a crystal-field picture, the corresponding absorption bands observed in numerous metallic compounds obeying different symmetry point groups are due to electronic excitations between these  $d$  levels. Supplementary excitation processes relative to the single one occurring in a pure octahedral symmetry field arise from lower symmetry fields. Neither the electronic spin functions nor the occupation numbers of the  $d$  levels are exactly specified in the originally defined and observed energy gaps. The  $(nd)$  electrons are empirically considered as a whole (involved in the quantity  $q$  left as a variable parameter), whereas the valence electrons of the ligands are inserted into the "frozen cores" of the respective atoms. The crystal-field model is at this stage a faithful mirror of the experimental point of view.

A first attempt to connect a great number of observed transition energies in metallic compounds is made by Tanabe et al.<sup>243</sup> in the frame of the crystal-field model. Considering octahedral compounds of the first-transition period and neglecting the overlap between the  $d$  orbitals and the ligand orbitals, these authors express in a set of diagrams the calculated excited-state energies as functions of the parametric ratio  $Dq/B$  where  $B$  is the Racah parameter corresponding to the *free ion*. The excited-state energies, as well as the corresponding wave functions related to well-defined configurations  $(nd)^q (q < 10)$  and multiplicities, are derived theoretically using the Griffith technique.<sup>244</sup> A best fit with the experimental spectra, that is, with the help of the quantities  $Dq$  and  $B$ , shows that smaller values of the latter ought to be used for the complex ion as compared to the  $B$ 's free-ion values. These actual  $B$  values are related, according to Schaeffer et al. to the so-called nephelauxetic effect,<sup>245</sup> characterizing an interelectron repulsion energy of a smaller magnitude for the ion cluster than for the corresponding gaseous state ion. This  $B$  reduction has tentatively been interpreted as a manifestation of an expansion of the unfilled metal  $d$  orbitals towards the ligand environment. Actually, a satisfactory quantum-mechanical interpretation of the mechanisms underlying the nephelauxetic effect is still not available.

### D. Solution by the Molecular Orbital Theory

The work of Sugano et al.<sup>246</sup> on the cluster  $(\text{NiF}_6)^{4-}$  (involved in the  $\text{KNiF}_3$  lattice) using a simplified approach of the molecular orbital model\* is the first quantum-mechanical calculation of the  $10Dq$  quantity. Although subjected later to severe criticisms, this work is the starting point towards the development of new ideas on this subject and more suitable methods of calculation. In view of the great amount of computational work needed when developing the assumptions underlying a pure crystal-field model within an LCAO-MO model, Sugano et al. made severe approximations: i. use of a pure "ionic" Hamiltonian, that is, the cluster is considered as a superposition of pure ionic entities  $(\text{Ni}^{2+} + 6\text{F}^-)$ , in which the overlap is not explicitly included; ii. use of a minimum basis set, the inner-shell Ni electrons, up to  $3p$  shells, being replaced by a core potential frozen in the actual wave function calculation; iii. only one- and two-center two-electron integrals and some three-center one-electron integrals are explicitly considered. A salient feature to note in the Sugano work is the important contribution of the covalence effects arising, curiously enough, from the antibonding  $d$  electrons corresponding to the  $e_g$  level, these effects being essential for approaching closely the experimental transition energy, that is,  $7250\text{ cm}^{-1}$  ( $+6.350\text{ cm}^{-1}$  theoretically).

In contrast to this result, Watson et al.,<sup>247</sup> using the same Hamiltonian operator in a more elaborate and rigorous integral formalism, find that covalent effects are due predominantly to the *bonding* ligand electrons pertaining to the same  $e_g$  level. However, as their final  $10Dq$  value was in complete disagreement with the observation, they conclude the inadequacy of both treatments.

A common insufficiency of these two preceding works lies in a proper definition of the mathematical form of the Hamiltonian and therefore of its eigenvalues. So, a difference of the latter quantities can hardly approach the physical content of the observed transition energy, that is, a single value of  $10Dq$  for all possible spectroscopic states arising from a definite electronic configuration of the metal.

\*Such an MO treatment involves an antibonding wave function

$$\psi^a = N^{-1/2}(\varphi - \lambda\chi)$$

which is a linear combination of a  $d$  atomic orbital,  $\varphi$ , and a combination,  $\chi$ , of ligand orbitals and, analogously, a bonding wave function

$$\psi^b = N^{-1/2}(\chi + \gamma\varphi)$$

which is orthogonal to  $\psi^a$ . The MO's of interest in a cubic field having a metallic character ( $d$  electrons) are  $\psi_{e_g}^a$  and  $\psi_{t_{2g}}^a$ , whereas the bonding orbitals  $\psi_{t_{2g}}^b$  and  $\psi_{e_g}^b$  are predominantly of ligand character. The numerical coefficients  $\lambda$  and  $\gamma$  are the covalency parameters of the MO model.

The conventional definitions of the orbital energies (eigenvalues) for open-shell systems, according to the Hartree-Fock-Roothaan procedure<sup>248</sup> are not directly suitable for a description of the experimental transition energy because the energies of the  $e_g$  and  $t_{2g}$  levels within the same configuration  $(nd)^q$  ( $q < 10$ ) may vary according to the species of spectroscopic states derived from that configuration [parameters  $a$ ,  $b$ ,  $\alpha$ ,  $\beta$  of (17) and (28) of the open-shell paper of Roothaan<sup>248</sup>]. Clearly this fact leads to serious ambiguities when matching the "clear-cut" phenomenological  $10Dq$  quantity which does not bother with concepts such as spin-up, spin-down and the relative level occupation numbers, both connected to theoretical expressions.

The first attempt to bridge the observed quantity with an orthodox, although semiempirical, MO treatment, inspired from the Roothaan model, was undertaken by Offenhartz,<sup>249</sup> who took as probes the complex ions  $\text{CrF}_6^{3-}$ ,  $\text{FeF}_6^{3-}$ , and  $\text{NiF}_6^{4-}$ , all corresponding to a  $d^1$  configuration. One merely replaces the open-shell Roothaan-Fock Hamiltonians (for closed- and open-shell parts of the open-shell system) by a single one, that is, the operator corresponding to the average state of the *entire*  $(nd)^q$  configuration. This means that neither the ground state nor the excited state still corresponds to definite spectroscopic states, a single set of MO's being responsible for a single observed quantity, in analogy with the crystal-field phenomenological definition. It is then possible to derive a set of MO's that better correspond to the usual analysis of molecular spectra in terms of electronic transitions. In this way one can incorporate the algebraic expressions of the mean-configuration orbital energies  $e_{t_{2g}}$  and  $e_{e_g}$ , as defined by the open-shell Roothaan formalism, into a unique energy expression giving the theoretical counterpart of the single observed quantity  $10Dq$ .

The  $d^1$  configuration systems treated by Offenhartz are but "heuristic cases" regarding the uniqueness of the energy expression matching the single observed (in an octahedral crystal field) quantity  $10Dq$ . Indeed, in the case of a  $d^n$  configuration system with  $n > 1$ , it is no longer possible<sup>250</sup> to define the latter unambiguously through a single energy expression (in the case of an octahedral crystal field), as the resulting energy expression in addition to the above mean values  $e_{e_g}$  and  $e_{t_{2g}}$ , contains extra terms such as  $\sum_{i,j} (2aJ_{ij} - bK_{ij})$ , the sum acting on singly occupied orbitals.<sup>248</sup>

However, for the hexafluoride complex anions mentioned above ( $d^1$  configuration systems), satisfactory results along these lines are obtained using, on the one hand, a simplified open-shell Hamiltonian, that is, in the ionic approximation, and, on the other hand, including in the Fock-Roothaan elements corrections for metal-ligand charge transfers, ignoring, however, monocenter charge rearrangements.<sup>251</sup> These corrections provide a way to make the *whole* set of occupied orbitals participate in the excitation process. The justification of the foregoing standpoint is strongly supported by a

recent *ab initio* work by Kleinman et al. on the  $(\text{NiF}_6)^{4-}$  cluster.<sup>252</sup> To avoid huge open-shell computations they start with a closed-shell type Hamiltonian where the  $a$  and  $b$  parameters of Roothaan's open-shell formalism are defined in terms of doubly occupied orbitals, but the fractional occupancy number  $f$  has the right value for open-shell MO's. In other words, they use an effective Hamiltonian equivalent to the Fock operator as defined in Section 1.F. A great change in the values of the coefficients of the orbitals is found to be responsible for the great difference in the final  $10Dq$  value, according to whether this quantity is obtained within the SCF ground state orbitals or by use of separate SCF calculations for the ground-state and excited-state orbitals respectively. This emphasizes the importance of the rearrangement of the electronic cloud in the excitation process where the full orbital set is concerned. The electron transfers metal→ligand and, to a lesser extent, ligand→metal are significant as shown by the great difference in magnitude of the MO coefficients of the  $d$  orbitals corresponding to a few consecutive iterations.

Let us stress that the widespread opinion of using an "ionic" Hamiltonian in the  $10Dq$  calculation is justified *only* if the covalency effects due to ligand electrons are properly introduced, and if the iterative SCF procedure leads to a real convergent solution.

It is worth mentioning the work of Moskowitz et al.<sup>253</sup> on  $(\text{NiF}_6)^{4-}$  using the Roothaan single Hamiltonian RHF method for the calculation of some excited-state wave functions and their corresponding energies. Transition energies roughly three times as great as the experimental value are found. Also, the free ion Racah parameter  $B$  for  $\text{Ni}^{2+}$  and that of the ion embodied in the cluster differ negligibly, in disagreement with the nephelauxetic effect. Both of these facts mean that a proper construction of the excited states involving a great flexibility of the basis set is necessary. Unrestricted HF calculations (UHF) give a substantial improvement of the  $10Dq$  value<sup>253</sup> in the case of the above cluster, that is,  $5976 \text{ cm}^{-1}$  ( $7250 \text{ cm}^{-1}$  experimentally). But the wave functions are no longer eigenfunctions of  $S^2$  nor of  $L^2$ , and, therefore, no longer eigenfunctions of the Hamiltonian fulfilling the (octahedral) symmetry of the  $\text{NiF}_6^{4-}$  ion. The calculated covalency parameters are also in reasonable agreement with experiment, but our preceding remark should be borne in mind. Other related papers using the UHF scheme have been published.<sup>254,255</sup>

Finally, we should like to discuss two papers, one by Wachters et al.<sup>256</sup> and the other by Hubbard.<sup>257</sup>

The first paper is an *ab initio*<sup>248,256</sup> satisfactory calculation of the  $10Dq$  parameter on  $\text{NiF}_6^{4-}$ , using a large Gaussian basis set. In this basis all the integral types are exactly computed. The value found is  $10Dq = E(^3T_{2g}) - E(^3A_{2g}) = 5.443 \text{ cm}^{-1}$ . Furthermore, this result is analyzed in terms of a

certain number of standard contributions, for example, the orthogonalization process of the starting ionic wave functions ( $T_{2g}$  and  $A_{2g}$ ) represents about 75% of the overall theoretical value. This process, occurring in the normalization of the respective wave functions, is closely associated with the repulsive energy of the  $d$  charge densities overlapping nearby ligand shells. It is also found that additional layers of (positive) point charges displaced around the basic cluster have a negligible incidence on the primitive cluster wave functions and can therefore be taken into account using the "unperturbed" cluster orbitals.

It will be noticed that no one has considered explicitly the contribution of the electronic correlation using CI or high-order perturbation calculations. In the standard Hartree-Fock independent particle model this correlation is neglected when constructing the Fock Hamiltonian operator. The electronic correlation problem is the one whose development in an *ab initio* framework, that is, using the molecular-orbital approach,<sup>258</sup> is still in its initial phase. On the other hand, Hubbard et al.,<sup>257</sup> using a simple valence bond approach among different electronic configurations for the metal ion as well as for the ligand anions, succeed in the case of the cluster  $(\text{NiF}_6)^{4-}$  and  $(\text{MnF}_6)^{4-}$  in deriving the contributions of certain correlation processes involved in the covalent parameters of the valence-bond theory. Nevertheless, these evaluations, which rest partly on the use of empirical data (i.e., spectroscopic data), show the major importance of "covalent" effects in contrast to a simple "ionic" model in deriving the  $10Dq$  parameter (theoretical value  $5400\text{ cm}^{-1}$ ) in such so-called ionic compounds.

## V. CONCLUSIONS

The first object of this review has been to present and discuss calculations of mono- and bielectronic observables on metallic complexes using a special semiempirical molecular orbital model deriving directly from the LCAO-SCF-Roothaan-Hartree-Fock theory, the latter being issued from the time-independent Schrödinger equation. Specifically, our derivations of, respectively, the Fermi contact term (isotropic part of the hyperfine interactions), the  $g$  tensor components (occurring in the Zeeman term), the nuclear quadrupole coupling constant, and the spin-spin dipolar interactions (contributing the zero-field splitting) have, to date, no counterparts in *ab initio* calculations presented for the metallic compounds envisaged here. This broad range of observables treated in conjunction with a great variety of transition-metal compounds, as well as the good correlations obtained with the observation, make us rather confident as to the sound parametrization involved in the construction of the corresponding approximate wave functions, as well as to the approximations made in the actual evaluations of these observables.



Secondly, this review provides a critical survey, issued from our own research work, of some molecular orbital formalisms applied mainly to transition-metal complexes.

It is worthwhile emphasizing that the whole review covers only a small fraction of a vast amount of studies in the field of the quantum-mechanical molecular orbital model. Important domains of investigation lie within the field of biochemistry, where great progress has been made this last decade in understanding the reactivity (including environment effects) and elucidating the electronic structures of fundamental molecules in living cells.<sup>259</sup>

### Acknowledgments

First, I am deeply grateful to Prof. I. Prigogine for having given me the opportunity to write this review and for his encouragement and unshaken enthusiasm during the patient elaboration of this work. It is my privilege to address my sincere appreciation to a number of colleagues and friends who have directly collaborated on part or the whole of the matters reported here. In this respect, it is a great pleasure to acknowledge the many years of close collaboration with my colleague and friend, Dr. C. A. ten Seldam, who wrote numerous very efficient programs and whose assistance in some difficult mathematical developments connected with some calculations of observables has been decisive. I am very grateful to my friend Prof. G. Berthier, who initiated me into doing the actual calculations of the molecular orbitals about 10 years ago. He accepted the heavy burden of critically reading the whole manuscript. Moreover, the many times we have been able to make use of his experience during discussions, which were often passionate, have helped us enormously in the realization of an important part of the results reported here. I am also indebted to Dr. B. Levy for a fruitful discussion on the configuration-interaction technique. In writing such a review being influenced by and therefore having reported about numerous works connected directly with the object of this manuscript is as natural as it is unavoidable. I take this opportunity to express my grateful thanks to Prof. J. de Boer and Prof. S. Wouthuysen, to the former for having allowed me, in the name of the executive committee of the Foundation for Fundamental Research on Matter, to accomplish this work, and to the latter for the prodigality of his encouragements throughout my work. Also, I cannot forget the stimulating atmosphere of the Van der Waals Laboratory, directed by Prof. N. J. Trappeniers, and last, but not least, my grateful thanks to Mrs. I. Geerling for her excellent typing.

### References and Notes

1. M. Delbrück, *Proc. Roy. Soc. (London), Ser. A*, **129**, 686 (1930).
2. E. Hückel, *Z. Physik*, **70**, 204 (1931); *ibid.*, **76**, 628 (1932); for EH method, see R. Pariser and R. G. Parr, *J. Chem. Phys.*, **21**, 466 (1953).
3. (a) Closed-shell systems, see C. C. J. Roothaan, *Rev. Mod. Phys.*, **23**, 69 (1951); (b) Open-shell systems, see C. C. J. Roothaan, *Rev. Mod. Phys.*, **32**, 179 (1960).
4. M. Born and J. R. Oppenheimer, *Ann. Physik*, **84**, 457 (1927).
5. P. G. Lykos and R. G. Parr, *J. Chem. Phys.*, **24**, 1166 (1956); *ibid.*, **25**, 1301 (1956).
6. P. O. Löwdin, *J. Chem. Phys.*, **18**, 365 (1950).
7. J. A. Pople, D. P. Sandry, and G. A. Segal, *J. Chem. Phys.*, **43**, S129 (1965).
8. See, for example, A. Streitwieser, Jr., *Molecular Orbital Theory for Organic Chemists*, Wiley, New York, 1961.
9. M. Goeppert-Mayer and A. L. Sklar, *J. Chem. Phys.*, **6**, 645 (1938).
10. W. Moffitt, *Proc. Roy. Soc. (London) Ser. A*, **210**, 245 (1951).

11. See, for example, R. G. Parr, *J. Chem. Phys.*, **20**, 1499 (1952).
12. M. Astier, G. Berthier, and P. Milli , *J. Chem. Phys.*, **57**, 5008 (1972).
13. R. Pariser, *J. Chem. Phys.*, **21**, 568 (1953).
14. M. Wolfsberg and L. Helmoltz, *J. Chem. Phys.*, **20**, 837 (1952).
15. C. J. Ballhausen and H. B. Gray, *Inorg. Chem.*, **1**, 111 (1962).
16. W. L. Yeranos and D. A. Hasman, *Z. Naturforsch.*, **A22**, 170 (1967).
17. M. D. Newton, F. P. Boer, and W. N. Lipscomb, *J. Am. Chem. Soc.*, **88**, 2367 (1966).
18. See J. C. Slater, *Quantum Theory of Molecules and Solids*, Vols. I and II, McGraw-Hill, New York, 1963 and 1965.
19. See S. T. Epstein, *The Variation Method in Quantum Chemistry*, Academic Press, New York, 1974.
20. H. C. Longuet-Higgins and J. A. Pople, *Proc. Phys. Soc. (London)*, **A68**, 591 (1955).
21. See C. K. J rgensen, *Int. J. Quantum Chem.*, (John Wiley, New York), **1**, 191 (1967).
22. (a) G. Berthier, P. Milli , and A. Veillard, *J. Chim. Phys.* **8** (1965); (b) G. de Brouck re, *Theor. Chim. Acta*, **19**, 310 (1970).
23. K. Ruedenberg, *J. Chem. Phys.*, **19**, 1433 (1951).
24. R. S. Mulliken, *J. Chem. Phys.*, **23**, 1833 (1955).
25. See Ref. 21.
26. K. Nishimoto and N. Mataga, *Z. Phys. Chem. (Frankfurt)*, **13**, 140 (1957).
27. G. Berthier, G. del Re, and A. Veillard, *Nuovo Cimento*, **X**, **44**, 315 (1966).
28. L. C. Cusachs, *J. Chem. Phys.*, **43**, Suppl., 157 (1965).
29. See, for example, C. K. J rgensen, *Oxidation Numbers and Oxidation States*, Springer-Verlag, Berlin, 1969.
30. H. Basch, A. Viste, and H. B. Gray, *Theor. Chim. Acta*, **3**, 458 (1966); *J. Chem. Phys.*, **44**, 10 (1966).
31. R. F. Fenske and D. D. Radtke, *J. Inorg. Chem.*, **7**, 479 (1968).
32. R. Pariser and R. G. Parr, *J. Chem. Phys.*, **21**, 466 (1953); *ibid.* **21**, 767 (1953).
33. See J. C. Slater, *Quantum Theory of Atomic Structure*, Vols. I and II, McGraw-Hill, New York, 1960.
34. See Ref. 33.
35. L. Di Sipio, E. Tondello, G. De Michelis, and L. Oleari, *Chem. Phys. Lett.*, **11**, 287 (1971).
36. G. Pilcher and H. A. Skinner, *J. Inorg. Chem.*, **24**, 937 (1962).
37. J. Hinze and H. H. Jaff , *J. Am. Chem. Soc.*, **84**, 540 (1962); *ibid.*, **85**, 148 (1963).
38. Y. Ellinger, A. Rassat, R. Subra, and G. Berthier, *Theor. Chim. Acta*, **10**, 289 (1968).
39. All the molecular exchange integrals  $K_{ij}$  with  $i \neq j$ , aside from those that cancel because of symmetry reasons, have been tabulated in the case of the cluster  $[\text{CrCl}_4](D_{4h})$ , using the Mulliken-Ruedenberg formulas.<sup>23</sup> They appear, indeed, to be small compared to the Coulomb  $J_{ij}$  integrals with  $i \neq j$ .
40. Let us remember that this difficulty arises because for an open-shell system,  $\sum_j^{\text{occ}} K_j$  for the  $\alpha$  spin-orbital functions is different from  $\sum_j^{\text{occ}} K_j$  for the  $\beta$  spin-orbital functions. (The summations extend over "occupied" orbitals.)
41. The LCAO form of the UHF equations for open-shell systems was derived independently by G. Berthier [*C. R. Acad. Sci.*, **238**, 91 (1954)] and by J. A. Pople and R. K. Nesbet [*J. Chem. Phys.*, **22**, 571 (1954)]. For a full account, see G. Berthier, *Molecular Orbitals in Chemistry, Physics and Biology*, A tribute to R. S. Mulliken, Academic Press, New York, 1964, p. 57.
42. W. Kolos and C. C. J. Roothaan, *Rev. Mod. Phys.*, **32**, 219 (1960).
43. H. M. James and A. S. Coolidge, *J. Chem. Phys.*, **1**, 825 (1933).

44. Citation taken from the excellent textbook written by C. A. Coulson, *Valence*, Oxford University Press, London, 1963, p. 124.
45. See, among other papers by these authors, J. Čížek and J. Paldus, *J. Chem. Phys.*, **47**, 3976 (1967); J. Paldus and J. Čížek, *J. Chem. Phys.*, **52**, 2919 (1970).
46. I. Fischer Hjalmar, *Ark. Fys.*, **11**, 259 (1957).
47. R. F. Prat, *Phys. Rev.*, **6**, 1735 (1972).
48. A. Veillard, *Chem. Commun.*, 1427 (1969).
49. A. Abragam and B. Bleany, *Electron Paramagnetic Resonance of Transition Ions*, Clarendon Press, Oxford 1970.
50. H. Kopfermann, *Nuclear Moments*, Academic Press, New York, 1958.
51. A. E. Siegman, *Microwave Solid-State Masers*, McGraw-Hill, New York, 1964.
52. J. Callaway, *Energy Band Theory*, Academic Press, New York, 1964; J. C. Slater, *Quantum Theory of Molecules and Solids*, Vols. I and II, McGraw Hill, New York, 1964 and 1965. See also J. Callaway, *Quantum Theory of the Solid State*, Vol. A (especially chapter 4) and Vol. B (especially chapter 5) Academic Press, New York, 1974.
53. C. A. Coulson and H. C. Longuet-Higgins, *Proc. Roy. Soc. (London), Ser. A*, **191**, 39 (1947).
54. P. O. Löwdin, *J. Chem. Phys.*, **18**, 365 (1950).
55. R. S. Mulliken, *J. Chem. Phys.*, **23**, 1833, 1841, 2338, 2343 (1955).
56. G. Berthier, J. Baudet, and M. Suard, *Tetrahedron*, **19** (1963), Suppl. 2, 1.
57. I. Fischer-Hjalmar, *J. Chem. Phys.*, **42**, 1962 (1965); *Molecular Orbitals in Chemistry, Physics and Biology*, A tribute to R. S. Mulliken, Academic Press, New York, 1964, p. 361.
58. See Ref. 23; see also, J. P. Dahl, *Acta Chim. Scand.*, **21**, 1244 (1967); K. Ruedenberg, *J. Chem. Phys.*, **34**, 1861 (1961).
59. J. R. Platt, *Handb. Phys.*, **37** (2), 173 (1961).
60. W. Kutzelnigg, G. del Re and G. Berthier, *Topics in Current Chemistry*, Vol. 22, Springer Verlag, Berlin, 1971.
61. W. Lipson, *Proc. Roy. Soc. (London), Ser. A*, **251**, 347 (1935).
62. B. Bleany, *Proc. Phys. Soc.*, **A63**, 407 (1950).
63. H. Hartmann and H. L. Schäfer, *Z. Phys. Chem. (Leipz.)*, **197**, 116 (1951).
64. C. K. Jørgensen, *Acta Chim. Scand.*, **11**, 73 (1957).
65. A. Carbonaro; A. Greco, and G. Dall'Asta, *Tetrahedron Lett.*, (1967) 2037.
66. G. Natta, V. Giannini, P. Pino, and A. Cassata, *Chim. Ind. (Milan)*, **47**, 524 (1965).
67. G. Wilke, *Angew. Chem.*, **75**, 10 (1963).
68. A. Yamamoto, K. Morifuji, S. Ikeda, T. Saito, Y. Uchida, and A. Misono, *J. Am. Chem. Soc.*, **90**, 1878 (1968).
69. G. Wilke and G. Bogdanovic, *Angew. Chem.*, **73**, 756 (1961).
70. R. Uttech and H. Dietrich, *Z. Kristallogr.*, **122**, 60 (1965).
71. A. Abragam and M. A. L. Pryce, *Proc. Roy. Soc. (London), Ser. A*, **205**, 135 (1951).
72. R. McWeeny, *J. Chem. Phys.*, **42**, 1717 (1965).
73. S. H. Hagen, "Elektronenspinresonantie van koperionen in ammoniumchloride," PhD. Thesis, University of Amsterdam, 1966.
74. F. S. Stibbe and N. J. Trappeniers, *18th Ampère Congress*, Nottingham, P. S. Allen, E. R. Andrew, C. A. Bates Eds., North Holland Publ. 1974, p. 137.
75. R. D. Willett, *J. Chem. Phys.*, **41**, 2243 (1964); A. W. Schlüter, R. A. Jacobson and R. E. Rundle, *Inorg. Chem.*, **5**, 277 (1966).
76. N. J. Trappeniers, G. de Brouckère, and C. A. ten Seldam, *Chem. Phys. Lett.*, **4**, 327 (1971). See footnote p. 267.
77. See, for example, R. S. Mulliken, C. A. Rieke, D. Orloff, and H. Orloff, *J. Chem. Phys.*, **17**, 1248 (1949); H. H. Jaffé, *J. Chem. Phys.*, **21**, 258 (1953). These references contain part of the analytical expressions that we have used in deriving the numerical values of the overlap integrals; we have calculated also other overlap integrals by the use of general recursion formulae.

78. G. de Brouckère, *Bull. Soc. Chim. Belg.*, **76**, 407 (1967).
79. L. Oleari, G. de Michelis, and L. Di Sipio, *Mol. Phys.*, **10**, 111 (1966).
80. G. de Brouckère, *Theor. Chim. Acta*, **19**, 310 (1970).
81. C. K. Jørgensen, F. M. Horner, W. E. Hatfield and F. Y. Tyree, Jr, *Int. J. Quantum Chem.*, **1**, 191 (1967).
82. A. Veillard, *Chem. Commun.*, 1427, (1969).
83. Ph. E. Stevenson and W. N. Lipscomb, *J. Chem. Phys.*, **50**, 3306 (1969).
84. Ph. Millié and G. Berthier, *Coll. Int. Cent. Natl. Rech. Sci. Paris*, **191**, 31 (1970).
85. Part of these results have been reported in Ref. 76.
86. J. Demuynck and A. Veillard, *Chem. Phys. Lett.*, **6**, 204 (1970).
87. R. F. Fenske, D. S. Martin, and K. Ruedenberg, *Inorg. Chem.*, **1**, 441 (1962).
88. H. Bash and H. B. Gray, *Inorg. Chem.*, **6**, 365 (1967); also F. A. Cotton and C. B. Harris, *Inorg. Chem.*, **6**, 369 (1967).
89. P. Ros and G. C. A. Schuit, *Theor. Chim. Acta*, **4**, 1 (1966).
90. B. N. Figgis, *Introduction to Ligand Fields*, Interscience, New York, 1966, p. 312.
91. G. de Brouckère and C. A. ten Seldam, unpublished results.
92. K. D. Carlson, C. R. Claydon, and C. M. Moser, *J. Chem. Phys.*, **46**, 4693 (1967).
93. K. D. Carlson and R. K. Nesbet, *J. Chem. Phys.*, **41**, 1051 (1964).
94. K. D. Carlson and C. A. Moser, *J. Phys. Chem.*, **67**, 2644 (1963).
95. G. Hertzberg, *Molecular Spectra and Molecular Structure. I. Spectra of Diatomic Molecules*, Van Nostrand, Princeton, 1950.
96. K. D. Carlson and C. M. Moser, *J. Chem. Phys.*, **44**, 3259 (1966).
97. See, for example, A. D. McLean and M. Yoshimine, *J. Chem. Phys.*, **47**, 3256 (1967).
98. G. de Brouckère and C. A. ten Seldam: unpublished results.
99. J. H. Gibbs, *J. Phys. Chem.*, **59**, 644 (1955).
100. F. Grimaldi, A. Lecourt, and C. Moser, *Trans. Faraday Soc.*, **2**, 59 (1968) (Symposium).
101. F. A. Cotton and Ch. B. Harris, *Proc. Natl. Acad. Sci. U.S.*, **56**, 12 (1966).
102. G. de Brouckère and C. A. ten Seldam, unpublished results.
103. P. S. Han, T. P. Das, and M. F. Rettig, *Theor. Chim. Acta*, **16**, 1 (1970).
104. J. H. Van Vleck, *Electric and Magnetic Susceptibilities*, Oxford University Press, London and New York, 1932, p. 186.
105. N. F. Ramsey, *Molecular Beams*, Oxford University Press, London and New York, 1956.
106. W. N. Lipscomb, M. T. P. *International Review of Science*, Physical Chemistry Ser. 1, Vol. 1, W. Byers Brown, Butterworth, London, 1972, p. 167.
107. T. Miyazaki and H. Shinoda, *Bull. Chem. Soc. Jap.*, **46**, 1216 (1973); H. Shinoda and T. Akugatawa, *Bull. Chem. Soc. Jap.*, **48**, 3431 (1975).
108. A. T. Amos and R. J. Crispin, *J. Chem. Phys.*, **63**, 1890 (1975).
109. T. Amos and J. Musher, *J. Chem. Phys.*, **49**, 2158 (1968).
110. H. F. Hameka, *Rev. Mod. Phys.*, **34**, 87 (1962).
111. G. B. Arrighini, M. Maestro, and R. Moccia, *J. Chem. Phys.*, **52**, 6411 (1971).
112. F. London, *J. Phys. Radium*, **8**, 397 (1937).
113. J. A. Pople, *J. Chem. Phys.*, **37**, 53 (1962).
114. G. G. Hall and A. Hardisson, *Proc. Roy. Soc. (London)*, Ser. A, **268**, 328 (1962).
115. A. T. Amos and H. G. Roberts, *J. Chem. Phys.*, **50**, 2375 (1969).
116. R. McWeeny, *Mol. Phys.*, **1**, 311 (1958).
117. J. A. Pople, J. W. McIver, Jr., and N. S. Ostlund, *J. Chem. Phys.*, **49**, 2960 (1968).
118. E. A. Laws, R. M. Stevens, and W. N. Lipscomb, *J. Chem. Phys.*, **54**, 4269 (1971).
119. P. E. Cade and W. N. Huo, *J. Chem. Phys.*, **47**, 654 (1967).
120. R. Ditchfield, D. P. Miller, and J. A. Pople, *J. Chem. Phys.*, **53**, 613 (1970).
121. R. Ditchfield, *J. Chem. Phys.*, **56**, 5688 (1972).

122. B. J. Ransil, *Rev. Mod. Phys.*, **32**, 239 (1960).
123. G. P. Arrighini, M. Maestro, and R. Moccia, *J. Chem. Phys.*, **49**, 881 (1968).
124. M. Karplus and H. J. Kolker, *J. Chem. Phys.*, **38**, 1263 (1963).
125. P. D. Ellis, G. E. Marciel, and J. W. McIver, *J. Am. Chem. Soc.*, **94**(12), 4069 (1972).
126. M. Karplus and J. A. Pople, *J. Chem. Phys.*, **38**, 2803 (1963).
127. J. W. Emsley, *J. Chem. Soc. A*, 2018, (1968).
128. Specialist Periodical Report, *Nuclear Magnetic Resonance*, Vol. I (1971), Vol. II (1972), Vol. III (1973), Chemical Society Burlington House, London.
129. N. F. Ramsey, *Phys. Rev.*, **91**, 303 (1953).
130. J. A. Pople, J. W. McIver, and N. S. Ostlund, *J. Chem. Phys.*, **49**, 2960 (1968).
131. Cl. Barbier and G. Berthier, *Int. J. Quantum Chem.*, **1**, 657 (1967).
132. R. C. Fahey, C. Graham, and R. L. Piccioni, *J. Am. Chem. Soc.*, **88**, 193 (1966).
133. K. Ruedenberg, *J. Chem. Phys.*, **19**, 1433 (1951).
134. C. Barbier, D. Gagnaire, G. Berthier, and B. Levy, *J. Magn. Resonance*, **5**, 11 (1971).
135. A. Denis and J. P. Malrieu, *Mol. Phys.*, **23**, 581 (1972).
136. For ethane, Cl. Barbier and G. Berthier (Ref. 137) have used three different SCF wave functions, determined respectively, by (a) W. E. Palke and W. N. Lipscomb, *J. Am. Chem. Soc.*, **88**, 2384 (1966); (b) R. M. Pitzer, *J. Chem. Phys.*, **46**, 4871 (1967); *ibid*, **47**, 965 (1967). The latter are still the best existing wave functions for this molecule.
137. Cl. Barbier and G. Berthier, *Theor. Chim. Acta*, **14**, 71 (1969).
138. Cl. Barbier, H. Faucher, and G. Berthier, *Theor. Chim. Acta*, **21**, 105 (1971).
139. Cl. Barbier, G. Berthier, B. Levy, Ph. Millie, and P. Noël, *J. Chim. Phys.*, **7-8**, 859 (1975).
140. R. A. Bernheim, D. J. Hay, T. R. Krugh, and B. J. Lavery, *J. Chem. Phys.*, **50**, 1350 (1969).
141. A. D. Buckingham and J. A. Pople, *Trans. Far. Soc.*, **59**, 2421 (1963).
142. I. Morishima, A. Mizuno, and T. Yonezawa, *Chem. Phys. Lett.*, **7**, 633 (1970).
143. H. Nakatsuji, H. Kato, I. Morishima, and T. Yonezawa, *Chem. Phys. Lett.*, **4**, 607 (1970).
144. H. A. Bethe and E. E. Salpeter, "Quantum Mechanics of One and Two Electron Systems, *Handb. Phys.*, **35**, 89 (1957).
145. See, for example, S. H. Hagen and N. J. Trappeniers, *Physica*, **47**, 165 (1970) and the references therein.
146. J. Itoh and Y. Yamagata, *J. Phys. Soc. Jap.*, **17**, 481 (1962); W. Mandema, "Protonspin-roosterrelaxatie in ammoniumchloride onder hoge druk," Ph.D. Thesis, University of Amsterdam, 1970.
147. S. H. Hagen and N. J. Trappeniers, *Physica*, **66**, 166 (1973). N. J. Trappeniers and S. H. Hagen, *Physica*, **31**, 251 (1965).
148. G. de Brouckère, N. J. Trappeniers and C. A. ten Seldam, *Chem. Phys. Lett.*, **21**, 230 (1973).
149. T. S. Reed, *J. Chem. Phys.*, **41**, 1488 (1964).
150. A. Forman and J. A. van Wijck, *J. Chem. Phys.*, **44**, 73 (1966).
151. J. Demuyne, A. Veillard, and V. Wahlgren, *J. Am. Chem. Soc.*, **95**, 5563 (1973).
152. A. T. Amos and L. C. Snijder, *J. Chem. Phys.*, **41**, 1973 (1964). A. T. Amos and G. G. Hall, *Proc. Roy. Soc. (London)*, *Ser. A*, **263**, 483 (1961).
153. W. Marshall, *Proc. Phys. Soc. (London)*, **78**, 113 (1961).
154. P. S. Bagus, B. Liu, and H. F. Schaefer III, *Phys. Rev.*, **2A**, 555 (1970).
155. R. E. Watson and A. J. Freeman, *Phys. Rev.*, **123**, 2027 (1961).
156. J. W. Moskowitz, C. Hollister, and C. J. Hornbach, *J. Chem. Phys.*, **53**, 2570 (1970).
157. D. E. Ellis, A. J. Freeman, and P. Ros, *Phys. Rev.*, **176**, 688 (1968).
158. H. C. Longuet-Higgins and A. J. Stone, *Mol. Phys.*, **5**, 417 (1962).
159. G. de Brouckère, N. J. Trappeniers, and C. A. ten Seldam, *Physica* **84B**, 295 (1976).
160. A. J. Stone, *Proc. Roy. Soc. (London)*, *Ser. A*, **271**, 424 (1962).
161. R. S. Mulliken, *Phys. Rev.*, **33**, 730 (1929); *Rev. Mod. Phys.*, **4**, 1 (1932).

162. See, for example, W. Low, *Paramagnetic Resonance in Solids*, Academic Press, New York 1960.
163. M. Blume and R. E. Watson, *Proc. Roy. Soc. (London)* Ser A **270**, 565 (1962).
164. G. Malli and S. Fraga, *Theor. Chim. Acta*, **7**, 80 (1967).
165. M. Blume and R. E. Watson, *Proc. Roy. Soc. (London)*, Ser. A., **270**, 127 (1962).
166. E. Clementi, *Tables of Atomic Functions*, Suppl. 2, IBM 1965. San José Research Lab. California.
167. A. P. Jucys, V. A. Kaminskas, and V. J. Kaveckis, *Int. J. Quantum Chem.*, **II**, 405 (1968).
168. G. de Brouckère, N. J. Trappeniers, and C. A. ten Seldam, see Ref. 159.
169. A. A. Hock and O. S. Mills, *Advances in the Chemistry of Coordination Compounds*, Macmillan, New York 1961, p. 604.
170. J. D. Dunitz and L. E. Orgel, *J. Chem. Phys.*, **23**, 954 (1955); R. E. Robertson and H. M. McConnell, *J. Phys. Chem.*, **64**, 70 (1960).
171. J. S. Griffith, *The Theory of Transition Metal Ions* Cambridge University Press, Cambridge, 1961, p. 437.
172. G. de Brouckère and C. A. ten Seldam, unpublished results.
173. J. Higushi, *J. Chem. Phys.*, **38**, 1237 (1963); *ibid.*, **39**, 1339 (1963).
174. Y. N. Chiu, *J. Chem. Phys.*, **39**, 2736 (1963).
175. S. A. Boorstein and M. Gouterman, *J. Chem. Phys.*, **39**, 2443 (1963); *ibid.*, **41**, 2776 (1964); *ibid.*, **42**, 3070 (1964).
176. C. Thomson, *Mol. Phys.*, **10**, 309 (1966); *ibid.*, **11**, 197 (1966).
177. M. Godfrey, C. W. Kern, and M. Karplus, *J. Chem. Phys.*, **44**, 4459 (1966).
178. J. H. van der Waals and G. ter Maten, *Mol. Phys.*, **8**, 301 (1964).
179. T. Amos and L. Snijder, *J. Chem. Phys.*, **43**, 2146 (1965).
180. M. Geller and R. W. Griffith, *J. Chem. Phys.*, **40**, 2309 (1964).
181. A. Dalgarno and J. T. Lewis, *Proc. Roy. Soc. (London)*, Ser. A., **233**, 70 (1965).
182. B. Levy and E. Kochansky, *Theor. Chim. Acta*, **12**, 138 (1968).
183. E. R. Cohen and J. W. M. Dumond, *Rev. Mod. Phys.*, **37**, 537 (1965).
184. A. D. McLachlan, *Mol. Phys.*, **6**, 441 (1963).
185. C. C. J. Roothaan, *J. Chem. Phys.*, **19**, 1445 (1951).
186. This was first noted for one-electron two center integrals by F. P. Prosser and C. H. Blanchard, *J. Chem. Phys.*, **36**, 1112 (1962).
187. J. W. Richardson, W. C. Nieuwpoort, R. R. Powell, and W. F. Edgell, *J. Chem. Phys.*, **36**, 1057 (1962); *ibid.*, **38**, 796 (1963).
188. R. E. Watson and A. J. Freeman, *Phys. Rev.*, **123**, 521 (1961).
189. R. R. Sharma, T. P. Das, and R. Orbach, *Phys. Rev.*, **149**, 257 (1966); *ibid.* **155**, 338 (1967); *ibid.* **171**, 378 (1968).
190. P. S. Han, T. P. Das, and M. F. Rettig, *J. Chem. Phys.*, **56**, 3861 (1972).
191. The interatomic distances are taken from *Table of Interatomic Distances and Configurations in Molecules and Ions*, Special Publication Nos. 11 (1958) and 18 (1965). The Chemical Society, Burlington House, London.
192. Ph. Millié, B. Levy, and G. Berthier, *Localisation and Relocalisation in Quantum Chemistry*, Vol. 1, O. Chalvet, R. Daudel, S. Diner, and J. P. Malrieu, Eds., D. Reidel Dordrecht, 1975, p. 59. See also J. Lennard-Jones and J. A. Pople, *Proc. Roy. Soc. (London)*, Ser. A., **202**, 166 (1950).
193. J. Ellinger, B. Levy, Ph. Millié, and R. Subra, *Localisation and Delocalisation in Quantum Chemistry*, Vol. 1, O. Chalvet, R. Daudel, S. Diner and J. P. Malrieu, Eds., D. Reidel Dordrecht, 1975, p. 283.
194. M. Tinkham, *Proc. Roy. Soc. (London)*, Ser. A, **236**, 535 (1956).
195. S. M. Blinder: *Adv. Quantum Chem.*, **2**, 47 (1965); R. G. Woolley, *Mol. Phys.*, **30**, 649 (1975).

196. J. Paviot and J. Hoarau, *C. R. Acad. Sci. (Paris)*, **C272**, 1718 (1971).
197. W. Sanger and J. Voittlander, *Chem. Phys.*, **9**, 183 (1975).
198. H. Faucher, unpublished results.
199. For a comprehensive treatment of the  $X\alpha$ -theory as well as a broad survey of its applications, we refer the reader to Slater's latest treatise: J. C. Slater, *The Self-Consistent Field for Molecules and Solids*, Vol. 4, McGraw-Hill, New York, 1974.
200. G. Berthier, *Adv. Quantum Chem.*, **8**, 183 (1974).
201. J. P. Dahl and C. J. Ballhausen, *Adv. Quantum Chem.*, **4**, 170 (1968).
202. J. A. Pople and D. L. Beveridge, *Approximate Molecular Orbital Theory*, McGraw-Hill, New York, 1970; J. N. Murrell and A. J. Harget, *Semi-empirical SCF MO Theory of Molecules*, Wiley, London, 1972.
203. M. Wolfsberg and L. Helmholz, *J. Chem. Phys.*, **20**, 837 (1952).
204. CNDO model: J. A. Pople, D. P. Sandry, and G. A. Segal, *J. Chem. Phys.*, **43**:S, 129 (1965); J. A. Pople and G. A. Segal, *op. cit.*, **43**:S, 136 (1965).
205. INDO model: J. A. Pople, D. L. Beveridge, and P. A. Dobosh, *J. Chem. Phys.*, **47**, 2026 (1967).
206. NDDO model: J. A. Pople, D. P. Sandry, and G. A. Segal, *J. Chem. Phys.*, **43**S, 129 (1965).
207. These algorithms refer to the so-called CNDO/1 and CNDO/2 parameterization. CNDO/1 parameterization: J. A. Pople and G. A. Segal, *J. Chem. Phys.*, **43**S, 136 (1965); CNDO/2 parameterization: J. A. Pople and G. A. Segal, *J. Chem. Phys.*, **44**, 3289 (1966).
208. G. C. Allen and D. W. Clack, *J. Chem. Soc. A*, 2668, (1970).
209. D. W. Clack and M. S. Farrimond, *J. Chem. Soc. A*, 299, (1971).
210. J. P. Dahl, *Acta Chem. Scand.*, **21**, 1244 (1967).
211. R. D. Brown and K. R. Roby, *Theor. Chim. Acta*, **16**, 175, 194, 278, 291 (1970); R. D. Brown and P. G. Burton, *op. cit.*, **18**, 309 (1970).
212. C. J. Ballhausen and H. B. Gray, *Molecular Orbital Theory* Benjamin, New York 1964; H. Basch, A. Viste, and H. B. Gray, *J. Chem. Phys.*, **44**, 10 (1966); H. Basch, A. Viste, and H. B. Gray, *Theor. Chim. Acta (Berl.)*, **3**, 458 (1965).
213. M. D. Newton, F. P. Boer, and W. N. Lipscomb, *J. Am. Chem. Soc.*, **88**, 2367 (1966).
214. M. D. Newton, F. P. Boer, and W. N. Lipscomb, *J. Am. Chem. Soc.*, **88**, 2353 (1966); F. P. Boer, M. D. Newton, and W. N. Lipscomb, *op. cit.*, **88**, 2361 (1966); M. D. Newton, F. P. Boer, and W. N. Lipscomb, *op. cit.*, **88**, 2367 (1966); W. E. Pake and W. N. Lipscomb, *op. cit.*, **88**, 2384 (1966).
215. J. A. Tossel and W. N. Lipscomb, *J. Am. Chem. Soc.*, **94**, 1505 (1972).
216. R. Manne, *Theor. Chim. Acta*, **6**, 299 (1966).
217. J. C. Slater, *Phys. Rev.*, **81**, 385 (1951); *ibid.*, **82**, 538 (1951).
218. R. Gaspar, *Acta Phys. Acad. Sci. Hung.*, **3**, 263 (1954).
219. W. Kohn and L. J. Sham, *Phys. Rev.*, **140A**, 1133 (1965).
220. F. Bloch, *Z. Phys.*, **57**, 545 (1929).
221. P. A. M. Dirac, *Proc. Cambridge Phil. Soc.*, **26**, 376 (1930); E. Wigner, *Phys. Rev.*, **46**, 1002 (1934).
222. The  $X\alpha$ -model using the muffin-tin potential predicts in case of the simple system  $C_2$  no bonding between the atoms [see J. C. Slater, *Int. J. Quantum Chem.*, Symposium, **8**, 81 (1974)]. Also, the calculated ionization energies of  $H_2O$ , CO compared badly with experimental data: J. W. D. Connolly and J. R. Sabin, *J. Chem. Phys.*, **56**, 5529 (1972); J. W. D. Connolly, A. Siegbahn, U. Gelius, and C. Nordling, *J. Chem. Phys.*, **58**, 4265 (1973).
223. J. W. D. Connolly and K. H. Johnson, *Chem. Phys. Lett.*, **10**, 616 (1971).
224. K. H. Johnson and F. C. Smith, Jr, *Chem. Phys. Lett.*, **10**, 219 (1971).
225. V. A. Gubanov, J. Weber and J. W. D. Connolly, *J. Chem. Phys.*, **63**, 1455 (1975).
226. K. H. Johnson and F. C. Smith, Jr, *Phys. Rev.*, **B5**, 831 (1972). K. H. Johnson, *Adv. Quantum Chem.*, **7**, 143 (1973).

227. It should be noted that the solution of the secular equation proceeds in a different way than in the SCF-LCAO method. The radial dependence of the basis functions, solution of the Schrödinger equation, is predetermined by numerical integration, and only the determination of the angular dependence is left for the secular matrix. This means that the basis set now becomes two dimensional, one degree of freedom being predetermined. The energy levels of the systems are related to the energy dependence of the coefficients of the scattered wavelets emitted by the atoms, and the zero's of the corresponding function give the required eigenvalues. These are found one at a time rather than simultaneously as in the LCAO methods.
228. M. Boring, J. H. Wood, and J. W. Moskowitz, *J. Chem. Phys.*, **63**, 638 (1975).
229. A. Rosen and D. E. Ellis, *Chem. Phys. Lett.*, **27**, 595 (1974).
230. D. E. Ellis and T. Parameswaran, *Int. J. Quantum Chem.*, **5**, 443 (1971).
231. H. Sambe and R. H. Felton, *J. Chem. Phys.*, **62**, 1122 (1975).
232. A. Rosen, D. E. Ellis, H. Adachi, and F. D. Averill, *J. Chem. Phys.*, **65**, 3629 (1976).
233. N. Rösch and K. J. Johnson, *Chem. Phys. Lett.*, **24**, 179 (1974).
234. V. Calder, D. E. Mann, K. S. Seshadri, M. Allavena, and D. White, *J. Chem. Phys.*, **51**, 2093 (1969).
235. M. Astier, G. Berthier, and Ph. Millié, *J. Chem. Phys.*, **57**, 5008 (1972).
236. B. Cook, *Theor. Chim. Acta (Berl.)*, **40**, 297 (1975).
237. J. A. Pople, *J. Am. Chem. Soc.*, **97**, 5306 (1975); W. J. Hehre, *op. cit.*, **97**, 5308 (1975).
238. M. J. S. Dewar, *J. Am. Chem. Soc.*, **97**, 6591 (1975).
239. R. Seeger and J. A. Pople, *J. Chem. Phys.*, **65**, 265 (1976).
240. J. A. Koningstein and G. Lucazeau, *Chem. Phys. (Neth.)*, **1**, (2), 112 (1973).
241. P. O'Donnell Offenhartz, *Atomic and Molecular Orbital Theory*, McGraw-Hill, New York, 1970. For a definition of the cubic crystal-field strength  $Dq$ , see H. L. Schäfer and G. Gliemann, *Basic Principles of Ligand-Field Theory*, Wiley, New York, 1969.
242. D. S. McClure, *J. Chem. Phys.*, **36**, 2757 (1962). P. Bloomfield, A. W. Lawson, and C. Rey, *J. Chem. Phys.*, **34**, 749 (1961).
243. Y. Tanabe and S. Sugano, *J. Phys. Soc. Jap.*, **9**, 753, 766 (1954).
244. J. S. Griffith, *The Theory of Transition-Metal Ions*, Cambridge University Press, London and New York, 1961.
245. C. E. Schaeffer and C. K. Jørgensen, *J. Inorg. Nucl. Chem.*, **8**, 143 (1958).
246. S. Sugano and R. G. Shulman, *Phys. Rev.*, **130**, 517 (1963).
247. R. E. Watson and A. J. Freeman, *Phys. Rev.*, **A134**, 1526 (1964).
248. C. C. J. Roothaan, *Rev. Mod. Phys.*, **32**, 179 (1960).
249. P. O'Donnell Offenhartz, *J. Am. Chem. Soc.*, **91**, 5699 (1969).
250. G. de Brouckère and C. A. ten Seldam, unpublished results.
251. P. O'Donnell Offenhartz, *J. Am. Chem. Soc.*, **92**, 2599 (1970).
252. B. Kleinman and M. Karplus, *Phys. Rev.*, **B3**, 24 (1971).
253. J. W. Moskowitz, C. Hollister, C. J. Hornback, and H. Basch, *J. Chem. Phys.*, **53**, 2570 (1970).
254. D. E. Ellis, A. J. Freeman, and P. Ros, *Phys. Rev.*, **176**, 688 (1968).
255. C. Hollister, J. W. Moskowitz, and H. Basch, *Chem. Phys. Lett.*, **3**, 185, 728 (1969).
256. A. J. H. Wachters and W. C. Nieuwpoort, *Int. J. Quantum Chem.*, **5**, 391 (1971).
257. J. Hubbard, D. E. Rimmer, and F. R. A. Hopgood, *Proc. Phys. Soc.*, **88**, 13 (1966).
258. P. V. Herigonte, *Electron Correlation in the Seventies*, Ischia Symposium, European Group of Theoretical Molecular Physics, (Cornelio Celsio 7, I 00161 Roma), 1970.
259. R. Daudel and B. Pullman Eds., *The World of Quantum Chemistry*, Reidel, Dordrecht, Holland, 1974. M. Kotani *Electronic Structure and Magnetic Properties of Hemoproteins, particularly of Hemoglobins*, *Adv. in Chem. Phys.*, **7**, 159 (1964).



# VARIATIONAL APPROACHES TO VIBRATION- ROTATION SPECTROSCOPY FOR POLYATOMIC MOLECULES

GRADY D. CARNEY

LUDWIG L. SPRANDEL AND C. WILLIAM KERN

*Department of Chemistry, The Ohio State University, Columbus, Ohio*

## CONTENTS

I. Introduction . . . . .	306
II. The Molecular Vibration-Rotation Hamiltonian . . . . .	307
III. Methods of Solution. . . . .	313
A. Perturbation Theory . . . . .	313
B. Variation Theory . . . . .	318
1. Diatomic Molecules . . . . .	318
2. Polyatomic Molecules . . . . .	323
IV. Applications of Variational Methods to Triatomic Molecules . . . . .	336
A. Literature Survey . . . . .	336
B. Linear Molecules . . . . .	337
C. Nonlinear Molecules . . . . .	341
1. Force Fields . . . . .	341
2. Relative Importance of Terms in the Vibrational Hamiltonian . . . . .	343
3. Comparison of SPF and Dunham Potential Functions . . . . .	347
4. Interpretation of Vibrational Wave Functions . . . . .	354
5. Dipole Moments and Infrared Band Intensities . . . . .	358
6. Rotational Constants . . . . .	365
7. Average Structures . . . . .	366
V. Spectral Predictions . . . . .	370
A. Infrared Spectrum of $\text{H}_3^+$ Isotopes . . . . .	370
B. <i>Ab Initio</i> Treatment of $^3\text{B}_1$ Methylene . . . . .	371
C. Application to Isotope Enrichment . . . . .	373
VI. Summary and Conclusions . . . . .	374
Acknowledgments . . . . .	376
References . . . . .	376

## I. INTRODUCTION

Developments<sup>1</sup> in laser technology and their widespread use in infrared spectroscopy have led to a need for new theoretical techniques that can be applied to vibrational-rotational (V-R) states that are perturbed significantly from the harmonic-oscillator and rigid-rotor limits. This is especially true for polyatomic molecules where the Schrödinger equation for nuclear motion cannot be solved by purely numerical methods, which are so successful for bound and scattering states in one dimension.

Until recently, studies of nuclear motion on a bound-state hypersurface have proceeded along two main lines. These are the construction of the proper V-R Hamiltonian operator, including its partitioning into successively smaller terms, and the subsequent problem of solving the corresponding perturbation equations. Emphasis has generally been directed toward the development of energy expressions corrected to no more than fourth order beyond the zero-order harmonic oscillator-rigid rotor solutions, with little attention being given to the use of the wave function for averaging molecular properties or to the computation of intensities.

In addition to improvements in measurement techniques, there have also been concomitant advances<sup>2</sup> in the machinery required to obtain molecular potential energy and property surfaces from first principles. Thus the usual procedure, based on low-order perturbation theory,<sup>3</sup> of using vibrational band origins and rotational data to derive molecular force fields<sup>4</sup> can now be supplemented by purely *ab initio* theory to obtain the molecular potential in an independent manner, not only near equilibrium, but also close to the atomic dissociation limits.

Although the perturbation method has been used extensively and successfully, it contains important shortcomings when information about highly excited V-R states is required. One practical problem is the low order to which the calculations must be constrained because of the tedious algebra encountered.<sup>5</sup> Typically, the energy expansion becomes intractable beyond second order. Another difficulty is that an expansion of the potential in a Taylor series about equilibrium has an unsatisfactory radius of convergence and leads to asymptotic behavior in the perturbation series.<sup>6</sup> Multiple degeneracies or resonances<sup>7</sup> also require special care and introduce notational and algebraic complexities.

To obviate these limitations of perturbation theory and to probe previously unexplored regions of the potential surface, an alternative approach for solving the general V-R Schrödinger equation has been developed.<sup>8-33</sup> This approach employs the variational principle and is patterned after electronic theory. The general strategy is to assume that the Hamiltonian operator including the potential is known and that the V-R wave function can

be expanded as a sum of products of one-phonon functions times symmetric top functions. The vibrational coordinates can either be "internal" coordinates corresponding to bond stretching and angle bending or normal coordinates that diagonalize the zero-order vibrational Hamiltonian in the usual perturbation sense. In the approaches taken by Carney and Porter<sup>31</sup> and by Bucknell et al.,<sup>14</sup> the one-phonon functions are either harmonic or Morse-oscillator-basis functions that are "adapted" to the potential but not explicitly optimized in a self-consistent field (SCF) sense. Lai and Hagstrom<sup>25</sup> proceed similarly, except that numerical rather than analytical basis functions are employed. By contrast, Sprandel and Kern<sup>19</sup> introduce an SCF step to obtain the energetically best vibrational product function, which then also generates "unoccupied" phonon states that can be used in a configuration-interaction like fashion to couple SCF modes with one another. Sprandel and Kern also circumvent analytical-basis functions by solving the SCF equations numerically. Handy et al.,<sup>34</sup> applied semiclassical scattering theory to bound states. All these methods lead to equivalent results, which show the limitations of perturbation theory as well as sensitivity to the variables used in the potential-energy expansion for the bent triatomic molecules to which they have been applied.

Complementary to these studies are those of Whiffen et al.,<sup>8,9</sup> Baraldi et al.,<sup>10</sup> Suzuki,<sup>11-13</sup> and Gribov and Khovrin,<sup>20-23</sup> who have investigated a number of molecules, including CO, HCl, OCS, CO<sub>2</sub>, and CS<sub>2</sub>, by similar methods.

The purpose of this Chapter is to review these new developments and to show that they are practical and powerful. We limit the scope of our subject mainly to nonlinear ABC molecules. Particular emphasis is given to the water molecule and its isotopes, which have been a fruitful testing ground with an abundance of experimental data. However, results for other molecules, including O<sub>3</sub>, NO<sub>2</sub>, ClO<sub>2</sub>, SO<sub>2</sub>, H<sub>2</sub>S, CO<sub>2</sub>, CS<sub>2</sub>, OCS, CH<sub>2</sub>, and H<sub>3</sub><sup>+</sup>, are also cited.

## II. THE MOLECULAR VIBRATION-ROTATION HAMILTONIAN

Analysis of nuclear motion begins with the classical Hamiltonian  $H = T + V$  for the V-R energy of the molecule. In contrast to the kinetic energy  $T$ , the potential function  $V$  is independent of the reference frame used to specify the coordinates and momenta of the nuclei. Transformation of the classical Hamiltonian  $H$  to quantum-mechanical form  $\hat{H}$  results in a second-order differential eigenvalue equation  $\hat{H}\Psi = E\Psi$ , whose solution yields the eigenenergies  $E$  and wave functions  $\Psi$  of the vibrating-rotating molecule.

For molecules with three or more atoms, the potential is not known accurately. In addition to the information contained in infrared and micro-

wave spectra about  $V$ , purely theoretical methods for small molecules have been developed so that *ab initio* potentials<sup>2</sup> can be obtained within the Born-Oppenheimer approximation. For our purposes this means that the molecular potential depends only on internuclear distances and not on any momenta associated with the relative motions of the nuclei. (Born-Oppenheimer "breakdown"<sup>35</sup> implies that  $V$  depends on these momenta.) Regardless of whether  $V$  is determined from *ab initio* theory and/or experiment, a large effort is required, especially when *ab initio* calculations are needed at many points over the potential hypersurface. This review, however, is not concerned primarily with the details of obtaining potential functions. Rather, assuming that  $V$  is known, we concentrate on obtaining the correct form of the nuclear kinetic operator  $\hat{T}$  and the solution of the V-R Schrödinger equation.

Numerous derivations of  $\hat{T}$  for polyatomic molecules have appeared in the literature.<sup>36-49</sup> The simplest expression is that obtained by Watson<sup>40</sup> starting from an earlier form of the Hamiltonian introduced in 1940 by Darling and Dennison.<sup>37</sup> Implicit in these derivations is the concept of an "equilibrium structure" of which two types are distinguished: linear and nonlinear systems containing  $N$  atoms. Nuclear motion in a nonlinear molecule requires  $(3N-6)$  degrees of freedom for vibration, and three each for the translation of, and rotation about, the center of mass. In a linear molecule, where there is one less rotational coordinate and one more of vibration, the derivation of  $\hat{T}$  is similar to that for a nonlinear molecule, although the two final results cannot be transformed "smoothly" from one to another.

The equilibrium structure is defined by a set of nuclear position vectors relative to the center of nuclear mass  $\mathbf{O}$ , which is taken as the origin of a molecule-fixed reference frame. This frame is usually attached to the molecule in the manner suggested by Eckart.<sup>48</sup> Vibrational motions are defined as nuclear displacements relative to the equilibrium structure in the Eckart frame. Rotational motions then consist of displacements of the reference frame about  $\mathbf{O}$ . In this manner the total angular momentum of the system is carried by the motion of the Eckart reference frame itself. Louck and Galbraith<sup>46</sup> have discussed the fundamental role of "Eckart vectors" from this point of view. The kinetic energy of a nonlinear  $N$ -atom system is most conveniently expressed in terms of Cartesian or rectilinear coordinates. These include the  $(3N-6)$  normal coordinates  $\mathbf{Q}$  of the molecule and any linear combination  $\mathbf{t}$  thereof,<sup>49</sup>

$$\mathbf{t} = \mathbf{L}\mathbf{Q} \quad (1)$$

in which the  $(3N-6) \times (3N-6)$  transformation matrix  $\mathbf{L}$  exists and has elements independent of both  $\mathbf{t}$  and  $\mathbf{Q}$ .

Using rectilinear coordinates, Wilson and Howard<sup>36</sup> have derived the kinetic energy operator  $\hat{T}_{\text{WH}}$  for a semirigid, asymmetrical top molecule. Their expression

$$\hat{T}_{\text{WH}} = \frac{1}{2} \mu^{1/2} \sum_{\alpha, \beta} (\Pi_{\alpha} - \pi_{\alpha}) \mu_{\alpha\beta} \mu^{-1/2} (\Pi_{\beta} - \pi_{\beta}) + \frac{1}{2} \mu^{1/2} \sum_k P_k \mu^{-1/2} P_k \quad (2)$$

is not Hermitian, but Darling and Dennison<sup>37</sup> have made it so by a transformation to the form

$$\hat{T}_{\text{DD}} = \frac{1}{2} \sum_{\alpha, \beta} \mu^{1/4} (\Pi_{\alpha} - \pi_{\alpha}) \mu_{\alpha\beta} \mu^{-1/2} (\Pi_{\beta} - \pi_{\beta}) \mu^{1/4} + \frac{1}{2} \sum_k \mu^{1/4} P_k \mu^{-1/2} P_k \mu^{1/4} \quad (3)$$

In (2) and (3),  $\mu_{\alpha\beta}$  is an effective reciprocal inertia tensor and  $\mu$  is its determinant. Both  $\mu_{\alpha\beta}$  and  $\mu$  depend on the instantaneous molecular geometry. The vector  $\Pi$  is the total angular momentum operator referred to the molecule-fixed axes; its components satisfy commutation relations

$$\Pi_{\alpha} \Pi_{\beta} - \Pi_{\beta} \Pi_{\alpha} = -i\hbar \Pi_{\gamma} \quad (4)$$

generated by a cyclic permutation of the axes. The customary positive sign on the right-hand-side of (4) is obtained if  $\Pi$  is referred to space-fixed axes. Because the operator  $\pi_{\alpha}$  depends on both vibrational coordinates  $Q_k$  and their conjugate momenta  $P_k$ ,  $\mu_{\alpha\beta}$  and  $\mu$  must be carefully manipulated when  $\hat{T}_{\text{DD}}$  is used.

Watson<sup>40</sup> greatly simplified  $\hat{T}_{\text{DD}}$  by proving that

$$\sum_{\alpha} \pi_{\alpha} \mu_{\alpha\beta} = \sum_{\alpha} \mu_{\alpha\beta} \pi_{\alpha} \quad (5)$$

Using commutation relations and sum rules, Watson rearranged  $\hat{T}_{\text{DD}}$  to obtain

$$\hat{T}_{\text{W}} = \frac{1}{2} \sum_{\alpha, \beta} (\Pi_{\alpha} - \pi_{\alpha}) \mu_{\alpha\beta} (\Pi_{\beta} - \pi_{\beta}) + \frac{1}{2} \sum_k P_k^2 + U_{\text{W}} \quad (6)$$

in which the order of the factors in the first term is immaterial on account of (5). The last term

$$U_{\text{W}} = -\frac{1}{8} \hbar^2 \sum_{\alpha} \mu_{\alpha\alpha} \quad (7)$$

is referred to as "Watson's term" and acts as a mass-dependent contribution to the potential energy, since it is independent of the vibrational momenta  $P_k$ .

The presence of  $\hbar^2$  in  $U_{\text{W}}$  and the commutator origin of  $U_{\text{W}}$  suggest, as Louck<sup>45</sup> points out, that the Watson term is purely quantum mechanical in

origin and has no classical analogue. Louck, working with the kinetic-energy expression for an  $N$ -particle system in a laboratory reference frame, has given an alternative derivation verifying  $\hat{T}_w$ . However, Wertheimer<sup>44</sup> has investigated the origin of  $U_w$ , concluding that the classical and quantum mechanical expressions for the V-R kinetic energy should have the same form.

Rather than using either  $\hat{T}_{DD}$  or  $\hat{T}_w$ , both of which are developed in the molecule-fixed reference frame, Bucknell, Handy, and Boys (BHB)<sup>14</sup> derived an alternative form

$$\hat{T}_{BHB} = -\frac{1}{2M} \nabla_G^2 - \sum_{i=1}^{N-1} \frac{1}{2m_i} \nabla_{iG}^2 + \frac{1}{2M} \sum_{i,j}^{N-1} \nabla_{iG} \cdot \nabla_{jG} \quad (8)$$

for the V-R kinetic-energy operator in the laboratory reference frame, thereby avoiding the origin of  $U_w$ . Their first term corresponds to the kinetic energy of the nuclear center-of-mass,  $N$  is the number of nuclei, and  $\nabla_{iG}^2$  is the Laplacian for the  $i$ th particle in terms of Cartesian coordinates in the center-of-mass laboratory-aligned reference frame. The nuclear center-of-mass is defined by

$$\mathbf{G} = \frac{1}{M} \sum_{i=1}^N m_i \mathbf{R}_i \quad (9)$$

and position vectors relative to the center-of-mass are given by

$$\mathbf{R}_{iG} = \mathbf{R}_i - \mathbf{G} \quad (10)$$

The coordinates  $\mathbf{R}_{NG}$  are absent from (8) owing to the introduction of  $\mathbf{G}$ . Margenau and Murphy<sup>47</sup> present a further discussion of the kinetic-energy expression in (8).

For the specific case of  $\text{H}_2\text{O}$ , Bucknell and Handy<sup>15</sup> calculated vibrational energies using  $\hat{T}_{BHB}$  and an "experimental" force field derived by Smith and Overend.<sup>50</sup> Whitehead and Handy<sup>16</sup> and Carney and Kern<sup>28</sup> have independently determined these same vibrational energies for  $\text{H}_2\text{O}$  using this force field and Watson's kinetic-energy operator  $\hat{T}_w$ . As described more fully in Section III, vibrational energies obtained using both types of kinetic-energy operators are numerically equal if, and only if,  $U_w$  is retained in  $\hat{T}_w$ . Carney and Porter<sup>31</sup> also find it necessary to include  $U_w$  in their vibrational analysis of  $\text{H}_3^+$ . For this molecule,  $\hat{T}_{DD}$  can be directly transformed to a special case of  $\hat{T}_w$ , thereby demonstrating the correctness of Watson's algebraic manipulation. Thus there appears to be ample evidence, at least for triatomic molecules, that Watson's form of  $\hat{T}_{DD}$  is indeed valid.

Meyer and Günthard<sup>39</sup> and Pickett<sup>43</sup> (MGP) have derived expressions for the V-R kinetic-energy operator of a general asymmetric top molecule in terms of curvilinear coordinates and their conjugate momenta. These coordinates are usually identified with instantaneous bond distances and

bond angles and are therefore mass independent (e.g., see Ref. 49). Such a formulation of the kinetic-energy operator is particularly attractive for investigating different isotopic species of a molecule or for describing large vibrational amplitudes. In the latter case, use of rectilinear vibrational coordinates may give a poor physical description of the system, as discussed by Pickett.<sup>43</sup>

Employing Pickett's notation, we write the kinetic-energy operator as

$$\hat{T}_{\text{MGP}} = \frac{1}{2} \hbar^2 \mathbf{p}^T \mathbf{G} \mathbf{p} + V' + \mathbf{P}^T \boldsymbol{\mu} \mathbf{P} + \mathbf{L} \cdot \mathbf{P} + \mathbf{P}^T \underline{\Delta} \mathbf{P} \quad (11)$$

The  $\mathbf{G}$  matrix is an instantaneous function of the molecular geometry but is not dependent on the choice of the rotating axis system. Its elements are identical to the  $G$  formulas of Polo<sup>51</sup> and Wilson et al.<sup>49</sup> The vector  $\mathbf{p}$  contains the vibrational momentum operators conjugate to internal vibrational coordinates  $\mathbf{q}$ , and  $\mathbf{P}$  is a vector involving the angular momentum operators. Identifying  $\mathbf{r}_\alpha$  as the instantaneous position vector of atom  $\alpha$  in the rotating coordinate system, a  $3 \times (3N - 6)$  matrix  $\mathbf{X}$  defined columnwise by

$$\mathbf{X}_t = \sum_{\alpha=1}^N m_\alpha \mathbf{r}_\alpha \times \frac{\partial \mathbf{r}_\alpha}{\partial q_t} \quad (12)$$

and a  $3 \times (3N - 6)$  matrix  $\mathbf{C}$  defined as

$$\mathbf{C} = \mathbf{I}^{-1} \mathbf{X} \quad (13)$$

are introduced, where  $m_\alpha$  is the mass of atom  $\alpha$ ,  $q_t$  is the  $t$ th internal vibrational coordinate, and  $\mathbf{I}$  is the  $3 \times 3$  instantaneous inertial tensor whose inverse equals  $2\boldsymbol{\mu}/\hbar^2$ . The elements of vector  $\mathbf{L}$  and the matrix  $\underline{\Delta}$  in (11) are then

$$L_\alpha = -\frac{1}{2} \hbar^2 \sum_{t,t'} (C_{\alpha t} G_{tt'} p_{t'} + p_{t'} G_{t't} C_{\alpha t}) \quad (14)$$

and

$$\underline{\Delta} = \frac{1}{2} \hbar^2 \mathbf{C} \mathbf{G} \mathbf{C}^T \quad (15)$$

The term  $V'$  in (11) behaves like a mass-dependent contribution to the potential, similar but not equal to  $U$ , in that it depends only on the coordinates and not on conjugate momenta. In general,

$$V' = \frac{1}{8} \hbar^2 \sum_{t,t'} \left[ \frac{\partial G_{tt'}}{\partial q_t} \frac{\partial \ln g}{\partial q_{t'}} + G_{tt'} \left( \frac{\partial^2 \ln g}{\partial q_t \partial q_{t'}} + \frac{1}{4} \frac{\partial \ln g}{\partial q_t} \frac{\partial \ln g}{\partial q_{t'}} \right) \right] \quad (16)$$

where

$$g = \frac{|\mathbf{I}|}{|\mathbf{G}|} \quad (17)$$

The sums  $t$  and  $t'$  go over the  $(3N - 6)$  generalized coordinates.

Using  $\hat{T}_{\text{MGP}}$  developed in terms of the two bond lengths and the bond angle for the water molecule, Sprandel<sup>19</sup> and Kern and Lai<sup>25</sup> and Hagstrom have calculated vibrational energies that are in excellent agreement with those obtained by Carney and Kern<sup>28</sup> and by Whitehead and Handy<sup>16,17</sup> for several force fields (see Section III). Therefore,  $\hat{T}_w$  appears to be numerically equivalent to  $\hat{T}_{\text{MGP}}$ , as expected.

To describe large amplitudes of vibration, Gribov<sup>20</sup> has an alternative approach to that used by MGP. He obtains

$$\hat{T}_G = \frac{1}{2} \tilde{p} \underline{\Xi} \tilde{p} \quad (18)$$

for the kinetic energy in a laboratory Cartesian frame, where  $\tilde{p}$  and  $\tilde{p}$  are, respectively, the row and column matrices of the Cartesian momenta of the nuclei, and  $\underline{\Xi}$  is a diagonal matrix of dimensionless reciprocal masses of the nuclei. The Cartesian momentum is given by

$$p_{r_i} = \frac{\partial T_G}{\partial \dot{r}_i} \quad (19)$$

where  $\dot{r}_i$  is the time derivative of  $r_i$ . Partial derivatives with respect to  $\dot{r}_i$  are related to derivatives with respect to the natural coordinate time derivatives  $\dot{q}_k$  by

$$\frac{\partial}{\partial \dot{r}_i} = \sum_k \left( \frac{\partial \dot{q}_k}{\partial \dot{r}_i} \right) \frac{\partial}{\partial \dot{q}_k} \quad (20)$$

so that

$$p_{r_i} = \sum_k p_{q_k} \left( \frac{\partial \dot{q}_k}{\partial \dot{r}_i} \right) \quad (21)$$

The  $\dot{q}_k$  and  $\dot{r}_i$  time derivatives are related by

$$\dot{\mathbf{q}} = \mathbf{B} \dot{\mathbf{r}} \quad (22)$$

where the matrix  $\mathbf{B}$  is independent of  $\mathbf{r}$  but does depend on  $\mathbf{r}$  and  $\mathbf{q}$ . Equation 21 now becomes

$$\mathbf{p}_r = \mathbf{B} \mathbf{p}_q \quad (23)$$

where

$$\mathbf{p}_q = \{p_{q_k}\} \quad (24)$$

Gribov then expresses the kinetic energy as

$$\hat{T}_G = \frac{1}{2} \mathbf{p}_q^T (\mathbf{B}^T \underline{\Xi} \mathbf{B}) \mathbf{p}_q \quad (25)$$

where  $\mathbf{B}^T \underline{\Xi} \mathbf{B}$  is given as a Taylor series expansion in the instantaneous, "natural" coordinates  $\mathbf{q}$ .



It is seen that Gribov's treatment is, in effect, a compromise between that of BHB and MGP. Gribov develops the kinetic energy in a laboratory Cartesian reference space, but the problem is transformed to the natural coordinate space for its numerical evaluation. Gribov's approach has not been verified by comparison to other studies in which the same molecular force field was used.

Although quantum-mechanical forms for the V-R kinetic energy of a linear molecule have also been derived, we do not discuss them in detail. Watson's form<sup>41</sup> is somewhat different from those derived by Nielsen,<sup>3</sup> Suzuki,<sup>12,13</sup> and Aliev,<sup>52</sup> which are cited in Section IV. Whiffen et al.,<sup>8,9</sup> and Whitehead and Handy<sup>16</sup> utilized Watson's Hamiltonian in their studies of the OCS molecule, while Suzuki<sup>12,13</sup> used the Nielsen-Overend type of Hamiltonian in his studies of CO<sub>2</sub> and CS<sub>2</sub>. The equivalence of the Hamiltonians of Watson, Gribov, and Nielsen for linear molecules has not been established so far by a direct nonperturbative numerical study of a common system.

### III. METHODS OF SOLUTION

#### A. Perturbation Theory

We begin by considering a polyatomic molecule in a nondegenerate but otherwise arbitrary state of vibration and assume that the potential energy in reduced normal coordinates is known through quartic terms. Using the notation of Nielsen<sup>3</sup> and expanding the potential in a Taylor series about equilibrium, we write the Watson Hamiltonian as

$$\hat{H} = \hat{H}^{(0)} + \lambda \hat{H}^{(1)} + \lambda^2 \hat{H}^{(2)} + \dots \quad (26)$$

where

$$\hat{H}^{(0)} = \frac{1}{2} \sum_i \omega_i (p_i^2 + q_i^2) + \frac{1}{2} \sum_g \frac{P_g^2}{I_{gg}^e} \quad (27)$$

$$\begin{aligned} \hat{H}^{(1)} = & \sum_{ijk} k_{ijk} q_i q_j q_k - \sum_g \left( \frac{P_g P_g}{I_{gg}^e} \right) - \frac{1}{2} \sum_{gg'} \sum_i \frac{P_g P_{g'}}{I_{gg}^e I_{g'g'}^e} \frac{a_i^{(gg')}}{(\omega_i)^{1/2}} q_i \\ & + \frac{1}{2} \sum_{gg'} \sum_i \frac{P_g}{I_{gg}^e I_{g'g'}^e} \frac{a_i^{(gg')}}{(\omega_i)^{1/2}} (p_{g'} q_i + q_i p_{g'}) \end{aligned} \quad (28)$$

and

$$\hat{H}^{(2)} = \sum_{ijkl} k_{ijkl} q_i q_j q_k q_l + \frac{1}{2} \sum_g \left( \frac{p_g^2}{I_{gg}^e} \right) - \frac{1}{2} \sum_{gg'} \sum_{ij} \left( \frac{P_g P_{g'}}{I_{gg}^e I_{g'g'}^e} \right) \frac{G_{ij}^{(gg')}}{(\omega_i \omega_j)^{1/2}} q_i q_j \quad (29)$$

The successive equations contain the harmonic, cubic, and quartic contributions to the vibrational potential energy, and  $\omega_i$ ,  $k_{ijk}$ , and  $k_{ijkl}$  are the cor-

responding expansion constants, referred to reduced normal coordinates. The last term in (27) gives the rigid-rotor motion; Coriolis and centrifugal distortion effects are part of  $\hat{H}^{(1)}$  and  $\hat{H}^{(2)}$ .

The vibrational wave function  $\psi_v$  and energy  $E_v$  corresponding to the Hamiltonian in (26) can be obtained by assuming convergent expansions

$$\psi_v = \psi_v^{(0)} + \lambda \psi_v^{(1)} + \lambda^2 \psi_v^{(2)} + \cdots \quad (30)$$

and

$$E_v = E_v^{(0)} + \lambda E_v^{(1)} + \lambda^2 E_v^{(2)} + \cdots \quad (31)$$

where  $\lambda$  is an ordering parameter. Substituting these into the Schrödinger equation and collecting terms in like powers of  $\lambda$ , we are led to the  $N$ th-order perturbation equation

$$\sum_{k=0}^N (\hat{H}^{(k)} - E_v^{(k)}) \psi_v^{(N-k)} = 0 \quad (32)$$

whose solutions take the form<sup>53-55</sup>

$$E_v = G + \sum_i^M \omega_i (v_i + \frac{1}{2}) + \sum_{i \leq j}^M x_{ij} (v_i + \frac{1}{2})(v_j + \frac{1}{2}) + \cdots \quad (33)$$

and

$$\begin{aligned} \psi_v = & \psi_v^{(0)} + \sum_{r \neq v}^{\infty} \sum_{l=1}^M a_r(l) \Phi_r(l) + \sum_{r,s \neq v}^{\infty} \sum_{\substack{l,m=1 \\ l \neq m}}^M b_{rs}(lm) \Phi_{rs}(lm) \\ & + \sum_{r,s,t \neq v}^{\infty} \sum_{\substack{l,m,n=1 \\ l < m < n}}^M c_{rst}(lmn) \Phi_{rst}(lmn) + \cdots \end{aligned} \quad (34)$$

In (34), the zero-order wave function

$$\psi_v^{(0)} = \chi_{v_1}(q_1) \chi_{v_2}(q_2) \cdots \chi_{v_l}(q_l) \cdots \chi_{v_M}(q_M) \quad (35)$$

for vibrational state  $v = (v_1, v_2, \dots, v_l, \dots, v_M)$  is singly, doubly, triply, and so forth, excited to produce the  $\Phi_r$ ,  $\Phi_{rs}$ , and  $\Phi_{rst}$  terms, respectively. The energy and wave-function expansion parameters are given in terms of the harmonic frequencies  $\omega_i$  and expansion constants of the potential energy

$$V = \frac{1}{2} \sum_{i=1}^M \omega_i q_i^2 + \sum_{ijk} k_{ijk} q_i q_j q_k + \sum_{ijkl} k_{ijkl} q_i q_j q_k q_l + \cdots \quad (36)$$

Given (36) and similar expansions for properties  $\mathcal{P}$  other than the energy, it can be shown<sup>55</sup> that vibrationally averaged properties also have a form analogous to (33). Specifically

$$\langle \mathcal{P} \rangle_v = \mathcal{P}'_0 + \sum_{i=1}^M A_i (v_i + \frac{1}{2}) + \sum_{i \leq j}^M B_{ij} (v_i + \frac{1}{2})(v_j + \frac{1}{2}) + \cdots \quad (37)$$

where the constants  $\mathcal{P}'_0$ ,  $A_i$ , and  $B_{ij}$  depend on the property expansion coefficients in addition to the force field.

The physical nature of these results can be seen if we examine them in one dimension, for which

$$\psi_v^{(0)} = [2^v v! \sqrt{\pi}]^{-1/2} H_v(q) \exp(-\frac{1}{2}q^2) \quad (38)$$

and

$$\psi_v^{(1)} = \frac{k_3}{6\omega\sqrt{2}} \{ [v(v-1)(v-2)]^{1/2} \psi_{v-3}^{(0)} + 9v^{3/2} \psi_{v-1}^{(0)} - 9(v+1)^{3/2} \psi_{v+1}^{(0)} - [(v+1)(v+2)(v+3)]^{1/2} \psi_{v+3}^{(0)} \} \quad (39)$$

These wave functions lead to the property average

$$\langle \mathcal{P} \rangle_v = \mathcal{P}_0 + (v + \frac{1}{2}) \left[ 2 \mathcal{P}_2 \frac{B_e}{\omega_e} + \mathcal{P}_1 \left( \frac{3B_e}{\omega_e} + \frac{\alpha_e}{2B_e} \right) \right] + \cdots \quad (40)$$

where  $\mathcal{P}_0$ ,  $\mathcal{P}_1$ , and  $\mathcal{P}_2$  are coefficients in the expansion  $[\xi = (R - R_e)/R_e]$

$$\mathcal{P} = \mathcal{P}_0 + \mathcal{P}_1 \xi + \mathcal{P}_2 \xi^2 + \cdots \quad (41)$$

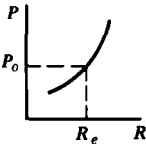
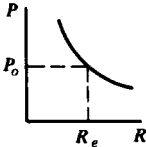
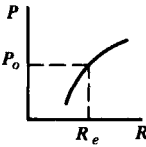
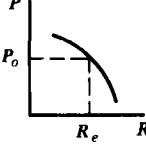
Clearly, we can distinguish four cases of (40). These are defined by the relative signs of  $\mathcal{P}_1$  and  $\mathcal{P}_2$ , as shown in Table I, corresponding to different curvatures in the  $\mathcal{P}$  versus  $R$  plots. "Large" effects are up to 20%, whereas "small" means a few percent or less.

Although these simplifications to one dimension provide insight, they are not useful from a quantitative standpoint for several reasons. First, accurate numerical solutions<sup>6,10</sup> of the one-dimensional Schrödinger equation are available. Second, when additional degrees of vibrational freedom are introduced, coupling between vibrational modes complicates the interpretation. In addition, the analysis becomes prohibitive when the theory is applied in third and higher orders to vibrating-rotating molecules, even in the diatomic case. The complexities originate from the unwieldy expressions for the non-diagonal matrix elements of the terms in (26). Thus, with each succeeding order of approximation, the required terms become more numerous and complex.

One device, called the contact transformation, was introduced by Van Vleck in 1929 to help manage the cumbersome bookkeeping of perturbation theory.<sup>56,57</sup> We do not go into the details of this method, except to state that when the Schrödinger equation is subjected to a transformation by a nonsingular operator

$$T = 1 + \lambda S_1 + \lambda^2 S_2 + \cdots \quad (42)$$

TABLE I.  
Relationship between signs of property expansion coefficients and size of  
vibrational averaging effects in one dimension.<sup>a</sup>

Sign of $P_1$	Sign of $P_2$	$P$ vs. $R$	Size of $\langle P \rangle_v - P_0$
Positive	Positive		Large; positive
Negative	Positive		Small; sign indeterminant
Positive	Negative		Small; sign indeterminant
Negative	Negative		Large; negative

a. See Eqs. (40) and (41).

the perturbation energies are eigenvalues of successive-order diagonal operators  $D_N$ . These depend on  $\hat{H}^{(0)}$  and lower-order operators  $S_{N-1}$ ,  $S_{N-2}$ ,  $\dots$ ,  $S_1$  through the commutation relations

$$[\hat{H}^{(0)}, iS_N] = V_N - D_N \quad (43)$$

when  $N=1$ ,  $V_1 = \hat{H}^{(1)}$ ; for  $N>1$ ,  $V_N$  involves multiple commutators of lower-order  $\hat{H}^{(N-1)}$ ,  $\hat{H}^{(N-2)}$ ,  $\dots$  and  $S_{N-1}$ ,  $S_{N-2}$ ,  $\dots$ . Further, if we now define the definite operator integral

$$I_N = \int_0^\infty e^{i\hat{H}^{(0)}\tau} V_N e^{-i\hat{H}^{(0)}\tau - \varepsilon\tau} d\tau \quad (44)$$

then<sup>58</sup>

$$iS_N = -i \lim_{\varepsilon \rightarrow 0} \left( I_N - \frac{1}{\varepsilon} D_N \right) \quad (45)$$

and

$$D_N = \lim_{\varepsilon \rightarrow 0} \varepsilon I_N \quad (46)$$

Contact transformation theory therefore replaces the principal task of traditional perturbation theory, namely, evaluating infinite sums of off-diagonal matrix elements divided by energy denominators, by the still formidable, but nevertheless more tractable, process of calculating  $I_N$  in (44).\*

Although contact transformation theory is an appealing way to systematize the application of perturbation theory to V-R spectroscopy, it has still not proved practical to carry the calculations beyond fourth order in the energy. Moreover, the energy expansion can be asymptotic. For example, it is known<sup>59</sup> that a one-dimensional harmonic oscillator perturbed by an odd-power potential  $\xi^N$  for  $N=3, 5, 7, \dots$  has no bound states; the even powers for  $N=4, 6, 8, \dots$  have been examined<sup>60-64</sup> by formal analyses and numerical calculations, with the essential result that the perturbation energy series diverges for all nonzero coupling strengths. When more than a single term is taken, the convergence behavior seems to depend on how the terms in the perturbing Hamiltonian are grouped<sup>6</sup>; that is, whether the complete anharmonic potential is taken as  $\hat{H}^{(1)}$ , or whether successively higher powers  $\xi^N$  belong to the corresponding  $\hat{H}^{(N-2)}$ .

These difficulties with perturbation theory are often relatively unimportant for low-lying vibrational states, especially when high accuracy is not required. However, for highly excited states or very shallow potentials, meaningful results must be obtained by circumventing a perturbation expansion and employing a full variational procedure, which we outline and apply in the following sections. We find also, using the variational principle, that the V-R wave functions, and therefore transition probabilities, are much easier to obtain than in the perturbation scheme. This is even true when degener-

\*For the one-dimensional first-order wave function in (39)

$$\psi_v^{(1)} = -iS_1\psi_v^{(0)}$$

where

$$iS_1 = -\frac{i}{2} \left[ \frac{1}{3}(pq^2 + q^2p) + \frac{4}{3}(p\hat{H}^{(0)} + \hat{H}^{(0)}p) \right]$$

and

$$D_1 = 0$$

acies, or near-degeneracies, occur among the energy levels. Special perturbation methods must be developed to handle these cases, producing yet another limitation inherent in this traditional approach.

## B. Variation Theory

To circumvent these disadvantages of perturbation theory, we introduce the linear variation method,<sup>65-68</sup> which has been used extensively in molecular electronic calculations.<sup>2</sup> For problems involving nuclear motion, this corresponds to diagonalization of a truncated matrix representation of the V-R Hamiltonian. In the remainder of this section, we discuss the methodology involved in the variational solution of V-R Schrödinger equations. In Section IV, results are given that demonstrate the accuracy and reliability of this approach.

### 1. Diatomic Molecules

To begin we consider selected studies of diatomic molecules from the viewpoint of what they offer in the solution of the more general polyatomic V-R problem where direct numerical solutions are not feasible. First we consider Suzuki's variational studies of the CO and HCl molecules,<sup>11</sup> and then proceed to Zetik and Matsen's<sup>69,70</sup> direct diagonalization approach. These two methods differ in the manner of evaluating the matrix elements over the potential function. We then explore various choices of the oscillator basis sets used to obtain the Hamiltonian in matrix form. Although we do not discuss them in this chapter, we refer the reader to the *ab initio* studies by Stevens et al.<sup>71</sup> and by Sachs and Hinze<sup>72</sup> for state-of-the-art applications to bound-state V-R spectroscopy. Lastly, we touch on the possible uses of variational solutions in scattering theory.

Following Suzuki,<sup>11</sup> we write the vibrational Hamiltonian in dimensionless normal coordinates

$$q = \left( \frac{\omega_e}{2B_e} \right)^{1/2} \frac{\Delta R}{R_e} \quad (47)$$

as

$$\hat{H}_v = \frac{1}{2}\omega_e(p^2 + q^2) + k_3q^3 + k_4q^4 + k_5q^5 + \cdots \quad (48)$$

and the V-R Hamiltonian as

$$\hat{H} = \hat{H}_v + B_e(J_x^2 + J_y^2)(1 - 2\gamma^{1/2}q + 3\gamma q^2 - \cdots) \quad (49)$$

where  $p = \hbar^{-1} \partial T / \partial q$ ,  $J_x = \hbar^{-1} P_x$ , and  $J_y = \hbar^{-1} P_y$ . The quantity  $\gamma = 2B_e/\omega_e$  represents "smallness" in the perturbation sense,  $B_e$  is the equilibrium rotational constant,  $\omega_e$  is the harmonic frequency, and the  $k_i$ 's are anharmonic

force constants. The  $k_i$ 's are related to the Dunham constants<sup>73</sup>  $a_i$  by

$$k_{i+2} = \frac{1}{2}\omega_e\gamma^{i/2}a_i \quad i = 1, 2, 3, \dots \quad (50)$$

From algebraic formulas for the nonvanishing matrix elements of  $\hat{H}_v$ , the contributions of each force constant  $k_i$  to the vibrational Hamiltonian matrix  $H_v$  can be represented with matrices  $A_i$  as

$$H_v = \sum_{i=2} k_i A_i \quad (51)$$

where  $k_2 = \omega_e$ . When a truncated set of  $m$  basis functions is chosen, an  $(m \times m)$  secular equation of the form

$$H_v \mathcal{L} = \mathcal{L} \mathbf{v} \quad (52)$$

results for  $\mathcal{L}$  and  $\mathbf{v}$ , the orthonormal eigenvectors and eigenenergies. Variational approximations to the true wave functions for  $\hat{H}_v$  are therefore given by

$$|v\rangle = \sum_n \mathcal{L}_{vn} |n\rangle \quad (53)$$

where  $|n\rangle$  are the basis functions and  $\mathcal{L}_{vn}$  are the corresponding eigenvectors from (52).

The V-R terms in (49) may be included explicitly in the development of  $H$  using (51) for each choice of the rotational quantum number  $J$ . The leading terms are

$$H_{v,J} = H_v + B_e J(J+1) \hbar^2 (1 - 2\gamma^{1/2} \mathbf{q} + 3\gamma \mathbf{q}^2 - \dots) \quad (54)$$

Direct diagonalization of  $H_{v,J}$  yields the V-R eigenfunctions and energies for the diatomic molecule. The rotational dependence is added to (53) as

$$|v\rangle_J = \sum_n \mathcal{L}_{vnJ} |n\rangle |J\rangle \quad (55)$$

where  $|J\rangle$  is a rigid rotor or spherical harmonic eigenfunction.

Vibrational energies for  $v \leq 6$  for CO and for  $v \leq 5$  for HCl were reported by Suzuki for a five-parameter potential function (through sixth-degree terms in  $q$ ). In these variational calculations, from 7 to 50 oscillator basis functions were used. Convergence of eigenvalues for HCl was appreciably slower than that for CO, but convergence was ultimately achieved with 30 harmonic-oscillator basis functions. In Table II comparisons of second- and fourth-order perturbation theories are made with the direct diagonalization procedure for vibrational energies and rotational constants. In the case of HCl, significant differences in band position and rotational constant were obtained between the variational and perturbation methods.

It should be borne in mind, as we continue our discussion below, that the

TABLE II  
Comparison of Calculated Frequencies and Rotational Constants ( $\text{cm}^{-1}$ ) for  $\text{HCl}^a$

Vibrational level $v$	Direct diagonalization I	Second-order PT II	Fourth-order PT III	Differences	
				I – II	I – III

---

Frequencies $\nu_v$					
1	2887.23	2885.45	2886.44	1.78	0.79
2	5676.36	5665.27	5669.67	11.09	6.69
3	8380.41	8339.44	8351.02	40.97	29.39
4	11022.48	10907.98	10931.85	114.50	90.63
5	13634.86	13370.87	13413.51	263.99	221.35

Effective rotational constants $B_v$					
0	10.440579	10.439966	10.440887	0.000613	–0.000308
1	10.139657	10.132792	10.138699	0.006865	0.000958
2	9.851493	9.825618	9.840339	0.025875	0.011154
3	9.590328	9.518444	9.545806	0.071884	0.044522
4	9.375818	9.211127	9.255101	0.164691	0.120717
5	9.224414	8.904096	8.968223	0.320318	0.256191

<sup>a</sup>Reference 11.

use of Dunham's form for the potential function expansion variable,  $\Delta R/R_e$ , is responsible to a large degree for these apparent differences. Use of a Simons-Parr-Finlan (SPF)<sup>74</sup> expansion variable,  $\Delta R/R$ , to develop the potential function would reduce significantly the difference in perturbation theory and variational results for the rotational constants.

The question of whether direct diagonalization and perturbation methods lead to the same force field is of fundamental importance. Anharmonic resonances and truncation of potential functions often limit the accuracy of the perturbation theory analysis as it is normally applied to obtain force constants that fit observed infrared data. By contrast, vibrational energies and wave functions are readily determined by direct diagonalization with a suitable basis set of oscillator functions.

Suzuki<sup>11</sup> evaluated changes in the eigenvectors arising from small changes in the force constants and determined resulting shifts in the vibrational frequencies  $\nu_i$ . Using these  $\nu_i$  and the derived rotational constants, he determined the force constants for both sixth- and fourth-degree potential func-



tions for CO and for HCl. Comparison of the variationally derived force constants with those derived from perturbation theory showed that the quadratic and cubic constants remain invariant. However, direct diagonalization is necessary to obtain the higher-order force constants satisfactorily. Suzuki<sup>12</sup> also utilized the direct diagonalization method to extract the dipole-moment derivatives of CO and HCl from the observed intensities.

Zetik and Matsen<sup>69,70</sup> and others<sup>71,72</sup> recognized that the electronic theory of small diatomic molecules has progressed to the point where reasonably reliable *ab initio* potential curves can be employed to obtain V-R energy levels. However, several possible difficulties must be kept in mind. For example, the relative error from point to point on an *ab initio* potential surface is difficult to quantify. Also, these potentials are obtained as a grid of points instead of in analytical form, which sometimes proves to be inconvenient.

Zetik and Matsen found that the general quadrature scheme introduced by Harris, Engerholm, and Gwinn (HEG)<sup>75</sup> was especially useful for evaluating matrix elements of the potential function. Cubic-spline interpolation was combined with numerical integration to determine directly the matrix elements of the Hamiltonian  $\hat{H}_v$ . The matrix representation of the vibrational coordinate in the oscillator basis was used to generate numerical quadrature algorithms. The eigenvalues  $\underline{\Lambda}$  of the coordinate matrix  $\mathbf{X}$  define the range of the argument of the potential function required; that is,

$$\lambda_{\min} \leq x \leq \lambda_{\max} \quad (56)$$

where

$$\mathbf{XC} = \mathbf{C}\underline{\Lambda} \quad (57)$$

and

$$X_{nm} = \langle n|x|m \rangle \quad (58)$$

The matrix representation of the potential function  $V(x)$  in the chosen basis is obtained by (1) diagonalizing the representation of  $x$ ; (2) replacing each diagonal element eigenvalue of  $\underline{\Lambda}$  with the potential at that value of  $x$ ; and (3) transposing this representation of  $V(x)$  back to the chosen oscillator basis set with the inverse transformation of  $\mathbf{C}$ . Matrix elements of the rotational terms are calculated, for a particular  $J$  value, by the same numerical procedure. The analytical oscillator basis is selected such that the matrix elements of the remaining terms appearing in the Hamiltonian operator are tractable.

Zetik and Matsen<sup>69</sup> tested the rate of convergence in energy as a function of harmonic-oscillator basis set size in their study of  $\text{H}_2$  using an *ab initio* potential function. Several methods were explored for choosing the parameters of the basis set. Vibrational energies were also reported by Matsen<sup>70</sup>

for several electronic states of  $\text{He}_2$ . The calculations of the vibrational intervals  $\Delta G(v + \frac{1}{2})$  (given in Table III) serve as sensitive tests of the quality of the *ab initio* potential functions.<sup>71,72</sup>

Following the methods of Suzuki and of Matsen for evaluating the vibration energies by the direct diagonalization method, it is convenient to choose analytical oscillator basis sets. Alternatives to the simpler harmonic-oscillator eigenfunctions have been explored along the lines that we now describe.

TABLE III  
*Ab initio* Vibrational Excitation Energies ( $\text{cm}^{-1}$ )  
for Molecular Helium in Various Electronic states<sup>a</sup>

Electronic state	Vibrational excitation	Excitation energy	
		<i>Ab initio</i>	Observed
$^3\Pi_g$	$\Delta G_{1/2}$	2103.5	1698.8
	$\Delta G_{3/2}$	2062.8	1628.4
	$\Delta G_{5/2}$	1925.1	1557.7
$^1\Pi_g$	$\Delta G_{1/2}$	2096.2	1696.9
	$\Delta G_{3/2}$	1911.7	1627.9
	$\Delta G_{5/2}$	1781.0	1558.7
$^3\Pi_u$	$\Delta G_{1/2}$	1573.5	1571.9
	$\Delta G_{3/2}$	1466.0	1482.3
$^1\Pi_u$	$\Delta G_{1/2}$	1581.3	1590.5
	$\Delta G_{3/2}$	1488.2	1510.5
$^3\Sigma_g^+$	$\Delta G_{1/2}$	1234.6	1480.0
	$\Delta G_{3/2}$	1005.9	1371.7

<sup>a</sup>Reference 70.

Locker<sup>76</sup> has investigated the use of sine functions as basis sets in variational calculations for bound states. For the higher energy levels, the eigenvalues calculated by using the sine basis sets are in much better agreement with the exact values than the results obtained by using harmonic-oscillator basis sets. Fues<sup>77</sup> and Morse potentials were used as test potentials, since their eigenenergies are well known, and since both incorporate anharmonic effects.

Greenawalt and Dickinson<sup>78</sup> have given matrix elements corresponding to Morse-oscillator basis sets and have found such basis sets to be more

rapidly convergent than harmonic-oscillator basis sets for diatomic molecules. Lesk<sup>79</sup> has found a way in which the parameters of harmonic-oscillator basis sets may be chosen in an optimum manner so as to improve the description of anharmonic wave functions. Shore<sup>80</sup> has employed cubic-spline basis functions in bound-state problems, obtaining eigenvalues to high accuracy. Of particular interest here is his comparison of eigenenergies for a Morse potential obtained by the cubic spline collocation method, the simple finite difference method, the Numerov method, and the cubic spline-variational method.

Both Chesick's<sup>81</sup> nonorthogonal Gaussian basis sets and Locker's<sup>76</sup> sine basis sets may be useful to describe variationally the higher vibrational states of polyatomic molecules. It was found that the distributed Gaussian basis sets are more effective than the harmonic-oscillator basis employed by Endres and Wilson<sup>82</sup> for the CH Morse oscillator, and that the Gaussian basis remains reasonably tractable even for linear triatomic molecules. Chesick<sup>81</sup> reported results for HCN and CH<sub>2</sub>.

Lin and Drake<sup>83</sup> have employed the variational method with harmonic-oscillator basis functions to examine both bound and continuum vibrational states of an anharmonic potential. Although there is no longer a variational-minimum principle for continuum eigenvalues, the low-lying continuum eigenfunctions were found to be in close agreement with the exact eigenfunctions evaluated at the same energy, provided that the internuclear distance was not too far from its equilibrium value. Hazi and Taylor's<sup>84</sup> stabilization (variational) method of calculating resonance energies is thus confirmed. Such studies may be of especial importance in regard to "pseudo" vibrational states of polyatomic molecules that have sufficient energy to undergo dissociation.

In studies of the dynamics of anharmonic oscillators, Endres and Wilson,<sup>82</sup> Endres,<sup>85</sup> and Dubrow et al.<sup>86</sup> have employed variational methods to examine the stationary states of oscillators with one and two degrees of freedom using harmonic and Morse models. Energies of low-lying vibrational states from both variational and semiclassical studies are found to be in good agreement when sufficiently large basis sets are used. However, the WKB approximation gives values for the higher energies that tend to be superior to those obtained variationally using harmonic-oscillator basis functions. This result for diatomic molecules may also be applicable to polyatomic systems.<sup>34</sup>

## 2. Polyatomic Molecules

Having discussed the basic methodology for the variational solution of diatomic V-R problems, we are ready to proceed to the more complex case of polyatomic systems. First, we discuss the structure of the equations to be

solved. Then the specific approaches taken by some different research groups are considered, following which, points concerning integration procedures and matrix diagonalization methods are mentioned.

To begin, we note that the V-R Hamiltonian of a polyatomic molecule can be written as a vibrational part and a part involving vibration-rotation interaction; that is

$$\hat{H} = \hat{H}_v + \hat{H}_{\text{vib-rot}} \quad (59)$$

where  $\hat{H}_v$  involves only vibrational coordinates and momenta and  $\hat{H}$  contains all the rotational and V-R interaction terms. Solution of the Schrödinger equation

$$\hat{H}\Psi = E\Psi \quad (60)$$

is achieved by diagonalization of the matrix representation of the Hamiltonian in an appropriate basis set. To this end,  $\Psi$  in (60) is expanded in products of vibrational wave functions  $\psi_n$  and symmetric-top eigenfunctions  $R_{J,K,M}(\theta, \phi, \varphi)$  as

$$\Psi_{JM} = \sum_{n,K} C_{nK}^{(JM)} \psi_n R_{J,K,M} \quad (61)$$

The sums are over the complete set of V-R basis states.

There are several important features about (61). First, the manner of obtaining the vibrational wave functions  $\psi_n$  is of importance. These wave functions are taken as eigenfunctions of the purely vibrational part of (59). We have

$$\hat{H}_v \psi_n = E_n \psi_n \quad (62)$$

where  $\psi_n$  may be taken as a CI-like expansion

$$\psi_n(t_1, t_2, \dots, t_{3N-6}) = \sum_v c_{v_1, v_2, \dots, v_{3N-6}}^{(n)} \chi_{v_1}(t_1) \chi_{v_2}(t_2) \dots \chi_{v_{3N-6}}(t_{3N-6}) \quad (63)$$

In (63) the  $\chi_{v_i}(t_i)$  are eigenfunctions of one-dimensional vibrational Hamiltonians of which there are  $(3N-6)$  of these corresponding to the  $(3N-6)$  vibrational coordinates  $t_i$  of the polyatomic molecule. We discuss below several approaches for obtaining these basis functions.

The rotational terms in (61) are constructed so that, for asymmetric tops, a wave function  $\Psi_{JM}$  is present for each value of the rotational angular momentum  $J$  and its projection  $M$ . For a given  $J$  we must sum over  $K$  in (61), since it is generally the matrix elements connecting  $K$  to  $K \pm 2$  states that are nonzero in the rotational bra-ket space. Following Carney and co-workers,<sup>28,31,32</sup> we write a supermatrix representation of the V-R Hamiltonian of (59) in the basis defined by (61); we have

	First vibrational state	Second vibrational state	Third vibrational state	
First vibrational state	$K_1$ $K_2$ $K_3$ $\vdots$ $\vdots$	$K_1 K_2 K_3 \cdots$	$K_1$ $K_2$ $K_3$ $\vdots$ $\vdots$	$K_1 K_2 K_3 \cdots$
Second vibrational state				$\cdots$
Third vibrational state				$\cdots$
	$\vdots$	$\vdots$	$\vdots$	(64)

There is a matrix of this form for each  $J$  and  $M$  value, since we have not included any operators that will mix states of different total angular momentum. Furthermore, the matrix elements between even and odd  $K$  states vanish, leading to two independent matrices for each  $J$ . We also notice that since there is no mechanism for the  $M$  states to interact in the absence of external fields, we have a  $(2J+1)$ -fold degeneracy. It is also important to realize that this matrix is Hermitian; in fact, the symmetric-top basis set can be chosen so that it is also real.<sup>32</sup> As many as 10 different vibrational states with  $J$  up to 5 can be readily accommodated in practical computations on a large-core digital computer.

Before proceeding to specific cases, we now examine the core of this entire development, namely, the solution of (62) to obtain a suitable set of vibrational eigenstates that are required in (61) and supermatrix (64). There are many variants on the way this can be accomplished. For example, we can introduce an analytical form for the one-phonon functions or proceed by direct numerical integration; we can directly diagonalize the vibrational Hamiltonian matrix or set up an intermediate self-consistent field (SCF) step to improve the convergence in (63). We also must decide on the appropriate vibrational coordinates for the problem. Should rectilinear coordinates be used, or should we remain in the space of central and valence force fields? All these possibilities have been investigated, with the essential result that each has its merits, but all lead, when fully converged, to identical numerical results. The salient features of these various procedures and comparative results for the  $\text{H}_2\text{O}$  molecule are given in Table IV. We now discuss each technique briefly.

Using a set of coordinates  $t_i$  that are linear combinations of the conventional rectilinear normal coordinates  $q_i$ , Carney and co-workers<sup>31,32</sup> have derived the V-R kinetic-energy operator for an ABC triatomic molecule with an isosceles equilibrium geometry.\* They obtained

$$\hat{T} = \hat{T}_v + \hat{T}_{\text{vib-rot}} \quad (65)$$

where

$$\hat{T}_v = \frac{1}{2\mu} \sum_i P_{t_i}^2 + \frac{(P_z^{\text{vib}})^2}{2I_{zz}^{\text{eff}}} \quad (66)$$

and

$$\begin{aligned} \hat{T}_{\text{vib-rot}} = & \frac{P_z(P_z - 2P_z^{\text{vib}})}{2I_{zz}^{\text{eff}}} + \frac{1}{2} \frac{I_{xx}}{I_{xx}I_{yy} - I_{xy}^2} P_y^2 + \frac{1}{2} \frac{I_{yy}}{I_{xx}I_{yy} - I_{xy}^2} P_x^2 \\ & + \frac{1}{2} \frac{I_{xy}}{I_{xx}I_{yy} - I_{xy}^2} (P_x P_y + P_y P_x) \end{aligned} \quad (67)$$

Equations 66 and 67 depend on the effective moment of inertia

$$I_{zz}^{\text{eff}} = \frac{\mu m_1 m_2 m_3}{\lambda^2 M} R^2 + 4\lambda t_1 \frac{R}{\gamma} \sin \theta + \mu t_1^2 \quad (68)$$

and the  $z$  component of the vibrational angular momentum

$$P_z^{\text{vib}} = t_3 P_{t_2} - t_2 P_{t_3} \quad (69)$$

\*For details of this derivation, see Ref. 32. We are only concerned here with the general form of the Hamiltonian and not with the detailed description of each term.

TABLE IV  
Features of Alternate Methods to Solve (62) and Some Representative Vibrational Energies ( $\text{cm}^{-1}$ ) for  $\text{H}_2\text{O}^a$

Investigators	Coordinate space	Basis set	Integration scheme	SCF	Number of configurations	Zero-point energy (000)	Excitation energies		
							(100)	(010)	(001)
Carney et al. <sup>b</sup>	"r"	Harmonic and Morse oscillators	Analytical HEG method <sup>g</sup>	No	220 <sup>j</sup>	4652	3717	1597	3821
Bucknell and Handy <sup>c</sup>	Rectilinear	Generalized harmonic oscillators	Gauss-Hermite quadrature	No	35	4646	3697	1560	3820
Whitehead and Handy <sup>d</sup>	Normal	Generalized harmonic oscillators	Gauss-Hermite quadrature	No <sup>h</sup>	84 <sup>k</sup>	—	3717	1597	3821
Lai and Hagstrom <sup>e</sup>	Valence	Numerical	HEG method <sup>g</sup>	No	128 <sup>j</sup>	4652	3717	1597	3821
Sprandel and Kern <sup>f</sup>	Valence	Numerical	Simpson's rule	Yes	27	4653	3718	1598	3822

<sup>a</sup>All calculations were performed with the experimental force field of Ref. 109, except for those of Bucknell and Handy which used the Smith and Overend force field of Ref. 50.

<sup>b</sup>Reference 26 and 28 through 30.

<sup>c</sup>References 14 and 15.

<sup>d</sup>References 16 and private communication.

<sup>e</sup>Reference 25.

<sup>f</sup>Reference 19.

<sup>g</sup>Reference 75

<sup>h</sup>Whitehead and Handy use a method based on Möller-Plesset theory to determine their basis functions.

<sup>j</sup>For these calculations, the number of configurations indicated is larger than actually needed to obtain converged results for the states given. Two quanta and higher excitation energies calculated by Carney et al., Lai and Hagstrom, and Whitehead and Handy are also in good agreement.

<sup>k</sup>Reference 17 uses 250 configurations for the potential of Sorbie and Murrell.<sup>18</sup>

Of particular significance is the fact that  $I_{zz}^{\text{eff}}$  depends only on coordinate  $t_1$ ; the remaining factors in (68), including  $\lambda$  and  $\gamma$ , are dependent only on masses and the equilibrium geometry of the molecule. Coordinates  $t_1$ ,  $t_2$ , and  $t_3$  are obtained by a nonlinear transformation of the symmetric stretching, the bending, and the asymmetric stretching internal valence coordinates, respectively, of the ABC molecule. These  $t$  coordinates are chosen to obtain the simplest possible expressions for (68) and (69).

Carney and Porter (CP) divide the vibrational Hamiltonian  $\hat{H}_v$  into a sum of three parts

$$\hat{H}_v = \sum_i h_i + \Delta\hat{T} + \Delta V \quad (70)$$

where

$$h_i = \frac{1}{2\mu} P_{t_i}^2 + V_i(t_i) \quad (71)$$

$$\Delta\hat{T} = \frac{1}{2I_{zz}^{\text{eff}}} (t_3 P_{t_2} - t_2 P_{t_3})^2 \quad (72)$$

and

$$\Delta V = V(t_1, t_2, t_3) - \sum_i V_i(t_i) + U_w \quad (73)$$

The term  $\Delta\hat{T}$  represents the additional kinetic energy contribution in which the vibrational momenta and coordinate operators are coupled. The potentials  $V_i(t_i)$  are cuts along  $t_i$  through the complete potential  $V(t_1, t_2, t_3)$ , including the Watson term  $U_w$ . In the CP method, harmonic or Morse-oscillator basis sets are introduced so that they satisfy the eigenvalue equation

$$h_i \chi_i(t_i) = \epsilon_i \chi_i(t_i) \quad (74)$$

by the usual basis-set-expansion and matrix-inversion techniques without SCF iterations. These eigenfunctions are used in (63) to form  $\psi_n(t_1, t_2, t_3)$ .

The matrix elements of  $\Delta\hat{T}$  over  $\psi_n$  can be evaluated analytically because the  $t_1, t_2$ , and  $t_3$  dependence in (68) and (69) leads to a product of one-dimensional integrals. Matrix elements of  $\Delta V$  over  $\psi_n$  can also be evaluated analytically when the potential is separable. However, when  $\Delta V$  is inseparable, or when it is otherwise convenient, Gauss-Hermite quadrature is used.<sup>75,87</sup> Orthogonality of the  $t_i$  coordinates allows factorization of the quadrature weights which are obtained at points defined by properties of the  $\chi_i(t_i)$ . Typically, 10 or fewer independent oscillators are introduced in each of the three dimensions, thereby limiting the basis and quadrature set to 1000 functions and grid points. An alternative is to retain the full set of 1000



but to restrict the summation in (63) by some criterion. For instance,

$$\sum_i v_i \leq L_{\max} \quad (75)$$

When  $L_{\max}=9$  there are 220 terms in the CI-like vibrational trial function; this number gives satisfactory precision and accuracy (see Section IV) for the vibrational energies  $E_n$  and the expansion coefficients  $c_{v_1, v_2, v_3}^{(n)}$ , which are obtained by diagonalization of  $\hat{H}_v$ .

Bucknell and Handy (BH)<sup>15</sup> employ a purely numerical integration scheme, based on Gauss-Hermite quadrature, for evaluation of the matrix elements  $\langle \psi_n | \hat{H}_v | \psi_m \rangle$  over a generalized harmonic-oscillator basis set

$$\chi(q) = \sum_m c_m q^m \exp(-\frac{1}{2}q^2) \quad (76)$$

in normal coordinate space  $q$ . If convergence within  $\pm 3 \text{ cm}^{-1}$  for the lowest 22 frequencies of  $\text{H}_2\text{O}$  is required, they find it necessary to use a  $250 \times 250$  secular matrix.

It is important to notice at this stage in the discussion that two main difficulties arise in the application of the CP and BH method to molecules containing more than three atoms. These can be illustrated by increasing the number of atoms to four. In the first place, the number of  $t_i$  or normal coordinates increases from three to six. This means that the number of oscillator basis functions must also be expanded considerably to ensure convergence of the band origins. We also see that the dimensionality of the secular matrix elements increases to six, meaning that we must evaluate integrals of the type

$$I = \int_{-\infty}^{\infty} \cdots \int_{-\infty}^{\infty} f(q_1, q_2, \dots, q_6) \exp\left(-\sum_{i=1}^6 q_i^2\right) dq_1 dq_2 \dots dq_6 \quad (77)$$

In fact, for  $N$  atoms the dimensionality of  $I$  will be  $3N-6$  for a nonlinear molecule. Since this is impractical, we require a more efficient integration procedure for the whole space with weight function of degree  $k=2L_{\max}$ . This problem has been investigated by numerical analysts<sup>88</sup> and, while the method to determine such an optimum scheme is not known *a priori*, it can be shown that at least  $(3N+L_{\max}-6)!/L_{\max}!(3N-6)!$  integration points must be used. This lower bound is compared in Table V with the simple-product number of one-dimensional points. The implication of these results is that if a near-optimum integration scheme exists, the CP and BH variational approaches may be extended directly to  $N>3$ ; otherwise, alternatives must be used.

A related variational approach has been suggested and tested by Sprandel and Kern (SK).<sup>19</sup> Their principal idea is to retain the entire kinetic and potential energy contributions to  $\hat{H}_v$  and obtain the "best" simple product function

TABLE V  
Comparison of Number of Integration Points Required for  
Simple Product and Optimum Schemes for Nonlinear  
Polyatomic Molecules Containing  $N$  atoms

$N$	$L_{\max}^a$	Simple Product	Optimum scheme
		$(L_{\max} + 1)^{3N-6}$	$(3N+L-6)!/L_{\max}!(3N-6)!$
3	5	216	56
	15	4096	816
4	5	46656	462
	15	$\sim 1.7 \times 10^7$	54264
5	5	$\sim 1.0 \times 10^7$	2002
	15	$\sim 6.9 \times 10^{10}$	$\sim 1.3 \times 10^6$

<sup>a</sup>Reference 17.  $L_{\max} = 5$  is sufficient to determine the fundamental frequencies of  $\text{H}_2\text{O}$  to within  $1 \text{ cm}^{-1}$ . A value of  $L = 15$  was needed to obtain band origins to within  $3 \text{ cm}^{-1}$  for the lowest 22 states of  $\text{H}_2\text{O}$ .

of the  $\chi_i$ . This corresponds to using only one term in the expansion of (63). Proceeding in this manner, it is found that a coupled set of integrodifferential equations result, but each equation depends only on one coordinate at a time. These equations may therefore be solved to self-consistency by direct numerical integration, thereby avoiding the necessity of introducing an analytical oscillator basis set. A related method has been developed by Lai and Hagstrom (LH)<sup>25</sup> for generating the product function with a model potential that depends on only one vibrational coordinate at a time. Sprandel and Kern proceed beyond the "best" or "model" product step to diagonalize the Hamiltonian matrix through use of a CI-like expansion of the trial vibrational wave function.

The SK and LH methods are convenient in that one can perform the calculations directly in the space of a central or valence force field without transforming to normal coordinates ( $q_i$ ) or some linear combination of them ( $t_i$ ). This is achieved by writing  $\hat{H}_v$  in terms of the instantaneous bond distances and angles. For the case of a nonlinear ABC molecule,

$$\hat{H}_v = \frac{-\hbar^2}{2\mu_1} \frac{\partial^2}{\partial R_1^2} - \frac{\hbar^2}{2\mu_3} \frac{\partial^2}{\partial R_2^2} - \frac{\hbar^2}{2} \left( \frac{1}{\mu_1 R_1^2} + \frac{1}{\mu_3 R_2^2} - \frac{2 \cos \theta}{m_2 R_1 R_2} \right) \frac{\partial^2}{\partial \theta^2}$$

$$\begin{aligned}
& -\frac{\hbar^2 \sin \theta}{m_2 R_1 R_2} \frac{\partial}{\partial \theta} + \frac{\hbar^2 \cos \theta}{2m_2} \left( \frac{1}{R_1} \frac{\partial}{\partial R_2} + \frac{1}{R_2} \frac{\partial}{\partial R_1} \right) \\
& -\frac{\hbar^2 \cos \theta}{m_2} \frac{\partial^2}{\partial R_1 \partial R_2} + \frac{\hbar^2 \sin \theta}{m_2} \frac{\partial}{\partial \theta} \left( \frac{1}{R_1} \frac{\partial}{\partial R_2} + \frac{1}{R_2} \frac{\partial}{\partial R_1} \right) \\
& + \frac{\hbar^2 \cos^3 \theta}{4m_2 R_1 R_2 \sin^2 \theta} - \frac{\hbar^2}{8} \left( \frac{1}{\mu_1 R_1^2} + \frac{1}{\mu_3 R_2^2} \right) (1 + \csc^2 \theta) + V(R_1, R_2, \theta) \quad (78)
\end{aligned}$$

where  $1/\mu_1 = 1/m_1 + 1/m_2$  and  $1/\mu_3 = 1/m_3 + 1/m_2$ . Now, to obtain the product solution

$$\psi_{ijk} = F_i(R_1)G_j(R_2)H_k(\theta) \quad (79)$$

Lai and Hagstrom introduce three equations of the form of (74), where

$$h_1 = \frac{-\hbar^2}{2\mu_1} \frac{d^2}{dR_1^2} + V(R_1, R_{2e}, \theta_e). \quad (80a)$$

$$h_2 = \frac{-\hbar^2}{2\mu_3} \frac{d^2}{dR_2^2} + V(R_{1e}, R_2, \theta_e) \quad (80b)$$

and

$$h_3 = \frac{-\hbar^2}{2} \left( \frac{1}{\mu_1 R_{1e}^2} + \frac{1}{\mu_3 R_{2e}^2} - \frac{2 \cos \theta_e}{m_2 R_{1e} R_{2e}} \right) \frac{d^2}{d\theta^2} + V(R_{1e}, R_{2e}, \theta) \quad (80c)$$

The subscript  $e$  denotes the equilibrium value of the variable. LH's partitioning of  $\hat{H}_v$  into three separate one-dimensional equations is like that of CP, except that valence internal coordinates are used. Once these equations are solved numerically (e.g., by the Numerov method), the complete vibrational Hamiltonian matrix  $\langle \psi_{ijk} | \hat{H}_v | \psi_{lmn} \rangle$  is formed by the HEG method and diagonalized to obtain the configuration interaction expansion.

The SCF equations are also similar to (74), with the difference that the effective one-dimensional Hamiltonian  $h_i$  for phonon  $i$  depends on solutions to all of the other one-phonon equations. The general method for solving the SCF equations is therefore an iterative procedure that converges when successive solutions agree within a specified tolerance. The vibrational energy corresponding to the "best" product  $\psi_{ijk}$  is

$$\tilde{E}_v = \langle \psi_{ijk} | \hat{H}_v | \psi_{ijk} \rangle \quad (81)$$

Using (78) and (79) for an  $AB_2$  molecule where  $M = m_2$  and  $m = m_1 = m_3$ , (81) becomes

$$\tilde{E}_v = \frac{-\hbar^2}{2} \frac{M+m}{mM} \left[ \varepsilon_i + \varepsilon_j - \varepsilon_k + \left\langle H_k \left| \frac{d^2}{d\theta^2} \right| H_k \right\rangle \left( \left\langle F_i \left| \frac{1}{R_1^2} \right| F_i \right\rangle + \left\langle G_j \left| \frac{1}{R_2^2} \right| G_j \right\rangle \right) \right] \quad (82)$$

The quantity  $(E_v - \tilde{E}_v)$ , where  $E_v$  is the converged CI vibrational energy, provides an overall measure of the "correlation" among modes. We find for  $\text{H}_2\text{O}$  that  $\tilde{E}_v$  gives the zero-point vibrational state energy to better than 0.3% accuracy. As the excitation level increases, the correlation contribution generally becomes larger. For the fundamentals these correlations contribute about  $12\text{ cm}^{-1}$  for the asymmetric stretch,  $14\text{ cm}^{-1}$  for the symmetric stretch, and  $30\text{ cm}^{-1}$  for the bend. Correlation effects may be smaller for excitation energies because of cancellation.

One distinct advantage of the SK approach is that it can be generalized straightforwardly to larger numbers of atoms. Consider a potential that is written as a sum of product functions in each variable. Not only are SCF equations<sup>8</sup> then solved in one dimension at a time, but effective one-phonon Hamiltonians in each variable contain "constants" which are no worse than one-dimensional integrals over the remaining vibrational coordinates. Whitehead and Handy<sup>17</sup> apply the vibrational counterpart of Möller-Plesset theory\* to achieve essentially self-consistency using analytical basis functions.

All the methods described here have their limitations when very high vibrational levels near the dissociation limit are required. Although this region has not yet been explored in detail for three dimensions or more in purely quantal treatments, it is clear that classical and semiclassical methods<sup>34</sup> are also of great interest in this region. The goal of the latter is to extend the WKB approximation, which has been widely applied in analyzing infrared spectra of diatomic molecules, to multidimensional systems. For such systems Miller<sup>89</sup> has recently argued that the semiclassical limit of eigenvalues can exist, even when a complete set of "good" quantum numbers cannot be specified to characterize that portion of the spectrum above the critical energy  $E_c$  where complete energy randomization occurs. Classical theory<sup>90</sup> appears to be very useful in establishing where  $E_c$  is actually located relative to the dissociation limit.

Semiclassical vibrational energies for  $\text{H}_2\text{O}$  and  $\text{SO}_2$  have been obtained recently by Handy et al.<sup>34</sup> For the states given in Table IV, their results agree with the fully quantal calculations to within  $10\text{ cm}^{-1}$  for the absolute energies and within 1 to  $5\text{ cm}^{-1}$  for the fundamental frequencies taken relative to the zero-point energy. For low-lying energies, semiclassical theory offers no special advantages; the results, of course, are slightly more approximate, but, more importantly, they are obtained with no more ease than the purely quantum-mechanical ones. When particular eigenvalues are required, however, the semiclassical approach may be preferable, especially in situations where individual states in the neighborhood of  $E_c$  are of interest.

\*See Ref. 2, Vol. 4, Chap. 1 for applications of the theory to electronic structure.

So far we have omitted detailed discussion of the techniques necessary to implement the variational V-R theory. Before proceeding, let us return to the HEG integration procedure<sup>75</sup> that is outlined earlier in this section. If we introduce basis functions for polyatomic molecules, we must diagonalize an  $N \times N$  matrix whose elements have the form

$$F_{ij} = \int_a^b \chi_i(x) f(x) \chi_j(x) dx \quad (83)$$

where the functions  $\chi_i$  are orthonormal and  $x$  corresponds to an internal coordinate. We first find the transformation  $\mathbf{C}$  that diagonalizes the  $\mathbf{X}$  matrix whose elements are

$$X_{ij} = \int_a^b \chi_i(x) x \chi_j(x) dx \quad (84)$$

For the general function  $f(x)$  appearing in (83), we then obtain the diagonal matrix  $\Phi$

$$\Phi = \mathbf{C} \mathbf{F} \mathbf{C}^{-1} \quad (85)$$

with elements

$$\Phi_{ij} = f(\lambda_j) \delta_{ij} \quad (86)$$

where  $\lambda_j$  is the  $j$ th eigenvalue of  $\mathbf{X}$ . The inverse of (85) gives the desired matrix

$$\mathbf{F} = \mathbf{C}^{-1} \Phi \mathbf{C} \quad (87)$$

The relation between this method and generalized Gauss quadrature for constructing a set of matrix elements of the form of (83) has been given by Dickinson and Certain.<sup>87</sup>

The elements of the  $\mathbf{X}$  matrix are well known for a harmonic-oscillator basis. For the Morse-oscillator basis functions  $\chi_v(x)$  satisfying

$$\begin{aligned} & \left[ -\frac{\hbar^2}{2\mu} \frac{d^2}{dx^2} + D(1 - e^{-ax})^2 \right] \chi_v(x) \\ &= \left[ a\hbar \left( \frac{2D}{\mu} \right)^{1/2} \left( v + \frac{1}{2} \right) - \left( \frac{a^2 \hbar^2}{2\mu} \right) \left( v + \frac{1}{2} \right)^2 \right] \chi_v(x) \end{aligned} \quad (88)$$

$\mathbf{X}$  can be obtained by the factorization method of Infeld and Hull,<sup>91</sup> who find for  $v < v'$

$$X_{vv'} = -\frac{2}{a} [(v' - v)(2\eta - v - v')]^{-1} \left[ \frac{v'!}{v!} \frac{\Gamma(2\eta - v' + 1)}{\Gamma(2\eta - v + 1)} (\eta - v)(\eta - v') \right]^{1/2} \quad (89)$$

where

$$\eta = \left( \frac{2\mu D}{a^2 \hbar^2} \right)^{1/2} - \frac{1}{2} \quad (90)$$

For the diagonal elements, Carney and Porter obtain

$$X_{vv} = \frac{1}{a} \left\{ \ln(2\eta + 1) - \Phi(2\eta - 2v) + \left[ \sum_{k=1}^v (1 + 2\eta - v - k)^{-1} \right] (1 - \delta_{0v}) \right\} \quad (91)$$

where  $\Phi(x)$  is the digamma function,<sup>92</sup>

$$\Phi(x) = \frac{d}{dx} \ln \Gamma(x) \quad (92)$$

The kinetic-energy integrals in the Morse-oscillator basis are

$$\left\langle v \left| \frac{d}{dx} \right| v' \right\rangle = a \left[ \frac{v'!}{v!} \frac{\Gamma(2\eta - v' + 1)}{\Gamma(2\eta - v + 1)} (\eta - v)(\eta - v') \right]^{1/2} (1 - \delta_{vv'}); \quad v' \geq v \quad (93)$$

$$\left\langle v \left| \frac{d^2}{dx^2} \right| v \right\rangle = -a^2(v + \frac{1}{2})^2 - (2\mu D)^{1/2} \frac{a}{\hbar} (v + \frac{1}{2}) \quad (94)$$

and

$$\begin{aligned} \left\langle v \left| \frac{d^2}{dx^2} \right| v' \right\rangle &= a^2 \left[ \frac{v'!}{v!} \frac{\Gamma(2\eta - v' + 1)}{\Gamma(2\eta - v + 1)} (\eta - v)(\eta - v') \right]^{1/2} \\ &\times \left[ \frac{1}{2} (v' - v - 1)(2\eta - v' - v - 1) - (v + 1) \right]; \quad v' > v \end{aligned} \quad (95)$$

The three-dimensional integration of a nonseparable potential-energy function is a generalization of the method used by Endres<sup>85</sup> for a nonseparable potential in two dimensions. In this case supermatrix  $\mathbf{X}^{(s)}$  is a direct product of the form

$$\mathbf{X}^{(s)} = \prod_i \mathbf{X}_i \quad (96)$$

where  $\mathbf{X}_i$  is a matrix of the coordinate  $x_i$  in the basis of  $N_i$  eigenfunctions  $\chi_i$  of  $h_i$ . When  $\mathbf{X}^{(s)}$  is used to calculate the full list of matrix elements  $\mathbf{F}^{(s)}$ , the result corresponds to that obtained using  $N_1 \times N_2 \times N_3$  vibrational configurations. Contraction of both the basis and quadrature set is effected when the configuration list is restricted to be less than  $N_1 \times N_2 \times N_3$ , which is the dimensionality of the full direct product space.

If, for a specific choice of internal coordinates and Hamiltonian operator, the anharmonic-oscillator eigenfunctions are not known, direct numerical integration can also be used to define the necessary matrix elements of the coordinate basis in the desired oscillator representation. For example, Lai<sup>25</sup> and Hagstrom determined by a finite difference method the numerical eigenfunctions for a separable oscillator-model Hamiltonian of the water molecule. Matrix elements of the internal coordinates were then evaluated by quadrature. Beyond that point, the general HEG procedure was employed.

An alternative numerical integration procedure is the polynomial expansion method described by Suzuki<sup>11,12</sup> for diatomic and linear triatomic molecules and by Carney et al.<sup>32</sup> for bent triatomic molecules. To evaluate matrix elements  $F_{nm}$  of a function  $F$ , we use the polynomial approximation

$$F \cong \sum_k A_k P_k \quad (97)$$

where  $A_k$  and  $P_k$  are the expansion coefficients and polynomial basis functions, respectively. For some oscillator basis sets, there are well-known analytical expressions

$$P_{nmk} = \langle n | P_k | m \rangle \quad (98)$$

for matrix elements of the polynomials  $P_k$ . Matrix elements of  $F$  are then readily obtained as

$$F_{nm} \cong \sum_k A_k P_{nmk} \quad (99)$$

In the case of multidimensional functions  $F$ , the polynomials  $P_k$ , which can be characterized by their degree  $k$ , consist of more than a single term.

The polynomial method has been used by Gribov and Khovrin,<sup>20-23</sup> by Carney et al.,<sup>32</sup> by Whiffen et al.,<sup>8,9</sup> and by Suzuki.<sup>11-13</sup> The HEG method, or Gaussian quadrature methods, have been used by Carney et al.,<sup>27-33</sup> by Handy et al.,<sup>15-17</sup> and by Lai<sup>25</sup> and Hagstrom. In some applications the polynomial and quadrature integration schemes are combined. For example, Sprandel<sup>19</sup> and Kern use the quadrature method to obtain numerical wave functions and integrals of powers of internal coordinates. Then matrix elements of the potential function are evaluated using the polynomial form of the potential function.

In perhaps all molecules except those involving only hydrogen atoms, nuclear masses are large enough that the polynomial expansion methods are likely to be useful. Carney et al.<sup>32</sup> have investigated this problem in detail for ozone using both the HEG and the polynomial integration procedures. However, for  $H_3^+$  it is essential that the HEG method be used because of the large vibrational amplitudes. Similar effects may be present in other hydrides (e.g.,  $NH_3$ ).

Although matrix diagonalization procedures<sup>93,94</sup> are not discussed here, it is important to realize that the vibrational Hamiltonian matrix is not "sparse" in the sense met in electronic structure calculations.<sup>95</sup> Direct diagonalization is therefore generally a time-consuming step in the solution of the variational V-R eigenvalue problem. However, if an SCF step of the type employed by Sprandel and Kern is introduced, then the extra effort of iterating to the best product function is likely to be returned with dividends

at the stage of diagonalizing the vibrational CI matrix. A definitive test of this point would be very worthwhile.

#### IV. APPLICATIONS OF VARIATIONAL METHODS TO TRIATOMIC MOLECULES

##### A. Literature Survey

The variational methodology described in Section III.B has been applied to  $\text{H}_2\text{O}$ ,  $\text{H}_2\text{S}$ ,  $\text{H}_3^+$ ,  $\text{CH}_2$ ,  $\text{ClO}_2$ ,  $\text{NO}_2$ ,  $\text{O}_3$ ,  $\text{SO}_2$ ,  $\text{CS}_2$ ,  $\text{OCS}$ , and  $\text{CO}_2$  and to selective isotopic variants. The molecules  $\text{CS}_2$ ,  $\text{OCS}$ , and  $\text{CO}_2$  are linear in their ground electronic states,  $\text{H}_3^+$  is a symmetric top, and the rest are asymmetric tops. The infrared spectra of  $\text{H}_2\text{D}^+$  and  $\text{CH}_2$  have not been observed, but since *ab initio* potential surfaces and dipole-moment functions are available,<sup>31,33</sup> their spectra can be predicted. There have been other nonperturbative, direct numerical treatments, such as those by Truhlar et al.<sup>96</sup> for HCN and by Handy et al.<sup>34</sup> for  $\text{H}_2\text{O}$  and  $\text{SO}_2$ ; the former investigates only the colinear degrees of vibrational freedom, and the latter uses semiclassical theory, as is mentioned earlier. We do not discuss these or other approximate approaches further, except to say that high-order (e.g., anharmonic) contributions in the kinetic- and potential-energy operators must generally be included to obtain results that can be compared meaningfully with experiment.

Of the studies cited below, different emphases and purposes are apparent. For example, Gribov and Khovrin,<sup>20-23</sup> Suzuki,<sup>11-13</sup> and Foord et al.<sup>9</sup> utilize the variational approach to extract anharmonic force constants from observed band structures and infrared intensities. Carney and Porter,<sup>31</sup> Carney and Kern,<sup>28</sup> Sprandel<sup>19</sup> and Kern, Whitehead and Handy,<sup>16,17</sup> Carney and Langhoff,<sup>33</sup> and Bucknell et al.<sup>14,15</sup> combine variational methods with *ab initio* force fields to predict V-R properties. Intermediate between these two types of studies are those on  $\text{H}_2\text{O}$  and  $\text{O}_3$  in which conventional experimentally derived force fields are combined with the variational approach to predict unknown observables and to determine optimum forms for the vibrational Hamiltonian, particularly the potential. For example, Carney et al.<sup>30</sup> have determined and assigned infrared band origins strictly on the basis of the properties of the wavefunctions and energies for the isotopic water molecules that contain tritium. These workers<sup>32</sup> also studied isotopic substitution effects in  $\text{O}_3$ .

A number of more technical studies of Carney and Porter,<sup>31</sup> Sprandel<sup>19</sup> and Kern, and Lai<sup>25</sup> and Hagstrom deal with choice of basis sets, coordinate representations, forms of the potential function, and computational feasibility. Methods of simplifying the variational calculations have also been



investigated. For example, Foord and Whiffen<sup>8</sup> use perturbation theory to approximate matrix elements of the Hamiltonian in their treatment of carbonyl sulfide. Suzuki<sup>12,13</sup> also followed this line in the studies of carbon disulfide and carbon dioxide.

Our subsequent discussion of variational methods in V-R spectroscopy is organized into those aspects that are, on the one hand, confirmatory in nature and, on the other, of more predicative interest. Illustrative studies of the former kind are presented in this section. In Section V work on  $D_3^+$ ,  $CH_2$ , and  $T_2O$  is given to exemplify the latter.

## B. Linear Molecules

Suzuki<sup>12</sup> has extended his approach for diatomic molecules to the case of three atoms in a line. The Hamiltonian derived by Goldsmith et al.<sup>97</sup>

$$\hat{H} = \hat{H}_v + \hat{H}_r + \hat{H}_c \quad (100)$$

is greatly simplified for the case of a symmetric, linear triatomic molecule. Here,  $\hat{H}_v$ ,  $\hat{H}_r$ , and  $\hat{H}_c$  are the vibrational, rotational, and Coriolis terms. Replacing the degenerate pair of bending normal coordinates by two new (cylindrical) coordinates, including  $r_2$ , Suzuki expresses  $\hat{H}_v$  as

$$\begin{aligned} \hat{H}_v = & \frac{1}{2} \sum_{s=1,3} \omega_s(p_s^2 + q_s^2) + \frac{1}{2} \omega_2(p_2^2 + r_2^2) + (k_{111}q_1^2 + k_{122}r_2^2 + k_{133}q_3^2)q_1 \\ & + k_{1111}q_1^4 + k_{1133}q_1^2q_3^2 + k_{3333}q_3^4 + (k_{1122}q_1^2 + k_{2222}r_2^2 + k_{2233}q_3^2)r_2^2 + \hat{H}'_v \end{aligned} \quad (101)$$

where

$$\hat{H}'_v = B_e(j_x^2 + j_y^2) \sum_{k=0}^K R_k q_1^k \quad (102)$$

The rotational and Coriolis contributions are

$$\hat{H}_r = B_e(J_x^2 + J_y^2) \sum_{k=0}^K R_k q_1^k \quad (103)$$

and

$$\hat{H}_c = -2B_e(j_x J_x + j_y J_y) \sum_{k=0}^K R_k q_1^k \quad (104)$$

In these equations  $R_k = (-1)^k(k+1)\gamma_1^{k/2}$ ,  $\gamma_1 = (2B_e/\omega_1)$ , and  $j_x$  and  $j_y$  are the dimensionless vibrational angular momenta. The totally symmetric normal coordinate  $q_1$  plays essentially the same role as  $q$  in diatomic molecules in that the anharmonic terms  $\hat{H}'_v$ ,  $\hat{H}_r$ , and  $\hat{H}_c$  are expanded as power series in  $q_1$  so that the bending and asymmetric motion coordinates  $r_2$  and  $q_3$  do not appear explicitly. This is convenient for numerical computations in which the

vibrational Hamiltonian matrix is directly diagonalized as described in Section III. Also, the Hamiltonian may be truncated easily at a desired order of approximation  $K$ .

One purpose of Suzuki's direct-diagonalization study of  $\text{CS}_2$  and  $\text{CO}_2$  was to compare the results with second-order perturbation treatments<sup>98-103</sup> in which third-order Fermi resonance corrections were utilized to obtain force fields from spectral term constants. These third-order parameters are complicated functions of the force constants and molecular geometry.<sup>98</sup>

Because the energy contributions of the quadratic through the quartic force constants are considered to "infinite order" of approximation (for sufficiently large vibrational-basis sets), only three terms beyond the quartic force field are required, namely, the quintic constants  $k_{11122}$ ,  $k_{12222}$ , and  $k_{12233}$ . In the case of  $\text{CO}_2$ , Suzuki<sup>104</sup> used the values of these constants reported by Chedin et al.<sup>99,100</sup> and found that these fifth-degree terms in the potential improved the agreement between the observed and variationally calculated vibrational energies and rotational constants.

However, truncation of the potential even at sixth degree for  $\text{CO}_2$  produces significant residual error. Use of the SPF representation<sup>74</sup> of the molecular force field instead of the normal coordinate representation has been shown to reduce the effect of truncation, at a given order in the potential function expansion, on the calculated band positions, as discussed by Chédin et al.<sup>99,100</sup> for  $\text{CO}_2$  and by Carney et al.<sup>29,31</sup> for the bent molecules  $\text{H}_2\text{O}$  and  $\text{H}_3^+$ . Similar results are also obtained for potentials of chemisorbed molecules.<sup>105</sup> Although Suzuki did obtain an experimental force field for  $\text{CS}_2$  using direct diagonalization, use of the normal coordinate representation of the potential complicates the comparison of perturbation and variationally derived force constants, as amplified further below.

A related and earlier approach for  $\text{CO}_2$  was developed by Vučelić et al.,<sup>24</sup> who determined *ab initio* force constants and dipole-moment derivatives. To obtain the vibrational frequencies for the system, the calculated potentials were fitted to a fourth-order polynomial in the internal coordinates, and the vibrational frequencies were calculated according to the variational approach of Heilbronner et al.<sup>101-103</sup> The fourth-order potential was used to take anharmonicity into account insofar as possible. Calculated and observed transitions are given in Table VI.

Foord et al.<sup>9</sup> have also used direct diagonalization to determine a 16-parameter force field for OCS based on curvilinear coordinates. It is seen from Table VII that while harmonic frequencies agree well among all sources, anharmonic contributions  $x_{ij}$  in the quantum-number expansion of the vibrational energy are more sensitive to the method of obtaining the force field from the observed data.

In Table VIII variational and perturbation energies are presented as

TABLE VI  
*Ab initio* and Observed Vibrational Transitions  
 (cm<sup>-1</sup>) in CO<sub>2</sub>

Upper state ( $n_1 n_2' n_3$ )	Lower state ( $n_1 n_2' n_3$ )	Calculated from quartic potential <sup>a</sup>	Observed frequency <sup>b</sup>
10 <sup>0</sup> 0	00 <sup>0</sup> 0	1232.8	1285.5 ( $\nu_1$ )
20 <sup>0</sup> 0	00 <sup>0</sup> 0	2578.6	—
30 <sup>0</sup> 0	00 <sup>0</sup> 0	4028.0	—
01 <sup>1</sup> 0	00 <sup>0</sup> 0	680.7	667.3 ( $\nu_2$ )
02 <sup>0</sup> 0	00 <sup>0</sup> 0	1409.7	1388.3
03 <sup>1</sup> 0	00 <sup>0</sup> 0	2176.9	1932.5
04 <sup>0</sup> 0	00 <sup>0</sup> 0	2980.5	—
00 <sup>0</sup> 1	00 <sup>0</sup> 0	2040.2	2349.3 ( $\nu_3$ )
00 <sup>0</sup> 2	00 <sup>0</sup> 0	4233.3	—
02 <sup>0</sup> 0	01 <sup>1</sup> 0	729.0	618.1
03 <sup>1</sup> 0	01 <sup>1</sup> 0	1496.2	1264.8
04 <sup>0</sup> 0	01 <sup>1</sup> 0	2299.8	1866
10 <sup>0</sup> 0	01 <sup>1</sup> 0	552.1	720.8
20 <sup>0</sup> 0	01 <sup>1</sup> 0	1879.9	2129.8
03 <sup>1</sup> 0	02 <sup>0</sup> 0	767.2	597.3
20 <sup>0</sup> 0	02 <sup>0</sup> 0	1168.9	1528
00 <sup>0</sup> 1	02 <sup>0</sup> 0	630.5	960.8
00 <sup>0</sup> 1	10 <sup>0</sup> 0	807.4	1063.6

<sup>a</sup>Reference 24.

<sup>b</sup>K. N. Rao, Int'l Astron. Union Symposium No. 65, 41 (1974). The labels for the 10<sup>0</sup>0 and 02<sup>0</sup>0 levels have been interchanged in accordance with G. Amat and M. Pimbert, *J. Mol. Spectrosc.* **16**, 278 (1965).

differences between observed and calculated results for several vibrational excitations of the OCS molecule. Inclusion of Fermi resonance terms in the perturbation analysis (column I) leads to an apparent satisfactory fit with the observed data, but use of this same force field in the more accurate variational scheme (columns II and III) reveals a significant discrepancy with the measurements. (Changes between columns II and III are due to differences in the variational basis sets.)

It is instructive to compare the variational approaches reported by Whiffen et al., Suzuki, and Whitehead and Handy. Suzuki<sup>11-13</sup> used the V-R Hamiltonian given by Goldsmith et al.,<sup>97</sup> which is equivalent to Aliev's

TABLE VII  
Empirical Spectroscopic Term Constants for the  
Vibrational Energies of OCS Obtained by Variational  
and Perturbation Methods

Parameter <sup>a</sup>	I <sup>b</sup>	II <sup>c</sup>	III <sup>d</sup>
$\omega_1$ (cm <sup>-1</sup> )	875.70	875.61	874.27
$\omega_2$ (cm <sup>-1</sup> )	523.62	524.64	524.20
$\omega_3$ (cm <sup>-1</sup> )	2092.46	2093.74	2094.15
$x_{11}$ (cm <sup>-1</sup> )	-4.32	-2.15	-3.25
$x_{12}$ (cm <sup>-1</sup> )	-7.16	-2.55	-3.14 <sup>e</sup>
$x_{13}$ (cm <sup>-1</sup> )	-2.97	-9.25	-2.53
$x_{22}$ (cm <sup>-1</sup> )	1.78	0.35	2.35 <sup>e</sup>
$x_{23}$ (cm <sup>-1</sup> )	-6.53	-7.60	-14.46 <sup>e</sup>
$x_{33}$ (cm <sup>-1</sup> )	-10.83	-11.44	-11.59
$x_{il}$ (cm <sup>-1</sup> )	-1.69	-0.014	-1.79 <sup>e</sup>
$\alpha_1$ (MHz)	20.26	19.86	18.88
$\alpha_2$ (MHz)	-10.28	-10.81	-10.56
$\alpha_3$ (MHz)	36.09	37.31	36.76
$q_e$ (MHz)	6.313	6.361	6.325
$D_{J(e)}$ (kHz)	1.281	1.305	1.283

<sup>a</sup>See Ref. 9 for a definition of the parameters.

<sup>b</sup>Obtained by perturbation theory from a variationally derived equilibrium geometry and molecular force field (Ref. 9).

<sup>c</sup>Obtained by A. Fayt, *Ann. Soc. Sci. Brux.*, **86**, 61 (1972) using a perturbation analysis of the observed spectrum.

<sup>d</sup>Obtained by Y. Morino and T. Nakagawa, *J. Mol. Spectrosc.*, **26**, 496 (1968) using a perturbation analysis of the observed spectrum.

<sup>e</sup>These values are not comparable as they exclude a Fermi resonance term.

Hamiltonian.<sup>52</sup> Whiffen et al.<sup>8,9</sup> and Whitehead and Handy<sup>16,17</sup> used the Watson Hamiltonian.<sup>41</sup> An important difference in the methods of Whiffen et al. and Whitehead and Handy is that the latter numerically integrated the Hamiltonian matrix elements. All these investigators employed harmonic-oscillator basis functions to expand their trial wave functions.

Foord and Whiffen<sup>8</sup> have observed infrared absorption spectra of OCS. From these data and other microwave measurements, the absolute values of the dipole moment in the equilibrium configuration and of the linear and

TABLE VIII  
Comparison of Calculated and Observed Energy  
Differences for OCS

Vibrational state ( $n_1 n_2 n_3$ )	$\nu_{\text{obs}} - \nu_{\text{calc}} (\text{cm}^{-1})$		
	I <sup>a</sup>	II <sup>b</sup>	III <sup>c</sup>
(10 <sup>0</sup> 0)	-0.01	-0.17	-0.32
(02 <sup>0</sup> 0)	0.38	3.81	-0.35
(20 <sup>0</sup> 0)	-0.13	-1.39	-2.00
(12 <sup>0</sup> 0)	-0.36	5.75	-3.46
(00 <sup>0</sup> 1)	0.00	-4.19	-15.96

<sup>a</sup>Comparison of ( $\nu_{\text{obs}} - \nu_{\text{calc}}$ ) for  $^{16}\text{O}^{12}\text{C}^{32}\text{S}$  calculated by Y. Morino and T. Nakagawa (MN), *J. Mol. Spectrosc.*, **26**, 496 (1968) using perturbation theory with adjustments for Fermi resonance.

<sup>b</sup>Comparison of ( $\nu_{\text{obs}} - \nu_{\text{calc}}$ ) calculated by Foord et al. using variational methods and MN's force field. See Ref. 9.

<sup>c</sup>Comparison of ( $\nu_{\text{obs}} - \nu_{\text{calc}}$ ) calculated by Whitehead and Handy using variational methods and MN's force field. See Ref. 16.

quadratic derivatives of the axial dipole component were determined using an anharmonic force field and direct diagonalization of the vibrational Hamiltonian.

## C. Nonlinear Molecules

### 1. Force Fields

To explore the relationship between the perturbation and variation methods further, let us consider quartic potential functions for the molecules  $\text{SO}_2$ ,  $\text{NO}_2$ ,  $\text{ClO}_2$ , and  $\text{H}_2\text{S}$ , which have been derived from infrared measurements and second-order perturbation theory. The variational V-R energies obtained with such potentials<sup>106</sup> (Table IX) show significant discrepancies with observed band origins in each case, particularly for  $\text{H}_2\text{S}$ , which has hydrogen atoms and therefore larger root-mean-square amplitudes. We therefore conclude that either the perturbation expansions that were employed to derive these potentials from the observed band origins are inadequately converged or that the constraints imposed by the Dunham expansion are more severe than had been previously supposed.

TABLE IX  
Vibrational Energies ( $\text{cm}^{-1}$ ) Obtained Using Quartic Experimental  
Potential Functions for Some Bent  $\text{AB}_2$  Molecules<sup>a</sup>

Vibrational state			$\text{SO}_2$		$\text{NO}_2$		$\text{ClO}_2$		$\text{H}_2\text{S}$	
$n_1$	$n_2$	$n_3$	VT	PT	VT	PT	VT	PT	VT	PT
0	0	0	1530	—	1877	—	1265	—	3299	—
0	1	0	517	518	759	750	451	445	1184	1183
1	0	0	1156	1151	1319	1320	945	943	2646	2615
0	0	1	1360	1362	1622	1618	1107	1110	2655	—
0	2	0	1027	—	1518	1498	902	—	2363	2354
2	0	0	2305	2296	2628	—	1882	1888	5272	5145
0	0	2	2711	2715	3220	3199	2203	2215	5308	5241
1	1	0	1671	1665	2073	—	1394	—	3807	3779
0	1	1	1873	1876	2373	—	1555	—	3816	3789
1	0	1	2505	2500	2922	2906	2036	2040	5274	5147

<sup>a</sup>Variational energies (VT) were calculated using quartic Dunham experimental force fields and are compared with the observed (PT) values. See Ref. 28 for additional details regarding the experimental force constants used in these calculations.

Using the variational approach, Lai<sup>25</sup> and Hagstrom performed several tests of Anderson's model potential,<sup>107</sup> which has the form

$$V(R_1, R_2, \theta) = V_D(R_1) + V_D(R_2) + A(R_1^2 + R_2^2 - 2R_1R_2 \cos \theta)^{-N/2} \\ - B/(R_1 + R_2)^N + C(R_1^2 + R_2^2 - 2R_1R_2 \cos \theta)^{-M/2} - A_\theta \cos(\theta - \theta_e) \quad (105)$$

where

$$V_D(R) = C' \left[ \left( \frac{2}{\xi^3 R} + \frac{1}{\xi^2} \right) e^{-\xi R} - \frac{F_D}{R} \right] \quad (106)$$

The constants in (105) and (106) can be adjusted to make (105) fit observed data. A variational calculation was first performed to determine the vibrational energies for the full potential, following which the calculation was repeated when  $V$  was expanded to second order. This truncated force field was then employed in a second-order perturbation calculation. The results are shown in Table X. The disparity between the last two columns, which were obtained with the truncated force field, suggests indeed that much of

TABLE X  
Effects of Potential-Function Truncation on Vibrational  
Energies ( $\text{cm}^{-1}$ ) of  $\text{H}_2\text{O}^a$

Vibrational state			Variational calculations		Second-order
$n_1$	$n_2$	$n_3$	I <sup>b</sup>	II <sup>c</sup>	perturbation theory
0	0	0	4795.51	4807.82	4782.41
0	1	0	1626.00	1642.15	1627.65
0	2	0	3242.10	3300.32	3247.17
1	0	0	3777.34	3825.70	3773.80
0	0	1	3943.97	3995.44	3940.93

<sup>a</sup>Reference 25.

<sup>b</sup>Full model potential was employed.

<sup>c</sup>Second-order approximation to model potential was used.

the difference between the variational and second-order perturbation approaches hinges on the higher-order force constants.

Lai and Hagstrom utilized the variational method to invert the band origin data known for  $\text{H}_2\text{O}$  and  $\text{D}_2\text{O}$  to obtain a quartic force field. However, because of limitations in the Dunham expansion form, the resultant higher-order force constants differ significantly from those obtained using second-order perturbation theory. Gribov and Khovrin have also utilized the variational approach to extract anharmonic force constants from the observed data for water,<sup>21</sup> hydrogen sulfide,<sup>22</sup> carbon dioxide,<sup>22</sup> and ammonia.<sup>23</sup> (The application to ammonia was not fully variational.) In their studies rather limited basis sets were used and the quadratic force constants were not optimized.

## 2. Relative Importance of Terms in the Vibrational Hamiltonian

To investigate the relative importance of various terms in the vibrational Hamiltonian, we follow the scheme of Carney and Porter<sup>31</sup> [see (70)], and write the Hamiltonian in the form

$$\hat{H}_v = \frac{1}{2\mu} \sum_i P_{i_i}^2 + V + \Delta\hat{T} + U_w \quad (107)$$

where  $\Delta\hat{T}$  represents all the nonseparable kinetic-energy terms that con-

tribute vibrational angular momenta, and  $U_w$  is a mass-dependent function identified by Watson.<sup>40</sup> The potential energy

$$V = \sum_n V_n P_n \quad (108)$$

is often written as a linear combination of polynomial terms  $P_n$  in the various types of internal coordinates.

As an example, *ab initio* coefficients for polynomial terms  $P_n$  are given in Table XI for  $H_3^+$  in the SPF variables

$$\rho_{ab} = (R_{ab} - R_e)/R_{ab} \quad (109)$$

where  $R_e$  is the equilibrium bond length of  $H_3^+$  in the equilateral geometry and  $R_{ab}$  is the instantaneous internuclear distance between atoms a and b.

TABLE XI  
Fifth-degree Simons-Parr-Finlan Expansion of the  
CI Potential Surface for  $H_3^+$ <sup>a</sup>

Coefficient number $n$	Polynomial terms $P_n^b$	Coefficient $V_n^c$
1	1.0	-1.335184
2	$\rho_1 + \rho_2 + \rho_3$	0.0
3	$\rho_1^2 + \rho_2^2 + \rho_3^2$	0.244944
4	$\rho_1\rho_2 + \rho_1\rho_3 + \rho_2\rho_3$	-0.036801
5	$\rho_1^3 + \rho_2^3 + \rho_3^3$	0.078313
6	$\rho_1^2(\rho_2 + \rho_3) + \rho_2^2(\rho_1 + \rho_3) + \rho_3^2(\rho_1 + \rho_2)$	-0.042076
7	$\rho_1\rho_2\rho_3$	0.217788
8	$\rho_1^4 + \rho_2^4 + \rho_3^4$	0.011167
9	$\rho_1^3(\rho_2 + \rho_3) + \rho_2^3(\rho_1 + \rho_3) + \rho_3^3(\rho_1 + \rho_2)$	-0.061533
10	$\rho_1^2\rho_2^2 + \rho_1^2\rho_3^2 + \rho_2^2\rho_3^2$	-0.037214
11	$\rho_1\rho_2\rho_3^2 + \rho_2\rho_3\rho_1^2 + \rho_1\rho_3\rho_2^2$	0.086770
12	$\rho_1^5 + \rho_2^5 + \rho_3^5$	-0.003403
13	$\rho_1(\rho_2^4 + \rho_3^4) + \rho_2(\rho_1^4 + \rho_3^4) + \rho_3(\rho_1^4 + \rho_2^4)$	-0.038229
14	$\rho_1^3(\rho_2^2 + \rho_3^2) + \rho_2^3(\rho_1^2 + \rho_3^2) + \rho_3^3(\rho_1^2 + \rho_2^2)$	-0.046858
15	$\rho_1\rho_2\rho_3^3 + \rho_1\rho_3\rho_2^3 + \rho_2\rho_3\rho_1^3$	-0.018078
16	$\rho_1\rho_2^2\rho_3^2 + \rho_2\rho_1^2\rho_3^2 + \rho_3\rho_1^2\rho_2^2$	0.064343

<sup>a</sup>See (108) and Ref. 31.

<sup>b</sup> $\rho_i = (R_{ab} - R_e)/R_{ab}$  where a and b are taken cyclic in pairs, and  $R_e = 1.6574$  Bohr.

<sup>c</sup> $\rho_i$  is dimensionless and the energy is evaluated in Hartrees.



For a fifth-degree expansion in these variables, only 16 parameters are required for  $D_{3h}$  molecular symmetry. The sizes of the higher-order force constants in Table XI show that the leading harmonic term in the SPF expansion ( $n=3$ ) and the cubic term ( $n=7$ ) are dominant. By contrast, in the usual Dunham and normal-coordinate expansions, the higher-order force constants become large and the expansion diverges.

The forms of (107) and (108) facilitate various levels of truncation. For instance, let us examine how the fundamental band positions change when we eliminate the terms  $\Delta\hat{T}$  and  $U_w$  from  $\hat{H}_v$ . From columns I and II of Table XII, we find upon subtraction of the zero-point energies that the  $\bar{\nu}_A$  band position\* is invariant to less than  $1\text{ cm}^{-1}$  but that the  $\bar{\nu}_E$  band position\* is red shifted by  $22\text{ cm}^{-1}$ . Omission of only the  $\Delta\hat{T}$  term gives to within  $1\text{ cm}^{-1}$  the same shifts in band origins as obtained for omission of both  $U_w$  and  $\Delta\hat{T}$ . Hence  $U_w$  lowers the energy of each state by nearly a constant amount  $(\hbar^2/8)\Sigma\mu_{xx}^0=27.4\text{ cm}^{-1}$ , while  $\Delta\hat{T}$  only raises the energy of states having a net vibrational angular momentum. In the (001) and (010) states, the contributions to the energy arising from  $\Delta\hat{T}$  and  $U_w$  are of opposite sign but nearly equal in magnitude. For the higher excitations and the ground state either  $\Delta\hat{T}$  or  $U_w$  dominates.

Alternatively, we retain  $\Delta\hat{T}$  and  $U_w$  terms in  $\hat{H}_v$  but systematically reduce the degree of the potential surface expansion. We then obtain the results given in columns III through V of Table XII. Since the force constants for quadratic SPF and Dunham expansions are the same, we also calculate eigenenergies for the Dunham quadratic potential as shown in column VI.

The quadratic Dunham potential gives  $\bar{\nu}_A$  and  $\bar{\nu}_E$  values that are blue shifted by 274 and  $241\text{ cm}^{-1}$ , respectively, relative to the quadratic SPF results. Hence, previous estimates of these fundamental frequencies that assume a Dunham force field are probably too large by about  $250\text{ cm}^{-1}$ . On the other hand, the quadratic SPF potential function values for  $\bar{\nu}_A$  and  $\bar{\nu}_E$  are red shifted from the values obtained with the fifth-degree SPF potential function by only 29 and  $31\text{ cm}^{-1}$ , respectively. Values for the  $\bar{\nu}_E$  fundamental band obtained with the cubic and quartic SPF potential functions differ from the fifth-degree SPF results by 0.5 and  $2.7\text{ cm}^{-1}$ , respectively, with the former being red shifted and the latter blue shifted. The corresponding shifts in  $\bar{\nu}_A$  values obtained from cubic and quartic SPF potentials are 38.4 and  $4.7\text{ cm}^{-1}$ . Both are blue shifted relative to the  $\bar{\nu}_A$  values obtained with the fifth-degree SPF force field.

From these considerations we conclude that the leading terms in the SPF force field give frequencies much closer to the converged values than do the

\*The *A* and *E* subscripts refer to the (100) state and to the doubly degenerate pair (010) and (001), respectively.

TABLE XII  
Hamiltonian Truncations and Their Effects on Vibrational Eigenenergies ( $\text{cm}^{-1}$ ) of  $\text{H}_3^+{}^a$

Vibrational state			Kinetic-energy truncations <sup>c</sup>		Potential-function truncations <sup>d</sup>				
$n_1$	$n_2$	$n_3$	Complete vibrational Hamiltonian <sup>b</sup>	I ( $\hat{H}_v - \Delta \hat{T}$ )	II ( $\hat{H}_v - \Delta \hat{T} - U_w$ )	III (fourth degree)	IV (third degree)	V (second degree)	VI <sup>e</sup> (second degree)
0	0	0	4345.28	4344.92	4371.67	4345.96	4351.56	4353.25	4426.04
0	1	0	6861.26	6838.83	6865.69	6864.55	6867.01	6836.85	7151.62
0	0	1	6861.44	6839.04	6865.90	6864.73	6867.16	6837.99	7151.62
1	0	0	7530.49	7530.16	7556.24	7535.95	7575.26	7509.41	7855.93

<sup>a</sup>See Ref. 31 for additional details concerning the method of calculating the vibrational energies.

<sup>b</sup>The complete Hamiltonian is defined with the fifth-degree SPF potential of Table XI.

<sup>c</sup>See (107) to identify truncated terms in the kinetic-energy operator.

<sup>d</sup>See (108) and Table X1 to identify truncated terms in the potential function. The full kinetic-energy operator was used in calculations III to VI.

<sup>e</sup>Quadratic Dunham expansion with the same force constants used in calculation V.

corresponding terms in a Dunham-type expansion. Thus, not only do the number and degree of the polynomial terms in (108) have significance in the variational calculations, but the results also depend strongly on the internal coordinate basis used to express  $P_n$ . The convergence of  $H_3^+$  band positions demonstrates the utility of the SPF polynomial form of the potential function. We discuss this point further in Section IV.C.3.

### 3. Comparison of SPF and Dunham Potential Functions

To provide additional evidence for the appropriateness of the SPF variables in cases where experimental confirmation is possible, we consider the ozone and water molecules. The Born-Oppenheimer potential for triatomics expanded as a power series has the form

$$V_R = \sum K_{ij} \Delta R_i \Delta R_j + \sum K_{ijk} \Delta R_i \Delta R_j \Delta R_k + \sum K_{ijkl} \Delta R_i \Delta R_j \Delta R_k \Delta R_l + \cdots \quad (110)$$

where the  $\Delta R$ 's are the displacements of the bond lengths and bond angles from equilibrium,  $\Delta R_1 = \Delta r_1$ ,  $\Delta R_2 = \Delta r_2$ , and  $\Delta R_3 = \Delta \theta$ . The SPF expansion has the form

$$V_\rho = \sum L_{ij} \rho_i \rho_j + \sum L_{ijk} \rho_i \rho_j \rho_k + \sum L_{ijkl} \rho_i \rho_j \rho_k \rho_l + \cdots \quad (111)$$

where  $\rho_1 = \Delta r_1/r_1$ ,  $\rho_2 = \Delta r_2/r_2$ , and  $\rho_3 = \Delta \theta$ . Here,  $r_1$  and  $r_2$  are the instantaneous bond lengths. The bond-length variables in the two expansions are related by

$$\Delta r_i = r_e \sum_{n=0}^{\infty} \rho_i^{n+1} \quad (112)$$

where  $r_e$  is the equilibrium bond length.

Experimentally derived quartic potential functions for  $O_3$  and  $H_2O$  have been reported recently. Barbe, Secroun, and Jouve (BSJ)<sup>108</sup> derived quadratic, cubic, and quartic force constants for  $O_3$  from an analysis of the infrared spectra of  $^{16}O_3$  and  $^{18}O_3$  at liquid nitrogen temperatures using second-order perturbation theory. Hoy, Mills, and Strey (HMS)<sup>109</sup> have determined a quartic potential for the water molecule using a similar procedure. Both potentials give an excellent fit to the observed data.

The BSJ and HMS potential functions ( $V_R$ ) for  $O_3$  and  $H_2O$  are developed in the traditional internal displacement coordinates  $\Delta R$ . Substitution of the expression for  $\Delta R$  [see (112)] into  $V_R$  followed by truncation to quartic terms results in the new potential  $V_\rho$ . The coefficients for both potential representations are given in Ref. 29.

To demonstrate that the SPF potentials are superior at large displace-

ments, contour maps of  $V_R$  and  $V_\rho$  for  $r_1$  and  $r_2$  varied separately with  $\theta = \theta_e$  are shown for  $O_3$  and  $H_2O$  in Figs. 1 and 2, respectively. In agreement with Simons' work<sup>110</sup> on  $CS_2$  and  $HCN$ , the  $V_\rho$  energy maps of both  $O_3$  and  $H_2O$  have improved qualitative features. The dissociation valleys are evident, indicating that a finite amount of energy is required to dissociate the molecule in contrast to the  $V_R$  surface which diverges. As Simons pointed out, this improved description occurs because  $\rho$  has the correct limiting behavior for bond stretching.

It is instructive to compare the  $V_\rho$  potential for  $H_2O$  in Fig. 2 with the more elaborate analytical function of Sorbie and Murrell (SM).<sup>18</sup> Their potential was constructed to be reasonably accurate over the whole three-dimensional coordinate space of the triatomic system, including the domain of the atom-diatom dissociation limits. For this purpose, terms were added to the HMS potential to accommodate the equilibrium properties of the diatomic fragments and to reproduce properties that depend on the potential-energy surface far from equilibrium. Although the  $V_\rho$  and SM potentials are similar over a large portion of the surface, the SM potential is superior at very large positive displacements where  $V_\rho$  predicts a significant barrier to dissociation and an incorrect atom-diatom limit. At negative displacements the SM potential is more repulsive than  $V_\rho$ . However, as shown below, the  $V_\rho$  potential predicts vibrational energies for bond-stretching motions that are superior to the SM potential. This seems especially significant, since  $V_\rho$  is much simpler and does not explicitly contain information about the equilibrium properties of the dissociation fragments.

To assess quantitatively how the vibrational energies change in the transition between the two potential expansions, a new potential  $V_\gamma$  is defined that is dependent on both  $V_R$  and  $V_\rho$  through a parameter  $\gamma$ :

$$V_\gamma = V_R + \gamma(V_\rho - V_R); \quad 0 \leq \gamma \leq 1 \quad (113)$$

Variation of  $\gamma$  from 0 to 1 transforms  $V_\gamma$  smoothly from  $V_R$  to  $V_\rho$ . An optimum value of  $\gamma$  can be selected on the basis of the agreement between the calculated vibrational energies and the observed band origins.

It is important to note that since  $V_R$  and  $V_\rho$  are equivalent through fourth-power terms, every  $V_\gamma$  transformed to normal coordinates will be identical to the normal force field through the fourth power as well. Hence, the second-order perturbation theory treatments that depend only on terms through the fourth power will give identical vibrational energies for any  $\gamma$ . By contrast, variational vibrational analysis is ideally suited for distinguishing different  $\gamma$  values because it includes the effect of higher-degree terms in the normal coordinate representation and is applicable to the case of noninfinitesimal vibrational amplitudes.

Although band positions derived from  $V_\rho$  are superior to those deter-

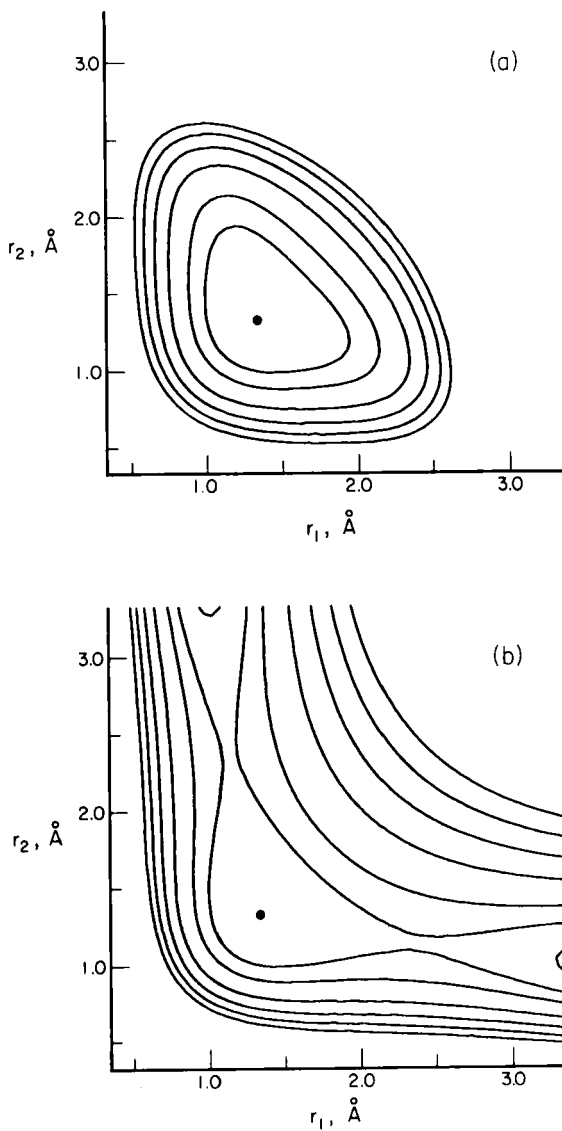


**Fig. 1.** Constant-energy contour maps for the  $^{16}\text{O}_3$  molecule using Dunham (a) and Simons-Parr-Finlan (b) expansions of the potential energy. The valence angle is fixed at the equilibrium value of  $116.8^\circ$ . Energy contours correspond to 1, 2, 4, 6, 8, and 10 eV above the energy of the equilibrium molecular structure, which is denoted by a dot in each figure.

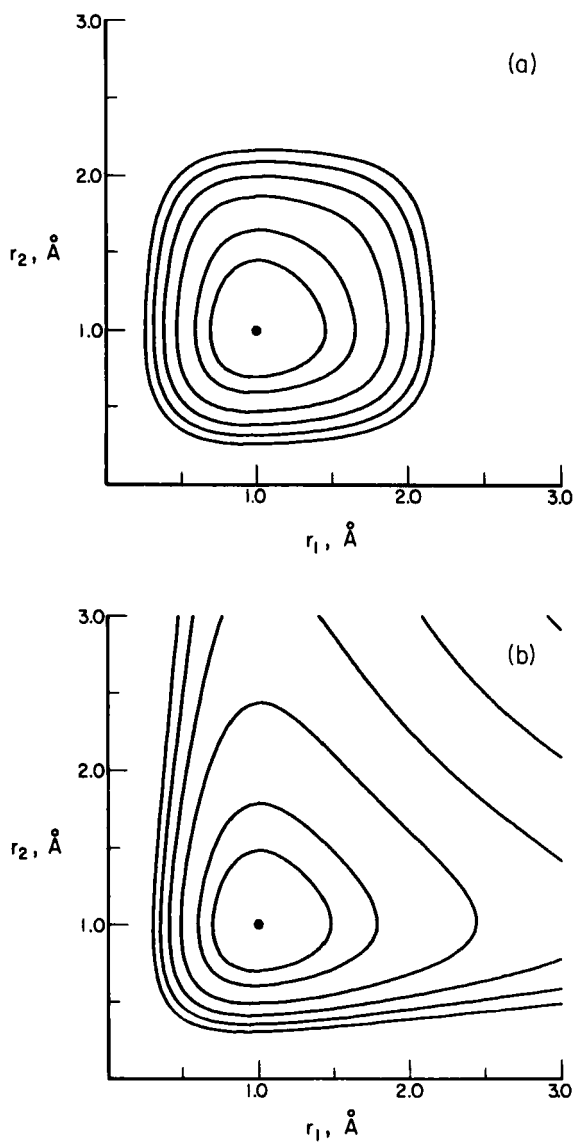


**Fig. 2.** Constant-energy contour maps for the  $\text{H}_2\text{O}$  molecule using (a) Dunham and (b) Simons-Parr-Finlan expansions of the potential energy. The valence angle is fixed at the equilibrium value of  $104.52^\circ$ . Energy contours correspond to 1, 2, 4, 6, 8, and 10 eV above the energy of equilibrium molecular structure, which is denoted by a dot in each figure.

mined by  $V_R$ , best agreement with experiment for  $O_3$  is obtained for a noninteger value of  $\gamma$ . In the bottom row of Table XIII we give the average deviation between calculated and observed values. The value of  $\gamma=0.75$  gives best agreement with the experimental observations. Another interesting feature of the  $O_3$  results is that the potential functions  $V_R$  and  $V_\rho$  produce vibrational energies that bracket the observed band origins, except for the (010) and (021) states that describe predominantly bending motions.

The  $H_2O$  molecule has much larger amplitudes of vibrational motion than

TABLE XIII  
Calculated Band Origins ( $\text{cm}^{-1}$ ) versus  $\gamma$  for  $^{16}O_3$

Quantum number assignments <sup>a</sup>			Calculated band origins <sup>b</sup>					Observed <sup>c</sup> band origins
$n_1$	$n_2$	$n_3$	$\gamma=0.0$	$\gamma=0.25$	$\gamma=0.50$	$\gamma=0.75$	$\gamma=1.0$	
0	1	0	700.1 (700.1)	700.1	700.1	700.0	700.0	700.9
0	0	1	1047.1(1047.1)	1045.7	1044.2	1042.7	1041.2	1042.1
1	0	0	1106.6(1106.6)	1105.3	1104.0	1102.6	1101.2	1103.1
0	2	0	1396.0(1395.8)	1396.0	1396.0	1396.0	1395.9	—
0	1	1	1728.4(1728.2)	1726.8	1725.1	1723.3	1721.5	1726.5
1	1	0	1796.8(1796.8)	1795.5	1794.1	1792.6	1791.0	1795.3
0	0	2	2077.5(2077.4)	2072.3	2066.8	2061.0	2054.9	2058.0
0	3	0	2086.9(2084.4)	2087.0	2087.0	2087.0	2087.0	—
1	0	1	2131.2(2131.1)	2125.4	2119.3	2112.9	2106.1	2110.8
2	0	0	2212.8(2212.8)	2209.4	2205.8	2202.2	2198.3	2201.3
0	2	1	2404.8(2402.8)	2403.0	2401.1	2399.1	2397.0	2409.5
1	2	0	2487.0(2485.4)	2485.5	2484.0	2482.3	2480.5	—
0	1	2	2742.3(2740.7)	2736.7	2730.7	2724.4	2717.6	2725.6
$\frac{1}{n} \sum  E_i^{\text{obs}} - E_i^{\text{calc}} $			8.6(8.6)	6.2	4.2	2.5	4.4	—

<sup>a</sup>The vibrational states are labeled by the predominant term in the wave function. The quantum numbers  $n_1$ ,  $n_2$ , and  $n_3$  denote symmetric stretch, bend, and asymmetric stretch, respectively. The energies are relative to the zero-point energies, which are 1456.0(1457.1), 1455.7, 1455.4, 1455.2, and 1454.8  $\text{cm}^{-1}$  for  $\gamma=0.0, 0.25, 0.50, 0.75$ , and 1.0, respectively.

<sup>b</sup>These are variational results calculated as a function of the parameter  $\gamma$  defined in (113). All calculations employ a 220-term vibrational wave function except for those in parentheses under  $\gamma=0.0$ , which are calculated using a 1140-term wave function. See Ref. 29 for details.

<sup>c</sup>Reference 108.

<sup>d</sup> $E_i^{\text{obs}}$ ,  $E_i^{\text{calc}}$ , and  $n$  are, respectively, the observed and calculated energies, and the number of band origins considered.

O<sub>3</sub> because of the lighter hydrogen atoms. Since a larger portion of the potential surface is being sampled by the vibrational motion, H<sub>2</sub>O should be a better test of the SPF expansion variable. For the same reason the variational calculations on H<sub>2</sub>O are more sensitive to basis-set incompleteness. Two independent variational vibrational calculations for H<sub>2</sub>O, each using the HMS potential ( $\gamma=0$ ) and the Watson Hamiltonian, were compared to test convergence. The results of these calculations should be the same in the limit of a complete basis set. The results of Lai<sup>25</sup> and Hagstrom (LH) were obtained with a large basis set ( $\sim 430$  expansion terms) and should therefore be essentially converged. The results in Table XIV, obtained with a 220-term wave function, differ only slightly from those of LH and, hence, problems of basis-set incompleteness should not bias our study of the  $V_\gamma$  potential surfaces. Whitehead and Handy<sup>16,17</sup> and Sorbie and Murrell<sup>18</sup> have reported energies for the quartic HMS potential for an 84-term wave function expansion. Their results are also in agreement with Table XIV.

As expected, the improvement shown in Table XIV for the calculated band origins of water when  $V_R$  is replaced by  $V_\rho$  is much greater than that found for O<sub>3</sub>. In fact, the improvement is dramatic for those states involving principally bond-stretching motions. For example, the (101) state differs by 271 cm<sup>-1</sup> from the observed value using  $V_R$  as compared to 11 cm<sup>-1</sup> when using  $V_\rho$ . This is substantially better agreement than the result for the SM potential, which is off by 66 cm<sup>-1</sup> for the same state. Overall, the average deviation from the experimental band origins is 92 cm<sup>-1</sup> for  $V_R$  but only 5 cm<sup>-1</sup> for  $V_\rho$ . In comparison, the average deviation using the SM potential is 15 cm<sup>-1</sup>. Only results for  $\gamma=0$  and 1 are presented in Table XIV, because, unlike ozone, best results are obtained for  $\gamma=1$ .

Another interesting question is whether the new  $V_\rho$  potential functions are capable of providing similar improvement in the vibrational energies of isotopically substituted molecules. For example, heavy-water molecules HDO and D<sub>2</sub>O have normal modes of vibration sufficiently different from those of H<sub>2</sub>O that new regions of the potential surface may be sampled by oscillatory motion of the atoms.

In Table XIV we present vibrational energies for selected states of HDO and D<sub>2</sub>O calculated with the HMS potential for both  $\gamma=0$  and  $\gamma=1$ . The  $\gamma=1$  results are again in excellent agreement with the observed band origins. These results, therefore, should provide good estimates of the positions of the bands that are so far unobserved. In particular, our results for the (020), (110), (120), and (002) bands of D<sub>2</sub>O and the (120) and (002) bands of HDO should be accurate to within several wave numbers. The ability to identify vibrational levels using variational analysis is especially important for HDO, since considerable uncertainty exists concerning the assignments of the excited vibrational states.



TABLE XIV  
Variational Vibrational Energies ( $\text{cm}^{-1}$ ) for  $\text{H}_2\text{O}$ ,  $\text{HDO}$ , and  $\text{D}_2\text{O}$  Using Modified HMS Potential Functions

Band Origins									
Quantum number assignments <sup>a</sup>				$\text{H}_2\text{O}$		$\text{HDO}$		$\text{D}_2\text{O}$	
				Calculated <sup>b</sup>	Observed <sup>c</sup>	Calculated <sup>b</sup>	Observed <sup>d</sup>	Calculated <sup>b</sup>	Observed <sup>d</sup>
$n_1$	$n_2$	$n_3$		$\gamma=0$	$\gamma=1$	$\gamma=0$	$\gamma=1$	$\gamma=0$	$\gamma=1$
0	1	0		1597	1596	1405	1404	1179	1178
0	2	0		3159	3156	2791	2787	2339	2338
1	0	0		3717	3659	2745	2724	2696	2674
0	0	1		3821	3758	3770	3709	2813	2788
0	3	0		4684	4679	4171	4159	3480	3478
1	1	0		5300	5237	4115	4101	3867	3844
0	1	1		5403	5335	5158	5092	3983	3957
0	4	0		6176	6169	5550	5529	4602	4599
1	2	0		6846	6777	5445	5438	5019	4993
0	2	1		6950	6877	6535	6461	5136	5108
2	0	0		7420	7211	5475	5378	5374	5292
1	0	1		7521	7261	6501	6421	5481	5378
0	0	2		7626	7453	7521	7529	5605	5532

<sup>a</sup>The quantum numbers  $n_1$ ,  $n_2$ , and  $n_3$  denote symmetric stretch, bend, and asymmetric stretch motions, respectively.

<sup>b</sup>The energies are relative to the zero-point energies cited in Ref. 29.

<sup>c</sup>See footnote b in Table XVIII for all observed  $\text{H}_2\text{O}$  bands except (040), which is given by C. C. Ferriso and C. B. Ludwig, *J. Chem. Phys.*, **41**, 1668 (1964).

<sup>d</sup>Taken from W. S. Benedict, N. Gailar, and E. K. Plyler, *J. Chem. Phys.*, **24**, 1139 (1956).

For both the  $O_3$  and water molecules with  $C_{2v}$  mass symmetry, the energies of the vibrational states involving one or more quanta in the bending mode, in particular the  $(0n0)$  states, are nearly independent of  $\gamma$ . This is not surprising, since the  $\Delta\theta$  variable was not changed. Thus  $\gamma$  is a parameter to be identified principally with the stretching motions of the molecule. Additional flexibility could be introduced by parameterizing  $\gamma$  as a function of  $\theta$ .

#### 4. Interpretation of Vibrational Wave Functions

The assignment of proper quantum numbers  $v=(n_1, n_2, n_3)$  to the vibrational wave functions  $\psi_v$ , defined as [cf. (63)]

$$\psi_v = \sum_{(i+j+k)=0}^{L_{\max}} c_{ijk}^{(v)} \chi_i(t_1) \chi_j(t_2) \chi_k(t_3) \quad (114)$$

and to the corresponding eigenenergies is often nontrivial. For purposes of illustration, we consider the case of ozone and investigate the matrix elements  $\langle \psi_v | Q_i | \psi_{v'} \rangle$ , where the  $Q_i$  are the usual normal coordinates. The normal frequencies for  $^{16}O_3$ , obtained using the Wilson FG matrix method,<sup>49</sup> are 1135, 716, and 1089  $\text{cm}^{-1}$  for the  $Q_1$  (symmetric stretch),  $Q_2$  (bend), and  $Q_3$  (asymmetric stretch) normal vibrations, respectively. Since the  $Q_i$  coordinates are linear in the space of the "t" coordinates (see Section III), the matrix elements  $\langle \psi_v | Q_i | \psi_{v'} \rangle$  are evaluated straightforwardly.

Those matrix elements required for the unambiguous assignment of the lowest 11 vibrational states of  $^{16}O_3$  are presented in Table XV and were computed with vibrational wave functions that included 1140 terms corresponding to  $L_{\max}=17$  in (114). The potential surface was that of Barbe et al.<sup>108</sup> It is to be expected, and indeed found, that the largest off-diagonal matrix elements of  $Q_i$  occur when  $|n_i - n'_i| = 1$ . Hence, after assigning the lowest energy to  $(000)$ , the fundamental states are identified by their large overlap with  $Q_i|000\rangle$ , as shown in the second to the fourth row of Table XV. Continuing in this manner, the overtone and combination bands are then determined by the magnitude of their matrix elements with the fundamentals, and so on. The assignments are facilitated by the existence of many more matrix elements than vibrational states and by an examination of the relative size of the expansion coefficients in (114). The higher-energy states are often more difficult to identify because the wave functions usually contain several terms in the expansion list,  $c_{ijk}^{(v)}$ , that may be large simultaneously. However, in molecules with  $C_{2v}$  or other mass symmetry, such as  $^{16}O_3$ , the assignment is simplified because the asymmetric stretching mode transforms according to a different irreducible representation than either the bending or symmetric stretching modes, as evidenced by exact zeros for some of the matrix elements in Table XV.

These state assignments can be checked and further interpreted by plotting

TABLE XV  
Assignments of Vibrational States for  $^{16}\text{O}_3$

Lower state $i^a$	Upper state $j^a$	Upper Matrix elements of the normal coordinates <sup>b</sup>			Assigned bands
		$Q_1$	$Q_2$	$Q_3$	
1	1	0.00744	0.00543	0.0	$\nu_0 \rightarrow \nu_0$
1	2	-0.00004	0.03875	0.0	$\nu_0 \rightarrow \nu_2$
1	3	0.0	0.0	0.03142	$\nu_0 \rightarrow \nu_3$
1	4	0.03060	-0.00012	0.0	$\nu_0 \rightarrow \nu_1$
2	2	0.00874	0.01042	0.0	$\nu_2 \rightarrow \nu_2$
2	5	0.00106	0.05479	0.0	$\nu_2 \rightarrow 2\nu_2$
2	6	0.0	0.0	0.03160	$\nu_2 \rightarrow \nu_2 + \nu_3$
2	7	-0.03053	0.00163	0.0	$\nu_2 \rightarrow \nu_1 + \nu_2$
3	3	0.01585	0.01005	0.0	$\nu_3 \rightarrow \nu_3$
3	6	0.00029	0.03927	0.0	$\nu_3 \rightarrow \nu_2 + \nu_3$
3	8	0.0	0.0	0.04388	$\nu_3 \rightarrow 2\nu_3$
3	10	0.03060	-0.00053	0.0	$\nu_3 \rightarrow \nu_1 + \nu_3$
4	4	0.01256	0.00667	0.0	$\nu_1 \rightarrow \nu_1$
4	7	0.00235	-0.03908	0.0	$\nu_1 \rightarrow \nu_1 + \nu_2$
4	10	0.0	0.0	0.03163	$\nu_1 \rightarrow \nu_1 + \nu_3$
4	11	-0.04252	-0.00128	0.0	$\nu_1 \rightarrow 2\nu_1$
5	5	0.01034	0.01607	0.0	$2\nu_2 \rightarrow 2\nu_2$
5	9	0.00274	0.06709	0.0	$2\nu_2 \rightarrow 3\nu_2$

<sup>a</sup>State indices  $i$  and  $j$  order the eigenenergies sequentially according to increasing energy.

<sup>b</sup>Matrix elements for normal coordinates are calculated using the exact definition of  $Q_i$ . The harmonic frequencies  $\omega_1=1135$ ,  $\omega_3=1089$ , and  $\omega_2=716\text{ cm}^{-1}$  are obtained for the  $Q_1$ ,  $Q_3$ , and  $Q_2$  vibrational modes, respectively. Matrix elements are calculated in angstroms using a 1140-term vibrational wave function. See Ref. 32.

maps of  $\psi_v$  as a function of the internal coordinates. Maps of this type exhibit nodal properties corresponding to the quantum numbers. In Figs. 3 through 8, we again consider  $^{16}\text{O}_3$  and employ the following notation: nodal surfaces are denoted by dotted lines, negative amplitudes by dashed lines, and positive amplitudes by solid lines. The maximum amplitude shown is for  $\psi_v = +0.8$ , and adjacent contours differ by a factor of  $\sqrt{2}$ . The origin of each map is at  $\Delta R_1 = \Delta R_2 = \Delta\theta = 0$ , where  $\Delta R_1$ ,  $\Delta R_2$ , and  $\Delta\theta$  are the internal displacement coordinates for ozone. The origin is positioned approximately at the center of each figure. The wave functions are plotted over the ranges

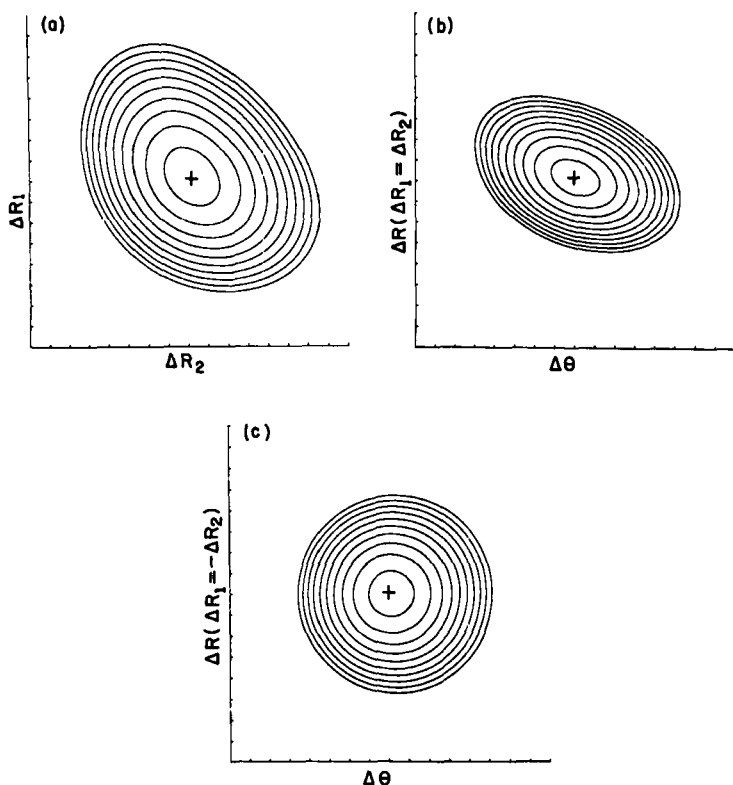


Fig. 3. Cross-sectional plots of the wave-function amplitude for the zero-point state (000) of vibration of ozone.

$-0.4$  to  $+0.4\text{\AA}$  for  $\Delta R_1$  and  $\Delta R_2$ , and  $-20$  to  $+20^\circ$  for  $\Delta\theta$ . The quantum number assignments are given in each figure legend or in the figure.

The zero-point vibrational state is shown in Fig. 3. Figures 4 and 5 show the fundamental and first overtone bending modes. The nodal behavior in the wave function amplitude is clearly exhibited. The wave functions for the (000), (010), and (020) states are totally symmetric in the asymmetric internal coordinate  $\Delta R$ , which is defined as  $\Delta R = |\Delta R_1| = |\Delta R_2|$  with  $\Delta R_1 = -\Delta R_2$ . The nodal structure of the (010) and (020) maps for the  $\Delta R_1$  versus  $\Delta R_2$  plane in which  $\theta$  is restricted by  $\Delta\theta = 0$  is a result of the linear dependence of the normal mode bending coordinate  $Q_2$  on both  $\Delta\theta$  and  $(\Delta R_1 + \Delta R_2)$ . Since

$$Q_2 = a\Delta\theta + b(\Delta R_1 + \Delta R_2) + \cdots \quad (115)$$

the nodal structure correlates with that of the quantity  $(\Delta R_1 + \Delta R_2)$  when

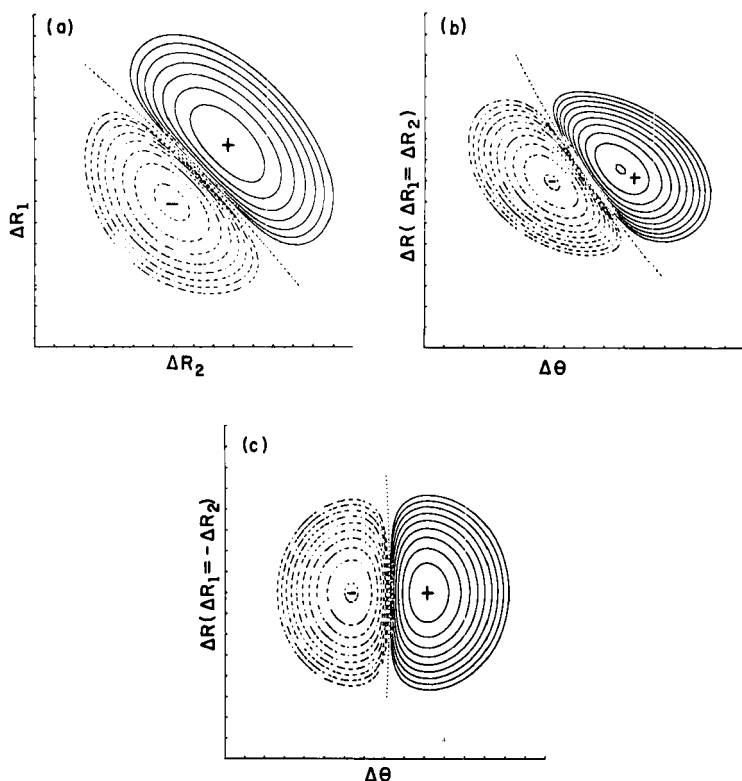


Fig. 4. Cross-sectional plots of the wave-function amplitude for the bending fundamental state (010) of vibration of ozone.

$\Delta\theta=0$ . This demonstrates the coupling of the bending and symmetrical stretching motions in  $\psi_v$ .

In Figs. 6a and 6b amplitude maps for the symmetrical stretching fundamental (100) are presented for  $\Delta R_1$  versus  $\Delta R_2$  with  $\Delta\theta=0$  and for  $\Delta R$  versus  $\Delta\theta$  with  $\Delta R_1=\Delta R_2$ . Figures 6c and 6d show the wave function of the (001) asymmetrical stretching state. In Fig. 6d, the  $\Delta R$  coordinate is defined with  $\Delta R_1 = -\Delta R_2$ . As expected, a single node appears in each wave function of Fig. 6. Amplitude maps for the first overtone in the symmetrical and asymmetrical vibrations are presented in Fig. 7. We see the presence of two nodal lines in these plots.

Wave function plots are given in Fig. 8 for some combination states. For the (110) state the presence of a node in the  $\Delta R(\Delta R_1=\Delta R_2)$  and  $\Delta\theta$  directions is clearly seen. The similarity among these maps occurs because the bending

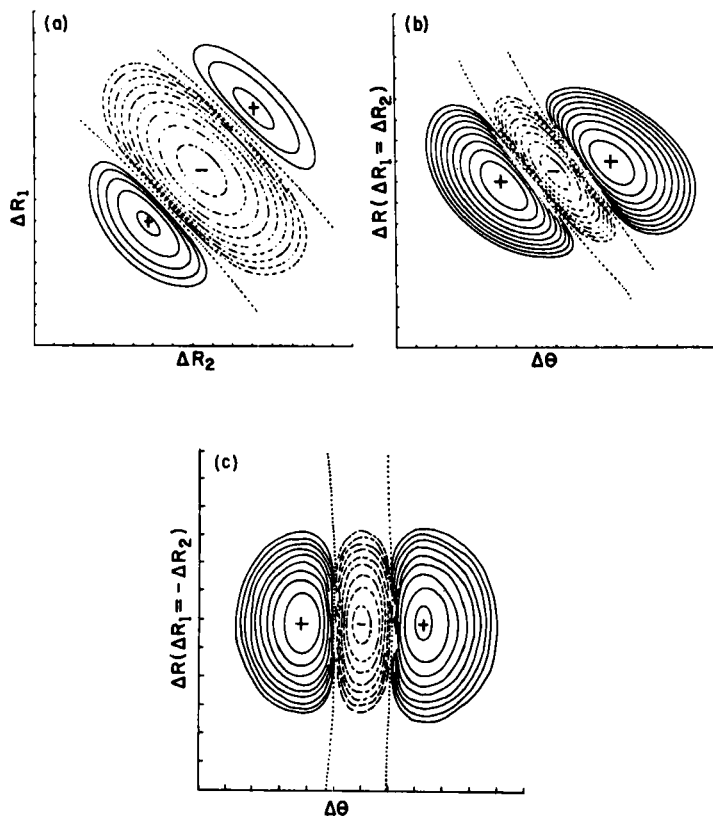


Fig. 5. Cross-sectional plots of the wave-function amplitude for the first bending overtone state (020) of vibration of ozone.

coordinate depends linearly on  $(\Delta R_1 + \Delta R_2)$ , as already noted.

Vibrational amplitude maps may also be useful for other purposes, for example, as an aid to interpreting the relative sizes of Franck-Condon factors. By an examination of maps for the vibrational states associated with the two electronic states, it should be possible to see by inspection where the largest overlap occurs and thereby infer which vibrational level is most likely to be occupied in a vertical transition.

### 5. Dipole Moments and Infrared Band Intensities

For a nonlinear  $AB_2$  molecule in a non-Eckart molecule-fixed reference frame (MFRF), the dipole-moment function  $\mathbf{M}$  is expanded in the form

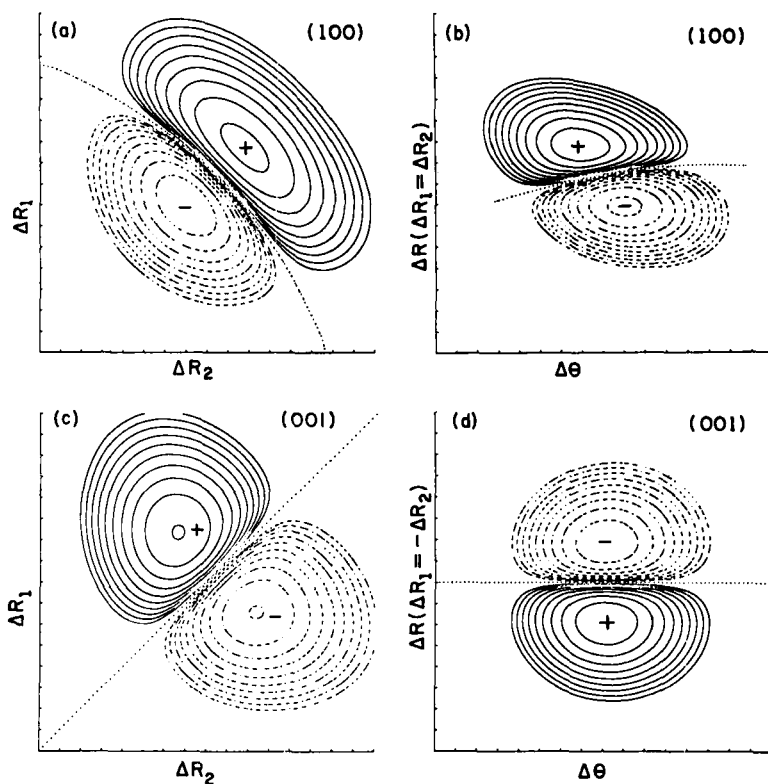


Fig. 6. Cross-sectional plots of the wave-function amplitude for the fundamentals in (a and b) symmetric and (c and d) asymmetric stretching states of vibration of ozone.

$$\mathbf{M} = \left\{ M_0 + \left( \frac{\partial M_s}{\partial \Delta R} \right)_0 (\Delta R_1 + \Delta R_2) + \left( \frac{\partial M_s}{\partial \Delta \theta} \right)_0 \Delta \theta + \cdots \right\} \hat{i} + \left\{ \left( \frac{\partial M_a}{\partial \Delta R} \right)_0 (\Delta R_1 - \Delta R_2) + \cdots \right\} \hat{j} \quad (116)$$

where  $M_0$  is the value of  $\mathbf{M}$  at the equilibrium geometry,  $(\partial M_s / \partial \Delta R)_0$  and  $(\partial M_s / \partial \Delta \theta)_0$  are its derivatives for symmetrical displacements, and the derivative  $(\partial M_a / \partial \Delta R)_0$  gives the rate of change of  $\mathbf{M}$  for asymmetrical displacements. The internal mass-independent vibrational displacements are denoted by  $\Delta R_1$ ,  $\Delta R_2$ , and  $\Delta \theta$ . The first derivatives of  $\mathbf{M}$  are therefore conveniently independent of the atomic masses (invariant to isotopic substitution). The unit directions  $\hat{i}$  and  $\hat{j}$  are taken to be parallel and perpendicular, respectively, to the instantaneous bisector of the valence angle  $\theta$ , and the

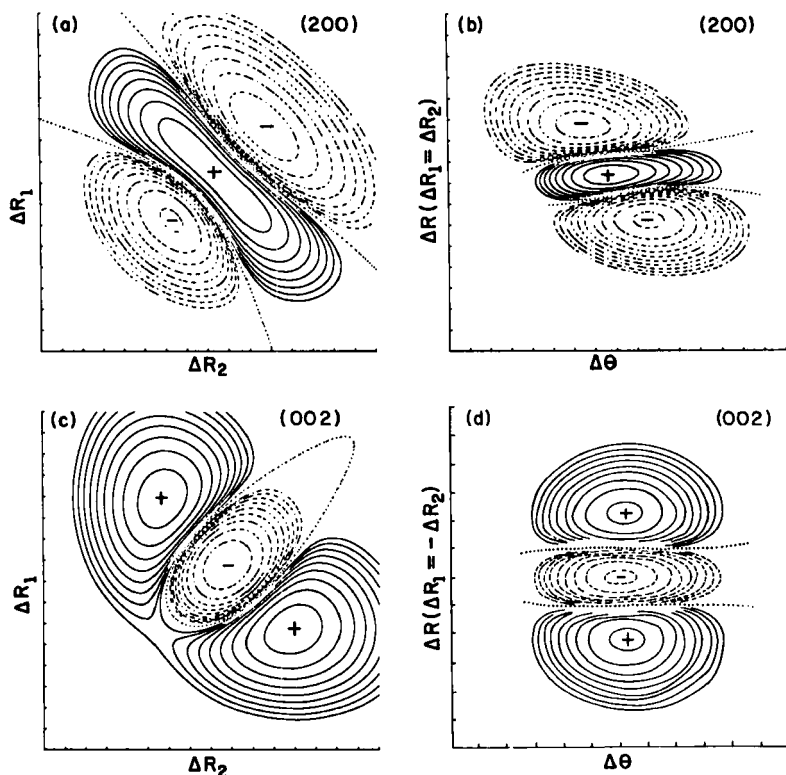


Fig. 7. Cross-sectional plots of the wave-function amplitude for the first overtone in (a and b) symmetric and (c and d) asymmetric stretching states of vibration of ozone.

origin of the MFRF is coincident with the A atom. In this coordinate system the molecular center-of-mass changes with geometry relative to the origin of the MFRF. This reference frame is customarily used in *ab initio* electronic calculations.

To determine infrared intensities, we must transform the dipole moment function  $\mathbf{M}$  to an Eckart MFRF appropriate for each isotopic species. The new dipole moment function

$$\mathbf{M}_E = \mathbf{R} \cdot \mathbf{M} \quad (117)$$

is obtained from  $\mathbf{M}$  by a rotation of unit directions in the plane of the molecule. In (117) the rotation matrix

$$\mathbf{R} = \begin{bmatrix} \cos \beta & -\sin \beta & 0 \\ \sin \beta & \cos \beta & 0 \\ 0 & 0 & 1 \end{bmatrix} \quad (118)$$



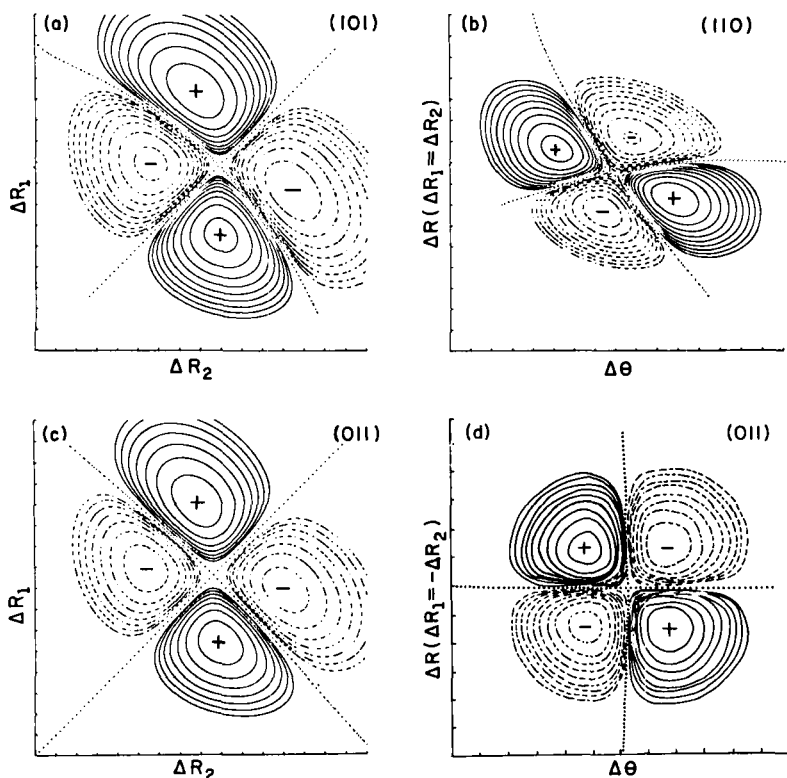


Fig. 8. Cross-sectional plots of the wave-function amplitude for the first combination states of vibration involving (a) symmetric and asymmetric stretching, (b) symmetric stretching and bending, and (c and d) asymmetric stretching and bending states of ozone.

depends on the instantaneous internal coordinates, the masses, and the equilibrium geometry through the angle of rotation  $\beta$ . The quantum mechanical matrix elements of  $\mathbf{M}_E$  involve the internal coordinates  $\Delta R_1$ ,  $\Delta R_2$ , and  $\Delta \theta$ , as well as  $\cos \beta$  and  $\sin \beta$ . If the magnitude of  $\beta$  is very small (e.g., when  $\Delta R_1 \cong \Delta R_2$ ), a Taylor series expansion of  $\mathbf{R}$  may be appropriate.

Choosing the water molecule for illustrative purposes, it is found that  $\langle 000 | \cos \beta | n_1, n_2, n_3 \rangle$  is sufficiently small for the fundamental bands of each isotopic species that only the leading term ( $M_0 \sin \beta$ ) in the expansion of the right-hand side of (117) for  $\mathbf{M}_E$  contributes to the isotope effect. The matrix elements of  $(M_0 \sin \beta)$  differ from zero in the case of the  $\nu_3$  bands for  $\text{H}_2\text{O}$ ,  $\text{D}_2\text{O}$ , and  $\text{T}_2\text{O}$ . For the molecules  $\text{HDO}$ ,  $\text{HTO}$ , and  $\text{DTO}$ , all modes contain significant mixtures of the asymmetric displacements. Additional terms in (117) involve products of  $\sin \beta$  or  $\cos \beta$  with powers of  $\Delta R_1$ ,  $\Delta R_2$ , and

$\Delta\theta$ . Typical results for the zero-point level are given in Table XVI. On the basis of such results,  $\langle v|\mathbf{M}_E|v'\rangle$  is found to be satisfactorily approximated, for fundamental excitations only, as

$$\begin{aligned} \langle v|\mathbf{M}_E|v'\rangle = & \left[ \left( \frac{\partial M_s}{\partial \Delta R} \right)_0 \langle v|\Delta R_1 + \Delta R_2|v'\rangle + \left( \frac{\partial M_s}{\partial \Delta\theta} \right)_0 \langle v|\Delta\theta|v'\rangle \right] \hat{i} \\ & + \left[ M_0 \langle v|\sin \beta|v'\rangle + \left( \frac{\partial M_a}{\partial \Delta R} \right)_0 \langle v|\Delta R_1 - \Delta R_2|v'\rangle \right] \hat{j} \quad (119) \end{aligned}$$

Since *ab initio* dipole-moment functions, including the equilibrium value  $M_0$ , the first derivatives, and a number of higher-order derivatives, are available for  $\text{H}_2\text{O}$ ,<sup>111</sup> the corresponding band strengths may be determined.

TABLE XVI  
Vibrational Averages for Internal Coordinate and  $\sin \beta$  and  $\cos \beta$   
Products for the Ground Vibrational States of Various Isotopes  
of Water

Matrix element <sup>a</sup>	Isotopic species					
	H <sub>2</sub> O	D <sub>2</sub> O	T <sub>2</sub> O	HDO	DTO	HTO
$\cos \beta$	0.99999	0.99999	0.99999	0.99975	0.99993	0.99950
$\sin \beta$	0.0	0.0	0.0	-0.00015	-0.00004	-0.00024
$(\Delta R_1 + \Delta R_2) \cos \beta$	0.03541	0.02576	0.02163	0.03059	0.02370	0.02853
$(\Delta R_1 + \Delta R_2) \sin \beta$	0.0	0.0	0.0	0.000139	0.00007	0.000197
$(\Delta R_1 - \Delta R_2) \cos \beta$	0.0	0.0	0.0	0.004948	0.002113	0.007068
$(\Delta R_1 - \Delta R_2) \sin \beta$	-0.000279	-0.000376	-0.000444	-0.000311	-0.000405	-0.000323
$(\cos \beta) \Delta\theta$	0.000482	-0.000174	-0.000513	0.000325	-0.000299	0.000370
$(\sin \beta) \Delta\theta$	0.0	0.0	0.0	-0.003160	-0.001358	-0.004436

<sup>a</sup>Units are angstroms and radians. See (118) for elements of the rotation matrix ( $\sin \beta$ ,  $\cos \beta$ ). Note,  $\sin \beta$  and  $\cos \beta$  are functions of  $\Delta R_1$ ,  $\Delta R_2$ , and  $\Delta\theta$ .

Variational vibration wave functions based on the HMS quartic force field,<sup>109</sup> modified to conform to the expansion form suggested by SPF,<sup>74</sup> are used to obtain IR band intensities for six isotopic molecules of water. Calculated results are given in Table XVII and compared with available experimental intensities in Table XVIII. The *ab initio* dipole-moment function is taken from Ref. 111. Each band corresponds to an excitation from the ground vibrational state. Quantum numbers for the upper states are given in the first column of Table XVII. The calculated band positions are given in parentheses along with the integrated band intensity.

TABLE XVII  
Calculated Band Intensities and Band Positions from the Ground States of Isotopic Water Molecules

Upper state				Integrated intensities in $\text{atm}^{-1} \text{cm}^{-2}$ at STP (Band positions in $\text{cm}^{-1}$ ) <sup>b</sup>										
$n_1$	$n_2$	$n_3^a$		H <sub>2</sub> O	D <sub>2</sub> O	T <sub>2</sub> O	HDO	HTO	DTO					
0	1	0	405	(1596)	214	(1179)	149	(995)	334	(1404)	326	(1333)	186	(1091)
0	2	0	2.11	(3156)	1.43	(2338)	1.31	(1976)	1.35	(2787)	1.65	(2643)	2.73	(2164)
1	0	0	51.6	(3659)	38.4	(2674)	34.7	(2240)	61.8	(2724)	45.1	(2302)	40.1	(2297)
0	0	1	192	(3758)	92.1	(2788)	58.2	(2367)	124	(3709)	131	(3717)	70.0	(2738)
0	3	0	0.0072	(4679)	0.0044	(3478)	0.0027	(2944)	9.06	(4159)	1.27	(3933)	0.076	(3221)
1	1	0	0.513	(5237)	0.172	(3844)	0.084	(3229)	6.92	(4101)	2.49	(3623)	6.42	(3385)
0	1	1	63.4	(5335)	25.4	(3957)	15.5	(3355)	29.4	(5092)	23.7	(5032)	14.2	(3819)
1	2	0	0.031	(6777)	0.018	(4993)	0.016	(4204)	0.071	(5438)	3.25	(4929)	0.340	(4451)
0	2	1	0.651	(6877)	0.293	(5108)	0.206	(4330)	0.044	(6461)	0.133	(6322)	0.165	(4882)
2	0	0	1.69	(7211)	0.815	(5297)	0.576	(4446)	2.52	(5378)	1.29	(4565)	1.25	(4538)
1	0	1	8.67	(7261)	3.98	(5378)	2.71	(4548)	0.741	(6421)	0.641	(6022)	0.583	(5026)
0	0	2	0.040	(7453)	0.0035	(5532)	0.0015	(4698)	5.07	(7259)	4.00	(7221)	2.03	(5392)

<sup>a</sup>The quantum numbers  $n_1$ ,  $n_2$ , and  $n_3$  denote symmetric stretch, bend, and asymmetric stretch motions, respectively.

<sup>b</sup>Band positions and zero-point energies are from Refs. 29 and 30.

TABLE XVIII  
Comparison of Experimental and *ab initio* Integrated Band Intensities for Vibrational  
Excitations from the Ground Vibrational States of H<sub>2</sub>O and HDO

Upper state			Integrated intensities (cm <sup>-2</sup> atm <sup>-1</sup> ) at STP		Band positions (cm <sup>-1</sup> )	
<i>n</i> <sub>1</sub>	<i>n</i> <sub>2</sub>	<i>n</i> <sub>3</sub>	Observed	Variational <sup>a</sup>	Observed <sup>b</sup>	Variational <sup>a</sup>
H <sub>2</sub> O						
0	1	0	285 <sup>b</sup> , 317 <sup>d</sup> , 265 <sup>e</sup> , (240–360) <sup>f</sup> , (316–395) <sup>f</sup>	405	1595	1596
1	0	0	9.73 <sup>b</sup> , 11.2 <sup>c</sup> , 13.1 <sup>c</sup> , 18 <sup>f</sup>	51.6	3657	3659
0	0	1	215 <sup>b</sup> , 243 <sup>g</sup> , 186.0 <sup>e</sup> , 189 <sup>f</sup> , (181–241) <sup>h</sup> , 180 <sup>i</sup>	192	3756	3758
0	2	0	2.06 <sup>c</sup> , 1.90 <sup>c</sup> , 1.77 <sup>b</sup> , 2.0 <sup>f</sup> , 3.5 <sup>m</sup>	2.11	3152	3156
1	0	1	(9.21–9.75) <sup>k</sup> , 20.1 <sup>b</sup> , 13.1 <sup>f</sup> , 17.1 <sup>m</sup>	8.67	7250	7261
0	2	1	1.35 <sup>k</sup> , 1.52 <sup>b</sup> , 1.3 <sup>f</sup> , 0.53 <sup>m</sup>	0.652	6872	6877
2	0	0	1.67 <sup>k</sup> , 1.42 <sup>b</sup> , 3.3 <sup>f</sup>	1.69	7201	7211
0	0	2	0.142 <sup>b</sup> , 3.3 <sup>f</sup>	0.040	7445	7453
1	2	0	0.095 <sup>b</sup> , 0.2 <sup>f</sup>	0.031	6775	6777
0	3	0	0.016 <sup>k</sup> , 0.2 <sup>f</sup>	0.0072	4667	4679
1	1	0	0.492 <sup>b</sup> , 0.5 <sup>f</sup>	0.513	5235	5237
0	1	1	24.34 <sup>b</sup> , 23.7 <sup>m</sup> , 25.3 <sup>f</sup>	63.4	5331	5335
HDO						
0	1	0	244 <sup>b</sup>	334	1403	1404
1	0	0	60.3 <sup>b</sup>	61.8	2724	2724
0	0	1	134.3 <sup>b</sup>	124	3707	3709

<sup>a</sup>Results were calculated using the 220-term variational wave functions of Refs. 29 and 30, which correspond to a SPF experimental potential surface defined by the HMS force constants. *Ab initio* dipole-moment derivatives from SCF–CI electronic calculations of Ref. 111 were also used.

<sup>b</sup>R. A. McClatchey, W. S. Benedict, S. A. Clough, D. E. Burch, R. F. Calfee, K. Fox, L. S. Rothman, and J. S. Garing, "AFCRL Atmospheric Absorption Line Parameters Compilation," AFCRL-TR-73-0096 Environmental Research Paper No. 434, Air Force Cambridge Research Laboratories, L. G. Hanscom Field, Bedford, Massachusetts, 1973.

<sup>c</sup>R. A. Toth, *J. Quant. Spectrosc. Radiat. Transfer*, **13**, 1127 (1973).

<sup>d</sup>W. S. Benedict and R. F. Calfee, ESSA Professional Paper 2, U.S. Government Printing office, Washington, D.C. 1967.

<sup>e</sup>J. M. Flaud and C. Camy-Peyret, *J. Mol. Spectrosc.*, **55**, 278 (1975).

<sup>f</sup>M. A. Hirshfeld, J. H. Jaffe, and G. Ross, *J. Quant. Spectrosc. Radiat. Transfer*, **6**, 311 (1966).

<sup>g</sup>Y. Ben Aryeh, *op. cit.*, **7**, 211 (1967).

<sup>h</sup>J. H. Jaffe and W. S. Benedict, *op. cit.*, **3**, 87 (1963).

<sup>i</sup>C. B. Ludwig, C. C. Ferriso, and C. N. Abeyta, *op. cit.*, **5**, 281 (1965).

<sup>j</sup>C. W. von Rosenberg, Jr., N. H. Pratt, and K. N. C. Bray, *op. cit.*, **10**, 1155 (1969).

<sup>k</sup>J. S. Margolis, Paper ME 9, Abstracts for 30th Symposium on Molecular Structure and Spectroscopy, Ohio State University, Columbus, Ohio, June 16–20, 1975.

<sup>l</sup>C. C. Ferriso and C. B. Ludwig, *J. Chem. Phys.*, **41**, 1668 (1964).

<sup>m</sup>Reference 112.

<sup>n</sup>G. L. Maclay, *J. Chem. Phys.*, **43**, 185 (1965).

The exact rotation matrix  $\mathbf{R}$  of (118) is found to be necessary in the calculation of those integrated intensities that involve overtones in the asymmetric stretching mode. Comparison of results for the exact  $\mathbf{R}$  analysis with results obtained by setting  $\mathbf{R}$  equal to a unit matrix shows that differences as large as 100% in the matrix elements  $\langle(000)|\mathbf{M}_E|(002)\rangle$  can occur for  $\text{H}_2\text{O}$ . On the other hand, the effect of this approximation is less severe for the fundamental bands and for combination bands involving only a single quanta of asymmetric stretching energy. For the  $\nu_3$  fundamental of  $\text{H}_2\text{O}$ , the error is as large as 9%, but for the  $\nu_1$  and  $\nu_2$  bands of  $\text{H}_2\text{O}$ , it is less than 1%.

In Table XVIII experimental and calculated integrated band intensities are given for multiple-quanta excitations from the ground vibrational state. Excellent agreement is obtained for the  $2\nu_2$ ,  $\nu_1 + \nu_3$ ,  $2\nu_1$ , and  $\nu_1 + \nu_2$  bands. The most widely quoted experimental value\* for the  $2\nu_2 + \nu_3$  band is larger than the theoretical value by almost a factor of 2, but the result of Penner and Varanasi<sup>112</sup> is in better accord with the present theoretical value for this band. For the  $\nu_2 + \nu_3$  band, the theoretical intensity is larger than the experimental value by nearly a factor of 3. For the  $\nu_1 + 2\nu_2$  and  $3\nu_2$  bands, the opposite is true. Except for the  $2\nu_3$  and  $\nu_2 + \nu_3$  two-quanta excitations, the theoretical results for the integrated band intensities are in satisfactory agreement with the observed values if we take into account the uncertainties associated with the latter.<sup>113</sup>

Unlike the situation for the fundamental bands, the calculated intensities for multiple-quanta excitations in some cases vary significantly with the force field. It is found that the overtone bands are the most sensitive. For example, changing from the HMS potential to a CI *ab initio* potential produces changes in the calculated intensities of the  $2\nu_2$ ,  $2\nu_3$ , and  $2\nu_1$  bands of -48, +97, and -27%, respectively.

## 6. Rotational Constants

In the variational method, the full V-R Hamiltonian

$$\hat{H} = \hat{H}_v + \hat{T}_{vr} + \hat{T}_c \quad (120)$$

is written in matrix form using eigenfunctions of the pure vibrational Hamiltonian  $\hat{H}_v$ . We follow Carney and Porter<sup>31</sup> by writing

$$\langle n | \hat{H} | m \rangle = E_n \delta_{nm} + \langle n | \hat{T}_{vr} | m \rangle + \langle n | \hat{T}_c | m \rangle \quad (121)$$

The rotational kinetic-energy operators  $\hat{T}_{vr}$  and  $\hat{T}_c$  depend only on the vibrational matrix elements and the angular momenta  $P_x$ ,  $P_y$ ,  $P_z$ . In matrix form, we obtain  $\mathbf{H}$  as

$$\mathbf{H} = \mathbf{E}^{(v)} + \frac{1}{2} [\mathbf{A}P_x^2 + \mathbf{B}P_y^2 + \mathbf{C}P_z^2 + \mathbf{D}(P_xP_y + P_yP_x)] + \frac{i}{\hbar} \mathbf{F}P_z \quad (122)$$

\*See the reference in footnote b of Table XVIII.

where  $E^{(v)}$  is the diagonal matrix of eigenvalues  $E_1, E_2, \dots$ , of  $\hat{H}_v$ . The Coriolis interaction operator  $\hat{T}_c$  yields the last term in  $H$  in which

$$\langle n | \hat{F} | m \rangle = \left\langle n \left| \frac{\hbar^2}{I_{zz}^{\text{eff}}(t_1)} \left( t_3 \frac{\partial}{\partial t_2} - t_2 \frac{\partial}{\partial t_3} \right) \right| m \right\rangle \quad (123)$$

contains the effective moment of inertia  $I_{zz}^{\text{eff}}(t_1)$ .

Equation 122 involves the angular momenta and the effective rotational constant matrices **A** through **F**. If the manifold of vibrational states does not contain states that are nearly degenerate, the off-diagonal elements of the rotational constant matrices are generally required only for high  $J$  states. However, for nearly degenerate vibrational states, the off-diagonal matrix elements of the so-called Coriolis interaction matrix **F** become necessary. The off-diagonal elements of **A** through **D** produce the Fermi-resonance and centrifugal distortion effects.

As an example, let us consider the effective rotational constants for ozone, which are known for only a few vibrational states of  $^{16}\text{O}_3$  and only for the (000) state of the isotopically substituted molecules. Recently, perturbation analyses of isotope effects on higher-order V-R constants was shown to require an anharmonic potential function.<sup>114</sup> Because the algebraic complexity of perturbation methods increases considerably upon isotopic substitution in bent  $\text{AB}_2$  molecules, variational procedures offer an attractive alternative. In Table XIX variationally determined values for the diagonal matrix elements of the **A**, **B**, and **C** matrices (referred to as rotational constants  $\bar{A}$ ,  $\bar{B}$ , and  $\bar{C}$ ) are presented for the four lowest vibrational states of six isotopically substituted ozone molecules. The diagonal matrix elements of **D** and **F** are zero. Off-diagonal elements are not reported, since they are generally much smaller than the diagonal elements. The experimental values that are included in parentheses in Table XIX are within 1% of the results computed with a 220-term vibrational wave function. Calculations with other basis sets show that these results are well converged. We conclude that the variational method represents a direct and accurate method of obtaining rotational constants of  $\text{AB}_2$  molecules.

## 7. Average Structures

The utility of the variational analysis can also be demonstrated by comparing average displacements of bond stretching and bending motions from equilibrium. Let us continue with  $^{16}\text{O}_3$  as our example and consider the average structures of Tanaka and Morino (TM),<sup>115</sup> which were determined from a perturbation analysis (PT) of microwave spectra for the five lowest vibrational levels enumerated in Table XX. The variational theory (VT) results were obtained with a 1140-term vibrational wave function. Although the overall agreement is satisfactory, several notable differences occur. In

TABLE XIX  
Effective Rotational Constants for Ozone Isotopes<sup>a</sup>

Isotopic species <sup>b</sup>	Rotational constants (cm <sup>-1</sup> ) <sup>c,d</sup>		
	$\bar{A}$	$\bar{B}$	$\bar{C}$
(000) vibrational state			
666	3.561(3.554)	0.445(0.445)	0.395(0.395)
668	3.495(3.488)	0.421(0.420)	0.374(0.374)
686	3.297(3.290)	0.446(0.445)	0.391(0.391)
868	3.429(3.422)	0.396(0.396)	0.354(0.354)
886	3.231(3.225)	0.421(0.420)	0.371(0.372)
888	3.164(3.158)	0.396(0.396)	0.351(0.351)
(010) vibrational state			
666	3.617(3.607)	0.444(0.444)	0.393(0.392)
668	3.547	0.419	0.373
686	3.350	0.444	0.390
868	3.478	0.395	0.353
886	3.280	0.419	0.370
888	3.211	0.395	0.350
(001) vibrational state			
666	3.512(3.501)	0.442(0.441)	0.390(0.391)
668	3.450	0.417	0.370
686	3.254	0.442	0.387
868	3.381	0.393	0.350
886	3.191	0.418	0.367
888	3.123	0.393	0.347
(100) vibrational state			
666	3.563(3.557)	0.444(0.443)	0.393(0.392)
668	3.495	0.419	0.372
686	3.297	0.444	0.390
868	3.433	0.394	0.353
886	3.229	0.419	0.369
888	3.166	0.394	0.350

<sup>a</sup>Calculated using a 220-term vibrational wave function. See Ref. 32.

<sup>b</sup>The isotopic species notation is 6=<sup>16</sup>O and 8=<sup>18</sup>O, with the central number corresponding to the apex atom.

<sup>c</sup> $\bar{A}$ ,  $\bar{B}$ , and  $\bar{C}$  are spectroscopic designations. They are related to those in (122) by the relations  $\bar{A}=pA$ ,  $\bar{B}=pA$ , and  $\bar{C}=pC$  where  $p=(h/4\pi c)$ . See (33) through (35) of Ref. 32 for details.

<sup>d</sup>Values in parentheses are experimental. See M. Lichenstein, J. J. Gallagher, and S. A. Clough, *J. Mol. Spectrosc.*, **40**, 10 (1971); R. H. Hughes, *J. Chem. Phys.*, **24**, 131 (1955) and *Phys. Rev.*, **85**, 717 (1952); L. Pierce, *J. Chem. Phys.*, **24**, 139 (1955); J. Bellet, B. Duterage, and J. C. Dysanemaecher, *C. R. Acad. Sci. (Paris)* **B279**, 287 (1974); T. Tanaka and Y. Morino, *J. Mol. Spectrosc.*, **33**, 538 (1970).

TABLE XX  
Average Structures in Specific Vibrational States for  $^{16}\text{O}_3$

Quantum numbers			$\Delta R = (R - R_{eq})(\text{\AA})$		$\Delta\theta = (\theta - \theta_{eq}) (\text{degrees})$	
$n_1$	$n_2$	$n_3$	VT <sup>a</sup>	PT <sup>b</sup>	VT <sup>a</sup>	PT <sup>b</sup>
0	0	0	0.00794	0.0075	-0.0183	-0.0167
0	1	0	0.01072	0.0090	+0.2704	+0.2834
0	0	1	0.01602	0.0158	-0.2160	-0.1666
1	0	0	0.01293	0.0127	-0.1495	-0.1666
0	2	0	0.01382	0.0104	0.5867	0.5833

<sup>a</sup>Variational results for a 1140-term vibrational wave function. See Ref. 32.

<sup>b</sup>Perturbation theory results. See Ref. 115.

particular, Tanaka and Morino predict equal values of  $\Delta\theta$  for both symmetric and asymmetric stretching, whereas the variational calculations predict a  $0.06^\circ$  difference. Also, they obtain a constant increase of about  $0.3^\circ$  in  $\Delta\theta$  per quanta of  $\nu_2$  excitation, whereas variational calculations show that this increment is slightly smaller in magnitude for a fundamental excitation but increases with additional  $\nu_2$  excitation. Similar differences are seen for  $\Delta R$ . Since variational results include higher-order kinetic and anharmonic terms in the Hamiltonian, they are expected to be more accurate.

The average and root-mean-square displacements in each of the fundamental states for six isotopic species of ozone (computed with a 220-term wave function) are given in Table XXI. The vibrational averaging methods using the quadrature formulation were applied by Carney et al.<sup>30,32</sup> to examine two types of basis-set dependence. One involves the nonlinear parameters that define the oscillator basis functions, and the other is the number of configurations retained in the variational wave function. The nonlinear parameters can be identified with the harmonic frequencies, or they can be scaled by changing the proportionality factor. In the limit of complete oscillator and CI basis representations, the precise value of the scale factor is unimportant. However, when truncations are made, thresholds for convergence must be established by varying the number of CI terms and the scale factor over limits appropriate to the molecule and vibrational states of interest. For the low-lying states of ozone, Carney et al.<sup>32</sup> found, at the 220-term CI level, that  $\Delta\theta$  and  $\Delta R$  change by 25 and 1%, respectively,



TABLE XXI  
Average Displacements and Root-Mean-Square Displacements for  
Isotopic Ozone Molecules

Isotopic species <sup>a</sup>	Vibrational averaged displacements <sup>b</sup>					
	$\Delta R_1$	$\Delta R_2$	$\Delta\theta$	$\sqrt{\Delta R_1^2}$	$\sqrt{\Delta R_2^2}$	$\sqrt{\Delta\theta^2}$
(000) vibrational state						
666	0.00794	0.00794	-0.0183	0.04504	0.04504	3.5831
668	0.00800	0.00765	-0.0217	0.04505	0.04434	3.5592
686	0.00773	0.00773	-0.0103	0.04438	0.04438	3.5276
868	0.00771	0.00771	-0.0246	0.04435	0.04435	3.5347
886	0.00743	0.00779	-0.0137	0.04365	0.04439	3.5029
888	0.00749	0.00749	-0.0172	0.04366	0.04366	3.4776
(010) vibrational state						
666	0.01072	0.01072	0.2704	0.04674	0.04675	5.6267
668	0.01062	0.01046	0.2624	0.04663	0.04631	5.5409
686	0.01044	0.01044	0.2681	0.04587	0.04587	5.6283
868	0.01036	0.01036	0.2538	0.04617	0.04617	5.4572
886	0.01017	0.01036	0.2607	0.04538	0.04577	5.5437
888	0.01009	0.01009	0.2532	0.04526	0.04526	5.4610
(001) vibrational state						
666	0.01606	0.01606	-0.2166	0.06912	0.06912	3.6089
668	0.01188	0.01943	-0.2189	0.06156	0.07403	3.6548
686	0.01557	0.01557	-0.1965	0.06795	0.06795	3.5517
868	0.01566	0.01566	-0.2257	0.06815	0.06815	3.5599
886	0.01873	0.01165	-0.1988	0.07257	0.06081	3.5839
888	0.01516	0.01516	-0.2051	0.06694	0.06694	3.5010
(100) vibrational state						
666	0.01293	0.01293	-0.1495	0.06055	0.06055	4.4796
668	0.01750	0.00835	-0.1576	0.06836	0.05160	4.4513
686	0.01263	0.01263	-0.1249	0.05990	0.05990	4.2967
868	0.01253	0.01253	-0.1604	0.05932	0.05932	4.5307
886	0.00826	0.01695	-0.1335	0.05137	0.06727	4.2760
888	0.01222	0.01222	-0.1381	0.05865	0.05864	4.3444

<sup>a</sup>See footnote b of Table XIX for isotopic species notation.

<sup>b</sup>Values refer to 220-term vibrational wave functions. See Ref. 32 for details. Results with a 1140-term vibrational wave function for (666) agree with these values within  $6 \times 10^{-4}$  units. Units are angstroms and degrees for distance and angular displacements.

when the harmonic frequencies are scaled by factors of up to 6. When the number of CI terms increases to 1140, these changes are reduced to 5 and 0.5%, respectively, thereby inferring closer realization of fully converged average properties.

Substitution of  $^{18}\text{O}$  for  $^{16}\text{O}$  at the terminal positions in  $^{16}\text{O}_3$  results in a significant difference in  $\Delta R$  between the bonds ( $\Delta R_1$  and  $\Delta R_2$ ) for states involving principally stretching motion. However, the sum of  $\Delta R_1$  and  $\Delta R_2$  for the symmetric stretching or the difference in the case of asymmetric stretching changes slowly, paralleling the small differences in reduced mass between isotopic species. For molecules with  $C_{2v}$  mass symmetry, the  $\Delta R$  displacement reflects the number of  $^{18}\text{O}$  atoms contained in the bond. Vibrational averaged structures using variational methods have also been reported for the water molecule.<sup>25</sup>

## V. SPECTRAL PREDICTIONS

The significant features of the variational approach include the retention of all terms in the V-R Hamiltonian, the possibility of using widely different forms and variables to describe the potential surface, and the ready applicability of the variational wave function. Section IV provides comparisons with experiment and perturbation calculations that demonstrate the accuracy and usefulness of the variational method outlined in Section III.B. In this section we consider three systems that are characterized by a lack of experimental infrared data and for which the variational results stand as predictions.

### A. Infrared Spectrum of $\text{H}_3^+$ Isotopes

Recent measurements of the infrared spectrum of  $\text{HD}^+$  suggest that similar techniques might be applied to  $\text{H}_3^+$ , whose vibrational spectrum is so far unobserved. Recently, the infrared absorption of  $\text{HD}^+$  ion was reported in the spectral region  $1900 > \bar{\nu} > 1600 \text{ cm}^{-1}$ .<sup>116</sup> Although extensive theoretical studies of  $\text{HD}^+$  exist in the literature, these measurements are the first to probe V-R excitation in the ground electronic state. Two principal features of the  $\text{HD}^+$  system were exploited. First, the spectral activity occurs in a region that is accessible by means of CO laser emission using Doppler-effect tuning. Second, dependence of ion-target gas-collisional processes on the internal V-R state of  $\text{HD}^+$  allows detection of the resonance IR excitation frequencies. The  $\text{D}_3^+$  system should also have these two characteristics in common with  $\text{HD}^+$  according to recent *ab initio* calculations for the isotopic  $\text{H}_3^+$  ions.<sup>27,31</sup> Collisional detection of  $\text{D}_3^+$  should be quite effective because of the known Jahn-Teller distortion on the geometry and dynamics of the

species involved. Of the molecular ions  $D_2^+$  and  $D_3^+$ , only the latter has an allowed IR spectrum.<sup>27</sup>

Having demonstrated for  $H_2O$  and  $O_3$  the suitability of combining the SPF potential function with the Watson kinetic-energy operator to determine the vibrational Hamiltonian, we consider *ab initio* predictions for  $H_3^+$  and its isotopic species. Using the fifth-degree potential function of Table XI, Carney and Porter determined the fundamental excitation energies for triatomic ions produced in electric discharges of  $H_2$  and  $D_2$ . Their results are shown in Table XXII. Of the vibrational excitations listed there, only the doubly degenerate infrared-allowed  $\bar{\nu}_E$  band of  $D_3^+$  appears to fall into the same frequency range in which the  $HD^+$  ion was observed. It is suggested that the IR spectrum of  $D_3^+$  could be monitored in an experiment similar to the one performed for  $HD^+$ .

TABLE XXII  
Fundamental Vibrational Excitation Energies ( $cm^{-1}$ )  
Relative to the Ground State  
for  $H_3^+$  Isotopic Species<sup>a,b</sup>

Quantum numbers			Molecular ions			
$n_1$	$n_2$	$n_3$	$H_3^+$	$D_3^+$	$H_2D^+$	$HD_2^+$
0	1	0	2516	1826	2203	1961
0	0	1	2516	1826	2329	2072
1	0	0	3185	2307	3000	2742

<sup>a</sup>Calculated using the fifth-degree SPF potential given in Table XI and a 220-term vibrational wave function.

<sup>b</sup>Ref. 31.

## B. *Ab Initio* Treatment of $^3B_1$ Methylene

Carney and Langhoff<sup>33</sup> have determined both potential and dipole-moment functions for the  $^3B_1$  state of  $CH_2$ . This molecule is of some importance in the oxidation of alkenes and alkynes. Accurate values for the band origins and intensities would perhaps facilitate monitoring IR absorption or emission lines to follow the extent of reactions in which  $^3B_1$   $CH_2$  is produced as an intermediate. At present, such spectroscopic quantities are not

available. Thus Carney and Langhoff have determined the vibrational frequencies using variational vibrational analysis of the *ab initio* potential function.

A judiciously chosen potential surface for the  $^3B_1$  state yields a fifth-degree Dunham expansion in the internal coordinates. The vibrational excitation energies were determined for the fifth-, fourth-, third-, and second-degree potentials to observe the effect of the truncation on the calculated band positions. The results at the electronic SCF level are given in Table XXIII.

TABLE XXIII  
Zero-Point Energies and Vibrational Excitation Energies ( $\text{cm}^{-1}$ ) for  $\text{CH}_2$  and  $\text{CD}_2$   
Using an SCF Potential Surface<sup>a,b</sup>

Vibrational state			$\text{CH}_2$				$\text{CD}_2$
$n_1$	$n_2$	$n_3$	Fifth degree	Fourth degree	Third degree	Second degree	Fifth degree
0	0	0	3991.9	3995.4	3932.1	3929.0	2946.9
0	1	0	1228.0	1233.3	1254.5	1268.3 <sup>c</sup>	934.7
0	2	0	2386.4	2395.4	2464.6	2526.2	1831.8
1	0	0	3195.9	3209.2	3016.6	3217.5 <sup>c</sup>	2308.6
0	0	1	3390.5	3415.4	3206.7	3426.5 <sup>c</sup>	2562.7

<sup>a</sup>Reference 33.

<sup>b</sup>Energies were calculated with a 220-term wave function using the methods discussed in Refs. 29, 30, and 32. Excited-state energies are relative to (000).

<sup>c</sup>Classical harmonic frequencies were calculated by Chu and Dahler<sup>117</sup> using an *ab initio* potential function calculated by Bender et al.<sup>118</sup> The results for (010), (100), and (001) are 1131, 3256, and  $3453 \text{ cm}^{-1}$ , respectively.

Values for the harmonic excitation energies calculated by Chu and Dahler<sup>117</sup> are also given. The Chu and Dahler results are nonvariational and were calculated using the *ab initio* CI potential reported by Bender et al.<sup>118</sup>

Although there is some variation in band origin with increasing degree of the SCF polynomial, the results appear to have essentially converged at fifth degree. However, the estimates of Chu and Dahler are less satisfactory because of the neglect of anharmonicity in the vibrational Hamiltonian operator.

### C. Application to Isotope Enrichment

The recent interest in isotopic separation suggests that a determination of the band origins for tritium-containing water might help to interpret the observed spectral features, as well as to provide useful information needed in attempts to enrich the tritium content of water. Only eight of the band origins of HTO, DTO, and T<sub>2</sub>O in Table XXIV have been observed. In every case Carney et al.<sup>30</sup> find good agreement with the variationally determined transition frequencies, which are based on the potential in Refs. 29 and 109. The calculated result for the (001) state of HTO is in better agreement with the recent work of Fayt and Steenbeckeliers<sup>119</sup> than the earlier work of Staats, Morgan, and Goldstein (SMG).<sup>120</sup> Also, the SMG

TABLE XXIV  
Vibrational Excitation Energies (cm<sup>-1</sup>) for HT<sup>16</sup>O, DT<sup>16</sup>O, and T<sub>2</sub><sup>16</sup>O

Vibrational state <sup>a</sup>			Band origins <sup>b</sup>					
			HTO		DTO		T <sub>2</sub> O	
<i>n</i> <sub>1</sub>	<i>n</i> <sub>2</sub>	<i>n</i> <sub>3</sub>	VT <sup>c</sup>	Observed	VT <sup>c</sup>	Observed	VT <sup>c</sup>	Observed
0	1	0	1333	1324 <sup>d</sup>	1091	—	995	995 <sup>d,f</sup>
0	2	0	2643	—	2164	—	1976	—
1	0	0	2302	2300 <sup>e</sup>	2297	—	2240	—
0	0	1	3717	3711 <sup>d</sup> , 3717 <sup>e</sup>	2738	2730 <sup>d</sup>	2367	2364 <sup>d</sup>
0	3	0	3933	—	3221	—	2944	—
1	1	0	3623	—	3385	—	3229	—
0	1	1	5032	—	3819	—	3355	3358 <sup>d</sup>
1	2	0	4929	—	4451	—	4204	—
0	2	1	6322	—	4882	—	4330	—
2	0	0	4565	—	4538	—	4446	—
1	0	1	6022	—	5026	—	4548	4537 <sup>d</sup>
0	0	2	7221	—	5392	—	4698	—

<sup>a</sup>The quantum numbers *n*<sub>1</sub>, *n*<sub>2</sub>, and *n*<sub>3</sub> denote symmetric stretch, bend, and asymmetric stretch, respectively.

<sup>b</sup>All energies are relative to the zero-point energies, which are calculated to be 3764, 3123, and 2850 cm<sup>-1</sup> for HTO, DTO, and T<sub>2</sub>O, respectively.

<sup>c</sup>Variational calculation.

<sup>d</sup>Reference 120.

<sup>e</sup>Reference 119.

<sup>f</sup>The value of 995.37 cm<sup>-1</sup> was determined in the vapor phase by R. A. Carpenter, et al., *J. Mol. Spectrosc.*, **44**, 197 (1972).

band origins of the (010) state of HTO and the (001) state of DTO appear to be too small. For all the bands considered in Table XXIV, the average deviation between calculated and observed values is only  $4.5\text{ cm}^{-1}$  with a maximum deviation of  $14\text{ cm}^{-1}$ .

The assignments for the states were made<sup>30</sup> on the basis of the  $\langle\psi_v|Q_i|\psi_{v'}\rangle$  matrix elements, where  $Q_i$  is a normal coordinate (see Section IV.C). The levels are denoted by the dominant term in the wave function, but significant mixing occurs for the higher-energy levels. However, we would expect the unobserved bands to fall within approximately  $15\text{ cm}^{-1}$  of the calculated values for all of the levels in Table XXIV.

These theoretical results, which are completely *ab initio* for  $\text{H}_3^+$  and  $\text{CH}_2$ , stand as predictions of vibrational energies, to be verified by subsequent measurements.

## VI. SUMMARY AND CONCLUSIONS

Both *ab initio* and experimentally derived force fields have been tested using variational methods to solve the V-R Schrödinger equation for bent and linear triatomic molecules. The analyses are suitable generalizations of earlier applications to diatomic molecules. Several different forms of the Hamiltonian operator for nuclear motion have been utilized, but only in the case of bent molecules are there presently sufficient data to establish their numerical equivalence.

Numerical and analytical basis functions have been employed to determine the V-R wave functions using several different techniques of evaluating the vibrational Hamiltonian matrix elements. These methods presently allow Hamiltonian matrices on the order of  $1000 \times 1000$  to be diagonalized. Suitable choices of oscillator or one-phonon basis sets may facilitate placement of the Hamiltonian matrix into the desired form for which currently available large matrix-diagonalization schemes are designed. Although molecular symmetry provides a way to reduce the order of the vibrational Hamiltonian matrix, isotopic substitution effects often preclude such a simplification. Apart from limitations of using finite basis sets, it has also been adequately demonstrated that there exist significant truncation errors, which are traceable to series expansions of molecular force fields and which affect both band positions and rotational constants.

Variational wave functions have been used to obtain average geometries, root-mean-square displacements, and dipole moments from infrared intensities. Comparisons with perturbation theory have been reported for a few cases.

Only a few variational results are available for V-R states of triatomic

molecules. There are presently no calculations on tetratomic and larger molecules in which the complete Hamiltonian has been employed. Use of an SCF-CI analogue to electronic theory appears to present one way in which larger numbers of vibrational modes may be treated. However, it will be necessary to develop efficient V-R basis-set-contraction schemes before the variational analysis will be competitive with perturbation methods. Use of the complete Hamiltonian in the former provides a test of the truncations implicit in the perturbation expansions.

Because the RKR method is used widely to extract two-body potentials from spectroscopic constants, additional study of the semiclassical method for triatomic molecules is needed. It is now known that quantum mechanical variational calculations produce eigenenergies in essential agreement with those determined by the semiclassical method, but the manner in which the semiclassical method should be formulated to obtain three-body molecular force fields from observed spectroscopic constants is unclear. The use of semiempirical potential functions (e.g., the LEPS potential) in variational vibrational analysis to complement SPF expansions about equilibrium seems particularly attractive. With such force fields, investigations of the density of states near the dissociation limits can be studied to identify the point at which quantum absorption of energy becomes statistical.

In regard to the interplay with experiment, it is emphasized that the *ab initio* studies of both  $\text{CH}_2$  and  $\text{H}_3^+$  need to be confirmed in the laboratory where the necessary technology appears now to exist.

An area of interest in electronic theory is that of vertical or Franck-Condon transitions. Spectral profiles in these spectra are related to the overlap of ground and excited V-R wave functions, each belonging to different electronic states of the molecule. Use of the variational method at a common reference geometry for definition of the vibrational basis set would allow a convenient means of evaluating the Franck-Condon factor, thereby helping to elucidate the nature of the upper vibrational state energy level density.

Another major area where variational theory could be used for polyatomic molecules is the inversion of spectral data to obtain force constants, especially the higher-order ones. This is generally a formidable task in that the solution is nonunique. Recently, Monte Carlo methods have been introduced as a way to identify the number of mathematically admissible solutions.<sup>121</sup> Use of rotational-constant anharmonicities allows the number of physically acceptable solutions to be narrowed. Applications of the SPF transformation and the variational method should allow still another narrowing of the number of admissible solutions, since the former extends the domain of convergence of Taylor series expansions into regions that variational theory readily accommodates.

This introduction to variational V-R spectroscopy is a survey of the

general theory and its range of applications. Although much progress has been made in developing the methodology to the point of practical utility, much remains to be done, particularly in extensions to larger molecules and to highly excited states of smaller systems, even those with three atoms. Future developments along these lines are likely to be most fruitful if carried out in conjunction with experimental programs.

### Acknowledgments

Many colleagues have provided significant help in compiling this review. Of special importance are our collaborators on much of the research summarized here: Dr. L. A. Curtiss, Dr. S. R. Langhoff and Dr. R. N. Porter. We are especially indebted to Dr. Langhoff for generating the vibrational amplitude maps in Figs. 3 through 8. The support of this research by the Battelle Institute Program fostered much fruitful collaboration under its auspices.

We would also like to thank Dr. N. C. Handy for sending us preprints of work at Cambridge. Correspondence with E. K. C. Lai and Professor D. H. Whiffen and discussions with Professor I. Shavitt have also been very helpful.

### References

1. For example, see *Chemical and Biochemical Applications of Lasers*, Vol. 1, C. Bradley Moore, Ed., Academic Press, New York, 1974.
2. *Modern Theoretical Chemistry: Electronic Structure Theory*, Vols. 3 (Methods) and 4 (Applications), H. F. Schaefer III, Ed., Plenum, New York, 1977.
3. H. H. Nielsen, *Rev. Mod. Phys.*, **23**, 90 (1951).
4. I. M. Mills, *Molecular Spectroscopy: Modern Research*, Vol. I, K. N. Rao and C. W. Matthews, Eds., Academic Press, New York, 1972, Chap. 5.
5. G. Amat, H. H. Nielsen, and C. Tarrago, *Rotation Vibration of Polyatomic Molecules*, Dekker, New York, 1971.
6. L. L. Sprandel and C. W. Kern, *Mol. Phys.*, **24**, 1383 (1972).
7. M. A. Pariseau, I. Suzuki, and J. Overend, *J. Chem. Phys.*, **42**, 2335 (1965).
8. A. Foord and D. H. Whiffen, *Mol. Phys.*, **26**, 959 (1973).
9. A. Foord, J. G. Smith, and D. H. Whiffen, *Mol. Phys.*, **29**, 1685 (1975).
10. I. Baraldi, F. Momicchioli, and M. C. Bruni, *J. Chem. Soc. (London), Faraday Trans. II*, **72**, 887 (1976).
11. I. Suzuki, *Bull. Chem. Soc. Jap.*, **44**, 3277 (1971).
12. I. Suzuki, *Bull. Chem. Soc. Jap.*, **48**, 3565 (1975).
13. I. Suzuki, *Bull. Chem. Soc. Jap.*, **48**, 1685 (1975).
14. M. G. Bucknell, N. C. Handy, and S. F. Boys, *Mol. Phys.*, **28**, 759 (1974).
15. M. G. Bucknell and N. C. Handy, *Mol. Phys.*, **28**, 777 (1974).
16. R. J. Whitehead and N. C. Handy, *J. Mol. Spectrosc.*, **55**, 356 (1975).
17. R. J. Whitehead and N. C. Handy, *J. Mol. Spectrosc.*, **59**, 459 (1976).
18. K. S. Sorbie and J. N. Murrell, *Mol. Phys.*, **29**, 1387 (1975).
19. L. L. Sprandel, *Diss. Abstr. Int.*, **35B**, 5577 (1975).
20. L. A. Gribov, *Opt. Spectrosc.*, **31**, 842 (1971).
21. L. A. Gribov and G. V. Khovrin, *Opt. Spectrosc.*, **36**, 274 (1974).
22. L. A. Gribov and G. V. Khovrin, *Opt. Spectrosc.*, **36**, 642 (1974).
23. L. A. Gribov and G. V. Khovrin, *Opt. Spectrosc.*, **37**, 257 (1974).



24. M. Vučelić, Y. Ohrn, and J. R. Sabin, *J. Chem. Phys.*, **59**, 3003 (1973).
25. E. K. C. Lai, Master's Thesis, Dept. of Chem., Indiana University, Bloomington, Indiana, 1975.
26. G. D. Carney, *Diss. Abstr. Int.*, **34B**, 1956 (1973).
27. G. D. Carney and R. N. Porter, *J. Chem. Phys.*, **60**, 4251 (1974).
28. G. D. Carney and C. W. Kern, *Int. J. Quant. Chem. Symp.*, **9**, 317 (1975).
29. G. D. Carney, L. A. Curtiss, and S. R. Langhoff, *J. Mol. Spectrosc.*, **61**, 371 (1976).
30. G. D. Carney, L. A. Curtiss, and S. R. Langhoff, *Appl. Spectrosc.*, **30**, 453 (1976).
31. G. D. Carney and R. N. Porter, *J. Chem. Phys.*, **65**, 3547 (1976); *Chem. Phys. Lett.* **50**, 327 (1977).
32. G. D. Carney, S. R. Langhoff, and L. A. Curtiss, *J. Chem. Phys.*, **66**, 3724 (1977).
33. G. D. Carney and S. R. Langhoff, "Ab-initio Study of the IR Spectrum of CH<sub>2</sub>," (unpublished, 1975).
34. N. C. Handy, S. M. Colwell, and W. H. Miller, *J. Chem. Soc. Fara. Discussions*, **62**, 29 (1977).
35. For a discussion of Born-Oppenheimer breakdown in diatomic molecules, see P. R. Bunker, *J. Mol. Spectrosc.*, **35**, 306 (1970).
36. E. B. Wilson, Jr. and J. B. Howard, *J. Chem. Phys.*, **4**, 260 (1936).
37. B. T. Darling and D. M. Dennison, *Phys. Rev.*, **57**, 128 (1940).
38. L. J. Bodi and C. F. Curtiss, *J. Chem. Phys.*, **25**, 1117 (1956).
39. R. Meyer and Hs. H. Günthard, *J. Chem. Phys.*, **49**, 1510 (1968).
40. J. K. G. Watson, *Mol. Phys.*, **15**, 479 (1968).
41. J. K. G. Watson, *Mol. Phys.*, **19**, 465 (1970).
42. B. J. Howard and R. E. Moss, *Mol. Phys.*, **19**, 433 (1970).
43. H. M. Pickett, *J. Chem. Phys.*, **56**, 1715 (1972).
44. R. Wertheimer, *Mol. Phys.*, **27**, 1673 (1974).
45. J. D. Louck, *J. Mol. Spectrosc.*, **61**, 107 (1976).
46. J. D. Louck and H. W. Galbraith, *Rev. Mod. Phys.*, **48**, 69 (1976).
47. H. Margenau and G. M. Murphy, *The Mathematics of Physics and Chemistry*, 2nd ed., Van Nostrand, New York, 1956, p. 411.
48. C. Eckart, *Phys. Rev.*, **47**, 552 (1935).
49. E. B. Wilson, Jr., J. C. Decius, and P. C. Cross, *Molecular Vibrations*, McGraw-Hill, New York, 1955.
50. D. F. Smith, Jr. and J. Overend, *Spectrochim. Acta*, **28A**, 471 (1972).
51. S. R. Polo, *J. Chem. Phys.*, **24**, 1133 (1956).
52. M. R. Aliev, *Opt. Spectrosc.*, **26**, 463 (1969).
53. C. W. Kern and R. L. Matcha, *J. Chem. Phys.*, **49**, 2081 (1968).
54. W. C. Ermler and C. W. Kern, *J. Chem. Phys.*, **55**, 4851 (1971).
55. B. J. Krohn, W. C. Ermler, and C. W. Kern, *J. Chem. Phys.*, **60**, 22 (1974).
56. J. H. Van Vleck, *Phys. Rev.*, **33**, 467 (1929).
57. W. H. Shaffer, H. H. Nielsen, and L. H. Thomas, *Phys. Rev.*, **56**, 1051 (1939).
58. A. M. Arthurs and P. D. Robinson, *Proc. Roy. Soc. (London)*, **A301**, 507 (1967).
59. H. A. Kramers, *Quantum Mechanics*, Dover Publications, New York, 1964, p. 194.
60. C. M. Bender and T. T. Wu, *Phys. Rev.*, **184**, 1231 (1969); see also, C. M. Bender, *J. Math. Phys.*, **11**, 796 (1970).
61. B. Simon, *Ann. Phys.*, **58**, 76 (1970).
62. S. N. Biswas, K. Datta, R. P. Saxena, P. K. Srivastava, and V. S. Varma, *Phys. Rev.*, **D4**, 3617 (1971).
63. G. R. Osche and G. J. Iafrate, *J. Chem. Phys.*, **56**, 1104 (1972).
64. W. K. McClary, *Commun. Math. Phys.*, **24**, 171 (1972).

65. J. W. Strutt (3rd Baron Rayleigh), *The Theory of Sound*, Vol. I, MacMillan, London, 1877; reprinted by Dover, New York, 1945, pp. 109 ff.
66. W. Ritz, *J. Reine, Angew. Math.*, **135**, 1 (1909).
67. J. K. L. MacDonald, *Phys. Rev.*, **43**, 830 (1933).
68. S. G. Mikhlin, *Variational Methods in Mathematical Physics*, MacMillan, New York, 1964.
69. D. F. Zetik and F. A. Matsen, *J. Mol. Spectrosc.*, **24**, 122 (1967).
70. F. A. Matsen, *Advances in Chemical Physics*, Vol. 21, Wiley-Interscience, New York, 1971, p. 1.
71. W. J. Stevens, G. Das, and A. C. Wahl, *J. Chem. Phys.*, **61**, 3686 (1974).
72. E. S. Sachs and J. Hinze, *J. Chem. Phys.*, **62**, 3367, 3377, 3384 (1975).
73. J. L. Dunham, *Phys. Rev.*, **41**, 713, 721 (1932).
74. G. Simons, R. G. Parr, and J. M. Finlan, *J. Chem. Phys.*, **59**, 3229 (1973).
75. D. W. Harris, G. G. Engerholm, and W. D. Gwinn, *J. Chem. Phys.*, **43**, 1515 (1965).
76. D. J. Locker, *J. Phys. Chem.*, **75**, 1756 (1971).
77. E. Fues, *Ann. Phys.*, **80**, 367 (1926).
78. E. M. Greenawalt and A. S. Dickinson, *J. Mol. Spectrosc.*, **30**, 427 (1969).
79. A. M. Lesk, *J. Chem. Phys.*, **49**, 3898 (1968).
80. B. W. Shore, *J. Chem. Phys.*, **58**, 3855 (1973); **59**, 6450 (1973).
81. J. P. Chesick, *J. Chem. Phys.*, **49**, 3772 (1968).
82. P. F. Endres and D. J. Wilson, *J. Chem. Phys.*, **46**, 425 (1967).
83. C. S. Lin and G. W. F. Drake, *Chem. Phys. Lett.*, **16**, 35 (1972).
84. A. U. Hazi and H. S. Taylor, *Phys. Rev.*, **1A**, 1109 (1970).
85. P. F. Endres, *J. Chem. Phys.*, **47**, 798 (1967).
86. R. Dubrow, D. Hatzenbuehler, W. Marx, E. Zahorian, and D. J. Wilson, *J. Phys. Chem.*, **72**, 2489 (1968).
87. A. S. Dickinson and P. R. Certain, *J. Chem. Phys.*, **49**, 4209 (1968).
88. A. H. Stroud, *Approximate Calculation of Multiple Integrals*, Prentice-Hall, Englewood Cliffs, New Jersey, 1971.
89. W. H. Miller, *J. Chem. Phys.*, **64**, 2880 (1976).
90. P. Brunner and J. W. Duff, *J. Chem. Phys.*, **65**, 3566 (1976).
91. L. Infeld and T. E. Hull, *Rev. Mod. Phys.*, **23**, 21 (1951).
92. *Handbook of Mathematical Functions*, M. Abramowitz and I. Stegun, Eds., Dover Publications, New York, 1965, Chap. 6.
93. J. Ortega, "The Givens-Householder Method for Symmetric Matrices," in *Mathematical Method for Digital Computers*, Vol. 2, A. Ralston and H. S. Wilf, Eds., Wiley, New York, 1967, pp. 94-115.
94. S. S. Kuo, *Numerical Methods and Computers*, Addison-Wesley, Reading, Mass., 1965, Chap. 9.
95. I. Shavitt, C. F. Bender, A. Pipano, and R. P. Hosteny, *J. Computational Phys.*, **11**, 90 (1973); I. Shavitt, *J. Computational Phys.*, **6**, 124 (1970); E. R. Davidson, *J. Computational Phys.*, **17**, 87 (1975).
96. D. G. Truhlar, R. W. Olson, A. C. Jeannotte II, and J. Overend, *J. Am. Chem. Soc.*, **98**, 2373 (1976).
97. M. Goldsmith, G. Amat, and H. H. Nielsen, *J. Chem. Phys.*, **24**, 1178 (1956); **27**, 838 (1957).
98. S. Maes, *Cahiers Phys.*, **14**, 125 (1960); *J. Mol. Spectrosc.*, **9**, 204 (1962).
99. Z. Cihla and A. Chédin, *J. Mol. Spectrosc.*, **40**, 337 (1971).
100. I. Jobard and A. Chédin, *J. Mol. Spectrosc.*, **57**, 464 (1975).
101. E. Heilbronner, Hs. H. Günthard, and R. Geril, *Helv. Chim. Acta*, **39**, 1171 (1956).
102. E. Heilbronner, H. Rutishauser, and F. Gerson, *Helv. Chim. Acta*, **42**, 2285 (1959).
103. E. Heilbronner, H. Rutishauser, and F. Gerson, *Helv. Chim. Acta*, **42**, 2304 (1959).

104. I. Suzuki, *J. Mol. Spectrosc.*, **25**, 479 (1968).
105. G. D. Carney and G. Wolken, Jr., *Chem. Phys. Lett.* **41**, 347 (1976).
106. J. Pliva, in *Critical Evaluation of Chemical and Physical Structural Information*, D. R. Lide, Jr. and M. A. Paul, Eds., National Academy of Sciences, Washington, D.C., 1974, Chap. 5.
107. A. B. Anderson, *J. Chem. Phys.*, **57**, 4143 (1972).
108. A. Barbe, C. Secroun, and P. Jouve, *J. Mol. Spectrosc.*, **49**, 171 (1974).
109. A. R. Hoy, I. M. Mills, and G. Strey, *Mol. Phys.*, **24**, 1265 (1972).
110. G. Simons, *J. Chem. Phys.*, **61**, 369 (1974).
111. B. J. Rosenberg, W. C. Ermler, and I. Shavitt, *J. Chem. Phys.*, **65**, 4072 (1976).
112. S. S. Penner and P. Varanasi, *J. Quant. Spectrosc. Radiat. Transfer*, **5**, 391 (1965).
113. A critical review of these data has been prepared by L. A. Pugh and K. N. Rao, *Molecular Spectroscopy: Modern Research*, Vol. II, K. N. Rao, Ed., Academic Press, New York, 1976, Chap. 4.
114. P. M. Parker, *J. Mol. Spectrosc.*, **58**, 344 (1975).
115. T. Tanaka and Y. Morino, *J. Mol. Spectrosc.*, **33**, 538 (1970).
116. W. H. Wing, G. A. Ruff, W. E. Lamb, Jr., and J. J. Spezeski, *Phys. Rev. Lett.*, **36**, 1488 (1976).
117. M. Y. Chu and J. S. Dahler, *Mol. Phys.*, **4**, 1045 (1974).
118. C. F. Bender, H. F. Schaefer III, D. R. Franceschetti, and L. C. Allen, *J. Am. Chem. Soc.*, **94**, 6888 (1972).
119. A. Fayt and G. Steenbeckeliers, *Comptes rendus, Ser. B*, **275**, 459 (1972). See also J. Bellet, G. Steenbeckeliers, and P. Stouffs, *Comptes Rendus, Ser. B*, **275**, 501 (1972).
120. P. A. Staats, H. W. Morgan, and J. H. Goldstein, *J. Chem. Phys.*, **24**, 916 (1956).
121. G. K. Speirs and V. Spirko, *J. Mol. Spectrosc.*, **56**, 104 (1975).

## AUTHOR INDEX

- Abbey, K. M., 123(97), 131(97), 137  
 Abragam, A., 224(49), 231(49, 71), 260(71), 265(71), 299  
 Abramowitz, M., 334(92), 378  
 Adachi, H., 290(232), 304  
 Adam, N. K., 121(88), 136  
 Agarwal, G. S., 43(49), 66  
 Alberty, J., 127(122), 137  
 Alder, B. J., 145(29), 146(32), 148(32), 149(32), 150(32), 151(32), 156(44), 173(29), 182(32), 199  
 Aliev, M. R., 313(52), 340(52), 377  
 Allavena, M., 285(234), 304  
 Allen, G. C., 285(208), 286(208), 303  
 Allen, L. C., 372(118), 379  
 Amat, G., 306(5), 337(97), 339(97), 376, 378  
 Amos, A. T., 251(108), 252(115), 264 (152), 300, 301  
 Amos, T., 248(109), 272(179), 300, 302  
 Anderson, A. B., 342(107), 379  
 Anderson, C. R., 68(10), 92(10), 97  
 Anderson, H. C., 140(6), 146(6), 183(6), 195(6), 198  
 Anderson, N., 196(92), 200  
 Andersen, O. S., 120(77, 78), 121(92), 123(77), 124(77, 92), 125(116), 136, 137  
 Arndt, R. A., 135(29)  
 Arrighini, G. B., 251(111), 254(111, 123), 300, 301  
 Arthurs, A. M., 196(90, 92), 200, 317(58), 377  
 Astier, M., 212(12), 285(235), 298, 304  
 Averil, F. D., 290(232), 304  
 Azuma, K., 100(22), 135  
 Babiker, M., 42(51), 66  
 Bagus, P. S., 264(154), 301  
 Ballhausen, C. J., 212(15), 284(201), 286(212), 298, 303  
 Bamberg, E., 68(12), 90(12), 97, 100(12, 33), 119(76), 124(76), 135, 136  
 Banos, A., 58(56), 66  
 Baraldi, I., 306(10), 315(10), 376  
 Barbe, A., 347(108), 351(108), 354(108), 379  
 Barber, N. M., 121(87), 136  
 Barbier, C., 258(134), 301  
 Barbier, C. I., 257(131), 258(131, 136, 137), 259(138, 139), 301  
 Barker, G. C., 131(124), 137  
 Barker, J. A., 140(4), 146(4, 30, 31), 148 (30, 31, 35), 149(30, 31, 36), 183(4), 195(4), 198, 199  
 Barlow, C. A., 125(115), 137  
 Barton, G., 42(51), 43(50), 66  
 Basch, H., 220(30), 221(30), 295(253, 255), 298, 304  
 Bash, H., 238(88), 300  
 Bässler, H., 21(37), 21(40), 23(37, 40), 24(40), 25(37, 40), 26(37), 65, 66  
 Baudet, J., 226(56), 299  
 Baumann, G., 100(13), 135  
 Bean, R. C., 100(5), 135  
 Bearman, R. J., 160(52), 188(52), 200  
 Begenisich, T., 68(7), 96  
 Bell, G. M., 125(114), 137  
 Bender, C. F., 335(95), 378  
 Bender, C. M., 317(60), 377  
 Benz, R., 136(75)  
 Bernheim, R. A., 259(140), 301  
 Berthier, G., 212(12), 216(22, 38), 219 (27), 221(22), 226(56), 228(60), 237(84), 249(192), 257(131), 258(131, 134, 136, 137), 259(138, 139, 192), 284(200), 285(235), 298, 299, 300, 302, 303, 304  
 Bethe, H. A., 261(144), 273(144), 301  
 Beveridge, D. L., 284(202, 205), 285(205), 303  
 Bird, R. B., 185(61), 188(61), 200  
 Biswas, S. N., 317(62), 377  
 Blanchard, C. H., 278(186), 302

- Bleany, B., 224(49), 230(62), 231(49), 299  
 Blinder, S. M., 257(195), 302  
 Bloch, F., 287(220), 303  
 Block, A. N., 37(46), 66  
 Blodgett, K. B., 2(11), 13(11), 65  
 Blume, M., 267(163, 165), 302  
 Bodi, L. J., 308(38), 377  
 Boer, F. P., 213(17), 219(17), 222(17),  
 286(213, 214), 298, 303  
 Bogdanovic, G., 230(69), 299  
 Boguslavskii, L. I., 131(126), 137  
 Bonifacio, R., 64(59), 66  
 Boon, J. P., 185(59), 200  
 Boorstein, S. A., 272(175), 302  
 Boring, M., 289(228), 304  
 Born, M., 120(80), 136, 205(4), 297  
 Boys, S. F., 306(14), 307(14), 310(14),  
 327(14), 336(14), 376  
 Bradshaw, R. W., 121(84), 136  
 Brdicka, R., 109(58, 62, 63), 136  
 Breedveld, G. J. F., 155(43), 199  
 Brout, R., 142(17), 199  
 Brown, R. D., 286(211), 303  
 Bruni, M. C., 306(10), 315(10), 376  
 Brunner, P., 332(90), 378  
 Bucher, H., 2(4), 13(4, 31, 32), 24(31),  
 57(4), 65  
 Buckingham, A. D., 259(141), 301  
 Bucknell, M. G., 306(14, 15), 307(14),  
 310(14, 15), 327(14, 15), 329(15), 335  
 (15), 336(14, 15), 376  
 Buff, F. P., 121(85, 86), 136  
 Bunce, A. S., 100(27), 135  
 Bunker, P. R., 308(35), 377  
 Burstein, E., 2(21), 42(21), 65  
 Butler, J. A. V., 115(71), 136  
  
 Cade, P. E., 253(119), 300  
 Calder, V., 285(234), 304  
 Callaway, J., 224(52), 299  
 Callen, H. B., 81(30), 97  
 Calvert, D., 125(114), 137  
 Carbonaro, A., 230(65), 299  
 Carlson, K. D., 232(92, 93, 94, 96), 300  
 Carnahan, N. F., 154(40), 199  
 Carney, G. D., 306(26, 27, 28, 29, 30, 31,  
 32, 33), 310(28, 31), 312(28), 324(28,  
 31, 32), 326(31, 32), 327(26, 29, 30),  
 335(27, 28, 29, 30, 31, 32), 336(28, 30,  
 31, 32, 33), 338(29, 31, 105), 342(28),  
 343(31), 344(31), 346(31), 353(29),  
 355(32), 363(29, 30), 364(29, 30), 365  
 (31), 367(32), 368(30, 32), 369(32),  
 370(27), 371(27, 31, 33), 372(29, 30, 32,  
 33), 373(30), 374(30), 377, 379  
 Carruthers, P., 142(17), 199  
 Cass, A., 90(43), 97, 120(81), 121(92),  
 124(92), 136, 137  
 Cassata, A., 230(66), 299  
 Certain, P. R., 328(87), 333(87), 378  
 Chan, H., 100(5), 135  
 Chance, R. R., 2(14, 18, 19), 3(18), 4(14,  
 24), 8(18), 9(18), 11(14), 13(14, 34, 35),  
 14(14), 15(14), 16(34, 35), 20(35), 21  
 (35, 39), 22(35), 23(18, 19, 39), 25(39),  
 34(44), 35(44), 37(45), 39(18), 40(19),  
 41(24), 42(18, 19, 24), 64(39), 65, 66  
 Chandler, D., 140(6), 146(6), 183(6),  
 195(6), 198  
 Chapman, S., 185(58), 186(58), 200  
 Chedin, A., 338(99, 100), 378  
 Chen, M., 148(35), 199  
 Chen, Y., 68(8), 74(19), 75(25), 78(19),  
 79(25, 26, 27), 80(26), 81(26, 29), 84(29),  
 85(29), 87(38), 88(36), 89(19, 38), 93(27,  
 48), 94(8, 19, 27, 48), 96, 97  
 Cheng, I. -Y., 196(86), 200  
 Cheng, I. -Y. S., 144(25), 171(25), 199  
 Chesnick, J. P., 323(81), 378  
 Chiu, Y. N., 272(174), 302  
 Chizmadzhev, Yu. A., 100(32), 135  
 Christy, R., 9(26), 14(26), 18(26), 25(26),  
 42(26), 65  
 Chu, M. Y., 372(117), 379  
 Ciani, S. M., 100(31, 35, 41), 109(64),  
 117(41), 123(99), 135, 136  
 Cihla, Z., 338(99), 378  
 Čížek, J., 224(45), 299  
 Clack, D. W., 285(208), 286(208, 209), 303  
 Clay, J. R., 121(86), 136  
 Claydon, C. R., 232(92), 300  
 Clementi, E., 267(166), 268(166), 302  
 Clemmow, P., 46(55), 58(55), 60(55),  
 63(55), 66  
 CNDO model: 284(204), 285(204, 207),  
 303  
 Co., K. U., 156(45, 47), 157(45), 158(45,  
 47), 159(47), 160(45), 161(47), 162(47),  
 164(47), 176(53), 177(53), 178(53), 179  
 (53), 181(53), 182(53), 193(75),

- 196(45, 47), 197(45, 96), 199, 200, 201  
 Cohen, E. R., 274(183), 302  
 Cole, K. S., 105(53), 136  
 Colquhoun, D., 68(11), 97  
 Colwell, S. M., 307(34), 323(34), 332(34), 336(34), 377  
 Connolly, J. W. D., 288(223, 225), 303  
 Conti, F., 68(4, 5, 16), 96, 97  
 Cook, B., 285(236), 304  
 Cook, G. A., 186(65), 188(65), 189(65), 200  
 Coolidge, A. S., 222(43), 298  
 Cotton, F. A., 243(101), 245(101), 300  
 Coulson, C. A., 222(44), 225(53), 299  
 Cowling, T. G., 185(58), 186(58), 200  
 Crispin, R. J., 251(108), 300  
 Croghan, P. C., 124(101), 137  
 Cross, P. C., 308(49), 311(49), 354(49), 377  
 Curtiss, C. F., 185(61), 188(61), 200, 308(38), 377  
 Curtiss, L. A., 306(29, 30, 32), 324(32), 325(32), 326(32), 327(29, 30), 335(29, 30, 32), 336(30, 32), 338(29), 353(29), 355(32), 363(29, 30), 364(29, 30), 367(32), 368(30, 32), 369(32), 372(29, 30, 32), 373(30), 374(30), 377  
 Cusachs, L. C., 219(28), 298  
  
 Dahl, J. P., 227(58), 284(201), 286(210), 303  
 Dahler, J. S., 372(117), 379  
 Dalgarno, A., 273(181), 302  
 Dall'Asta, G., 230(65), 299  
 Danielli, J. F., 100(17), 135  
 Darling, B. T., 308(37), 309(37), 377  
 Das, G., 318(71), 321(71), 322(71), 378  
 Das, T. P., 246(103), 281(189), 283(190), 300, 302  
 Datta, K., 317(62), 377  
 Daudel, R., 297(259), 304  
 Davis, H. T., 185(57, 59, 60), 187(60, 68), 188(68, 69, 70), 194(76, 77), 198(97), 200, 201  
 Davson, H., 100(17), 135  
 de Bock, A., 186(64), 188(64), 200  
 de Brouckere, G., 216(22), 221(22), 231(76), 233(78), 235(80), 237(80, 85), 238(76), 239(91), 241(98), 246(102), 263(148), 265(159), 267(76, 168), 268(159), 272(172), 294(250), 298, 299, 300, 301, 302, 304  
 Decius, J. C., 308(49), 311(49), 354(49), 377  
 De Felice, L. J., 68(4, 5, 15), 96, 97  
 De Groot, S. R., 86(34), 97  
 Delahay, P., 127(121), 131(128), 137  
 Delbruck, M., 205(1), 297  
 de Levie, R., 100(42), 102(44, 46, 47, 48), 103(44, 46, 47), 104(44), 105(130), 107(48, 55), 109(48), 114(67), 120(47, 79), 123(97), 125(55), 128(44), 130(67), 131(67, 97), 136, 137  
 del Re, G., 219(27), 228(60), 298, 299  
 de Michelis, G., 234(79), 300  
 Demuyne, J., 237(86), 238(86), 263(86, 151), 300, 301  
 Denim, V. V., 121(89), 136  
 Denis, A., 258(135), 301  
 Dennison, D. M., 308(37), 309(37), 377  
 Derksen, H. E., 68(1), 92(1), 96  
 Devanathan, M. A. V., 125(111), 137  
 Dewar, M. J. S., 285(238), 304  
 Dickinson, A. S., 322(78), 328(87), 333(87), 378  
 Dietrich, H., 230(70), 299  
 Diller, D. E., 186(63), 200  
 Dionne, V. E., 68(11), 97  
 Dirac, P. A. M., 287(221), 303  
 Di Sipio, L., 221(35), 234(79), 298, 300  
 Ditchfield, R., 254(120, 121), 300  
 Dobosh, P. A., 284(205), 285(205), 303  
 Dolph, C. I., 197(94), 201  
 Drake, G. W. F., 323(83), 378  
 Drexhage, K. H., 2(5, 6, 7, 8, 9), 10(6, 7, 8, 9), 13(5, 6, 7, 8, 9, 31), 15(6, 7), 16(7, 8, 9), 17(5, 6, 7, 8), 18(36), 19(36), 20(6, 36), 21(6, 9), 22(6), 24(31), 30(5, 6, 7, 8, 9), 43(5, 6, 7, 8, 9), 50(5, 6), 57(5, 6, 7, 8, 9), 64(5, 6, 7, 8, 9), 65  
 Dubrow, R., 323(86), 378  
 Duff, J. W., 332(90), 378  
 Dumond, J. W. M., 274(183), 302  
 Dunham, J. L., 319(73), 378  
 Dunitz, J. D., 271(170), 302  
  
 Eckart, C., 308(48), 377  
 Edgell, W. F., 279(187), 302  
 Eggers, F., 100(40), 135  
 Ehrenstein, G., 100(9), 135

- Eichner, J., 100(5), 135  
 Eisenberg, M., 90(42), 97, 100(11, 39), 135  
 Eisenman, G., 100(8, 31, 35, 41), 109(64, 66), 117(41), 123(99), 135, 136, 137  
 Ellinger, J., 259(193), 302  
 Ellinger, Y., 216(38), 298  
 Ellis, D. E., 264(157), 265(157), 289(229, 230), 290(232), 295(254), 301, 304  
 Ellis, P. D., 255(125), 301  
 Elson, J., 2(21), 42(21), 65  
 Emch, G. G., 195(78), 200  
 Emsley, J. W., 255(127), 301  
 Endres, P. F., 323(82, 85), 334(85), 378  
 Engerholm, G. G., 321(75), 327(75), 328(75), 333(75), 378  
 Epstein, S. T., 214(19), 298  
 Erdey-Gruz, T., 115(72), 136  
 Ermler, W. C., 314(55), 362(111), 377(54), 379  
 Ershler, B. V., 125(113), 137  
 Esin, O. A., 125(112), 137  
 Eyring, H., 115(73), 136
- Fahey, R. C., 258(132), 301  
 Farrimond, M. S., 286(209), 303  
 Fassett, J. R., 70(20), 74(20), 75(20), 81(20), 84(20), 97  
 Faucher, H., 259(138, 198), 301, 303  
 Fayt, A., 373(119), 379  
 Feldberg, S., 120(78), 125(116), 136, 137  
 Felton, R. H., 290(231), 304  
 Fenske, R. F., 220(31), 238(87), 298, 300  
 Ferrell, R., 2(23), 45(23), 65  
 Ferrell, R. A., 40(47), 66  
 Feshbach, H., 169(50), 199  
 Fettiplace, R., 90(39), 97  
 Finkelstein, A., 90(43, 44), 97, 120(81), 121(92), 124(92), 136, 137  
 Finlan, J. M., 320(74), 338(74), 362(74), 378  
 Fippis, B. N., 238(90), 300  
 Fisher, M. E., 140(7), 184(56), 198, 200  
 Fischer Hjalmar, I., 224(46), 226(57), 227(57), 269(57), 299  
 Fishman, H. M., 68(2, 6), 87(6), 96  
 Fleck, M., 2(5), 13(5, 31), 17(5), 24(31), 30(5), 43(5), 50(5), 57(5), 64(5), 65  
 Flory, P. J., 125(106), 137  
 Foord, A., 306(8, 9), 307(8, 9), 313(8, 9), 335(8, 9), 336(9), 337(8), 338(9), 340(8, 9), 341(9), 376  
 Forman, A., 262(150), 263(150), 301  
 Förster, T., 23(41), 66  
 Fowler, R. H., 72(22), 97  
 Fraga, S., 267(164), 302  
 Franceschetti, D. R., 372(118), 379  
 Freeman, A. J., 264(155, 157), 265(157), 279(188), 293(247), 295(254), 301, 302, 304  
 Frisch, H. I., 142(16), 199  
 Frumkin, A. N., 125(108), 137  
 Fuchs, M., 120(77), 123(77), 124(77), 136  
 Fuchs, R., 40(48), 45(53), 57(48), 66  
 Funck, T., 100(40), 135  
 Fues, E., 322(77), 378
- Gage, P. W., 92(45), 97  
 Gagnaire, D., 258(134), 301  
 Galbraith, H. W., 308(46), 377  
 Gallavotti, G., 144(24), 199  
 Garito, A., 46(54), 66  
 Gartenhaus, S., 195(80), 200  
 Gaspar, R., 287(218), 303  
 Geller, M., 273(180), 302  
 Geril, R., 338(101), 378  
 Gerischer, H., 66(58)  
 Gerson, F., 338(102, 103), 378  
 Giannini, V., 230(66), 299  
 Gibbs, J. H., 242(99), 300  
 Ginsburg, S., 123(98), 137  
 Glasstone, S., 115(73), 136  
 Godfrey, M., 277(177), 302  
 Goel, N. S., 121(85, 86), 136  
 Goepfert-Mayer, M., 210(9), 211(9), 216(9), 297  
 Goldman, D. E., 136(51)  
 Goldsmith, M., 337(97), 339(97), 378  
 Goldstein, J. H., 373(120), 379  
 Goldstein, R. A., 171(51), 200  
 Gordon, L. G. M., 90(39), 97, 100(10), 135  
 Gorter, E., 100(16), 135  
 Gosman, A. L., 193(74), 200  
 Gouterman, M., 272(175), 302  
 Graham, C., 258(132), 301  
 Grahame, D. C., 125(109), 137  
 Gray, H. B., 212(15), 220(30), 221(30), 238(88), 286(212), 298, 300, 303  
 Gray, P., 140(11), 142(11), 199  
 Greco, A., 230(65), 299

- Greenawalt, E. M., 322(78), 378  
 Greene, R. F., 81(30), 97  
 Grell, E., 100(40), 135  
 Grendel, F., 100(16), 135  
 Grevendonk, W., 186(64), 188(64), 200  
 Gribov, L. A., 306(20, 21, 22, 23), 307(20, 21, 22, 23), 312(20), 335(20, 21, 22, 23), 336(20, 21, 22, 23), 343(21, 22, 23), 376, 377  
 Griffith, J. S., 271(171), 292(244), 302, 304  
 Griffith, R. W., 273(180), 302  
 Grigorev, P. A., 131(127), 137  
 Grimaldi, F., 243(100), 300  
 Gubanov, V. A., 288(225), 303  
 Gubbins, K. E., 185(62), 200  
 Guidotti, D., 37(46), 66  
 Günthard, Hs. H., 308(39), 310(39), 338(101), 377, 378  
 Gwinn, W. D., 321(75), 327(75), 328(75), 333(75), 378  
  
 Hagen, S. H., 231(73), 262(73, 145, 147), 266(145, 147), 299, 301  
 Hall, G. G., 252(114), 300  
 Hall, J. E., 90(42), 97, 100(11), 123(93), 135, 137  
 Hameka, H. F., 251(110), 252(110), 300  
 Hammerstein, A., 197(95), 201  
 Han, P. S., 246(103), 283(190), 300, 302  
 Handy, N. C., 306(14, 15, 16, 17), 307(14, 15, 34), 310(14, 15, 16), 312(16, 17), 313(16), 323(34), 327(14, 16, 17), 329(15), 332(17, 34), 335(15, 16, 17), 336(14, 15, 16, 17, 34), 340(16, 17), 341(16), 352(16, 17), 376, 377  
 Hanley, H. J. M., 186(63), 200  
 Hansma, P. K., 42(52), 66  
 Harary, H., 125(117), 137  
 Hardisson, A., 252(114), 300  
 Harris, Ch. B., 243(101), 245(101), 300  
 Harris, D. W., 321(75), 327(75), 328(75), 333(75), 378  
 Hartmann, H., 230(63), 299  
 Hasman, D. A., 212(16), 298  
 Hass, G., 24(42), 25(42), 66  
 Hatfield, W. E., 237(81), 300  
 Hatzenbuehler, D., 323(86), 378  
 Hay, D. J., 259(140), 301  
 Haydon, D. A., 90(39, 41), 97, 100(6, 10, 28), 121(90), 125(90), 135, 137  
 Hazi, A. U., 323(84), 378  
 Heeger, A., 46(54), 66  
 Heilbronner, E., 338(101, 102, 103), 378  
 Helmholtz, L., 212(14), 222(14), 284(203), 298, 303  
 Henderson, D., 140(4), 146(4, 30, 31), 148(30, 31, 35), 149(30, 31, 36), 183(4), 195(4), 198, 199  
 Herigonte, P. V., 296(258), 304  
 Herreman, W., 186(64), 188(64), 200  
 Hertzberg, G., 232(95), 300  
 Hider, R. C., 100(27), 135  
 Higushi, J., 272(173), 302  
 Hill, T. L., 68(17, 18), 73(18, 23), 79(27), 84(23), 87(38), 89(38), 93(27, 48), 94(27, 48), 97, 140(10), 142(10), 176(54), 199, 200  
 Hinze, J., 221(37), 298, 318(72), 321(72), 322(72), 378  
 Hirschfelder, J. O., 185(61), 188(61), 200  
 Hitchcock, P. B., 126(119), 137  
 Hladky, S. B., 90(39, 41), 97, 100(6, 28), 109(57), 123(96), 135, 136  
 Hoarau, J., 257(196), 303  
 Hock, A. A., 271(169), 302  
 Hodgkin, A. L., 87(37), 89(37), 93(37), 97  
 Hollister, C., 264(156), 295(253, 255), 301, 304  
 Hopgood, F. R. A., 295(257), 296(257), 304  
 Hornbach, C. J., 264(156), 295(253), 301, 304  
 Horner, F. M., 237(81), 300  
 Hosteny, R. P., 335(95), 378  
 Howard, B. J., 308(42), 377  
 Howard, J. B., 308(36), 309(36), 377  
 Hoy, A. R., 347(109), 362(109), 379  
 Hsu, K., 124(102), 137  
 Hubbard, J., 295(257), 296(257), 304  
 Hubbell, W. L., 126(118), 137  
 Hüchel, E., 205(2), 297  
 Huggins, M. L., 125(107), 137  
 Hull, T. E., 333(91), 378  
 Huo, W. N., 253(119), 300  
 Hust, J. G., 193(74), 200  
 Huxley, A. F., 87(37), 89(37), 93(37), 97  
  
 Iafrate, G. J., 317(63), 377



- Ikeda, S., 230(68), 299  
 Ikenberry, L. D., 188(73), 189(73), 200  
 Inacker, O., 13(30, 32, 33), 15(30), 16(30), 19(30), 25(33), 65  
 INDO model: 284(205), 285(205), 303  
 Infeld, L., 333(91), 378  
 Itoh, J., 262(146), 301  
 Ivanov, V. T., 100(37), 135
- Jaffe, H. H., 221(37), 298  
 Jähnig, J., 86(32), 97  
 Jain, M. K., 100(34), 135  
 James, H. M., 222(43), 298  
 Jancovici, B., 195(81), 200  
 Jeannotte, A. C., II, 336(96), 378  
 Jobard, I., 338(100), 378  
 Johnson, K. H., 288(223, 224), 289(226), 303  
 Johnson, K. J., 290(233), 304  
 Johnson, P., 9(26), 14(26), 18(26), 25(26), 42(26), 65  
 Jørgensen, C. K., 216(21), 230(64), 233(64), 234(66), 237(81), 292(245), 298, 299, 300, 304  
 Jouve, P., 347(108), 351(108), 354(108), 379  
 Jucys, A. P., 267(167), 302
- Kallman, H., 21(38), 64(38), 66  
 Kaminskas, V. A., 267(167), 302  
 Karplus, M., 254(124), 255(126), 277(177), 295(252), 301, 302, 304  
 Kato, H., 260(143), 301  
 Katz, B., 68(9), 92(9), 96  
 Katz, I., 121(92), 124(92), 137  
 Kaveckis, V. J., 267(167), 302  
 Keizer, J., 70(21), 71(21), 86(33), 97  
 Kern, C. W., 277(177), 302, 306(6, 28), 310(28), 312(28), 314(55), 315(6), 317(6), 324(28), 327(28), 335(28), 336(28), 342(28), 376, 377(53, 54)  
 Ketterer, B., 114(69), 124(69), 131(69), 136(75)  
 Khachatryan, A. G., 195(79), 200  
 Khovrin, G. V., 306(21, 22, 23), 307(21, 22, 23), 335(21, 22, 23), 336(21, 22, 23), 343(21, 22, 23), 376, 377  
 Kirkwood, J. G., 143(22), 145(29), 156(44), 171(22), 173(29), 199  
 Kirtley, J., 42(52), 66
- Kishimoto, U., 100(22), 135  
 Kleinman, B., 295(252), 304  
 Kliever, K., 45(53), 66  
 Kliever, K. L., 40(48), 57(48), 66  
 Klochkoy, V. V., 124(105), 137  
 Knight, P. L., 11(29), 34(29), 35(29), 64(29), 65  
 Knoll, W., 123(100), 137  
 Kochansky, E., 273(182), 302  
 Kohn, W., 287(219), 303  
 Kolb, H. A., 68(12), 90(12), 97  
 Kolker, H. J., 254(124), 301  
 Kolos, W., 222(42), 298  
 Koningstein, J. A., 290(240), 304  
 Kopfermann, H., 224(50), 299  
 Koutecky, J., 109(58, 61), 136  
 Kozak, J. J., 143(19, 20), 144(25), 150(34), 151(34), 152(34), 154(37, 41), 156(45, 46, 47), 157(45), 158(45, 47), 159(47), 160(45), 161(47), 162(47), 164(46, 47), 165(46), 167(46), 171(25, 51), 173(41), 175(34), 176(46, 53), 177(41, 53), 178(46, 53), 179(53), 180(37, 41), 181(53), 182(53), 183(46), 191(41), 193(75), 195(82, 83), 196(45, 47, 86), 197(45), 198(75), 199, 200, 201(93)  
 Kramers, H. A., 317(59), 377  
 Krasne, S., 100(8, 35), 123(99), 135, 137  
 Krasnoselskii, M. S., 168(49), 196(49), 199  
 Krespi, V., 90(43), 97  
 Krohn, B. J., 314(55), 377  
 Krugh, T. R., 259(140), 301  
 Ku, J. S., 154(38), 187(66), 188(66), 199, 200  
 Kubo, R., 81(31), 97  
 Kuhn, H., 2(1, 2, 3, 4, 5, 12), 3(12), 4(12), 11(12), 12(12), 13(1, 2, 3, 4, 5, 13, 30, 31, 32, 33), 15(30), 16(30), 17(5), 19(30), 22(12), 24(12, 31), 25(12, 33), 30(5), 38(12), 43(5), 50(5), 57(1, 2, 3, 4, 5), 64(5), 65  
 Kuo, S. S., 335(94), 378  
 Kurczewska, H., 21(40), 23(40), 24(40), 25(40), 66  
 Kutzelnigg, W., 228(60), 299
- Lai, E. K. C., 306(25), 307(25), 312(25), 327(25), 330(25), 334(25), 335(25), 336(25), 342(25), 343(25), 352(25), 370(25), 377

- Laidler, K. J., 115(73), 136  
 Lamb, W. E., Jr., 370(116), 379  
 Langhoff, S. R., 306(29, 30, 32, 33), 324  
 (32), 325(32), 326(32), 327(29, 30), 335  
 (29, 30, 32, 33), 336(30, 32, 33), 338(29),  
 353(29), 355(32), 363(29, 30), 364(29,  
 30), 367(32), 368(30, 32), 369(32), 371  
 (33), 372(29, 30, 32, 33), 373(30), 374  
 (30), 377  
 Langmuir, I., 13(10), 65  
 Laprade, R., 100(31, 35, 41), 117(41), 135,  
 136  
 Larkin, D., 120(79), 136  
 Latorre, R., 100(9), 135  
 Luger, P., 68(12), 90(12), 97, 100(12, 30),  
 114(69), 116(74), 120(83), 122(83),  
 123(83), 124(69), 131(69, 125), 135,  
 136, 137  
 Lavery, B. J., 259(140), 301  
 Laws, E. A., 235(118), 300  
 Lax, M., 74(24), 82(24), 97  
 Lea, E. J. A., 124(101), 137  
 Lebedev, A. V., 131(126), 137  
 LeBlanc, O. H., Jr., 109(59), 136  
 Lebowitz, J. L., 140(2), 142(16), 198, 199  
 Lecar, H., 100(9), 135  
 Lecourt, A., 243(100), 300  
 Lee, T. D., 144(28), 190(28), 199  
 Lee, Y-T, 142(15), 183(15), 199  
 Lekner, J., 142(13), 158(13), 195(13), 199  
 Lemberg, H. L., 37(46), 66, 195(84), 200  
 Lesk, A. M., 323(79), 378  
 Lesslauer, W., 131(125), 137  
 Levine, S., 125(114), 137  
 Levy, B., 258(134), 259(139), 249(192),  
 259(192, 193), 301, 302  
 Levy, R., 273(182), 302  
 Levy, S., 125(116), 137  
 Lewinson, V. A., 145(29), 173(29), 199  
 Lewis, J. T., 273(181), 302  
 Liberman, Ye. A., 124(104, 105), 137  
 Lin, C. S., 323(83), 378  
 Lincoln, W. W., 150(34), 151(34), 152(34),  
 154(39), 155(42), 156(46), 164(46),  
 165(46), 167(46), 173(39), 175(34),  
 176(39, 46), 178(46), 180(39), 183(46),  
 199  
 Lipscomb, W. N., 213(17), 219(17), 220(17),  
 237(83), 247(106), 248(106), 251(106),  
 253(118), 286(213, 214), 287(215),  
 298, 300, 303  
 Lipson, W., 230(61), 299  
 Liu, B., 264(154), 301  
 Locker, D. J., 322(76), 323(76), 378  
 London, F., 251(112), 300  
 Longuet-Higgins, H. C., 215(20), 222(20),  
 225(53), 265(158), 266(158), 271(158),  
 298, 299, 301  
 Louck, J. D., 308(45, 46), 309(45), 377  
 Lovett, R., 196(87, 88), 200  
 Low, W., 266(162), 302  
 Lowdin, P. O., 209(6), 226(54), 297, 299  
 Lowry, B. A., 188(69), 200  
 Lucazeau, G., 290(240), 304  
 Luks, K. D., 150(34), 151(34), 152(34),  
 154(33, 37, 38, 39, 41), 155(33, 42), 156  
 (45, 46, 47), 157(45), 158(45, 47), 159  
 (47), 160(45), 161(47), 162(47), 164(46,  
 47), 165(46), 167(46), 173(33, 39, 41),  
 175(34), 176(33, 39, 46, 53), 177(41, 53),  
 178(46, 53), 179(53), 180(37, 39, 41),  
 181(53), 182(53), 183(46), 187(66, 68),  
 188(33, 66, 68, 70), 190(33), 191(41),  
 192(33), 193(75), 194(77), 196(45, 47),  
 197(45), 198(75), 199, 200, 201  
 Lykos, P. G., 207(5), 297  
 McCarty, R. D., 193(74), 200  
 McClary, W. K., 317(64), 377  
 McClure, D. S., 291(242), 304  
 McConnell, H. M., 126(118), 137  
 MacDonald, J. K. L., 318(67), 378  
 Macdonald, J. R., 125(115), 137  
 McIver, J. W., 255(125), 256(130), 301  
 McIver, J. W., Jr., 253(117), 300  
 McLachlan, A. D., 274(184), 302  
 McLaughlin, I. L., 194(76, 77), 200  
 McLaughlin, S., 100(39), 109(64, 65, 66),  
 120(78), 124(65, 103), 125(116, 117),  
 135, 136, 137  
 McLean, A. D., 241(97), 243(97), 300  
 McWeeny, R., 231(72), 252(116), 299, 300  
 Maes, S., 338(98), 378  
 Maestro, M., 251(111), 254(111, 123), 300,  
 301  
 Magleby, K. L., 92(46), 97  
 Malli, G., 267(164), 302  
 Malrieu, J. P., 258(135), 301  
 Mann, D. E., 285(234), 304  
 Manne, R., 286(216), 303

- Marciel, G. E., 255(125), 301  
 Margenau, H., 308(47), 310(47), 377  
 Mark, M. A., 146(32), 148(32), 149(32),  
 150(32), 151(32), 182(32), 199  
 Markin, V. S., 100(32), 114(68), 124(105),  
 131(127), 135, 136, 137  
 Marshall, W., 264(153), 301  
 Martin, D. S., 238(87), 300  
 Marx, W., 323(86), 378  
 Mason, R., 126(119), 137  
 Mataga, N., 219(26), 298  
 Matcha, R. L., 377(53)  
 Matsen, F. A., 318(69, 70), 321(69, 70),  
 378  
 Maun, E. K., 156(44), 199  
 Mazur, P., 86(34), 97  
 Mead, C. A., 90(42), 97, 100(11), 123(93),  
 135, 137  
 Melman, P., 64(57), 66  
 Meyer, A., 68(3), 96  
 Meyer, H., 13(32), 65  
 Meyer, R., 308(39), 310(39), 377  
 Mikhlin, S. G., 318(68), 378  
 Miledi, R., 68(9), 92(9), 96  
 Miller, A. H., 13(34, 35), 16(34, 35), 20(35),  
 21(35), 22(35), 65  
 Miller, D. P., 254(120), 300  
 Miller, I. R., 100(26), 135  
 Miller, M. A., 188(70), 200  
 Miller, W. H., 307(34), 323(34), 332(34,  
 89), 336(34), 377, 378  
 Millié, P., 212(12), 216(22), 221(22), 298  
 Millie, Ph., 237(84), 259(139), 249(192),  
 259(192, 193), 285(235), 300, 301, 302,  
 304  
 Mills, I. M., 306(4), 347(109), 362(109),  
 376, 379  
 Mills, O. S., 271(169), 302  
 Milonni, P. W., 11(29), 34(29), 35(29),  
 64(29), 65  
 Miracle-Sole, S., 144(24), 199  
 Misono, A., 230(68), 299  
 Miyazaki, T., 251(107), 300  
 Mizuno, A., 260(142), 301  
 Möbius, D., 2(3, 4), 13(3, 4, 31), 21(37),  
 23(37), 24(31), 25(37), 26(37), 57(3, 4),  
 65  
 Moccia, R., 251(111), 254(111, 123), 300,  
 301  
 Moffat, M. J., 143(19, 20), 199  
 Moffitt, W., 210(10), 297  
 Momicchioli, F., 306(10), 315(10), 376  
 Monroe, E., 143(22), 171(22), 199  
 Montal, M., 100(23, 24), 135  
 Moore, C. Bradley, 306(1), 376  
 Moore, L. E., 68(6, 14), 87(6), 96, 97  
 Moraal, H., 144(27), 199  
 Morawitz, H., 64(59), 66  
 Moreira, H., 102(44, 46, 47), 103(44, 46,  
 47), 104(44), 120(47), 128(44), 136  
 Morf, W. E., 100(36), 135  
 Morgan, H. W., 373(120), 379  
 Morifuji, K., 230(68), 299  
 Morino, Y., 366(115), 368(115), 379  
 Morishima, I., 260(142), 301  
 Morse, P. M., 169(50), 199  
 Moser, C., 243(100), 300  
 Morawitz, H., 2(13, 17), 11(17), 13(13),  
 42(17), 64(13, 17), 65  
 Moser, C. M., 232(92, 94, 96), 300  
 Moskowitz, J. W., 264(156), 289(228),  
 295(253, 255), 301, 304  
 Moss, R. E., 308(42), 377  
 Mott, N. F., 104(52), 136  
 Mueller, P., 90(40), 97, 100(1, 2, 3, 4, 13,  
 14, 15, 19, 20, 21, 23), 129(19, 20, 21),  
 135  
 Muller, R. U., 90(44), 97  
 Mulliken, R. S., 218(24), 226(55), 233(77),  
 242(77), 266(161), 298, 299, 301  
 Murphy, G. M., 308(47), 310(47), 377  
 Murphy, W. C., 37(46), 66  
 Murrell, J. N., 306(18), 348(18), 352(18),  
 376  
 Musher, J., 248(109), 300  
 Myers, V. B., 121(90), 125(90), 137  
 Nakadomari, H., 125(116), 137  
 Nakatsuji, H., 260(143), 301  
 Natta, G., 230(66), 299  
 NDDO model: 284(206), 285(206), 303  
 Neher, E., 68(13, 14), 90(13), 92(47), 97  
 Nesbet, R. K., 232(93), 300  
 Neumcke, B., 100(30, 33), 109(60), 114  
 (69), 120(83), 122(83), 123(83), 124(69),  
 131(69), 135, 136  
 Newton, M. D., 213(17), 219(17), 222(17),  
 286(213, 214), 298, 303  
 Nielsen, H. H., 306(3, 5), 313(3), 315(57),  
 337(97), 339(97), 376, 377, 378

- Nieuwpoort, W. C., 279(187), 295(256),  
302, 304
- Nishimoto, K., 219(26), 298
- Noble, B., 196(91), 200
- Noble, D., 123(98), 137
- Nöel, P., 259(139), 301
- O'Donnell Offenhartz, P., 291(241), 294  
(249, 251), 304
- Ohrn, Y., 306(24), 338(24), 339(24), 377
- Oleari, L., 234(79), 300
- Olson, R. W., 336(96), 378
- Oppenheimer, J. R., 205(4), 297
- Orbach, R., 281(189), 302
- Orgel, L. E., 271(170), 302
- Orloff, D., 233(77), 242(77), 299
- Orloff, H., 233(77), 242(77), 299
- Ortega, J., 335(93), 378
- Osche, G. R., 317(63), 377
- O'Stein, D., 64(57), 66
- Ostlund, N. S., 253(117), 256(130), 300,  
301
- Otto, A., 2(20), 42(20), 65
- Ovchinnikov, Yu. A., 100(37), 135
- Overend, J., 306(7), 310(50), 327(50), 336  
(96), 376, 377, 378
- Pagano, R. E., 100(26), 135
- Paldus, J., 224(45), 299
- Palyvos, J., 194(77), 200
- Parameswaran, T., 289(230), 304
- Pariseau, M. A., 306(7), 376
- Pariser, R., 212(13), 220(32), 298
- Parker, P. M., 366(114), 379
- Parr, R. G., 207(5), 212(11), 220(32),  
297, 298, 320(74), 338(74), 362(74), 378
- Parry, J. M., 125(110), 137
- Parsegian, A., 120(82), 136
- Parsegian, V. A., 126(120), 137
- Parsons, R., 125(110), 137
- Pastur, L. A., 144(26), 199
- Paviot, J., 257(196), 303
- Penner, S. S., 379(112)
- Penrose, O., 140(2), 198
- Percus, J. L., 142(18), 199
- Perman, W. H., 124(102), 137
- Perram, J. W., 121(87), 136
- Petersen, D. C., 100(25), 135
- Phase Transitions and Critical Phenomena,  
140(9), 198
- Philpott, M. R., 2(17), 11(17, 28), 34(28),  
35(28), 42(17), 64(17, 28), 65
- Piccioni, R. L., 258(132), 301
- Pickett, H. M., 308(43), 310(43), 311(43),  
377
- Pilcher, G., 221(36), 298
- Pino, P., 230(66), 299
- Pipano, A., 335(95), 378
- Platt, J. R., 227(59), 299
- Plesner, I. W., 88(36), 97
- Pliva, J., 341(106), 379
- Polo, S. R., 311(51), 377
- Pople, J. A., 212(7), 215(20), 222(20),  
252(113), 253(117), 254(120), 255(126),  
256(130), 259(141), 284(202, 204, 205,  
206), 285(204, 205, 206, 207, 297), 297,  
298, 300, 301, 303, 304
- Porter, R. N., 306(27, 31), 310(31), 324  
(31), 326(31), 335(27, 31), 336(31),  
338(31), 343(31), 344(31), 346(31),  
365(31), 370(31), 371(31), 377
- Poussart, D. J. M., 68(6), 87(6), 96
- Powell, R. R., 279(187), 302
- Prat, R. F., 224(47), 299
- Prausnitz, J. M., 155(43), 199
- Prock, A., 2(14, 18, 19), 3(18), 4(14, 24),  
8(18), 9(18), 11(14), 13(14, 34, 35), 14  
(14), 15(14), 16(34, 35), 20(35), 21(35,  
39), 22(35), 23(18, 19, 39), 25(39), 34  
(44), 35(44), 37(45), 39(18), 40(19), 41  
(24), 42(18, 19, 24), 64(39), 65, 66
- Prosser, F. P., 278(186), 302
- Pryce, M. A. L., 231(71), 260(71), 265(71),  
299
- Pugh, L. A., 365(113), 379
- Pullman, B., 297(259), 304
- Radtke, D. D., 220(31), 298
- Ramsey, N. F., 246(105), 256(129), 300,  
301
- Rangarajan, S. K., 103(50), 105(130), 131  
(129), 136, 137
- Ransil, B. J., 254(122), 301
- Rao, K. N., 365(113), 379
- Rassat, A., 216(38), 298
- Raveche, H. J., 196(85), 200
- Ree, F. H., 142(15), 183(15), 199
- Ree, T., 142(15), 183(15), 199
- Reed, T. M., 185(62), 200
- Reed, T. S., 262(149), 263(149), 301

- Requena, J., 90(39), 97  
 Rettig, M. F., 246(103), 283(190), 300, 302  
 Rice, S. A., 37(46), 66, 140(11), 142(11, 13, 14), 158(13), 164(48), 171(48), 179(48), 185(57, 59), 188(69, 73), 189(73), 195(13, 14, 82, 83, 84), 199, 200  
 Richardson, J. W., 279(187), 302  
 Richter, J., 131(125), 137  
 Richter, P. H., 86(32), 97  
 Rieke, C. A., 233(77), 242(77), 299  
 Rimmer, D. E., 295(257), 296(257), 304  
 Ringsheim, H. P., 90(39), 97  
 Ritchie, R., 2(22), 45(22), 65  
 Ritz, W., 318(66), 378  
 Roberts, H. G., 252(115), 300  
 Robertson, C. R., 121(84), 136  
 Robertson, J. D., 100(18), 135  
 Robinson, P. D., 317(58), 377  
 Robinson, P. O., 196(92), 200  
 Roby, K. R., 286(211), 303  
 Roder, H. M., 186(63), 200  
 Roothaan, C. C. J., 205(3), 214(3), 215(3), 216(3), 221(3), 222(42), 278(185), 294(248), 295(248), 297, 298, 302, 304  
 Roper, L. D., 135(29)  
 Ros, P., 238(89), 264(157), 265(157), 295(254), 300, 301, 304  
 Rösch, N., 290(233), 304  
 Rosen, A., 289(229), 290(232), 304  
 Rosenberg, B. J., 362(111), 379  
 Ross, S. L., 80(28), 97  
 Rudin, D. O., 90(40), 97, 100(1, 2, 3, 4, 19, 20, 21), 127(19, 20, 21), 135  
 Ruedenberg, K., 217(23), 220(23), 223(23), 238(87), 258(133), 298, 300, 301  
 Ruelle, D., 140(1), 144(23), 184(23), 195(1), 198, 199  
 Ruff, G. A., 370(116), 379  
 Rutishauser, H., 338(102, 103), 378  
 Ruyschaert, J. M., 100(26), 135  
 Sabin, J. R., 306(24), 338(24), 339(24), 377  
 Sachs, E. S., 318(72), 321(72), 322(72), 378  
 Saito, T., 230(68), 299  
 Sakmann, B., 92(47), 97  
 Salpeter, E. E., 261(144), 273(144), 301  
 Sambe, H., 290(231), 304  
 Sandry, D. P., 212(7), 284(204, 206), 285(204, 206), 297, 303  
 Sängner, W., 257(197), 303  
 Saxena, R. P., 317(62), 377  
 Schaeffer, C. E., 292(245), 304  
 Schaefer, H. F., 264(154), 301  
 Schaefer, H. F., III, 306(2), 308(2), 318(2), 376  
 Schafer, F. P., 2(5), 13(5, 31), 17(5), 24(31), 30(5), 43(5), 50(5), 57(5), 64(5), 65  
 Schäfer, H. L., 230(63), 299  
 Schoenwald, J., 2(21), 42(21), 65  
 Schrod, I. B., 154(33, 37, 38, 41), 155(33), 173(33, 41), 176(33), 177(41), 180(37, 41), 187(66), 188(33, 66), 190(33), 191(41), 192(33), 199, 200  
 Schuit, G. C. A., 239(89), 300  
 Schwarz, G., 86(35), 97  
 Secroun, C., 347(108), 351(108), 354(108), 379  
 Seeger, R., 290(239), 304  
 Segal, G. A., 212(7), 284(204, 206), 285(204, 206, 207), 297, 303  
 Seidah, N. G., 102(46, 47, 48), 103(46, 47), 107(48), 109(48), 120(47, 79), 136  
 Sengers, J. V., 185(57), 187(67), 200  
 Seshadri, K. S., 285(234), 304  
 Shaffer, W. H., 315(57), 377  
 Sham, L. J., 287(219), 303  
 Sharma, R. R., 281(189), 302  
 Shavitt, I., 335(95), 362(111), 378, 379  
 Shepherd, W. C., 100(5), 135  
 Shikov, V. M., 125(112), 137  
 Shinoda, H., 251(107), 300  
 Shipley, G. G., 126(119), 137  
 Shkrob, A. M., 100(37), 121(89), 135, 136  
 Shore, B. W., 323(80), 378  
 Shulman, R. G., 293(246), 304  
 Siebenga, E., 68(3), 96  
 Siegman, A. E., 221(51), 231(51), 299  
 Silbey, R., 2(14, 18, 19), 3(18), 4(14, 24), 8(18), 9(18), 11(14), 13(14, 34, 35), 14(14), 15(14), 16(34, 35), 20(35), 21(35), 22(35), 23(18, 19), 34(44), 35(44), 37(45), 39(18), 40(19), 41(24), 42(18, 19, 24), 64(39), 65, 66  
 Simon, B., 317(61), 377  
 Simon, S., 100(25), 135  
 Simon, W., 100(36), 135  
 Simons, G., 320(74), 338(74), 348(110),

- 362(74), 378, 379  
 Skinner, H. A., 221(36), 298  
 Skinner, S. M., 102(43, 45), 136  
 Sklar, A. L., 210(9), 211(9), 216(9), 297  
 Slater, J. C., 213(18), 220(33), 287(217), 288(199), 298(34), 303  
 Smejtek, P., 124(102), 137  
 Smith, D. F., Jr., 310(50), 327(50), 377  
 Smith, F. C., Jr., 288(224), 289(226), 303  
 Smith, J. G., 306(9), 307(9), 313(9), 335(9), 336(9), 338(9), 340(9), 341(9), 376  
 Smith, W. R., 146(31), 148(31), 149(31, 36), 199  
 Snijder, L., 272(179), 302  
 Snijder, L. C., 264(152), 301  
 Sommerfeld, A., 2(16), 5(16), 6(16), 41(16), 65  
 Sondermann, J., 13(31), 24(31), 65  
 Sorbie, K. S., 306(18), 348(18), 352(18), 376  
 Speirs, G. K., 379(121)  
 Sperling, W., 2(5), 13(5, 31), 17(5), 24(31), 30(5), 43(5), 50(5), 57(5), 64(5), 65  
 Spezeski, J. J., 370(116), 379  
 Spirko, V., 379(121)  
 Sprandel, L. L., 306(6, 19), 307(19), 312(19), 315(6), 317(6), 327(19), 329(19), 335(19), 336(19), 376  
 Srivastava, P. K., 317(62), 377  
 Staats, P. A., 373(120), 379  
 Stanley, H. E., 140(8), 181(8), 198  
 Stark, G., 116(74), 123(100), 136(75), 137  
 Starling, K. E., 154(40), 199  
 Steenbeckeliers, G., 373(119), 379  
 Stegun, I., 334(92), 378  
 Steinbach, J. H., 68(11), 97  
 Stern, E., 2(23), 40(47), 45(23), 65, 66  
 Stern, O., 107(54), 136  
 Stevens, C. F., 68(7, 10), 92(10, 46), 96, 97  
 Stevens, R. M., 253(118), 300  
 Stevens, W. J., 318(71), 321(71), 322(71), 378  
 Stevenson, Ph. E., 237(83), 300  
 Stibbe, F. S., 231(74), 239(74), 279(74), 299  
 Stone, A. J., 265(158, 160), 266(158), 301  
 Stranahan, G., 195(80), 200  
 Stratton, J., 5(25), 7(25), 28(25), 37(25), 39(25), 58(25), 65  
 Streitweiser, A., Jr., 209(8), 297  
 Strey, G., 347(109), 362(109), 379  
 Stroud, A. H., 329(88), 378  
 Strutt, J. W., 318(65), 378  
 Stuart, C. A., 196(85), 200  
 Suard, M., 226(56), 299  
 Subra, R., 216(38), 259(193), 298, 302  
 Sugano, S., 292(243), 293(246), 304  
 Suzuki, I., 306(7, 11, 12, 13), 307(11, 12, 13), 313(12, 13), 318(11), 320(11), 321(12), 335(11, 12, 13), 336(11, 12, 13), 337(12, 13), 338(104), 339(11, 12, 13), 376, 379  
 Szabo, G., 100(8, 31, 35, 41), 109(64, 66), 117(41), 121(91), 123(93), 124(91), 135, 136, 137  
*Table of Interatomic Distances and Configurations in Molecules and Ions*, 231(191), 239(191), 267(191), 272(191), 302  
 Tafel, J., 115(70), 136  
 Tago, Y., 154(39), 173(39), 176(39), 180(39), 199  
 Takagi, M., 100(22), 135  
 Tanabe, Y., 292(243), 304  
 Tanaka, T., 366(115), 368(115), 379  
 Tarrago, C., 306(5), 376  
 Taylor, H. S., 323(84), 378  
 Teorell, T., 136(49)  
 ter Maten, G., 272(178), 302  
 ten Seldam, C. A., 231(76), 238(76), 239(91), 241(98), 246(102), 263(148), 265(159), 267(76, 168), 268(159), 272(172), 294(250), 299, 300, 301, 302, 304  
 Tews, K. H., 2(15), 7(15), 11(15, 27), 13(15, 27, 30, 32), 15(30), 16(30), 18(15), 19(30), 65  
 Thiele, E., 188(72), 200  
 Thomas, K. M., 126(119), 137  
 Thomas, L. H., 315(57), 377  
 Thomson, C., 272(176), 302  
 Throop, G. J., 160(52), 188(52), 200  
 Tilak, B. V. K. S. R. A., 125(111), 137  
 Tien, H. T., 100(19, 20, 21, 38), 127(19, 20, 21), 135  
 Tillman, P., 13(31), 24(31), 65  
 Tinkham, M., 302(194)  
 Tomita, K., 81(31), 97  
 Tondello, E., 221(35), 298  
 Topaly, V. P., 124(104, 105), 137  
 Tossell, J. A., 287(215), 303

- Trappeniers, N. J., 231(74, 76), 237(85),  
 238(76), 239(74), 262(145, 147), 263  
 (148), 265(159), 266(145, 147), 267  
 (76, 168), 268(159), 279(74), 299, 300,  
 301, 302  
 Truhlar, D. G., 336(96), 378  
 Tyree, F. Y., Jr., 237(81), 300  
  
 Uchida, Y., 230(68), 299  
 Urry, D. W., 100(7), 135  
 Uttech, R., 230(70), 299  
  
 Vainberg, M. M., 196(89), 200  
 van der Waals, J. H., 272(178), 302  
 Van Vleck, J. H., 246(104), 300, 315(56),  
 377  
 Van Vliet, K. M., 70(20), 74(20), 75(20),  
 81(20), 84(20), 97  
 van Wijck, J. A., 262(150), 263(150), 301  
 Varanasi, P., 379(112)  
 Varma, V. S., 317(62), 377  
 Vaubel, G., 21(37), 23(37), 25(37), 26(37),  
 65  
 Veillard, A., 216(22), 219(27), 221(22),  
 224(48), 237(82, 86), 238(86), 263(86,  
 151), 298, 299, 300, 301  
 Verlet, L., 140(5), 146(5), 183(5), 195(5),  
 198  
 Verveen, A. A., 68(1, 3, 15), 92(1), 96, 97  
 Viste, A., 220(30), 221(30), 298  
 Vlasov, A. A., 143(21), 199  
 Voittländer, J., 257(197), 303  
 Volmer, M., 115(72), 136  
 Vucelic, M., 306(24), 338(24), 339(24), 377  
 Vukadin, D., 114(67), 130(67), 131(67),  
 136  
  
 Wachters, A. J. H., 295(256), 304  
 Wahl, A. C., 318(71), 321(71), 322(71),  
 378  
 Wahlgren, V., 263(151), 301  
 Walz, D., 107(56), 136  
 Wanke, E., 68(4, 5, 16), 96, 97  
 Watson, J. K. G., 308(40, 41), 309(40),  
 313(41), 340(41), 344(40), 377  
 Watson, R. E., 264(155), 267(163, 165),  
 279(188), 293(247), 301, 302, 304  
 Waylonis, J., 24(42), 25(42), 66  
 Weber, J., 288(225), 303  
 Weeks, J. D., 140(6), 146(6), 183(6), 195  
 (6, 82, 83), 198, 200  
 Wei, L. Y., 123(94, 95), 137  
 Wertheim, M. S., 188(71), 200  
 Wertheimer, R., 308(44), 310(44), 377  
 Wescott, W. C., 100(19, 20, 21), 127(19,  
 20, 21), 135  
 Whiffen, D. H., 306(8, 9), 307(8, 9), 313  
 (8, 9), 335(8, 9), 336(9), 337(8), 338(9),  
 340(8, 9), 341(9), 376  
 White, D., 285(234), 304  
 White, S. H., 100(25), 135  
 Whitehead, R. J., 306(16, 17), 310(16),  
 312(16, 17), 313(16), 327(16, 17), 332  
 (17), 335(16, 17), 336(16, 17), 340(16,  
 17), 341(16), 352(16), 376  
 Widom, B., 141(12), 183(12), 199  
 Wiegand, J., 13(31), 24(31), 65  
 Wilke, G., 230(67, 69), 299  
 Willett, R. D., 231(75), 272(75), 299  
 Willig, F., 66(58)  
 Wilson, D. J., 323(82, 86), 378  
 Wilson, E. B., 308(36), 309(36), 377  
 Wilson, E. B., Jr., 308(49), 311(49), 354  
 (49), 377  
 Wilson, K. G., 184(55, 56), 195(55), 200  
 Wing, W. H., 370(116), 379  
 Wolfsberg, M., 212(14), 222(14), 284(203),  
 298, 303  
 Wolken, G., Jr., 338(105), 379  
 Woo, B. Y., 123(94, 95), 137  
 Wood, J. H., 289(228), 304  
 Wu, T. T., 317(60), 377  
  
 Yafuso, M., 100(25), 135  
 Yamagata, Y., 262(146), 301  
 Yamamoto, A., 230(68), 299  
 Yang, C. N., 144(28), 190(28), 199  
 Yeranov, W. L., 212(16), 298  
 Yermishkin, L. N., 131(127), 137  
 Yonezawa, T., 260(142), 301  
 Yoshimine, M., 241(97), 243(97), 300  
 Young, D. A., 142(14), 146(32), 148(32),  
 149(32), 150(32), 151(32), 164(48),  
 171(48), 179(48), 182(32), 195(14), 199  
  
 Zahorian, E., 323(86), 378  
 Zetik, D. F., 318(69), 321(69), 378  
 Zingsheim, H. P., 68(13), 90(13), 97  
 Zobel, O. J., 130(123), 137  
 Zwanzig, R. W., 140(3), 142(3), 143(3), 198

## SUBJECT INDEX

- Admittance, 111, 117
- Adsorption, 125
  - isotherm, 125
- Argon, 175
- Average structures, 366
- Barrier profile, 123
- Basic charge distributions expansions, 278
- BBGKY formulation, 140
- Bifurcation point, 111, 143, 169, 170
- Bifurcation properties, 143
- Bifurcation theory, 195
- Born energy, 120, 121
- Brout- Carruthers expansion, 142
- Carriers, 116, 120
- Closed kinetic system, 69
- Close-packing density, 162
- Coexistence, 181
  - envelope, 181
  - region, 197
  - boundary locus, 171
- Cole-Fisher, 142
- Complementary variational principles, 11, 196, 197
- Complex Poynting vector, 6
- Compressibility equation-of-state, 172
- Conductance fluctuation, 90
  - in liquid bilayer membranes, 90
  - in nerve axon membrane, 93
  - in postsynaptic end plate, 91
- Conservation relation, 73
- Constant-field approximation, 103
- Contact term, Fermi, F., 260-261
  - see also* First order one-electron properties
- Continuous branch of eigenvectors, 169
- Continuum, 101
  - models, 101
  - representation, 184
- Correlation operator, electronic, 273-274, 276
  - Corresponding states description, 155
  - Critical compressibility factor, 173
  - Critical exponents, 11, 142, 180, 184
  - Critical isotherm, 180
  - Critical phenomena, 140
  - Critical point, 180, 181
- Davis-Rice-Sengers theory, 186
- Dense fluid periodic region boundary locus, 171
- Dense liquid-solid transition, 172
- Dielectric displacement, 101
- Diffusion, 108
- Dipolar Interactions, spin-spin, 260, 261
  - see also* Second-order two-electron properties
- Dipole moment, electric, 241-243
  - see also* First-order one-electron properties
- Dipole potential, 121, 124
- Double layer, 107
- Double perturbation technique, 273, 274
- Drude metal, 39
- Dyadic Green's function method, 2
- Electronic structures, 233-329
- Electronic transitions and ab initio approach, 295
  - and crystal-field approach, 292
  - '10 Dq' problem, 290
  - nephelauxetic effect, 292
  - semiempirical MO approach, 294
  - simplified MO approach, 293
  - valence bond approach, 296
- Elementary chemical reaction, 71
  - nonregular, 72
  - regular, 72
- Energy equation of state, 172, 175
- Energy flux method, 2
- Energy transfer, 1



- Enskog theory, 185, 186  
 Exchange-correlation potential function, 287  
 Existence and uniqueness of the solutions, 143  
 $\theta$ -Expanded YBG equation, 145  
 First order one-electron properties:  
   closed-or open shell systems, dipole moment electric, 241-243  
   open shell systems, contact term Fermi, F., 261-264  
 First and second order proper ties:  
   open shell systems, spin Hamiltonian, 260, 261  
 Flat isotherms, 176  
 Forster transfer, 21  
 Fourier-transform method, 169  
 Frechet derivative, 169  
 Fresnel coefficients, 27  
 Gas-liquid coexistence, 162  
   behavior, 165  
   region, 11, 154, 173, 190  
 Gas liquid interface, 198  
 Gas liquid transition, 11, 142, 172  
 Green's function method, 2  
 Griffith inequalities, 182  
 Gyromagnetic factor  $g$ , electronic, 260, 261  
   *see also* Second-order one-electron properties  
 Hard-sphere fluid, 140  
 Hamiltonian, 306, 307  
 Hartree-Fock, *see* MO calculation scheme, 286  
 Hartree-Fock theory, coupled, 246-248  
 Hyperfine interactions, anisotropic, 261, 260  
   *see also* Second order one-electron properties  
 Hyperfine interactions, transferred, 260, 261  
   *see also* First order one-electron properties  
 Image forces, 210, 213  
 Image methods, 10  
 Integration methods, 327  
   HEG 327, 331, 333, 335  
   polynomial expansion method, 335  
   Simpson's rule, 327  
 Interfacial kinetics, 110  
 Inversion, 186-188  
   in  $K_r$ , 187  
   in the  $\eta_s$  function, 186  
   loci, 188  
   temperature, 188  
 Ionic displacement, 101, 110, 128  
 Irreducible cluster integral, 143  
 Ising model, 194  
 Isothermal compressibility, 159, 197  
 Kirkwood-Salsburg (KS equations), 144  
 Kirkwood superposition approximation, 11, 154, 180  
 Kirkwood YBG equation, 156  
 Krasnosel'skii theorem, 168, 169  
 Langmuir-Blodgett technique, 12  
 Lattice-gas model, 183  
 Lennard-Jones fluid, 142  
 LCAO approximation:  
   discarding muffin-tin and exchange correlation potentials, 289, 290  
   in ab initio MO scheme, 214  
   in semiempirical MO schemes, 207  
 Lipid bilayer, 100  
 Long-range behavior, 167  
 Long-range order, 142  
 Lower bound, 144, 171  
   on limit of stability, 144  
   on stability of a pure phase, 171  
 Mataga-Nishimoto, 219  
 Matrix elements, 211-215, 216-220  
   in discrete variational method, 289  
   in Goepfert-Mayer-Sklar method, 210  
   in Huckel:  
     extended method, 211-213  
     simple method, 209  
   in our semiempirical MO scheme, 216-220  
   in Roothaan SCF method, 214, 215  
 Matrix elements evaluations:  
   MO ground state:  
     use of spectroscopic terms, 220  
     use of (VSIE), 221  
 Maxwell construction techniques, 173  
 Mayer expansion, 142  
 Mechanical stability, 196

- Membrane thickness, 123
- Metallic complexes electronic structures,  
and related molecular observables,  
229, 230, 231
- Membrane thickness, 123
- Mixtures of simple fluids, 194
- MO calculation schemes:  
all electrons nonempirical, 286  
CNDO, and its serious shortcomings, 212,  
284, 285  
derived from CNDO, 285  
derived from Wolfsberg-Helmholtz, 286  
Goeppert-Mayer-Sklar, 210  
Hartree Fock, 214  
Huckel, extended, and its shortcomings,  
210, 211  
simple and its shortcomings, 207-209  
INDO, 285  
NDDO, 285, 286  
our model of, 215  
Roothaan, 214  
UHF, 221, 285, 286  
Wolfsberg-Helmholtz, 284  
 $\alpha$ , and its shortcomings, 287-289
- Modified Lennard-Jones 12-6 intermolecu-  
lar potential, 145
- Molecular beam experiments, 141
- Molecular dynamics, 146
- Molecules studied, 323  
diatomic – list, 335  
triatomic – list, 323, 326, 336
- Monte Carlo, 146
- Muffin-tin, 288
- Multicenter integrals:  
angular momentum, 268  
correlation operator, electronic, 276  
Coulomb, exchange, 217, 223, 227  
dipolar, spin-spin, 277  
electric field gradient, 245
- Noise power spectrum, 70, 86, 87  
differentiation between systems, 86  
eigenvalue method, 79  
irreversible thermodynamic approach,  
81  
master equation approach, 75  
matrix expression, 84, 85  
peaking phenomenon, in, 86, 87  
rate constant determination from, 89  
relation to time correlation function, 78
- Nonclassical critical exponents, 184
- Nonclassical values, for attendant critical ex-  
ponents, 11
- Nonlinear equations, 143  
integral, 196
- Nonradiative energy transfer, 6
- Nuclear spin-spin coupling, indirect, 260,  
261  
*see also* Second order one-electron proper-  
ties
- Observables/classification, 240, 241
- Odd multiplicity, 170
- Open kinetic system, 88
- Pair correlation function, 145  
hard sphere, 145
- Percus Yevick equation, 147
- Percus-Yevick (JPY) results, 142  
theory, 142
- Perfect mirror problem, 10
- Perturbation theories, 145, 186, 306, 313,  
315, 317, 320  
contact transformation, 317  
Nth order perturbation equation, 314
- Phase transformations, 143
- Phase transition, 143
- Plane wave spectrum method, 45
- Plasma frequency, 39
- Polarizability, electric, 260, 261  
*see also* Second order one-electron proper-  
ties
- Population analysis:  
Coulson and Longuet-Higgins, 225  
Mulliken, 226
- Population indices, and observable calcula-  
tions, 227, 228
- Positive tailing, 162
- Potential energy surface (function) (force  
field), 319-321  
*ab initio*, 321, 322, 328, 329  
Dunham's form, 320, 345, 347  
experimental, 342, 365  
force constants, 320, 321  
LEPS potential, 375  
SPF form, 371, 375  
Taylor series, 361  
truncation, 320  
Watson's term, 313, 338, 352
- Potential functions:

- exchange correlation, 287
- Mataga-Nishimoto, 219
- muffin-tin, 288
- Mulliken-Ruedenberg, 217, 223
  - see also* Multicenter integrals
- "Pressure" equation of state, 172, 175
- Pressure function, 172
- Propagation of attractive correlations, 184
- Quadrupole, 28
- Quadrupole coupling constant, nuclear eq., 243, 246, 260, 261
  - see also* First order one electron properties
- Radiative decay constant, 3
- Redlich-Kwong equation, 172
- Reference frame, 310
  - Eckart, 308
  - laboratory, 310
  - molecule-fixed, 310
- Relaxation matrix, 75
- Renormalization group theories, 184
- Rotational constants, 319, 320
- Scaling hypothesis, 182
- Second order one electron properties:
  - open shell system gyromagnetic factor  $g$ , electronic, 265-272
  - open or closed shell systems:
    - Hartree-Fock theory coupled, 246-248
    - hyperfine interactions, anisotropic, 259, 260
    - nuclear spin-spin coupling, indirect, 256-259
    - polarizability, electric, 249-251
    - shielding, magnetic, 251-255
    - susceptibility, magnetic, 251-255
- Second order two-electron properties, open shell systems dipolar interactions, spin-spin, 272-283
- Secular equations, solution of, 289, 323
  - in discrete variational method, 289
  - in multiple-scattering wave method, 289
  - in our MO model, 232
- Self diffusivity, 186
- Shear viscosity  $\eta$ , 154
- Shear viscosity  $\eta_s$ ,
  - see also* Second order one-electron properties
- Single barrier models, 114
- Solid-liquid transition, 142
- Spherical nonpolar molecules, 175
- Spin Hamiltonian, 260, 261
- Spin orbit coupling constant:
  - atomic, 267
  - molecular, 266, 268
- Spin-spin dipolar integrals, monocentric, 280
- Square-well potential function, 140, 141
- Stability analysis, 176, 184
- Stability of solutions, to nonlinear equations, 143
- Stratified medium, 34
- Supercritical simple fluids, 155
- Superposition approximation, 111, 142, 143, 145
- Surface plasmon modes, 1
- Surface polaritons, 41
- Thermal conductivity, 154, 186
- Thin film enhancement effect, 23
- Three capacitor model, 141
- Torus, 109
- Total energy, calculation of, 222
- Transition state, 288
- Transport behavior of classical fluids, 186
- Transport properties, 185, 197
- "Truncated superposition approximation," 11, 154, 175, 180
- Unexpanded YBG equation, 11, 155, 181
- Van der Waals equation of state, 172
- Vibrational basis functions, 317, 319, 322
  - analytical, 322
  - cubic spline, 321, 323
  - harmonic oscillator, 317, 319, 322, 323
  - Morse oscillator, 323, 334
  - nonorthogonal Gaussian, 323
  - numerical, 321
  - sine functions, 322, 323
- Vibrational CI, 332
- Vibrational coordinates, 326
  - cartesian, 324, 326
  - curvilinear, 338
  - dimensionless normal, 329
  - internal, 328
  - normal, 326, 327

- rectilinear, 326, 327
- reduced normal, 314
- Vibrational SCF, 326
- Vibrational wavefunctions, 314, 324, 354
  - assignment of quantum numbers, 353
- plots, 354-358, 361
- Yang-Lee theory of phase transition, 144
- YBG nonlinear integral equation, 184
- Yvon-Born-Green (YBG) theory, 140
- Zwanzig expansion, 142